

**NEW ENVIRONMENTS FOR NEUROPHYSIOLOGICAL
INVESTIGATIONS**

by
Arvindra Singh Sehmi

Statement of Originality

A thesis submitted in fulfilment of the requirements for the degree of Doctor of Philosophy in the Department of Engineering, The University of Leicester, England. All work recorded in this thesis is original unless otherwise acknowledged in the text or by references. No part of it has been submitted for another degree in this or any other University.

A handwritten signature in black ink, appearing to read 'A.S. Sehmi', with a horizontal line underneath the name.

A.S. Sehmi
October 1988

UMI Number: U016430

All rights reserved

INFORMATION TO ALL USERS

The quality of this reproduction is dependent upon the quality of the copy submitted.

In the unlikely event that the author did not send a complete manuscript and there are missing pages, these will be noted. Also, if material had to be removed, a note will indicate the deletion.



UMI U016430

Published by ProQuest LLC 2015. Copyright in the Dissertation held by the Author.
Microform Edition © ProQuest LLC.

All rights reserved. This work is protected against
unauthorized copying under Title 17, United States Code.



ProQuest LLC
789 East Eisenhower Parkway
P.O. Box 1346
Ann Arbor, MI 48106-1346

X751538905

I would like to dedicate this thesis to my late grandmother, and to my parents as a mark of my love and respect for them.

Acknowledgements

The writer of any thesis owes a vote of thanks to family, friends, and colleagues who contribute, sometimes unwittingly to its content, or spur the writer on towards its completion. This thesis is no exception, and I would like to acknowledge the following people in particular, and to offer them my sincere thanks.

Professor Barrie Jones has supervised the project from its inception, giving inspiration, valuable support and offering constructive suggestions. His contribution has not been confined to academic matters, and I would also like to thank him for his enormous help, understanding, and sincere friendship during my many years as a university student.

The project was begun at the University of Sussex and continued at the University of Leicester. Friends and colleagues at both of these universities deserve a mention, in particular Salih, George, Ashok, and John who, among other things, kept me in touch with the University during the 18-month-long *three months* that I spent at Medelec Ltd.

The Overseas Research Student's award scheme (governed by the Committee of Vice Chancellors and Principals) and Medelec Ltd kindly agreed to provide sponsorship and the facilities to complete my work. Dr. Neil Robinson was instrumental in organising Medelec's sponsorship, including a three month secondment to the Turing Institute, and, in addition, gave me valuable guidance. Many other friends and colleagues helped me during this period including Paulette who collected the majority of the raw evoked potential data.

A *special* Thank-You is reserved for my parents, Chhani and Mohini, sister Sonia, brother Mandhi, and my extended family in England, who have always been there to help me when I needed them.

Finally, there are the friends who make you take a break when you need it, and admonish you when you're slacking ! For this bullying, I would like to thank Anuj, Mauro, Salih, Steven, Isobel, Claire, Diane and Alison (who, aslo,, prufe red and helped to colllate the the thisis fro mi ?).

Thank you all very much !

“My work has always tried to unite the true with the beautiful and when I had to choose one or the other I usually chose the beautiful.”

Hermann Weyl

Table of Contents

ABSTRACT

LIST of ABBREVIATIONS

INTRODUCTION

CHAPTER ONE

- **The Background of Electrodiagnosis**

1.1 Animal Electricity	1-1
----------------------------------	-----

CHAPTER TWO

- **Muscle Electrophysiology, Computing Techniques in Electromyography (EMG) and EMG-Force Dynamics**

2.1 The Electrophysiology of Skeletal Muscle	2-1
2.2 Computer-Aided Electromyography	2-3
2.3 Quantitative Methods in EMG Analysis	2-5
2.3.1 Time Domain Analysis Techniques	2-5
2.3.2 Decomposition of the Electromyogram	2-9
2.3.3 Frequency Domain Analysis Techniques	2-11
2.3.4 Turning Points Spectral Analysis	2-13
2.4 The Modelling of Emg-Force Dynamics	2-15
2.4.1 The Integrated EMG (IEMG) and Force	2-18

CHAPTER THREE

- **A Computer System for Control and Digital Signal Processing Applications**

3.1 Introduction	3-1
3.2 Instrument Specification	3-3
3.2 SPC Hardware Organisation	3-5
3.2.1 General Hardware Description	3-5
3.2.2 The Signal Acquisition Processor (SAP)	3-6
3.2.3 The Signal Acquisition Card (SAC)	3-7
3.2.4 The Dual Plane Memory (DPM)	3-8
3.3 SPC Software Organisation	3-9
3.3.1 General Software Description	3-9
3.3.2 The Host Resident Kernel Program	3-10
3.3.3 The Host Resident Graphics Utilities Package	3-12
3.3.4 The Sap Resident Monitor Program	3-12
3.3.5 The SAP/HOST Communication Protocols	3-14
3.4 Simulated EMG Spectral Analysis in the SPC	3-18
3.5 Further Developments to the SPC	3-19
3.6 Discussion	3-20

CHAPTER FOUR

● **A Controllable Force Generator and Transducer System
for Muscle Investigations**

4.1 Introduction 4-1
4.2 Current Loading Methods and their Limitations 4-2
4.3 The Controllable Magnetic Muscle Load and Force Transducer (Magload) 4-4

CHAPTER FIVE

● **Magnetic Load Design and Experimental Results**

5.1 The Muscle Load Design Overview 5-1
5.1.1 Static Design Considerations 5-2
5.1.2 Dynamic Design Considerations 5-6
5.1.3 Additional Considerations and Features 5-8
5.2 Results and Discussion 5-10

CHAPTER SIX

● **Features and Uses of Brainstem Auditory Evoked Potentials (BAEPs)**

6.1 Introduction 6-1
6.2 Brainstem Auditory Evoked Potentials (BAEPs) 6-3
6.2.1 Origin of BAEP Components 6-3
6.2.2 Methods of Recording BAEPs 6-5
6.2.3 Clinical Uses of the BAEP 6-6

CHAPTER SEVEN

● **Quantitative Analysis and Interpretation of EPs**

7.1 Introduction 7-1
7.2 ERP Estimation by Latency-Corrected Averaging 7-3
7.2.1 Method 1 (due to Woody): 7-3
7.2.2 Method 2 (due to McGillem and Aunon): 7-4
7.3 ERP Estimation by Digital Filtering 7-6
7.4 Computer Identification of Features in BAEPs 7-9
7.5 General Knowledge-Based System Concepts 7-14
7.5.1 Rule-Based Systems 7-14
7.5.2 Network-Based Systems 7-16
7.6 Inexact Reasoning in Expert Systems 7-19
7.6.1 Certainty Factor Calculations in MYCIN 7-20
7.6.2 Uncertainty in PROSPECTOR 7-21
7.6.3 Fuzzy Certainty Factor Calculations in EPAXIS 7-24

CHAPTER EIGHT

- **Computer-Assisted Analysis of Single Response BAEPs**

8.1	Introduction	8-1
8.1.1	Event Analysis Algorithm Summary	8-2
8.2	Data Acquisition - Equipment and Procedure	8-4
8.3	The Event Binning Process	8-6
8.4	Data Simulations and Some Intermediate Results	8-9
8.5	Adaptive Selection of Peak Discrimination Factor	8-13
8.5.1	Frequency Distributions of Single Response Deflections	8-14
8.6	Spike Rejection and Adaptive Low Pass Filtering	8-16
8.7	The Effects of Sub-Averaging and Filtering on the Event Binning Process	8-18
8.7.1	Event Binning with Sub-Averaged Responses	8-19
8.7.2	Event Binning with Filtered Single, and Sub-Averaged, Responses	8-22
8.8	A Model of the Synchronous Summation of Noise Events	8-23
8.9	Latency Variability and Component Trajectories	8-27
8.10	Significance Testing of BAEP Components	8-32
8.11	Enhanced Averaging by Intelligent Trial Selection	8-35
8.12	Event Analysis Case Studies	8-38
8.12.1	Case Study A	8-38
8.12.2	Case Study B	8-41
8.12.3	Case Study C	8-43
8.13	Discussion	8-46

CHAPTER NINE

- **Discussion and Conclusions**

.....	9-1
-------	-----

REFERENCES and BIBLIOGRAPHY

APPENDICES

- A Published Paper on the SPC
 - Hailstone, J.H., Jones, N.B., Parekh, A., Sehmi, A.S., Watson, J.D. and Kabay, S., "Smart instrument for flexible digital signal processing".
- B1 MAGLOAD: Design Calculations
- B2 MAGLOAD: Circuit Diagrams
- B3 MAGLOAD: Tabulated Results
- B4 Published Paper on EMG-Force Modelling and MAGLOAD
 - Jones, N.B., Sehmi, A.S. and Lago, P.J., "An EMG-force measuring system for assessing muscle condition".
- C1 Published Paper on EPAXIS Expert System
 - Sehmi, A.S., "Epaxis: An expert system for automatic component labelling in evoked potentials".
- C2 Source Code for EPAXIS Expert System Program

APPENDICES (cont.)

D1 Source Code for Event Analysis Program

D2 Source Code for Data Simulation and Related Programs

D3 Event Analysis: Results for Bin Cancellation Simulations

D4 Event Analysis: Results for Latency Variability Recovery Experiments

D5 Normal Latency Values for Short Latency BAEPs

D6 Published Paper on Event Analysis

- **Sehmi, A.S., Robinson, N.L., Charles, A.J. and Robinson, P.M., “New developments in computer applications in neurology”.**

New Environments for Neurophysiological Investigations

by
Arvindra Singh Sehmi

ABSTRACT

The main topics of research are in the sub-areas of neurophysiology that are concerned with measurement of the electrical activity arising from contracting muscle (EMG) and from the surface of the scalp (EEG). Investigations are restricted to the surface-recorded interference pattern EMG, and to the EEG waveform recorded in response to sensory stimulation, known as the evoked potential (EP). The EMG and EP are representative of two important classes of signal commonly encountered in engineering, namely random noise-like and deterministic non-stationary. The thesis describes work on the development of a variety of new techniques and methods of analysis for application in neurophysiology and electrodiagnosis.

- A general purpose signal processing computer has been built which incorporates a high level of *user-machine ergonomics*. Turning Points Spectral estimation of the interference pattern EMG is simulated on this computer to demonstrate its flexibility for constructing analysis and control applications.
- Some emphasis is placed on methods of improving the quality of acquired EMG data for use in the analysis of the dynamics of the neuromuscular system. In this respect, the author describes the design of a fully *controllable muscle loading* system which uses *dc electromagnetic suspension* technology. The above computer can be used to control this muscle load for accurate *loading protocols* in EMG-Force modelling experiments.
- Techniques involved in the design and construction of the computer lead to higher-level program and data analysis specifications which employ *Artificial Intelligence* (AI) computing methods. These AI methods, in conjunction with some of those techniques which were used for EMG analysis, are applied to the investigation of *single-trial* EPs.
- A suite of adaptive EP analysis procedures, which include a prototype *fuzzy expert system*, facilitate the extraction of EP component *latency variability estimates*, and also provide automatic *selective single-trial averaging*. The latter selective averaging facility, can be used to enhance underlying activity and to examine the relationships that might exist between different components in the EP.

List of Abbreviations

The following lists common lexical abbreviations used in the text. Mathematical abbreviations and notational conventions are fully described prior to the points at which they are used.

AI	Artificial Intelligence
ADC	Analogue to Digital Converter
APWF	A Posteriori Wiener Filter
ASW	Analogue Switch
BAEP	Brainstem Auditory Evoked Potential
BIN	Event Accumulator Bin
CMRR	Common Mode Rejection Ratio
CNS	Central Nervous System
CNTR	Control Port
CRDFT	Canonically Registered Discrete Fourier Transform
DAC	Digital to Analogue Converter
DATA	Data Port
DFT	Discrete Fourier Transform
DMA	Direct Memory Access
DPM	Dual Plane Memory
DTW	Dynamic Time Warping
ECG	Electrocardiogram, Electrocardiography
EEG	Electroencephalogram, Electroencephalography
EMG	Electromyogram, Electromyography
EMI	Electromagnetic Interference
EP	Evoked Potential
EPSP	Excitatory Post Synaptic Potential
EPAXIS	Evoked Potential Analysis and Expert Interpretation System

ERP	Event Related Potential
ES	Expert System
FDC	Floppy Disk Controller
FFT	Fast Fourier Transform
FIR	Finite Impulse Response Filter
GAV	Grand Average
HSTPRO	Host Processor Protocol Handler Program
I/O	Input and Output
IEMG	Integrated Electromyogram
IIR	Infinite Impulse Response Filter
IKBS	Intelligent Knowledge Based System
IPL	Inter Peak Latency
ISR	Interrupt Service Routine
KB	Knowledge Base
KBS	Knowledge Based System
LCA	Latency Corrected Average
MA	Mean Amplitude
MAGLOAD	Controllable Magnetic Muscle Loading Device
MDAC	Multiplying Digital to Analogue Converter
MMSE	Minimum Mean Square Error Filter
MU	Motor Unit
MUAP	Motor Unit Action Potential
MUAPT	Motor Unit Action Potential Train
PDF	Peak Discrimination Factor
PROM	Programmable Read Only Memory
PRVEP	Pattern Reversal Visual Evoked Potential
PWM	Pulse Width Modulation
NT	Number of Turns

RAM	Random Access Memory
S&H	Sample and Hold Amplifier
SAC	Signal Acquisition Card
SAP	Signal Acquisition Processor
SAPCWI	SAP Control Word Interpreter Program
SAPMON	SAP Monitor Program
SAPPRO	SAP Protocol Handler Program
SAPRST	SAP Reset Program
SCC	Single Card Computer
SNR	Signal to Noise Ratio
SPC	Signal Processing Computer
SSEP	Somatosensory Evoked Potential
STAT	Status Port
TVAP	Time Varying A Posteriori Wiener Filter
VDU	Visual Display Unit
VHF	Very High Frequency

Introduction

The main topics of research that this thesis will address are in the sub-areas of neurophysiology that are concerned with measurements involving the electrical activity arising from contracting muscle and from the surface of the scalp. The electrical signals are known as the electromyogram (EMG) and electroencephalogram (EEG) respectively. The author restricts investigations to the surface-recorded interference pattern EMG, and to the EEG waveform recorded in response to sensory stimulation, known as the evoked potential (EP). Since the electrogenesis of EMG and EP signals in man is at the cellular level, there is much interest and value to be gained from the extraction of both quantitative and qualitative descriptors of these signals. The descriptors should lead us to a deeper understanding of some aspects of the biophysical mechanisms that govern bioelectric signal generation. In this respect, the EMG and EP signals can be used to locate and identify gross anatomical features of their respective origins, and they can also be used to model the dynamic behaviour of their associated neuromuscular / neural systems.

Due to the recent advances in electronics and computer engineering, there is a wider availability of small, relatively inexpensive, and powerful computers. It has also become more realistic to consider the benefits of integrating what may have been distinct analysis methodologies under the unified control and/or supervision of a computer. Attempts to integrate several, possibly complex, procedures have been impeded in the past by the problems of ensuring simple user-machine interactions. To circumvent this problem in a computer-based environment, techniques to create sophisticated external data links and internal graphical and tactile interfaces to the underlying analysis procedures are available.

These advances have provided new opportunities for rapid, on-line, digital signal processing of electrophysiological data and the comprehensible display of results. Two important classes of signal that are commonly found in engineering are the random noise-like signal and the non-stationary deterministic signal. The analysis methods available for these types of signal are also applicable to EMG and EP since EMG data is usually represented by random-noise models and EP data by non-stationary, deterministic models. The quantitative analysis of random-noise signals is generally performed by spectral estimation techniques, whereas non-stationary deterministic signal estimation is usually accomplished by averaging and/or filtering.

EMG and EP signals differ significantly in their noise content and also in the relative amounts of inherent quantifiable information. The noise and information contents are mutually related. The raw EMG signal has a high signal-to-noise ratio and often it contains an excess of quantifiable information which makes subsequent interpretation confusing. Despite the excessive information content, extraction of a statistically significant set of signal quantifiers from the EMG is very difficult because of the noise-like nature of this signal. Spectral averaging techniques help to reduce the information content in EMG signals to a manageable size, and they provide the additional benefit of allowing a reduction in the variance of the noise in the spectral estimate.

In contrast to the EMG, the EP has a low signal-to-noise ratio and the problem in this case becomes one of extracting as much information as possible from the data. The non-stationary, deterministic model of the signal makes averaging one of the most effective estimation methods available. EPs, though, are not *exactly* deterministic, and averaging tends to under-perform for this and other reasons. Spectral estimation methods are not widely used to quantify the EP, since the additive noise and signal power bands overlap in the frequency domain. Digital filtering of the EP has been investigated extensively by many researchers and is now gaining some popularity.

The EMG from a contracting muscle can be used with concurrent muscle force measurements to model the dynamics of muscles. The noise-like features of the EMG can, however, cause the model estimation procedures to become unstable. Careful control of the *quality* of the EMG during data acquisition reduces restrictions that must be placed on the choice of modelling algorithm (Lago, 1979).

The work presented in this thesis concerns the development of a variety of new techniques and methods of analysis for application in both clinical and research-based EMG and EP studies. There is some emphasis on methods of improving the quality of acquired EMG data for use in the analysis of the dynamics of the neuromuscular system. Spectral estimation of the EMG as outlined by Lago (1979) is simulated on a general purpose signal processing computer which exhibits a high level of user-machine ergonomics in its design. This computer can also be used to control an instrument that will provide accurate muscle loading protocols for EMG-Force modelling experiments. The lessons that were learnt in the design and construction of the computer, pointed the way towards higher-level program and analysis specifications that embraced techniques from Artificial Intelligence (AI). These AI techniques, in conjunction with some of the techniques which were used for EMG analysis, were applied to the investigation of EPs.

The integrated system comprising the general purpose computer and the controllable muscle load, and an another comprising several suites of EP analysis programs, constitute those *environments* which are referred to in the title of this thesis. The techniques used to create these environments and to analyse the data are of interest, not only in neurophysiology and electrodiagnosis, but also in several areas of engineering.

A brief summary of the chapters that follow is provided below to introduce the order of reading:

- Chapter One gives a short resumé of the history of electrodiagnosis as we know it today.
- Chapter Two provides a literature review of some of the quantitative methods in EMG analysis that have evolved in the last three decades. The author shows that the accurate control of force and its measurement is of importance, both in quantitative EMG analysis and in the modelling of EMG-Force dynamics.
- Chapter Three discusses the development and specification of a flexible menu-driven signal processing computer. The computer has been configured to perform a simulation of the EMG Turning Points Spectral Analysis procedure (Jones and Lago, 1983) which is described in chapter two.
- Chapter Four and Chapter Five address the problem of providing accurate, controlled and repeatable forcing protocols in EMG investigation and in the modelling of EMG-Force dynamics. A computer-controlled static and dynamic loading system and force transducer which uses dc electromagnetic suspension technology is described. Results are given showing the force control that is achievable.
- Chapter Six introduces the Brainstem Auditory Evoked Potential (BAEP) and some of its uses through a concise literature review. This review is provided because the analysis methods used in chapter three for EMG signals are extended later into the EP signal domain.
- Chapter Seven describes some procedures in the quantitative and qualitative analysis of evoked potentials. The difficulty of performing the qualitative analysis task introduces a requirement for intelligent knowledge-based programming methods (i.e. Expert Systems (ESs)). The methodology behind expert systems programming is presented through a description of some well known ESs that incorporate inexact reasoning mechanisms.
- Chapter Eight discusses a non-linear adaptive signal processing technique that has been developed for automatically detecting significant events in the BAEP. This analysis is pursued further and applied to the automatic enhancement and scoring of BAEP data. The technique is equally applicable to other evoked potentials.
- Chapter Nine concludes this work with a discussion, recommendations for further research, and application possibilities for the ideas that have been investigated.

Chapter One

The Background of Electrodiagnosis

1.1 Animal Electricity

The early history of electrodiagnosis was significantly affected by the two great wars. A large number of survivors from both World Wars bore peripheral nerve injuries. The postwar interest in the treatment and care of these and similar patients received further impetus from the advances in electronic technology taking place at the time. It was much earlier in the eighteenth century, however, that the interest in *animal electricity* led to the birth of electrodiagnosis.

Duverney (1700), a French anatomist, performed the initial classic experiment of electrically stimulating a frog muscle (Morgan, 1868). The first published report on muscle contraction using static electricity (with a Leyden jar as the source of stimulus) was by Kratzenstein (1746) who two years earlier had used it to straighten out the contracted finger of a paralysed woman. In the following years many reports appeared on electrotherapy for the purpose of curing paralysis and other diseases. In 1758, Beccaria noted that the contractions arising from electrical stimulation were stronger than those observed from mechanical stimulation (Colwell, 1922). An explanation was required for the muscle's increased response arising from electrical stimuli travelling along neural pathways. Seven years later in 1795 Fontana guessed that "*if it be not electricity, it may be something however very analogous to it*". Nearly three decades later Galvani began his series of experiments with muscle contraction in the frog.

Galvani noted a relationship between electricity and muscle contraction. His belief that the body generated this electricity led him to call it *animal electricity*. He observed that this *electricity* arose not from muscle, but from nervous tissue especially the brain, and that the nerves were the conductors whose oily sheaths prevented the dispersion of electricity. Galvani compared the muscle to Leyden jars, as the receptacles of animal electricity. Thus the *frog current* was a nerve current and not one of muscular origin.

In 1792, Volta wrote of Galvani's work, "*it contains one of the most beautiful and surprising discoveries and the germ of many others*" (Volta, 1816). A year later Volta objected with, "*It is thus that I have discovered a new law, which is not so much of a law of animal electricity but they are in*

reality the effects of a weak artificial electricity which is excited in a manner of which there is no doubt, by the simple application of two plates of different metals ” (Volta, 1793). Galvani’s works imply that the phenomena belong to some forms of spontaneous animal electricity.

The confusion arose in assigning the source of animal electricity. Volta insisted that a current source and the muscle formed part of a *closed circuit* so as to produce contractions. Galvani proved that a muscle could be stimulated by placing the free end of a nerve across a muscle without the intervention of metals, showing that electricity could be generated by animal tissue. Later Volta’s *pile* was constructed and used to investigate stimulation thresholds. Volta’s invention nearly extinguished any arguments in favour of electricity of muscular origin. This was because all the effects which Galvani attributed to animal electricity could be produced with Volta’s battery.

It was not until Nobili improved the galvanometer that further advances were made in electrophysiology. In 1838, Matteucci proved conclusively that contracting muscle generated electricity (Matteucci, 1844). In 1851, DuBois-Reymond obtained readings of muscle responses from the arm of a man using jars of liquid as electrodes. This was probably the first demonstration of electromyography as we know it today.

Electrotherapy in the form of electropuncture became popular as the distinction between, and location of, motor and sensory nerves became more apparent. Duchenne tried to establish a routine of treatment using cloth-covered electrodes for percutaneous stimulation. He was one of the first to use faradic stimulation and in one case produced contractions with a current of such high intensity that he admits to having produced a fracture of the cervical vertebrae. Heidenhein (Biedermann, 1898) noticed that occasionally, in the presence of disease a muscle might respond better to continuous current even though it failed to respond to faradic current. Baierlacher (Neumann, 1865) reported having made this observation in the paralysed muscles of a twenty eight year old woman and as a direct result of this, Erb credited Baierlacher with the discovery of electrodiagnosis. This observation was explained by Neumann in 1864 (Neumann, 1865) when he used a mechanical device to interrupt continuous current. He noticed that interruptions exceeding a certain rate had no effect on paralysed muscle. The first important conclusion in electrodiagnosis was thus made - the duration of current was the critical factor in eliciting a muscular contraction.

Piper (1912) recorded voluntary contractions in the forearm flexors of man in 1907 with the string galvanometer. He believed that the distinctive rhythms found in each muscle indicated the rate of stimuli received from the central nervous system. Proebster (1928) described spontaneous irregular action potentials in the denervated muscles of a boy with a traumatic plexus birth lesion and in another patient with long-standing poliomyelitis. Proebster used a recording galvanometer

and tested muscle in voluntary as well as in electrically induced contractions, and it is to him that most authors give credit for the beginning of clinical electromyography (EMG). At about this time, Adrian (Adrian and Bronk, 1929) introduced the coaxial needle electrode and the loudspeaker to EMG. This enabled observations of the potentials from single motor units in the muscle and monitoring of the intensity and quality of the complex electrometer record.

Lindsley (1935) made the first tracings of a patient with myasthenia gravis and noted the marked fluctuations in amplitude of the motor unit responses to contraction. In 1941 Denny-Brown and Nevin recorded the characteristic potentials of myotonia. In the same year, Buchthal and Clemmensen validated neurogenic and myogenic findings in muscular atrophy with clinical EMG, and Hofer obtained rhythmic potentials in rigid muscles at rest in patients with Parkinsonism. In 1950, Bayer demonstrated an increase in the size of muscle potentials with increases in the force of contraction (Lenman, 1959).

Until the middle of the present century, most electrodiagnostic exploration was conducted in the muscle. In 1948, Hodes, Larrabee and German stimulated nerves at two different points and by correlating the temporal difference in muscle response with distance, were able to determine conduction velocity. Liberson found that conduction occurs in both directions and that the portion of the impulse which is antidromic returns through the reflex arc. This permitted yet another recording to be taken from the muscle supplied by the stimulated nerve and is known as the F-wave response. Single fibre EMG as described by Ekstedt, did not appear until 1964, at which time it allowed the recording of jitter. The increasingly useful information available from EMG, caused its use to spread with considerable speed.

At about the same time as EMG was beginning its foundations with Galvani, Caton (1875) presented an account of the spontaneous electrical activity of the brain, of motor potentials and of sensory evoked responses (EP) at the Annual Meeting of the British Medical Association in Edinburgh. He reported that *“When any part of the grey matter is in a state of functional activity, its electric current usually exhibits a negative variation. On the areas shown by Dr Ferrier to be related to rotation of the head and to mastication, negative variation of the current was observed to occur whenever these two acts respectively were performed. Impressions through the senses were found to influence the currents in certain areas; e.g., the currents of that part of the rabbit’s brain which Dr Ferrier has shown to be related to movements of the eyelids, were found to be markedly influenced by stimulation of the opposite retina by light ”*.

Caton's experiments on the brain of the rabbit were carried out using a Thompson galvanometer which would not have been capable of following the rapidly changing potentials of the electroretinogram (Halliday, 1968). He was more likely to have measured the relatively slow changes in the voltage of the cortical surface. Since that time all advances in this field (as was the case in EMG) had to await the discovery and application of improved methods of transduction.

With the development of the thermionic valve differential amplifier (Adrian and Matthews, 1934) and of signal averaging techniques (Dawson, 1951, 1954) researchers were able to investigate the possible existence of repeated and similar electrical responses in the electroencephalogram (EEG) in response to sensory stimulation (i.e. evoked potentials, EPs).

Modern-day EMG and EP investigations involve the use of a vast array of tools and techniques to perform qualitative and quantitative measurements of the electrophysiological activity. The tools used to obtain the data for investigation are designed to retain as many inherent characteristics as possible in the presence of much distracting and occluding influences (e.g. radio frequency noise and tissue noise). The techniques used to analyse the data are designed to remove (and/or ignore) distracting information and enhance (and/or extract) those features of interest. Some of these tools and techniques will be presented in the sections of this work that are concerned with *collection* and *control* of EMG data and computer-aided *analysis* of EMG and EP data.

Chapter Two

Muscle Electrophysiology, Computing Techniques in Electromyography (EMG) and EMG-Force Dynamics

This chapter presents a simplified account of muscle electrophysiology. Following this is a brief account of the literature published recently on quantitative analysis of the interference pattern EMG. Later the relationship between the EMG and resultant force in the modelling of muscle dynamics is examined.

2.1 The Electrophysiology of Skeletal Muscle

Human skeletal muscle consists of striations of muscle fibres enclosed in the sarcolemma membrane and terminated by tendons, Fig.[2.1(a)]. Typical fibre diameters range from 5 to 100 microns and a typical muscle may have as many as a million fibres. Individual fibres are made up of parallel sub-units called myofibrils which consist of longitudinally repeated units termed sarcomeres which are bounded by the so-called z lines. The sarcomeres are the fundamental elements that contribute towards muscular contraction following electric stimulation.

Fig.[2.1(b)] shows a single load bearing or *extrafusal* muscle containing fibres which form the main mass of the muscle. These are responsible for generating forces or causing changes in muscle length. They are innervated by a class of nerve cell found in groups of nuclei located in the grey matter of the ventral horn of the spine. This group, called the α -motor neurones, have cell bodies whose diameters range from 25 to 100 μm and have long processes, from 8 to 20 μm in diameter, called *axons* (Rosenberg et al., 1982). These axons conduct nerve impulses to the extrafusal muscle fibres. The α -motor neurones terminate on the *motor end plates* attached to the extrafusal muscle fibre. The nerve impulse is a localised voltage change approximately 100 μV in amplitude and 1ms in duration that occurs across the membrane surrounding the nerve-cell body and axon. It is propagated along the axon at a velocity of about 50 to 120 m/s, the exact velocity being partly dependent on the diameter of the axon. Nerve impulses are often referred to as *action potentials* or, because of their relatively short duration, as *spikes*. Action potentials can be propagated repetitively to produce spike trains having mean frequencies which may vary from one pulse every few seconds to several hundred pulses per second. When the nerve impulse reaches the junction between the axon and the muscle fibre, a series of complex electro-chemical events lead to a wave of depolarisation sweeping over the entire muscle fibre and resulting in contraction of the muscle fibre. Each terminal branch of a single α -motor neurone axon innervates one extrafusal fibre of

SKELETAL MUSCLE ORGANISATION

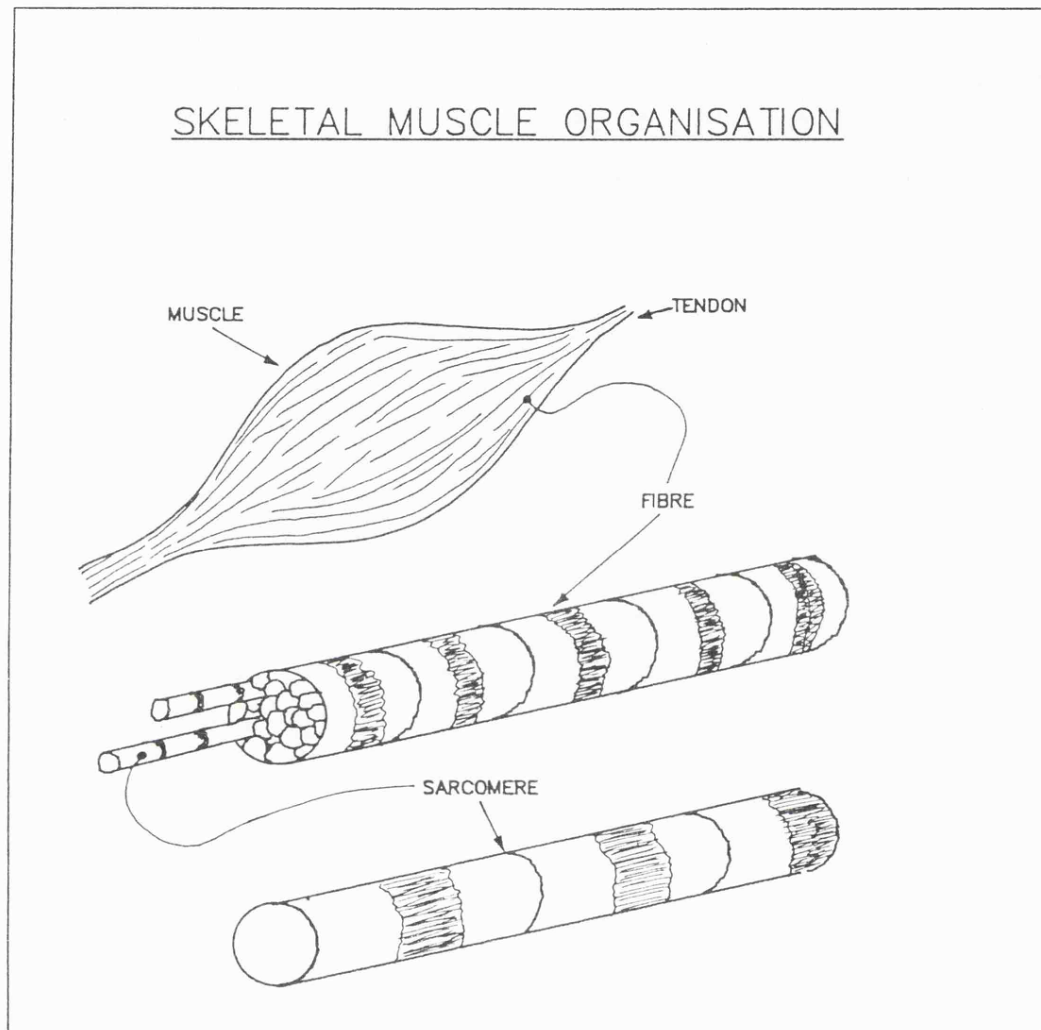


Fig.[2.1(a)] Schematic of human skeletal muscle showing the major structures it contains.

one muscle, and all the extrafusal muscle fibres innervated by a single α -motor neurone lie within the same muscle. This collection of muscle fibres and one α -motor neurone is called a *motor unit*. The groups of motor units making up a skeletal muscle vary in size and number, depending upon the function of that muscle.

The force of contraction of the entire muscle may be graded by increasing the number of active motor units within a muscle and by altering the frequency of the nerve impulses reaching the muscle over the axons of the α -motor neurones. A train of nerve impulses will hence produce a series of *force twitches* that combine and result in a sustained force level.

An important component of this motor unit system is the *muscle spindle* (see Fig.[2.1(b)]). This is a complex sensor that responds to imposed length and velocity changes and is thought to provide information which is important in the control of movement and in the maintenance of posture. The fibres within the muscle spindle, the *intrafusal fibres*, transmit length and velocity information to the spinal cord through the sensory afferent axons (types Ia and Ib). In addition these intrafusal fibres are innervated by the γ -motor or *fusimotor* neurones. These are thought to modify (modulate) the response of the muscle spindle sensory endings to imposed length changes. This modulating information is obtained from neighbouring segments within the spinal cord, the higher neural centres, and from within the muscle itself through deformation of the intrafusal muscle fibres. In the latter, deformation is caused by length changes imposed on the parent muscle which distorts the fine terminals of the sensory axons.

The neuromuscular system thus contains complex processes that can be likened to a servomechanism that controls muscle force and length. The basic measurable unit of activity required for analysis of this system is the electric field associated with the muscle membrane depolarisation. This can be measured with concentric needle or surface electrodes. The motor unit action potential (MUAP), as it is called, thus provides the basic currency of neuromuscular system identification and electromyography (EMG).

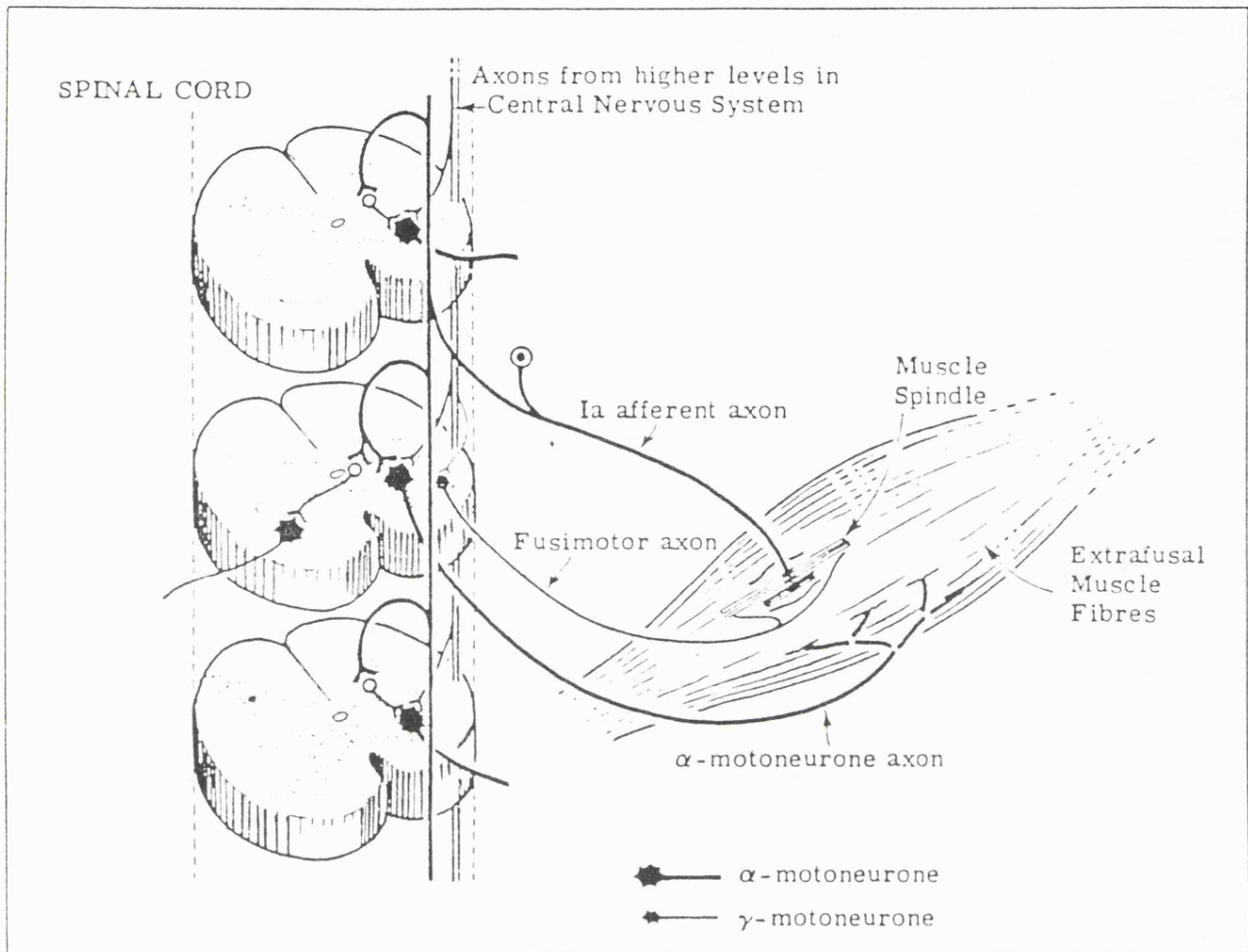


Fig.[2.1(b)] Diagram of some of the pathways connecting a muscle spindle and its parent muscle to the spinal cord. The neuronal circuits within this system are also shown. (Taken from ROSENBERG et. al., 1982).

2.2 Computer-Aided Electromyography

Electromyography has major relevance in non-invasive clinical neuromuscular investigation, diagnosis and motor control studies in man. Electromyographic recordings involving the concentric needle electrode were introduced by Adrian and Bronk in 1929 to record motor unit action potentials in human muscle. In normal muscle, the amplitude of a MUAP recorded with such an electrode may range from 10 to 300 μ V. The number of phases (slope reversals) of MUAPs recorded with bipolar needle electrodes may range from one to four with the following distribution: 3% monophasic, 49% biphasic, 37% triphasic, and 11% quadriphasic (Buchthal et al., 1954). MUAPs having more than four phases are usually indicative of abnormal muscle tissue. The time duration of MUAPs ranges from 1 to 13ms (De Luca, 1979). The above parameters are greatly affected by the type of needle used and the geometric arrangement of the active muscle fibres of each motor unit with respect to the recording site.

MUAPs undergo characteristic changes in voltage, duration and waveform shape after pathological loss of motor axons or muscle fibres. The correlations that exist between EMG potentials and the pathological changes of motor units are the basis of the clinical uses of quantitative EMG in neuromuscular diseases, as pioneered by the works of Kugelberg, Buchthal, Lambert, Hausmanowa-Petrusewicz and many others over the last thirty years (Desmedt (ed), 1983).

EMG, as it is generally carried out, relies principally on visual inspection of the changes in potential displayed on the oscilloscope, and auditory interpretation of the signals when they are played through a loudspeaker. The simple data provided is useful and often adequate to establish or confirm a diagnosis in a variety of neuromuscular disorders. The method is, however, subjective to some degree, and a great deal depends on the experience of the operator.

Attempts to use computers in EMG were made in the early 1970s to obtain objective results that could be presented in a quantitative, reproducible and practical manner. These practical methods were intended to reveal information essential for the integration of computer-aided EMG into daily use at EMG laboratories. Computers may be used either for the diagnosis of motor disorders in clinical neurology, or for monitoring and research revalidation, orthopaedic surgery, clinical pharmacology, sports medicine, human physiology and psychology. State-of-the-art automatic analysers can process input data, control various examination protocols or menus, host programmable modules (stimulators, filters, amplifiers, recorders, etc.), and generate databases of patient data. A new generation of computer-aided EMG machines incorporating the attributes of Artificial Intelligence to create *expert systems* will almost certainly be available in a primitive form

within the next decade. Expert systems will be used to augment the skills of the electromyographer or his assistant by providing advice on planning neuromuscular investigations based on the interpretation of patient symptoms and test results. Such *co-operative* systems will use a set of coded relationships, or rules, that embody the steps employed in arriving at a diagnosis, coupled with a data bank of anatomical and procedural facts on EMG.

2.3 Quantitative Methods in EMG Analysis

As mentioned in the previous section, diagnostic EMG studies focus most attention towards the isolation of individual action potentials in the belief that their visually identifiable features will reveal any motor unit disorders. Fig.[2.2] shows a selection of normal and pathological MUAPs as measured with concentric needle electrodes. Though examination of individual action potentials may be satisfactory, in some cases false negatives can occur. These arise in the early stages of disease, either because an active pathological unit is not close enough to the recording site to be detected, or because it may be close enough but inactive due to its high activation threshold. Also false positives arise as many normal motor units exhibit a small percentage of polyphasic action potentials. It is thus desirable to investigate maximal contractions involving all motor units in the vicinity of the needle electrode in order to provide additional information. Unfortunately these large contraction levels cause MUAPs from several motor units to overlap and interfere producing a signal which is difficult to interpret, as in Fig.[2.3]. Various analytical techniques have been developed to evaluate (characterise) the interference pattern EMG in both time and frequency domains. The methods that have evolved in these domains are discussed in the following sections.

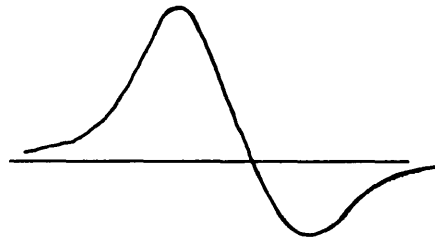
2.3.1 Time Domain Analysis Techniques

The early analogue methods of EMG quantification included the RMS value, the zero crossing rate and, counting the number of spikes in a one second epoch.

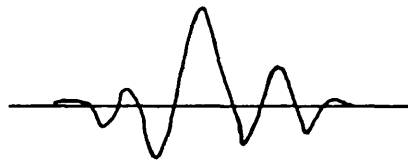
The RMS measurement has advantages over many of the other methods of mean voltage measurement in that it is a precise and standard measure of any continuous time waveform. It does not require the insertion of filters or time constants other than those normally used to limit the bandwidth of the EMG recording. RMS measurement may yet prove of diagnostic value when used as one of a group of measurements made automatically during computerised analysis (Hayward, 1983).

The zero crossing rate is related to total activity but is not well correlated with generated force (Fusefeld, 1971, 1972, 1978). In this instance recordings were made from a single point in the deltoid, using monopolar electrodes. The healthy patients in the control group were able to control the force of contraction, whereas those patients in the study who suffered from primary muscle diseases, failed to control it. The inadequate control of force in the test group of patients is unfortunately expected, but nevertheless undesirable, and it is an example of one significant source of error arising between the separate groups in the same experiment.

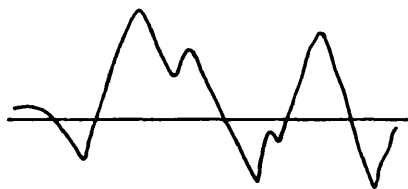
SOME MOTOR UNIT ACTION POTENTIALS



NORMAL



BECKERS MUSCULAR
DYSTROPHY



INHERITED
MOTOR-SENSORY
NEUROPATHY

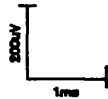


Fig.[2.2] A selection of normal and pathological MUAPs as measured with a bipolar concentric needle electrode (adapted from JONES and LAGO, 1983).

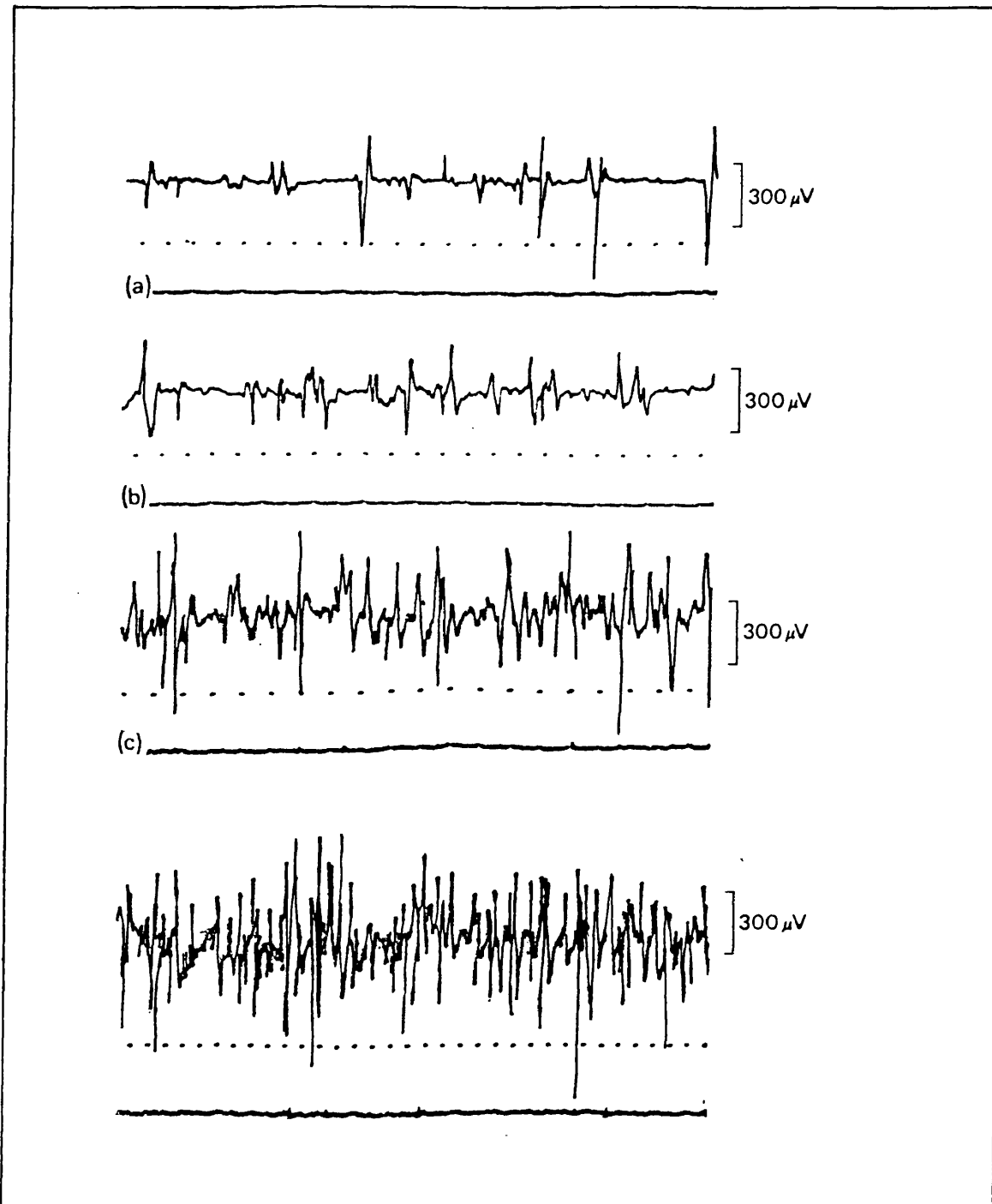


Fig.[2.3] MUAPs from normal first dorsal interosseus muscle during progressively more powerful contractions. In the interference pattern (c), individual units can no longer be clearly distinguished. The time scale is 10ms (taken from LENMAN and RITCHIE, 1970).

The counting of positive or negative excursions in the EMG (spikes) was first performed manually on photographic records by Bergstrom (1958). Automatic methods of spike counting (e.g. Close et al., 1966) were introduced but the usefulness of these methods was limited by a lack of validated results. In addition, the need to standardise the electronic technique for both healthy subjects and patients was not appreciated at the time (Hayward, 1983).

The method of turns analysis was introduced by Willison in 1963. It involved counting the number of amplitude increments contained in the slope between phase reversals of the waveform. Turns analysis was conceived as a tool to improve the certainty of diagnosis of muscular dystrophy. Willison's mechanical apparatus recorded the turns count in increments whose amplitude was chosen by the user (usually $100\mu\text{V}$). The elegance in this method was that measurements were related only to the previous reference point and not to any reference baseline of the signal. The method was planned for incorporation into the clinical environment as opposed to just being used in the research laboratory, but was extremely time-intensive and so was not popular.

The above technique was automated by Fitch (1967) and produced as its output two pulse trains derived from the interference pattern EMG. The first was an indication of the times of occurrence of phase reversals in the signal. The other was an indication of the times of occurrence of amplitude increments between phase reversals of the waveform. These pulse trains provided the turns (NT) and amplitude counts respectively. The turns count was normalised in time to simplify comparisons. The mean amplitude (MA) was the ratio between NT and the amplitude count. The MA represents the average amplitude of all the individual components that have been measured in the EMG. The information contained in the two pulse trains is sufficient to reconstruct the original signal provided that the amplitude threshold is sensitive enough (about $100\mu\text{V}$).

Turns analysis and some of its variations has found more widespread use in the laboratory than any other method to date as workers in other fields gained experience with it. The turns count gives a crude estimate of the rate at which the neural impulses are firing. It has diagnostic significance since the neural impulses give rise to MUAPs that contain a number of phases. These reversals of direction in the interference EMG over a fixed time have also been shown to correlate with the percentage of polyphasic action potentials measured from single motor units (Daube, 1981). The Fitch analyser has been used (Rose and Willison, 1967) to demonstrate the differences between normal, dystrophic and partially denervated muscle, and to investigate the effect of age in normal subjects (Hayward, 1977). Developments of this device have also allowed histogram displays showing the relative frequency of various times between reversals, i.e. the inter-peak intervals. Differential diagnosis of limb girdle syndrome has been provided from this information (Willison, 1971). Comparison of these methods made by Troup et al. show that amplitude and turn counts and integrated EMG are not linearly related and that the amplitude count is a more reliable

measure of the intensity of muscle activity than the integrated EMG. Hayward (1983) points out, however, that even control values show significant differences from one laboratory to another. Therefore, in order to enable valid comparisons to be made between results of turns analysis (and other methods) in different individuals and in different muscle groups, many aspects of the way in which the EMG is recorded need to be standardised. These include, as with the zero crossings method above, the sites at which muscles are to be sampled, the way in which the muscles are to be activated, and the force of contraction (Hayward, 1983).

The lack of force control in diseased patients is a typical problem when using sprung load cells and standard weights, because the level of force (and inertial forces associated with the latter) is invariably in the patient's control. The problem becomes more acute:

- as the demanded forcing level increases,
- if the patient suffers from the advanced stages of neuromuscular disorder, or
- if the patient is young, and/or unable to understand the clinicians explicit instructions on the forcing protocol.

The range of maximum force developed in healthy subjects also varies considerably with the method of force generation used (Hayward and Willison, 1973). Such problems could also account for the limited amount of research being conducted with dynamic measurements on diseased patients using the time domain techniques that have been mentioned above.

Some dynamic measurements were conducted by Fugelsang-Frederiksen et al. (1977, 1978, 1981) from vastus medialis in healthy subjects. In this case, a ramp of activity was controlled by visual feedback of the force signal by asking the subject to match the output of a ramp generator (calibrated for a 0-20Kgf over 27 seconds). In a normal subject, the mean amplitude ratio was constant over this wide force range showing an independence of this ratio with increasing force. Analysis of the turns-amplitude / force curves showed a phase relationship between electrical activity and mechanical effect as the force is increasing or decreasing. No results were reported for abnormal subjects and again it can be assumed that this method of force control is not practicable in such situations. It does however have considerable potential for application in muscle physiology within the research laboratory.

A commercial implementation of the Fitch analyser (Medelec Ltd., 1978) has recently been modified to incorporate Stalberg's alterations to the turns/amplitude technique (Stalberg et al., 1983). To make the method of turns and amplitude counting insensitive to force level and hence easier to use, a plot of turns (NT) versus mean amplitude (MA) was introduced. The relationship is linear for low to medium force but skews for forces exceeding 50% of maximal. This occurs because, as the mean amplitude increases almost linearly with force, the number of turns reaches a

saturation level before maximal force is approached. This is due to the superposition of individual MUAPs and would suggest that the mean amplitude ratio is not independent of force as was the case in the observation of Fugelsang-Frederiksen mentioned above. The ratio should decrease as contraction forces approach the maximum. Stalberg's method is sensitive in detecting myopathies and gives the same yield as conventional measurements in neuropathies.

A new technique using turns and amplitude measures (Nandedkar et al., 1986) attempts to create a set of parameters that are more representative of the way an electromyographer would visually quantify an EMG response. The *upper centile amplitude* is derived from the histogram of turns amplitudes (using a 100 μ V threshold) and represents the amplitude of the largest spikes in the interference pattern EMG. An *activity* measure indicates how *full* the interference pattern is. This is essentially a quantification of the total baseline existence of the EMG. The complexity of the EMG is reflected in the *number of small segments* parameter. This parameter is calculated by counting the number of small turns (segments) that exist for a short time (i.e the low-amplitude, high-frequency components). This last parameter is a non-specific, but sensitive characteristic of neuromuscular disorders because small segments are produced by complex or polyphasic MUAPs.

2.3.2 Decomposition of the Electromyogram

The EMG analysis methods described above provide much information on muscle physiology but fail to adequately describe the neuromuscular system at the spinal level. The control scheme that governs muscle contraction and the control of force is effected through the neuronal connections from several subsystems. These can be both at the spinal level and from higher centres in the central nervous system (Andreassen, 1978). A *window* into the central nervous system is opened through analysis of the discharge sequences obtained from individual motor units, the motor unit action potential train (MUAPT). The statistics of the times of occurrence of MUAPs in the MUAPT are greatly affected by small detection errors of as little as one percent (Shiavi and Negin, 1973). This problem, in addition to interfering MUAPs, means that highly reliable decomposition methods are essential to investigate the patterns of neuronal activation or *firing* of individual motor units during high force-level contractions.

Attempts have been made (Bergmans, 1971; Prochazka et al., 1972, 1973; Guiheneuc et al., 1983; Le Fever and De Luca, 1984; McGill et al., 1985) to automate completely or partially the detection and identification of MUAPs from the interference pattern.

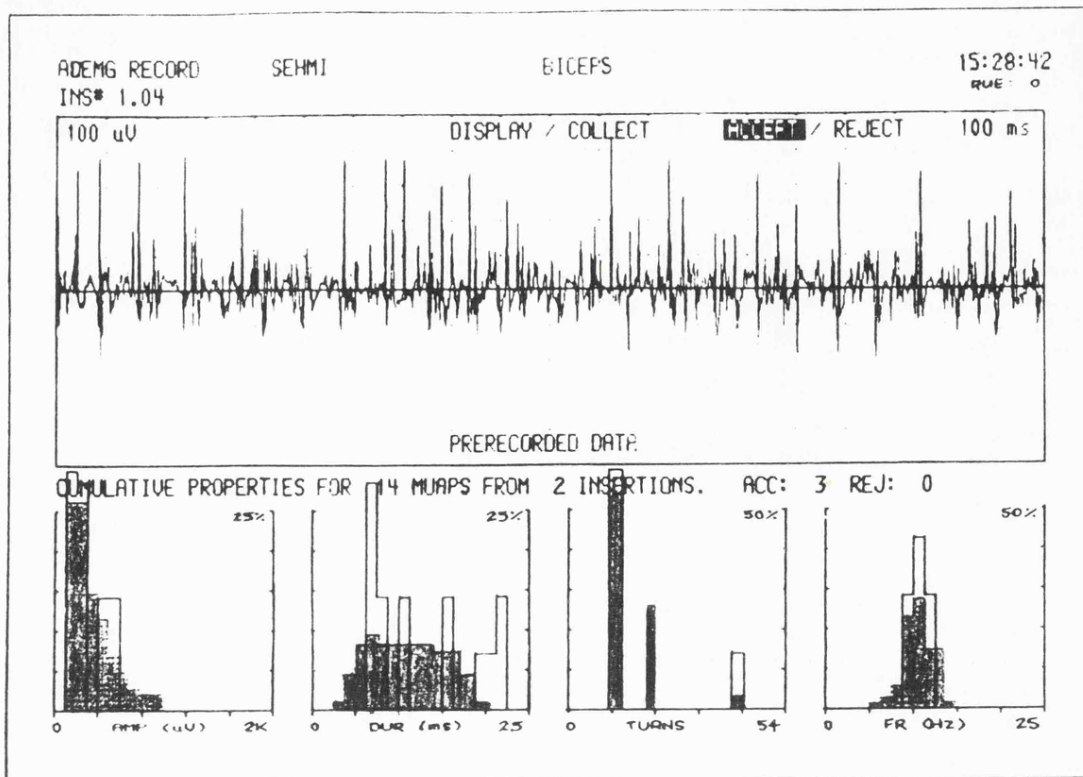
Bergmans (1971) developed two programs having different degrees of human interaction. Detection of MUAPs was performed using a software delay line, a *sliding window* of fixed duration and thresholds set using potentiometers. Provision was made for detection of five different potentials using point-to-point comparison. Two consecutive potentials identical to one of the five templates and separated by at least 23ms from each other was the criteria used for acceptance. Superimposed potentials were rejected. The template matching was sensitive to artifacts and noise and resulted in both false positives and false negatives. Once a potential was recognised by the program, the operator was allowed to confirm or deny acceptance. The program was too time-intensive and was modified to give the task of recognising potentials to the operator.

Prochazka et al. (1972, 1973) developed a system to accommodate small changes in the action potential shapes and superimpositions. The operator selects four different MUAPs with a manually adjusted amplitude threshold. These four MUAPs constitute the original templates for subsequent classification. The computer then sorts and averages all detected potentials into the template *bins* based on a minimum mean square error calculation. Unrecognised potentials are held separately for later decomposition by subtracting templates from them. The choice of template(s) used to resolve a superimposition is made by the operator. The end of analysis is preceded by a statistical evaluation of the firing frequency. Accuracies of between 95% and 100% have been claimed for signals containing up to six MUAPs.

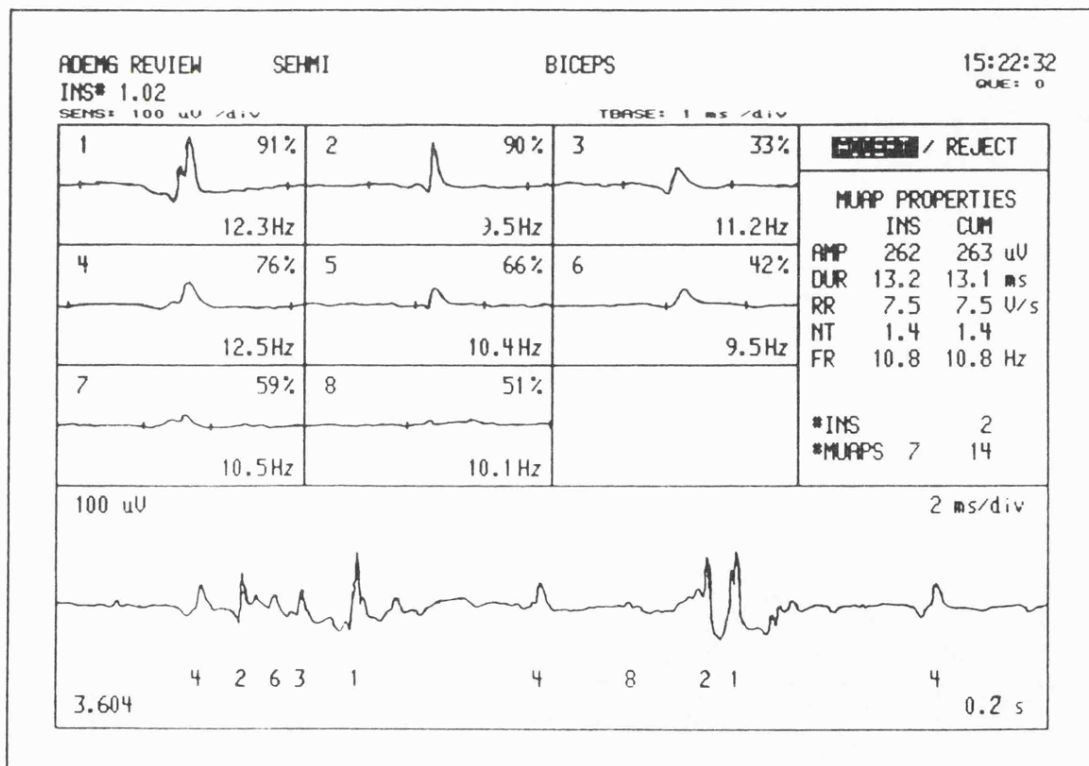
A fully automatic decomposition scheme on EMG obtained at up to 30% force-level has been devised by McGill et al. (1985). The EMG is differentiated to transform the MUAPs in the signal into sharp spikes which are easily identifiable. Those spikes that exceed a certain threshold have their Canonically Registered Fourier Transform (CRDFT) computed. The CRDFT is computed by taking the discrete Fourier transform (DFT) of the spike followed by an interpolation of the trigonometric polynomial specified by the DFT coefficients. The DFT is then rotated in such a way that the peak of the continuous waveform underlying the samples will lie at the midpoint of the analysis interval. This then forms the *canonical* template for matching with other MUAPs treated in a similar way. The CRDFT is independent of the arbitrary phase of the spikes, and therefore serves to align the peaks of the spikes in the frequency domain. It is claimed that the procedure allows a lower sampling frequency to be used so reducing memory usage and processing time. To a certain degree, identification of spikes belonging to the same train is performed using the shape and regularity of MUAP firing as criteria. Representations of the true MUAP shapes are obtained by averaging MUAPs in the raw EMG using the identified trains of sharp spikes as triggers. Analysis time for a 10 second epoch of EMG has been reported to be 90 seconds. It is hard to see how this is going to be accurate as superimpositions are not resolved resulting in weak approximations of the firing statistics (recall the observation of Shiavi and Negin, 1973).

One of the most advanced recognition programs applied to MUAPs has been developed by Le Fever and De Luca (1982). A special electrode which permits three channel recordings from the same motor unit is used. The recordings offer identification of interfering potentials and those potentials that have similar shapes. All channels are sampled at 50 KHz to reduce error during alignment of templates with unclassified MUAPs. All channels are then compressed by storing only those segments of activity exceeding a noise threshold set by the operator. Pattern recognition is performed with information from the discharge timings of detected MUAPs using a manually assisted statistical analysis. The algorithm is based upon a maximal a posteriori estimation of the probability of the moment each MUAP present in the recording will fire. If the new MUAP and the template are found to have been produced by the same unit then the template is updated to compensate for random variations in the MUAP waveform. Otherwise, it is considered to be a new motor unit firing, and is treated as the initial estimate for the new template. The method is capable of resolving superimposed MUAPs. The program is time-consuming, but the reliable determination of firing rates of up to eight MUAPs that is achieved at *maximal* contraction is not yet possible using any other method.

A commercial implementation (Nicolet Inc., 1986) of the method due to McGill et al. (1985) produces the results shown in Fig.[2.4(a)] to Fig.[2.4(c)].

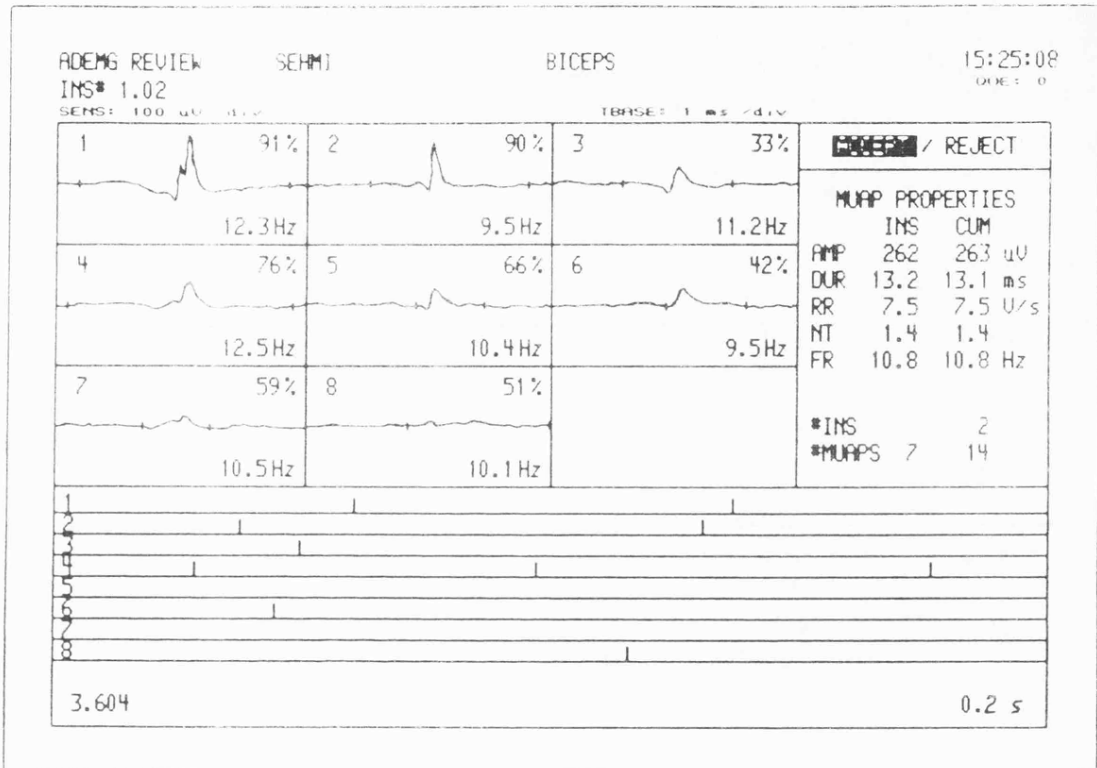


(a)



(b)

Fig.[2.4]. (a) Results of a decomposition on 10s of EMG data recorded with concentric needle electrodes from the biceps at low contraction (approx. 30% MVC). (b) Eight isolated MUAPs with cumulative shape and innervation statistics.



(c)

Fig.[2.4] (c) The eight MUAPs with segments of their corresponding times of occurrence. MUAPs occurring at these points will give rise to the EMG segment in the lower widow of (b).

2.3.3 Frequency Domain Analysis Techniques

Frequency domain or harmonic analysis is generally performed using the well known Fourier transform. This can be understood as a decomposition of the signal into sinusoidal components of different frequencies, or into travelling waves of different length in the case of propagating action potentials. The strength of the components as a function of the frequency constitutes the spectrum of the signal. One aspect of spectral analysis is that it offers a means of detecting periodicities hidden within deterministic or random signals (e.g. Interference pattern EMGs).

Numerical signal analysis, with the use of discrete Fourier transforms implemented on digital computers, has increased the possibilities of manipulating the EMG signals in ways not possible with any analogue filter bank analyser or the techniques already mentioned in the previous sections.

The digitised signal is first multiplied by a time window. This is because only a finite record length can be used to estimate the spectrum of the signal. The finite record length causes errors in the estimate through *leakage* to adjacent spectral components. This leakage can be reduced if the signal is smoothly tapered down towards both ends of the record. The conversion to the frequency domain is then done with a discrete Fourier transform. Normally a fast Fourier transform (FFT) devised by Cooley and Tuckey (Brighman, 1974) is used to reduce computational time and effort. A subsequent calculation of squared absolute values of the transformed signal gives the power spectrum. Mathematically the power spectrum $G(j\omega)$ can be represented in terms of the Fourier amplitude $\Psi(j\omega)$ by the following formula:

$$G(j\omega) = \lim_{T \rightarrow \infty} (1/2T) |\Psi(j\omega)\Psi(-j\omega)| \dots \dots \dots \text{Eq.[2.1]}$$

These Fourier components are the results of a Fourier transform:

$$\Psi(j\omega) = \int_{-T}^{+T} \Phi(t)\exp(-j\omega t)dt \dots \dots \dots \text{Eq.[2.2]}$$

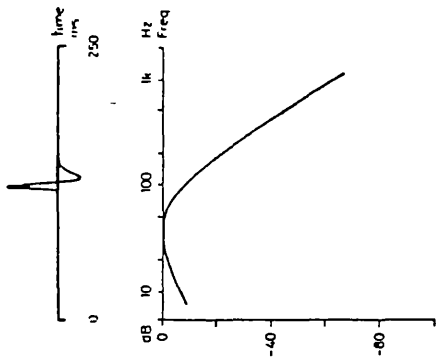
where $2T$ is the length of the observation interval.

Apart from its mathematical function of time to frequency domain transformation, the transform can be considered as an averaging of the time dependent signal $\Phi(t)$ with an oscillating weighting function. It can also be interpreted as a correlation between the signal and an oscillating function. $\Psi(j\omega)$ is thus sensitive to the occurrence of periodic components in the signal.

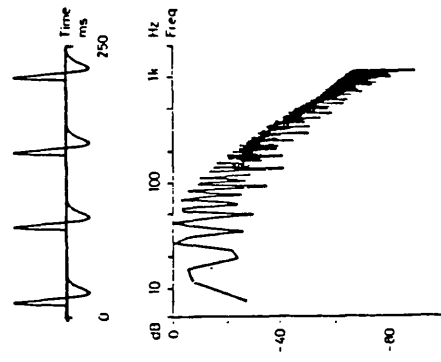
The usefulness of the FFT as a tool in signal analysis is seen in Fig.[2.5(a)] to Fig.[2.5(d)]. A computer generated biphasic action potential, as seen in normal muscles, and the corresponding power spectrum is shown in Fig.[2.5(a)]. Fig.[2.5(c)] illustrates the result of summing the biphasic potentials such as might be generated during a maximal contraction. The potentials have been randomly distributed over the observation interval and the total signal has the character of random noise. The power spectrum now contains large fluctuations but in the mean it has the same shape as that of the individual signals. Hence the spectrum of randomly summated signals essentially reflects the properties of the individual components. Another case of particular interest is the temporal summation which occurs in the spectral analysis of MUAP trains. Fig.[2.5(b)] depicts the spectrum of a series of single MUAPs arriving in a regular sequence. Here the spectrum is characterised by a number of peaks occurring at frequencies equal to the repetition rate and its harmonics. Also in this case the spectrum envelope has essentially the same shape as that of the individual signals in the pulse train. In Fig.[2.5(d)] the signals have been assumed to arrive in bursts with small relative time differences, having been distributed over the observation interval with a dispersion having a standard deviation of approximately 1.2% of the length of the observation interval. A dramatic change is produced in the power spectrum of the signal as compared with that of the original signal. In this case the plot reveals several properties of the signal which are hidden from visual inspection of the time sequence results.

The above example is an indication that spectral analysis can reveal underlying mechanisms of the EMG signal rather than describing details of the shape of the signal. It is this property of the Fourier transform that provides the interrelations between spectral measures and other characteristics of the signal, such as changes in the duration of a signal with otherwise unchanged form causing a change in the spectrum. Thus for example, the duration per phase in a MUAP will have an effect on the positioning of the spectral features on the frequency axis. For MUAPs with irregular phases one can show that the zero crossing frequency (indicative of the average duration per phase) is essentially a function of the rate of spectral decrease on the high frequency side (Rice, 1944, 1945). Note the connection established with a time domain characteristic. Also, as fatigue in muscle increases, the nerve conduction velocity increases (Lindstrom et al., 1970) which in turn leads to MUAPs of increased duration. This produces a similar effect in the spectrum as the above. Indeed the tracking of the median frequency (Stulen and De Luca, 1982) provides an index of localised muscle fatigue. Additionally information concerning the average firing rate and firing rate variations (Lago and Jones, 1981) can be obtained from the power spectrum.

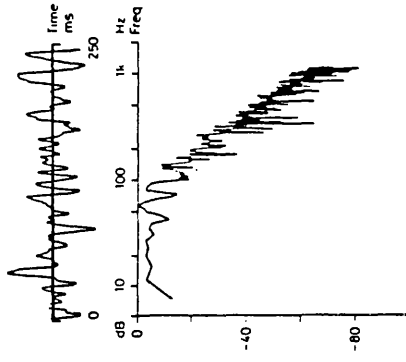
These methods, however, continue to be used only as research tools mainly because the spectral shape is influenced by a variety of phenomena which interact in a very confusing manner. In particular motor neurone firing time statistics and time delay variations (Lago and Jones, 1977) influence the spectral profile as well as the conduction velocity and MUAP shape (other problems



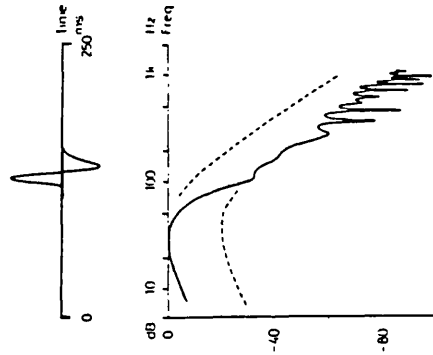
a Computer-generated action potential and its power spectrum.



b Pulse train of computer-generated action potentials with power spectrum. The distinct peaks in the line spectrum occur at frequencies equal to the repetition rate and its harmonics. The envelope through the peaks has essentially the same shape as the spectrum of the single potential.



c Summation of approximately 1,000 computer-generated action potentials randomly distributed over the observation interval and the resulting power spectrum. In the mean, the spectrum has the same shape as that of the single potential shown in figure 3.



d Summation of 100 potentials occurring in a burst with a Gaussian time dispersion having a standard deviation of 3 ms. At low and high frequencies the spectrum has the same shape as that of the individual potentials. The low frequency part of the spectrum is shifted upwards, as compared with the high frequency part, an amount proportional to the number of signal sources (fibers in the unit). The frequency at which the transition from the upper to the lower curve occurs is inversely proportional to the standard deviation of the time dispersion of the individual contributions in the unit.

Fig.[2.5] Illustration of the usefulness of the Fourier transform in EMG analysis (taken from LINDSTROM and PETERSEN, 1983).

are associated with baseline drift, needle movement, size of the innervation zone, synchronisation and cross-talk). Correct interpretation of the spectral shape is thus extremely difficult and many conflicting results have been reported. The dilemma is further increased because the spectrum of interference EMG can be shown to be the product of a function derived from the pooled motor neurone pulse train spectrum $\phi(\omega)$ and the spectrum of the *average* action potential $|H|^2$ (see Fig.[2.6]). Significantly different action potentials can also produce similar spectra because the spectra do not contain any phase information.

In general it seems that the EMG spectral data yields useful information readily when it is processed so as to enhance a particular feature such as the peak frequency, the average firing frequency or the median frequency. The spectrum in full detail is not easy to interpret.

2.3.4 Turning Points Spectral Analysis

The information of most interest, relating to the existence of multiphasic (abnormal) potentials, is contained in the time locked groups of turning points within the interference pattern EMG, as recognised by Willison (1963) and others. This information exists in the power spectrum of the EMG itself but is overwhelmed by the other influences already described above. If however spectral analysis is performed on the point process describing the EMG, then much of the distracting information from the power spectrum can be removed.

This technique (Lago and Jones, 1983) involves marking only significant turning points in the interference pattern EMG. The selection of significant peaks is performed after a noise reduction process and then peak amplitude comparisons with a peak discrimination factor is used. This limits the acceptance of artifactual deflections along a wave due to noise. Once the markers have been assigned, a 0-1 binary sequence is obtained upon which an FFT is performed. The processing sequence resulting in the turning points spectrum is illustrated in Fig.[2.7].

A prime attraction of this method lies in the fact that the spectral shape arising from normal muscle producing a predominance of biphasic or triphasic potentials is reasonably simple. Fig.[2.8(a)] and Fig. [2.8(b)] show this. More complex shapes arise from more complex potentials as in Fig.[2.8(c)] and Fig.[2.8(d)].

Research work on inferring the shape of the action potentials from the turning points spectrum is currently being conducted by colleagues (Jones, Lago, and Parekh). The first area of investigation involves the creation of standard spectra, representative of normals and of known disorders, which are characterised by their mean and first two principle components. It is then intended that new spectra should be classified by observing which standards they are closest to. The second approach concerns preprocessing the sequence of time markers that represent significant peaks in

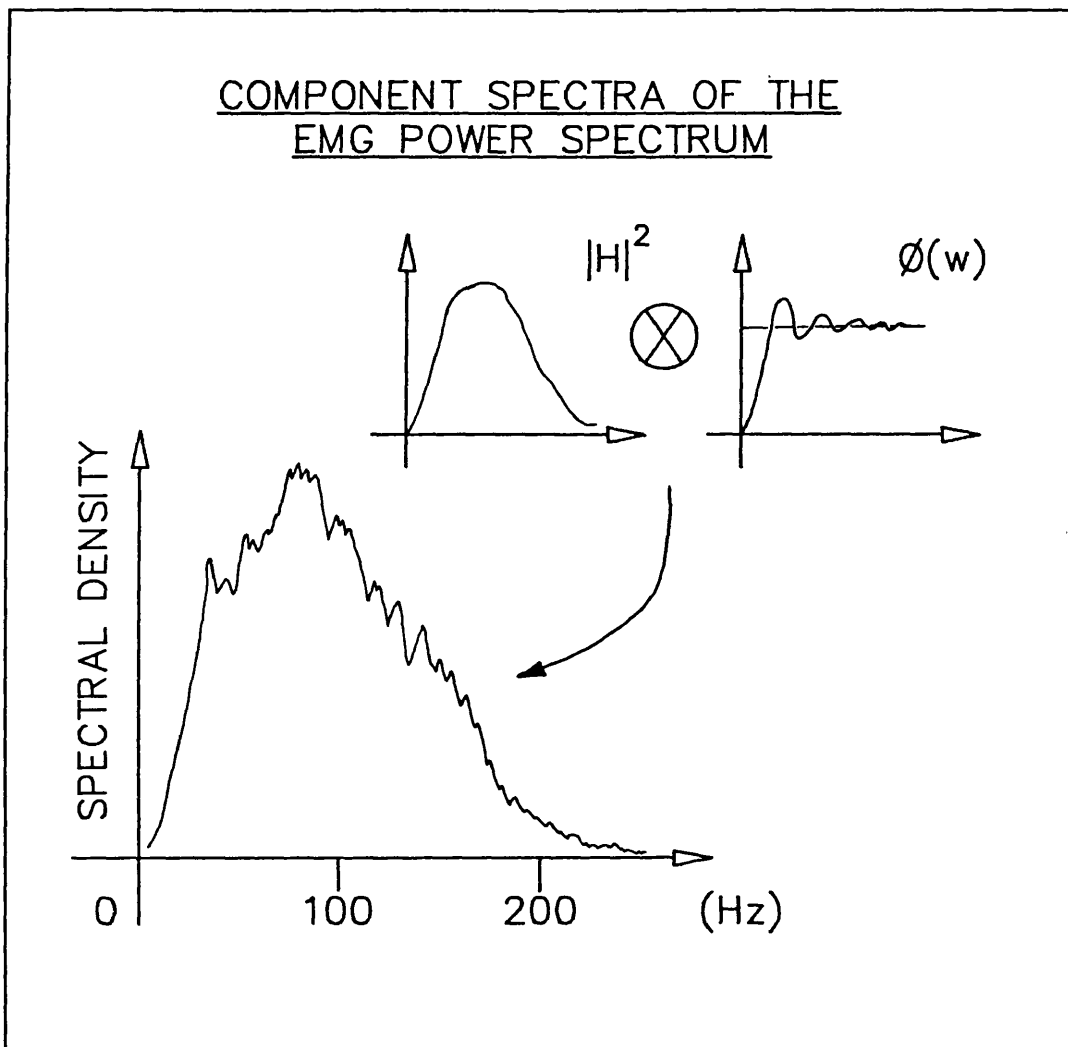


Fig.[2.6] Component spectra of the EMG power spectrum
(adapted from JONES and LAGO, 1983).

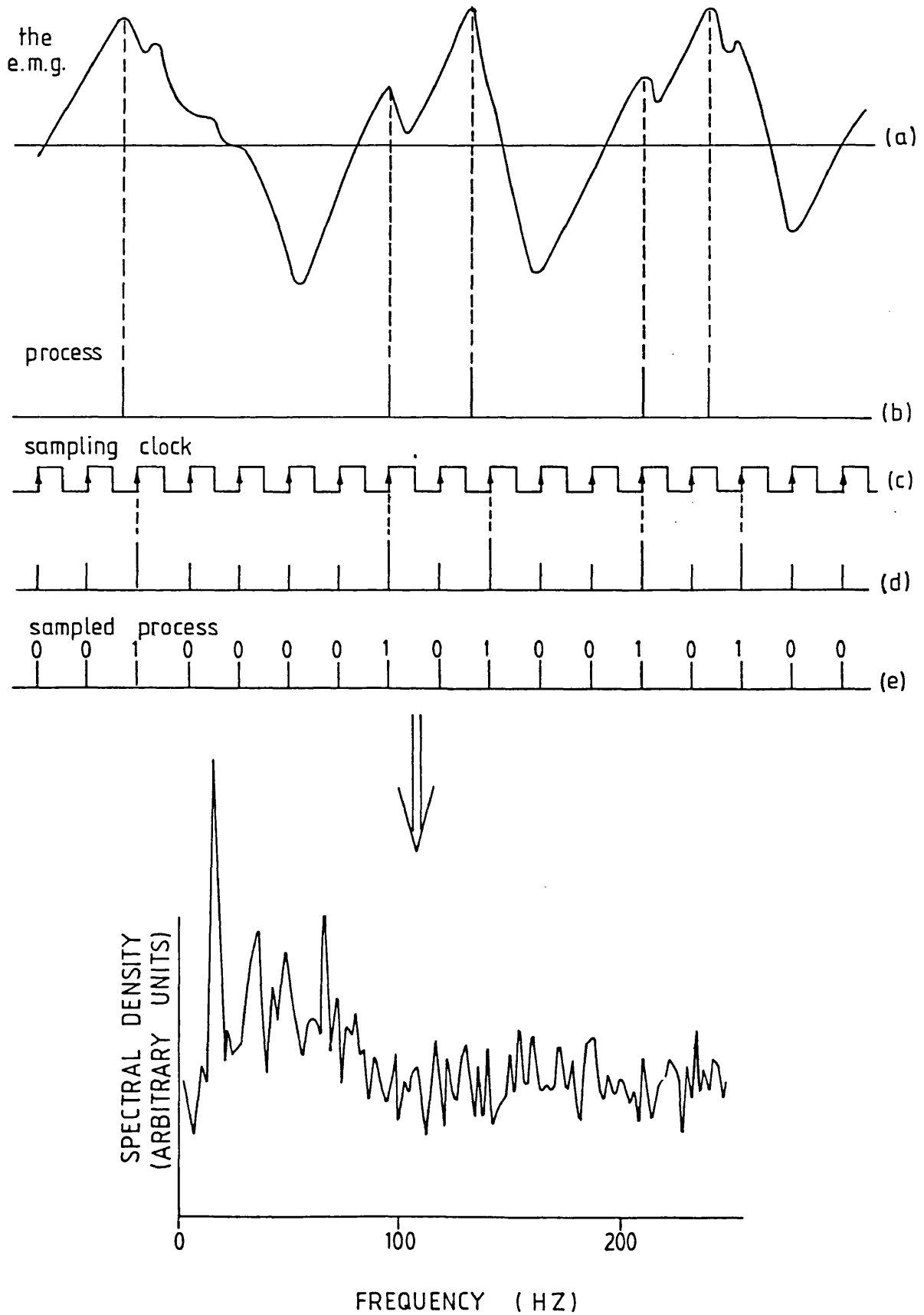


Fig.[2.7] Processing sequence to extract significant turning points (maxima) from the interference pattern EMG and subsequent power spectrum (taken from SEHMI, 1983).

the EMG in such a way as to produce marker sequences which have spectra of the type in Fig.[2.8(a)]. This preprocessing, called *splitting* involves the allocation of successive markers to two or more sequences in a cyclic order, shown in Fig.[2.9]. It can be shown that the number of splitting processes required to obtain simple spectra as in Fig.[2.8(a)] is related to the number of positive phases in the action potential. For example, the sequence of turning points related to the interference pattern EMG of the spectrum of Fig.[2.8(c)] would require at least a four way split to produce the flat simple spectrum of Fig.[2.8(a)]. The reasoning behind this is that these myopathic potentials, having four positive phases, will spatially summate but maintain the grouping and time locked sequencing that is hidden in the resultant interference EMG at moderate to high contraction levels. An alternative process of thinning successively allocates the events of the original sequence at random to two new sequences. In either case the objective is to remove the clustering effect of the time locked sequence of turning points (mentioned earlier) so that they can be considered as each marking only one turning point of the action potential. Fig.[2.10] shows the thinning and splitting process applied to a synthetic EMG made up of action potentials with four positive phases.

Despite considerable experience gained using the methods described in the sections above, few are used routinely in most clinical situations. This is presumably because an adequate set of diagnostic standards (results interpretation criteria and normative databases) and examination procedure standards (use of standard electrodes and forcing protocols) do not exist. Additionally on-line computing facilities incorporating these methods have not been developed and/or perfected for use in the clinical environment (the exception to this is the turns-amplitude analysis of Stalberg et al., (1983)). Furthermore incorrect classification of patients using automatic analysis of the interference EMG in controlled situations is known although not well documented (Jones and Lago, 1983).

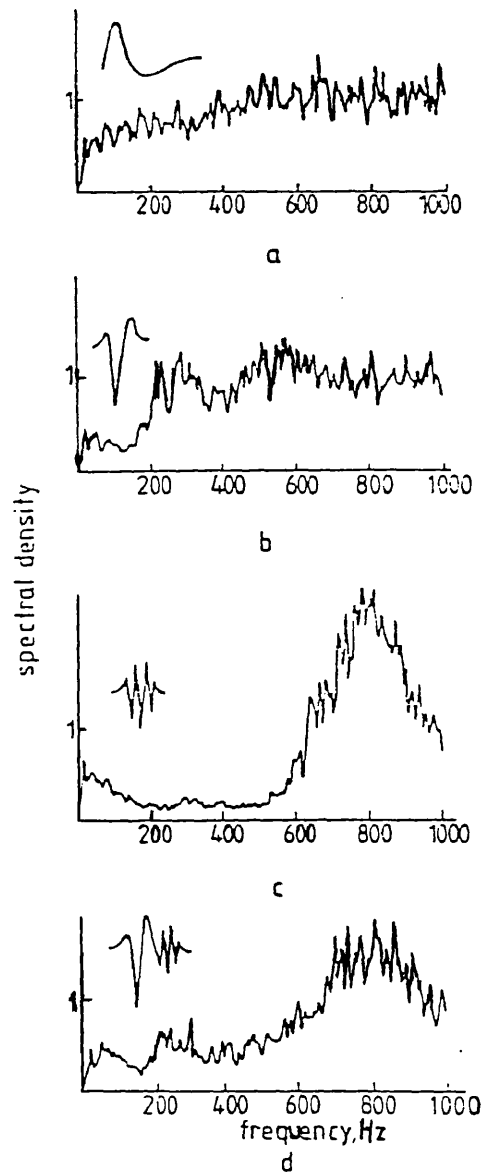


Fig.[2.8] Some EMG turning point spectra and the associated action potentials
 (a) normal biphasic, (b) normal triphasic, (c) myopathic,
 (d) initial neurogenic. (Simulations, taken from LAGO and JONES, 1983).

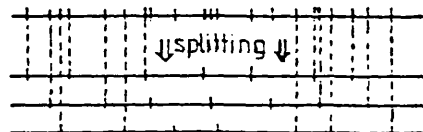


Fig.[2.9] The splitting process applied to the turning points sequence. This example is a 1:3 split (i.e. $n = 3$).

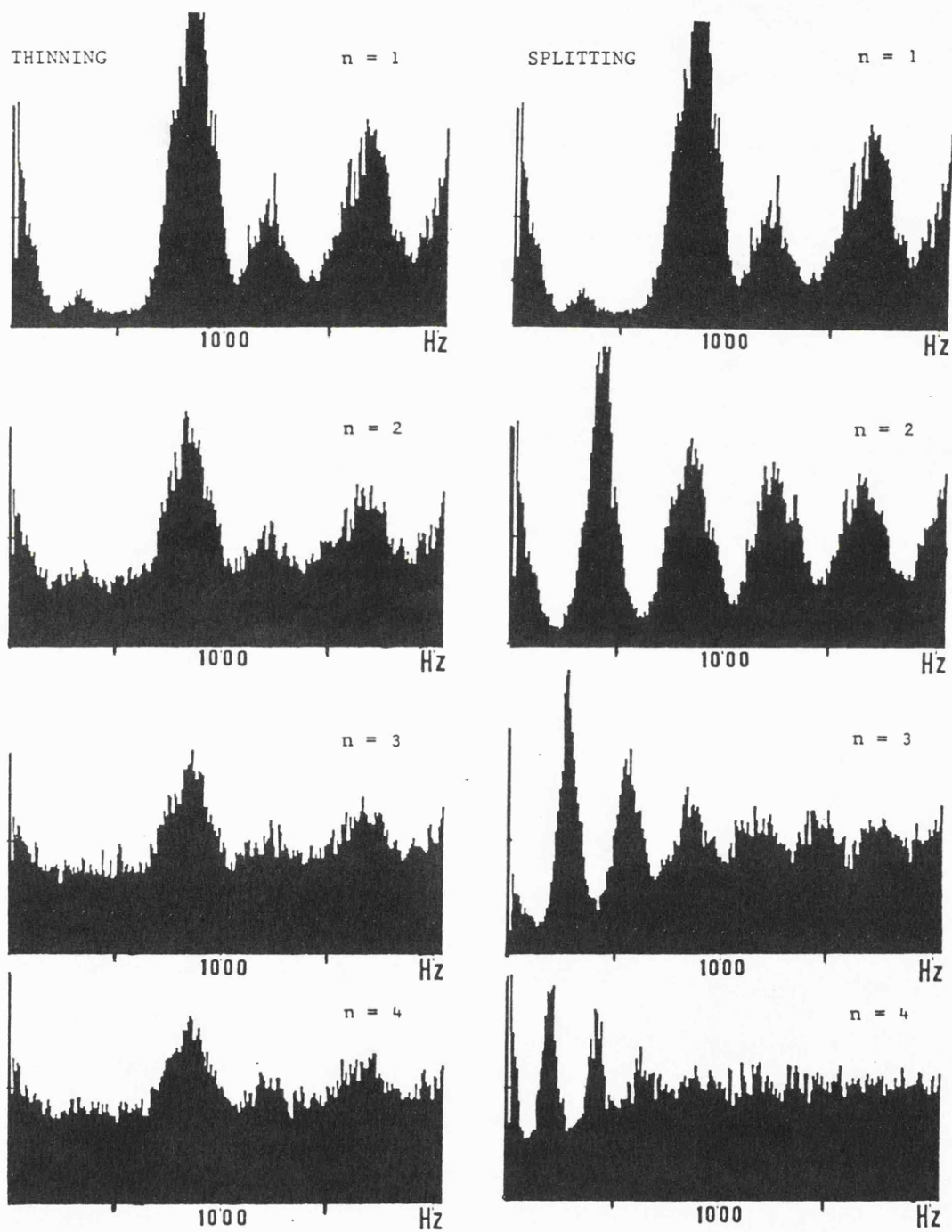


Fig.[2.10] The thinning and splitting processes applied to interference pattern EMG simulated with quadriphasic action potentials (taken from LAGO and JONES, 1983).

2.4 The Modelling of Emg-Force Dynamics

This section is intended to provide information on some of the muscle modelling procedures that have been tried by several researchers. The accurate control of force in these experiments is highlighted to give the reader an insight into the problems that can occur without it. EMG-force modelling is a quantitative technique that is used in EMG investigations, and hence this resumé is purposely included in this chapter. Nevertheless, a definite binding exists between the ideas that follow, and those that resulted in the work described in chapters four and five which are concerned with the accurate control of muscle loading.

In-vitro experiments to determine the mechanical properties of muscle have been conducted by Wilkie (1956) in a series of isometric (constant length) and isotonic (constant force) contraction experiments. Wilkie used simple apparatus consisting of a lever arm pivoted about its centre and a dissected frog sartorius muscle clamped to one end. By applying loads at one end of the lever and tetanising the muscle at the other, he was able to determine the following:

- (a) tetanic tension-length curve,
- (b) isometric stress-strain curve,
- (c) isotonic contraction-time curve,
- (d) force-velocity curve, and
- (e) the active-state curve.

These curves are directly related to the three element (non-linear) elastic model of Hill (1938), Fig.[2.11]. The parallel elastic component (PEC) represents the elasticity of the passive muscle and of the joint. The *force generator* is mimicked by the contractile component (CC), and the series elastic component (SEC). The CC transmits its force through the SEC and together they represent the elasticity of the tendons and ligaments. Wilkie's experimental results are shown in Fig.[2.12(a)] to Fig.[2.12(d)]. The characteristics show the typical static and dynamic non-linearities associated with contracting soft tissue. Fig.[2.12(b)] illustrates a set of isotonic shortenings of muscle against various loads. This indicates the following:

- an increase in latency to the point when the muscle has developed isometric tension equal to the isotonic load,
- a decrease in the maximum shortening, and
- a decrease in the initial velocity of shortening, i.e. the initial slope of the curve, decreases with increasing contraction force.

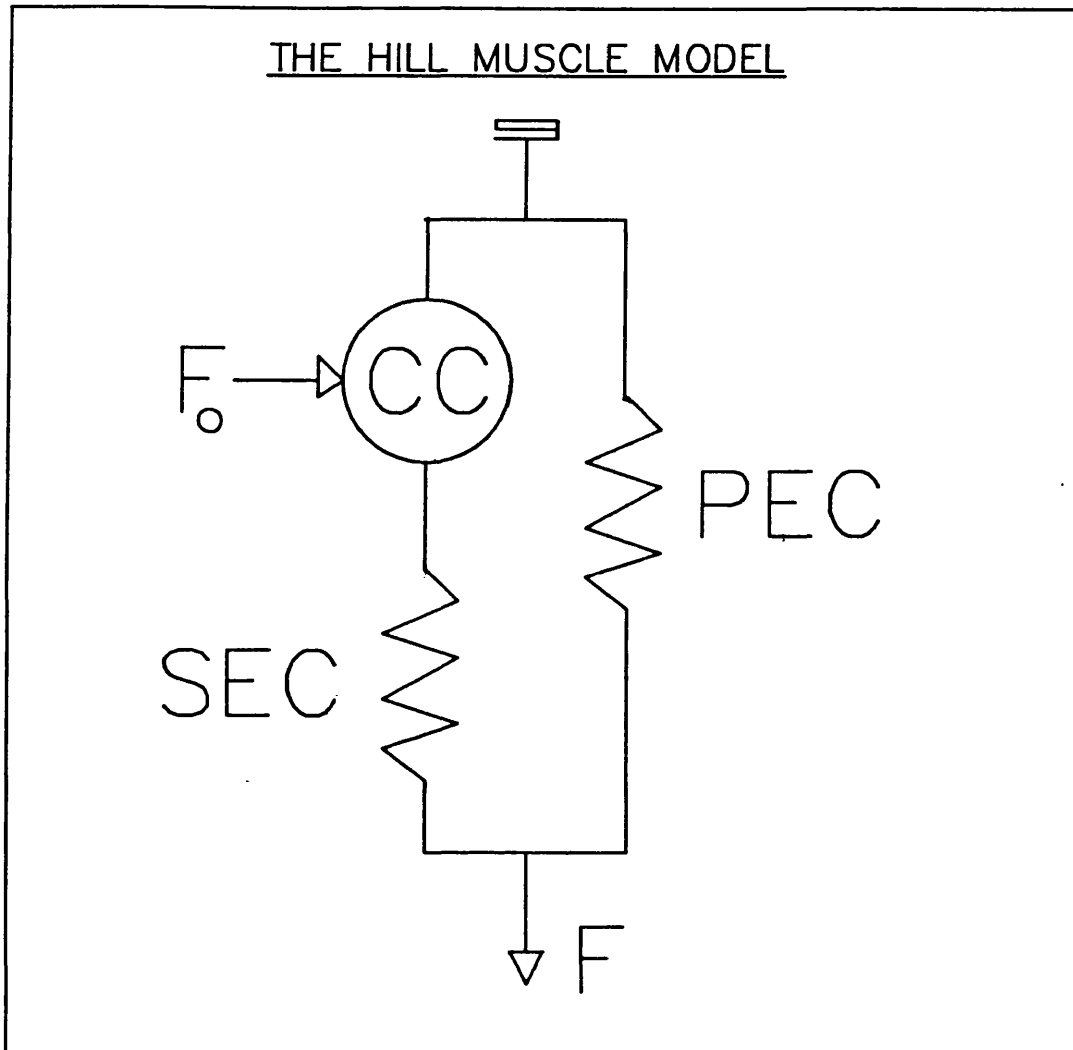


Fig.[2.11] The parallel elastic model of muscle (HILL, 1983).
PEC: Parallel Elastic Component; SEC: Series elastic component; CC: The Contractile component; F_o : The Active State; F: Load.

From Fig.[2.12(b)] Wilkie deduced that when the velocity of shortening is zero (at the plateau points) then the tension developed by the muscle is only a function of its length. However, this is only strictly true when the muscle length is near its in-vivo length. The plot of the isotonic force against the initial velocity of shortening gives the characteristic of Fig.[2.12(c)]. This has been described by Hill (1938) using the equation:

$$V = b(F_0 - F)/(F + a) \quad \dots \dots \dots \text{Eq.[2.3]}$$

where $V = dx/dt =$ velocity, $F =$ force, $F_0 =$ maximum isometric tension. The parameters a and b have the dimensions of force and velocity respectively and are in fact functions of muscle length as can be deduced from Fig.[2.12(a)]. The curve shows that even when there is no load on the muscle the velocity has a certain limited value. It does not become infinite as would that of an undamped elastic body. Under isometric conditions, when the velocity is zero, the force is maximal. The non-linearity suggests that if the system is a viscous-elastic one, then the viscosity must be non-linear.

The active-state curve (interrupted line) of Fig.[2.12(d)] describes the isometric tension which the CC can develop (or bear at any instant without lengthening) at any point in time. To measure this, the effect of the SEC must be removed by quick stretch or by sudden isotonic loading. The experimental conditions are arranged such that sudden isotonic loading occurs after a change in length greater than the amount by which the SEC contributes to the tension developed by the muscle (from the stress-strain curve). In this way the twitch-like tension developed solely by the CC was measured (Ritchie, 1954). Under these conditions the tensions produced after various durations of tetanus, must pass through the active-state curve. The peak points are selected since the CC and SEC are at constant length during this part of the twitch. Therefore the tension produced at this point must be due to the CC only.

Dynamic models based on Eq.[2.3] have been developed by many researchers (Hof and Van Den Berg, 1981; Glantz, 1977; Bawa, Mannard and Stein, 1976; Rees et al., 1986). An example is the thirteen parameter electrical analogue due to Hof and Van Den Berg (1981) for investigations on the gastrocnemius-soleus complex. The characteristics describing the PEC and SEC can be determined experimentally or by heuristic mathematical descriptions of their probable forms. Hof and Van Den Berg (1981) used a logarithmic expression for the SEC derived from the inverse relationship existing between the SEC compliance (reciprocal of elasticity) and the active state (Ritchie and Wilkie, 1958). The PEC was modelled on exponential data obtained from the literature. The driving signal for their analogue, to give the active state characteristic, was chosen to be the rectified and smoothed EMG as this is the most convenient measureable signal representative of the neuronal input to the CC. As would be expected in such a model, the proliferation of parameters requires an equal amount of calibration procedures when used with different subjects and in different muscles. The models have been relatively hard to use for in-vivo

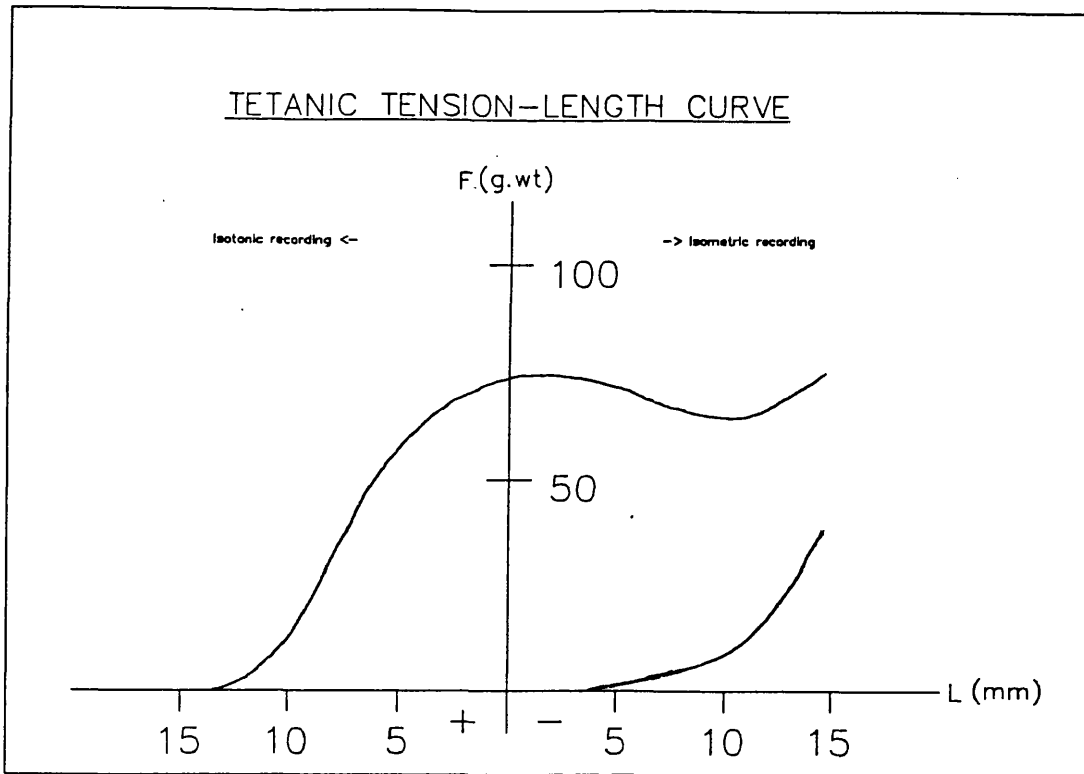


Fig.[2.12(a)] Tetanic tension length curve in stimulated muscle (upper curve) and stress-strain curve for resting muscle (lower curve) (taken from WILKIE, 1956).

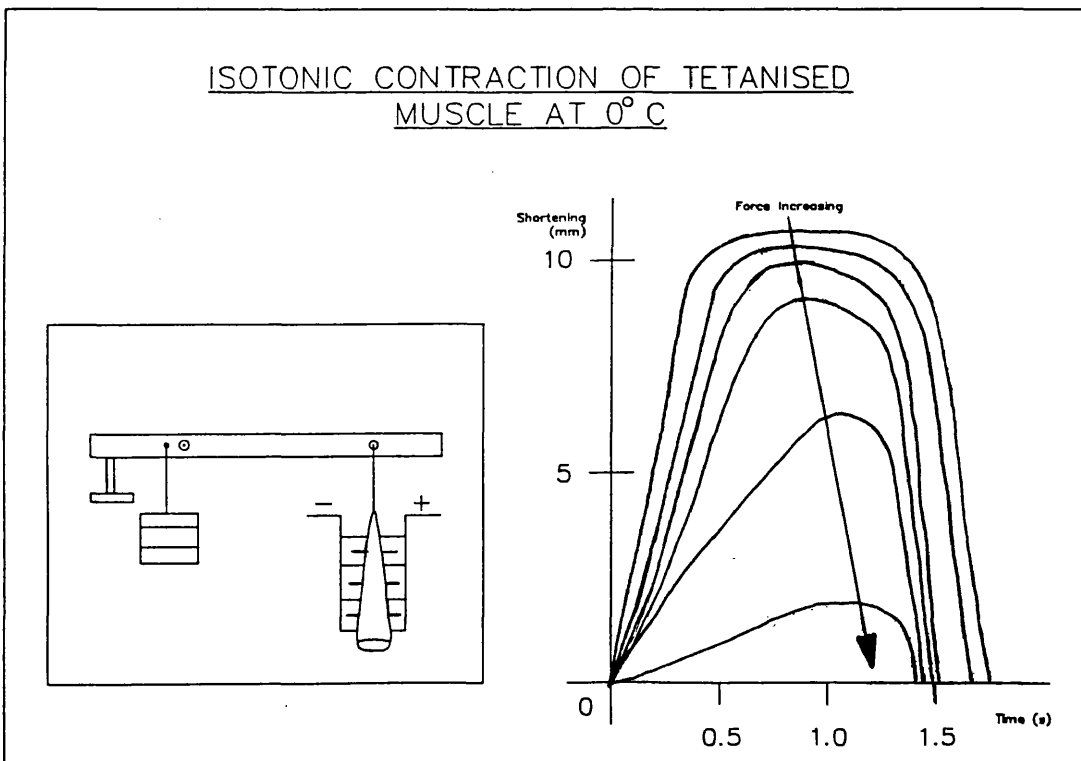


Fig.[2.12(b)] Isotonic contraction of tetanised muscle at zero degrees celsius. a: arrangement of apparatus; b: curves showing contraction at various tensions (taken from WILKIE, 1956).

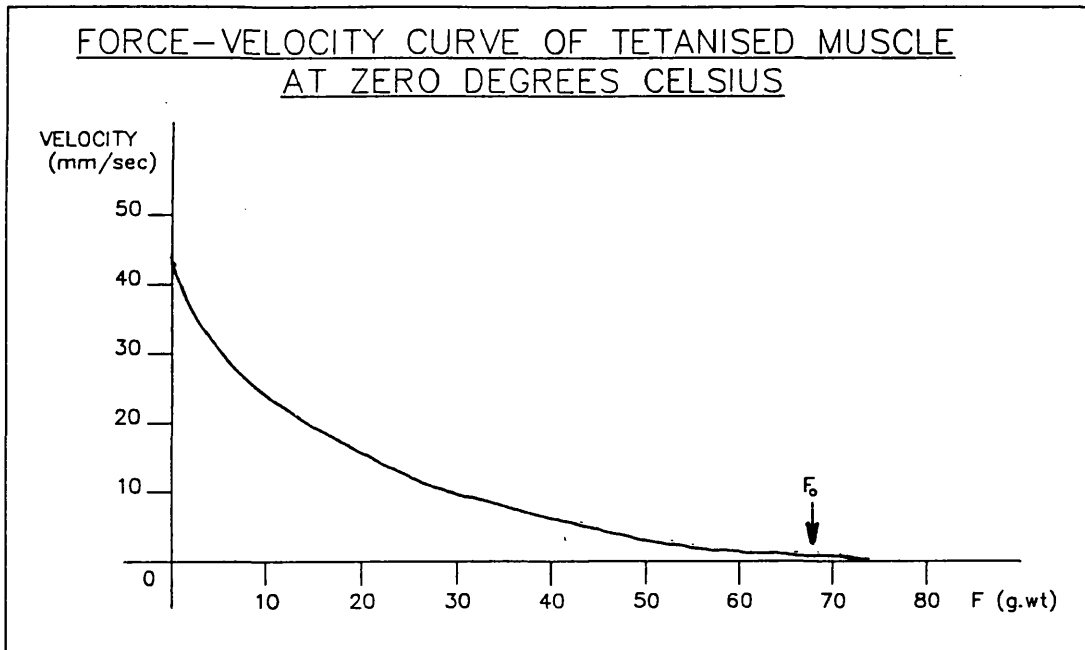


Fig.[2.12(c)] Force-Velocity curve of tetanised muscle at zero degrees celsius (taken from WILKIE, 1956).

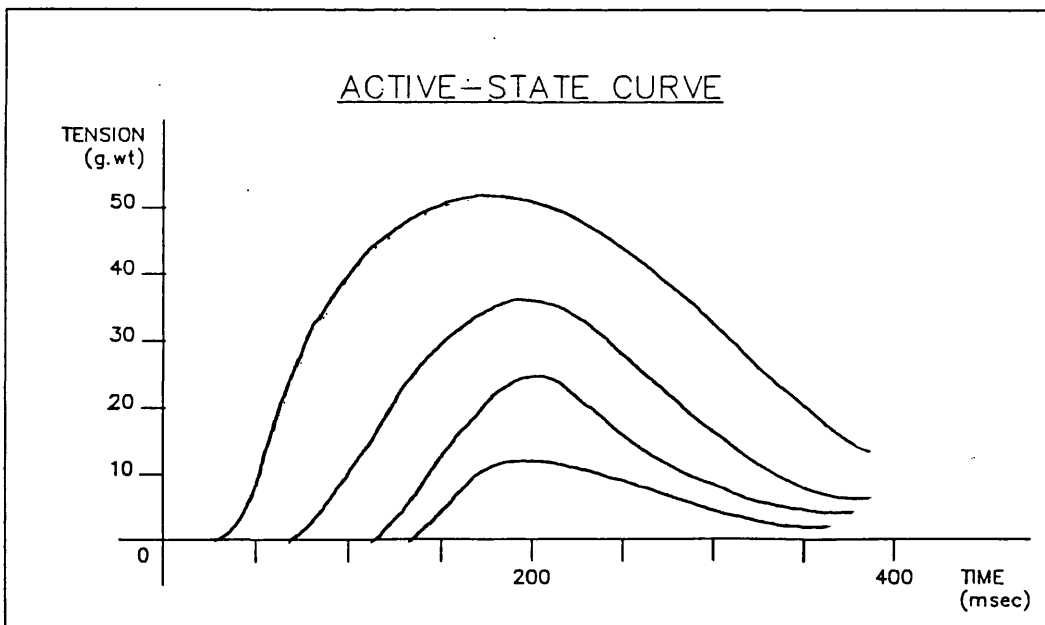


Fig.[2.12(d)] Active-state curve obtained from experimental tension-time curves (taken from WILKIE, 1956).

investigations for this reason and that the parameters specifying the elements of the model are non-linear (Jones, 1986). Although some of the results obtained are promising, the models will be difficult to use routinely.

For routine studies, a simpler approach is necessary employing linear models of the muscle dynamics. In order to study the system with linear descriptions one must assume that either the force or length are regarded as constant and also that the effects of fatigue are carefully considered. The latter is important when large records of EMG data are required. This demands longer periods of contraction leading to variations in the EMG signal itself which in turn is used to drive some of these models. One method of in-vivo linear modelling is to first estimate the *average* isometric twitch response experimentally. This can be done by supramaximally stimulating the muscle, synchronously averaging the resulting response and then fitting this response to a parameterised mathematical equation (Milner-brown et al., 1973). The equation used could take the form of a linear combination of two exponentials to account for the rising and decaying parts in the twitch response: $f(t) = A\exp(-\alpha t) - B\exp(-\beta t)$.

Another method is to take the smoothed and rectified EMG as a close representative of neuronal activity and then relate it to the actual force produced by an appropriate system identification method. The impulse response of such a model then provides the average twitch response. Bekey et al. (1966) investigated the human triceps muscle using an on-line parameter tracking procedure implemented on an analogue computer. The rectified EMG-force relationship was successfully described by a second order differential equation when using short bursts of rhythmical voluntary contraction. The reasons for their particular forcing protocol and choice of model were not explained. Other second order models have been reported by Cogshall et al. (1970), Gottlieb et al. (1971), Mannard et al. (1973), Crosby (1978), Lago (1979), and Zahalak (1979).

Lago (1979) points out that in an almost noise-free situation all modelling algorithms will yield, essentially, the same estimates for parameters. However the presence of noise in the majority of input data is such that the choice of modelling algorithm and data collection procedure must obey precise criteria to produce reliable and non-oscillatory results. In addition to the need for restricting the muscle length and velocity of contraction for isometric and isotonic investigations respectively, it is particularly important in isometric conditions to constrain the tension such that the data lies on or near the linear portion of Fig.[2.12(a)].

No studies so far reported have demonstrated that a linear EMG-force model can be made totally independent of the force pattern. The reasons for the residual dependence of the models on the force pattern demanded are still conjectural. The problems of EMG-force non-linearity is, however, a likely cause. An example of a yet unexplained EMG-force relationship is shown in

Fig.[2.13], where bursts of EMG can be seen when the force has dropped to almost zero. These details of the EMG should be interpreted as noise as far as identification algorithms are concerned (Jones et al., 1987).

2.4.1 The Integrated EMG (IEMG) and Force

Clinicians and physiologists have sought to quantify the total activity, which is closely related to the generated force, and also the fluctuations which contain information on the constituent action potentials. Although much literature exists on the relationship between the EMG and force (Brigland and Lippold, 1954; Troup and Chapman, 1972; Lloyd, 1971; amongst others) the results of these experiments are not quite in agreement (Metral and Gasser, 1981). The mathematical relationships postulated have included linear, non-linear, quadratic and even linear followed by an exponential. These discrepancies can be attributed to the variations in experimental procedure used. First, and most likely, is the contraction protocol used (both static or dynamic and isometric or isotonic) and muscle or muscle group investigated. Second, a confusion between smoothed and integrated (averaged) EMG (IEMG) exists in terms of the time constants used for the electronic integration and the prior rectification, be it half or full wave. Finally, the effects of fatigue have not been carefully evaluated.

One definition of the IEMG is equivalent to measuring the area under the fully rectified signal for three arbitrarily chosen sub-intervals of period $\frac{1}{6}$ sec to give a total integration period of $\frac{1}{2}$ sec (Lippold, 1952). Another version is to use the full-wave rectified signal followed by an RC low pass filter (Inman et al., 1952). The time constant was chosen subjectively to compromise between an output smooth enough to permit *useful* analysis and such that it would be small enough to yield a desired accuracy. Hof and Van Den Berg (1981) used a third order averaging filter (Garland et al., 1972) and a time constant (T) of approximately 25ms. According to physiological data (Edman, 1970) T should be very short. However one would prefer to have a large T to obtain sufficient smoothing of the rectified signal. Hof and Van Den Berg (1981) determined their time constant by applying a step input to the summing point of their integrator and selected a T such that their non-linear Hill model did not produce any noticeable slowing down of the step response.

Using the gastrocnemius-soleus muscle group and surface electrodes, a linear relationship has been found between the area-type IEMG and the isometric tension throughout the normal contraction range (Lippold, 1952). De Vries (1962) have also reported a linear relationship with the same IEMG method as Lippold at very low levels of contraction in the elbow flexors with surface electrodes. The rectified and electronically smoothed IEMG has revealed a linear relation with a time delay (Inman et al., 1952). Thus, by and large, it was generally accepted that the IEMG

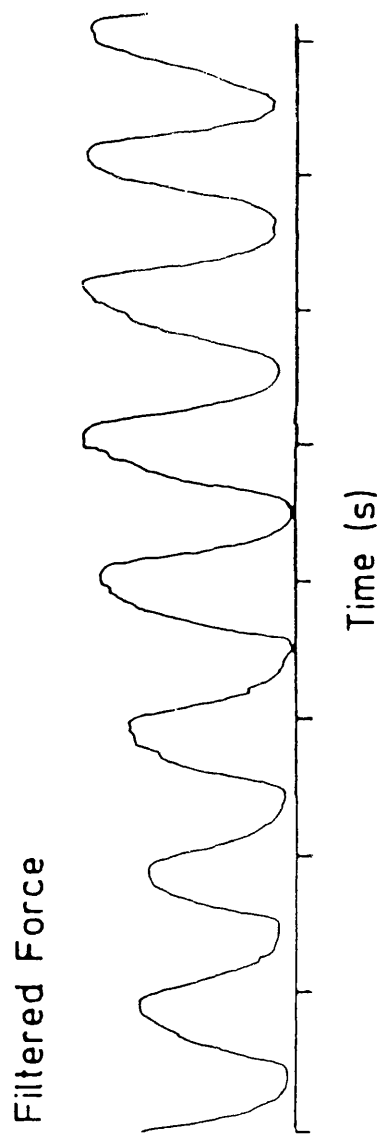
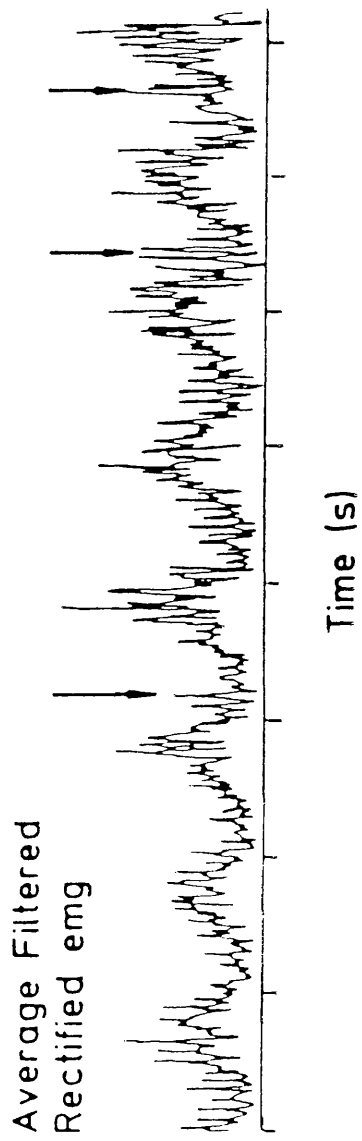


Fig.[2.13] EMG and Force waves. departures from assumed model are indicated (taken from JONES et. al., 1987).

provided a reasonable index of muscle activity for most of the larger and smaller muscles with short tendons. However, Bigland and Lippold (1954) observed that certain muscles, such as the tibialis anterior, have given rise to quadratic relations under isometric conditions.

Under isometric isotonic conditions it is not possible to describe the IEMG with any form of numerical index (due to the variations between muscles and subjects) and the qualitative information obtained has not been very useful for physiological studies. In order to provide an insight into the recruitment, firing frequency and synchronisation of active motor units it is more appropriate to investigate other applications of the IEMG in situations that are closely related to normal voluntary effort. The use of dynamic forcing protocols is necessary in these situations.

Bigland and Lippold (1954) studied the relationship between the IEMG and tension at various velocities of shortening in voluntary contraction. For constant velocity anisotonic tests on the calf muscles, a linear relation between IEMG and velocity of shortening and lengthening was found. Also less electrical activity was required during the lengthening, or negative velocity phase. This finding is in agreement with the force-velocity relationship determined by Hill (1938). For isotonic and varying velocity tests, a linear relation was again found, although in the lengthening phase the electrical activity remained constant. The constant electrical activity points were used to draw a family of force-velocity curves and were once again in agreement with the Hill equation.

Gottlieb and Aggarwal (1971) investigated the relation between the foot torque and the IEMG from the soleus muscle. The actual foot torque was compared with the output from two cascaded first order low pass filters (producing a second order function) using the IEMG as input. Isometric *step* and *ramp* force tracking was employed and one of the time constants was said to be related to the active state although it was not specified how exactly, apart from the response shape that was obtained. The muscle twitch response obtained from this model was not similar to that actually measured. The conclusion was, that if the EMG should undergo any dynamic changes of its own which are independent of the applied torque (e.g. through the stretch reflex loop), then the model was bound to reveal less information on the muscle dynamics (cf. Fig.[2.13]).

Metral et al. (1981) recorded the surface EMG from the extensor carpi radiales of normal human subjects during voluntary isometric anisotonic contractions. A bi-linear relation was obtained between the IEMG and force. It was stressed that the pursuit task had to be perfectly linear to obtain this relation. Otherwise, often a good parabolic fit was obtained with correlation coefficient greater than 0.98. The first linear trend occurred up to 50% maximum contraction in agreement with Milner-Brown et al. (1973). The second linear trend of higher slope above 50% suggested a rapid increase in IEMG attributable to the recruitment of higher threshold motor units having large amplitude action potentials. A subsequent analysis of the relationship between the running

sum of the IEMG and increasing force produced a fit to the sum of two increasing exponentials. The first exponential was taken to represent the contractile properties of the muscle (tension-length), and the second taken to represent motor unit recruitment on the basis of the parameter variations with changing muscle length and rate of tension increase.

Chapter Three

A Computer System for Control and Digital Signal Processing Applications

3.1 Introduction

This chapter provides a description of the main elements in a flexible and ergonomically efficient computer for use in basic digital signal processing, data acquisition and external instrument control tasks. The computer architecture is such that the reconfiguration for different procedures is relatively straightforward. To-date, the computer has been configured for two analysis procedures. It has wider use in the control of, and acquisition of data from, the muscle load which is described in chapter four. Experience gained with this Signal Processing Computer (SPC), and the emergence of new computer and software technologies, point the way towards a greater emphasis on the use of commercial hardware and high level programming languages. This should allow for shorter research and development timescales in order to create analysis environments that embody the basic philosophy and functionality of the SPC.

Today instrumentation in almost every field is becoming increasingly *smart* or intelligent. This is primarily because the incorporation of a microprocessor and its associated software allows more complicated analysis to be performed and permits a more complex configuration than in a conventionally designed instrument. The rapid proliferation of advanced instrumentation ownership among the general public has put demands on the system designer to obscure most of the complexity of the the instrument behind an interface that is *user friendly*. Lack of time to consult systems that perform complex analyses is an important consideration in the specification and design of today's computers which must be relatively quick, especially in a clinical environment where time is often a critical factor. There is little doubt that, through the use of suitable software and the associated interface hardware, instrument ergonomics can be maximised in terms of user friendliness.

A significant problem with most of the digital signal processing systems available today is the rigidity of the user interface adopted. As a result of this, an inordinate amount of time is required to consult the system and its associated manuals. The SPC was designed for use either by those with no expertise in digital signal processing or in situations where the user is unable to pay much attention to the instrument. Such situations may arise in the operating theatre or outpatient clinic. The SPC uses a menu-driven user interface to maximise ease of interaction. The system allows

entry of analysis parameters, patient details etc. in a convenient manner by presenting the user with a page of options on the screen, and allowing him to depress the appropriate software-monitored (soft) keys. The small number of keys used to control the instrument obviates the need for an alphanumeric keyboard, although this can be connected if required. Relabelling of the keys and the use of branching menus allows the user to progress through signal acquisition, processing and display of results with the knowledge that all options have already been considered by the system programmer. Furthermore, the instrument exists as a single portable unit, containing the display unit with its soft-keys, a 5¹/₄ inch floppy disk drive and various data acquisition and programmable processing cards.

3.2 Instrument Specification

The computer was required to perform on-line analysis of data that had previously been analysed off-line and this led to real-time data throughput being considered. The normal pre-requisite for real-time analysis is a small (dedicated) mini or microcomputer. In an attempt to overcome the development of a dedicated system restricted to only one or a group of analysis methods, a strategy of flexible application was adopted based on generic software and simple, but versatile hardware. This would enable the creation of dedicated systems based on re-configurations of the various system modules. The modules comprise a suite of software routines and programmable hardware which together allow the construction of multiple and independent applications by a programmer familiar with signal processing and the basic system concepts.

By real-time analysis one most often intends to convey the idea of very fast processing of data whilst it is being acquired. In practice, however, real-time analysis is performed on-line at a speed appropriate to the amount of time allowable before the display of results or the execution of actions. The advantages of doing an analysis in real-time are as follows and were considered important requirements for this computer system:

- Immediate availability of information to the user. This leads to greater throughput and makes repetition of experiments, where validation is necessary, relatively easy.
- System and analysis parameter settings can be optimised rapidly by examining the full or partial results of a data analysis.
- Controlled variables can be continually monitored and adjusted in accordance with experimental and ambient conditions.
- The fact that complex results can be obtained quickly makes it possible to design and implement other investigation procedures that would otherwise be impracticable or overlooked.

The disadvantages highlighted when considering real-time analysis were:

- Real-time programs are more complex than others with regard to the difficulty of design and coding and with regard to testing, debugging, and implementation.
- A good source of test data (simulated or real) is essential for test purposes.

Two applications in clinical signal processing were specified for development in the computer:

- The first was acquisition and processing of blood flow and pressure signals during surgery. In this application, derived from Butler et al. (1980) and Law et al. (1983), the surgeon would be presented with flow, pressure, or ECG displays, or vascular impedance modulus or phase characteristics to assist in the assessment of the vascular system.
- The second application area was implemented as a simulation in this work and is intended to demonstrate a potential use of the computer in an electromyography outpatient clinic. A description of the analysis procedure used (Turning Points Spectral Analysis of the Interference Pattern EMG (Lago and Jones, 1983)) has been presented in chapter two (Sec.[2.3.4]).

These analyses required the instrument to be capable of sampling at least three channels of information (e.g. blood flow, blood pressure, and ECG). To accommodate electromyographic investigations and to adhere to the philosophy of flexibility in other medical, biological, and industrial applications, the system was required to facilitate acquisition of up to four multiplexed channels with 8 or 12 bits resolution at a nominal sampling frequency of 3.3 kHz.

The software was designed to aid both straightforward reconfiguration and ease of interaction with the instrument. The SPC should also be easy to expand and to this end the use of commercial boards adhering to the S-100 bus standard was specified. This will enable additional boards to be bought from manufacturers and the present ones to be updated.

Experience gained at the Graduate Division of Biomedical Engineering, University of Sussex has shown that computer equipment developed for research into new applications of clinical signal processing should be easily operated by clinical personnel as well as research staff. Previously, the fashion has been to employ general-purpose computers with command structures more appropriate to technical users. The 'flexible friendly computer' is intended to aid algorithm development and evaluation by clinical staff.

HARDWARE

In order to minimize 're-invention of the wheel' and avoid unnecessary development time and expense, the computer was based upon a standard S-100 bus system with a single mini-floppy drive and using three commercial cards. To this was added an in-built 5.5" display surrounded by program-definable keys, and a four channel analogue acquisition sub-system. Signal processing and data acquisition are partitioned between the main Z80-based computer and the acquisition processor with inter-processor communication taking place via a dual-plane memory, permitting truly concurrent processing.

SOFTWARE

The combination of a branching menu structure with an integral graphics display surrounded by program-definable 'soft' keys allows the operator to control computer functions without resort to an alphanumeric keyboard. In addition to the menu structure, a series of utilities are provided for the developer of signal processing algorithms. These include a package of maths utilities such as Fast Fourier Transforms, a graphics package and signal acquisition firmware. The packages can be accessed via most popular languages available under the, now dated but still standard, CP/M operating system.

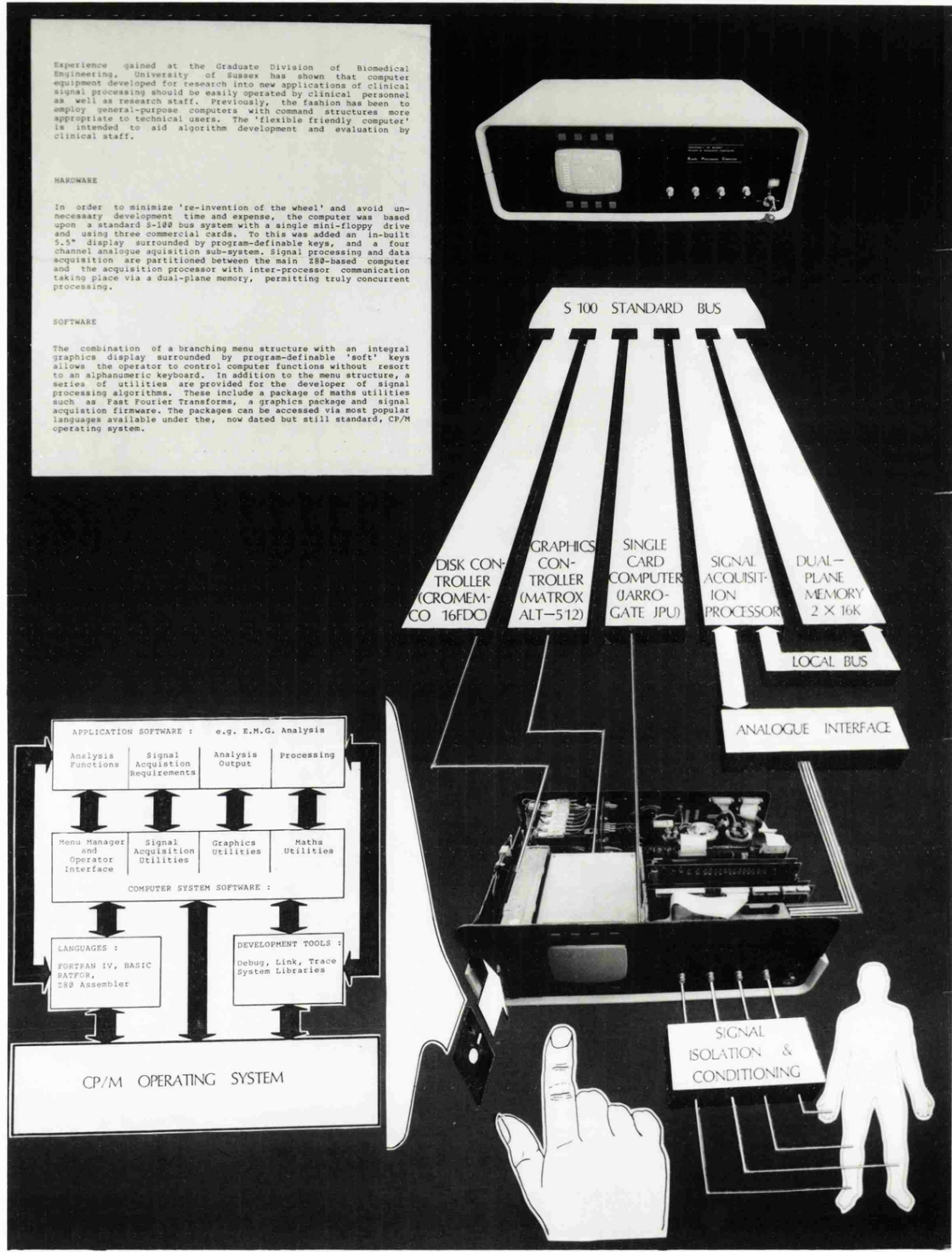


Fig.[3.1] The interaction of system modules (both Hardware and Software) in the SPC.

3.2 SPC Hardware Organisation

The specification of the SPC outlined in Sec.[3.1] has been translated into the system shown in Fig.[3.1], which clearly illustrates the way system software interacts with hardware to provide a simple patient/user interface. The hardware schematic diagram in Fig.[3.2] shows both the individual elements of the SPC and their communication links across the S-100 bus.

3.2.1 General Hardware Description

The SPC is essentially a dual-processor computer containing six boards, three of which are standard commercial boards. One of the two processors (6 MHz Zilog Z80B) resides in the commercial Single-Card Computer (SCC) together with 64 kbytes of RAM, three serial ports, three parallel ports, and two counter-timers. The second processor (4 MHz Zilog Z80A) resides in the Signal Acquisition Processor (SAP) board. This was initially designed by Hailstone and Watson in 1983, and subsequently modified by Hailstone and Sehmi during 1984, to cater for EMG acquisition and analysis. The SAP is intended to control signal acquisition of up to four channels of input data and also to drive XY plotter outputs for obtaining hard copies of results via the Signal Acquisition Card (SAC). To ensure control over the processors, a hierarchical arrangement had to be adopted, giving rise to a *host* and *slave* processor configuration. The SCC is considered the host processor and the SAP, the slave or satellite processor.

Through host-resident communication protocol programs and slave-resident monitor programs, the host is able to control the slave processor by passing coded messages (i.e. control data) across the data lines of the S-100 bus and these are then decoded and executed (the handshaking mechanism will be explained later in the software section). Using a similar handshaking method to transfer acquired data to the host from the slave would be very time consuming. A Dual Plane Memory (DPM) (Watson, 1983) was the solution implemented for this (non-control) data transfer between the slave and host processors because it allows two independent 16 kbyte blocks of data (i.e. memory *planes*) to be accessed separately by both the host and slave processors. The host processor can force the SAP to interchange these planes of data *immediately* by issuing a single plane-swap command using the communication protocol programs. The above dual-processor arrangement allows for signal acquisition on the SAP and signal processing on the SCC, thus permitting concurrent operation.

The remaining (commercial) boards are the floppy disk controller, and the graphics controller. A Cromemco 16K floppy disk controller (FDC) card provides disc Input/Output (I/O) and other facilities such as boot-strapping the operating system from disk on power-up. This facility is required to obviate the need for a keyboard terminal and VDU monitor for loading the operating

SPC HARDWARE

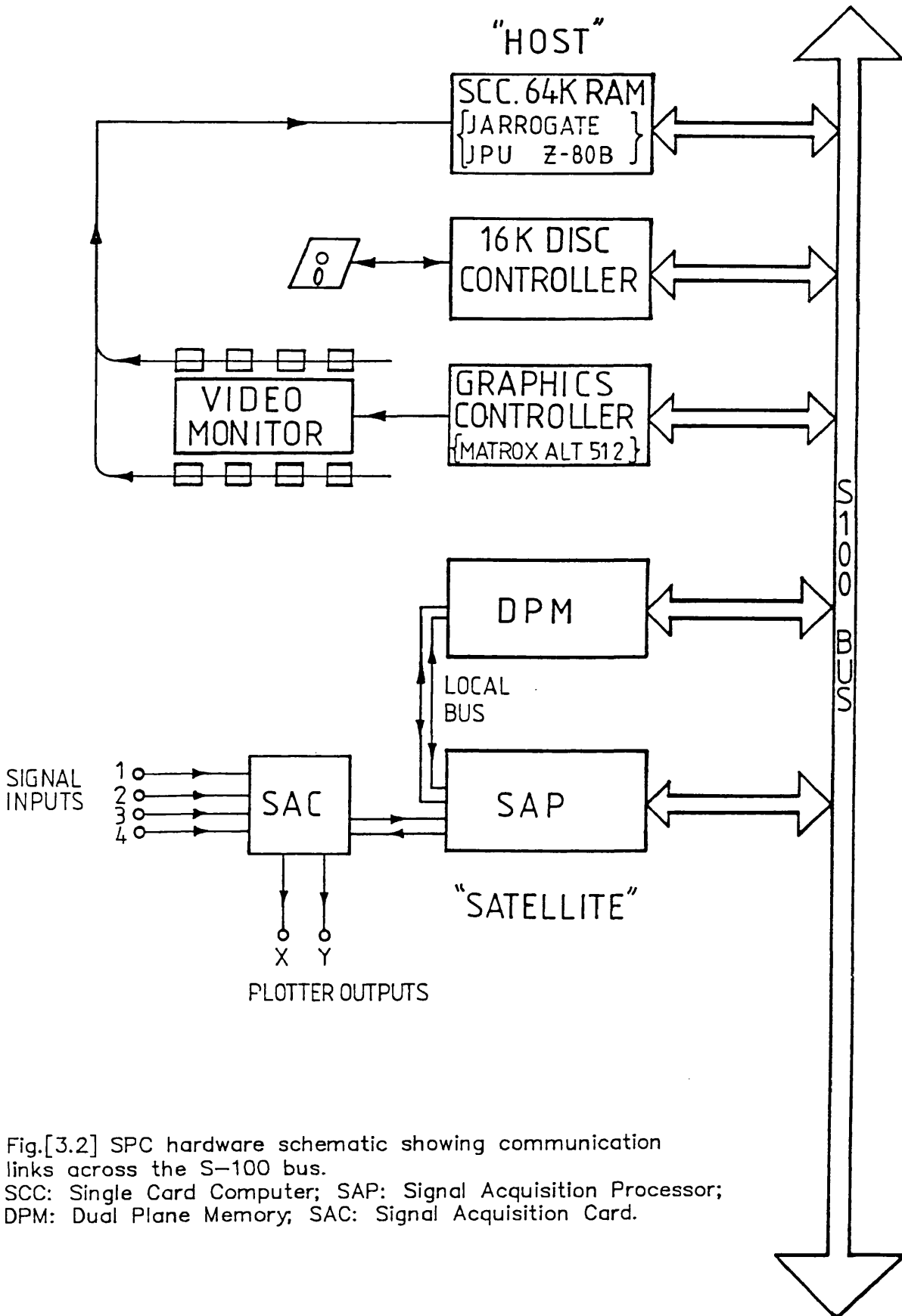


Fig.[3.2] SPC hardware schematic showing communication links across the S-100 bus.
 SCC: Single Card Computer; SAP: Signal Acquisition Processor;
 DPM: Dual Plane Memory; SAC: Signal Acquisition Card.

system and executable files of an application. The RS232 serial line on the FDC allows the connection of a terminal and monitor for local (i.e. on the machine) program development (edit, compile, link, run, and debug) through disk-based operating system facilities. A Matrox ALT 512 graphics controller provides logical overlay of two 256 x 256 resolution video planes on a seven inch diagonal display monitor. An external VHF connection is provided to drive larger monitors.

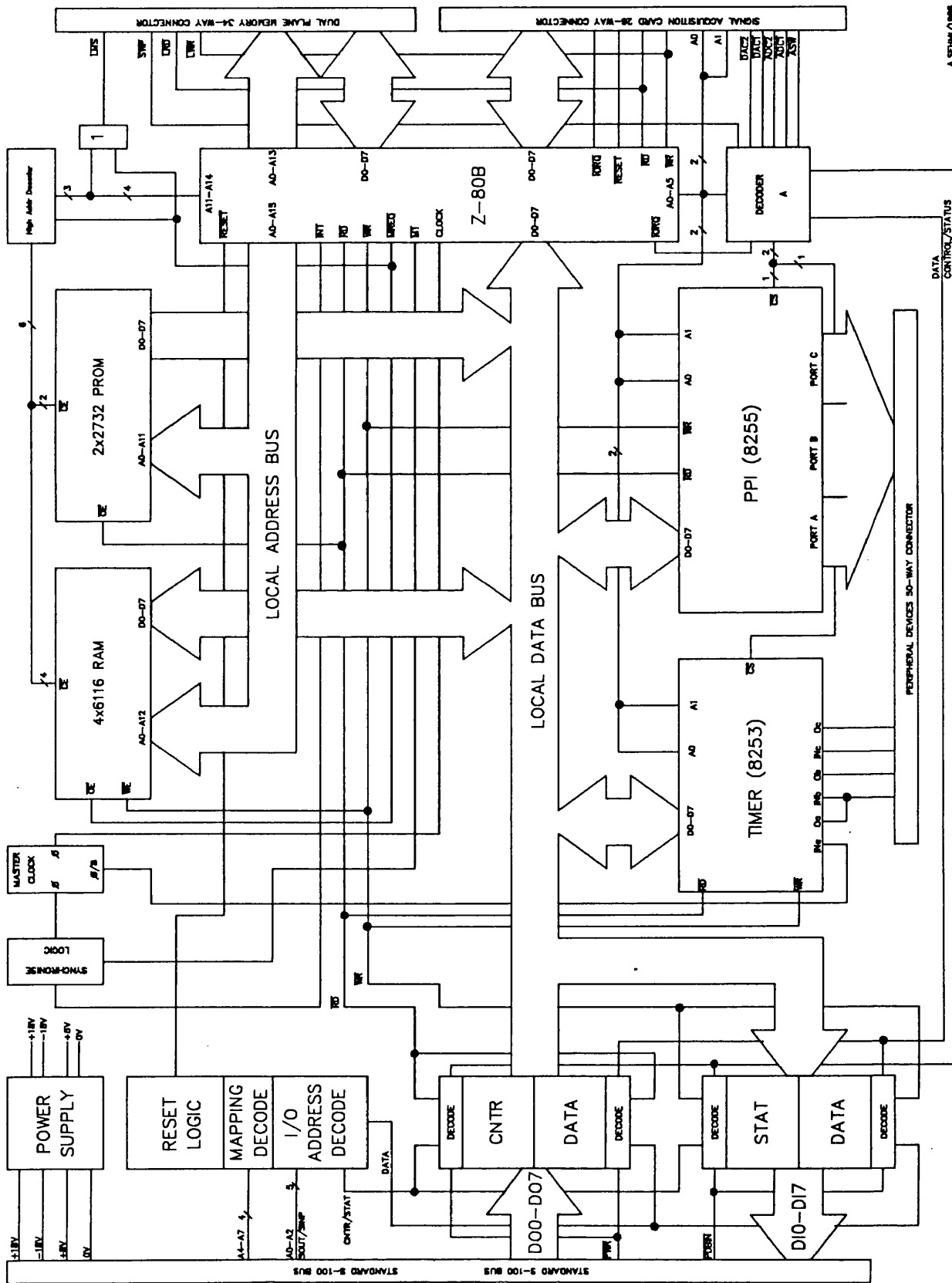
The non-commercial hardware modules and how they interact with each other is described briefly in the following three sections.

3.2.2 The Signal Acquisition Processor (SAP)

Fig.[3.3] shows a schematic diagram of this slave processor board as it existed prior to the new developments to be mentioned later. The main features of this board are the use of a local bus to communicate with 8 kbytes of local PROM, 24 kbytes of local RAM of which the last 16 kbytes are a plane in the DPM, the timer, I/O and protocol-communication ports, and the remote S-100 bus. The memory chips are addressed in the order in which they have just been mentioned. To the right of the schematic diagram are the control, data and address signals used to interface the DPM and SAC. Decoder A provides all the I/O mapped control signals for the SAC and a single control signal for the DPM. The SAC control (select) signals are used to address the analogue to digital converter (ADC) and the multiplying digital to analogue converters (MDACs), and to select the analogue switches (ASWs) for multiplexing data into the computer. The DPM control signal is used to swap the planes in the DPM. In addition, decoder A also provides control signals for the peripheral parallel interface, programmable interval timer, and the host-slave communication protocol ports. The latter are the route through which the SAP exchanges control information with the host processor along the S-100 bus.

The SAP/host interface has its base address set in host I/O space and can be changed with switches. The interface base address is fixed in SAP I/O space. The control-data (CNTR/DATA) port is read-only and hence an input port (with respect to the SAP), and the status-data (STAT/DATA) port is write-only and hence an output port. During normal operation the host loads the CNTR port with a data byte that contains bit-coded information. This informs the SAP whether to expect an additional data byte through the input DATA port, in the case of a SAP-settable function, or whether to send data to the output DATA port, in the case of a SAP-readable function. The SAP will update its STAT port with a coded data byte whenever it is executing a task that has been requested by the host. In this way the host always has the immediate SAP status available for interrogation. When the SAP is idle it polls the host's *ready* and *read/set* flags that are set through the CNTR port and will respond accordingly. A similar communication protocol exists within the host processor which is more complicated because it is required to

SIGNAL ACQUISITION PROCESSOR



A.52844/1086

Fig.[3.3] Schematic of the Signal Acquisition Processor (SAP).

interpret and act upon more information from the SAP status byte. A description of this protocol and its interaction with the SAP communication protocol will be treated separately in the section on software organisation.

The programmable interval timer (Intel 8253) is organised as two related and one independent 16-bit counter-timers, with all modes of operation being software programmable (i.e. settable) by the SAP under host control.

The arrangement described above will enable interrupt driven signal acquisition to be performed. The sampling interval can be adjusted easily by changing the count values that are loaded into the counter timers. At the end of each sampling interval the SAP is interrupted on a counter time-out and an interrupt service routine (ISR) acquires a byte of data through the SAC. The multiplexing of more than one channel of data is performed by the ISR in the monitor program residing in the SAP. The ISR outputs a data word to the analogue switches thereby selecting the correct input channel to sample.

The peripheral parallel interface (Intel 8255) is not dedicated and could be used to interface additional peripheral devices such as a printer or various alarm devices to signal any error conditions should the SPC be configured as a monitoring instrument.

3.2.3 The Signal Acquisition Card (SAC)

This board had not been fully integrated into the SPC at the time the author had completed the simulation suite of programs (for EMG Turning Points Spectral Analysis) running on the SCC. Several elements remained to be added and debugged in the SAP board. This procedure was taken up by a colleague (Kabay, 1985) who was required to correct and implement the following:

- The synchronisation of trigger timing between Sample and Hold (S&H) Amplifier and Analogue to Digital Convertor (ADC).
- The implementation of programmable anti-aliasing filters for automatic selection of cut-off frequency, bandwidth and roll-off.

The schematic of Fig.[3.4] shows the main elements of the signal acquisition card. These are:

- a bank of analogue switches (ASW) used for input data multiplexing,
- two 12-bit multiplying digital to analogue converters (MDAC) used for automatic offset adjustment and programmable gain control respectively,
- one 12-bit analogue to digital converter (ADC) with integrated 10V reference for conversion of input data to a form useable by the computer, and
- a sample and hold amplifier used to enable accurate conversion of input data during the sampling interval.

Two analogue switches are used to put the gain MDAC into the bipolar mode for plotting purposes. The SAC is interfaced directly to the SAP through the SAP local data bus and several control signals.

The intended operation of the SAC is largely software driven and is explained in some detail later in Sec.[3.3.4].

3.2.4 The Dual Plane Memory (DPM)

A schematic diagram of this board is shown in Fig.[3.5]. The DPM comprises two planes, each consisting of 16 kbytes of static RAM, and is configured such that one plane resides in the memory space of the host processor and the other resides in the memory space of the SAP. The former plane in host memory space is *phantomed* through the S-100 bus and can be selected to be on any one of the four 16 kbyte boundaries of the SAP's full address space. An output control signal from the DPM board logic provides the necessary phantoming signal. When this signal becomes active, the host processor board will automatically disable its own currently addressed memory location thereby allowing only the DPM memory location at the same address to be accessed. The other DPM plane is accessed through the local bus between the SAP and the DPM board. Under host control the SAP can initiate a plane swap which is used to transfer acquired data to the SCC (host) from the SAP. This is the main use of the DPM although it could be used to transfer data and executable programs to the SAP from the SCC.

More detailed descriptions of the plane reversal procedure under software control are given in Sec.[3.3.5]. The DPM feature in the SPC provides data throughput at much faster rates than could be obtained using direct data bus utilisation techniques such as I/O and direct memory access (DMA). The transition time for a plane swap is equivalent to the execution time of the single output instruction needed to negate the SAP plane swap control signal and is approximately 1.7 μ s. DMA methods using the Z80 family of processing logic having the same memory bandwidth would take typically 7 to 8ms.

3.3 SPC Software Organisation

The software for the SPC is written in a mixture of RATFOR and Z-80 Assembly Language. A large part of the author's work was concerned with the development and specification of the SPC software and it is for this reason that a thorough explanation is provided.

3.3.1 General Software Description

The SPC software can be divided into three major modules:

- (i) **Host-resident kernel program:** this suite of macros and dedicated subroutines provides the nucleus of generic user-configurable programs to run the desired application on the SPC. The kernel provides any number of screen pages each with its own menu. With each page is a RETN key function used to access the previous menu page and seven programmer definable key functions, one of which provides up to three pages of HELP information. These pages describe in detail the usage of the remaining key functions which might, for example, set the parameters for subsequent data analysis. By attaching a page (with its own key function definitions) to the key function definition of a preceding page, a branching tree structure can be built to any depth limited only by the available memory space. A simple three-level tree structure is shown in Fig.[3.6]. The kernel program also handles the SAP communication protocol.
- (ii) **Host-resident graphics utilities package:** this provides graphics primitives to display computed results in a visual format. This is attractive to a clinician, e.g. a physician, and has the added advantage of being able to convey trends or patterns in computed results more readily than a numerical listing.
- (iii) **SAP-resident monitor program:** this communicates with the host processor through the SAP-local-bus/S-100 interface. The SAP monitor executes the instructions asked of it by the host and consistently updates its status messages which can then be looked at by the host. Various functions may be set or read in the SAP by the host. The settable functions include the sampling frequency, number of input channels, analogue signal gain and offset using the MDACs, and DPM plane swaps.

These modules can be combined to create an integrated system application during the program writing stage. The design of the software modules allows a structured and systematic reconfiguration method for the SPC task handling capabilities. The ability to program in a high level language for floating point calculations is beneficial where speed is unimportant. Assembler programs can be used for speed optimisations.

The SPC software will now be described with the aid of flow diagrams. These will show the general operation of the major macros and subroutines but will not represent them exactly as they currently exist, since they have all undergone improvements implemented by Kabay (personal communication, 1988) to incorporate hardware changes in the SAC and new signal processing utilities. Detailed software listings of the current programs are available from the Department of Engineering at the University of Leicester (c/o Professor N.B. Jones). Attention will be paid to the communication protocol existing between the SAP and Host processors (under routines SAPPRO and HSTPRO respectively). A brief overview of the implementation of MUSCLE, the EMG Turning Points Spectral Analysis simulation package for the SPC is then given.

3.3.2 The Host Resident Kernel Program

The kernel is concerned with the overall control and co-ordination of the instrument, and the prompting of and display of information to the user. The prompting is organised as a menu page and selection of options is made by depressing the appropriate (*soft*) key from those surrounding the menu page. Depressing a menu soft-key leads to any one of the following actions being performed:

- The execution of a function previously attached to that key during the program writing stage. This function may change the screen display into another menu page, with prompting of further options.
- Display of computed results.
- Simple message display (e.g. HELP information).

The soft-keys are always monitored for activation. Whether they have a function attached to them or not is entirely up to the programmer during the instrument configuration period. Soft-key functions exist as subroutines and therefore always return to the *parent* menu page unless the function generates a new menu page, in which case the function is a *child* as in Fig.[3.6]. The kernel also performs the protocol operations with the SAP.

All menu pages are generated by specifying the macro SPCKEY (see Fig.[3.7]). This macro writes the user defined menu and soft key legends to the screen through SETMEN. SPCKEY then monitors the keys with GETKEY and will transfer control to the selected subroutine when a key is depressed. At the end of each key scan the status of the SAP is checked by means of the protocol handler HSTPRO. SPCKEY contains two reserved key functions: Key 1 is used to step up the *menu tree* to the immediate parent menu page and Key 2 is used to access the user defined HELP pages. Keys 3-8 are initially undefined and can be used to generate the child menu pages in the menu tree by specifying a new instance of the macro SPCKEY in the subroutine attached to the key definition. For each instance of SPCKEY the programmer must provide the key legends, the menu and help texts, and the subroutines attached to the Keys 3-8.

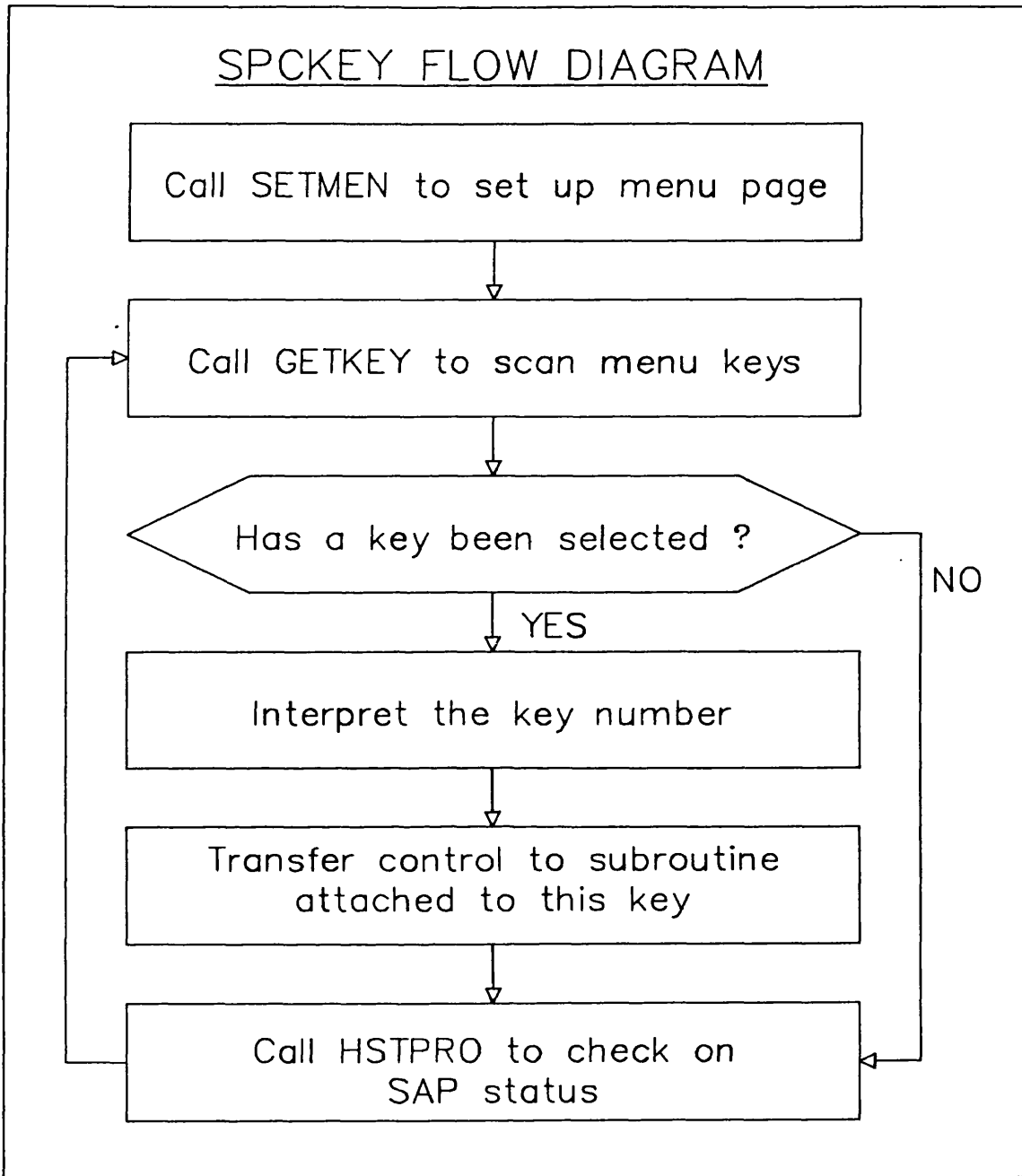


Fig.[3.7] Flow diagram of SPCKEY used to generate menu pages. These menus can be attached to key definitions from higher level menu pages giving the tree structure of Fig.[3.6].

A suite of SAP function calls are provided to aid the programmer in setting and reading SAP parameters (i.e. SAP settable and SAP readable functions respectively). These functions load the relevant control and data words corresponding to the desired action, and then, by invoking HSTPRO, the control and data words are sent to the SAP CNTR and DATA ports (see Fig.[3.3], Sec.[3.2.2]). The SAP then executes the requested command under SAPPPO, in the SAP monitor program. The SAP settable functions provided are:

(i) Immediate Control Functions

- Activate DPM plane swap (SAPMPS)
- Start signal acquisition (SAPST)
- Stop signal acquisition (SAPSP)
- Transfer Data/Program via DPM (SAPXFR)
- Execute transferred program (SAPXEC)
- Plot transferred data (SAPPLT)

(ii) Control Functions With Data

- Data/Program start low addressbyte (ASDPAL)
- High address byte (ASDPAH)
- Data/Program length low byte (ASDPLL)
- High byte (ASDPLH)
- Set sampling interval low byte (ASSIL)
- Set 8 or 12-bit A/D conversion (ASWDLN)
- High byte (ASSIH)
- Set input channel number (ASCSPC)
- Set gain MDAC low byte (ASGNL)
- High byte (ASGNH)
- Set offset MDAC low byte (ASOFL)
- High byte (ASOFH)
- Automatic input signal gain set (ASAGN)
- Automatic input signal offset set (ASAOFF)
- Set data plotting time base interval (ASPTI)

The parameter values used to set the SAP with the functions in (ii) above can be read from the SAP by the host using similar functions that are prefixed ARxxxx instead of ASxxxx.

The SPCKEY flow diagram describing the essential operations of the kernel program is given in Fig.[3.7]. Note that a similar flow diagram describes each instance of the SPCKEY macro at each non-terminal node of the menu tree in Fig.[3.6]. Terminal nodes can only originate from a parent SPCKEY macro, and each macro must have a parent macro except for the Level 1 root macro (in which case the 'parent' accessed through the RETN key is the CDOS operating system).

3.3.3 The Host Resident Graphics Utilities Package

Primitive subroutines for the Matrox ALT-512 graphics board are provided in this package, called GRAPH which is written entirely in Z-80 Assembly language. The host resident kernel program uses these whenever it has to write to the display screen to draw graphics and print text, etc. The graphics board has a display field consisting of two 256 x 256 planes of video RAM. It contains its own refresh memory, TV sync and video generator, and all I/O for the S-100 bus. Each dot (pixel) is addressable via the X-Y registers. The X-Y, dot colour (black or white), clear, plane select, status flags, and display mode control registers can be accessed by the host processor via six input and two output ports.

A selection of graphics primitives in GRAPH allow the user to perform simple drawing tasks. Functions are available to plot and position points on the screen, draw lines and axes, and print characters in standard and greek fonts. The spatial orientation and size of the printed characters can also be specified. Different graphics screen modes enable the display of logical combinations of the video planes. Additional functions allow the storage and retrieval of graphics images to and from specified files on disk.

Together these primitives are sufficient to create adequate screen displays for the menu pages, and displays of computed results in the form of graphs and charts.

3.3.4 The Sap Resident Monitor Program

Tasks related to input data acquisition, SAP configuration, and communication with the host processor are performed by SAPMON. The primary or foreground task is to monitor the SAP control port (see Fig.[3.3], Sec.[3.2.2]) for host requests which are then executed as secondary or background tasks after the immediate SAP status has been made available to the host through the SAP status port. The foreground task is always returned to, and the SAP status updated, when the background task is completed. This concept can be illustrated with the flow diagram of Fig.[3.8].

Within the SAP monitor program reside several major subroutines:

- **SAPPRO:** This handles the SAP/Host protocols. The CNTR port is polled and the control words are read when signalled by the host. SAPPRO continually updates SAP status by loading its STAT port with a status word. The host can then interrogate this port when necessary to co-ordinate message transfer. This constitutes a simple handshake mechanism implemented under software control.

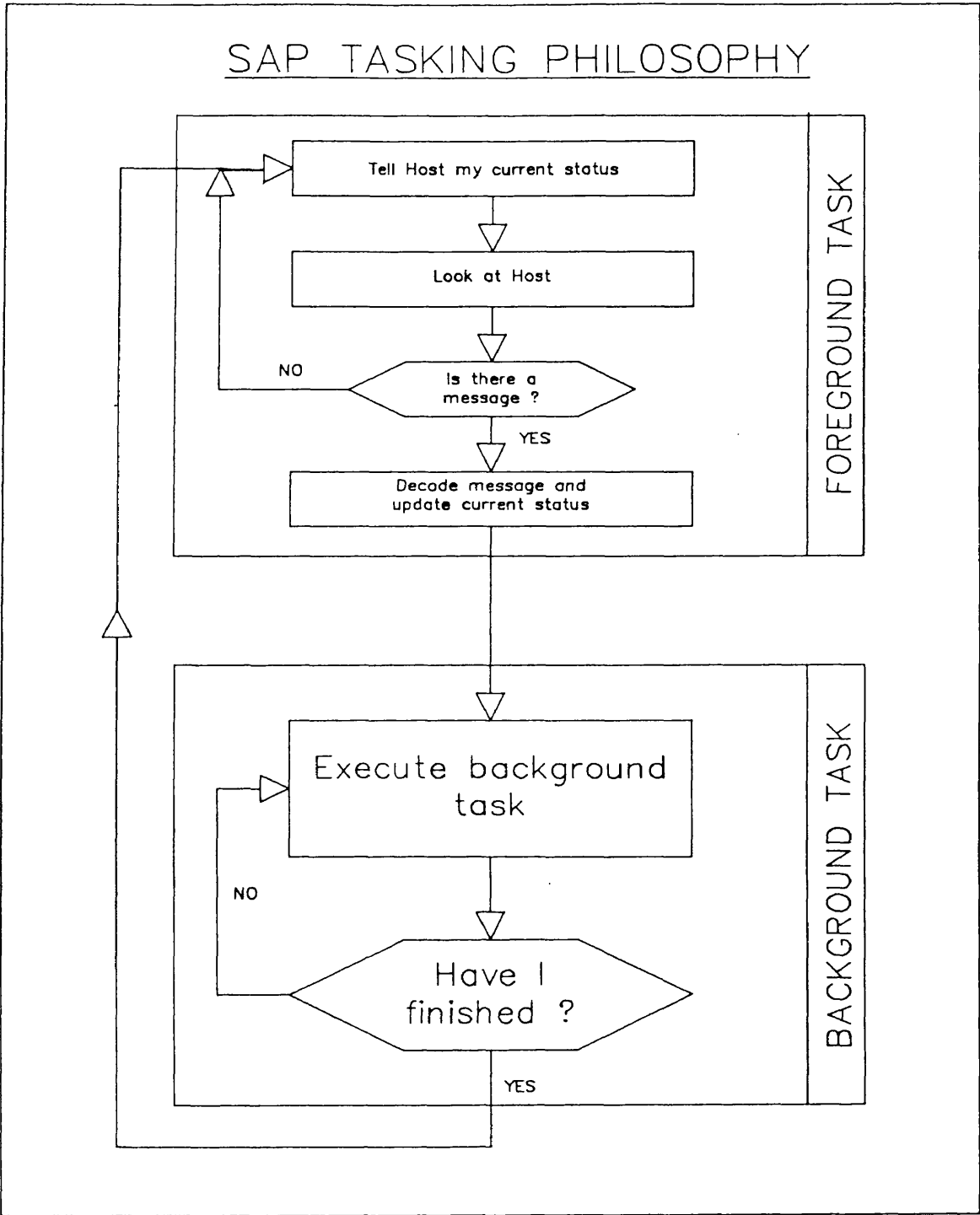


Fig.[3.8] SAP-resident monitor program flow diagram showing the split tasking philosophy adopted. The primary loop is the foreground task which monitors host requests.

- **SAPCWI:** This interprets the host control word that is obtained through the SAP control port under SAPPRO. The interpreted command is then executed and SAPPRO is re-entered. All set and read functions that the host can request of the SAP (see Sec.[3.3.2]) are performed by the corresponding *slave* subroutines in the SAP monitor program.
- **SAPRST:** This performs SAP initialisation after a hardware reset or software controlled reset from the host processor. SAPRST sets the stack pointer, performs a RAM test, selects plane 1 of the DPM, sets up the signal acquisition card (SAC) with default values for the input channel, gain and offset, and loads a default sampling interval count for the interrupt timers and a default A/D conversion word length. Control is then transferred to SAPPRO.

Signal acquisition under SAPMON is interrupt driven to allow the host to be monitored during input samples. This fits into the general philosophy of foreground and background tasking. The signal acquisition is thus considered a task of secondary priority relative to that of monitoring the host. With this arrangement the acquisition of data can be terminated if this is required by the host application. The start and stop commands are issued through the CNTR port in the manner described above. If SAP default values are not to be used, then the host application program must use the SAP set functions under the kernel program to select the A/D conversion word length, sampling interval, and the gain and offset values per input channel. The sequence of events that occurs during interrupt driven signal acquisition is illustrated in Fig.[3.9].

On receiving a *start signal acquisition* command from the host, START will set up a vector address for the correct interrupt service routine (12 or 8-bit) and load the programmable interval timers with the interval counts corresponding to the selected sampling interval. The STAT port is updated signalling *acquisition under way* to the host and then the Z-80 maskable interrupt is enabled before returning to SAPPRO. When the timer times-out, the SAP is interrupted and the vectored interrupt service routine (ISR) is executed. The interrupt is disabled and each channel specified for input is in turn set up with a gain and an offset by loading the MDACs with the appropriate 12-bit data words. The specified channels are multiplexed and sampled, and the digitised data is loaded into the DPM. The interrupt is enabled and SAPPRO re-entered to monitor the host. At this point the SAP could be interrupted again by the timer or alternatively stopped by a command from the host. The end of data acquisition causes the interrupt to be disabled.

Once the DPM plane in SAP memory space has been filled with data the acquisition ISR will request a plane swap command from the host by setting a flag in the STAT port. SAPPRO is re-entered to monitor the host reply. The host should then acknowledge causing a plane swap.

INTERRUPT DRIVEN SIGNAL ACQUISITION

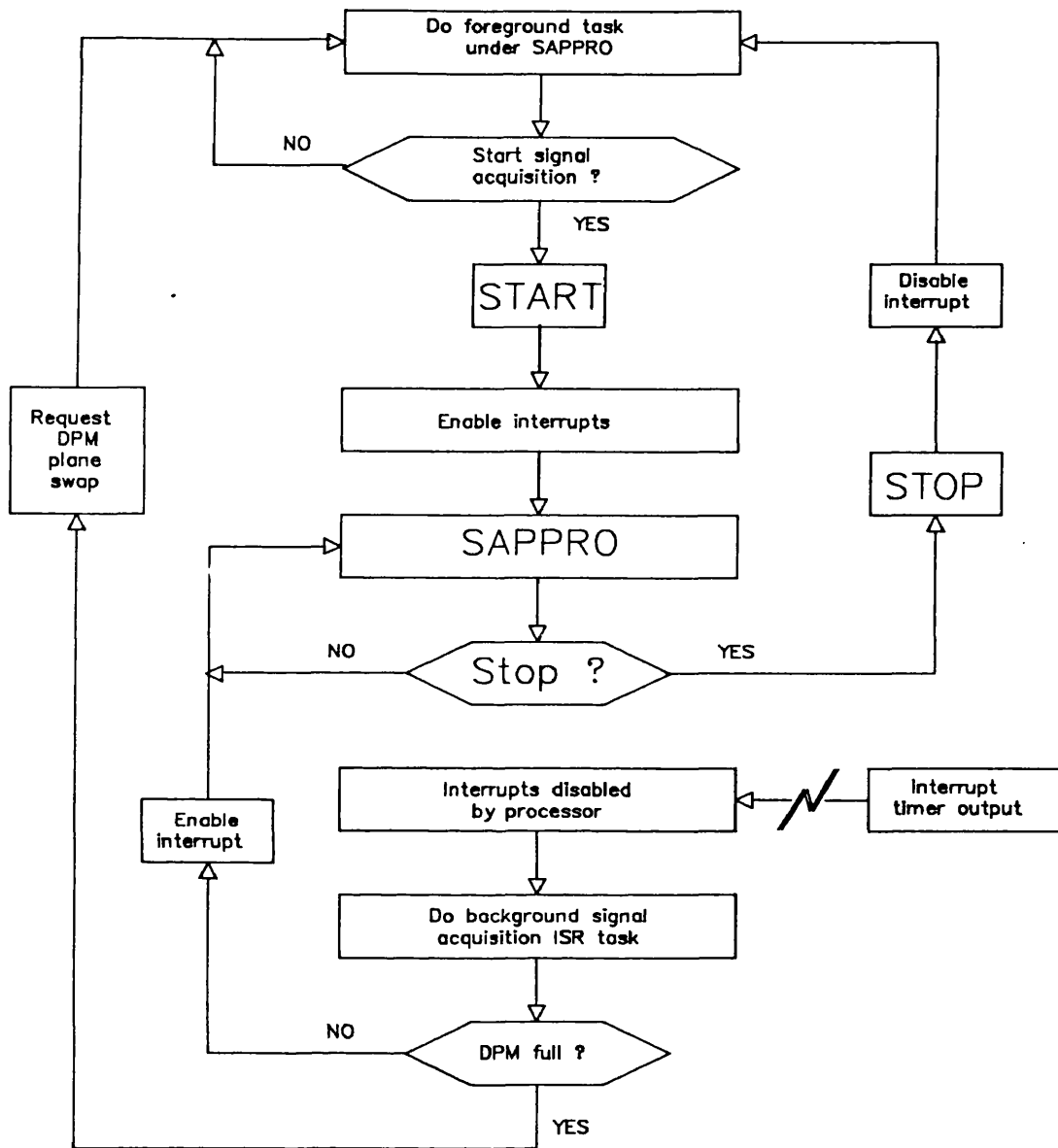


Fig.[3.9] The event sequence for interrupt-driven signal acquisition.

The host should restart SAP signal acquisition again if more data is needed. This time data is channelled into the conjugate DPM plane. During data acquisition by the SAP, the host could be storing the previous plane of DPM data onto disk for later processing. In this manner therefore, with judicious choice of sampling frequency, it is possible to acquire multi-channel records of data which occupy more memory than is directly addressable by an 8-bit microprocessor.

Other powerful facilities provided under SAPMON are the ability to execute programs or plot data transferred to it from the host via the DPM.

3.3.5 The SAP/HOST Communication Protocols

A full discussion of these protocols in the sections above would not have been appropriate since these dealt specifically with local descriptions of the main software modules in the SPC. The protocols are necessarily interactive and will be explained together.

SAPMON, the SAP-resident monitor program contains the protocol handling subroutine, SAPPRO. The host-resident kernel program communicates with the SAP through HSTPRO. Both these programs utilise the control/data (CNTR/DATA) and status/data (STAT/DATA) ports in the SAP. These ports are I/O mapped in both the host: via the S-100 bus, and the SAP: via the local bus (See Fig.[3.3], Sec.[3.2.2]). The CNTR port, set by the host processor application program through HSTMON, and read under SAPPRO, is assigned the following configuration:

The SAP/HOST CoNTRol Port



- 7-3: SAP function codes
- 2: SAP Read or Set function (R/S)
- 1: HOST ReaDY signal (RDY)
- 0: SAP software controlled ReSeT (SAPRST)

Similarly the STAT port which is loaded by SAPPRO, and read by the host under HSTPRO, has the configuration below:

The SAP/HOST STATus Port



- 5: SAP sending ERRor code to HOST (ERR)
- 4: SAP sending DaTA to HOST (DTA)
- 3: Current DPM Memory Plane (CMP: 0 = Plane 1, 1 = Plane 2)
- 2: SAP Requesting a DPM Plane Swap (RPS)

- 1: SAP currently ACQuiring data (ACQ)
- 0: SAP ACKnowledges HOST is ready (ACK)

Some of the following will have been mentioned briefly above. However, for the sake of clarity and completeness in this section, it is necessary to restate a few facts.

Fig.[3.10] describes SAPPRO. This is SAPMON's foreground task in relation to Fig.[3.8]. Since the SAP responds to host initiated commands, the top loop in SAPPRO monitors the SAP CNTR port to see if the host is ReaDY to request that a task be performed. When the host is ready it activates RDY in the control word, and SAPPRO will respond by setting the STAT port status word ACKnowledge (ACK) bit low, and DaTA (DTA) bit high. The control word is then tested for the type of function that is to be performed. In the case of a read function, SAPPRO must tell the host that data is being sent to it via the output DATA port by making DTA active. In the case of a set function, data to be used must be obtained from the input DATA port. Both function types reset ACK for the next cycle of SAPPRO.

The other status bits that SAPPRO can use to flag certain conditions to the host are ERR, CMP, ACQ, and RPS. The ERRor flag is followed by an error code that HSTPRO will submit for interpretation and user notification. The Current Memory Plane signal is provided only for background information. It could be used as an indicator of which plane is being accessed in display format design or during SAP reset procedures. ACQ and RPS are used extensively during SAP data acquisition. The former flags that data ACQuisition is under way and the latter Requests a DPM Plane Swap when a plane has been filled. The response of the host to these signals was designed for EMG data acquisition of at least 32 kbytes of data sampled at 1 kHz. This allows for 15 seconds of 12-bit data and sufficient spectral resolution to interpret gross changes in the form of the turning points spectra up to 500Hz. Over 95% of the power of surface EMG is contained within this frequency range, therefore this bandwidth can be regarded as adequate for the majority of EMG spectral methods.

Unlike SAPPRO, the host protocol handler (HSTPRO) does not function as a foreground task module within the host application program. It is invoked once at each execution of SPCKEY (See Fig.[3.7], Sec.[3.3.2]) to check SAP status as part of the major task which is the application program. Also, HSTPRO must be called explicitly by any application subroutines attached to SPCKEY key functions if they require SAP activation.

HSTPRO is summarised briefly with the aid of Fig.[3.11]. On entry into this subroutine a CHanGe flag in the host-resident kernel program is examined to determine whether the application program wants to activate the SAP. Either a read function is performed as the default action or

SAPPRO: SAP PROTOCOL HANDLER

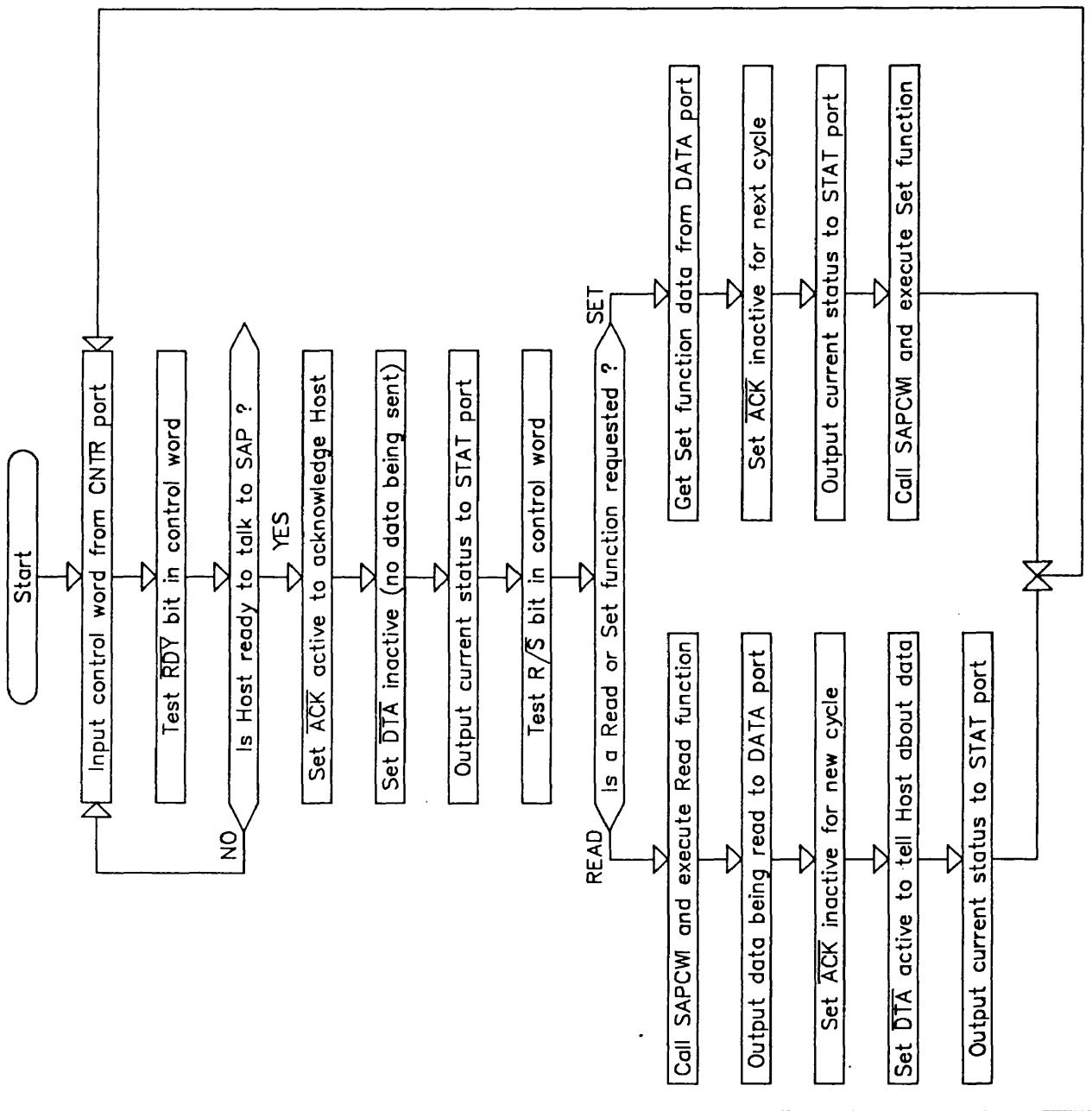


Fig.[3.10] SAP-resident protocol handler flow diagram describing how commands from the host processor are effected.

HSTPRO: HOST PROTOCOL HANDLER

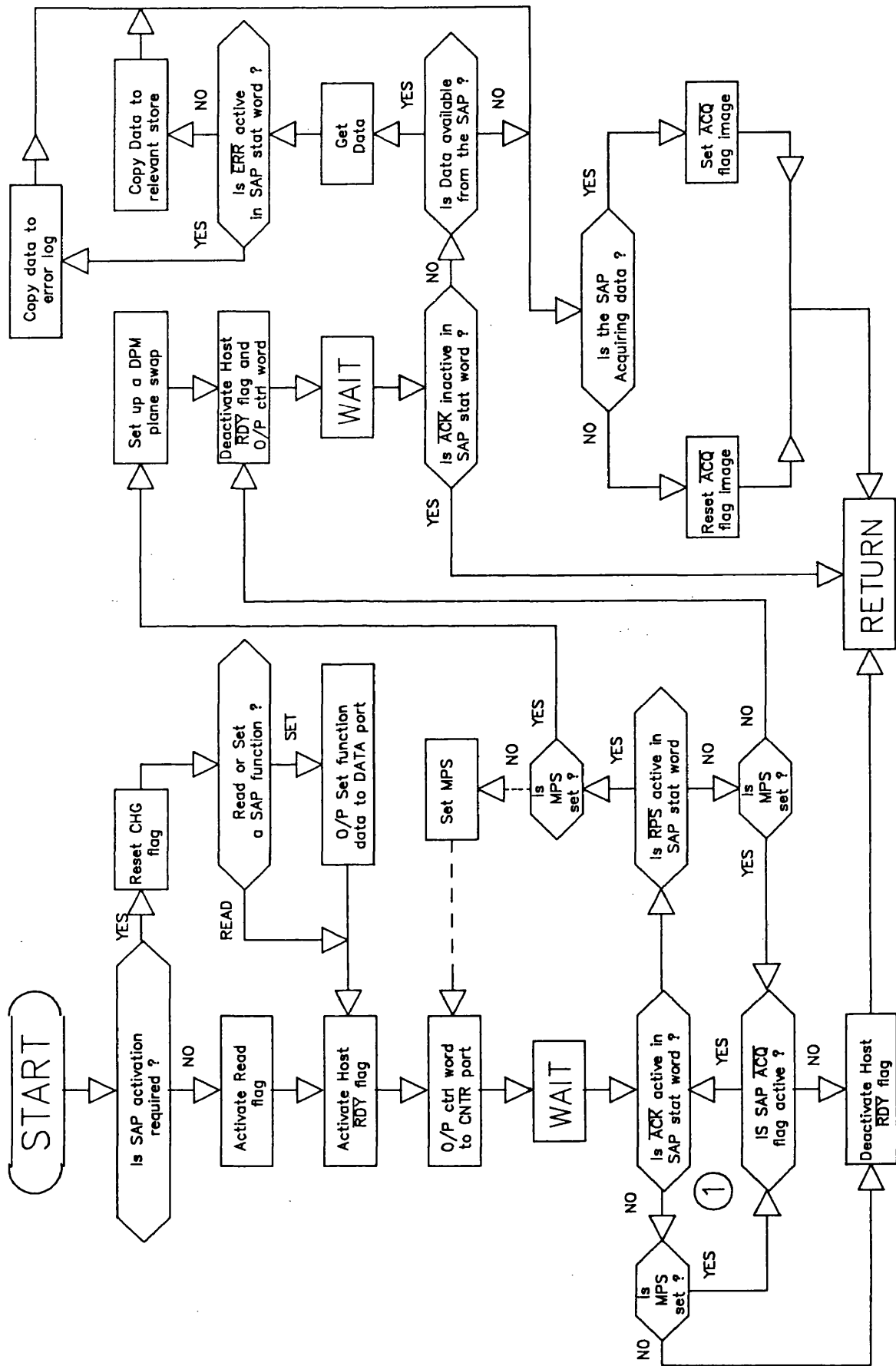


Fig.[3.11] Host-resident protocol handler flow diagram. This allows control over the SAP by SPC application programs.

else the set function is flagged and the DATA port is loaded with the relevant set function data byte. ReaDY is activated and the CNTR port updated so that the SAP can respond according to the decode of the higher order bits in the control word (Sec.[3.3.4]). The host is notified by the SAP that this control word has been received through the ACKnowledge flag in the SAP status word. The host RDY flag is de-activated and, if SAP ACK has been turned off under SAPPRO, then HSTPRO is left. If ACK is still active, then the SAP status word is examined to determine the DaTA and ACQuisition flag states. If data is available, the ERRor state is then determined or else the ACQ flag is copied into the a kernel program flag image and HSTPRO is subsequently left.

The Control of DPM Plane Swapping

The above description accounts for much of the work that HSTPRO performs. The portions of Fig.[3.11] that test and react to, the MPS and RPS flags conduct the SAP/HOST communication during signal acquisition. MPS is the name given to the host control function bit pattern assigned to a Memory Plane Swap, and RPS is the SAP status flag that Requests a Plane Swap from the host. This part of Fig.[3.11] is considered critical in the control of the timing of DPM plane swaps during EMG data capture.

The performance of the protocol outlined below has only been tested by the author under debug conditions (in the Summer of 1984) since the SAC was not fully functioning (as indicated in Sec.[3.2.3]). Debug tests did show that the intended sequencing of operations and DPM plane swapping were operational. Providing an example of the sequence of actions that an application program would have to perform for EMG data capture, will simplify the explanation of this segment of the HSTPRO flow diagram.

The SAP is set up for interrupt driven signal acquisition as described in Sec.[3.3.4]. At this point the ACQ is active through SAPMON. The SAP ACK flag is inactive and, between data samples, SAPPRO monitors the host control word for DPM swap or stop acquisition commands. During data capture into the first DPM plane, the host application program would have triggered the SAP immediate command: SAPMPS (Sec.[3.3.2]). HSTPRO responds by setting the local Memory Plane Swap (MPS) flag active. In this case the loop 1: ACK active? → MPS? → ACQ active?, is entered under HSTPRO.

When the first DPM plane has been acquired, data acquisition is stopped by not re-enabling the interrupt (Sec.[3.3.4]) and SAPPRO activates ACK and RPS. As a result HSTPRO signals a DPM plane swap and the application program restarts signal acquisition by invoking the SAP function START again. The RPS flag will become active under SAPPRO at the end of the second DPM

plane data capture, but will not be recognised by the application program until the first plane has been processed. Should more than two planes of data be required, the processing undertaken by the application program would have to be restricted to simple operations such as data transfer to another memory block, or even writing the data to disk, before reSTARTing the next DPM plane data capture. This is necessary to ensure that the data around the 16 kbyte boundary of the DPM planes remains contiguous when swapped into core memory space or stored on disk. In essence, the processing of the DPM plane in host memory space under the application program must take less time than it takes for the SAP to fill the DPM plane in its memory space. In this way temporal discontinuities in the signal at a DPM plane boundary can be minimised.

To save communication time, HSTPRO can be edited to include the dashed-line branch in Fig.[3.11]. This allows HSTPRO to turn the MPS signal on and off by itself for continuous plane swapping. SAPMON's interrupt service routines would also have to be edited to *re-enable* the interrupt flip flop after a completed DPM plane data capture process instead of leaving it *disabled* (see Fig.[3.9]), and to count the required number of plane swaps before de-activating the ACQ flag, thus allowing HSTPRO to return to the application program.

The other combinations of RPS and MPS tests that are present in HSTPRO simply ensure that the DPM planes are not swapped unless the application program is also ready to do so. In addition, by demanding a plane swap before entering HSTPRO, one is able to swap DPM planes outside periods of data acquisition (e.g. transferring data to SAP for plotting), in which case a plane swap can occur without an active RPS flag signal from the SAP.

Kabay has since changed the protocol to suit his application and data acquisition strategy (personal communication, 1988). These changes will be described briefly at the end of this chapter.

3.4 Simulated EMG Spectral Analysis in the SPC

The SPC has been configured for a simulation of EMG spectral analysis using the tools available in the Host resident kernel program. Some twenty instances of the macro SPCKEY are used to give an equal number of menu pages together with their corresponding key definitions. The major menu pages (the non-terminal nodes in the resulting tree structure) are used to select data acquisition and EMG analysis parameters, and to provide control and manipulation of the graphical display of computed results. The SAP can be set up according to various options selectable in menu pages emanating from the root menu. These include a start and stop signal acquisition control and the sampling interval. Menu pages are provided so that spectral and simple time domain analysis procedures can be performed. In the former the user can select the EMG record length and the number of data points on which an FFT is to be performed. In the case of Turning Points Spectral analysis, the simulated EMG data (due to Parekh, 1986) is first reduced to a 0-1 binary sequence, as described in Sec.[2.3.4], before performing the power spectral estimation. The time domain analysis options are: Zero crossings per second, mean value, rectified mean value, mean square value, and the displayed record length. All analysis routines were implemented in RATFOR for ease of coding, even though this proved to be expensive on memory.

Owing to the limited memory space available in the computer (48 kbytes), for running the full application program, some non-terminal node menu pages perform a memory overlay. This essentially means that all current information must be stored in parameter data files on disk before reloading the next selected menu page and all its child menu pages. Although this does take time it was effective because the spectral and time domain analyses are arranged as distinct overlays.

Some of the typical display formats that have been obtained in the application program MUSCLE are illustrated in Fig.[3.12]. These are from left to right:

- the root menu,
- one help page,
- data acquisition and EMG analysis parameter selection,
- results display selection,
- FFT routine parameter selection,
- raw EMG data display,
- EMG power spectral density display, and
- the EMG turning points spectral density display.

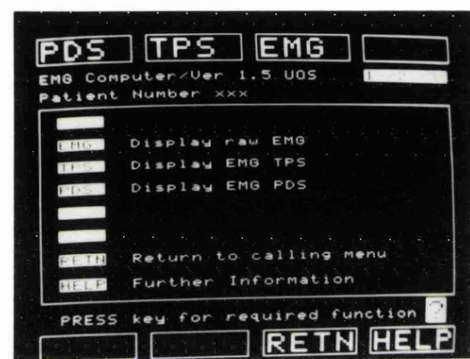


Fig.[3.12] Some display formats available under 'MUSCLE', the EMG Turning Points Spectral Analysis Application for the SPC.

3.5 Further Developments to the SPC

This section will outline the additional developments that have been made to the SPC by Kabay following Hailstone's, Watson's and the author's initial work on the basic design and specifications of the firmware.

The SPC has been taken to completion by Kabay. He has followed the design principles laid down by the initial team of workers already mentioned in the text above. Kabay has configured the SPC for Vascular Impedance Calculations (Butler et al., 1980). A list of changes and enhancements to the SPC have kindly been provided by him and these are given below:

[A] Hardware

- The SAC now contains anti-aliasing filters using digital switched capacitor filters (type Motorola MF10) providing programmable cut-off frequency, bandwidth and roll-off characteristics.
- The SAC multiplexer is buffered to prevent voltage loading errors.
- The input amplifier has been replaced by a high quality instrumentation amplifier to minimise dc offset and to improve CMRR and frequency response.
- Synchronisation between the S&H amplifier and ADC has been improved.

[B] Software

- Automatic setting of input gain and offset for each channel selected by the operator.
- The ISR for data acquisition contains provision for the settling time of the gain and offset control DACs when two or more channels of data are being acquired.
- Automatic de-multiplexing of digitised data stored as 8 or 12 bit ADC words.
- A Real-time coherent averaging utility has been provided using channel 1 data for the averaging trigger reference. Up to 128 frames of triggered data can be acquired for improvements in signal to noise ratio in noisy environments. The trigger selection menu provides a zoom facility to increase resolution of the trigger point in the data acquired through channel 1.
- Automatic delay compensation between input channels to offset software overheads.

3.6 Discussion

The primary purpose of this chapter has been to explain the contributions of the author in the developments of the SPC. The SPC has evolved through the contributions of several workers over the last six years and has been taken to completion recently (Hailstone et al., 1986, reproduced in Appendix [A]). It has been shown how simple building blocks of fairly low technology can be combined to provide flexibility and ease of interaction with the computer system.

The SPC design philosophy is as important as its intended function in the areas of EMG and cardiovascular data processing. Today, however, there are available more effective methods for creating similar functionality and ease of use for less effort and in far lower time spans. In this respect, cheap personal computers (IBM PC and compatibles) and the wealth of programming languages and programming environments (e.g. C, Prolog, Windows, MetaWindows, etc.) must be considered. The real-time functionality of the SPC can be achieved using a PC under PCDOS and plug-in commercial data acquisition cards containing DPM-type memory buffers. The man-machine interface can be designed using a windows environment and all SPC signal processing and control functions can be implemented in a modern high level language with virtually no serious speed limitations.

Using techniques based on artificial intelligence (AI), developed in recent years, and now available for the PC, we now have new opportunities for instrument design. The use of expert systems technology will permit instrument designs that provide traditional analytical capabilities with interpretation and evaluation of the results. Ultimately it will be possible to control the instrument behaviour during data acquisition and analysis according to expert knowledge about the task domain.

The author will show in a later chapter how some of these ideas have been taken into consideration for Event Analysis in Evoked Potentials (EPs). Much of the design strategy adopted for the SPC has been used to create an EP analysis package written in the C language contained in a PC-based environment and controlling external data acquisition hardware (Appendix [D1]). Expert interpretation of the analysis results is then provided by an expert system written in Prolog (Appendix [C1 and C2]).

As it stands the SPC still has considerable potential for use. The muscle load, described in the next chapter, can be controlled easily by the SPC. The computer can be programmed to output forcing patterns and concurrently analyse the actual force and EMG signals measured from the subject under test. With respect to the work that has been done on EP analysis, the SPC can be used to

drive electronic stimulators for the provision of sensory stimuli to the patient. Cognitive EP studies sometimes use complex patterns of mixed stimuli which can also be programmed into the machine.

Chapter Four

A Controllable Force Generator and Transducer System for Muscle Investigations

4.1 Introduction

As mentioned in Sec.[2.3], the study of EMG provides information concerning the structure and functioning of the motor units (MU) it represents. Also, associated with any muscular contraction is the generation of a force and a change in length of muscle. In Sec.[2.4] it was determined that relationships between EMG-force and muscle length-shortening velocity are both of interest in determining the dynamics of the neuromuscular system.

Linear models to study the dynamics of the neuromuscular system have been considered by researchers because:

- (i) When the muscle contraction is isometric and surface electrodes are used, it is known that the static relationship between EMG and force is linear for many, but not all, muscles (Milner-brown and Stein, 1975; Lawrence and De Luca, 1983).
- (ii) The elementary force wave (force twitch) generated as the result of a single motor neurone pulse can last up to 100ms, whereas the corresponding component of the EMG (the MUAP) is over in much less than ten milliseconds. Hence, a linear model can be assumed such that the model's impulse response will have the characteristics of some 'average' or 'representative' force twitch (Jones et al., 1987).

The relationships describing the mechanics of muscle are highly non-linear making linear modelling unsuitable for EMG-force dynamics in non-isometric conditions. Ideally one would prefer to have the muscle (or muscle group) under investigation subjected to both isotonic and isometric contractions. In addition the provision of dynamic force variations at nearly constant muscle length is desirable for certain forms of neuromuscular investigation. Quantitative EMG studies used in the characterisation of the neuromuscular system, would also benefit from having such controllable muscle loads.

The usefulness of linear dynamic models in situations where non-isometric conditions do exist (e.g. biomechanics of sport) can therefore be said to be somewhat limited. However, in sports medicine for example, there is potential value in knowing the dynamics of force build up and decay in athletes using theoretically sound means of monitoring changes in muscle characteristics during

training and recovery from injury, even if there is a restriction to isometric conditions. Linear modelling is therefore worth pursuing and it should benefit from better methods of force control and measurement (Jones et al., 1988, reproduced in Appendix [B4]).

This chapter and the next describe the development and design of a system for controllable muscle loading and force transduction for use in EMG-force modelling and quantitative EMG investigations. The system described will enable production and measurement of deterministic forcing patterns from the patient under test.

4.2 Current Loading Methods and their Limitations

Much of the literature regarding neuromuscular investigation stresses the importance of obtaining interference pattern electromyograms (EMG) *under isotonic conditions*. *Isometric* loading is considered to be of lesser importance but, nonetheless, desirable. Fig.[4.1] shows some of those methods most frequently used in current clinical practice. Static, or constant force, loading can be achieved using a set of standard weights. In situations where load cells and springs are used, the patient must compress and extend them to produce just the right amounts of load level and dynamic force variation. The amount of force produced is monitored using strain gauge transducers and/or calibrated meters. Other more complicated techniques are used in situations where patients exert contractions isometrically against a force transducer. One complicated technique uses suitable apparatus to stabilise and support the joints involved in the test, such that their spatial geometries minimise force interference from non-targetted muscle groups. The measured force controls the vertical position of a horizontal target line on an oscilloscope, and the patient attempts to match this with a second line. A microprocessor controls the position of the target line causing it to either move up and down or remain stationary at a fixed level (Le Fever and De Luca, 1982).

The methods of muscle loading mentioned above suffer from three major drawbacks. First, and most important, is that the accuracy of isotonic loading is determined by the patient's motor and sensory control abilities. The success of the examination depends on the full co-operation of the patient. The patient must concentrate and be able to contract and relax his muscles in a deterministic, predictable manner at the request of the investigator. This degree of co-operation is not always obtained, especially in severe cases of neuromuscular disorder and in young children.

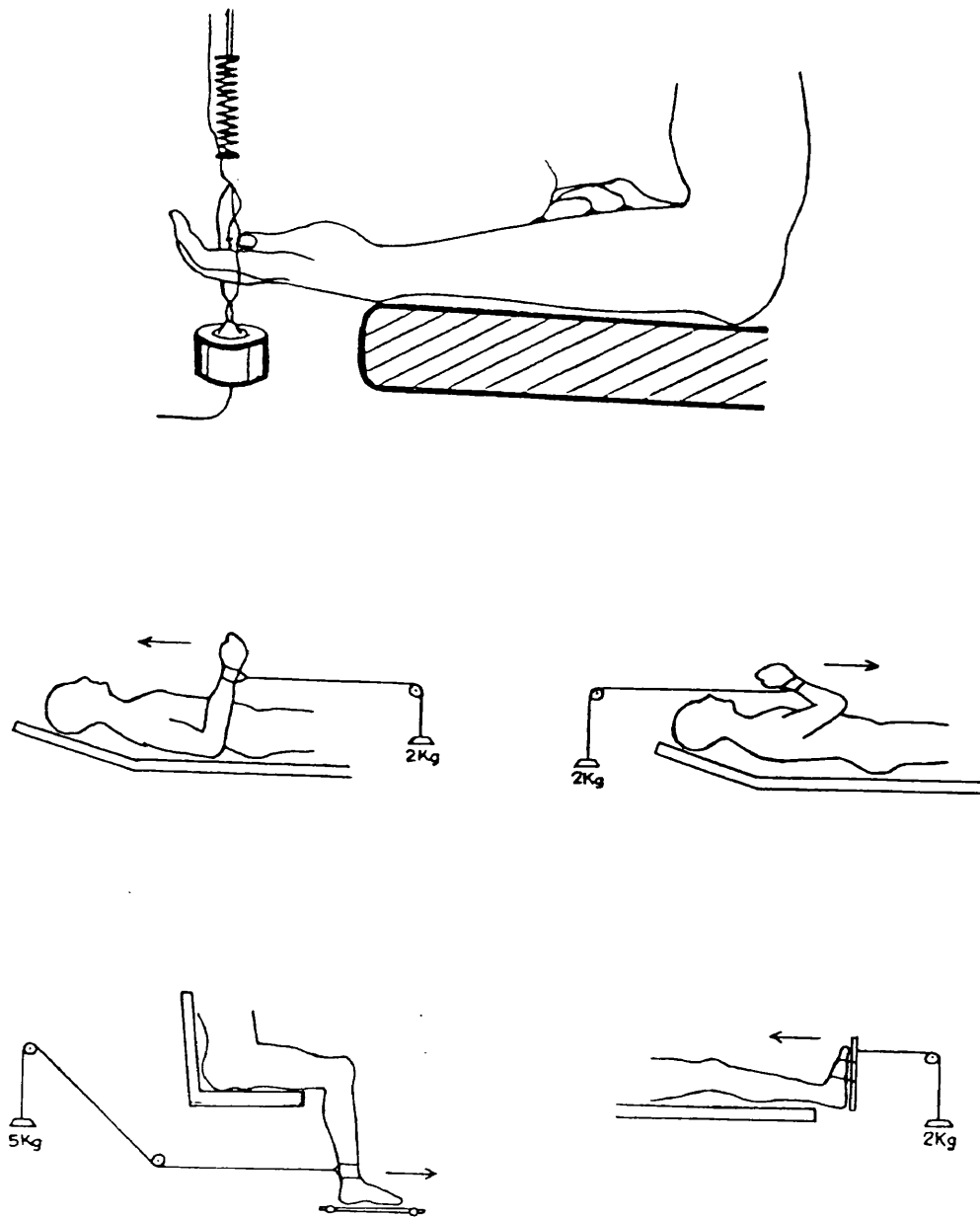


Fig.[4.1] Extant methods of muscle loading (taken from JOHNSON, 1978 and HAYWARD, 1977).

Second, since a full interference EMG is produced under conditions of powerful contraction (large force levels), the patient often cannot maintain a spring or load cell at a constant compressed length for large static loading. At large static loading levels maintaining a standard weight motionless to minimise inertial forces also becomes difficult and for dynamic measurement on muscles, springs and weights are even more difficult to control.

Finally, when dynamic variations in the load are required, they must be reproducible in their amplitude and frequency both during and across individual tests. Repeated loading sequences should (a) be kept to a minimum and (b) occur after long resting intervals, especially when the patient's muscle is examined with a needle electrode which can be painful. Frequent repetitions as a result of unsatisfactory loading sequences must therefore also be avoided. Such conditions cannot be achieved with any confidence using current methods. The limitations can cause patient trauma and discrepancies in results across separate trials and muscle testing procedures because of the inconsistent forcing protocols that are used.

It is necessary therefore to have systems where:

- (a) static levels and dynamic changes in muscle loading are under the control of the examiner,
- (b) the load remains constant when required irrespective of small patient movements,
- (c) static and dynamic variations in loading are repeatable, and
- (d) a virtually constant muscle length is achieved during dynamic loading.

The goal of point (d) can be achieved using visual feedback through the patient and is based on the constant length requirements only. In other words, the patient is not asked to follow a moving force target but to maintain a constant position target. The assumption we make is that manual patient control over muscle length alone, is simpler with the assistance of visual position feedback than attempting to control both force and muscle length independently and simultaneously. This assumption has been confirmed in tests. The advantages of this approach are apparent under dynamic loading conditions where the frequency of force variations can alter slowly.

STEEL BALL SUSPENSION

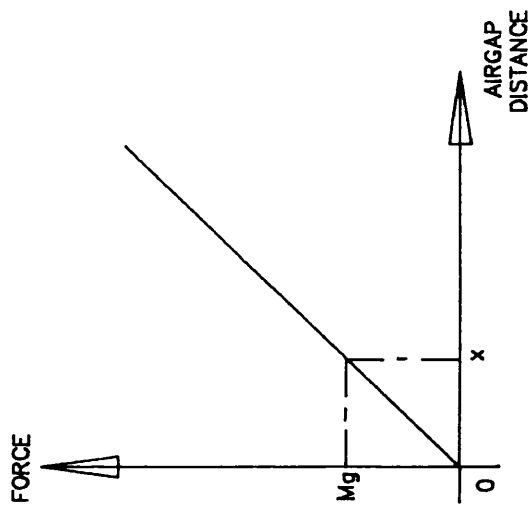
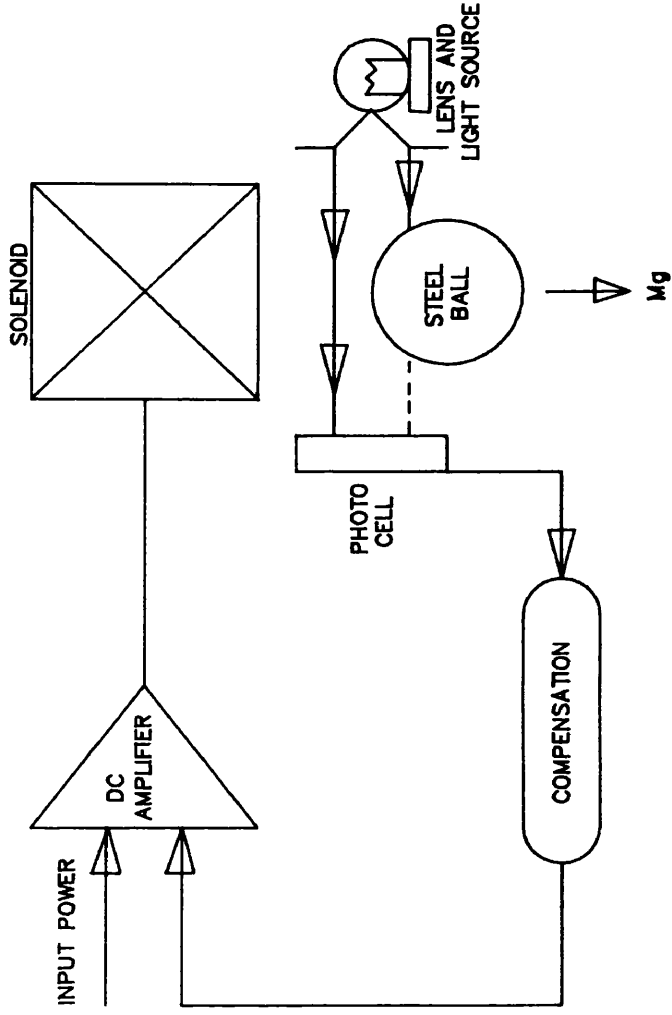


Fig.[4.2] Illustration of the principle of Magnetic Suspension where the weight of the steel ball is matched by the force of attraction of the solenoid.

4.3 The Controllable Magnetic Muscle Load and Force Transducer (Magload)

A useful loading device will produce a relationship between force and muscle length that is constant over a range of variation in muscle length. To provide this characteristic and in addition provide dynamic loading, the control of a d.c. electromagnet was proposed and developed. The familiar open-loop inverse square law characteristic of the solenoid (electromagnet) is reshaped over a limited airgap distance using closed-loop force feedback.

The device design closely follows techniques derived from the field of magnetic suspension. The principle of magnetic suspension may be illustrated by considering the steel ball suspension system shown in Fig.[4.2]. A steel ball is attracted upwards by an iron-cored solenoid. The ball interrupts a beam of light falling onto a phototransistor. The collector current in this phototransistor is then used as a measure of the vertical height of the steel ball. This measurement is then used to control the current through the solenoid so that the ball is restored to an equilibrium position at which the force of gravity is exactly opposed by the attractive force of the solenoid. This is shown in the graph accompanying Fig.[4.2].

Magload differs from the steel ball suspension mainly in the type of feedback signal used. The light source and phototransistor (a position transducer) of the suspension system are replaced by a transducer system which measures the force (or equivalent parameter) produced by the solenoid. Additionally, the steel ball is replaced by a steel reaction plate attached to, or somehow interacting with, the patient. Strictly speaking there is no suspension, but the methods used to control solenoid current are similar. This type of arrangement constitutes the core of Magload. The force of attraction between the solenoid and the reaction plate is kept constant over a 30mm airgap (corresponding to a restricted patient movement) by using the force feedback to control the current through the solenoid.

Technical drawings of the complete mechanical assembly are shown in Fig.[4.3(a)] and Fig.[4.3(b)]. These show the main assembly, which is pivoted about a horizontal axis, and the reaction plate attached to and positioned in front of, the fixed electromagnet. The patient interacts with this system using the horizontal rod above the pivotal axis of the main assembly. This rod can be adjusted vertically to provide a mechanical advantage of up to $2^{1/2}$ times the attractive force of the magnet with a correspondingly increased arc of movement. The free space behind the electromagnet is used to house the electronic control circuitry.

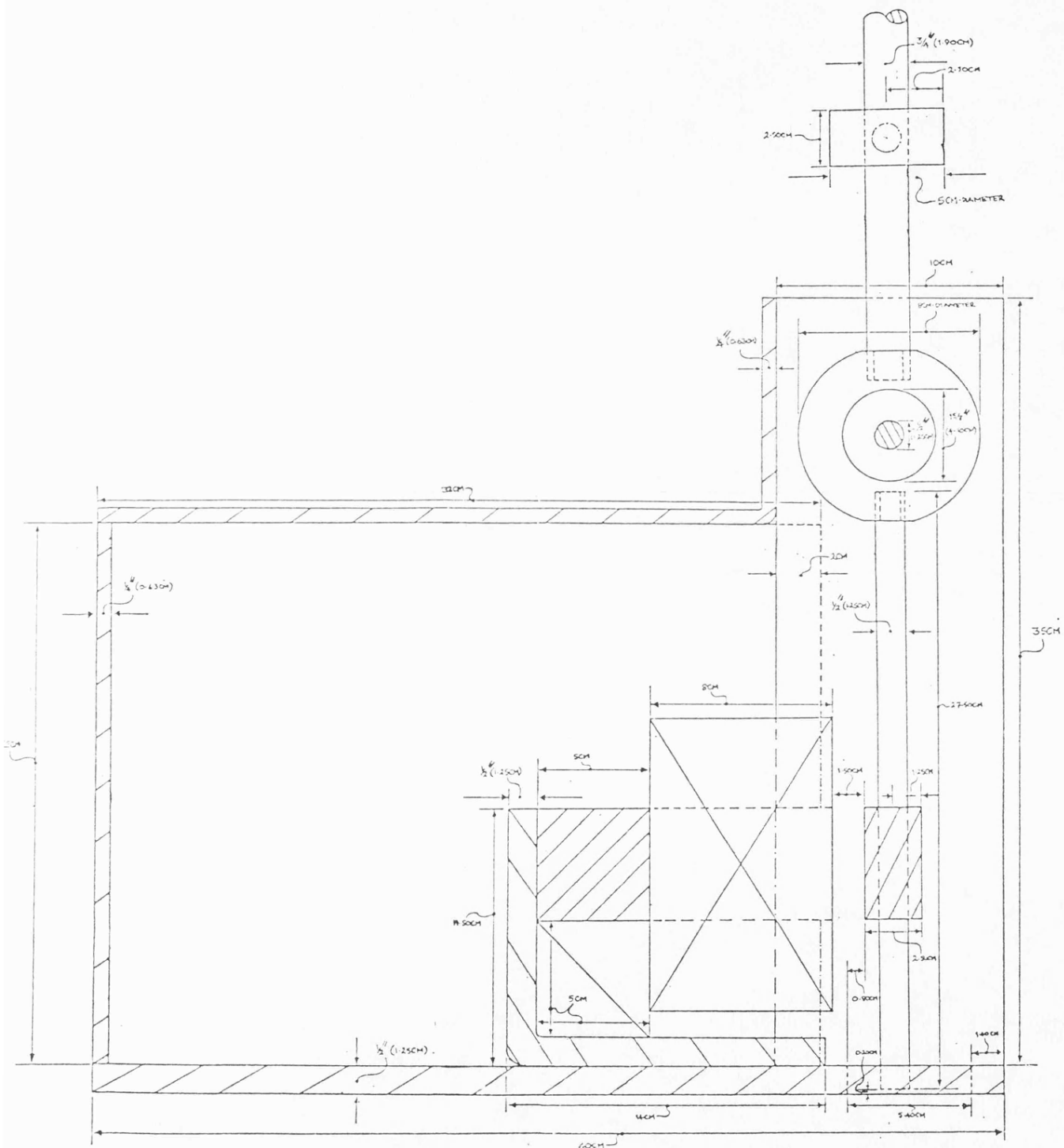


Fig.[4.3(a)] Side view of MAGLOAD mechanical assembly.

A better view of the major elements in the main assembly is shown in the photographs of Fig.[4.4]. The dimensions of the cylindrical rods making up this system were calculated using simple bending moment theory. A 2:1 safety factor was used to avoid bending when maximum designed loads are present at the reaction plate. The inertia of the main assembly was calculated using both theoretical and trifilar suspension methods. The values were within 10% of each other. The average value for the inertia is 0.367 Kgm^2 .

The fluctuations in airgap length about a nominal value are related to the variations in contracting muscle length. These airgap fluctuations are presented visually to the patient who must maintain them at a minimum. Therefore the nominal airgap distance can be held approximately constant. If the airgap changes, the electromagnet system reacts to keep the force constant throughout the available airgap. The constant force characteristic that has been achieved, effectively simulates the force-extension characteristic of a very long spring several meters in length. Fig.[4.5] shows the system in use. In this example the biceps muscle of the patient is being tested. The elbow joint is secured to an adjustable platform. The force pattern is controlled remotely, either manually by the investigator or with a computer (e.g. the SPC in chapter three).

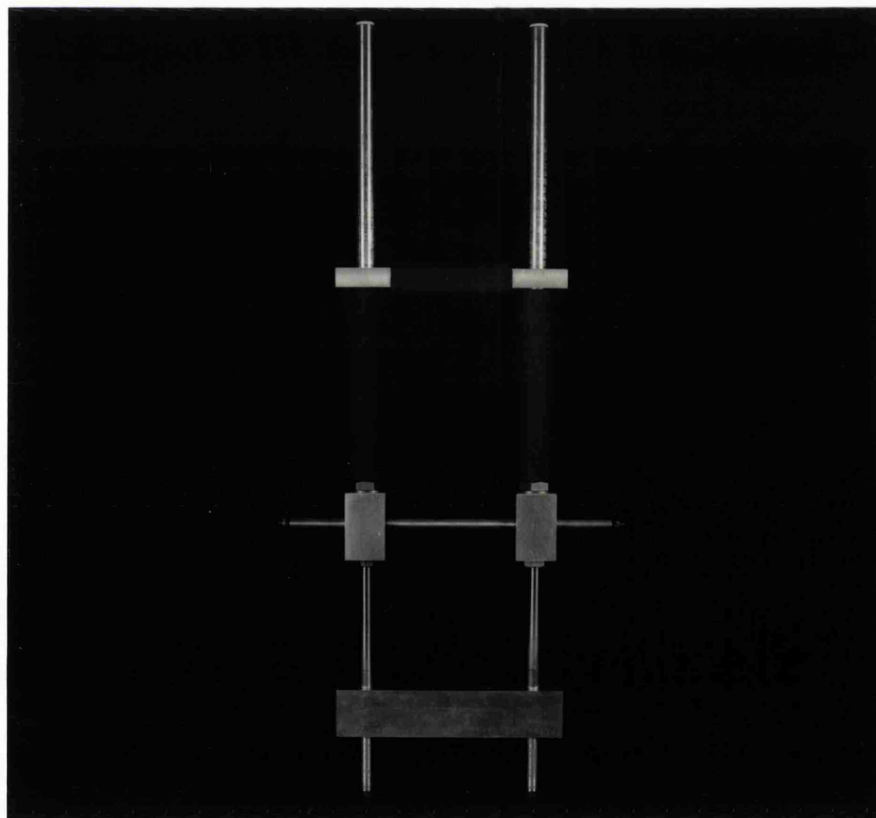
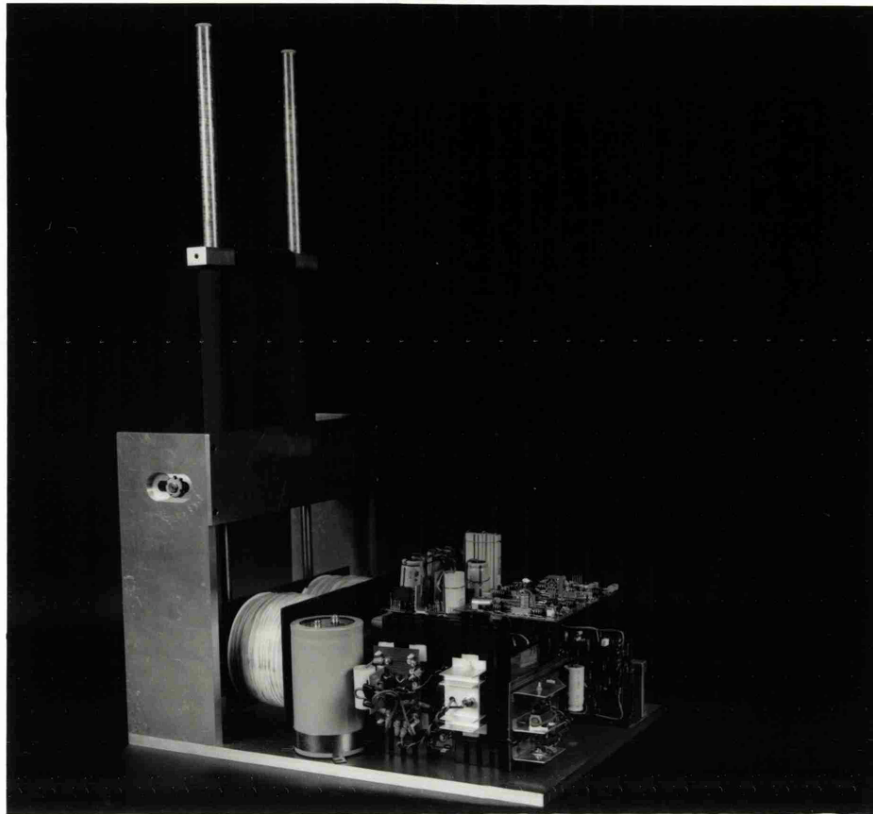


Fig.[4.4] The reaction plate, pivot, and adjustable bar of the main assembly.



Fig.[4.5] Illustration of the Magnetic Load (MAGLOAD) force measurement system in use.

Chapter Five

Magnetic Load Design and Experimental Results

This chapter considers the design of the magnetic muscle load (Magload). The design enables complete control over both static and dynamic forcing patterns. Experimental results will be given and the chapter will end with a discussion of the likely uses for Magload. Detailed schematic diagrams of the magnetic and electronic control circuits are provided in Appendix [B2].

5.1 The Muscle Load Design Overview

It was required that the electromagnet be capable of providing 250N force at a nominal airgap of 20mm. This force level was chosen subjectively by observing students perform weight training exercises at the University gymnasium. The nominal airgap distance was chosen from a compromise between allowing small movements for the subject, and the magnet-amplifier design constraints. The latter constraints primarily relate to the size of the magnet, power output, and the corresponding complexity of the control amplifier system. A U-shaped magnet capable of providing up to 500N at this airgap was designed such that the required maximum load is achieved at power dissipation levels not necessitating forced cooling. A U-shaped magnet was selected for its simplicity of construction. Magnetic circuit design is an iterative procedure, as is apparent from calculations available in Appendix [B1], and a simple magnet shape was necessary for the prototype stages.

The following notation is used in the electromagnet design:

- a - Pole face area (m^2)
- A_w - Window area (m^2)
- B - Electromagnet flux density (T)
- F - Force produced by electromagnet (N)
- ξ - Forcing ratio
- I - Steady state load current (A)
- i - Instantaneous load current (A)
- l - Mean turn length (m)
- L - Inductance of coil windings (H)
- N - Number of turns
- NI - Ampere-turns
- P - Power dissipation (W)
- R - Resistance of coil (Ω)
- S - Reluctance of airgap

ELECTROMAGNET SYSTEM DESIGN PROCEDURE

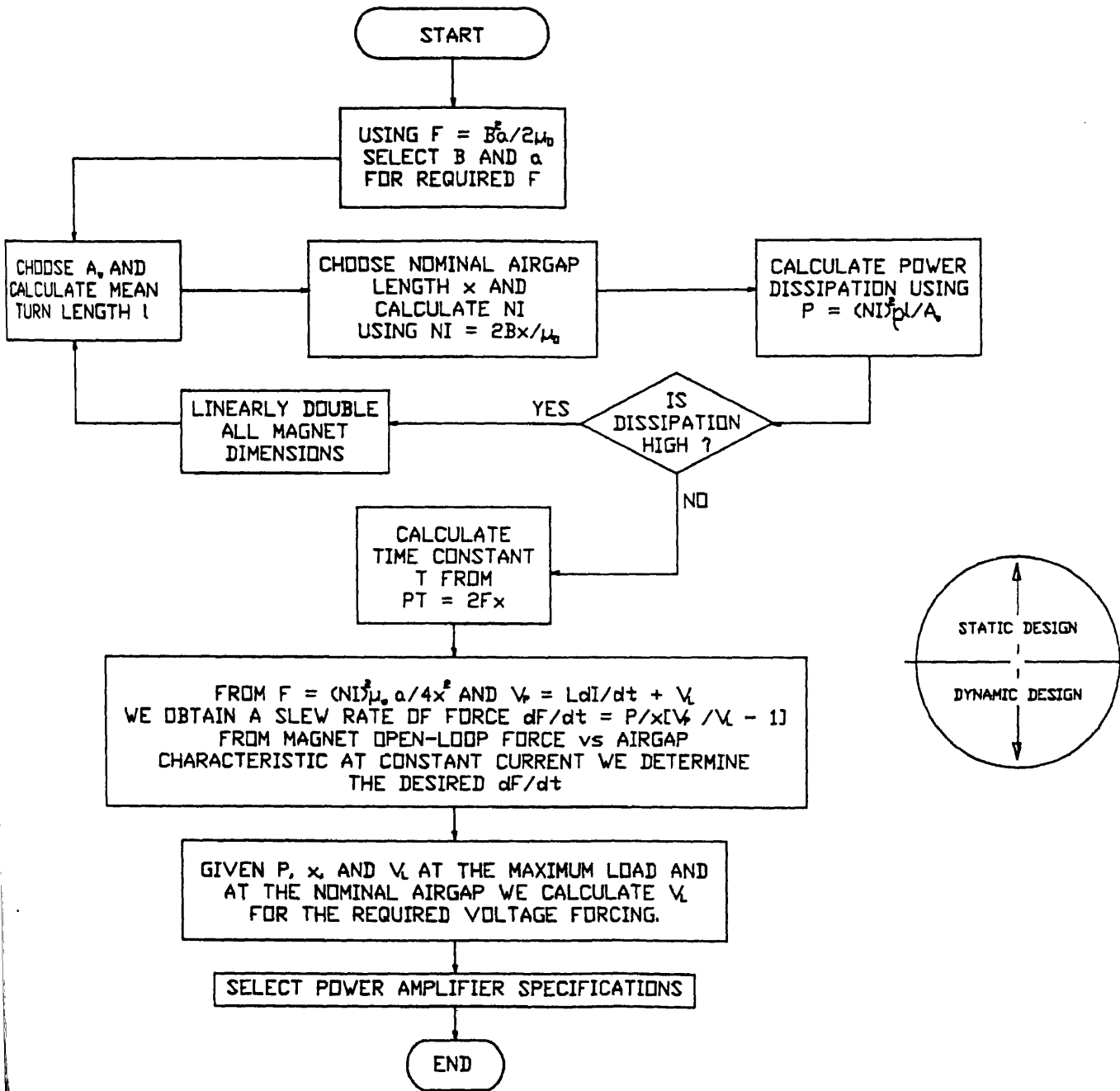


Fig.[5.1] Summary of static and dynamic design procedures used for the magnetic load system.

- V_p - Supply voltage (V)
- V_l - Load voltage (V)
- x - Airgap distance (m)
- μ_o - Permeability of free space
- ρ - Resistivity of coil windings (m)
- b - Coil wire cross section area (m²)
- τ - Coil time constant (Sec)

Before examining the detailed design aspects of Magload, an appreciation of the general design procedure adopted is provided in Fig.[5.1]. This shows a partition between the static and dynamic design considerations employed. Each of these will be discussed in turn below.

5.1.1 Static Design Considerations

This section is concerned mainly with the design and testing of the magnetic circuit. A magnet consists of the core and the coil each of which must be designed correctly for maximum overall efficiency. Consider the simple magnetic circuit of Fig.[5.2]. Assuming that the magnetic flux density is the same throughout the core (i.e. no flux leakage), the force on the reaction plate exerted by the electromagnet may be computed by considering the change in stored energy in the airgap when work is done in changing the airgap length x by an amount $2\Delta x$. The force required acts through half this distance.

Force x Distance = Energy per Unit Volume x Change in Volume of Airgap

$$\text{i.e. } F \cdot \Delta x = (B^2 / 2 \mu_o) \cdot 2a\Delta x$$

therefore:

$$F = B^2 a / \mu_o$$

or for a single pole:

$$F = B^2 a / 2 \mu_o \dots \dots \dots \text{Eq.[5.1]}$$

The ampere turns required to produce a flux density B are:

$$NI = 2Bx / \mu_o \dots \dots \dots \text{Eq.[5.2]}$$

Combining Eq.[5.1] and Eq.[5.2] gives:

$$F = (NI)^2 \mu_o a / 8x^2 \dots \dots \dots \text{Eq.[5.3]}$$

This equation suggests that for a given current and airgap, the force will increase with pole face area. The choice of pole face area is also influenced by amplifier design, since the inductance (and hence time constant) of the coil depends on the dimensions of the pole face.

It is also evident from Eq.[5.3] that the force-airgap distance and force-current characteristics will be highly non-linear. Other factors important in the design of the magnet are:

- saturation in the magnetic core,
- flux leakage,
- power loss in the coils, and
- magnet weight.

Changes in magnet parameters result in changes to other magnet parameters and in the magnet operating conditions. A useful illustration of these interactions is shown in Fig.[5.3].

Eq.[5.3] holds under the ideal condition of infinite permeability of the iron paths and therefore the absence of any flux leakage. Mild steel is used in this application and the mild steel core possesses reluctance of a significant magnitude compared to the airgap reluctance. This leads to large flux leakages and higher flux densities in the limbs of the magnet than in the airgap. An operating point of 0.65T was chosen to avoid saturation in the magnet core (2.0 wb/m² (T) for mild steel). This ensures that the mild steel core remains in the linear region of the magnetisation curve at its maximum force level of 250N and nominal airgap of 20mm. This precaution is also necessary to reduce power dissipation (i.e. use of lower coil currents) and, because of the control system, to allow for transient fluctuations in coil current, and hence flux density, when the airgap changes due to patient movements. Increasing the magnet's dimensions also helps to limit saturation in the core, e.g. increasing the pole face area increases flux leakage, thereby reducing flux density.

The size of the magnet coil is determined by the design of the magnet limbs and poles. The choice of using a high voltage and low current design for the coil or vice versa is influenced predominantly by the amplifier requirements and to a lesser extent by the coil itself (i.e. magnetic material, coil windings guage, and insulation properties). Two important parameters in the coil design are the power required to produce the required ampere-turns NI, and the time constant of the coil τ , i.e. the ratio of its inductance L to its resistance R.

Using a linearised model of Eq.[5.3] we can gain an insight into the role played by the coil time constant in any attempt to control the force developed by the magnet. At the nominal airgap, the magnet current (i.e. current through the coils of the magnet) generates a certain force, and any displacement x from this position results in a change i in the current. If we assume that the change in force of attraction f is a linear function of the airgap x and current i , then:

$$f = -k_1 x + k_2 i \quad \dots \dots \dots \text{Eq.[5.4]}$$

where k_1 is the force per metre at constant current, and k_2 is the force per ampere at constant airgap. These can be determined experimentally for a given magnet.

The relationship between the magnet current and supply voltage V_p is:

$$RI + L di / dt = V_p \dots \dots \dots \text{Eq.[5.5]}$$

In Laplace transform notation Eq.[5.4] and Eq.[5.5] become:

$$F(s) = -k_1 X(s) + k_2 I(s)$$

$$I(s) = (k_3 / (1 + s \tau)) \cdot V_p(s) \dots \dots \dots \text{Eqs.[5.6]}$$

Eqs.[5.6] produce an open-loop description of force:

$$F(s) = -k_1 X(s) + (k_2 k_3 / (1 + s \tau)) \cdot V_p(s) \dots \dots \dots \text{Eq.[5.7]}$$

The quantity that can be controlled directly by the amplifier system is the voltage across the magnet coils. This voltage will in turn alter the coil current and hence the force produced. The coil time constant τ represents the lag in coil current behind the controlling voltage. This application required holding the force constant over the operating range of airgaps, and the task was accomplished by holding the airgap flux constant using a primary flux feedback loop. In this way the non-linear force-airgap characteristic becomes very nearly linear. Therefore, the force is now independent of the airgap, or in Eq.[5.4] the constant k_1 reduces to zero.

The flux loop hence changes the open-loop system Eq.[5.7] to:

$$F(s) = (k_2 k_3 / (1 + s \tau)) \cdot V_p(s) \dots \dots \dots \text{Eq.[5.8]}$$

which is a simple first order lag, and so the linearisation using flux feedback control leaves the force variations proportional only to i . The speed of fluctuations in i is largely determined by the time constant of the magnet coils. Since the time constant of the coil is large, this leads to a narrow bandwidth for the overall response of the control system. A large forcing voltage capability is therefore necessary to obtain a high bandwidth for the system. This will allow transient current and force variations to occur quicker than is dictated by the coil time constant. The transient changes in force with varying airgap will then be sufficiently rapid to make the force produced by the magnet *appear* constant to the patient competing with the system.

The *apparently* constant nature of the transmitted force relies on the assumption that the fastest possible twitch response that can be produced by human muscle is slower than the worst-case response time of the magnet to demanded force alterations. Such worst-case response times for the magnet are achieved by forcing fast voltage changes across the magnet coils, and they are concerned with the dynamic design of the system to be discussed in the next section.

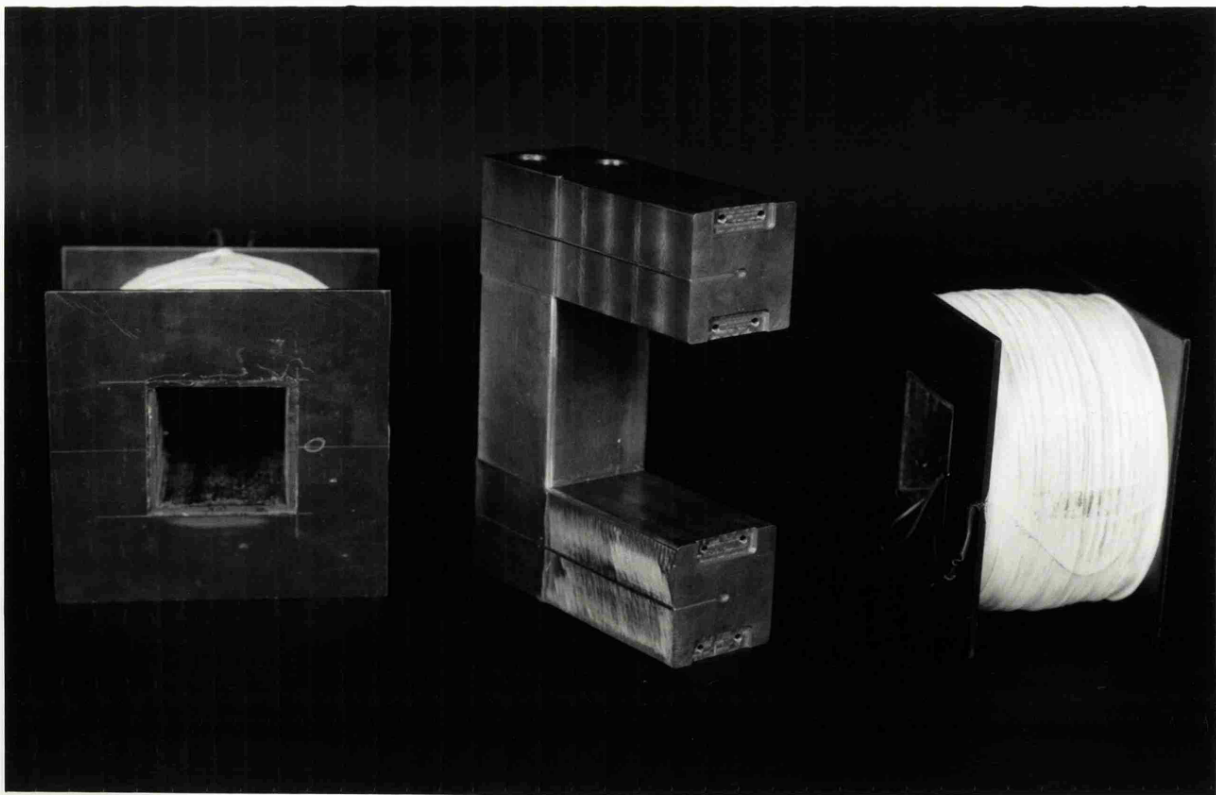
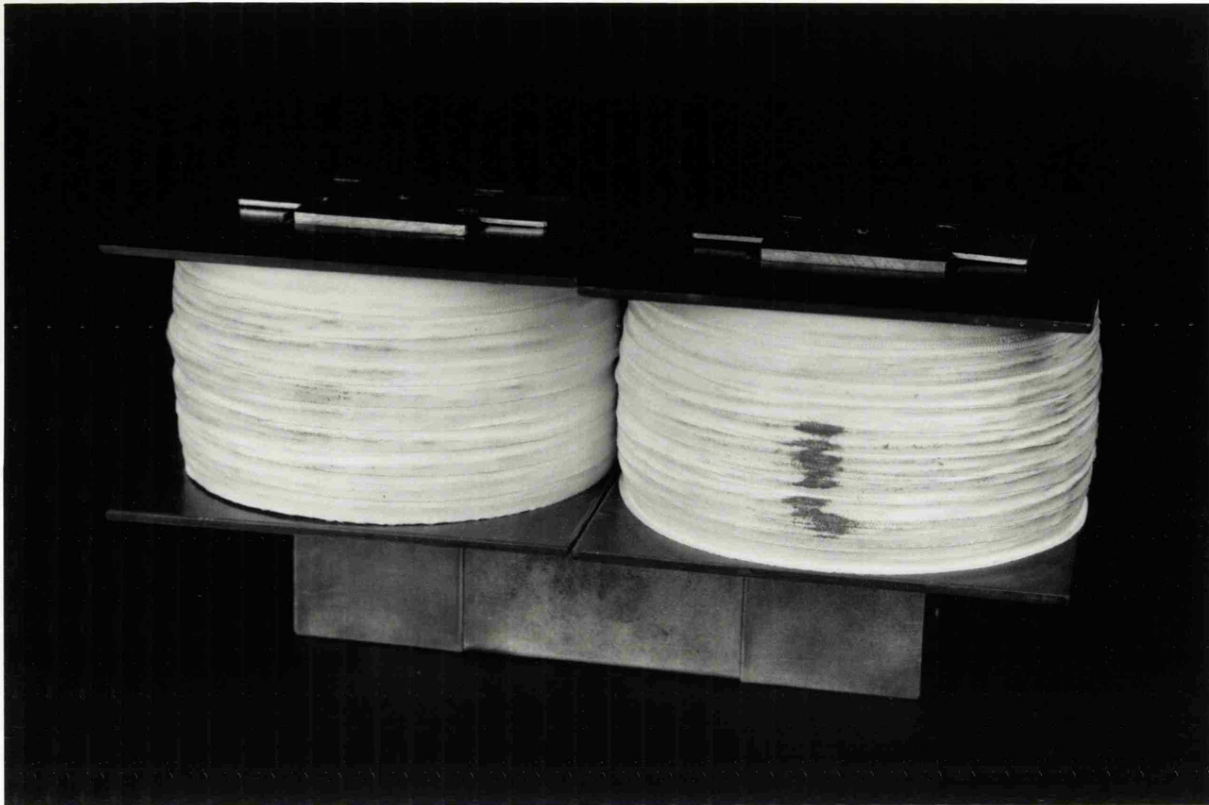


Fig.[5.4] The Electromagnet core and coils showing the recess in the pole faces used to mount the flux transducers.

A photograph of the core and coils is shown in Fig.[5.4] and their corresponding dimensions are shown in Fig.[5.2].

The static *open-loop* characteristics of the magnet are:

- (i) the Force F vs Airgap x at constant current I , and
- (ii) the Force F vs Current I at constant airgap x .

These characteristics were found experimentally using the arrangement shown in Fig.[5.5] with the magnet coils connected in parallel. The measurements taken can be found in Appendix [B3], and the curves obtained are shown in Fig.[5.6] and Fig.[5.7]. The cantilever arrangement illustrated in Fig.[5.5] was necessary to distribute (share) the test loads evenly between the two pole faces of the U-shaped magnet.

STATIC OPEN-LOOP MEASUREMENT TEST RIG

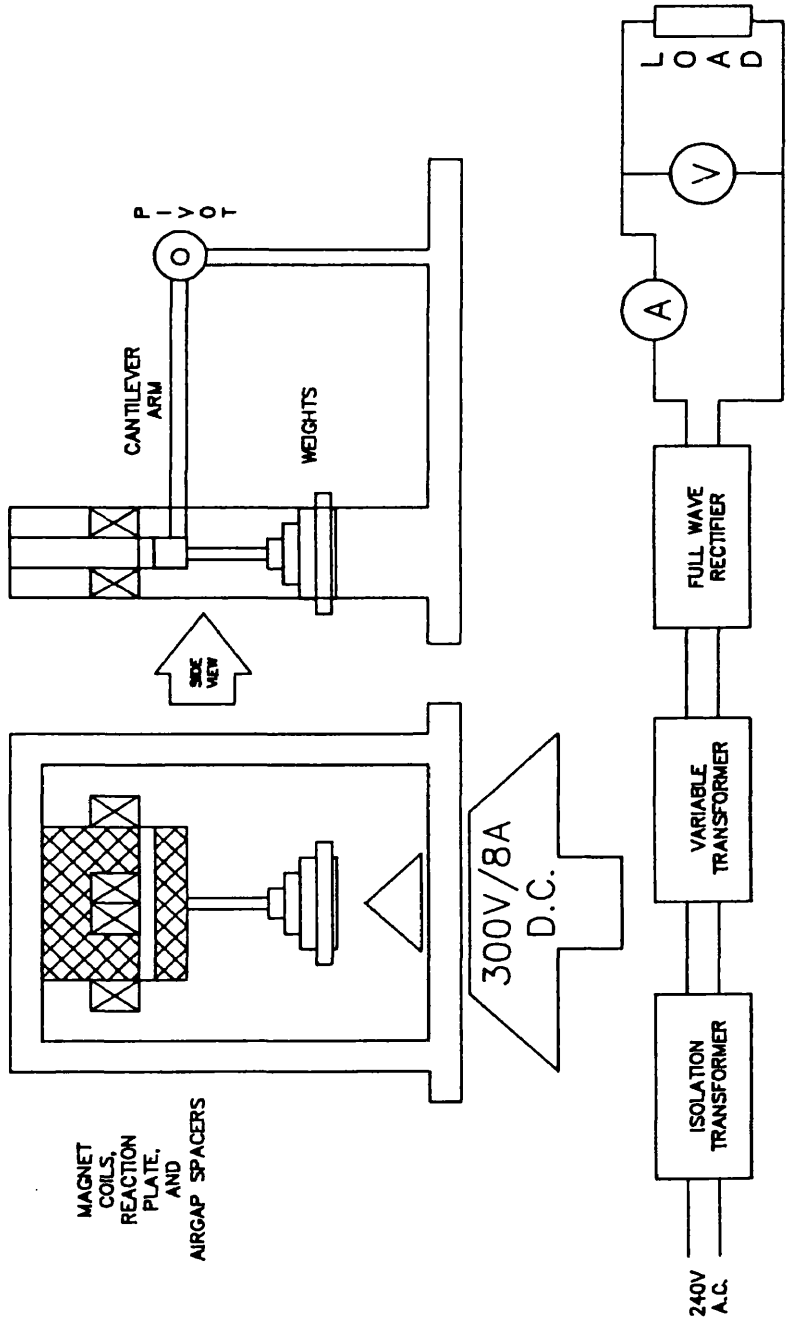


Fig.[5.5] Experimental arrangement used to measure the static open-loop characteristics the electromagnet. The airgap is adjusted using a set of wooden spacers, each one having a different width. The current is varied using the 8A, 240V variable transformer and rectifier circuit.

Magload: FORCE Vs AIRGAP @ Constant Current (Open-loop)

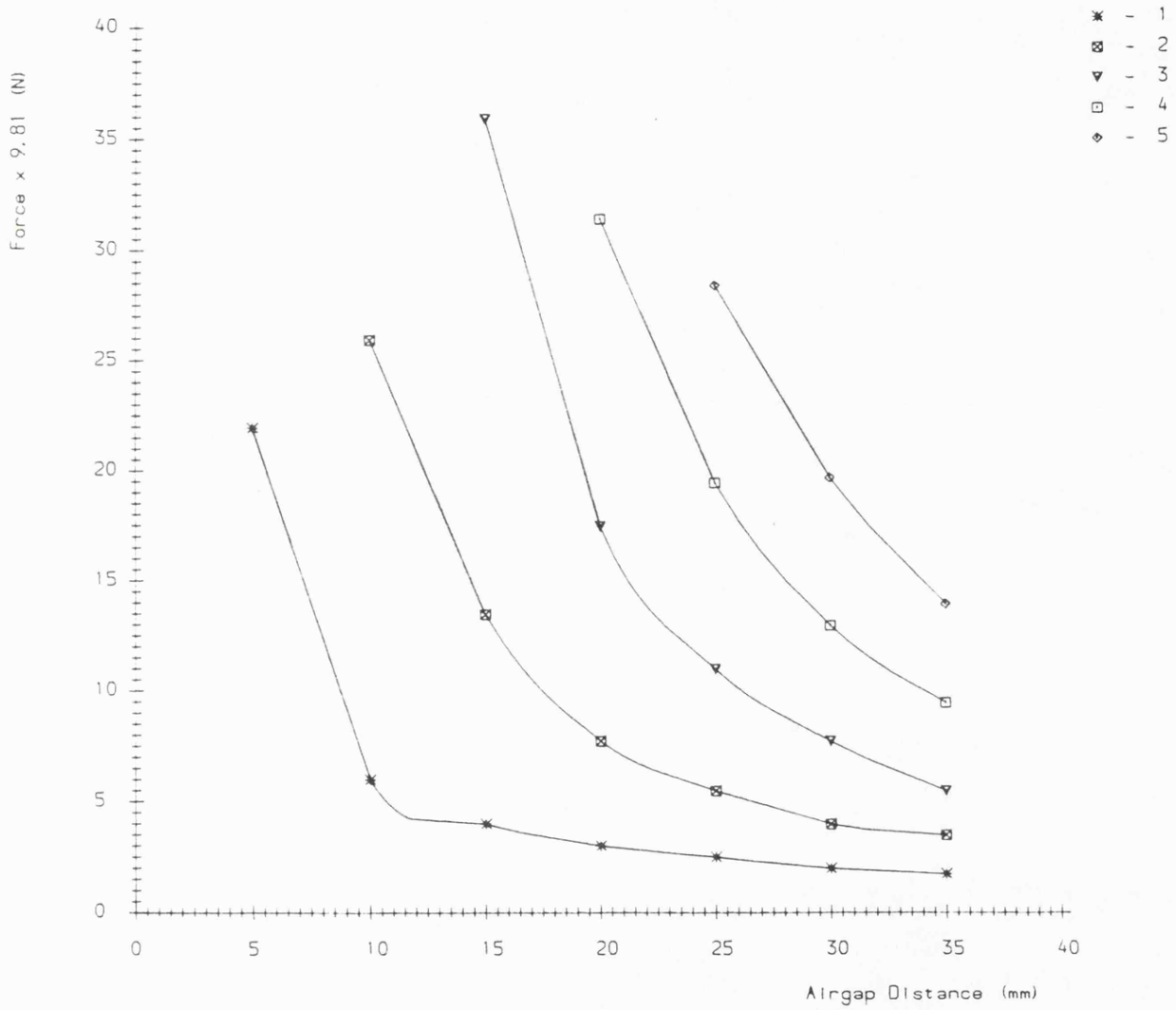


Fig.[5.6] Open-loop inverse square law characteristic of the electromagnet at constant current.
(Curves 1-5 were obtained at 1-5 Amps respectively)

Magload, FORCE Vs CURRENT • Constant Airgap (Open-loop)

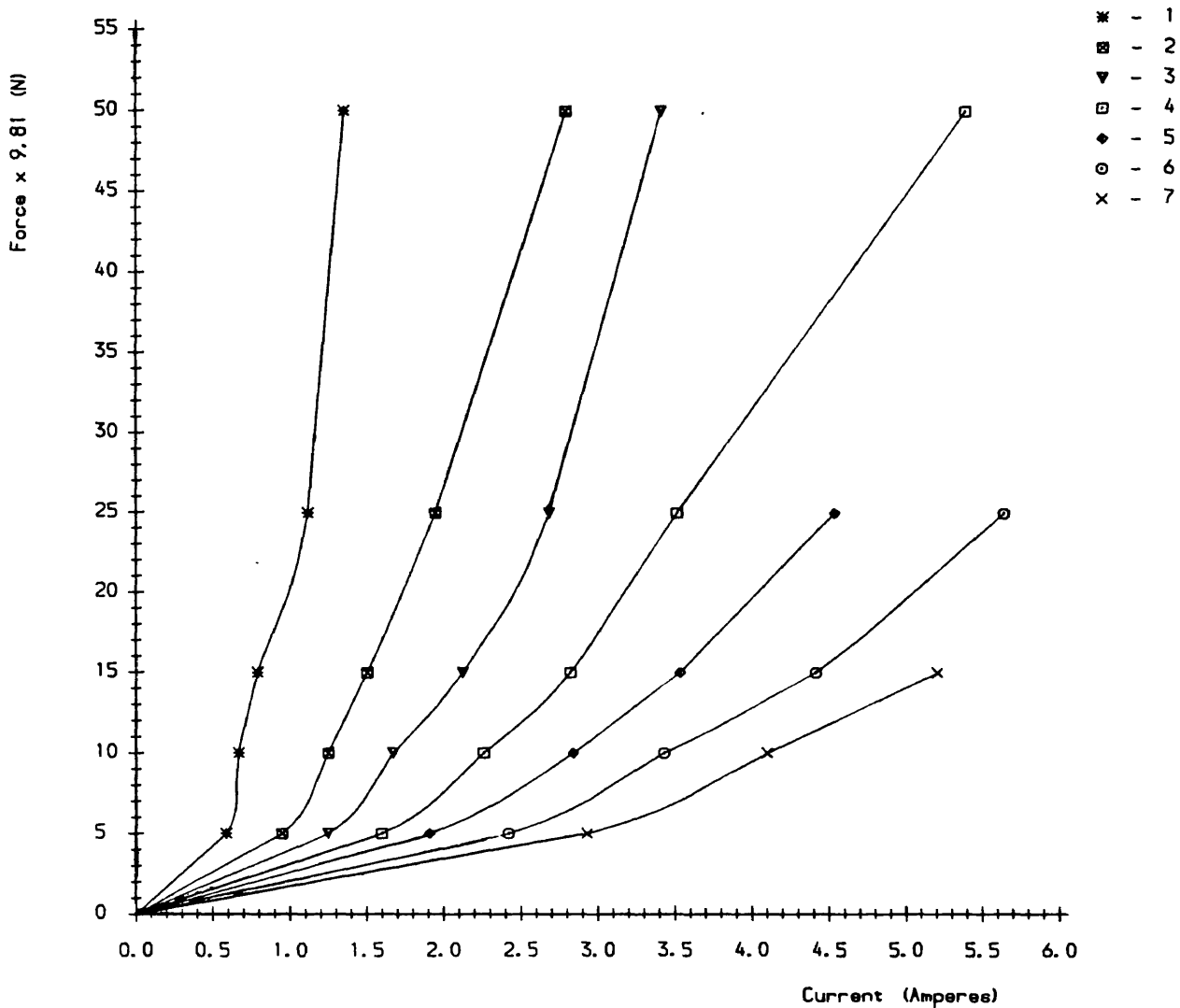


Fig.[5.7] Open-loop square law characteristic of the electromagnet at constant airgap. (Curves 1-7 were obtained at 5-35 mm (5mm increments) respectively)

5.1.2 Dynamic Design Considerations

The design of the static behaviour of Magload concerned the magnetic circuit alone, and was discussed in the previous section. The coil requirements evolving from static considerations are closely linked with the power amplifier design in dynamic considerations. This link mainly relates to the ability to force voltage changes across the electromagnet windings at rates faster than are dictated by the coil time constant.

Due to the amount of power which is dissipated in the magnet (see Appendix [B1]), the current in the magnet is not controlled by a Class A amplification system. Instead, to maximise amplifier efficiency and lower power supply rating, the electronics to drive the magnet use Class D amplification methods employing the principles of Pulse Width Modulation (PWM).

The technique of PWM is illustrated in Fig.[5.8] which shows the currents and voltages in the transistor amplifier and magnet. By varying the ratio of the On to Off time of the drive transistor amplifier an average current can be maintained in the magnet. As a result of this, an average force is produced by the magnet. The force required at the nominal airgap can be set by adjusting this On-Off ratio. Any instantaneous changes in airgap, and hence instantaneous force, result in the On-Off ratio being altered through the flux feedback loop, keeping the force constant and equal to the preset level.

The overall control scheme for the magnet is shown in Fig.[5.9]. The position signal provides the patient with a visual indication of the location of the reaction piece in the airgap. This helps the patient to maintain approximate isometric conditions with the force being held constant (or varying) by the control system. Positive current feedback is used in a minor controlling loop to boost the response of the system at large airgaps (i.e. greater than the nominal 20mm gap). This effectively overcomes attractive force losses due to flux leakage. Since the major feedback signal (flux) is proportional to the controlled variable (force), no compensation is used. This feature has the advantage that the flux feedback signal can be used directly as an indication of the force output of the system. Hence, the magnetic load functions as both the *controller* and the *transducer* of muscle loading patterns. The time constant for the magnet is 57.2ms (see Appendix [B1]) suggesting a bandwidth of approximately 17.5Hz. The average isometric twitch response of muscle is in the region of 25ms for a group of very fast motor units and rises to as much as 100ms with slower motor units (Lago, 1980). Therefore, in order to achieve a response time for the system which is quicker than the duration of the fastest average isometric twitch response, there is a need to obtain a bandwidth for the system which is at least greater than twice that dictated by the magnet time constant.

5.1.2 Dynamic Design Considerations

The design of the static behaviour of Magload concerned the magnetic circuit alone, and was discussed in the previous section. The coil requirements evolving from static considerations are closely linked with the power amplifier design in dynamic considerations. This link mainly relates to the ability to force voltage changes across the electromagnet windings at rates faster than are dictated by the coil time constant.

Due to the amount of power which is dissipated in the magnet (see Appendix [B1]), the current in the magnet is not controlled by a Class A amplification system. Instead, to maximise amplifier efficiency and lower power supply rating, the electronics to drive the magnet use Class D amplification methods employing the principles of Pulse Width Modulation (PWM).

The technique of PWM is illustrated in Fig.[5.8] which shows the currents and voltages in the transistor amplifier and magnet. By varying the ratio of the On to Off time of the drive transistor amplifier an average current can be maintained in the magnet. As a result of this, an average force is produced by the magnet. The force required at the nominal airgap can be set by adjusting this On-Off ratio. Any instantaneous changes in airgap, and hence instantaneous force, result in the On-Off ratio being altered through the flux feedback loop, keeping the force constant and equal to the preset level.

The overall control scheme for the magnet is shown in Fig.[5.9]. The position signal provides the patient with a visual indication of the location of the reaction piece in the airgap. This helps the patient to maintain approximate isometric conditions with the force being held constant (or varying) by the control system. Positive current feedback is used in a minor controlling loop to boost the response of the system at large airgaps (i.e. greater than the nominal 20mm gap). This effectively overcomes attractive force losses due to flux leakage. Since the major feedback signal (flux) is proportional to the controlled variable (force), no compensation is used. This feature has the advantage that the flux feedback signal can be used directly as an indication of the force output of the system. Hence, the magnetic load functions as both the *controller* and the *transducer* of muscle loading patterns. The time constant for the magnet is 57.2ms (see Appendix [B1]) suggesting a bandwidth of approximately 17.5Hz. The average isometric twitch response of muscle is in the region of 25ms for a group of very fast motor units and rises to as much as 100ms with slower motor units (Lago, 1980). Therefore, in order to achieve a response time for the system which is quicker than the duration of the fastest average isometric twitch response, there is a need to obtain a bandwidth for the system which is at least greater than twice that dictated by the magnet time constant.

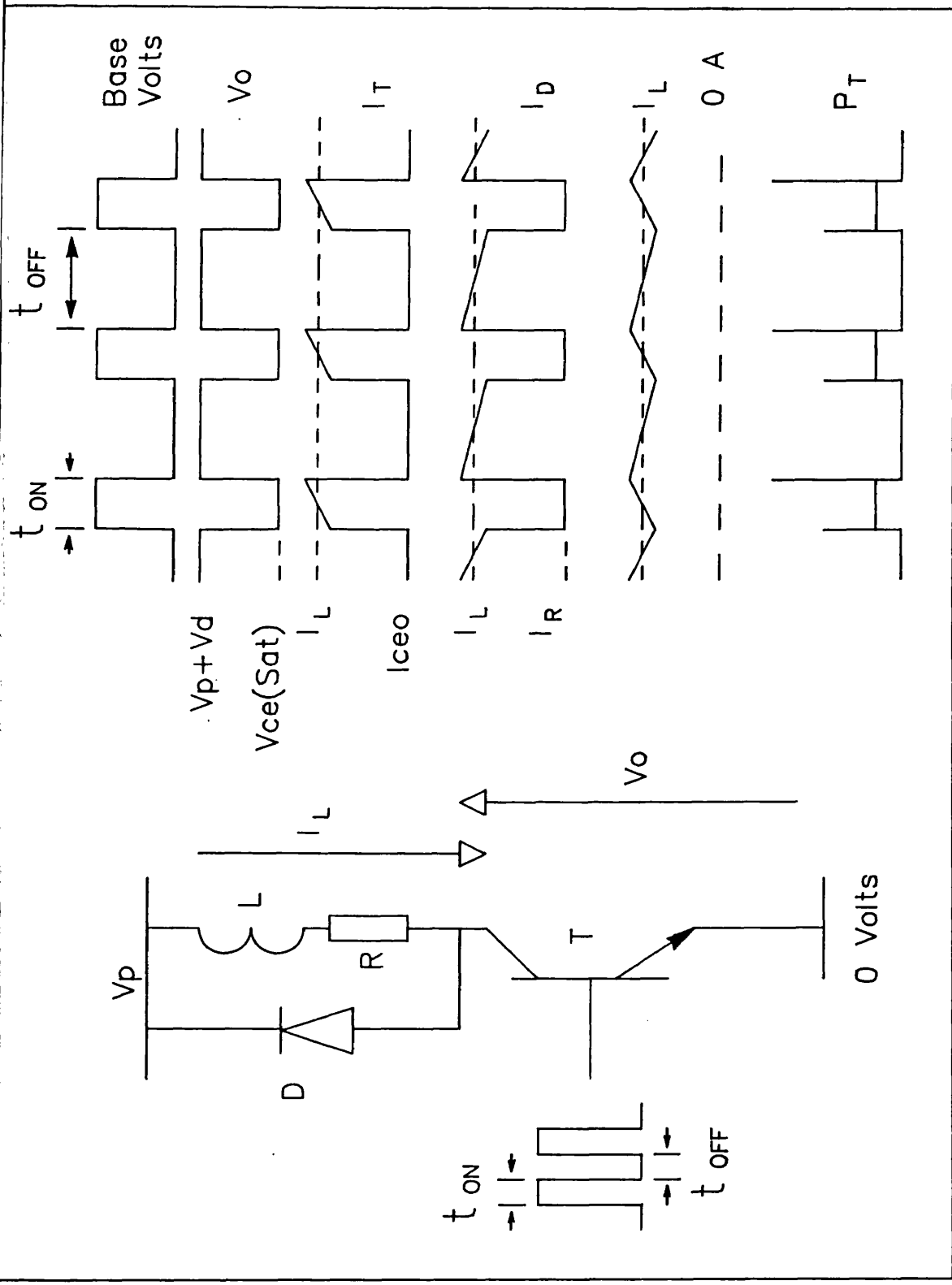


Fig.[5.8] Currents and voltages in a Class D (PWM) amplifier.

ELECTROMAGNET CONTROL SCHEME

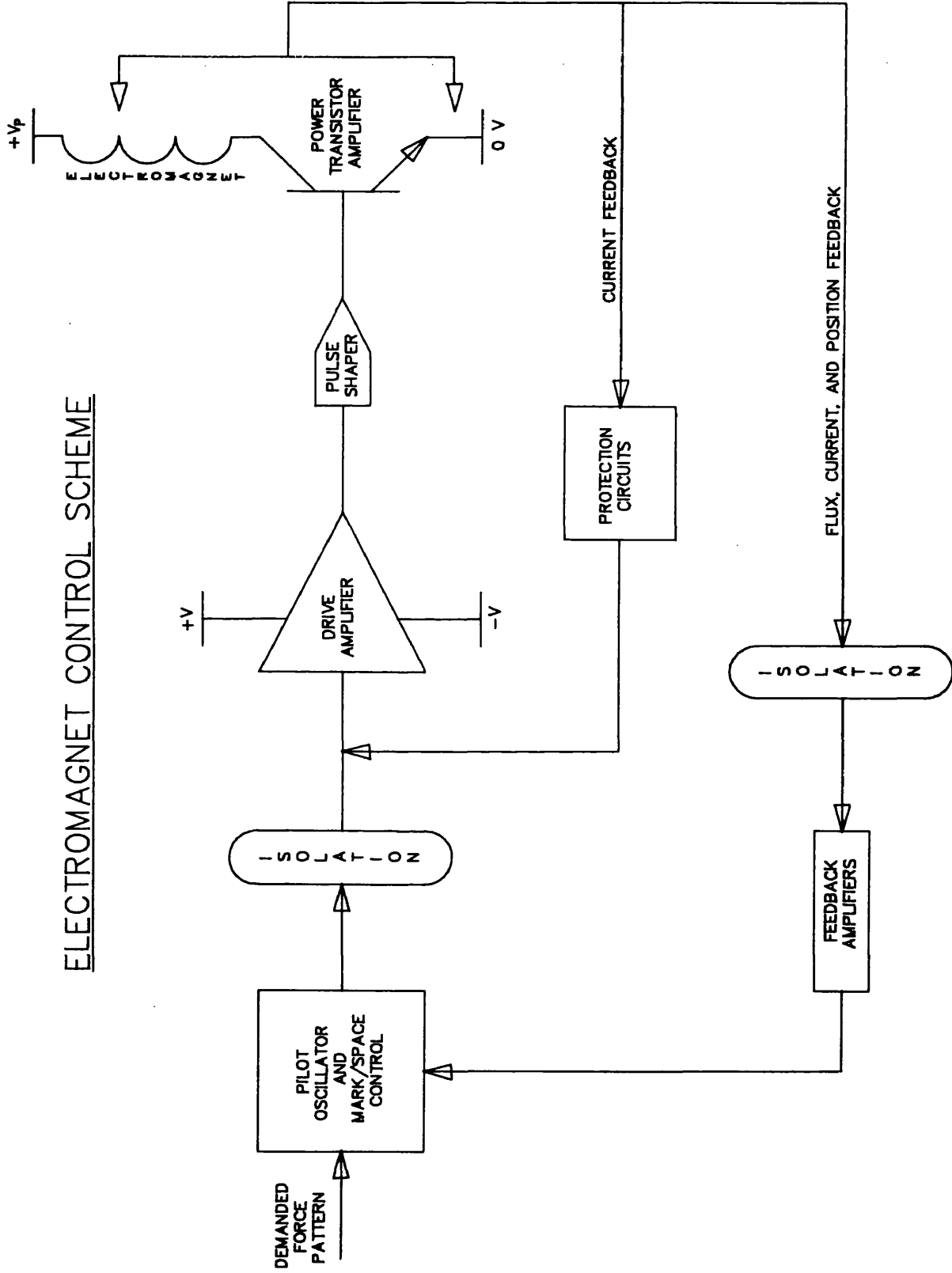


Fig.[5.9] Control scheme used in MAGLOAD.

To obtain a high bandwidth for the control system through voltage forcing we consider the behaviour of the magnet in relation to the supply voltage as follows (Whorlow, 1978):

The total force is given by:

$$F = ((NI)^2 \mu_0 a) / 4x^2 \dots \dots \dots \text{Eq.}[5.9]$$

Therefore:

$$dF / dt = (2N^2 \mu_0 a) / 4x^2 \cdot I di / dt \dots \dots \dots \text{Eq.}[5.10]$$

Combining Eq.[5.5] and Eq.[5.10]:

$$\begin{aligned} dF / dt &= (2N^2 \mu_0 a I) / 4x^2 \cdot (V_p - IR) / L \\ &= [2N^2 \mu_0 a \cdot (I^2 R) \cdot (V_p / R - 1)] / 4x^2 L \end{aligned}$$

Since $L = N^2 / S$, $S = 2x / \mu_0 a$, $P = I^2 R$, and $V_1 = IR$

$$dF / dt = (P / x) \cdot (V_p / V_1 - 1) \dots \dots \dots \text{Eq.}[5.11]$$

The quantity V_p / V_1 describes the voltage forcing ratio ξ in the positive direction when the drive transistor amplifier is turned on. ξ is the ratio of the supply voltage to the steady state voltage drop across the resistive part of the magnet when a quiescent current I is being maintained with the full supply across the magnet. When the drive transistor amplifier is turned off this current still flows due to the inductance of the coils and is recirculated through the power supply by the freewheeling diode. By virtue of this recirculated current flow, a voltage V_1 will exist across the resistive part of the magnet and provides the negative voltage forcing of current through the coils since the inductive drop is now in a direction opposite to that of the resistive drop. The difference between V_p and V_1 determines the rate at which the decaying inductive current falls when the drive transistor is off. The more V_1 approaches V_p , the less decay there will be in the inductive current; consequently there will be a lower current ripple. Values of V_1 less than one half of the supply voltage result in inadequate forcing and the ripple current increases.

This can be shown easily from Eq.[5.5]:

$$L di / dt = (V_p - V_1) \dots \dots \dots \text{Eq.}[5.12]$$

This represents the forcing of current in the magnet in the positive direction. In the negative direction :

$$L di / dt = V_1 \dots \dots \dots \text{Eq.}[5.13]$$

Hence for equal positive and negative forcing we equate Eq.[5.12] and Eq.[5.13] and it emerges that:

$$\xi = V_p / V_1 = 2 \dots \dots \dots \text{Eq.}[5.14]$$

If ξ is required less than 2 then the circuit of Fig.[5.10(a)] is adequate. Otherwise the equal positive and negative voltage forcing circuit of Fig.[5.10(b)] must be implemented (Hodkinson, 1975). This circuit is more complex to drive however, requiring the use of an inverter amplifier to drive the topmost PNP transistor when an NPN type can not meet power requirements.

The required value of ξ is obtained by first defining the quantity dF / dt . This represents the slewing rate of force generated by the magnet-amplifier combination and is related to the forced current variations in the magnet. To demonstrate the selection of a slewing rate of force, we refer to Fig.[5.7] and assume we are operating at the nominal airgap of 20mm and at a force of 10N. A movement of 10mm, to 30mm, caused by the patient would make it necessary for the magnet to produce the equivalent of approximately 30N at 20mm. The period of growth for this force must be quicker than the time taken for an average isometric twitch response to rise and decay. Thus, taking 20ms as a reasonable response time for the build-up of magnetic force, we find that:

$$dF / dt = (200 / 20 \times 10^{-3}) = 10kNs^{-1} \dots \dots \dots \text{Eq.[5.15]}$$

By substituting the power dissipation value of 350W (see Appendix [B1]) and nominal airgap of 20mm in Eq.[5.11], ξ is found to be approximately 1.5. Therefore at the maximum specified force of 500N and nominal airgap of 20mm, a single-ended amplifier as in Fig.[5.10(a)] is sufficient for the current variations needed in this application. Appendix [B1] explains the choice of supply voltage based on this value of ξ .

5.1.3 Additional Considerations and Features

The large amounts of power that are being switched through the magnet cause concern for the safety of both user and patient. In this respect the use of PWM means that the switching signals can be transmitted to the power amplifier through galvanic or optical isolation units. Magload uses optical isolation to separate the patient, user, and low voltage control circuits from the high power modules. In addition, there are protection circuits for the power amplifier, and monitor circuits for the high voltage reservoir capacitor.

An opto-isolated primary operations sequencer maintains orderly and safe use of Magload. The primary sequencer will give permission to drive the system only when all control circuit board voltages are stable, the power amplifier base drive is off, and there is no mains disturbance. When a start command is issued, the high voltage reservoir capacitor is charged and the base drive enabled. At this point the user can introduce desired forcing reference patterns. A stop command, mains disturbance, or current overload will discharge the reservoir capacitor and disable the base drive. The force reference pattern must be turned off before permission to start can be reissued.

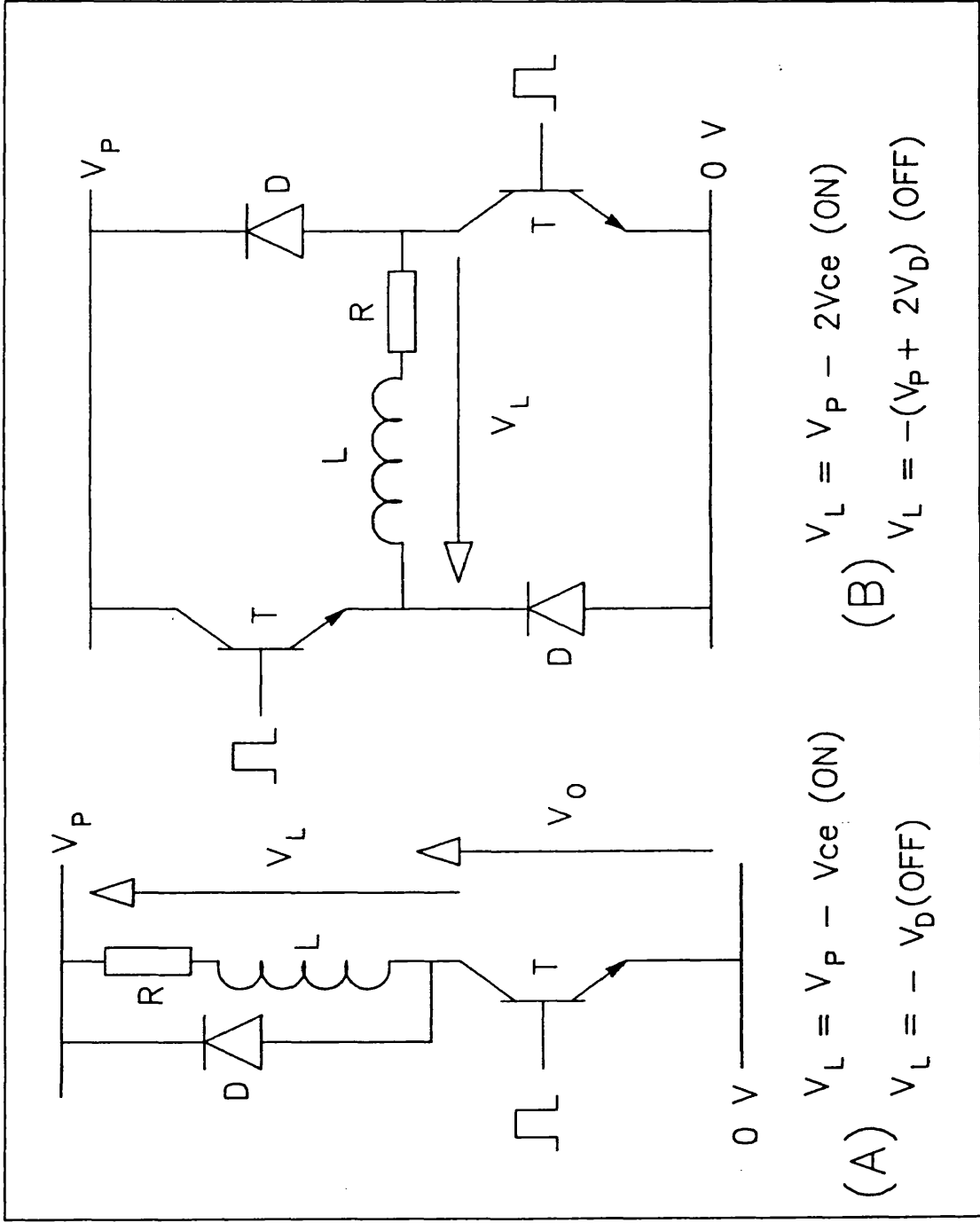


Fig.[5.10] (a) Single-ended class D amplifier with inductive load, and (b) dual-transistor class D amplifier with equal positive and negative forcing capability.

The force reference input can be controlled with a local waveform generator providing d.c., sinusoidal, and triangular voltages. The force pattern can also be controlled through the digital to analogue output of a computer.

5.2 Results and Discussion

The experimental arrangement of Fig.[5.11] was used to measure the static *closed-loop* characteristics of the controllable muscle load. A load cell was connected horizontally between the middle of the pull rod of the main assembly and a screw arrangement that was secured to the rear of the main frame. A static force level was then set with the control d.c. voltage reference. Various airgaps were produced, by adjusting the screw arrangement, and the corresponding force was read from the calibrated load cell meter. This was repeated at ten different force levels. The results obtained from this experiment are shown graphically in Fig.[5.12] and are tabulated in Appendix [B3].

At large force levels and airgaps the effects of flux leakage are noticeable. These effects occur despite the minor current control loop that is used to boost the response at large airgaps. Another factor that contributes to this non-linearity is the geometric misalignment of the pole faces and reaction plate throughout the total available airgap. This can be improved by including another minor control loop using the position of the reaction plate as the feedback signal. A more favourable approach, would be to re-design the main assembly such that the reaction plate remained parallel to the pole faces during the stroke length, and/or to re-design the magnet for minimal flux leakage.

As mentioned earlier, the inertia of the main assembly is 0.367 Kgm^2 . The effect of this on force control is assumed to be negligible as visual position feedback is used to maintain approximate isometric conditions. Visual position feedback helps to minimise any accelerations of the main assembly, due to patient tremor for example, and as such will maximise the ease with which a patient is able to perform a force pursuit exercise.

Frequency and time responses of the system were measured using an Ono Sokki CF-910 mini FFT analyser. The input signal to Magload (channel A in the analyser) consisted of the d.c. reference force level additively combined with 20Hz bandlimited white noise. The output from Magload (channel B in the analyser) was taken directly from the flux force transducer mounted on the pole face of the electromagnet. This transducer is linear up to 2.0T. Fig.[5.13] shows the input reference voltage and the voltage measured from the flux transducer. Fig.[5.14(a)] to Fig.[5.14(d)] show the frequency response of the system and the coherence function relating the test signal to the output at increasing force levels. The frequency responses therefore represent the transfer function between the delivered and demanded forces in the system.

STATIC CLOSED-LOOP MEASUREMENT TEST RIG

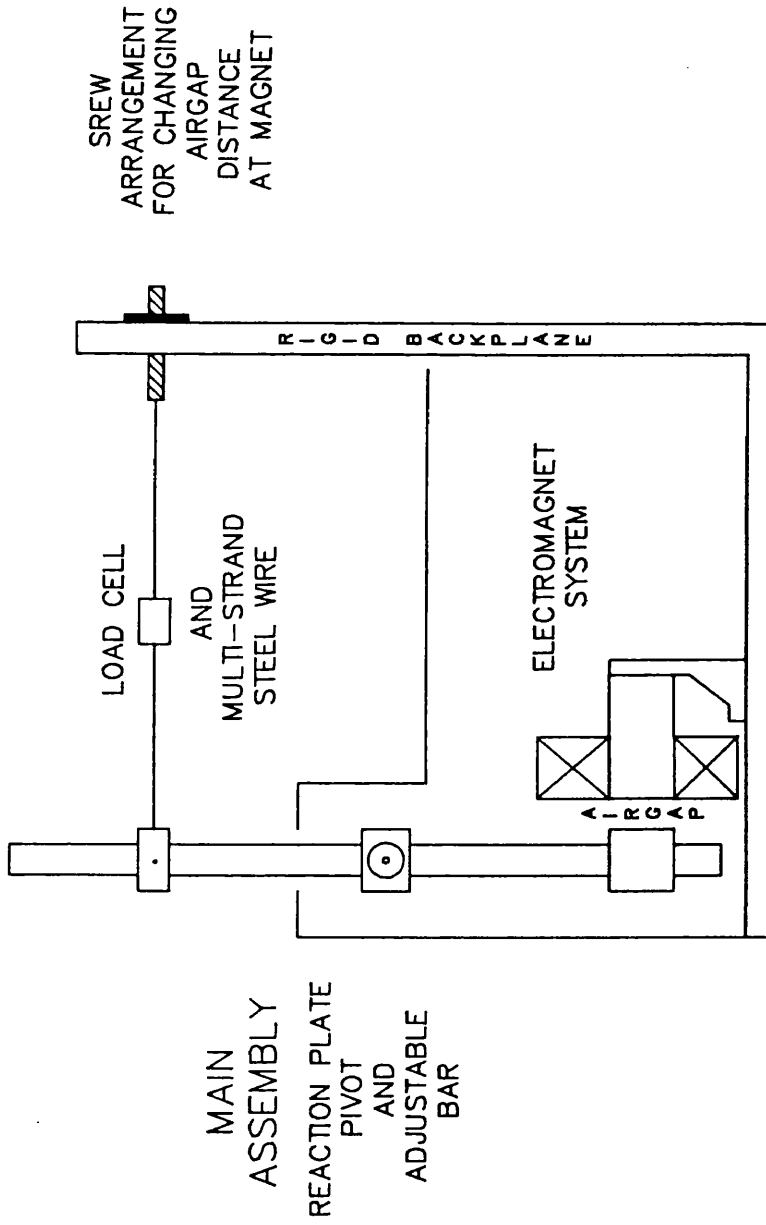


Fig. [5. 11] Experimental arrangement used to measure the static closed-loop characteristics of the electromagnet-amplifier system.

Magload: FORCE Vs AIRGAP (Closed-loop)

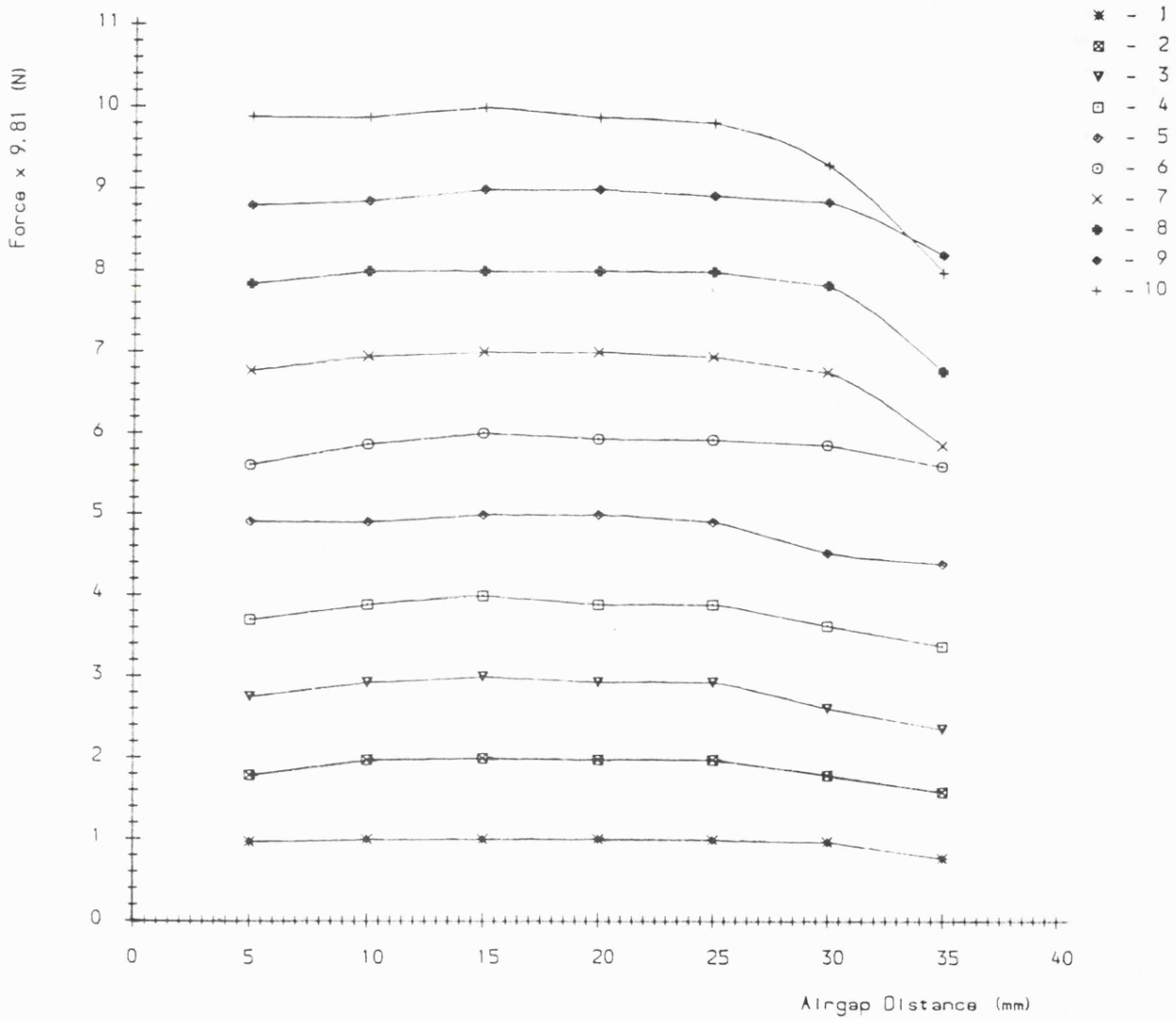


Fig.[5.12] Static closed-loop characteristic for MAGLOAD showing a high degree of linearity between 5mm and 30mm airgaps at ten force levels.

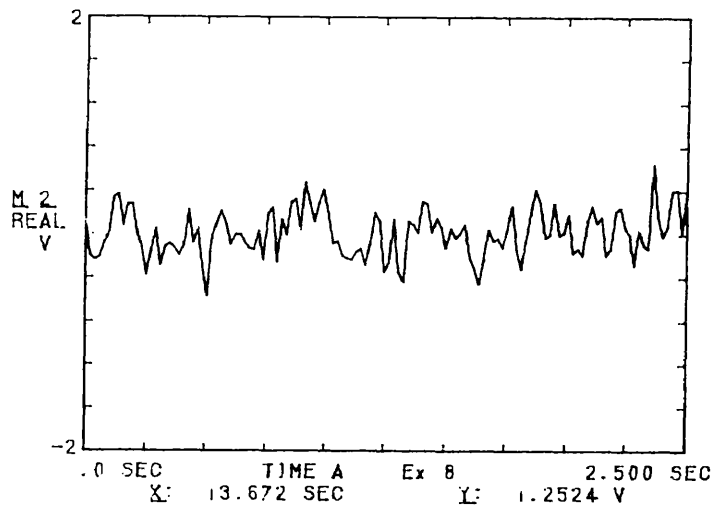
The magnitude and phase plots exhibit some minor periodic resonances of unknown origin. They may arise from coupling between the large inductance of the magnet and the mains reservoir capacitor ($LC = 1.25H \times 2000F = 0.05Hz$). These resonances persist in the magnitude plots up to the higher force levels whereas they are attenuated in the phase plots. The phase plots are almost linear and roll off at $-2.25^\circ / Hz$ to -45° at 20Hz. The coherence remains high at all force levels throughout the frequency range. Using a higher bandwidth noise it is found to go to zero at 50Hz before returning to a high value and remaining above 0.75 up to 100Hz (not shown).

There is an improvement in the coherence functions as the d.c. force level is increased. This can be attributed to a small limitation of the system. We recall that in Sec.[5.1.2] a forcing ratio of 1.5 was determined for the magnet-amplifier configuration. This suggested that a single-ended transistor amplifier was sufficient to provide the required voltage forcing. This was, however, only true at the maximum designed force and nominal airgap. In this particular system, the load voltage V_1 decreases at lower force levels and with decreasing airgaps. The implication of this is that the forcing ratio increases and the current ripple in the magnet increases leading to lower values in the coherence function. If this situation was detrimental to the performance of the system then the circuit of Fig.[5.10(b)] would have to be used to maintain equal positive and negative current forcing voltages across the magnet drive transistor. The PWM switching frequency was made as high as possible (20KHz) to avoid substantial current ripple. Higher switching frequencies would necessitate more complex drive circuitry to control the power dissipation in the magnet transistor amplifier at turn-on, and particularly at turn-off.

Various forms of forcing are of interest in the study of the dynamic properties of muscle (see Sec.[2.4]). Current research work in EMG decomposition and fatigue being conducted by the author's colleagues involves the use of Magload to provide accurate long duration ramp force patterns. A small magnetic device based on the ideas behind Magload has been built by an undergraduate student for testing the small muscles in the hand. This device uses a bobbin-shaped electromagnet with tapered ends containing a cylindrical reaction piece passing through its centre and lying along its vertical axis. Using a Class A drive amplifier, the magnet is capable of providing static forcing levels up to 0.5N that remain nearly constant over a 2cm stroke length. It should be possible to incorporate a flux or current feedback loop into this system to improve linearity and enable controlled dynamic forcing.

Fig.[5.15] shows a diagram of an improved magnet design that could be implemented in the future in similar systems to Magload. The diagram shows a cylindrical magnet having an E-shaped axial cross section. The coil is wound around the short central pole at one end of the hollow cylinder, and the remainder of the cylinder contains a freely moving disc which would function as the reaction plate. In this way the flux paths are restricted to the cylinder walls, the airgap between the

MAGLOAD. A:1/P(2kg dc + wh noise) B:0/P(flux/for)01:05
20Hz A:DC/ 2V B:DC/ 2V INST 0/16 DUAL 1k



MAGLOAD. A:1/P(2kg dc + wh noise) B:0/P(flux/for)01:05
20Hz A:DC/ 2V B:DC/ 2V INST 0/16 DUAL 1k

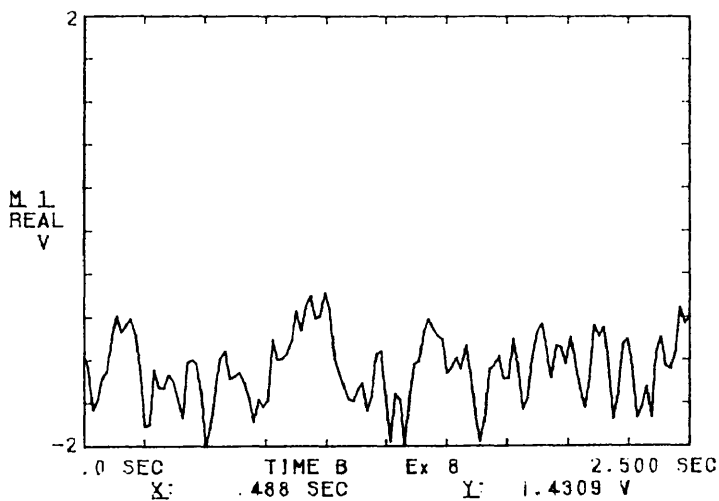


Fig.[5.13] Demanded (top) and output (bottom) force voltage waveforms. The demanded force pattern is d.c. + 20Hz bandlimited white noise. The d.c. reference represents a 20N static force level.

MAGLOAD. A:1/P(2kg dc + wh noise) B:0/Piflux/for01:05
20Hz A:DC/ 2V B:DC/ 2V INST .0/16 DUAL 1k

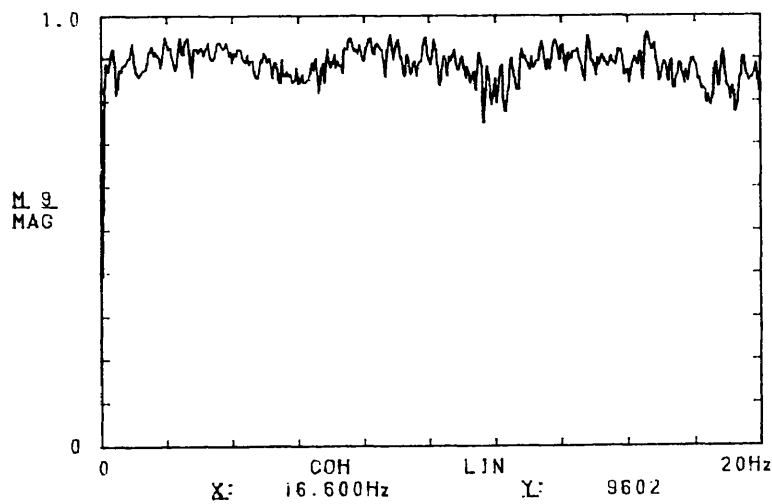
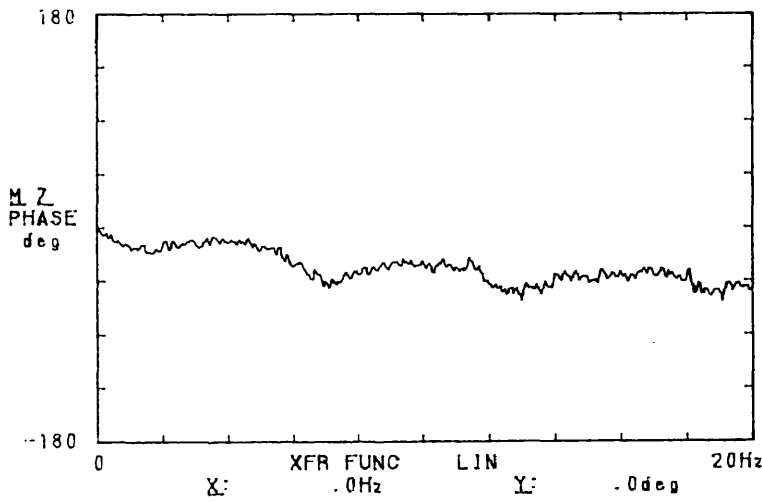
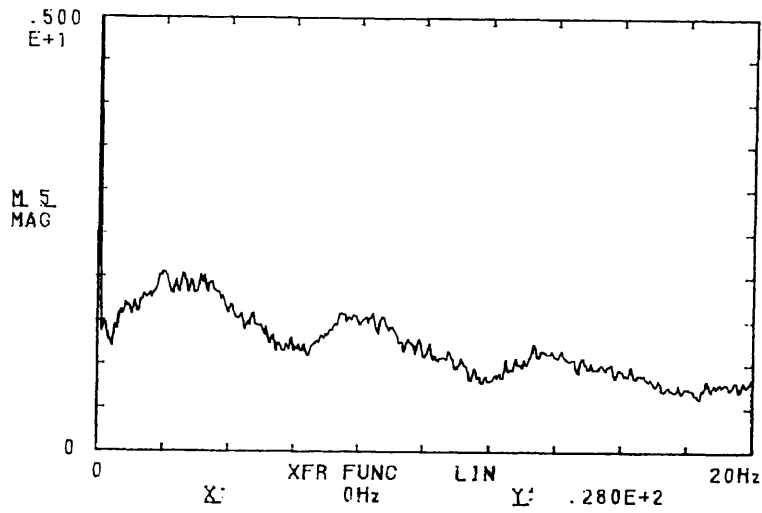


Fig.[5.14(a)] Frequency response of the system at 2Kg
d.c. reference plus white noise.
TOP: Magnitude.
MIDDLE: Phase.
BOTTOM: Coherence function.

MAGLOAD. A:1/P(4kg dc + wh noise) B:0/P(flux/for0i:15
20Hz A:DC/ 2V B:DC/ 2V INST 0/16 DUAL 1k

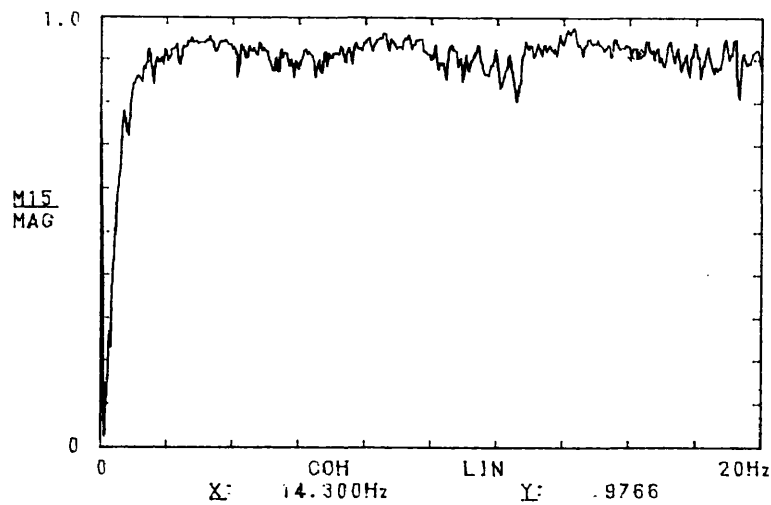
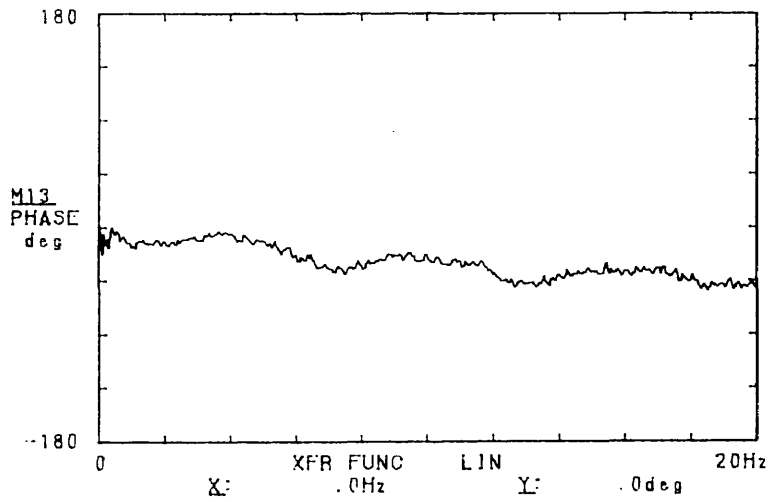
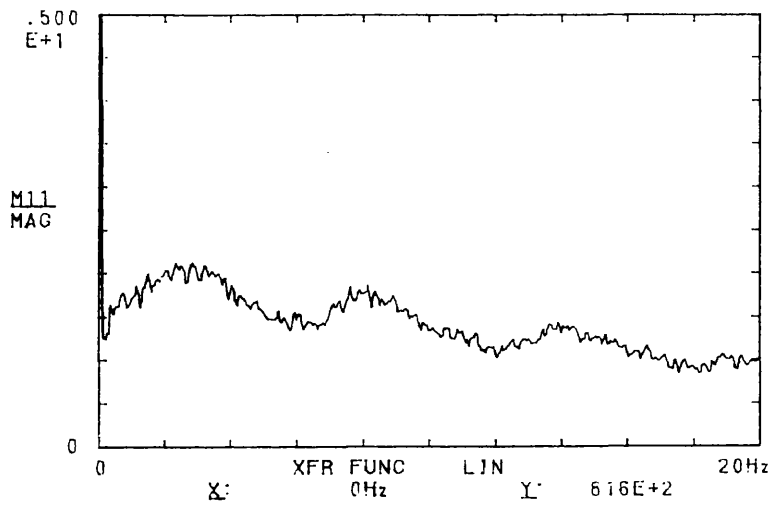


Fig.[5.14(b)] Frequency response of the system at 4Kg d.c. reference plus white noise.

TOP: Magnitude.

MIDDLE: Phase.

BOTTOM: Coherence function.

MAGLOAD. A:1/P(6kg dc + wh noise) B:0/Piflux/far01:35
20Hz A:DC/ 2V B:DC/ 2V INST 0/16 DUAL 1k

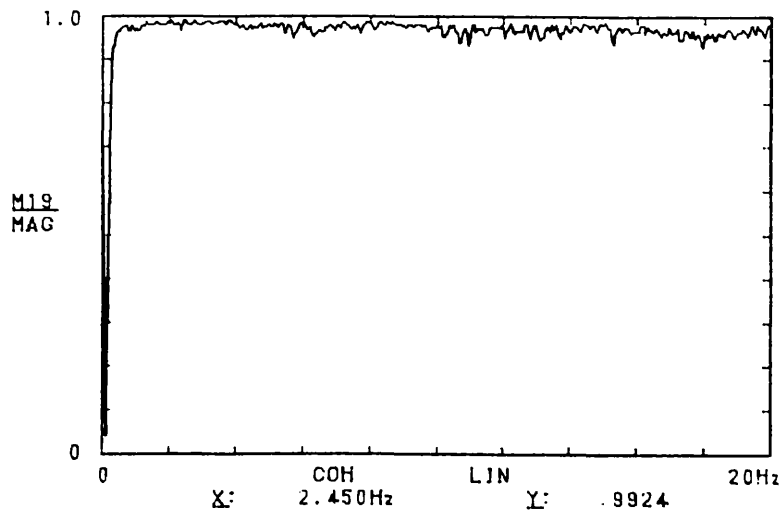
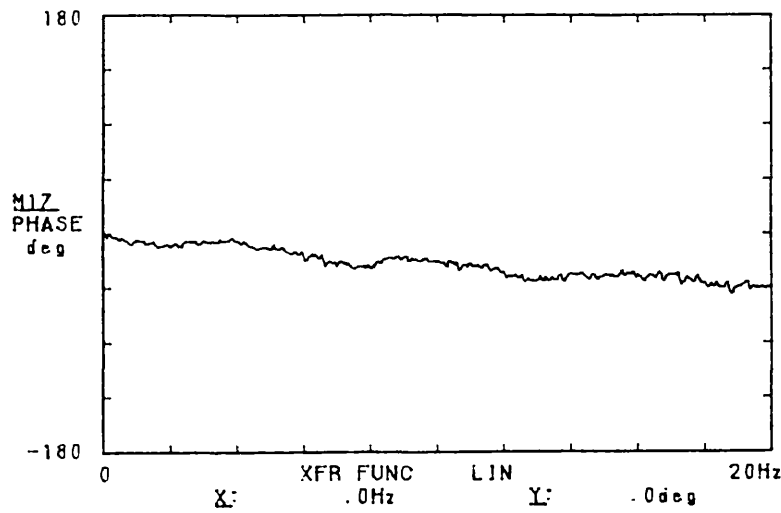
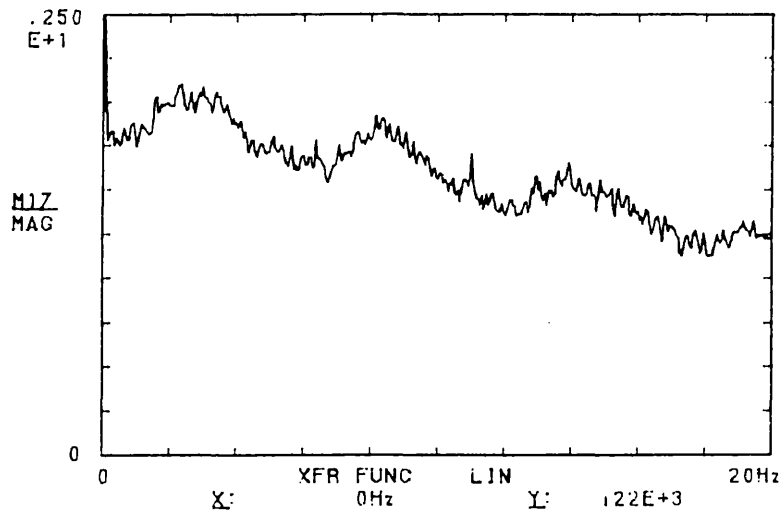


Fig.[5.14(c)] Frequency response of the system at 6Kg d.c. reference plus white noise.

TOP: Magnitude.

MIDDLE: Phase.

BOTTOM: Coherence function.

MAGLOAD. A:1/P(8kg dc + wh noise) B:0/P(flux/for01:40
20Hz A:DC/ 2V B:DC/ 2V INST 0/16 DUAL 1k

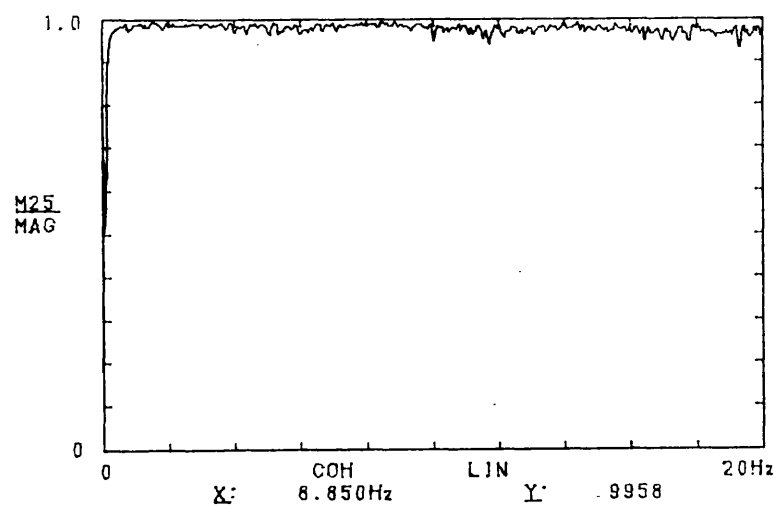
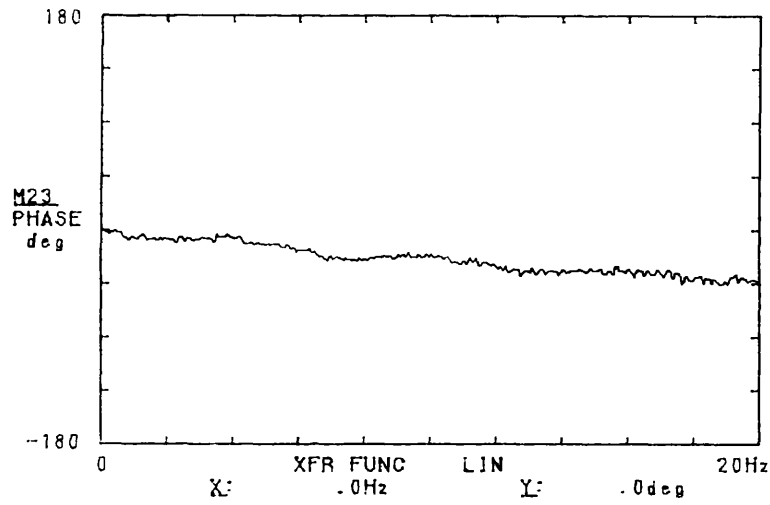
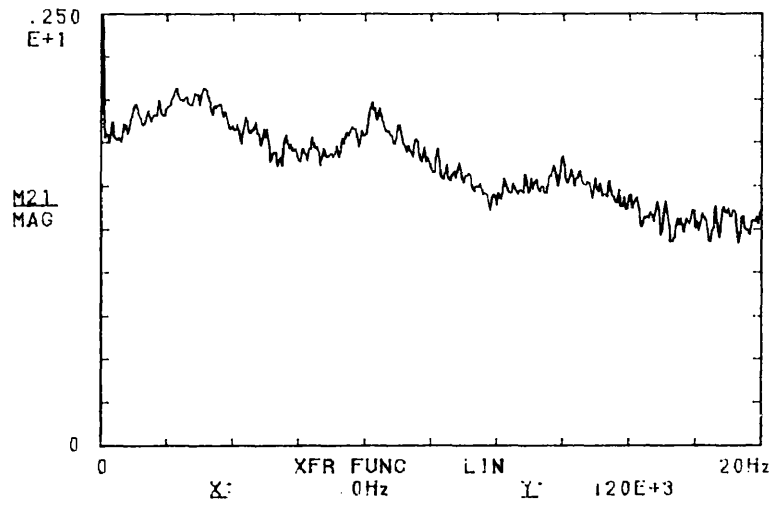


Fig.[5.14(d)] Frequency response of the system at 8Kg d.c. reference plus white noise.
TOP: Magnitude.
MIDDLE: Phase.
BOTTOM: Coherence function.

central pole face and disc, and the airgap between the disk circumference and cylinder wall. If airgap between the disc circumference and the inner surface of the cylinder wall is narrow, then friction throughout the full stroke of the disc will be minimal because there will be an equal force of attraction between the cylinder wall and the total disc circumference. The reaction plate remains parallel to the pole face because of the circumferential force on the disk and the geometrical constraints of the magnet construction. The latter and the constrained flux paths will minimise flux leakage. Another advantage of this method is the 50% reduction in power dissipation, yet producing the same amount of force as can be produced by an equivalent U-shaped magnet. The use of a single pole implies that both the force F and airgap x will be reduced by a factor of 2, so the power P will be reduced by a factor of 4. Hence, for the same force, the current I must be increased by a factor of 2 which in turn increases the power by a factor of 2. The effective decrease in the power will therefore be 50%.

From the above discussion, it is evident that there is virtually no restriction on the forcing protocols that can be designed with Magload and more flexibility is obtainable under computer control. Magload will faithfully and repeatedly reproduce demanded force patterns, and it will also provide a direct measure of the force produced. The main disadvantage of the current Magload system is its expense and weight. Fig.[5.16] shows some of the interactions that are possible with the Magload system.

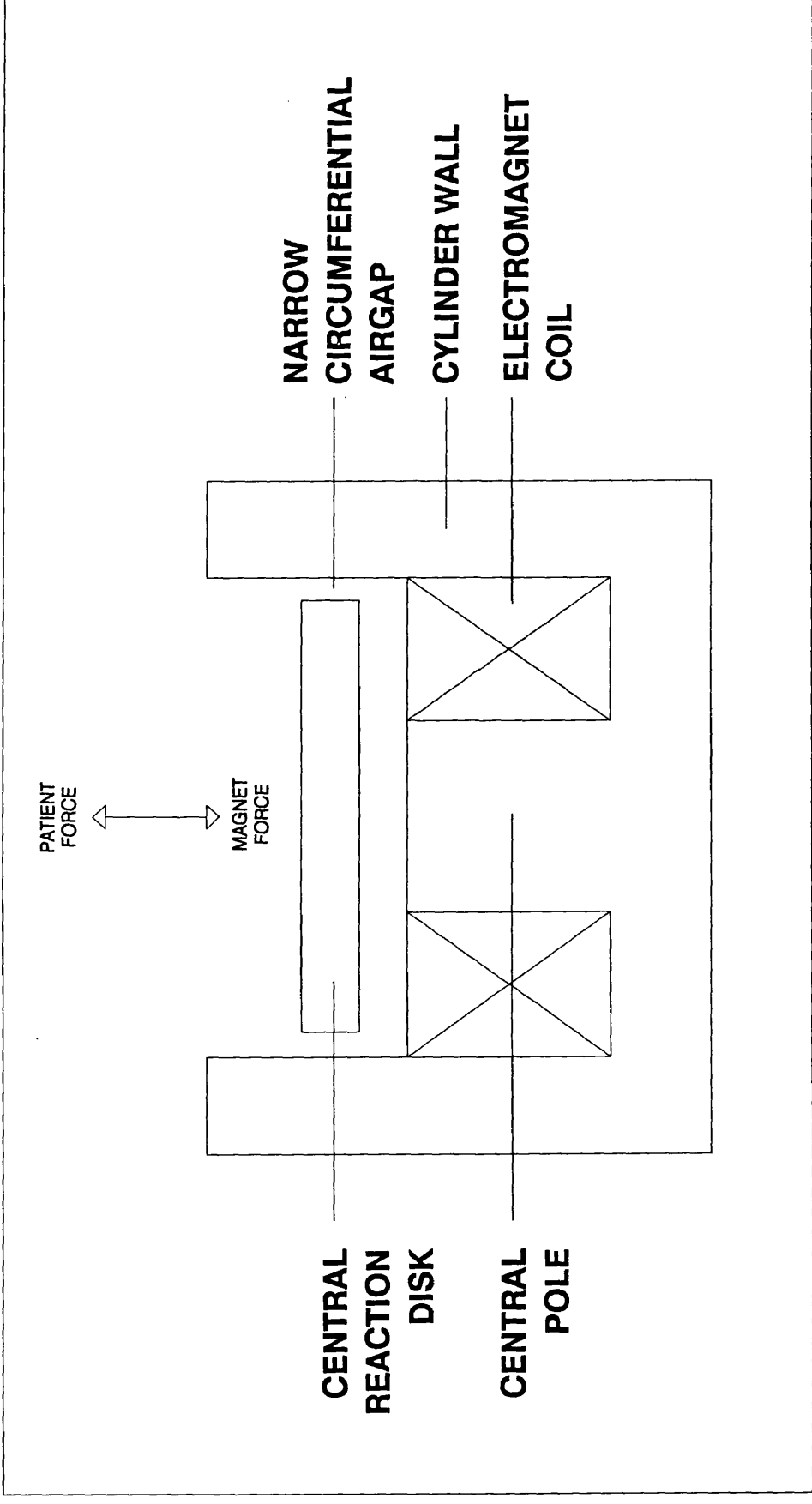


Fig. [5.15] Diagram showing the E-shaped axial cross-section of a cylindrical magnetic circuit.

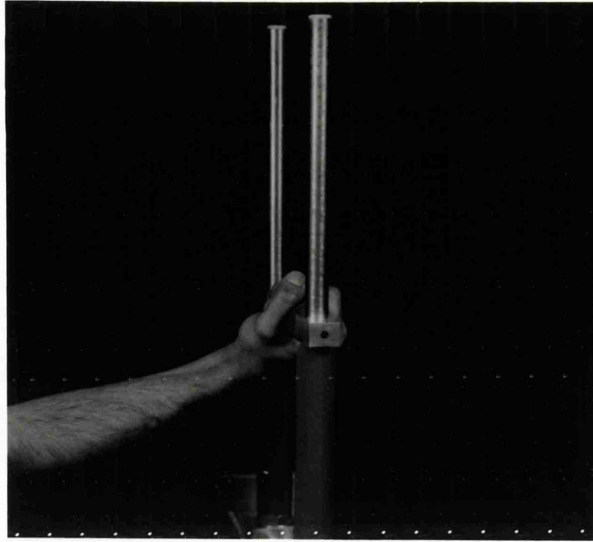


Fig.[5.16] Illustration of some of the useful subject interactions with the MAGLOAD system.

Chapter Six

Features and Uses of Brainstem Auditory Evoked Potentials (BAEPs)

6.1 Introduction

Physical or sensory stimulation of the human peripheral nervous system and/or some psychological process will, under normal circumstances, result in changes to the on-going electrical activity of the central nervous system (CNS). These variations in voltage are known as event related potentials (ERPs). Evoked potentials (EPs) are ERPs that follow a sensory stimulus. Emitted potentials occur in the absence of any evoking stimulus and are normally associated with the cognitive function of the CNS.

ERPs are generated by a polarisation of charge across the membranes of cells in the nervous system. They can often be seen as a wave or group of waves in the electroencephalogram (EEG) even when recorded on the cortex at a distance from their origin. The morphology of the measured potential depends on the geometry of the active membranes with respect to the recording site(s), on the synchronisation of activity between cells, and on the impedance of the volume conductor in which the cells are active. Amorphous collections of cells and/or little synchronisation between the cells, makes it difficult to record potentials at a distance. Therefore, ERPs offer a limited (though useful) look at the processes of the nervous system. Furthermore, overlapping potential fields from different groups of simultaneously active cells make it difficult to distinguish between those measurements that are associated and are not associated with the evoking event.

Most ERPs are indistinguishable in routine EEG recordings because of their inordinately low amplitudes (0.1 to 2 μ V) and the interference of background cerebral electrical activity and electromyographic (EMG) artifacts (Chiappa, 1982). Isolation of the ERP from overlapping potentials generated by cells that are not related to the event is usually performed by filtering and averaging. Filtering usually involves restricting the frequency response of the recording system to those frequencies present in the ERP. Averaging exploits the non-stationary time locked nature of an ERP with its related stimulus and assumes that background EEG activity is a stationary random noise process that will be uncorrelated with both the ERP and the stimulus.

The information contained in the structure of features (feature events or waves) in averaged sensory EPs provides important insights into the sensory systems that is not available through other clinical tests (Picton, 1988). A major use is in the assessment of the neurological condition of the sensory receptor. The presence or absence of EP waves and their latencies are the primary characteristics used in clinical interpretation. The presence of a normal EP generated by the brain is reasonable evidence for correct function in the peripheral receptor. Absence of a normal EP is indicative of pathology in the sensory end-organ, the generator mechanism for the EP, or the neural pathways between them.

Over the past decade, several methods have been developed to study the EP. Of these, pattern-shift visual, brainstem auditory, and short-latency somatosensory EPs have come into routine clinical use and are now firmly established as valuable clinical tools. EPs are widely used to assess hearing in infants who cannot respond reliably in behavioural tests (Picton, 1988). They are also used to confirm the presence of lesions in the sensory system when demyelinating disease (e.g. in the optic nerve) is suspected because of indications in another area of the central nervous system. This is particularly relevant to:

- the diagnosis of multiple sclerosis,
- determination of the anatomical distribution of a disease process, and
- monitoring continuously the integrity of a pathway that cannot be examined clinically because of anaesthesia (Chiappa, 1982; Halliday, 1982; Colon et al., 1983).

Therefore, EPs will often be used to study patients with multiple sclerosis, nervous system tumours, trauma and stroke. EPs also have important uses in intra-operative monitoring procedures, and in intensive care environments, as well as in infants whose sensory systems cannot be accurately assessed. These tests provide sensitive, quantitative information complementing standard clinical neurological examination.

In this study the author has developed a procedure to analyse the short latency acoustically evoked brainstem electrical activity or brainstem auditory evoked potential (BAEP). Therefore, the remaining section of this chapter presents a simple description of BAEP-related physiology, recording techniques, and clinical uses.

6.2 Brainstem Auditory Evoked Potentials (BAEPs)

This section provides a general appreciation of the physiology and uses of the BAEP in auditory investigations.

6.2.1 Origin of BAEP Components

The output of the cochlea and VIII nerve can be examined using techniques pioneered by Portmann and co-workers in the late 1960s (Halliday, 1982). The more central connections of the VIII nerve comprised of brainstem pathways provide the BAEP potential in response to an acoustic transient (click) which is generated by passing a 0.1 msec pulse through shielded headphones. The BAEP is most effectively obtained with a high intensity click stimulus and can contain up to seven components within the following 10ms. These are labelled I-VII according to Jewett's (1970) classification. There is considerable evidence that at least the first five components correspond to the successive activation of peripheral and pontomedullary (cochlea, spiral ganglion, and eighth nerve), pontine (cochlear nucleus, superior olivary nucleus, and lateral lemniscus tracts and nuclei), and midbrain (inferior colliculus) portions of the brainstem pathway (Stockard et al., 1978). Volume-conducted acoustic nerve and brainstem potentials recorded with electrodes at the vertex (electrode, Cz) and mastoid (electrode, Ai) are shown in the diagram of Fig.[6.1].

The precise correlations of scalp-recorded BAEP components with deep sub-cortical structures are unknown (Stockard et al., 1978) and they are certainly more complex than is suggested by Fig.[6.1]. The BAEP generators within the brain might be serially or non-serially linked, simultaneously active, or have sustained activity. Hence there cannot be a direct correspondence between different components in the BAEP and different anatomical loci. However, the degree of correspondence that does exist, permits one to use the latencies of the early wave components I-V as indirect measures of sensorial registration of the stimulus along the brainstem pathway. More precisely, the inter-peak latency (IPL) of waves I and III is a measure of conduction in the extra-axial and pontomedullary segments of the auditory pathway and the III-V IPL is a measure of conduction in the more rostral pontine and midbrain segments of the pathway.

Wave I of the BAEP is a negative potential recorded at the ear being stimulated (the ipsilateral side). This is a manifestation of the VIII nerve action potential generated in response to the click stimulus in the segment of the nerve near to the cochlea. Waves II and III are thought to emanate from the cochlear nucleus and superior olivary complex respectively. There is some evidence (Buchwald et al., 1975) that wave II is connected with the VIII nerve since this component disappears when connections of this nerve to the brainstem are destroyed ipsilaterally, but not

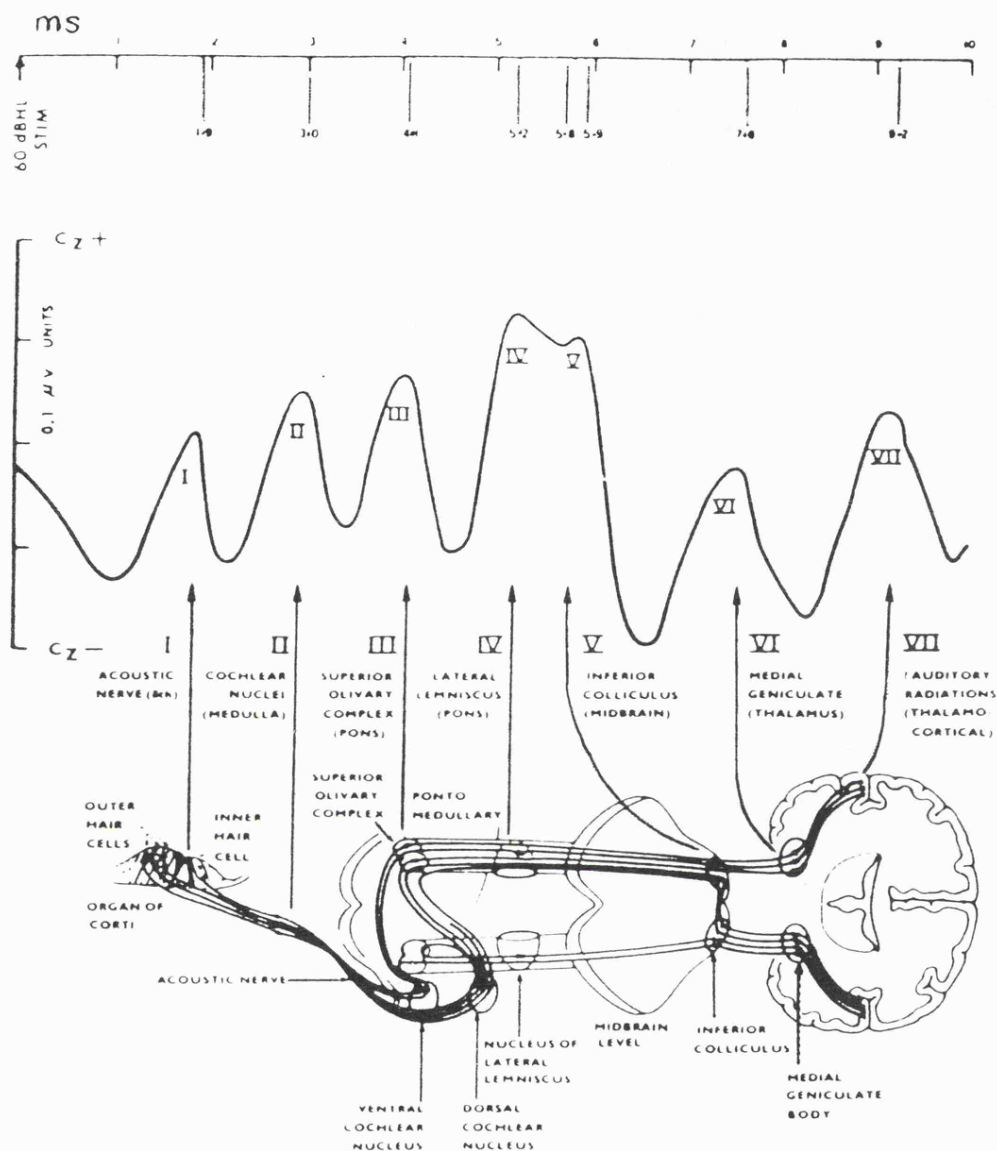


Fig.[6.1] Diagram of normal latencies at 60dBSL for components I through VII. Lesions at different levels of the auditory pathway tend to produce response abnormalities in the components, although the affected component(s) does not specify the precise generator(s) of the response (taken from Stockard et al., 1977).

contralaterally. The generator sites for components IV and V are difficult to locate. Lesions in the mid and upper pons, in the region of the lateral lemniscus and inferior colliculus, produce abnormalities in both waves but do not stop the generation of either. The majority of workers in this field appear to agree that there is no complete answer available yet. In terms of clinical interpretation however, there is no difference between the two possibilities as they lie so close to one another (Chiappa, 1982). It is unknown whether the BAEPs reflect activity of groups of neurones or the action potentials in fibre tracts or a combination of both. A further complication regarding BAEP generator locations is that the surface recorded potential components are the summation of electrical activity of many thousands of neurones and their processes. The electrically active sites are dispersed in anatomically discrete nuclei and tracts between which there is much interaction.

6.2.2 Methods of Recording BAEPs

In routine clinical practice, patients should be tested in the supine position and sedated whenever there is significant artifactual muscle activity. Ideally the patients should be asleep. To record BAEPs, repeated clicks at *about* 10 Hz (to avoid mains synchronisation) are generated in high quality shielded earphones as described earlier. Monaural stimulation is used because normal responses from one ear can obscure abnormal responses from the other during binaural stimulation and so the contralateral (nonstimulated) ear is masked with white noise. BAEPs are normally recorded with rarefaction (where the initial movement of tympanic membrane is outward) or, their opposite, condensation clicks. Different polarities produce different wave morphologies, amplitudes, and latencies, and on some occasions the BAEP is pathological with a single click polarity only. Alternating clicks can cancel stimulus artifact and cochlear microphonics (a nerve action potential prior to wave I) since these are click-phase sensitive. However, this is not used routinely because the waves produced are an average representation of the waveforms elicited with either polarity alone.

Electrode derivations (montage) for BAEP measurements conform to the international 10-20 standard. One electrode is placed at the vertex Cz, and the other two are placed over the primary auditory areas left and right, on or in the region of the earlobes ipsilaterally Ai, and contralaterally Ac.

Due to the extremely small amplitudes, which range from 0.1 to 2 μ V, between 1000-4000 responses are measured for averaging. At least two similar averages must be obtained from each ear, thus providing a simple estimate of the reliability of the recording. The decision as to how many responses to average is determined by the degree of inter-trial variability of IPLs; the I-III, III-IV, and I-V IPLs should not vary by more than 80 μ sec at most between trials. If they do, then louder clicks and/or patient sedation should be used (Stockard et al.,1978).

If the intertrial criteria for reproducibility is met then the measurements will almost always be made from the sum of the averages in each trial. Fig.[6.2] shows the 95% confidence limits for normal BAEP wave component latencies at various intensity levels (obtained from Wessex Regional Audiology Centre). Stimulus intensity is adjusted to 60-70 decibels above sensation (or hearing) threshold level (dBSL/DBHL). The contralateral ear is masked with 30-40 dBSL white noise. The stimulus intensity has a large influence on the BAEP. Decreasing the intensity, produces a longer latency and a decrease in amplitude, especially of waves II, IV, and VI. In cases where there is difficulty in identifying wave V (or the IV/V complex), reducing stimulus intensity to 0-10 dBSL may help to identify this component since it is selectively preserved near threshold. Because of this, the plot of Wave V Latency as a function of Stimulus Intensity is used to

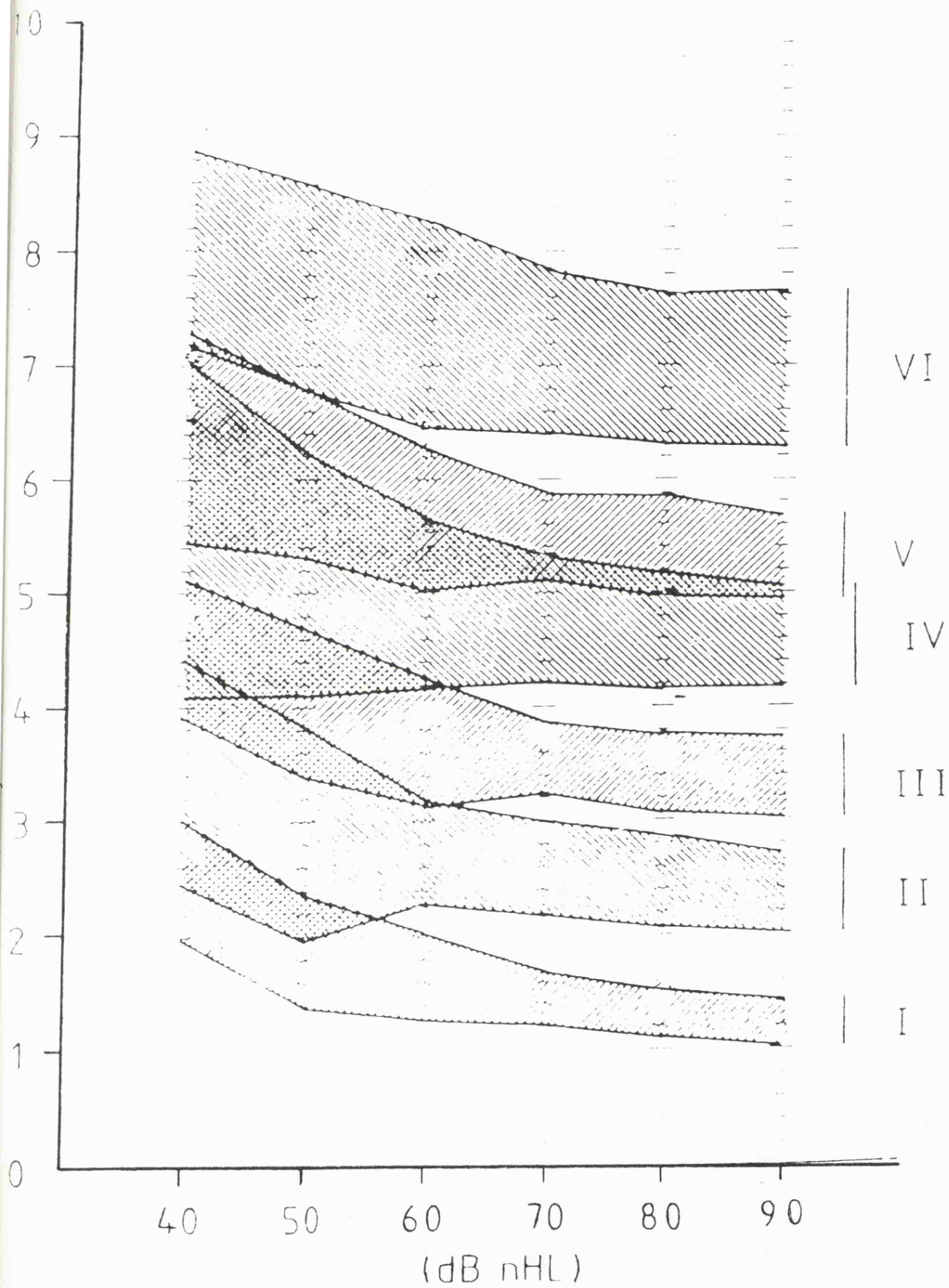


Fig.[6.2] 95% confidence limits for normal BAEP wave component latencies across intensity levels 40 to 90 dB SL (dBHL). (Wessex Regional Health Authority).

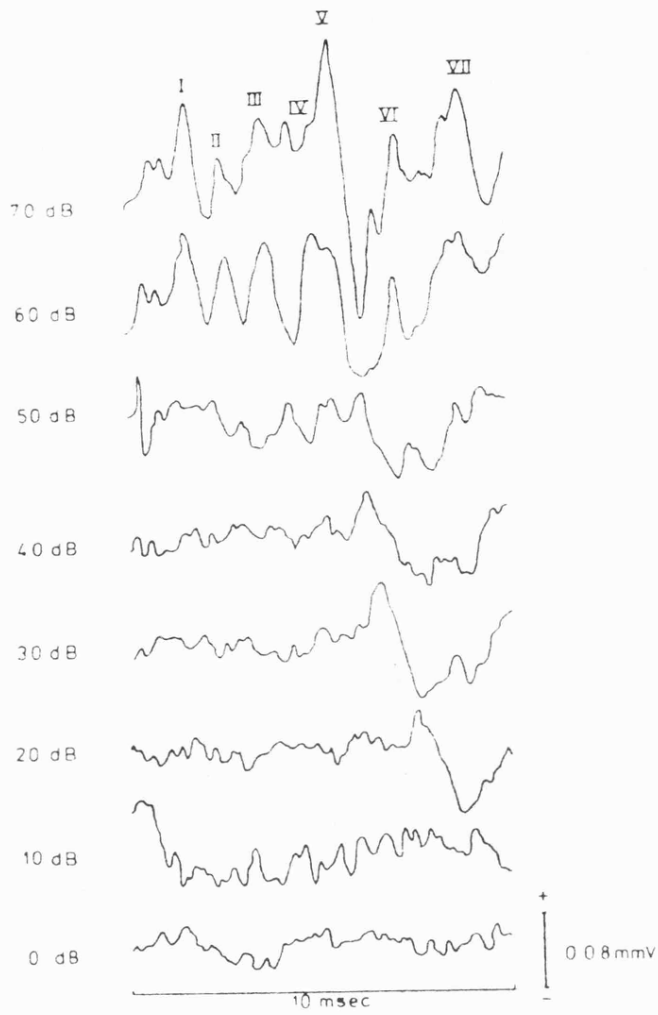


Fig.[6.3] The persistence of wave V as function of stimulus intensity (taken from Colon et al., 1983).

characterise the BAEP. Fig.[6.3] shows the persistence of wave V at low intensity levels. The complete test, at several intensity levels, should take one hour to complete and possibly up to two hours in an intensive care unit.

6.2.3 Clinical Uses of the BAEP

Non-pathological factors such as age, sex, temperature, and technical factors such as stimulus rate, stimulus polarity, electrode derivations, and amplifier filter settings can affect the morphology of the BAEP. It would be out of context to expand any further on this matter save to say that with constant test conditions reproducibility can be excellent making the BAEP an important electrophysiological test. Stockard et al. (1978) provide a thorough treatment of the non-pathologic factors influencing BAEPs. The clinical interpretation of BAEPs is based almost entirely on the IPLs which reflect conduction properties of the brainstem auditory tract. IPLs are seldom affected by changes in the stimulus intensity and disorders of the peripheral hearing apparatus, although the absolute latencies of the wave components are affected.

[A] Multiple Sclerosis

Brainstem auditory evoked potentials may reveal a clinically unsuspected demyelinating lesion as in multiple sclerosis (MS). Though pattern-shift visual and short-latency somatosensory EPs provide better diagnosis because of their less complex morphology, the stability of wave V in the BAEP lends itself equally well to identification and interpretation in MS. Robinson et al. (1982) investigated MS using binaural stimulation and recording from two channels of the standard BAEP electrode montage. They tried to identify component V in all records, arbitrarily defining it as being the most negative-going potential in the latency range 5.5-10 msec. Three types of abnormality in the BAEP were found to exist with the occurrence of MS. First, there is an increase in wave V latency and the earlier components may lie within normal limits. Second, acute degradation of the BAEP makes wave V identification impossible, despite clear post-auricular muscle reflex and middle-latency components. Finally, wave V has a greatly reduced amplitude in comparison with a normal and well formed component III.

[B] Acoustic Neuromas

This is a tumour arising on the VIII nerve and usually causes deafness. It is the most common of the space-occupying lesions in the cerebello-pontine angle. The detection of these lesions is of considerable importance as the tumours are usually benign and can be removed with little trauma when detected at an early stage. The BAEP in some patients with acoustic neuromas do not contain a wave I and the I-III interval cannot be determined. In these cases it is necessary to use an external auditory canal needle electrode in an attempt to demonstrate wave I. In a group of 25

patients with acoustic neuromas and five with cerebello-pontine angle meningiomas, all had abnormal BAEPs on the side with the tumour. Five had normal CAT scans and two had normal standard audiometric findings. The incidence of false-positive tests was low, i.e. a pronounced abnormality in the I-III or I-IV IPL without a tumour detected with radiographic contrast study of the posterior fossa. Patients with large acoustic neuromas may also have BAEP abnormalities of the III-V IPL after stimulation of the contralateral ear. This is thought to be caused by the complex distortion and cross-compression of brain-stem structures. The condition improves after removal of the tumour (Chiappa et al., 1982)

[C] Other Nervous-System Diseases and Uses

BAEP abnormalities have been reported in other diseases of the myelin and various leukodystrophies. Diseases connected with the degeneration of the spinal dorsal-root ganglia, axons, and posterior columns (e.g. Friedreich's ataxia and Charcot-Marie-Tooth disease) exhibit abnormal BAEPs. Chiappa et al. (1982) postulate that the same process of degeneration occurs in the auditory system homologues of these structures, viz. the spiral ganglia, the auditory nerve, and its central connections. The BAEP has proved useful in assessing the irreversibility of brain damage resulting in coma due to anoxia, hepatic failure, or drug abuse. Starr (1976) studied patients certified clinically brain dead i.e. having no vestibulo-ocular reflex, no pupillary reactions, and no spontaneous respiration. In these patients any auditory evoked potentials originating from brainstem structures (waves II-V) were absent. Wave I, from the VIII nerve, was present, but with prolonged latency. High doses of anaesthetic agents (and barbiturates) do not seriously alter the BAEP, even when the electroencephalogram is isoelectric. Hashimoto et al. (1980, 1981) have reported using the BAEP to monitor the hazardous procedure of posterior fossa surgery, e.g. on the arterial tree. Another area of much attention is the use of the BAEP in paediatric applications. Screening for hearing defects is more easily performed electrophysiologically in infants because the conventional behavioural hearing tests may not be practicable. Several investigators have reported the use of BAEP monitoring in sudden infant death syndrome (cot death) and mental retardation.

Chapter Seven

Quantitative Analysis and Interpretation of EPs

The first half of this chapter will consider some analytical methods that have been developed to study EPs, and will highlight some of the obstacles that need to be surmounted. The interpretation (i.e. labelling or scoring) of the EP waveform is then considered. This leads on to a brief discussion of knowledge based systems and their possible application in the problem of interpreting and scoring the EP.

7.1 Introduction

The simplest model of an EP consists of the sum of an invariant (non-stationary) signal and random noise. In this model the noise is assumed to be primarily due to background EEG activity that is uncorrelated with either the stimulus or the noise from another application of the stimulus. This additive model accounts for biological artifacts, such as high frequency EMG activity, and non-biological instrumentation and electromagnetic interference (EMI) noise.

It is worth noting that the EP model differs from the model of interference and needle EMG, in that the EMG exhibits statistical stationarity similar to that of the additive noise. In the latter case the noise is mainly non-biological and due to EMI. Another difference between the two models is that the signal to noise ratios (SNR) are not comparable. EP feature extraction and analysis techniques are hampered by the low SNR obtainable in single responses and they are encouraged by the fact that significant features are deterministic. The converse is true for EMG analysis techniques (see chapter two). It is because of these fundamental differences that one rarely applies the approaches adopted in EMG analysis to EP analysis, unless the problems of low SNR in the EP are dealt with carefully prior to, or during analysis.

In the previous chapter we saw that ensemble averaging is used to extract the EP signal from additive noise, and is based on the prior assumptions of the simple EP model mentioned above. This provides an unbiased estimate of the signal at increased SNR which improves as the number of single response EPs contributing to the average increases. The assumption of an invariant signal implies that the *population of cells* which generates the EP responds in the same way to each occurrence of the eliciting stimulus. The assumption is a reasonable one for some, but not all cases. Changes in the degree of adaptation and habituation and level of attention and fatigue can affect the EP, particularly in late waves that are usually associated with higher cognitive function.

Therefore, the same stimulus can evoke different responses resulting in variations to the latency and/or amplitude of the EP. For such cases, biased estimates with lower than expected SNRs result from averaging the signal (Ruchkin, 1988).

It is now a generally accepted premise that EP signals do exhibit variability (Aunon et al., 1981). Although one of the most important problems in EP research is still signal extraction, more recently there has been an increased interest in the determination of the variability associated with the signal (Madhavan et al., 1985; McGillem et al., 1985).

The effect of latency variation upon the averaged signal waveform resembles that of a low pass filter, since attenuation of fine-detail, high-frequency activity occurs. Ruchkin has shown mathematically (1965) that this phenomenon can be expressed in terms of a linear filtering operation. The original signal corresponds to the filter input, the latency-blurred average corresponds to the filter output, and the filter's frequency response is the Fourier transform of the probability density function of the latency. He states that if the effective range of latency variation is T seconds, then there will be heavy attenuation of the average signal waveform at frequencies above $1/2T$ Hz and relatively little attenuation at lower frequencies.

It may be desirable to reduce the distortion caused by latency variability if the features of interest are seriously obscured. The possibility of achieving this depends on whether the SNR is sufficiently high, so that the data can be effectively analysed on a single response (i.e. single trial) basis before averaging, thereby permitting extraction of signal latencies and quantification of the variability on a trial-to-trial basis.

7.2 ERP Estimation by Latency-Corrected Averaging

Computation of averages by this method requires filtering single trials, estimating the latency of features, and then aligning the corresponding features by shifting each trial in time. The alignment procedure is followed by averaging across trials to produce the latency-corrected average (LCA).

Woody (1967) and McGillem and Aunon (1977) have developed methods for LCA. Woody's method has been employed by several laboratories and the latter method is beginning to obtain wider clinical use and evaluation (Ruchkin, 1988). The descriptions given below refer to the more general ERP signals.

7.2.1 Method 1 (due to Woody):

This method uses adaptive correlation detection. The approach cross-correlates a template representative of the ERP under study with single trials of the response in order to estimate the latency of significant features. The single trials are then corrected for their individual latency variations whence a new average response is computed. The conventional average is chosen as the initial template. Iterations with each new LCA can be done until no further improvements are obtained. The convergence criterion is based on the average of the cross-correlation coefficients between each trial suitably shifted by its estimated latency and the template.

There is no guarantee of convergence for the process. Woody's simulation studies determined that (a) convergence to the true ERP response waveform occurred if the rms SNR was greater than 0.2, and (b) the choice of initial template was not critical. Ruchkin (1988) has found that the rms SNR should be above 0.4 to 0.5 for reliable convergence to occur. The performance of Woody's method can be improved by prefiltering the data, thereby increasing the SNR. Tukey (1978) suggests prewhitening the data and template in the pass band, thereby increasing the fidelity of the peak of the cross-correlation function. It is not known whether this suggestion has been implemented.

The Woody procedure is capable of compensating for shifts in the latency of the entire waveform but cannot cope with random shifts in the individual components of the ERP. Furthermore, the possible existence of strong components such as alpha waves, causes the Woody procedure to align to them (Aunon and Sencaj, 1978). Also, this procedure can produce, from noise-only data, LCAs that appear to contain perfectly plausible signals (McGillem et al., 1985; Ruchkin, 1988).

7.2.2 Method 2 (due to McGillem and Aunon):

This method was devised to overcome limitations of the method due to Woody described above. It is non-iterative and deals with multiple peaks in the analysis epoch. The LCA procedure is aided by initially filtering the single trials of ERP data with a Wiener-like minimum mean square error filter which selectively attenuates at those frequencies where the SNR is low. After filtering, the peaks in the ERP are found by cross-correlating the single trials with a template having the general shape of the peaks. Histograms for the number of peaks found at each latency (sampling point) are constructed for both positive and negative peaks. Positive peaks add one unit to the positive peaks latency bin and negative peaks subtract one unit from the negative peaks latency bin. These two latency bins together constitute a *polarised* histogram which is then subjected to a running average over the analysis epoch.

The zero crossings of the running average provide estimates of the boundaries of the latency range of positive and negative peaks in the ERP. A nonparametric sign test at a specified confidence level is used to reject the null hypothesis that the samples in the latency ranges are drawn from a zero mean population (McGillem et al., 1981). In another report (Aunon and Sencaj, 1978), the parametric student's t-test is used instead, to test the hypothesis that the samples are drawn from a zero mean normal distribution. This procedure partitions the latency interval into regions of significant ERP component activity. For each significant region, the responses containing an identifiable peak in that region are aligned, so that peaks coincide. The latency-corrected waveforms are then averaged over a specified range in the vicinity of the peak, and the result is reproduced at the mean latency for that particular component.

Statistics of the latencies of the peaks in each LCA segment provide measures of component variability. Since the latency variability for each component is different, and there can be differences in the set of trials that contribute to the LCA of each component, the LCA of the whole waveform is reproduced as a series of disjoint LCA segments over time. Some components may be omitted if the significance tests failed to reject the null hypothesis.

For the two methods outlined above, it is not known in general how much error in latency measurements may be introduced. Simulation studies by the authors of method 2 suggest that reliable results are obtained for rms SNRs at or above 0.5 (-6 dB) and that relatively flat *polarised* histograms are produced with noise only data which can be readily distinguished from data with a signal content.

Ruchkin (1988) states that the ability of method 2 to cope with (a) multiple component variability and (b) not needing a starting cross-correlation template as with method 1, are the major criteria that will make method 2 a more satisfactory technique for dealing with variable latency data. Somehow, it was overlooked that there is still the need to specify a peak detection template, hypothesis testing significance levels, and component averaging ranges.

In a recent paper, the authors (McGillem et al., 1985) have reported an improvement to method 2 by converting the disjoint LCA segments into a smooth curve using least-squares fitting of power series (i.e. Chebyshev polynomials or Fourier series). However, where components were omitted in the LCA generation stage, the approximating functions behaved erratically and required the use of various compensation techniques. The compensations included the use of the conventional average as an approximation to missing components. Using invariant simulated data embedded in noise at different SNRs, the authors claim that the computed measures of latency variability are accurate to less than one sampling interval. This appears to suggest that computed variability measures using LCA are entirely due to the signal and not due to the ongoing EEG noise.

7.3 ERP Estimation by Digital Filtering

Averaging is a means of reducing additive noise interference. Noise attenuation can also be obtained using linear digital filtering techniques. Since linear filters are frequency selective, they can improve the SNR when the signal and the noise do not occupy the same frequency bandwidth and the noise model is additive. Filtering will not generally reduce variance in amplitude and latency of components when noise modulates the signal randomly (e.g. through random fluctuations in membrane potential and the metabolic state of the generator cells). The major benefits of simple linear filtering of ERP data are:

- A reduction in the number of trials used to obtain clear average responses thereby minimising the effects of habituation etc. and random noise modulation.
- Single trial measurements are possible in situations of high SNR and high frequency separation of signal and noise (e.g. with slow late waves associated with cognitive ERPs such as the N200 and P300).
- Digital filters can exhibit zero phase shift distortion and input data need not be irrevocably transformed.

The use of filters for smoothing the average ERP can be done on either the individual trials before summation or simply on the average alone. Both these will produce the same result since the operations of averaging and filtering are both linear. If an estimate of the latency variability of the filtered data is required, then the data must be filtered on a trial-to-trial basis because the variance computation is non-linear (Ruchkin, 1988).

There are three types of filters that are commonly used in ERP estimation. The first may be called *conventional* digital filters which achieve their action by computing a weighted sum of amplitudes over a finite range of adjacent sampled data points of the input. These are known as finite impulse response (FIR) filters (Lynn, 1971). The second are called *recursive* or *autoregressive* and are more sophisticated conventional digital filters that generate output values by operating on both the weighted input and previous output data points. These are known as infinite impulse response (IIR) filters (Lynn, 1977; Taylor and MacFarlane, 1974). Implementation of IIR and FIR filters requires the specification of the weighting function used. The discrete Fourier transform of the filter weighting function is the frequency transfer function of the filter. Therefore, one may use a rough knowledge of signal and noise spectra when formulating a filter weighting function. The main advantage of the above types of filter is the computational economy and the possibility of implementing these filters on-line. The main disadvantage is that the specification is largely

pragmatic and empirical. The filters are not optimal in the sense that noise interference is only reduced to a pre-determined minimum for stationary noise. In fact the noise and signal characteristics may change over time from one stimulus delivery to the next.

The third type of filter used in ERP estimation attempts to reach optimal noise rejection performance in each trial by minimising the expected mean square difference between the filter output and the actual signal. These *a posteriori* Wiener-like filters (McGille and Aunon, 1977; De Weerd and Martens, 1978; Ruchkin, 1988) assume that:

- both signal and noise processes have stationary statistics,
- signal and noise are uncorrelated,
- the analysis epoch is of infinite duration, and
- the power spectra of the signal and the noise are known exactly.

The transfer function of such filters $G(j\omega)$ is given by $S(j\omega)/(S(j\omega) + N(j\omega))$ where $S(j\omega)$ and $N(j\omega)$ are the power spectra of the signal and the noise respectively. From this relationship it is seen that $G(j\omega)$ attenuates heavily at frequencies where the noise power is greater than the signal power and approaches unity in the reverse situation.

The application of a posteriori Wiener-like filters (APWF) to ERPs is obviously less optimal than is suggested by the transfer function $G(j\omega)$ and the assumptions associated with its formulation. ERPs are transitory, generally having high frequency, short duration and short latency components and low frequency, long duration and long latency components. Furthermore, the analysis epoch is, of course, finite. The effectiveness of APWF is further limited by the fact that only the power spectrum $[S(j\omega) + N(j\omega)]$ is measurable directly. The individual component spectra must be estimated from the average spectrum of the individual trials and the spectrum of the average. DeWeerd (1981) points out that this method of spectral estimation is only valid for deterministic signals and is therefore at odds with the APWF assumptions again. Additionally, he states that the SNR must be high before the estimates can be considered close enough to the *true* signal and *true* noise spectra for a reliable determination of $G(j\omega)$. This situation can only occur with prolonged averaging of ERPs, which in turn decreases the initial need for APWF.

The transitory nature of an ERP results in the power contribution of high frequency and low frequency components being averaged over the entire analysis interval. This happens because the transients do not usually occupy the entire interval, and so the power is underestimated. DeWeerd (1981) has suggested the use of his time varying a posteriori filter (TVAP) to take into account the transient property and corresponding temporal power distribution of the ERP. TVAP has been formulated to operate on the averaged ERP only; hence it is intended exclusively for smoothing and cannot be used for latency variability measurements.

McGillem and Aunon, (1977) employ Wiener's minimisation of the squared error between the signal and its estimate in their MMSE filter (Sec.[7.2.2]). The MMSE filter derivation depends on the general Wiener assumptions already mentioned, apart from the finite duration of the ERP, which is accounted for. This filter was developed for use on single trial ERPs and not on average ERPs, and so it is possible to use it for latency variability investigations. Its use in this respect is adequate provided that the latency variability does not render the average ERP an invalid estimate of the single trial responses (Ruchkin, 1988).

No one is currently in a position to state which type of filtering technique discussed above is best for ERP estimation. Carlton and Katz (1980) and Boston (1983) have compared the performance of a posteriori filters and conventional digital filters. The results of these studies were obtained from simulations, somatosensory ERPs, and auditory brainstem ERPs, and indicate that the time invariant a posteriori filters are not, or are only marginally, better than conventional filters. TVAP may offer a better performance over conventional filters, but this remains to be seen (Ruchkin, 1988).

7.4 Computer Identification of Features in BAEPs

Some of the ideas behind the ERP estimation methods described above are the basis of automatic BAEP feature extraction techniques reported in the literature. Several researchers have attempted to analyse the average response to locate significant wave components (Gabriel et al., 1980; Fridman et al., 1982) without much success except in the simpler cases where the wave components can be visually separated. The common element in all these techniques is to maximise SNR in the average BAEP, thus making it sufficiently *clean* to be examined by an algorithmic peak detection processor.

The problem that one often faces is that the BAEP components can be embedded in residual noise thereby making the peak location inaccurate. Gabriel et al. (1980) filter their data using a quadratic, seven-point, least squares fit. They then use zero crossings in the derivative of the filtered data with time windows to locate and label (according to Jewett's (1970) classification) the BAEP features. The placement of these windows in time and their width is based on normal latency values obtained from the literature. It has been reported that a 98% peak detection accuracy for waves I, III and V can be achieved to within ± 2 sampling points with 65-75 dBHL BAEP data. They were unable to resolve the IV/V complex however, and go on to say that peaks that are not clearly defined in the average are still generally recognised as the *appropriate* peaks, even though they may not be labelled correctly. These inadequacies have not been considered to be a problem as they suggest (for normal data only) that their algorithm can be useful in training personnel in the identification of BAEP waves, and that it can provide a check against the judgement of experienced examiners. In our experience, the detection and localisation of BAEP waves requires additional knowledge besides that obtainable through an examination of the averaged response only. This is due, of course, to the variability of the data across trials.

Fridman et al. (1982) used an informal approach to the filtering of BAEP data before the detection of peaks. BAEPs were *optimally* filtered on a subaverage-to-subaverage basis. The total number of trials used was 2000 with each subaverage containing 200 trials. Fridman et al. reasoned that the SNR is largest over the frequency range in which the phase variance of the power spectra of single subaverages is the smallest. The same reasoning was applied to the ratio of the amplitudes of total averaged data and subaveraged data power spectra. The passband was defined to lie in the region of maximum SNR as determined by these criteria. Peak detection was done simply on an examination of the zero crossings of the derivative of the filtered sequence with no indication as to how the components were labelled correctly. It would appear from their results that exactly five components had to be found before being serially assigned the labels I-V. The filtering procedure was therefore being used, and relied upon, to extract the exact number of

components expected in a BAEP. It is difficult to see how such a technique can be used to resolve complex components and to distinguish between multiple peaks in the vicinity of any single component. Nevertheless, the resulting amplitude and latency statistics obtained from the filtered data were reported to be significantly more reliable than those obtained from unfiltered data.

In their paper on the evaluation of BAEPs using dynamic time warping (DTW), Picton et al. (1988) give a brief insight into the true complexity associated with the automatic selection of BAEP components. Their DTW technique provides a simple means of demonstrating differences between waveforms by stretching or shrinking portions of one temporal sequence to make it similar to another reference sequence. The reference template waveform was constructed from the hierarchical combination of pairs of normal BAEPs by DTW. This normal template is then used to assess the morphology of test BAEPs by determining the amount of warping necessary to fit the test BAEP to the normal template. Distortion measures obtained from this procedure are then used in conjunction with the location of peaks in the normal template to identify peaks in the test BAEP.

Picton et al. used three approaches to identify peaks of the BAEP: First, manual peak identification was used, which, as the authors' quite rightly state, is simple to perform and quite difficult to describe. However, in normal waveforms, waves I, III, and V were identified as follows:

- Wave I was identified as the most prominent peak after 1.2 msec and before the waveform moved negatively towards the baseline.
- Wave III was the first prominent peak occurring at least 1.5 msec after wave I.
- Wave V occurred at least 1.3 msec after wave III as the most prominent positive wave or the second of two prominent positive waves or the last positive wave prior to the waveform moving negatively towards the baseline. This disjunction of conditions is probably an attempt by the authors' to *home-in* on the elusive wave V in the possible presence of a wave IV/V complex and/or early wave VI.
- The procedure is complemented with an identification of the waves in the reverse direction in time, starting with wave V as the most prominent positive peak preceding the most prominent negative-going shift in the waveform after 5.0 msec.

In cases of ambiguity, additional information was obtained from a comparison between the ipsilateral and contralateral recordings. Additionally, the effects of changing the stimulus intensity or rate of stimulation were used to determine the exact location of the waves. Wave V should remain visible and shifted towards a longer latency at lower intensities and faster rates (Sec.[6.2.2]). Waves I and III are larger in the ipsilateral recording and wave I is readily observed at high intensities and slower rates.

The second peak detection approach adopted by Picton et al. was that of Fridman et al. (1982) using zero crossings of the filtered BAEP. This method has already been described above. Finally, the DTW technique was used against a normal template.

Results of the second and third approaches measured against the manual approach in 96 normal BAEPs showed that the zero crossing method obtained errors of 1%, 3% and 26% in the detection of waves I, III, and V respectively. The DTW approach produced corresponding errors of 0%, 2%, and 26%. In 40 abnormal BAEPs, the error values were 3%, 13% and 60% for the zero crossing method and 5%, 3%, and 18% for the DTW method. The most common errors for the DTW method were cited as being the selection of wave VI instead of wave V, the selection of the second wave in bifid components, the inability to resolve the IV/V complex, and the inability to distinguish between cochlear-microphonics (Sec.[6.2.2]) and wave I. The most common errors encountered in the zero crossing method were as suggested in the description given above.

Many approaches to BAEP peak identification do not examine responses at the single-trial or small subaverage level to reject artifacts which will affect the identification process. The rejection of artifactual activity is important (Schulman-Galambos and Galambos, 1975), and is normally performed manually by simply halting data acquisition whilst observing the accumulation of the average on the CRT screen. The removal of offending trials should be performed on an automatic basis when considering computer-based peak identification.

Feature extraction in BAEPs using the procedural (algorithmic) or deterministic techniques encountered in the discussions so far, seems unlikely to attain the levels of reliability necessary for routine clinical use. The complexity involved must suggest a re-evaluation of the decision models used. The complexity will obviously increase in situations of abnormal morphology of the waveform, where irregular shifts in the latency of components, multiple components, and/or the absence of components can occur. A problem exists in the special case of BAEP feature identification because the qualitative information contained in the BAEP is difficult to describe quantitatively. A personal view is that in order to allow the analysis of BAEPs to provide both qualitative as well as quantitative information, it is necessary to couple the powerful algorithmic techniques available on the one hand, with symbolic interpretation techniques on the other. This view also applies to other ERPs. The algorithmic methods can be used to extract quantitative values and symbolic descriptors of the data. These symbolic descriptors can then serve as the database of facts upon which a *knowledge-based system* (KBS) will perform reasoning for qualitative interpretation of the data.

Research work that will be described in the next chapter addresses the problems associated with BAEP analysis with the above thoughts in mind. A method called 'Event Analysis' has been developed to identify and characterise the important waves contained in the BAEP. In this study, wave components are identified by analysing the ensemble of responses that comprise the averaged BAEP. The results from a group of analysis procedures are then interpreted by a prototype knowledge-based, or as it is sometimes called, expert system. This *expert system* (ES) contains some of the subjective methods of decision making that a human expert might use to locate the *best* possible position of wave components (see Appendix [C1]).

The foregoing discussions have pointed out some of the important underlying characteristics of the BAEP that are of interest to the clinician, mainly with respect to the extraction of the latency variability of wave components. 'Event Analysis' provides these quantitative statistics. Additional information using these statistics is inferred for the construction of new average waveforms. The new averages are obtained by separating single trials into homogeneous sets of those trials which contain specific combinations of significant peaks. The selection of the group of significant peaks in the initial set is currently performed manually. Ultimately, this initial set will comprise those peaks that have been selected by an enhanced and validated version of the prototype ES.

The author's first thoughts on the implementation of an ES were directed towards the interpretation of quantitative results from some standard and widely used EMG and/or EP analyses. The large amounts of data and qualitative results available for normal subjects, made these areas good candidates to commence investigations involving the *intelligent* interpretation of the results from various analyses. Later, it became apparent, through the author's work on BAEP analysis, that an ES approach could be used for qualitative BAEP feature extraction and interpretation. The ideas that are behind the prototype that was constructed, can nevertheless be applied in simple EMG data interpretation. Moreover, the techniques of Artificial Intelligence that are now available, can be applied to the planning of EP and EMG data analysis procedures (Fuglsang-Frederiksen and Jeppesen, 1987; Andreassen et al., 1987).

The implementation of the prototype ES for BAEP interpretation (called EPAXIS) was carried out at the Turing Institute (Glasgow, Scotland) during a period of secondment from Leicester University between October 1987 and January 1988. The system was implemented in Quintus Prolog (Ver. 2.0) under Unix BSD 4.2 on a Sun Microsystems 3/50 minicomputer. It was later ported onto an IBM PC-AT in SD-Prolog (Ver. 1.2) under MS-DOS 3.30 (Appendix [C2]). The research work conducted at the Institute is reproduced in the publication included in Appendix [C1]. What follows is a brief description of knowledge-based system techniques, some of which were used in the construction of the prototype ES. This description should help to clarify

the implementation details contained in Appendix [C1]. A similar description was included in a specification for expert system techniques in quantitative EMG analysis for the EMG-equipment manufacturer Medelec Ltd (Woking, Surrey) in 1985.

7.5 General Knowledge-Based System Concepts

Knowledge-based systems behaving in an apparently intelligent way have evolved over the last decade (Kulikowski, 1980). Both KBSs and conventional computer programs have knowledge about the problem domain and information on how to manipulate that knowledge. The distinction lies in the manner of representation of the knowledge used. Conventional programs have *implicit* knowledge, that is *usually* opaque, about domains that are static and formalised. KBSs have *explicit* knowledge, that is transparent, about domains that are *usually* subjective and judgemental. Central to a KBS is an inference mechanism which uses the knowledge contained in the knowledge-base (KB) to reason about the problem domain. The explicit separation of knowledge from inference provides flexibility and enhanced transparency, especially in terms of altering or modifying the systems behaviour.

A classification of KBSs due to Hayes-Roth and Waterman (1979), suggests two distinct types of KBS, namely, rule-based and network-based systems. There is nothing rigid in this classification scheme, and indeed it is quite common to combine these two models of knowledge representation and their principles in the construction of specific KBSs.

7.5.1 Rule-Based Systems

Problem solving and intelligent, expert-like behaviour can be simulated to a certain degree using if-then type rules of the form:

IF (antecedent) THEN (consequence), or

IF certain facts are known to be true (or false)
THEN arrive at an appropriate conclusion.

These are also known as production systems. Problem solving can be thought of as a transition from a specified state to a goal state through application of rules governed by a strategy. To implement a production system three types of knowledge are necessary. First, *declarative* knowledge is the facts pertaining to the problem domain. Second, *procedural* knowledge provides the basis for manipulating the state descriptions, and finally, *control* knowledge specifies how such manipulations can be effected. Sometimes, however, it is not easy to distinguish between procedural and control knowledge.

If the control strategy of a system is:

(a) start with a collection of facts (declarative knowledge),

- (b) apply all the applicable rules related to the known facts (using procedural knowledge and directed by control knowledge),
- (c) derive new facts and eventually the solution to the problem,

then the system is said to have adopted a data-directed or forward chaining inference. Goal-directed or backward chaining starts with an unproven hypothesis and attempts to match this with the facts known about the problem. The rules in the KB are in fact used to derive more information about their premises.

Another aspect of the control strategy involves the type of search technique adopted in matching the facts and knowledge about the facts. Search techniques commonly used are breadth first, depth first, and a combination of both using heuristic pruning. Heuristic pruning involves an examination of the current search path and obtaining some measure of confidence for it. The measure of confidence is sometimes specified using basic common sense reasoning or rules-of-thumb. If the confidence measure at the current node in the search path falls below a threshold, then all solutions below this node are eliminated, and the search continues along another path from a node higher up in the search space.

The classic example of an if-then type production system is MYCIN which was developed for the diagnosis of infectious diseases (Shortliffe, 1976; Shortliffe et al., 1979). MYCIN is a backward-chaining deduction system. The primitive facts in MYCIN are stored as triples in the form (Context - Parameter - Value). A *context* is some real-world entity that the system is currently reasoning about, for example, it may be an *organism* of sorts. A *parameter* is an attribute of the context, such as *identity* or *strain*. The *value* is an instance of the parameter, for example, it might be the *actual name* of the organism such as *streptococcus*. With each triple there is an associated certainty factor (CF) with a value between -1 (negation) and +1 (certainty). A rule premise contains a conjunction of triples, and each rule will have a CF attachment to its conclusion. At the start of a consultation there will be many triples in the knowledge base, some of which will have empty values. Certain triples represent the goals of the consultation and these will obviously be unfilled at the start. MYCIN begins with a list of possible diagnoses and uses the production rules to work towards the primitive facts. Eventually, primitive facts which are known, from clinical observations and laboratory results, enable the empty ones to be instantiated (i.e. filled). MYCIN uses a theory of inexact reasoning to obtain cumulative CFs for each conclusion made through the invocation of premises in a rule. These CF calculations are discussed later in Sec.[7.6.1].

A context tree is used as part of the control strategy to specify the organisation of knowledge. The system can explain its conclusions by examining both the context tree and the individual rules that have been used to infer the conclusions. Use of MYCIN-like systems has highlighted some of the

problems related to human engineering. MYCIN-type rules can cope with a degree of uncertainty in their rules and factual base, but it is difficult to extend the rules and facts to reflect any uncertainty that may occur in quantified variables (Nilsson, 1980). Finally, it is not easy to express a given piece of knowledge in the form of a rule, and the meaning of some of the rules in the system may not be immediately comprehensible to an uninitiated user, even when such rules are coded in English.

7.5.2 Network-Based Systems

An example of a network-based system is PROSPECTOR (Duda and Hart, 1977). It was developed to assist field geologists in the evaluation of sites for the existence of certain ore deposits, and for the selection of favourable drilling locations. The knowledge in PROSPECTOR is captured in a series of hierarchical models consisting of spaces, which are in turn connected by rules to form a network. The concept of a *space*, is simply a place holder for some evidence or a hypothesis. Each space has an a priori probability value indicating how true it is. At the start of a run these probabilities are usually low. The rules connecting the spaces specify how the probability values are propagated from one space to the next as the run proceeds and evidence is accumulated up the network. The network rules in PROSPECTOR may be logically combined. In comparison to, say MYCIN, the lower spaces in the hierarchy can be likened to the premise part in a production, and the higher spaces can be likened to the action part. Similarly, the connecting rules between spaces can be likened to the mechanism for inexact reasoning.

The implementation of inexact reasoning in PROSPECTOR involves the computation of rule strengths which are defined by likelihood ratios for sufficiency (LS) and necessity (LN) (see Sec.[7.6.2]). PROSPECTOR does not create new spaces in the same way as MYCIN will create new facts using its rules. The system is concerned solely with the propagation of probability values through the network of spaces constituting its models. Also, the inference network has no understanding of the context of the rules and the geological relationships between spaces. Therefore, PROSPECTOR uses a classification of minerals in the form of a semantic net to enable it to perform associative deductions. For example, the user will not be consulted about the implications of the presence of sulphides, when it has already determined some information on pyrite (as pyrite is a member of the sulphide group). The top level structure of PROSPECTOR is thus a collection of spaces forming the nodes of an inference network. At the lower level is the semantic net, with its nodes contained within the spaces if they are unique to the spaces, or with its nodes appearing outside the spaces if they can be referred to by other statements.

Some systems attempt to arrange the knowledge in the task domain into several distinct *chunks* or frames of knowledge. A frame may be thought of as a collection of rules all of which relate to a particular aspect of a problem. Frames are then linked in a network that encompasses the entire problem domain.

PIP (Present Illness Program) is a frame-based system developed at MIT providing expert advice in the diagnosis of renal diseases and related disorders (Szolovitz et al., 1978). Knowledge in this system is organised in frames. A frame in PIP contains all the information related to a particular hypothesised disease. The information in these frames is typically:

- *Triggers* which activate the hypothesis frame.
- A set of *findings* linked by rules characterising the disease state.
- A set of *relations* describing the inter-relationships between different frames, e.g., information as to whether the current state can be complicated by other disorders.
- A section where conflict resolution is effected.
- A section where an estimate of likelihood for the current frame is calculated.

PIP maintains a matching and a binding score. The former determines the degree of congruence between observed findings and expected values. The latter is just a ratio of the expected number of findings for the current hypothesis to the total number of reported findings. These scores are then combined to give a local score. Finally the local score is updated to reflect the effect of other frames on the current frame and to give a likelihood estimator for the frame. A hypothesis frame is activated if the conditions specified in the frame trigger are satisfied. The hypothesis frame can be in the active, semi-active or inactive state, depending on the value of the binding score.

Another frame-based system which has had impressive success is INTERNIST, the computer consultant for internal medicine (Pople and Myers, 1974). In INTERNIST, every diagnosis D_i has a set of manifestations $\{M_j\}$. These M_j are associated with an *evoking strength* and a *frequency* count. The evoking strength ($L[di / mi]$) is defined as a number in the range 0-5 characterising the likelihood of disease D_i causing manifestation M_j . The frequency count is the likelihood that a patient having disease D_i exhibits manifestation M_j . The control strategy for this system lies in an exhaustive search of the disease hierarchy. A heuristic measure of the reliability of the diagnosis reached is computed based on evoking strength, frequency count, manifestations explained and/or unexplained by the current or other frames (Szolovitz et al., 1978). Frame-based systems are better at capturing the causal reasoning mechanisms which model the human way of thinking than say, if-then systems. Frame-based systems are also referred to as semantic networks.

CASNET is a causal associated network for diagnosing disease states in glaucoma (Kulikowski, 1980). The network nodes in CASNET consist of real, physiologically distinct, states. A set of tests provide evidence and likelihood as to which one of the dysfunctional states the patient is in. Some of the nodes are termed the starting states, and some the final states. Causal connections between nodes are represented as links, with link strengths specifying the likelihood of one node being causally responsible for another node. For every node a number called the *status* of the node is computed based on simple tests. The node is confirmed or denied depending on the value of this status. A *weight* value is also computed which for each node, provides the strength of the causal associations of the nodes under consideration to all its surrounding confirmed and denied nodes. An acceptable path in the network is a path connecting any starting node to any final node which does not contain any denied nodes. This path constitutes the diagnosis, and the nodes in the path hold the explanations of the diagnosed disease state. The control strategy here attempts to confirm nodes and find an acceptable path based on the weight value computed for nodes.

The approach taken by the author to interpret results from event analysis is a combination of rule-based system techniques and knowledge representation in frames. This has resulted in a suite of programs called EPAXIS that reason with symbolic information generated by the analysis programs. The frames of knowledge contain certainty factor attachments which are propagated through the inference network using methods derived from fuzzy logic (Zadeh, 1979). Further details of this reasoning mechanism are given in the next section.

7.6 Inexact Reasoning in Expert Systems

The knowledge-based systems presented so far all use some form of inexact reasoning and heuristics. The reasons for this are threefold:

- (i) The data and knowledge is unreliable.
- (ii) The data and knowledge is not static.
- (iii) The search space for solutions is potentially very large.

With ideal and/or simple KBSs, the knowledge and data do not lead to false, inexact, or tentative conclusions. Once conclusions have been made by such a system, there is no need to modify or retract facts in the light of new information (i.e. the system is displaying monotonic reasoning). In real-world applications data can be noisy and error-prone due to extraneous measurements and missed observations. Additionally, the knowledge captured in the system can be ill-specified in terms of its consistency and correctness. A single line of reasoning, not supporting multiple arguments and multiple conclusions, is therefore inadequate for many *ill-conditioned*, i.e. heuristic, tasks.

Many systems which employ heuristics defend their methodology only on the basis of the results they have produced. The approaches have been criticised for being unnecessarily fabricated. For example, MYCIN's own formalism for reasoning with uncertainty could have been replaced by the thoroughly studied Bayes' theorem. Bayes' rule could be used to calculate the probability of a disease given some evidence from the a priori probability of the disease and the conditional probabilities relating the observations to the diseases (Stefik et al., 1983). The amounts of data being considered are so large, however, that conditional independence of observations must often be assumed. The need to resort to an assumption of independence is often seen to undermine the merits of the rigorous statistical model (Stefik et al., 1983). The PROSPECTOR system seeks a compromise by replacing the observations with subjective estimates of prior probabilities.

Another approach to inexact reasoning that is divergent from classical predicate logic is fuzzy logic (Zadeh, 1979). Zadeh's theory of approximate reasoning provides characterisation of linguistic variables, e.g. high amplitude, mild polyphasicity, early latency etc., by a mapping of the numerical values of the variables in a fuzzy set into corresponding *possibility* values. For example the fuzzy proposition *X has high amplitude* is characterised using the fuzzy set:

- ($X \in (0,10)$), 0.1)
- ($X \in (10,100)$), 0.3)
- ($X \in (100, \infty)$), 0.7)

The interpretation of the proposition *X has high amplitude* is then taken to be *X may be less than 10* with a possibility 0.1 of having a high amplitude, between 10 and 100 with a possibility 0.3 of having a high amplitude, and so on. The possibility value has no direct relationship to a probability value. Conceptually, it represents the degree of certainty with which the value of an attribute is believed to be true. The possibility value is usually determined from a continuous function related to the (fuzzy) set of values for an attribute (variable). There will be more said about fuzzy sets in Sec.[7.6.2].

We will now consider briefly the mechanisms of inexact reasoning implemented in MYCIN and PROSPECTOR. This will be followed with a description of the fuzzy reasoning mechanism that was implemented in the prototype ES described in Appendix [C1].

7.6.1 Certainty Factor Calculations in MYCIN

When MYCIN makes a conclusion using its rules, a primitive fact will be added into its dynamic database together with a computed certainty factor for this fact. This certainty factor (CF) is computed from:

- (i) the combined certainty factors of the individual clauses in the rule premise,
- (ii) the certainty factor attachment of the rule, and possibly from the
- (iii) certainty factor of the original primitive fact if it existed already in the dynamic database.

The operation performed in (i) is simply the minimum CF of the premise clauses. This is multiplied by the CF attachment of the rule to give a certainty factor CR. CR is stored together with the primitive fact in the conclusion provided the conclusion does not already exist. If the conclusion already exists with a certainty factor of CI, then the computation in (iii) is done as follows:

$$CF = CI + CR(1 - CI) \quad \text{for } CR, CI > 0.$$

$$CF = -(|CI| + |CR|(1 - |CI|)) \quad \text{for } CR, CI < 0.$$

$$CF = \frac{CI + CR}{1 - \min(|CI|, |CR|)} \quad \text{for } CI, CR < 0, |CR|, |CI| \neq 1.$$

$$CF = 1 \text{ with a combination of } 1 \text{ and } -1 \text{ for } CR, CI.$$

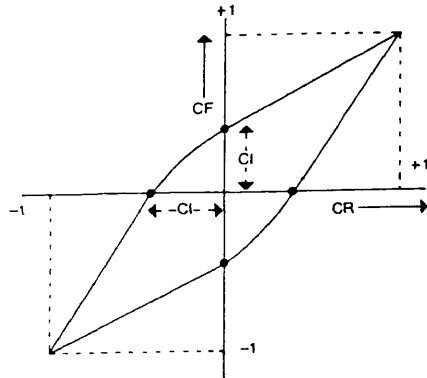


Fig.[7.1(a)] Certainty factor interpolation in MYCIN.

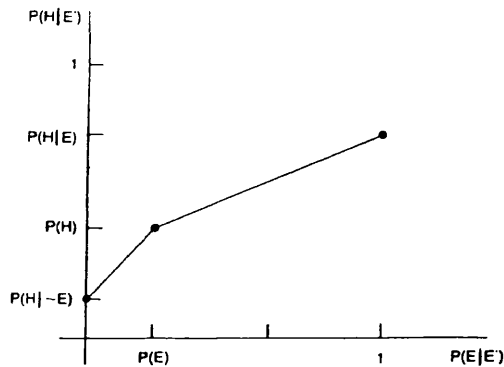


Fig.[7.1(b)] Piecewise linear interpolation for dealing with uncertain evidence in PROSPECTOR.

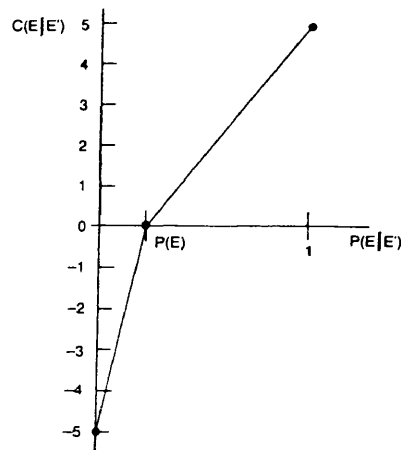


Fig.[7.1(c)] The relationship between user-input certainty values and probability values used to calculate the odds allocated to hypothesis spaces (i.e. using the relationships for (b)).

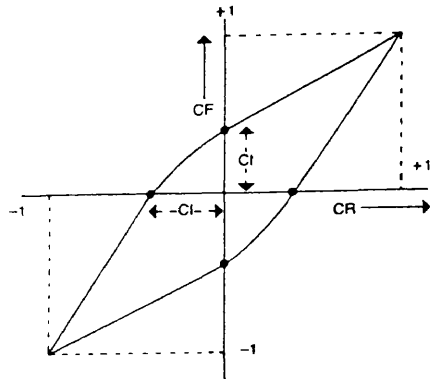


Fig.[7.1(a)] Certainty factor interpolation in MYCIN.

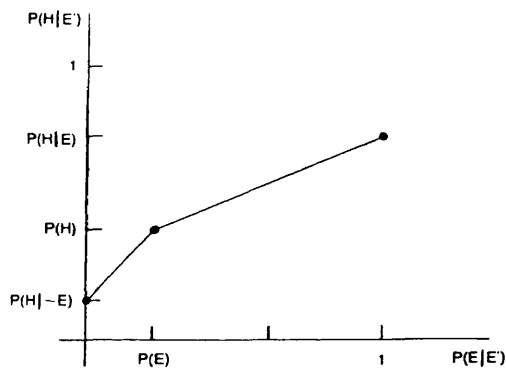


Fig.[7.1(b)] Piecewise linear interpolation for dealing with uncertain evidence in PROSPECTOR.

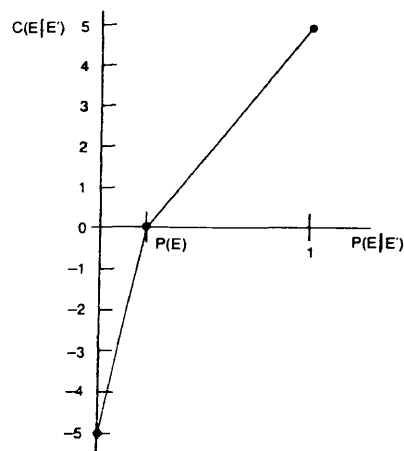


Fig.[7.1(c)] The relationship between user-input certainty values and probability values used to calculate the odds allocated to hypothesis spaces (i.e. using the relationships for (b)).

Using these formulae, MYCIN is able to cope with non-monotonic judgemental reasoning. Shortliffe (1976), provides a formalised description of the epistemology which is loosely based upon Bayes' theorem. The variation in the computed CF is shown in Fig.[7.1(a)], (Alty and Coombs, 1984).

7.6.2 Uncertainty in PROSPECTOR

As we have seen already, PROSPECTOR, has a rule strength between spaces using the LS and LN ratios. LS and LN measure the degree to which a change in probability of one space will affect the probability of another. One way to visualise this arrangement is in terms of source spaces and target spaces. The source spaces contain facts used as evidence at lower levels in the PROSPECTOR model hierarchy, and the target spaces contain hypotheses at higher levels in this hierarchy. The target spaces are, in turn, the source spaces for higher level spaces, and so on. The top level of the hierarchy represents the goal of the model. This interpretation then reduces to a production rule representation having probabilistic attachments through the rule strength formalism; a vague similarity with a rule-based system is evident.

The propagation of probability values in the model is driven by Bayes' theorem relating the hypotheses H to the evidence E:

$$P(H|E) = P(E|H) \cdot \frac{P(H)}{P(E)} \dots \dots \dots \text{Eq.[7.1]}$$

where $P(H|E)$ is the conditional probability of H being true given E, and $P(E|H)$ is the conditional probability of E existing given H. $P(H)$ and $P(E)$ are the prior probabilities of H and E respectively; these being estimated by the expert during the formulation of a PROSPECTOR model. Given that $P(\text{not } X) = P(\sim X) = 1 - P(X)$, it can be shown that:

$$P(\sim H|E) = P(E|\sim H) \cdot \frac{P(\sim H)}{P(E)} \dots \dots \dots \text{Eq.[7.2]}$$

Dividing Eq.[7.1] and Eq.[7.2] gives:

$$\frac{P(H|E)}{P(\sim H|E)} = \frac{P(E|H)}{P(E|\sim H)} \cdot \frac{P(H)}{P(\sim H)}$$

therefore, if odds $O(X) = P(X)/(1 - P(X))$ then:

$$O(H|E) = \frac{P(E|H)}{P(E|\sim H)} \cdot O(H) \dots \dots \dots \text{Eq.[7.3]}$$

or, this equation may be rewritten as:

$$O(H|E) = LS \cdot O(H)$$

which is the odds version of Bayes' theorem and relates, through the likelihood ratio LS, how the odds of H change with an observed true E. Similarly:

$$O(H|\sim E) = LN \cdot O(H)$$

informs us how to calculate the new odds of H given that E is definitely untrue using the likelihood ratio LN.

LS and LN therefore provide a means of changing the prior odds of H if E is true and E is untrue respectively. One or the other is used as the rule strength depending upon whether E is true or untrue. They are related by the equation:

$$LN = \frac{(1 - LS \cdot P(E|\sim H))}{(1 - P(E|\sim H))} \dots \dots \dots \text{Eq.[7.4]}$$

and generally $1 \leq LS \leq \infty$ and $0 \leq LN \leq 1$ so that, for example, statements like: *if there is fire then there is smoke* can be made with a reasonable amount of certainty. A problem does exist however, since one may want to state that *the presence of E will increase the odds on H, but the absence of E will have no effect*, i.e. in this case $LS > 1$, and $LN = 1$ which is inconsistent with Eq.[7.4] and probability theory. PROSPECTOR, nevertheless, has methods of dealing with this inconsistency.

The decision to use either LS or LN depends on whether or not E or $\sim E$ are known with certainty. This is not usually the case, and in a perfect world it would be dealt with by a linear interpolation (Alty and Coombs, 1984). If E is known to be true with evidence E', e.g. $P(E|E')$, then:

$$P(H|E') = P(E|E') \cdot P(H|E) + (1 - P(E|E')) \cdot P(H|\sim E)$$

One problem with this linear interpolation approach, is that when the network is set up, all nodes are assigned prior odds. Since LN and LS relate the prior odds across the network, an expert would have great difficulty in setting up a completely consistent network. The model building experts usually give the prior odds of nodes and the LN, LS values in a subjective manner. Thus the network will usually be mathematically inconsistent. If E' is the evidence that causes the user to suspect the presence of E, then the probability of H will be altered to $P(H|E')$. This will be between $P(H|\sim E)$ and $P(H|E)$. If $P(H|E')$ has the value 0 then $P(H|E')$ should be $P(H|\sim E)$.

When $P(E|E')$ has the value 1, $P(H|E')$ should have the value $P(H|E)$. If, however, we know nothing about E (i.e. $P(E|E') = P(E)$) then the prior odds on H should not change. Thus $P(H|E') = P(H)$. These three points give us the relationship between $P(H|E')$ and $P(E|E')$ as shown in Fig.[7.1(b)].

This technique in PROSPECTOR overcomes the problem of inconsistent LN, LS and prior odds assigned to the network by the expert, thereby eliminating erroneous propagation of probabilities. It yields the relationships below for the piecewise approximations in Fig.[7.1(b)]:

$$P(H|E') = P(H|\sim E) + \frac{(P(H) - P(H|\sim E))}{P(E)} \cdot P(E|E')$$

for $0 \leq P(E|E') \leq P(E)$, and

$$P(H|E') = P(H) + \frac{(P(H|E) - P(H))}{(1 - P(E))} \cdot (P(E|E') - P(E))$$

for $P(E) \leq P(E|E') \leq 1$.

The same piecewise approximation technique is used to map user input probability values to the prior odds allocated to the spaces that prompt for that user input. The user supplies a certainty factor $C(E|E')$ between 5 (the queried value is definitely true) and -5 (definitely not true). A value of 0 for $C(E|E')$ has no effect on the prior probability, and the extreme values force the probability to 1 or 0.

The graph of $C(E|E')$ against the prior probability $P(E)$ is shown in Fig.[7.1(c)]. The piecewise approximation relationships are:

$$P(E|E') = P(E) + \frac{C(E|E')}{5} \cdot (1 - P(E))$$

for $C(E|E') > 0$, and

$$P(E|E') = P(E) + \frac{C(E|E')}{5} \cdot P(E)$$

for $C(E|E') \leq 0$.

Suppose the user supplied the value of 3 for the certainty of a piece of evidence E which had a prior probability $P(E) = 0.6$ in the PROSPECTOR network. The adjustment made to the prior probability would then be $0.6 + (3/5)(0.4) = 0.44$.

or, this equation may be rewritten as:

$$O(H|E) = LS \cdot O(H)$$

which is the odds version of Bayes' theorem and relates, through the likelihood ratio LS, how the odds of H change with an observed true E. Similarly:

$$O(H|\sim E) = LN \cdot O(H)$$

informs us how to calculate the new odds of H given that E is definitely untrue using the likelihood ratio LN.

LS and LN therefore provide a means of changing the prior odds of H if E is true and E is untrue respectively. One or the other is used as the rule strength depending upon whether E is true or untrue. They are related by the equation:

$$LN = \frac{(1 - LS \cdot P(E|\sim H))}{(1 - P(E|\sim H))} \dots \dots \dots \text{Eq.[7.4]}$$

and generally $1 \leq LS \leq \infty$ and $0 \leq LN \leq 1$ so that, for example, statements like: *if there is fire then there is smoke* can be made with a reasonable amount of certainty. A problem does exist however, since one may want to state that *the presence of E will increase the odds on H, but the absence of E will have no effect*, i.e. in this case $LS > 1$, and $LN = 1$ which is inconsistent with Eq.[7.4] and probability theory. PROSPECTOR, nevertheless, has methods of dealing with this inconsistency.

The decision to use either LS or LN depends on whether or not E or $\sim E$ are known with certainty. This is not usually the case, and in a perfect world it would be dealt with by a linear interpolation (Alty and Coombs, 1984). If E is known to be true with evidence E', e.g. $P(E|E')$, then:

$$P(H|E') = P(E|E') \cdot P(H|E) + (1 - P(E|E')) \cdot P(H|\sim E)$$

One problem with this linear interpolation approach, is that when the network is set up, all nodes are assigned prior odds. Since LN and LS relate the prior odds across the network, an expert would have great difficulty in setting up a completely consistent network. The model building experts usually give the prior odds of nodes and the LN, LS values in a subjective manner. Thus the network will usually be mathematically inconsistent. If E' is the evidence that causes the user to suspect the presence of E, then the probability of H will be altered to $P(H|E')$. This will be between $P(H|\sim E)$ and $P(H|E)$. If $P(H|E')$ has the value 0 then $P(H|E')$ should be $P(H|\sim E)$.

When $P(E|E')$ has the value 1, $P(H|E')$ should have the value $P(H|E)$. If, however, we know nothing about E (i.e. $P(E|E') = P(E)$) then the prior odds on H should not change. Thus $P(H|E') = P(H)$. These three points give us the relationship between $P(H|E')$ and $P(E|E')$ as shown in Fig.[7.1(b)].

This technique in PROSPECTOR overcomes the problem of inconsistent LN, LS and prior odds assigned to the network by the expert, thereby eliminating erroneous propagation of probabilities. It yields the relationships below for the piecewise approximations in Fig.[7.1(b)]:

$$P(H|E') = P(H|\sim E) + \frac{(P(H) - P(H|\sim E))}{P(E)} \cdot P(E|E')$$

for $0 \leq P(E|E') \leq P(E)$, and

$$P(H|E') = P(H) + \frac{(P(H|E) - P(H))}{(1 - P(E))} \cdot (P(E|E') - P(E))$$

for $P(E) \leq P(E|E') \leq 1$.

The same piecewise approximation technique is used to map user input probability values to the prior odds allocated to the spaces that prompt for that user input. The user supplies a certainty factor $C(E|E')$ between 5 (the queried value is definitely true) and -5 (definitely not true). A value of 0 for $C(E|E')$ has no effect on the prior probability, and the extreme values force the probability to 1 or 0.

The graph of $C(E|E')$ against the prior probability $P(E)$ is shown in Fig.[7.1(c)]. The piecewise approximation relationships are:

$$P(E|E') = P(E) + \frac{C(E|E')}{5} \cdot (1 - P(E))$$

for $C(E|E') > 0$, and

$$P(E|E') = P(E) + \frac{C(E|E')}{5} \cdot P(E)$$

for $C(E|E') \leq 0$.

Suppose the user supplied the value of 3 for the certainty of a piece of evidence E which had a prior probability $P(E) = 0.6$ in the PROSPECTOR network. The adjustment made to the prior probability would then be $0.6 + (3/5)(0.4) = 0.44$.

One last point to consider is the logical combinations of probability values between the spaces in the PROSPECTOR model. Combination with the logical operators AND, OR, and NOT is effected using Fuzzy Set theory (Zadeh, 1979). For AND, the minimum probability is taken. For OR, the maximum probability is taken, and NOT simply negates the probability.

7.6.3 Fuzzy Certainty Factor Calculations in EPAXIS

EPAXIS is an acronym for EP Analysis and eXpert Interpretation System. It is a suite of programs used to automatically score the auditory brainstem evoked potential. The expert system part is provided in Appendix [C1] and the (event) analysis part is will be described in the next chapter. EPAXIS uses fuzzy certainty factors for its uncertainty mechanism, mainly because the fuzzy sets used, can be specified easily from the normative values of latency variability quoted in the literature. Usually the numbers of the fuzzy set will be normally distributed about their central value since this is expected when a measurement is subject to a large number of small disturbances. Therefore, using two terms (i.e. the mean and standard deviation), permits the error specification to be invariant for many types of measurement. This is an important advantage in EP analysis. Bayes' theorem, as we have seen, is difficult to implement because of the need to supply prior probabilities. Medelec Ltd. have conducted their own normal data study with the aid of the event analysis program, and these values will be substituted into EPAXIS in the future.

In Sec.[7.4] some methods of feature identification in BAEPs were discussed. The techniques produced results that provided no sensitivity and specificity information for latency labels of the features detected. In some cases it was even possible to allocate the wrong labels to features; this being confirmed visually after the fact. Unfortunately, this approach is unsatisfactory because it would be difficult to express the degree of pathology connected with the features in the BAEP using their latency values. There is also no way to incorporate provision of a set of features that fit the selection criteria for a particular BAEP component. Since manual feature selection can be highly judgemental, providing such possibilities in a system for feature selection might be more acceptable to a clinician.

The rules that EPAXIS contains are modelled on the judgemental processes that an expert uses for BAEP scoring. The data provided by event analysis are examined by EPAXIS rules in the early stages of a goal-directed reasoning process. Candidate choices for features are given fuzzy values which are propagated through the search space towards the final goal of finding waves I-IV. Hence, the quantitative results are easily assigned qualitative descriptions for the system to reason with.

The method by which fuzzy values are assigned to the data relies on the definition of a fuzzy model for the normal brainstem potential. The model is described next, and in fact is comprised of two parts, namely, the procedural and the declarative model components.

[A] The Fuzzy Procedural Model (Database)

The fundamental primitive for information modelling is propositional statements of the form: *an attribute of an object has a particular value*. This is represented in the Prolog language as the symbolic structure:

Object Attribute Value.

We may express that *a component wave of the BAEP occurs at position X* by writing:

Wave position_is X.

As soon as *Wave* does not occur exactly at *X* then we have introduced an amount of imprecision, where *X* does not exactly reduce to one element in the domain U_{Wave} (universe of discourse) of the variable *Wave*. *X* is then the set of mutually exclusive possible values for *Wave*. In the imprecise proposition above, the set *X* may not have clear boundaries. Then *X* is what Zadeh (1979) has named a fuzzy set and *Wave position_is X* is said to be a fuzzy proposition. A fuzzy set *X* say, is described by means of a membership function μ_X . This is a function mapping from the domain U_{Wave} to the interval [0,1]. A value of 1.0 represents full membership and a value of 0 represents non-membership. Intermediate values of μ_X for U_{Wave} represent partial membership.

The fuzzy set (Π_X) of values which the results of event analysis (*X*) can take for a wave component (*Wave*) in the domain of BAEP waves (U_{Wave}), is given uniquely by the fuzzy membership function (μ_X). The membership function for the domain U_{Wave} is shown in Fig.[7.2]. This is termed the *fuzz function* and enables assignments of reliability or *fuzz* to the results of the event analysis algorithm and the peaks in the averaged BAEP response.

Referring to Fig.[7.2], peaks in the bin segment shown, have their *fuzz* computed by a simple interpolation through a mapping of their times of occurrence onto the *fuzz function*. For example, the bin peak at 'B' maps to a *fuzz* of 1.0 indicating full membership of *X* in U_{Wave} and 'A' maps to a *fuzz* of 0.8 indicating partial membership of *X* in U_{Wave} .

Zadeh also calls Π_X the possibility distribution. Its identification can be subjective since the definition of μ_X can be subjective. The importance of this distribution is the order it imparts on the domain U_{Wave} and it should contain all possible values of *Wave*. In this application, μ_X has

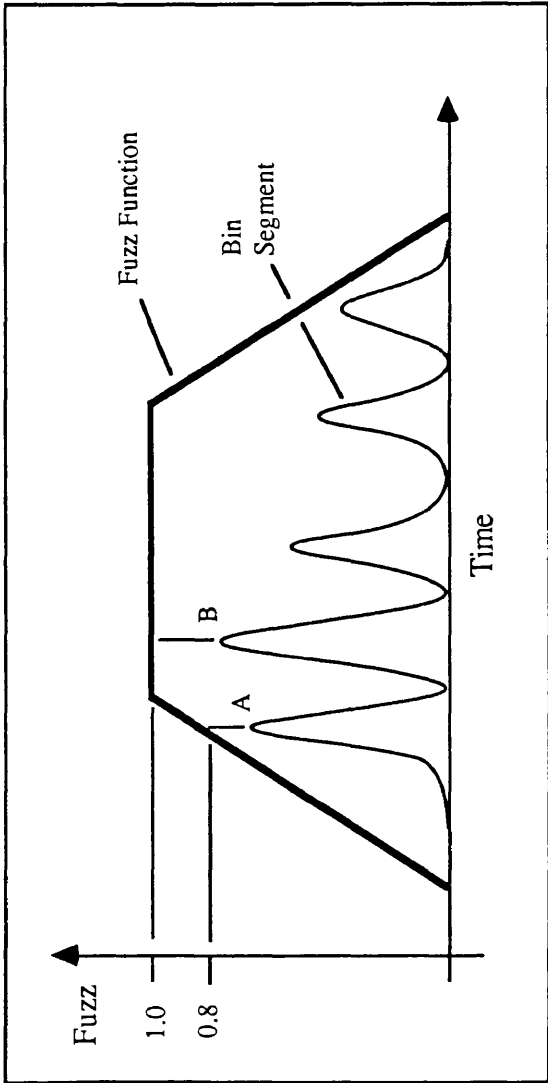


Fig.[7.2] The 'Event Analysis' algorithm produces a histogram (bin) of peaks similar to that produced in Method 2 (Sec.[7.2.2]). A mapping of the bin peaks onto the fuzz function provides a measure of reliability for the these peaks, and in turn, for the corresponding averaged BAEP peaks if they exist.

been estimated from a linear approximation to the normal statistical distribution of the individual components in the BAEP. This can be altered dynamically in EPAXIS since the model descriptions are generic. The flexibility that this provides is important in maintaining the separation between the components in the expert system as a whole and for its adaptability to other EP domains.

Fig.[7.3] illustrates the complete fuzzy procedural model for the BAEP. The fuzz functions are located along the time axis at the normal mean values (initially) for each component wave of interest.

Prolog descriptions for each wave are constructed via the execution of the declarative model (explained later) when required. The generic Prolog structures for a fuzzy function (or fuzzy latency window) are:

```
fuzzwindow(WaveNumber, Anchor, [P, Q, R, S]).  
modifs(WaveNumber, [a, b, c, d]).  
current_shift(WaveNumber, Shift).
```

where [P, Q, R, S] are defined in terms of the modifiers [a, b, c, d]. The modifiers are set to constant values, but conceptually they can be continuous functions of time that modulate their respective fuzz function regions. The Prolog predicate `current_shift/2`, is used to relocate the anchor point for the fuzzy function along the time axis.

This structure means that the fuzzy functions can adopt any suitable form and location. The description adopted for the prototype system is simple. The modifiers for each wave in the current implementation of EPAXIS are: [0, 1, 2, 1]. This results in fuzzy function descriptions: [P, Q, R, S] = [0, Sd, 2 . Sd, Sd], where Sd is the normal latency standard deviation for a particular wave component. Hence, the total width of each fuzzy function is 4 standard deviations. The extents of the spread either side of the anchor point (normal mean latency value for the component wave) correspond to the 99% confidence limits (note that the distribution of latencies for BAEP components is assymetric).

We have seen how the results of the event analysis algorithm can be assigned reliability measures. To reason effectively with these *tagged* data requires the declarative model and the inference machine (rule interpreter) to be compatible at the higher level.

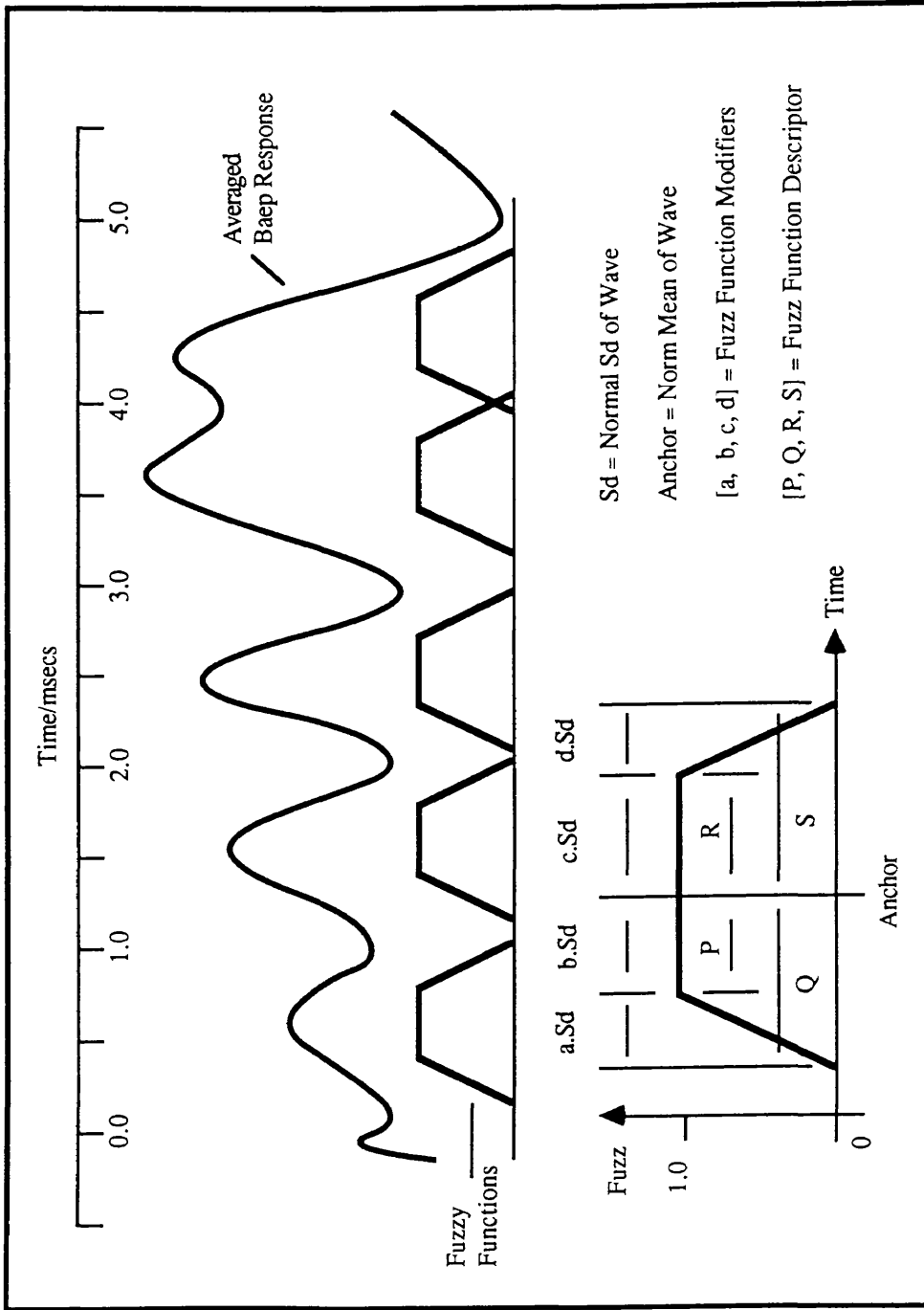


Fig.[7.3] A fuzzy procedural model for Brainstem EPs.

[B] The Fuzzy Declarative Model (Knowledge Base)

This model attempts to capture the expert decision making processes used to interpret (label) a BAEP. The fuzzy procedural model described above makes it possible to formulate propositions of the form:

Object Attribute FuzzyValue.
FuzzyValue = Value + Fuzz.

Furthermore we can formulate the consequence of fuzzy propositions by using rules or productions:

if: Object Attribute FuzzyValue
then: ObjectX AttributeX ValueX.

The value *ValueX* of object *ObjectX* is concluded with the fuzzyness *Fuzz* (in *FuzzyValue*) of object *Object*.

The certainty with which a proposition holds is expressed with a propositional attachment called the *certainty factor, cf*. Therefore we can write:

if: ObjectX AttributeX FuzzyValueX cf CF
then: ObjectY AttributeY ValueY.

The value *ValueY* of object *ObjectY* is concluded with a combination of the fuzzyness *FuzzX* of object *ObjectX* and the cf attachment *CF* : [0.0, 1.0]. This in effect allows the modeller to express the reliability or confidence with which a proposition is being made when the object value is completely true. If the object value is fuzzy, then this is reflected nevertheless through a combination of fuzzy and certainty values.

The production *if contralateral recording is available then contra_wave_V position_is X*, produces a piece of evidence that may be needed for reasoning whilst the antecedent is true, but the evidence is not terribly important if the antecedent is false. To prevent the assertion of the consequent with a low certainty value in the absence of a contralateral recording, another extension to our existing formalism is required. In this case we must assign a weighting to evidence for truth and a weighting to evidence for falsehood:

if: ObjectX AttributeX FuzzyValueX cf CF wt (WtT,WtF)
then: ObjectY AttributeY ValueY

The combined fuzzy value for object *ObjectX* is calculated in two stages:

$$[1] \text{ Fuzz} = \text{FuzzX} \cdot \text{CF}$$

Introducing the clause weights (WtT, WtF) we obtain a total reliability for the antecedent proposition in the production rule. This is termed the *fuzzy reliability factor (FRF)*:

$$[2] \text{ FRF} = \frac{WtF + \text{Fuzz}(WtT - WtF)}{\max(WtT, WtF)}$$

The value *ValueY* of object *ObjectY* is concluded with the fuzzyness *FRF* of object *ObjectX*. Fig.[7.4] illustrates the variation of the clause weight (*FRF*) with the certainty factor attachment (or combined fuzzy value) of the rule proposition. The contribution of truth and falsehood to the declarative interpretation of an antecedent proposition (and how much this contributes to the assertion of consequent propositions), is determined by the truth and falsehood weights. Adjustments of these weights is equivalent to an adjustment of the slope of the line in Fig.[7.4]. The steeper the positive slope, the higher is the contribution of truth of antecedents in the assertion of consequents, and the less falsehood detracts. Negative slopes have the same effect as negation of the antecedent propositions. Use of weights that produce negative slopes is not recommended as it obscures the declarative content of the rules.

Rules containing conjunctions of antecedents get their individual *FRF*s combined before the assertion of a consequent using the following relationships:

$$\text{ClauseWtA} = WtFA + \text{FuzzA}(WtTA - WtFA)$$

$$\text{ClauseWtB} = WtFB + \text{FuzzB}(WtTB - WtFB)$$

etc...

$$\text{FRF} = \frac{\text{ClauseWtA} + \text{ClauseWtB} + \dots + \dots}{\max(WtTA, WtFA) + \max(WtTB, WtFB) + \dots + \dots}$$

where a clause weight *ClauseWtX* is the individual *FRF* of a single antecedent *X* in the conjunction. If consequent has a certainty factor attachment, then the *FRF* calculated as above is combined with this as in stage [1] above.

These ideas are employed in a structured declarative model (knowledge base of rules) with a rich syntax. The grammar for the rules is summarised below in Backus-Naur Form:

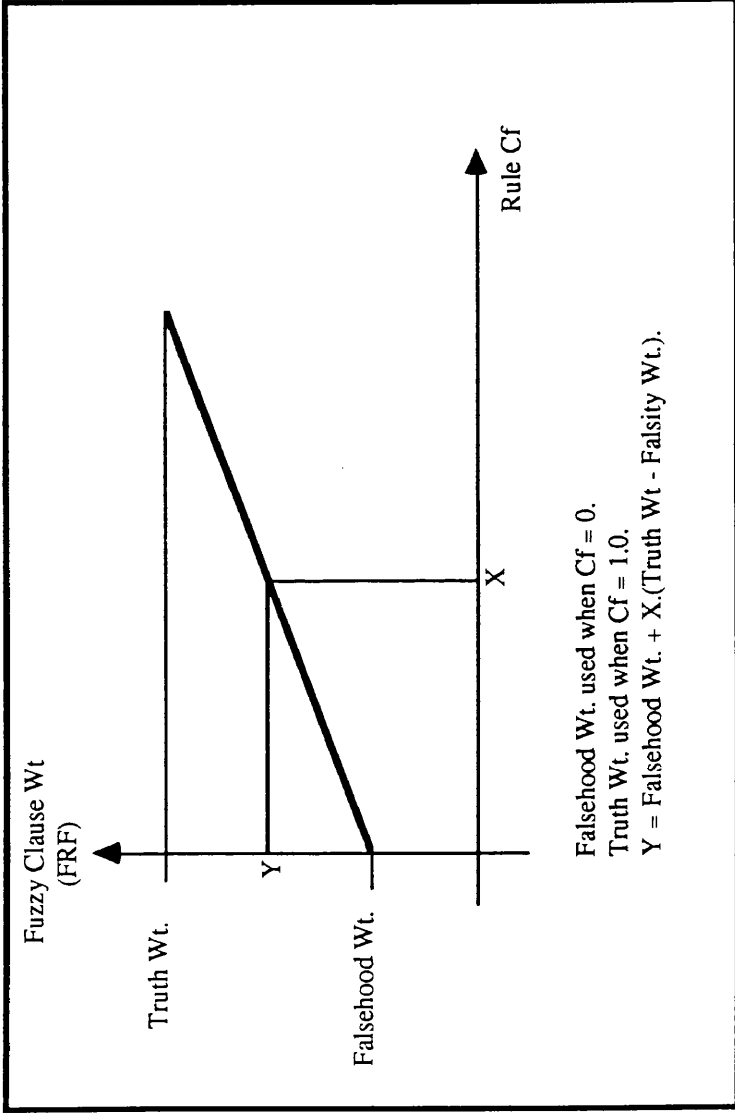


Fig.[7.4] Variation of FRF with rule certainty factor.

Rule Grammar

```
rule ::=
    (term) :: if (antecedent)
    then (consequent).
antecedent ::=
    (antecedent) && (antecedent)
    | (antecedent) or (antecedent)
    | (antecedent) cf (number)
    | (antecedent) wt (weightT, weightF)
    | (antecedent) cf (number) wt (weightT, weightF)
    | (term).
consequent ::=
    (consequent) && (consequent).
    | (consequent) cf (number).
    | (term).
term ::=
    any Prolog term.
number ::=
    [float : (0.0, 1.0)].
weightT, weightF ::=
    [float : (0.0, 5.0)].
```

The effectiveness of the above fuzzy descriptions of data and the use of a fuzzy reasoning mechanism will only be determined through an extensive validation study. It is hoped that this work will continue in the future and that the expert system will be extended to encompass other EP domains. A sample run of EPAXIS and comments on the author's experience so far with the representation scheme are provided in Appendix [C1].

Chapter Eight

Computer Assisted Analysis of Single Response BAEPs

8.1 Introduction

We have seen that the major features in the averaged ERP are due to components common to all the individual responses (trials). In the special case of ERP data, ensemble averaging can be an inadequate estimation of the ERP. The averaging process will obscure any subtle variations within and between the components of the individual responses. Individual responses are related to the excitability of the corresponding generator sites in the central nervous system (Sec.[6.2.1]) and so, it is possible therefore, that the information contained in these variations is clinically more important than the gross information contained in the average response. The ability to extract such information will greatly improve the understanding, and/or confirm existing observations, of the underlying relationships between the components of ERPs.

In Sec.[7.2] various techniques were introduced for the analysis of single response ERP data. Several factors that are common to these techniques can be identified quite readily:

- Analysis is performed on a single response or small sub-average basis.
- The single responses are digitally filtered before further analysis. This filtering usually assumes that the noise which is combined additively with the ERP signal can be described by a wide band stationary model.
- An enhanced average ERP is obtained by summing the preprocessed single responses. The number of single responses used in total during the entire analysis procedure is usually of the same order as would be used in the conventional averaging process.
- In some cases, an attempt is made to identify the major components of the ERP in the averaged response.

To date, some efforts have been made to estimate the latency variability associated with ERP components. In particular, the analysis procedure due to McGillem and Aunon (1985), mentions some experiments that are currently being pursued to obtain latency variability information (Sec.[7.2.2]).

In this investigation, single response ERP data is analysed using a specialised peak detection algorithm which reduces it to a sequence of *events*. Hence, the procedure is called *Event Analysis*. The events detected within each response are *synchronously summed* to provide estimates of the locality of major components in the ERP and, in turn, estimates of the component latency variability.

Much of the development work for event analysis was conducted using BAEPs as the input data because they exhibit a very low SNR and sometimes a very complex component structure. Other ERPs tend to have better noise characteristics and simple component structure, with the possible exception of very long latency emitted potentials (i.e. above 1 sec). However, as it is not firmly established what the true component structure of these emitted potentials actually is, and because they are usually of high amplitude, we can assume that BAEPs provide a good basis for the validation and incremental construction of generic and robust ERP analysis algorithms. Reference will therefore be made to BAEPs only from now on, in spite of the fact that the event analysis procedure is itself a non-specific procedure. In reading the text, the phrase *single response* can be freely interchanged with the phrase *small sub-average*, unless the latter is stated explicitly.

8.1.1 Event Analysis Algorithm Summary

The approach taken by the author to analyse BAEP data, differs from that taken by other researchers in several respects. The following points will serve to highlight why event analysis is different to other techniques, and also they will provide the reader with a resumé of the analysis procedure before details are discussed in the next sections:

- (a) The additive noise model of BAEP data (Sec.[7.1]), where the measured single response x is the sum of a non-stationary signal s plus random noise n , is interpreted in terms of an additive combination of a signal event sequence $\{E_s\}$ and a noise event sequence $\{E_n\}$. That is, after event extraction, the measured single response event sequence $\{E_x\}$ is given by:

$$\{E_x\} = \{E_s\} + \{E_n\} \quad \dots \dots \dots \text{Eq.[8.1]}$$

- (b) Normally no filtering is performed on the single responses prior to event extraction. A form of adaptive prefiltering is available however, and it may be invoked if the original data is severely contaminated with high frequency noise.
- (c) Synchronous summation of $\{E_x\}_m$ over M trials, giving $\{E_X\}$, produces an *event bin* which effectively partitions the averaged response X into component and non-component regions. The reduction of data to an event sequence has the distinct advantage of being immune to large amplitude artifacts in the single responses. This makes it possible to

observe features in the *event bin* which are related to corresponding features in the averaged response. Some features in the average response, which are detected in the event bin, may be *smearred out* and not visually identifiable; even though they do exist at the level of the constituent single responses.

- (d) A basic knowledge based interpretation of BAEPs is performed as discussed in the last chapter (and Appendix [C1]). This interpretation procedure is intended to locate and label the *most* significant five components in the BAEP. Currently, the significant components are selected manually on the basis of observable features in the event bin, observable features in the averaged BAEP response, and latency variability statistics.
- (e) Several different latency corrected and enhanced averages are then produced automatically, by intelligent trial selection, following the determination of significant components.
- (f) Multiple representations of the same waveform produced after (e) provide sufficient information for the analysis of relationships between components.
- (g) The number of trials needed for analysis, in comparison to conventional BAEP estimation methods, is reduced, in general, by a factor of between 32 and two. This depends on whether single responses or small sub-averages are used as input. The trial reduction factors are based on normal BAEP estimations which use 2048 trials for analysis.
- (h) Advances have been made towards the accurate estimation of signal-related latency variability to within ± 2 sample points ($\pm 0.08\text{ms}$).
- (i) Event analysis is generic in terms of its applicability to all ERPs because of the adaptive analysis procedure adopted.
- (j) The algorithm has been used to provide fast and reliable estimates of component latencies in an EP normal data study (conducted by Robinson and Robinson of Medelec Ltd., Woking, Surrey - between January and March, 1988).
- (k) The algorithm has achieved sufficient performance to warrant its implementation on the next generation of multi-purpose EMG/ERP machines currently being developed at Medelec Ltd. It is being re-structured for real-time ERP analysis in a hybrid microprocessor architecture (using the TMS 32020C Digital Signal Processor and the MC68000). The main use of event analysis in this context, will be to enable automatic component labelling, and the provision of latency variability estimates.

8.2 Data Acquisition - Equipment and Procedure

A Medelec Mystro MS25 five-channel amplifier system and a Medelec ST10 stimulator was used as the stimulation protocol controller and stimulation source respectively. Two MS25 analogue outputs are connected to a CED 1401 data acquisition system. The CED 1401 contains 16, 12-bit analogue to digital conversion inputs. The acquisition hardware is driven by software written in the C language running on an IBM PC-AT computer with all inter-communication being effected via a CED 1401 interface card. The driver program initialises the CED 1401 for data acquisition at a sampling rate of 25 kHz. The CED 1401 then waits for a succession of triggers from the MS25, thus enabling it to acquire data from both analogue inputs. Each trigger signal is synchronised with a 50% delayed delivery of the auditory stimulus. This causes the ipsilateral and contralateral channel recordings to be digitised in a pre and post stimulus format before being held in the CED 1401 2 MByte mass memory. Both channels consist of 1024, 20ms trials, with each trial containing 500, 16-bit words split between the pre and post stimulus periods. At the end of data acquisition, all data is sent to the computer for storage in archive files on hard disk and subsequent analysis. Fig.[8.1] is a schematic representation of the data acquisition setup that was used.

After data acquisition, it is possible to control the CED 1401 with the driver program in order to make small subaverages from the data. The 2 Mbyte mass memory limit dictates the maximum size and number of subaverages obtainable. The usual protocol adopted in our tests consisted of the acquisition of 1024 trials per channel, each of which could be reduced to subaverages containing a maximum of 16 single trials (i.e. a minimum of 64 subaverages per channel).

Filter cut-offs were set at 100 Hz and 1.5 kHz, the stimulation repetition rate was 5 Hz, and the contralateral ear was masked with 40 dBSL white noise. Stimulation intensities used were from 20 dBSL to 80 dBSL.

It is worthwhile noting that the filter roll-offs are -20dB / decade and -40dB / decade at the low and high ends of the pass band respectively. The filter settings provide sufficient aliasing protection and *some* limiting of high frequency EMG artifacts, which would otherwise overload the input analogue to digital convertors. Higher order, filter roll-off characteristics, in the upper end of the pass band, could remove nearly all EMG artifactual activity at the expense of severe phase distortion. The phase distortion is not desirable, so improved response fidelity is often achieved using post acquisition, zero-phase digital filtering (Sec.[7.3]).

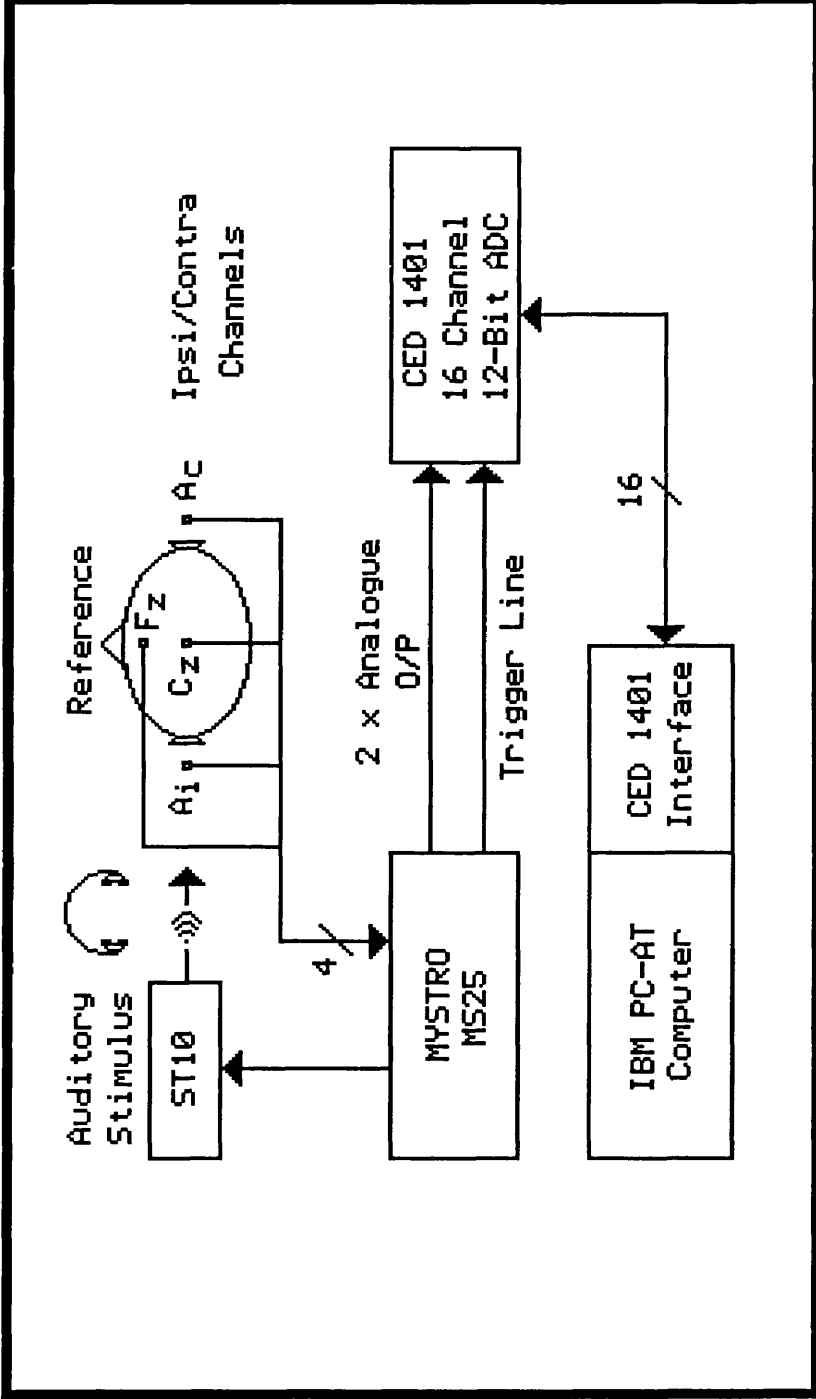


Fig. [8.1] The experimental setup used for the acquisition of BAEP data. A similar setup can be used for all other ERPs when different stimuli and electrode derivations are employed.

In the discussion section of chapter three (Sec.[3.6]), it was suggested that the functionality of the SPC could be achieved, and improved upon, in several ways. The types of system mentioned immediately above provide an analysis environment with greatly improved capability and performance compared with the SPC. An important aspect of using this type of environment, has been the short time-scale required for the development of the event analysis algorithm (less than 1¹/₂ man-years). Additionally, the ease with which real data can be acquired, has enabled a largely data-driven approach to be adopted in the development process, with simulations being used primarily for confirmative and demonstrative purposes. These points contrast well with the overall SPC development and algorithm implementation strategy.

8.3 The Event Binning Process

The event binning process (item (c), Sec.[8.1.1]) relies on the following three sub-processes:

- (i) First, a peak detection algorithm is applied to a digitised single response BAEP to extract events.
- (ii) Second, the events are extracted from all the trials comprising the averaged BAEP response.
- (iii) Finally, synchronous summation of the events across all trials is performed, to provide estimates of the locality of BAEP components.

In sub-process (i), an event is assigned to the point where a pair of maxima enclose a minimum such that the amplitude differences between the maxima and the enclosed minimum are larger than an arbitrary threshold value. This threshold value is termed the peak discrimination factor, or PDF (not to be confused with the probability density function). The method of event extraction used in this analysis is similar to that implemented prior to the calculation of Turning Points Spectra of interference pattern EMGs (Lago and Jones, 1983), which was described in Sec.[2.3.4] and simulated on the SPC (Sec.[3.4]). The difference lies in making certain that an event is assigned only at points where there is maximal separation, in amplitude terms and with respect to the chosen PDF value, between the pair of maxima and the enclosed minimum.

The sequence of N digitised data points following the m^{th} stimulus is $d_0, d_1, \dots, d_{N-1} = \{d_n\}_m$. The stimulus is delivered M times giving $N \times M$ data points in total. A turning point is defined as a change in sign of the gradient, where a traversal from positive to negative gradient indicates a maximum and the converse indicates a minimum. The maxima $d_{mx/i}$ and $d_{mx/ii}$ which enclose a minimum $d_{mn/j}$ and precede the minimum $d_{mn/jj}$, must satisfy all of the following conditions:

$$| d_{mx/i} - d_{mn/j} | > \text{PDF} \quad \dots \quad \text{Eq.}[8.2]$$

$$| d_{mx/ii} - d_{mn/j} | > \text{PDF} \quad \dots \quad \text{Eq.}[8.3]$$

$$| d_{mx/ii} - d_{mn/jj} | > \text{PDF} \quad \dots \quad \text{Eq.}[8.4]$$

where the indices satisfy: $mx/i < mn/j < mx/ii < mn/jj$

such that a significant event can be assigned to the maximum $d_{mx/i}$ occurring at the index value (sampled point) mx/i . A significant event is also assigned to the minimum $d_{mn/j}$ occurring at the index value mn/j . Note that the true latency of events, is the index value, multiplied by the sampling interval, and that this will be assumed to be understood from here onwards.

Event extraction commences with a default maximum $d_{mx/0}$ and a default minimum $d_{mn/0}$ being set to the largest polarised integer values the computer can hold, thereby ensuring that Eq.[8.2] is true at the start of analysis in the current sequence. Then a candidate minimum $d_{mn/j}$ is compared with the minimum that was found immediately prior to it, and the lower-amplitude minimum of the two is assigned to $d_{mn/j}$. The lower minimum is used in the PDF comparison with the candidate maximum $d_{mx/ii}$ as in Eq.[8.3]. When this condition succeeds, a minimum $d_{mn/jj}$ is found that makes Eq.[8.4] true, confirming that significant events occur at times mx/i and mn/j . During this latter phase of analysis, any maxima found along the waveform are compared with the maximum $d_{mx/ii}$, and the higher-amplitude maximum of the two is assigned to $d_{mx/ii}$. The updating procedure conceptually *slides* the $1^{1/2}$ wave template, described by Eqs.[8.2-8.4], backwards in time by 1 wave, and then the search cycle repeats to obtain another pattern of peaks that fit the template and conditions just described. Implicit in this one wave *backward slide*, is that Eq.[8.2] is automatically satisfied in all the subsequent search cycles. In this way, valid events represent those peaks enclosing the deepest troughs with respect to the chosen PDF value.

The strength of performing peak detection in the manner described above is demonstrated in Fig.[8.2], which shows an uncharacteristic BAEP waveform that contains large amounts of high frequency noise and spike artifacts. Peaks and troughs have been found successfully in both the smoothed and unsmoothed versions of the same potential. The smoothed BAEP was produced by two convolutions with a 3-point, unit area, triangular window. It has fewer turning points detected in it, since the convolution process has diminished the amplitude of some of the original *noisy* turning points.

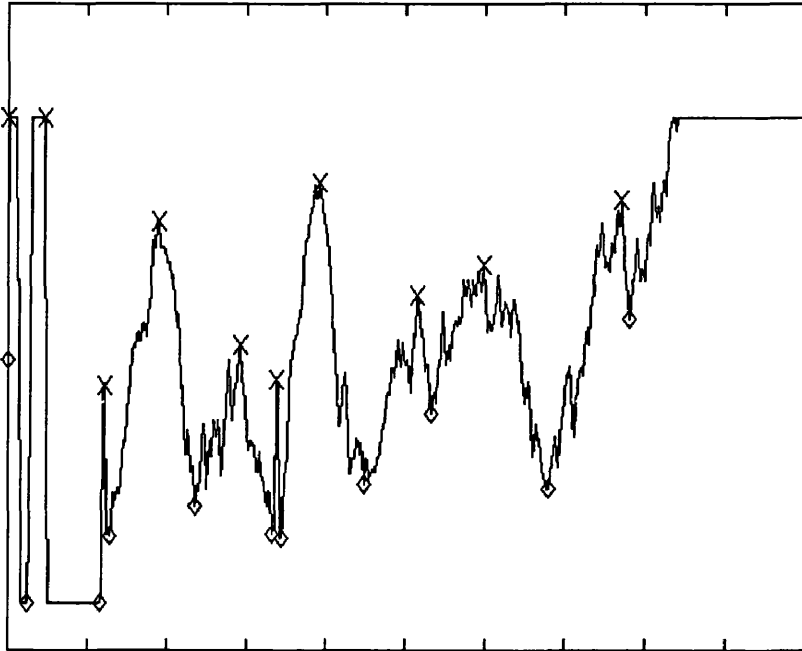
Eq.[8.1] can be rewritten to reflect the fact that the data sequence $\{d_n\}_m$ contains both maxima mx , and minima mn events:

$$\begin{aligned}
 \{E_x\} &= \{E_{x/mx}\} + \{E_{x/mn}\} \\
 \{E_s\} &= \{E_{s/mx}\} + \{E_{s/mn}\} \\
 \{E_n\} &= \{E_{n/mx}\} + \{E_{n/mn}\} \\
 \{E_{x/mx}\} + \{E_{x/mn}\} &= \\
 \{E_{s/mx}\} + \{E_{s/mn}\} + \{E_{n/mx}\} + \{E_{n/mn}\} & \dots \dots \dots \text{Eq.[8.5]}
 \end{aligned}$$

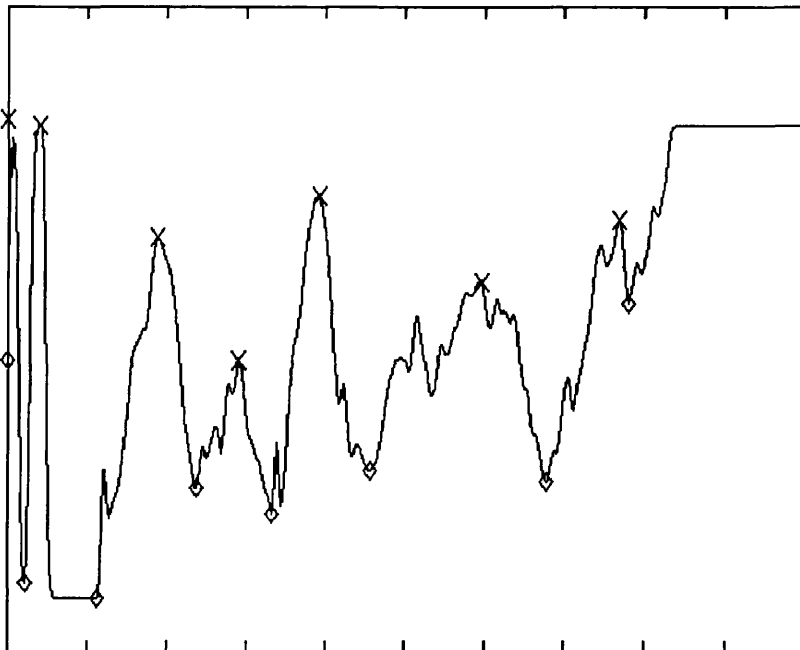
A more realistic model of the event detection sub-process, requires the incorporation of an event detection error term, so that Eq.[8.1] now becomes:

$$\begin{aligned}
 \{E_x\} &= \{E_s\} + \{E_n\} - \{E_{err}\} \dots \dots \dots \text{Eq.[8.6]} \\
 \text{where: } \{E_{err}\} &= \{E_{err/mx}\} + \{E_{err/mn}\}
 \end{aligned}$$

The objectives of event extraction are:



(a) BAEP data which contains a few spikes and high frequency noise around the peaks.



(b) A smoothed version of the above data.

Fig.[8.2] Locations of peaks and troughs as found with the peak detection algorithm. In both (a) and (b), the same PDF value of 30 ordinates has been used. The maximum peak-to-peak deflection of the two traces is approximately 220 ordinates.

- to reduce $\{E_n\}$ to zero, and
- to maximise the term $(\{E_s\} - \{E_{err}\})$ by a judicious choice of PDF value.

If these objectives can be achieved, then $\{E_x\}$ will contain nearly all of the signal-related events in $\{d_n\}_m$.

Sub-process (ii), simply applies sub-process (i) to all the individual trials in the averaged BAEP response, and simultaneously invokes sub-process (iii).

In sub-process (iii), a $1 \times N$ integer array $B[N] = b_0, b_1, \dots, b_{N-1}$, is maintained, where the b_n represent accumulator bins for the number of occurrences of significant events (both maxima and minima) at times n across the ensemble of M signal sequences. To enable an improvement in the registration of stimulus-related events only, and not noise-related events, the elements b_n in the array $B[N]$ are decremented at points where significant event-minima occur, and incremented at points where significant event-maxima occur. This method of summing events, simulates *averaging of significant events* across all the responses, apart from the omission of the formal division by N . Therefore, event-maxima are labelled with '+1', event-minima with '-1', and all other points in $\{d_n\}_m$ are labelled with '0'.

The polarised labelling and summation process, assumes that low counts will occur in $B[N]$ when noisy epochs of data are temporally synchronised across a large set of trials. We note that, with noisy data, there should be an equal probability of finding temporally synchronous event-maxima and event-minima across trials.

The accumulator bin count or event bin is formally described by:

$$b_n = \sum_{m=1}^M \{E_x\}_m$$

$$\text{where: } E_x = \begin{cases} 1 & \text{at Event Maxima} \\ -1 & \text{at Event Minima} \\ 0 & \text{Elsewhere} \end{cases}$$

$$\text{and, } \{E_x\} = B[N] = \{b_n\}, \text{ for } n = 1, 2, \dots, N \dots \dots \dots \text{Eq.[8.7]}$$

8.4 Data Simulations and Some Intermediate Results

Several programs were written to simulate data having the general characteristics of BAEPs. These programs are included in Appendix [D2], and they were used extensively for the validation of event analysis and for the demonstration of results.

Four sets of noise data are used in conjunction with a single set of simulated signal data. The noise and signal data each contain 64 trials of 500 data points each. Two of the noise files contain real background EEG, recorded as described in Sec.[8.2], but without the use of any evoking stimulus and contralateral channel masking. The remaining two noise files contain simulated pink noise. Both of the latter noise data files were produced by generating random deviates having poisson and gaussian amplitude distributions respectively, and then bandlimiting each of them in the frequency domain between 300 Hz and 1.5 kHz. The simulated signal is a 1 kHz, exponentially decaying, sine wave. The pre-stimulus period of this sine wave is clamped to zero, and the exponential decay begins in the post-stimulus period, decaying to 0% at the end of the trial record.

The noise files are individually added to the signal file, to produce four simulated data sets. Prior to addition, the noise and signal data are normalised. After combination, the data is maximally scaled. The data so produced, allows one to test the event analysis algorithm with a deterministic signal, having similar noise characteristics to the BAEP. The use of an exponentially decaying sine wave, and pre-normalisation, enables investigations to be conducted at SNRs varying from 0 dB down to -28 dB within the post-stimulus period. This range of SNRs, is sufficient to cover the worst case SNR expected in a BAEP, even at the lowest stimulus intensities.

Most of the illustrations presented from now on, will be in a similar format to that shown in Fig.[8.3]. The upper window contains the grand averaged response of 64, zero-mean, single trials or small sub-averages (GAV), and the lower window contains the corresponding event bin (BIN). Only post-stimulus period data are shown, which consist of 250 sampled points acquired at 25 kHz. These 10ms epochs of data are delimited by the 1ms interval marks in each window. GAV amplitude values are provided in terms of absolute ordinates, without reflecting the scaling required to fit the data in the window. For real BAEP data, each GAV ordinate represents approximately 0.25nV. BIN amplitude values represent the actual values contained in the event bin.

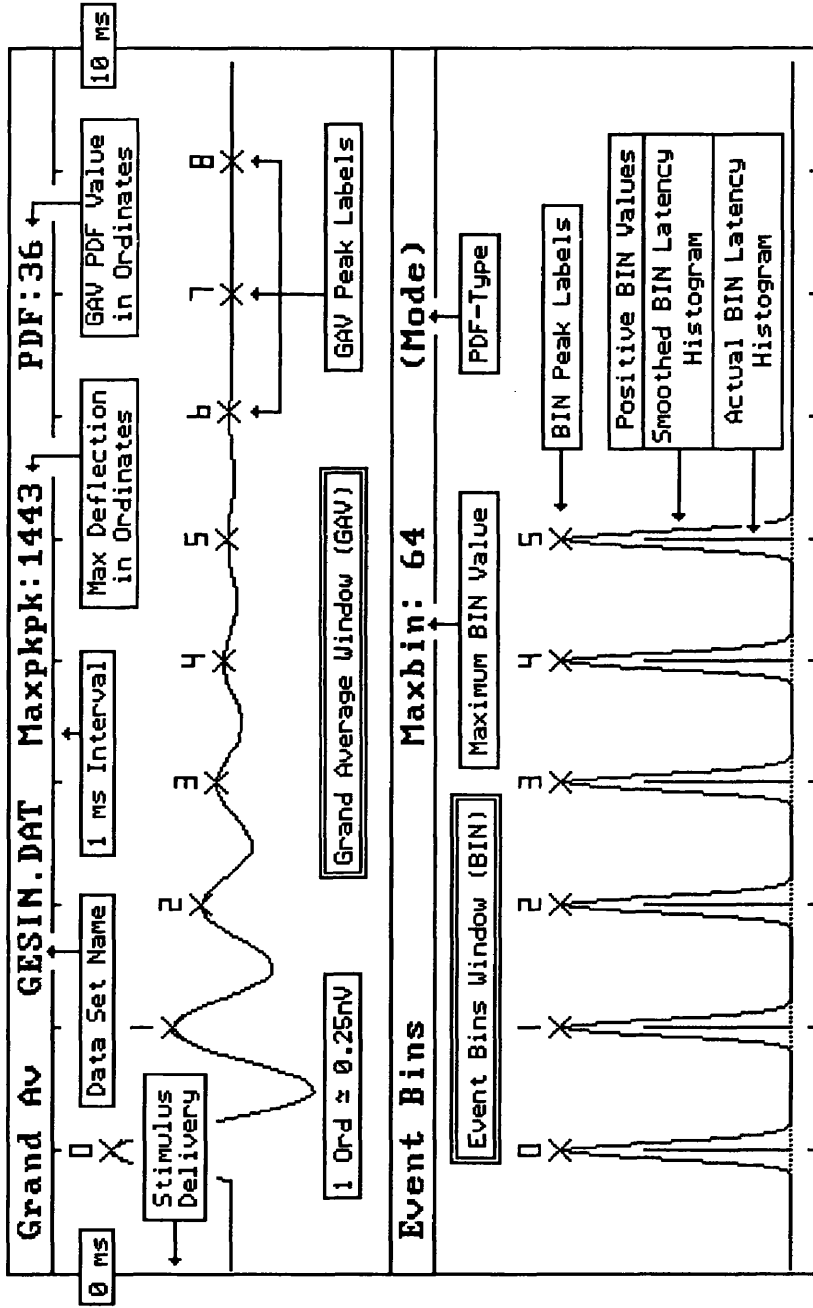


Fig.[8.3] A sample of the graphical display format for the results in the text. It shows explanations for the various screen attributes that are available. These displays have been derived directly from the Event Analysis result screens. The menu bars and cursors are not shown for clarity.

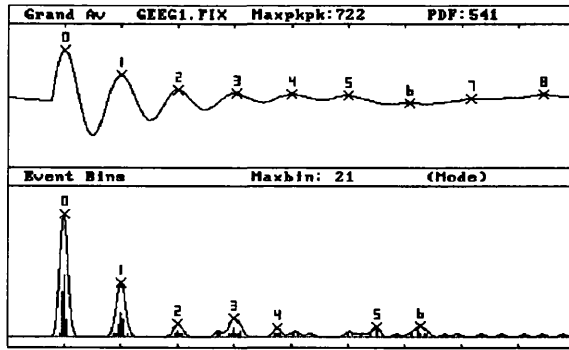
In all diagrams the BIN is displayed in two forms:

- (a) Discrete vertical lines show the latency histograms of the positive half of the event bin. This format was chosen so as to emphasise the correlation between features in the BIN and those in the GAV. Note, there no relation is implied between those peaks in the GAV and those peaks in the BIN that have the same numeric labels.
- (b) A smoothed version of the latency histogram is shown as the continuous line forming an envelope over (a). This curve was produced on an empirical basis, in order to transform the latency histogram into smooth segments that can be partitioned easily in the computer, using the *same* peak detection algorithm that was used to create the histogram initially.

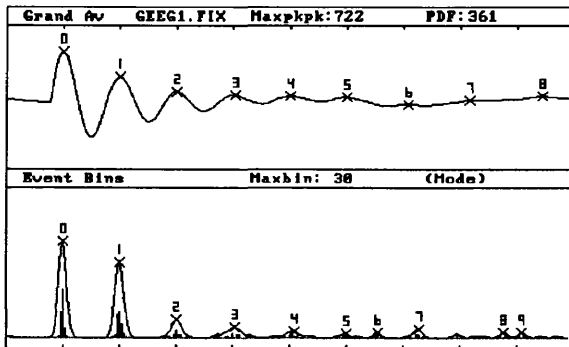
Several smoothing functions were tried in (b), and the best performance was achieved with two passes of a three point moving average followed by a convolution with a three point triangular window. During the early stages of the algorithm development, it was determined that the widths of the smoothing functions should be as small as possible, so as not to artificially distort the inherent structure of (a).

Figs.[8.4(a) - 8.4(c)] show a selection of event bins that have been generated from one of the above simulated data sets at different settings of PDF. The noise data file used in this example contains single trials of spontaneous background EEG. These diagrams serve to illustrate all of the points that have been discussed in the last section. The structuring in the BIN becomes more pronounced in the vicinity of GAV peaks as the PDF value is reduced from 75% to 25% of the maximum peak-to-peak deflection. The accuracy with which the BIN delimits GAV features (*throughout* the record), improves as the PDF value is reduced. Hence, the power to resolve events during the binning process increases at lower PDF values. The BIN structuring is also affected by the gradual change in SNR along the waveform. Peaks in the BIN are less pronounced as the SNR decreases. Nevertheless, Figs.[8.4(b) and 8.4(c)] show BIN peaks which are very nearly spaced at the 1ms intervals of the peaks in the GAV. Accurate segmentation of the GAV into component and non-component regions is hence likely to be successful at low PDF values and at SNRs as low as -20 dB (the SNR is 0 dB at 1ms [GAV peak '0'], and -20 dB at 7ms [GAV peak '6']).

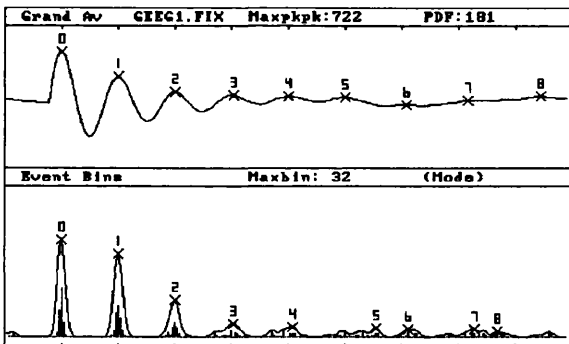
The ability to segment the BAEP is the first step towards the automatic detection of its components, and the subsequent estimations of their latency variability. Fig.[8.4(d)] shows the superior results obtained for the segmentation by using a PDF value which has been chosen adaptively on a single trial basis. This method of PDF selection will be described in the next section.



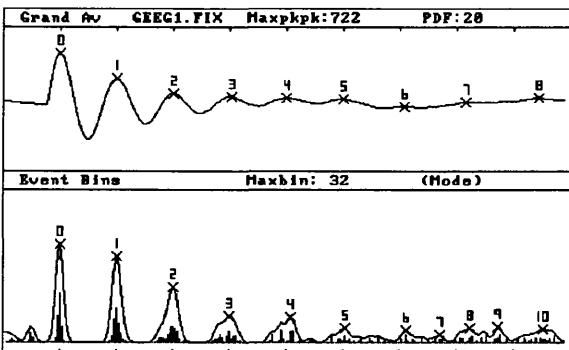
(a) PDF value = 75% of Maxpkpk.



(b) PDF value = 50% of Maxpkpk.



(c) PDF value = 25% of Maxpkpk.



(d) PDF value is determined adaptively.

Fig.[8.4] The effect of the PDF value on the structuring that occurs in the event bin (BIN). The PDF value per single trial varies from 75% of the maximum peak-to-peak deflection, to one that is determined adaptively.

Figs.[8.5(a) - 8.5(c)] display the same GAV data as in Fig.[8.4]. The BIN in this case is produced by modifying the event binning process, such that synchronous summation in the event bin occurs with event maxima only. That is, in Eq.[8.7], the event minima are labelled with '0' when detected, instead of '-1'. This prevents *cancellation* of event-maxima by event-minima in the event bin $B[N]$. It can be seen from these results, that there is a degradation in BIN structuring compared to that obtained using bin cancellation in Fig.[8.4]. The BIN structure is worse in regions of low SNR, and the latency histograms take on a remarkably uniform distribution. McGillem and Aunon (1977), have observed a similar distribution when random noise data was analysed with their MMSE filter and peak detection algorithm (Sec.[7.2.2]).

At a later stage, the author gives a probabilistic model of the bin cancellation process in order to quantify its effectiveness in noise-event suppression. However, at this point a heuristic explanation is offered which requires the restatement of Eq.[8.5] in terms of the *set* of single event sequences $\{E_x\}_m$ that comprise the BIN sequence $\{E_X\}$:

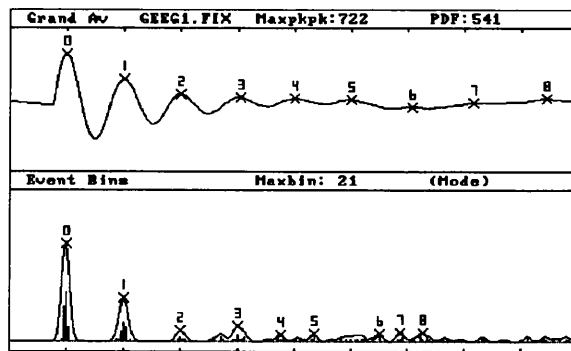
We know that: $\{E_X\} = \sum_{m=1}^M \{E_x\}_m$

where: $E_x = \begin{cases} 1 & \text{at Event Maxima} \\ -1 & \text{at Event Minima} \\ 0 & \text{Elsewhere} \end{cases}$

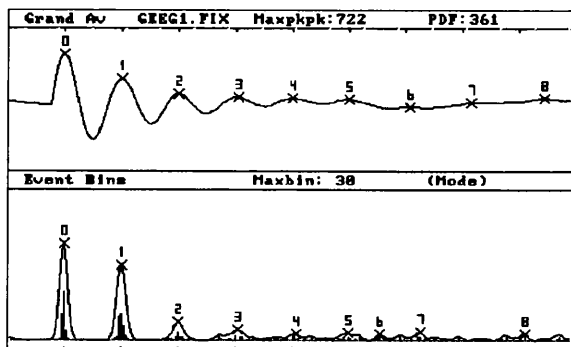
Therefore, from $X = \sum_{m=1}^M (s + n)_m = S + N$, we can rewrite Eq.[8.5] as:

$$\{E_{X/mx}\} + \{E_{X/mn}\} = \{E_{S/mx}\} + \{E_{S/mn}\} + \{E_{N/mx}\} + \{E_{N/mn}\} \dots \dots \dots \text{Eq.[8.8]}$$

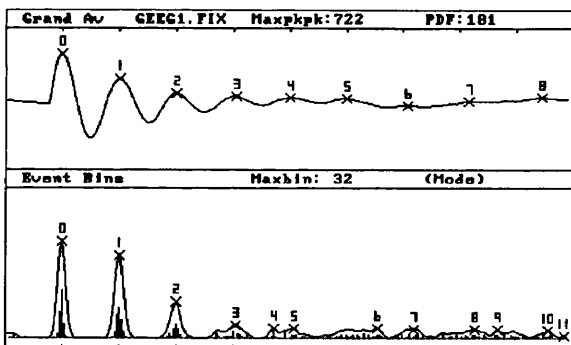
The peak detection algorithm described previously, was designed to minimise the number of events detected in the term $(\{E_{N/mx}\} + \{E_{N/mn}\})$. If, however, the noise-events $\{E_{N/mx}\}$ and $\{E_{N/mn}\}$ are erroneously detected within the single trials, then it is probable that the summation of the polarised numeric labels assigned to these events ('±1'), will tend towards zero across all trials, as the number of trials tends towards infinity. If bin cancellation is not used, then the sum of the individual $\{E_{n/mn}\}_m$ in the term $\{E_{N/mn}\}$, is not available to diminish the sum of the individual $\{E_{n/mx}\}_m$ in the term $\{E_{N/mx}\}$. This causes the event bin $\{E_X\} = B[N]$, to accumulate values which become uniformly distributed in noisy epochs of data. Bin cancellation can, therefore, be thought of as a *low pass event filter* that is computationally very efficient.



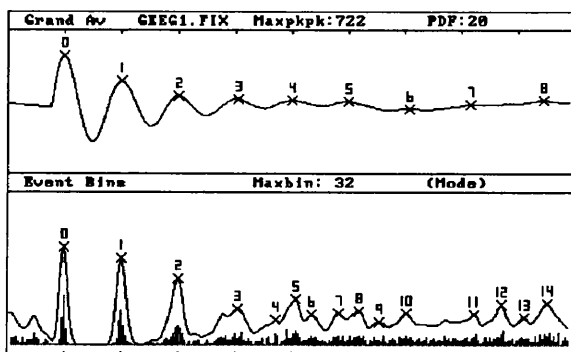
(a) PDF value = 75% of Maxpkpk.



(b) PDF value = 50% of Maxpkpk.



(c) PDF value = 25% of Maxpkpk.



(d) PDF value is determined adaptively.

Fig.[8.5] Results obtained from the same data used in Fig.[8.4]. In this case the event bins have been computed without the use of bin cancellation. This causes substantial loss of structure in the BIN.

Some cancellation is also expected to occur between the terms $\{E_{S/mx}\}$ and $\{E_{S/mn}\}$. The non-stationary assumption used for BAEP data, makes it reasonable to say that events in these terms will rarely occur within the same temporal space across trials, and if they do, then it will happen with negligible frequency. Additionally, a physiological phenomenon exists that supports the statistical argument. It has long been known, that sensory stimulation will actually reduce, rather than increase, the spontaneous activity of the brain. This observation due to Berger (1929), follows from the fact that the alpha rhythm of the brain is at its maximum excitation only when one is completely relaxed. These background brainwaves, the major source of noise in all ERPs, decrease in amplitude following tactile or auditory stimulation. A similar reduction can be induced by voluntary movements or even mental arithmetic. Berger suggests that this is a generalised response of the brain correlating with attention. ERPs, therefore, actually suppress background EEG activity. So, the use of synchronous summation of events will be enhanced in the region of the ERP components, since the temporal separation of true maxima and minima events will be less affected by EEG noise.

Comparing Fig.[8.4] and Fig.[8.5] again, we can conclude, that the use of a bin cancellation technique will provide better estimates of the locality of BAEP features when the data is contaminated with noise and the SNR is low.

8.5 Adaptive Selection of Peak Discrimination Factor

A deficiency in the peak detection method as it stands at this point in the discussion, is that it relies on some knowledge of what value to assign to the PDF. The use of similar peak detection algorithms by both Parekh (1987) and Lago and Jones (1983), for EMG turning points spectral analysis, incorporated an empirical choice of the PDF value. Their PDF values were usually set to about 3% of the maximum peak-to-peak signal deflection, since this provided the sufficient and repeatable peak discrimination in the analysis and subsequent classifications of turning point spectra that they were seeking. Additionally, the high SNR obtainable, the random, noise-like nature, and perhaps, the fact that general characteristics of the EMG were being investigated in the frequency domain, made it unnecessary to be very strict with the choice of PDF value. The main difference between EMG signals and EPs in this context, is that in the former case the PDF is being used to reduce information content, and in the latter case the PDF is being used to maximise information content. It follows, therefore, that the choice of a PDF value must be dealt with carefully.

The BAEP has a particularly large noise content even after averaging. Fridman et al. (1982) have estimated that the SNR is at best 1:1 based upon an average of 200 trials. This suggests that contamination of the BAEP by EEG, EMG and movement artifact is quite substantial, and that a judicious choice of PDF for peak selection would be difficult to make. Simply standardising on one PDF value, for use across the entire ensemble of BAEPs, is unlikely to be successful in segmenting the averaged BAEP, and this was demonstrated in Fig.[8.4]. Too large a PDF value, will result in events being missed, and too low a PDF value, will cause extra noise events to be detected which do not *cancel out* in the available number of trials.

Event analysis incorporates a PDF value specification which is performed adaptively prior to the event binning process. An estimate of the *noise* in each sequence $\{d_n\}_m$ is computed, and the value obtained is then used as the PDF. In this way we can compensate for transient changes affecting the assumed statistical stationarity of background EEG activity. This *noise* estimate does not lend itself to a calculation of the SNR, as it is not a measure of signal power. The estimate is calculated solely for its appropriateness to this analysis. Peak detection algorithms which incorporate an amplitude threshold criterion, require, as a rule of thumb, a threshold value that will be greater than the most common noise deflections, but less than the deflections associated with the peaks that are being sought. If this requirement can be achieved, then it should enable the inclusion of those fluctuations arising from true signal components, and the omission of those fluctuations arising from noise.

8.5.1 Frequency Distributions of Single Response Deflections

Individual responses are processed by the specialised peak detection algorithm (sub-process (i)) described in Sec.[8.3]. The PDF value is set to zero at this point, so that all maxima and minima turning points are found. The distribution of amplitude differences between adjacent maxima and minima (max/min deltas), is determined using a discrete-valued histogram. The statistics of this frequency distribution provide estimators for the characteristic noise deflections contained within the single responses. Histograms are computed for both the *noise-only* pre-stimulus record, and the post-stimulus record. The frequency distributions are different for all subjects, and different for all the individual responses in the same data set. The event binning process is then performed using PDF values obtained from this noise amplitude information. The two main processes now needed for event analysis are summarised in Fig.[8.6].

The response-specific PDF value, used in the event binning process, is determined from the *mode* of the post-stimulus frequency distribution. The author has found that there is no significant difference in results, when either the pre-stimulus or post-stimulus mode value is used. This result was expected, since the two distributions consistently have similar shape.

The amplitude differences in the two halves of the data sequence $\{d_n\}_m$ (i.e. over $n = [1, N/2]$, and $n = [(N/2 + 1), N]$), thus provide another *pair* of sequences, each being denoted by $\Delta_0, \Delta_1, \dots, \Delta_{P-1} = \{\Delta_p\}_m$. Construction of the frequency distribution $H[\Delta_p]_m$ from the sequence $\{\Delta_p\}_m$, requires a subjective choice of the optimal classwidth CW to be used. The choice of this parameter depends on the amount of resolution required, and to a lesser degree on the sample size. Too high a resolution (many classes or small CW) will lead to multimodal distributions, and too low a resolution will tend to obscure the important information in the distribution. Dixon et al. (1983), suggest that in order to obtain a smooth histogram, the number of classes NC should be approximately equal to the square root of the sample size. The class width is then found by dividing the range of data by NC , i.e. :

$$\text{Class Width, } CW = \frac{[\Delta_p]_{\max} - [\Delta_p]_{\min}}{\text{Number of Classes, } NC} \dots \dots \dots \text{Eq.[8.9]}$$

The mode value of $H[\Delta_p]_m$, Δ_{md} , is then given by the *end* value of the class containing the highest number of observations. The mean value is also calculated from the distribution:

$$\bar{\Delta} = \sum_{i=1}^{NC} \left[\left(\frac{f_i}{P} \right) \cdot (CW/2 + CW \cdot (i - 1)) \right] \dots \dots \dots \text{Eq.[8.10]}$$

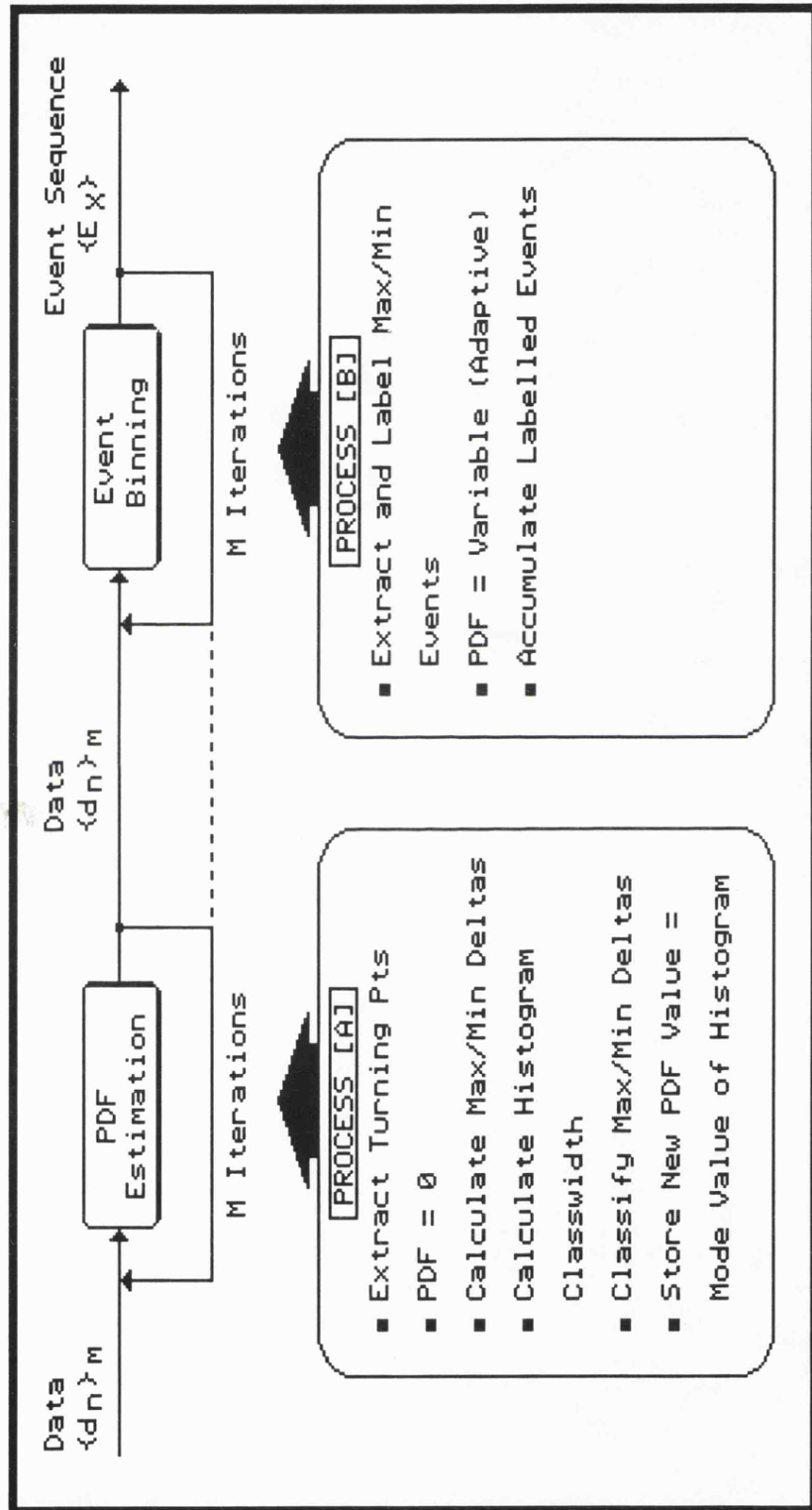


Fig. [8.6] Schematic diagram of the adaptive PDF calculation and subsequent event binning process. The dotted line indicates that the two separate iteration loops can be combined into one *super - process*, so as to enable a predominantly parallel execution architecture for more rapid execution in multi-tasking and/or multi-processor environments.

where f_i is the frequency of occurrence of the observation in the i^{th} class, and P is the total number of observations. The ratio f_i / P is, therefore, the relative frequency in the i^{th} class. The maximum number of observations usually seen on either side of the stimulus, is in the range 50 to 100. NC is hence chosen to be about 10 (i.e. $\sqrt{P_{\text{max}}} = \sqrt{100}$), and accordingly an optimal CW for pre-stimulus and post-stimulus histograms can be calculated for each of the M response sequences $\{d_n\}_0$ to $\{d_n\}_{M-1}$.

The implementation of Eq.[8.9] produced reasonably good performance, in that structuring was observed in the BIN in most cases. This suggested that the PDF values were being optimally selected on a single response basis. Examination of $H[\Delta_p]_m$, however, often showed that the effect of outlying observations (i.e. a large $[\Delta_p]_{\text{max}}$) reduced the resolution in $H[\Delta_p]_m$, and the mode class sometimes contained too high a percentage of the observations in $\{\Delta_p\}_m$. The solution to this problem was to double the number of classes for increased resolution, and to compute the CW on the grounds that high amplitude *spikes* (i.e. outliers) will be drawn from near the upper decile of the distribution describing the sequence $\{\Delta_p\}_m$. We assume that this distribution is normal, so the new range of data used in Eq.[8.9] is, the mean μ , plus one standard deviation σ , (i.e. giving $P(\Delta_p \leq 0.84)$). Eq.[8.9] is now modified to read:

$$\text{Class Width, } CW = \frac{[\Delta_p]\mu + [\Delta_p]\sigma}{\text{Number of Classes, } NC = 20} \dots \dots \dots \text{Eq.[8.11]}$$

Multimodality in $H[\Delta_p]_m$, due to the increased resolution, is rarely observed, although it is expected in situations of very low SNR.

Fig.[8.4(d)], shows how the use of the adaptive PDF value has resulted in a significant improvement in the correlation of BIN features with GAV features, compared to that obtained with a trial selection of PDF values, as in Figs.[8.4(a), (b), and (c)].

Fig.[8.5(d)] shows the high sensitivity obtained with the adaptive PDF value, resulting in an expected uniform BIN distribution in regions of low SNR when no bin cancellation is employed, (Sec.[8.4]).

8.6 Spike Rejection and Adaptive Low Pass Filtering

The problems associated with large amplitude spikes and residual high frequency noise in the data have been described earlier with respect to averaging of BAEP data. Unfortunately, reduction of the data into a sequence of turning points is not immune from these artifacts, and erroneous spikes will be regarded as valid events during the binning process. To a certain degree, these spikes can be smoothed out of the original data by *heavy* filtering, but one would risk incomplete suppression of large spikes and lose fidelity in the BAEP components. The techniques described below, provide spike rejection during the event binning process, and *soft* filtering of the data which retains much of the response fidelity.

An extra class in $H[\Delta_p]_m$, Δ_{spk} , is defined to hold observations lying outside the interval $([\Delta_p]_\mu + [\Delta_p]_\sigma)$, and is used to implement a spike-rejection criteria during event analysis. For example, the high frequency, large amplitude spikes in the data of Fig.[8.1(a)], can be rejected during the event binning process, by using the value of Δ_{spk} , and some knowledge of the distribution of *latency* intervals between maxima and minima turning points in $\{d_n\}_m$. The latency intervals in the two halves of the data sequence $\{d_n\}_m$ (i.e. over $n=[1, N/2]$, and $n=[(N/2 + 1), N]$), give a *pair* of sequences denoted by $(\Delta t)_0, (\Delta t)_1, \dots, (\Delta t)_{P-1} = \{(\Delta t)_p\}_m$. The desired histogram $H[(\Delta t)_p]_m$, is constructed in a similar manner to $H[\Delta_p]_m$. Spike rejection is performed by comparing all events, prior to binning, with the spike class value Δ_{spk} , and the latency interval mode class value $(\Delta t)_{md}$. If the event is drawn from both classes simultaneously, then the event is rejected, because it is of high frequency and large amplitude.

$H[(\Delta t)_p]_m$ contains information related to the characteristic frequencies that exist in the response sequence $\{d_n\}_m$. The timing information that is available, in terms of the number of sampling points between commonly occurring fluctuations in the signal, is used to adaptively specify the width w of a simple, first-order, linear-phase, autoregressive moving average filter. The filter can be invoked prior to the event binning process. It is derived from the rectangular linear-phase filter of $2k + 2$ equal weights (Taylor and MacFarlane, 1974), and has the transfer function:

$$H(z) = \frac{E(z)}{D(z)} = \frac{1 - z^{2k+2}}{z^k(1 - z)}$$

if $k = w/2 - 1$, then by inverse z-transform:

$$e_n = e_{(n-1)} + [d_{(n+w/2)} - d_{(n-w/2)}]$$

and for unity gain at dc:

$$e_n = e_{(n-1)} + (1/w) \cdot [d_{(n+w/2)} - d_{(n-w/2)}] \dots \dots \dots \text{Eq.[8.12]}$$

where: $w = 2 \cdot (\Delta t)_{md}$

Since $(\Delta t)_{md}$ approximates the most common intervals defined by the times of occurrence of adjacent maxima and minima, the factor 2 in $(w = 2 \cdot (\Delta t)_{md})$, makes w approximate the actual *event* intervals defined by the times of occurrence of adjacent minima. Since w is usually found to be between four and twelve sample points wide, the first transmission zero in the frequency response will lie between 2 kHz and 6 kHz. This range of frequencies is above the high cut-off of the input analogue filters and will ensure that residual high frequency power is attenuated. Zero-phase is restored by a unit leading shift of all data points in the filtered sequence $\{e_n\}_m$.

8.7 The Effects of Sub-Averaging and Filtering on the Event Binning Process

The event analysis procedure seeks to provide a simple method to determine BAEP component latency variability using a small data set. It has already been said how useful latency variability information alone might be for the clinician. Nevertheless, in reality clinicians may view this information with some scepticism if it is not provided in conjunction with the traditional, and normally reliable, estimations of the averaged response. Performing an averaging procedure on a *small* set of single responses requires data of sufficiently high quality to yield an acceptable response estimate. In the case of scalp recorded BAEPs, the data is only likely to have sufficient signal power in responses obtained at the highest intensity levels. The main objective then, in the context of producing good, clinically acceptable, BAEP estimations, is to ensure that the SNR is increased before averaging.

The SNR in single responses can be improved by the filtering process described in the last section. Additionally, at the expense of an increase in the *total* number responses, we can improve the SNR by averaging within contiguous subsets of single responses. Increases in SNR result in improved estimations of the BAEP. However, because of the *small* number of trials being analysed, and because these trials might be either filtered or sub-averaged, it is possible that the bin cancellation assumptions of Eq.[8.8] will be violated. The effects of filtering or sub-averaging on bin cancellation are due to the attenuation of high frequency random noise fluctuations. Referring to Eq.[8.8], we recall that for bin cancellation to operate as a *low pass event filter*, the term $(\{E_{N/mx}\} + \{E_{N/mn}\})$ should tend towards zero as the number of responses tends towards infinity, because the noise-events are random and uncorrelated between trials. If the filtering and sub-averaging operations adversely affect the noise-event distribution in both the temporal and the spatial dimensions, then as far as the peak binning process is concerned, it is likely that the error in the term $(\{E_{N/mx}\} + \{E_{N/mn}\})$ will increase.

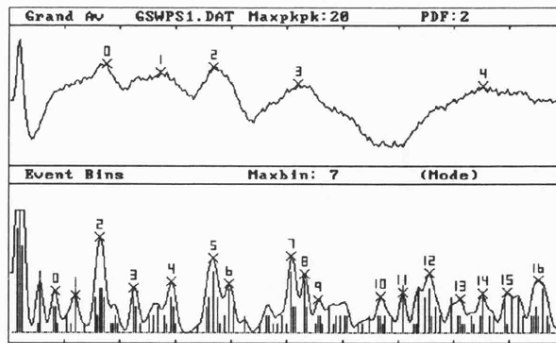
If we model the detection of noise-events across trials by a discrete random binomial process, then it will be possible to predict the error in event-counts for different probabilities of event detection. The author will discuss this probability model later in Sec.[8.8]. At this point we note that there exists a trade-off between providing *clean* BAEP averages and ensuring that bin cancellation is maximised for adequate BIN structuring when *small* numbers of single responses are being analysed.

8.7.1 Event Binning with Sub-Averaged Responses

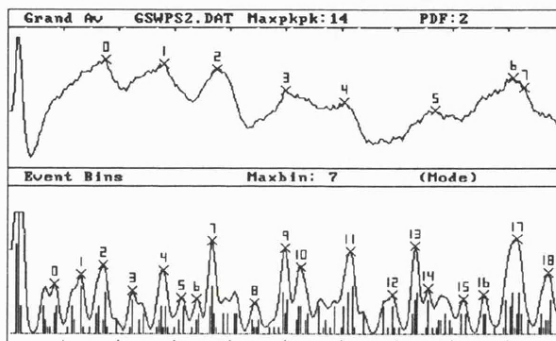
As before, we assume that the single response is $x_m = (s + n)_m$, where the signal s is time-invariant, and the noise n is additive, statistically stationary, and uncorrelated with either s or the stimulus. The individual component latency variabilities across all x_m will be entirely due to the variance of n in x_m . In reality, the components in s exhibit a degree of variability, so the measured variance will be due to both s and n in x_m . If we create small sub-averages $x_i = \sum (s + n)_i$, consisting of i consecutive single responses, and make the reasonable assumption that all the s in the sub-averages $[x_i]_m$ are time-invariant provided i is sufficiently small, then the contribution to the error in measured latency variance due to n , can be reduced by the number of responses i per sub-average. The use of sub-averages in event analysis will, therefore, yield a maximum likelihood estimation of the latency variability.

The results shown in Fig.[8.7] were obtained by performing the event binning process as illustrated in Fig.[8.6]. The different sets of data consisted of sub-averages generated from single BAEP responses recorded ipsilaterally at a stimulus intensity of 60 dB from a normal adult male. Each set of data consisted of 64 sub-averages, and the number of single responses per sub-average was varied by powers of two from set to set. As the size of the sub-averages increases, so does the total number of responses in the GAV. This is reflected in the improved quality of the GAV as we progress from Fig.[8.7(a)] to Fig.[8.7(d)]. In Fig.[8.7(a)] there is residual high frequency noise and a complex wave IV/V component in the GAV at peak '3'. Fig.[8.7(d)] contains hardly any residual noise and exhibits separation of wave IV at GAV peak '3' and wave V at GAV peak '4'.

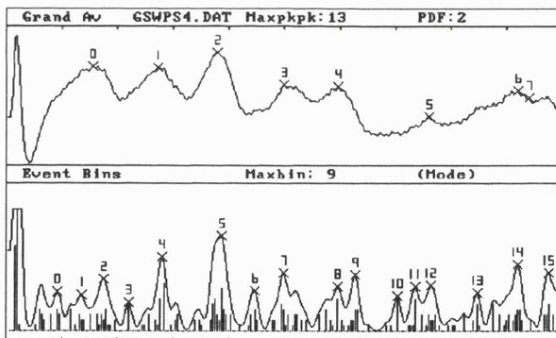
In all cases the structuring that exists in the BIN in the vicinity of GAV components is evident. Fig.[8.7(a)] shows very good BIN structuring, despite the fact that the sub-averages contain only one response each. There is a broad BIN peak in the vicinity of the inflection in the GAV between GAV peak '3' and GAV peak '4', corresponding to the underlying wave V in the wave IV/V complex. This BIN peak becomes more prominent as the sub-average size increases. The small variability in wave V, which results in a point of inflection at low response counts, is revealed by the bifid BIN peaks ('7' and '8') in Fig.[8.7(d)], despite the good wave V representation in the GAV. On serial examination of Figs.[8.7(a) - 8.7(d)], one is able to observe the developments of the bifid BIN peak and wave V. In this data, a close coupling between waves IV and V is suggested, first by the complex component at low response counts, and second by the simultaneous occurrence of bifid BIN peaks at higher response counts. This hypothesis can be tested with an intelligent averaging method described later.



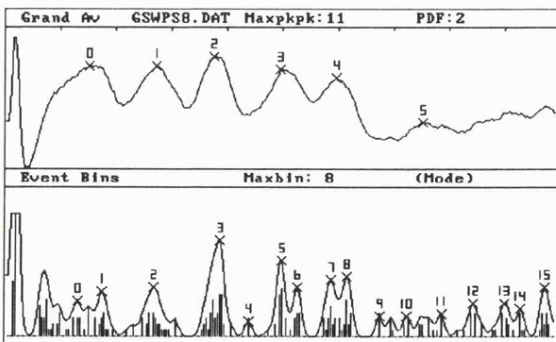
(a) 1 response/sub-average = 64 responses in total.



(b) 2 responses/sub-average = 128 responses in total.

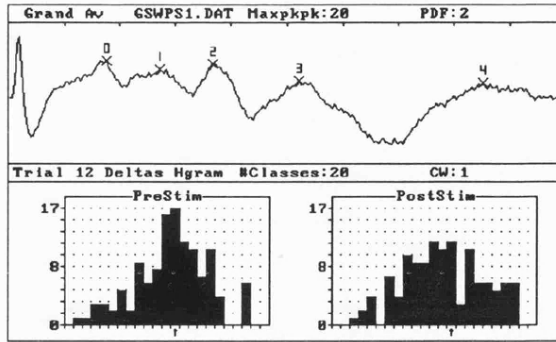


(c) 4 responses/sub-average = 256 responses in total.

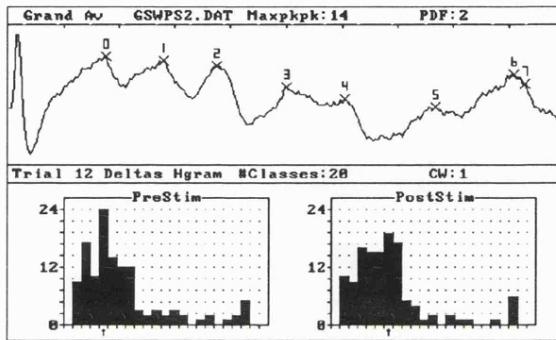


(d) 8 responses/sub-average = 512 responses in total.

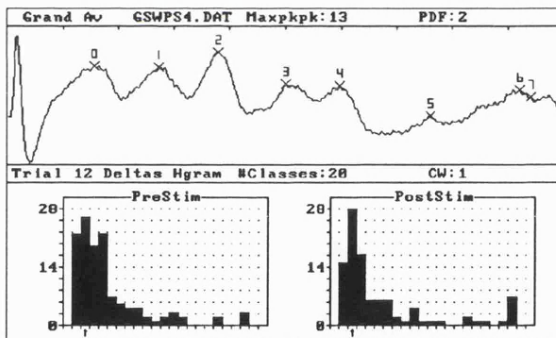
Fig.[8.7] The effects of increasing the sub-average size on BIN structure and the shape of the GAV response.



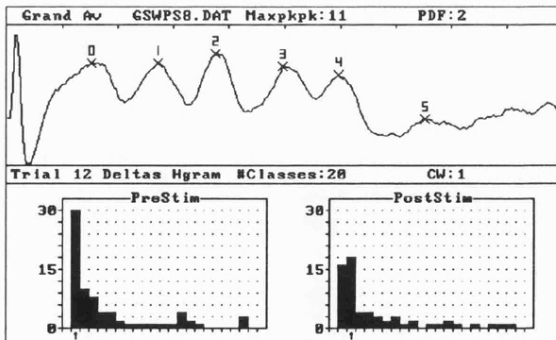
(a) 1 response/sub-average - distributions are approximately normal.



(b) 2 responses/sub-averages - distributions are diverging from normality.



(c) 4 responses/sub-average - distributions are becoming Poisson-like.



(d) 8 responses/sub-average - distributions are Poisson-like.

Fig.[8.8] The effects of increasing the sub-average size on the distributions of adjacent maxima and minima amplitude differences, in both the pre-stimulus and post-stimulus periods, of the single response sub-averages (trial #12 was selected arbitrarily).

The BIN structuring is slightly better in Fig.[8.7(a)] than it is in Fig.[8.7(b)], and thereafter it improves significantly. In Fig.[8.7(a)], it would seem that the bin cancellation process has successfully produced BIN segmentation. However, the increased activity in the BIN of Fig.[8.7(b)], suggests that the random distribution of polarised noise-events in Eq.[8.5] (i.e. $\{E_n/m_x\}$ and $\{E_n/m_n\}$) has been altered, effectively increasing the error in the event bin $\{E_X\}$. The return to improved BIN segmentation in Fig.[8.7(c)] and Fig.[8.7(d)] is almost certainly due to the higher SNR and the low pass gaussian filtering obtained through making larger sub-averages. Therefore, in this latter case, the advantages of the low frequency event filtering have been superseded by the increase in SNR.

Figs.[8.8(a) - 8.8(d)] illustrate the frequency distributions $H[\Delta_p]_m$, of amplitude differences between adjacent maxima and minima, calculated as described in Sec.[8.5.1] for the adaptive selection of PDF values. The same data sets as in Fig.[8.7] were used. $H[\Delta_p]_m$ changes progressively from approximately normal to Poisson as the size of the sub-average increases. This behaviour supports the explanations given above for the effects of sub-averaging on BIN segmentation. We can see, as was previously noted in Sec.[8.5.1], that the two $H[\Delta_p]_m$ produced from each side of the stimulus have very similar shape. Hence, either of the mode values $[\Delta_{md}]_m$ of $H[\Delta_p]_m$, can be used to approximate the response-specific PDF values.

The following points are given in summary of what has been said so far in this section:

- The random nature of additive noise means that the benefits of bin cancellation are most apparent when single response or low SNR data is being analysed.
- The use of sub-averages, results in a trade-off between obtaining good BIN segmentation using a small number of responses, and the provision of good quality averaged BAEPs which normally requires a large number of responses.
- The interest in obtaining latency variability estimates, means that the size of the sub-averages must be both small enough to preserve signal variability information, and large enough to offset adverse effects on bin cancellation.

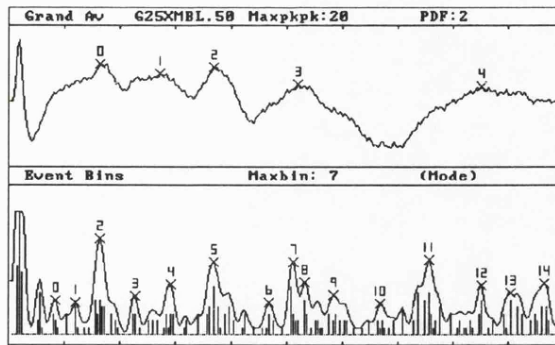
The use of ERPs for real-time monitoring of the central nervous system in intensive care units and during surgical operations, means that automated analysis procedures must be optimised for speed. Very recently, the author has made a short investigation into another form of sub-averaging which generates combinatorial averages of single responses from small sets of the data. These combinatorial averages retain some of the advantages of both bin cancellation and small sub-averages, without actually having to increase the *total* number of single responses when the size of the sub-average is increased.

Combinatorial averaging is simply a careful re-structuring of the order in which the original ensemble of data is combined. If, for example, we want to analyse an ensemble of 64 responses and specify a sub-average size of four, then a data set of 65 responses is acquired and divided into 13 subsets of five responses each. Five sub-averages are produced from the five possible combinations of four single responses within each subset. This results in a total of 65 sub-averages, 64 of which will be analysed. These sub-averages have an improved SNR because they contain more responses, but the SNR of their grand average will not be different to that achievable by averaging the original ensemble of single responses. This *local* improvement in SNR indicates that the BIN structuring (and GAV segmentation) will be better than that obtainable with no sub-averaging.

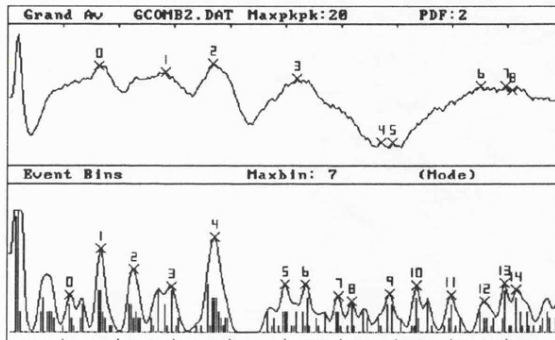
Figs.[8.9(a) - 8.9(d)] shows the results of combinatorial averaging using the same data set as in Fig.[8.7(a)] (i.e. 64 single responses). All GAVs in Fig.[8.9] are the same as expected, but the BIN structures show marked differences as the combinatorial sub-average sizes increase. The broad peak in the BIN of Fig.[8.7(a)] at wave V is no longer present in Figs.[8.9(b) - 8.9(d)]. These instead, now show a pronounced peak in the vicinity of the GAV inflection. It is difficult to predict where the benefits of higher SNR start to replace the benefits of bin cancellation. Given the small amount of work done in this one area, the author is only in a position to guess where this optimal point lies. Examination of both BIN representations (discrete and smoothed) shows that good BIN structure relies on the *dense* clustering of discrete BIN values. This characteristic is present in Fig.[8.9(c)] and the clustering starts to weaken in Fig.[8.9(d)]. The optimal point, therefore, probably lies between sub-average sizes of four and eight responses, in which the noise variance will be attenuated by between 25% and 12.5% respectively.

As was found with the normal sub-averaging process, when the sub-average size is small, the noise variance will be attenuated less, helping bin cancellation. The signal can be considered invariant within the sub-average, so we can expect an unbiased latency variability estimate. When the sub-average size is large, the noise variance will be attenuated more, which is detrimental to bin cancellation. The signal can no longer be considered invariant within the sub-average, so we can expect a biased latency variability estimate, despite the increase in SNR per sub-average.

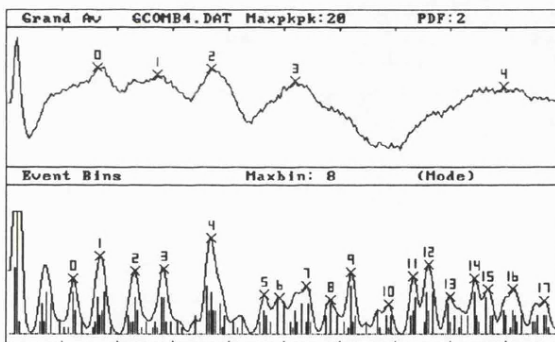
Fig.[8.10] shows the frequency distributions $H[\Delta_p]_m$ corresponding to the combinatorially averaged data. We can see how the distributions remain normal longer than was the case in Fig.[8.8] as the sub-average size increases. This averaging method is not fully evaluated, though there is strong evidence that it will prove to be useful in the analysis of low intensity BAEPs due to the retention of benefits arising from *both* sub-averaging and bin cancellation. The important



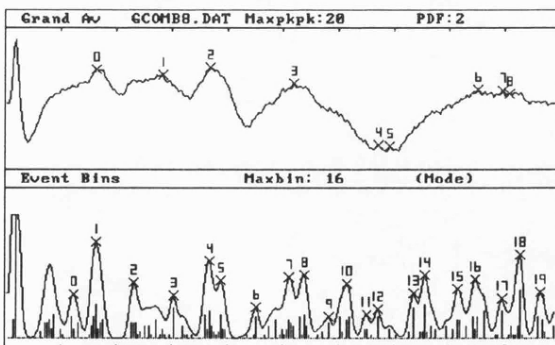
(a) 1 response/sub-average = 64 responses in total.



(b) 2 responses/sub-average = 64 responses in total.

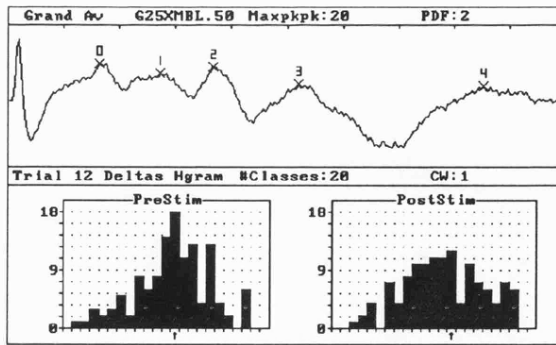


(c) 4 responses/sub-average = 64 responses in total.

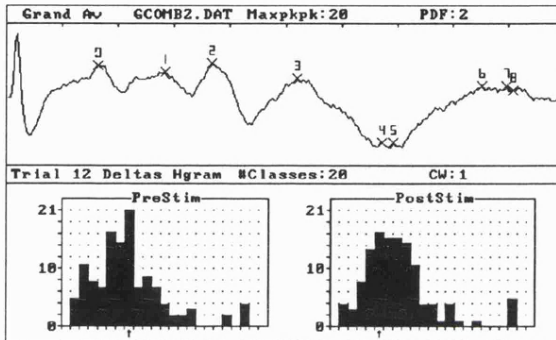


(d) 8 responses/sub-average = 64 responses in total.

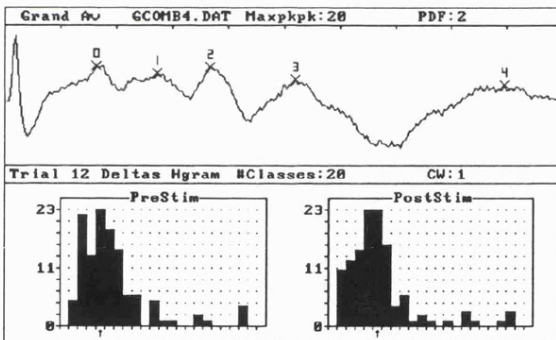
Fig.[8.9] The effect of increasing the sub-average size on BIN structuring, when the sub-averages are generated combinatorially. The total number of responses in all cases will remain the same, despite the increase in sub-average size.



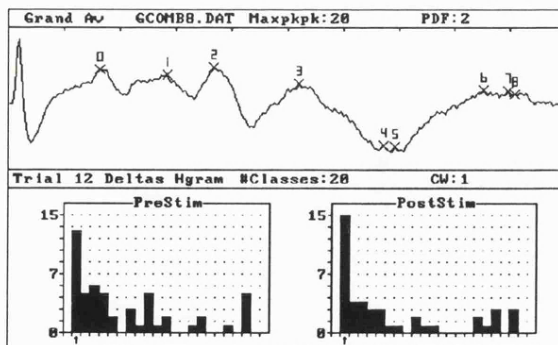
(a) 1 response/sub-averages - distributions are approximately normal.



(b) 2 responses/sub-average - distributions are approximately normal.



(c) 4 responses/sub-average - distributions are diverging from normality.



(d) 8 responses/sub-average - distributions are Poisson-Like.

Fig.[8.10] The effect of increasing the sub-average size on the distributions of adjacent maxima and minima amplitude differences, in both the pre-stimulus and post-stimulus periods, of the combinatorial sub-averages.

point about this form of averaging, is that all the assumptions for event analysis are preserved, i.e. the author has been careful not to obscure latency variability information by keeping sub-averages small, and the noise is still randomly distributed.

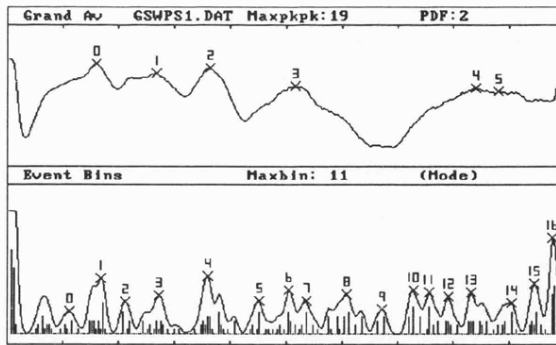
8.7.2 Event Binning with Filtered Single, and Sub-Averaged, Responses

The detailed discussion on sub-averaging given above has, hopefully, provided the reader with a clear understanding of how the SNR in sub-averages influences BIN structure. Adaptive low pass filtering was discussed in Sec.[8.6], and this procedure is useful for achieving improved SNRs in the ensemble of single responses and sub-averages prior to event analysis.

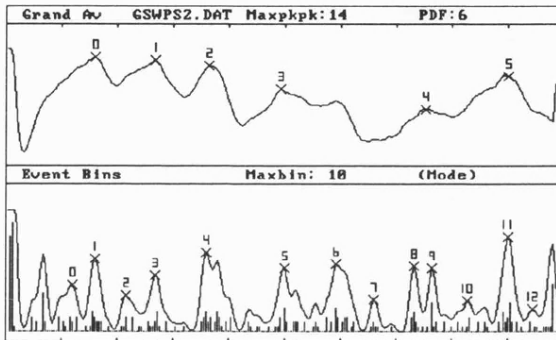
The results given in Figs.[8.11 - 8.14] correspond to the filtered representations of the data sets used in Figs.[8.7 - 8.10]. In general there is an improvement in both the quality of the GAV and the features in the BIN. In all cases the progress of structuring in the BINs follows a similar pattern to that of their unfiltered counterparts. The $H[\Delta_p]_m$, however, behave quite differently, in that none contain normal distributions of adjacent maxima and minima amplitude differences, but are more Poisson-like. This suggests that the benefits of bin cancellation are of lesser importance with filtered data than with unfiltered data, and that the major benefit is obtained through an increase in the SNR.

Although there is no dramatic improvement in the BIN structures of Figs.[8.11 and 8.13] over Figs.[8.7 and 8.9], we have achieved enhanced estimations of the averaged responses, albeit at the expense of another computational process. Since the parameters for the adaptive filtering are obtained through the application of generic event analysis functions, the integration of adaptive filtering into the kernel processes outlined by Fig.[8.6] was straight-forward in programming terms. There is no major disadvantage in the use of the adaptive filter, so it would be entirely up to the user of the suite of event analysis programs to decide for or against its invocation.

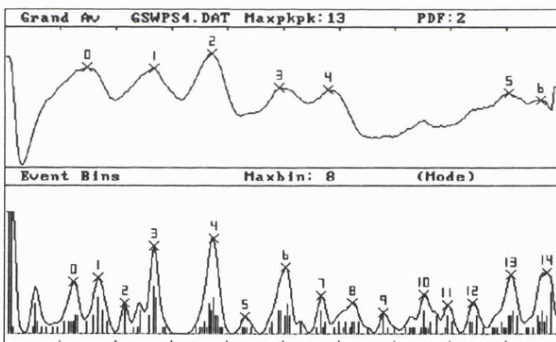
One is unable to predict the *exact* (non-frequency dependent) effects that any filtering process will have on amplitude variations in individual responses. This further increases the difficulty of making a judicious choice of PDF value. Hence, it is another argument for the use of an adaptive PDF estimation procedure.



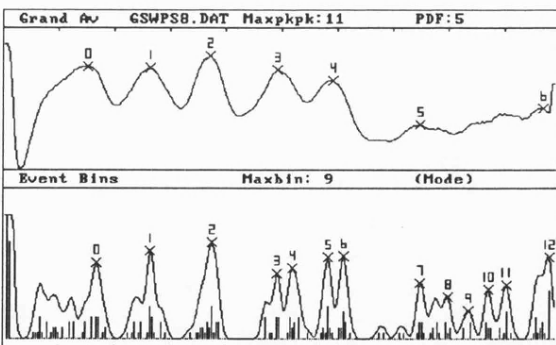
(a) 1 response/sub-average = 64 responses in total.



(b) 2 responses/sub-average = 128 responses in total.

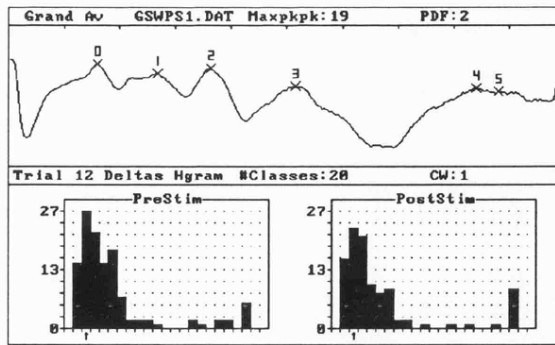


(c) 4 responses/sub-average = 256 responses in total.

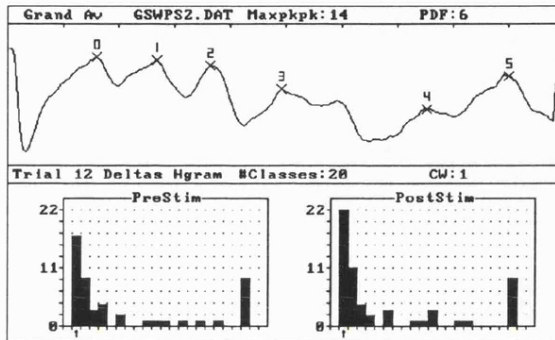


(d) 8 responses/sub-average = 512 responses in total.

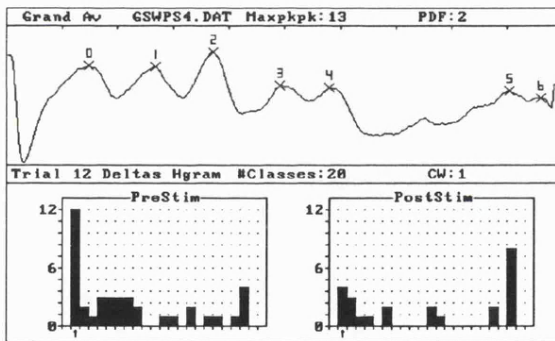
Fig.[8.11] Results obtained with filtered representations of the data sets used in Fig.[8.7]. BIN structuring is improved due to a reduction in much of the distracting noise at the single trial level. The appearance of the GAV is much better than in Fig.[8.7].



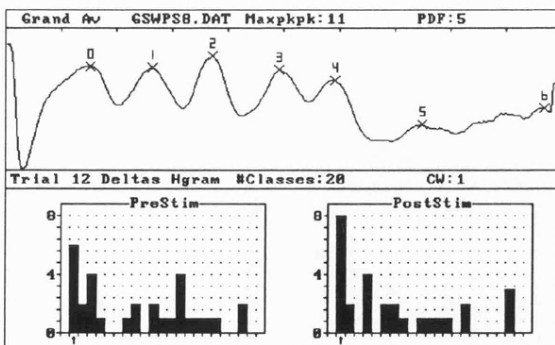
(a) 1 response/sub-average - distributions are approximately Poisson.



(b) 2 responses/sub-average - distributions are Poisson-like.

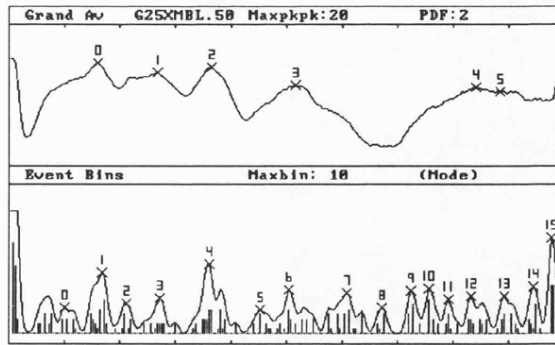


(c) 4 responses/sub-average - distributions are Poisson-like.

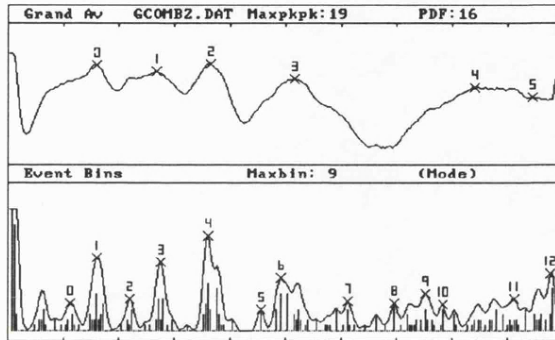


(d) 8 responses/sub-average - distributions are Poisson-like.

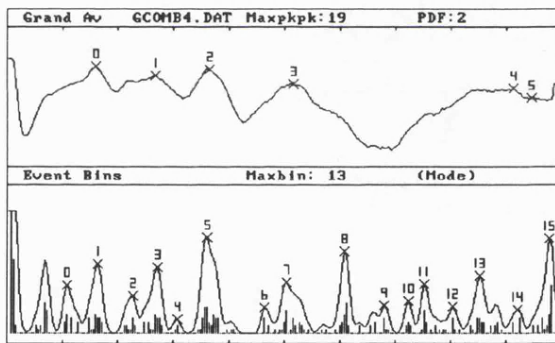
Fig.[8.12] Results obtained with filtered representations of the data sets used in Fig.[8.8]. The filtering procedure has altered the frequency distributions $H[\Delta p]_m$.



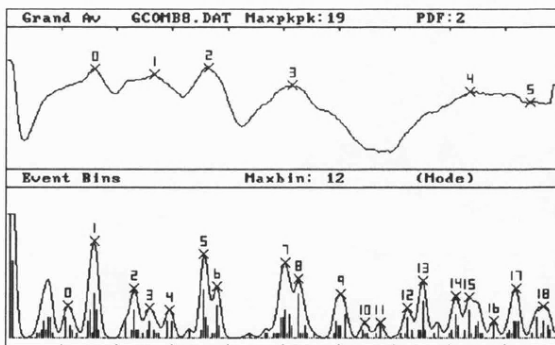
(a) 1 response/sub-average = 64 responses in total.



(b) 2 responses/sub-average = 64 responses in total.

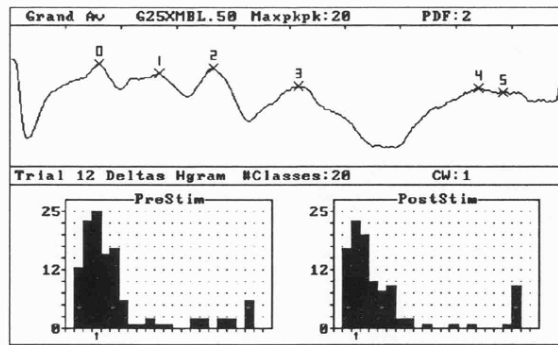


(c) 4 responses/sub-average = 64 responses in total.

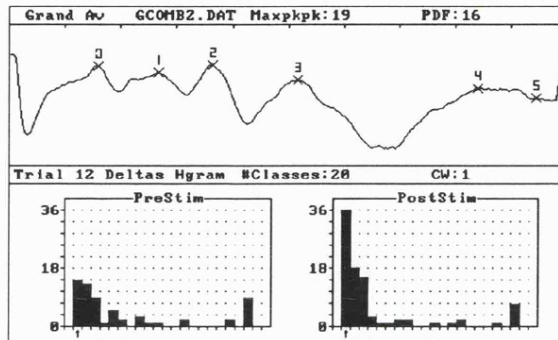


(d) 8 responses/sub-average = 64 responses in total.

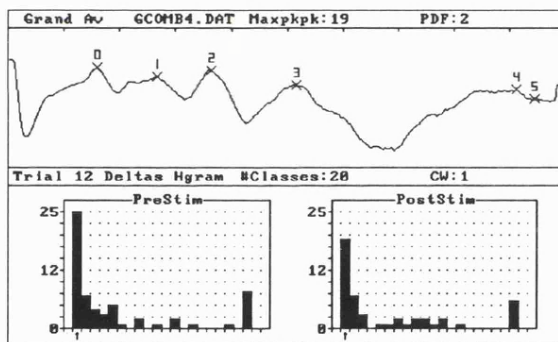
Fig.[8.13] Results obtained with filtered representations of the data sets used in Fig.[8.9]. BIN structuring is improved and the appearance of the GAV is much better than in Fig.[8.9].



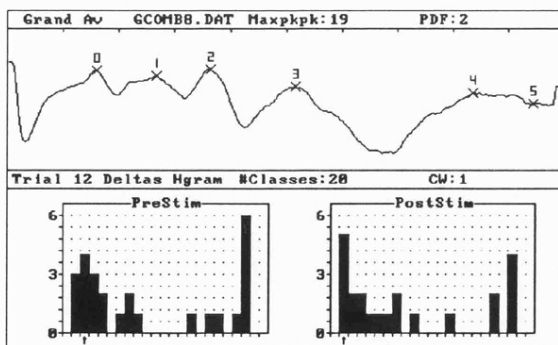
(a) 1 response/sub-average - distributions are approximately Poisson.



(b) 2 responses/sub-average - distributions are Poisson-like.



(c) 4 responses/sub-average - distributions are Poisson-like.



(d) 8 responses/sub-average - distributions are Poisson-like.

Fig.[8.14] Results obtained with filtered representations of the data sets used in Fig.[8.10]. The filtering procedure has altered the frequency distributions $H[\Delta p]_m$ in a similar way to that in Fig.[8.10].

8.8 A Model of the Synchronous Summation of Noise Events

The last section has emphasised the importance of the bin cancellation process for BIN structuring when single responses or small sub-averages are being analysed. In addition, filtering can be used to enhance both the BIN and the GAV. The author has also mentioned the advantages which can be gained from a reduction in the total number of trials required for an interpretation of the BAEP. From a commercial point of view, one can argue that providing trial reduction in conjunction with latency variability information, is the immediate task that must be addressed in BAEP research. For the first time then, it might be possible to seriously consider the use of BAEPs (and other EPs), for real-time monitoring of the central nervous system.

The fast generation of averages depends on both the stimulus repetition rate and the total number of responses acquired. In most circumstances, it is better to use low stimulus repetition rates where one can observe all the wave components in the BAEP (Sec.[7.4]). It follows that the total number of responses used is the main issue that must be considered when a fast averaging procedure is designed.

Although an automatic fast averaging procedure has not yet been implemented by the author, the modelling of bin cancellation with noise events has produced an insight into how this can be achieved with the existing kernel programs. As it stands, event analysis generates probability values for the events that are detected. The remainder of this chapter will make it clear to the reader how these probability values are calculated. For the time being, it is sufficient to say that all detected events, within and across trials, occupy a two dimensional *space* which is used to ascertain this probability. This *local* event-probability p , can be used to provide criteria for stopping data acquisition during fast averaging.

The two event analysis processes depicted in Fig.[8.6] can be implemented as a single process, and for each iteration of this *super-process*, the value of p can be re-calculated. We restate Eq.[8.6] which is:

$$\{E_x\} = \{E_s\} + \{E_n\} - \{E_{err}\}$$

and reiterate the objectives of event extraction which are:

- to reduce $\{E_n\}$ to zero, and
- to maximise the term $(\{E_s\} - \{E_{err}\})$ by adaptive PDF value estimation.

With a small trial size, the sum of terms $\{E_n\}_m$ across M responses may contribute to the error in the event bin $B[N]$. Certainly, if p is very low, then the numbers of $\{E_{n/mn}\}_m$ and $\{E_{n/mx}\}_m$ found in $\{E_n\}_m$ will be small, and their relative proportions are not likely to differ significantly, therefore resulting in an error. Determination of the probability of having an error, on the basis of the value p , will in turn allow the analysis to be driven in real-time, and terminated when an acceptable value of p is reached.

The *acceptable* value of p depends on an *acceptable* error contribution from $\{E_n\}_m$. When this value of p is reached, then one can assume confidently, that the BIN structuring is adequate and that the BIN may exhibit an acceptably small error in its event counts. At this point, the analysis should be in a reasonably good position to proceed with the latency variability estimations. The idea of dynamically monitoring the quality of the results from the analysis should prove to be very useful for knowledge based interpretation of the BAEP in an extended version of the EPAXIS expert system, since the results will contain the maximum amount of quantitative information for the expert system to reason with.

The probability model for bin cancellation with noise events utilises the generation of pairs of independent discrete random binomial processes. A pair of binomial processes represent a series of noise events $[E_{n/mx}]$ and $[E_{n/mn}]$, which are assumed to be drawn from the same temporal location in their corresponding event sequences $\{E_{n/mn}\}_m$ and $\{E_{n/mx}\}_m$ across M independent trials (i.e. they are synchronised). Furthermore, we assume that an event will always occur in each trial, and, therefore, we are subject to the constraint that the total number of the maxima and minima events does not exceed the total number of trials M . We know that with optimal bin cancellation, the sum of the polarised labels attached to all of the $[E_{n/mx}]$ and $[E_{n/mn}]$ should give a zero value in $\{E_X\}$ when there are no signal-related events $\{E_S\}$; see Eq.[8.8]. In order to simulate an error-count β in the event bin after M trials, it is only necessary that the total number of occurrences, of both $[E_{n/mx}]$ and $[E_{n/mn}]$, differs by β .

The discrete binomial probability $P(X = m)_M$ of obtaining m events in M trials, at an event probability p , is given by:

$$P(X = m)_M = {}^M C_m \cdot p^m \cdot p^{(M-m)}$$

$$\text{where } {}^M C_m \text{ is the binomial coefficient} = \frac{M!}{m! \cdot (M-m)!}$$

The discrete error probability $P(X = \beta)_M$ of obtaining an error of β in M trials is calculated for both the positive and negative errors $\beta = 0, \pm 1, \dots, \pm \text{MaxErr}$ (10), at several values of p up to 0.5. For each value of β , the trial size M is varied as $M = 4, 8, 12, \dots, \text{MaxTrials}$ (128). For each

of these values of M , a partial error probability $P(X = \beta)_m$ is calculated for each of the consecutive trials $m = 0, 1, \dots, M/2$. These represent the probability associated with just *one* of the possible ways in which an error of β can be generated in M trials. $P(X = \beta)_m$ is given by:

$$P(X = \beta)_m = P(X = m)_M \cdot [P(X = m + \beta)_M + P(X = m - \beta)_M], \quad \text{for } M - \beta \leq m \leq \beta,$$

$$P(X = \beta)_m = P(X = m)_M \cdot P(X = m + \beta)_M, \quad \text{for } m < M - \beta, \text{ and}$$

$$P(X = \beta)_m = P(X = m)_M \cdot P(X = m - \beta)_M, \quad \text{for } m > \beta.$$

The total error probability $P(X = \beta)_M$ for all the different ways of generating an error of β at one value of M is then given by:

$$P(X = \beta)_M = \sum_{m=0}^{M/2} P(X = \beta)_m \dots \dots \dots \text{Eq.[8.13]}$$

A plot of $P(X = \beta)_M$ versus M , is just one of the family of curves of error probability for all values of β . Another representation of the information contained in this family of curves is the cumulative error probability. In order to generate this family of curves, the values $P(X \leq \beta)_M$ for all trials M and β are calculated from the $P(X = \beta)_M$ values after computing Eq.[8.13]:

$$P(X \leq \beta)_M = 1.0 - \sum_{\beta = \text{MaxErr}} P(X = \beta)_M \dots \dots \dots \text{Eq.[8.14]}$$

This gives the probability of obtaining an error of less than β in M trials at a particular event probability value p . $P(X \leq \beta)_M$ is only an estimate, since $\text{MaxErr} \ll \infty$. The simulation results and their corresponding graphs are included Appendix [D3]. The simulation programmes are available in Appendix [D2]. An example of one family of curves for $P(X = \beta)_M$ is given in Fig.[8.15] for $p = 0.1$. This shows that the probability of obtaining small error counts is high when the trial size is small. As the trial size approaches 100, the curves at all values of β converge rapidly to a low error probability value. The bin cancellation error actually rises from $M = 4$ to about $M = 40$ for $\beta = [1 \text{ to } 5]$, before attaining a very shallow exponential decay beyond $M = 40$. This would seem to suggest that, without the aid of filtering and/or averaging to improve the SNR of single responses, reliance on bin cancellation for producing structure in the BIN is feasible only with a critical trial size of about 40. We must remember, however, that the latter statement is only valid for an event probability p of 0.1, and that the critical trial size must be increased at lower values of p .

Referring to Fig.[8.15], the efficacy of fast averaging can be predicted when a value of p is reached by mapping from the trial number on the abscissa to the error probabilities on the ordinate at various values of β . Alternatively, we could first establish an acceptable error count (e.g. five), and

Probability ($P(X=\beta)M$) of Bin Cancellation Error (β) for Increasing Numbers of Trials (M) at $p=0.10$.

Curves for $\beta = 0$ to 5 - Top to Bottom

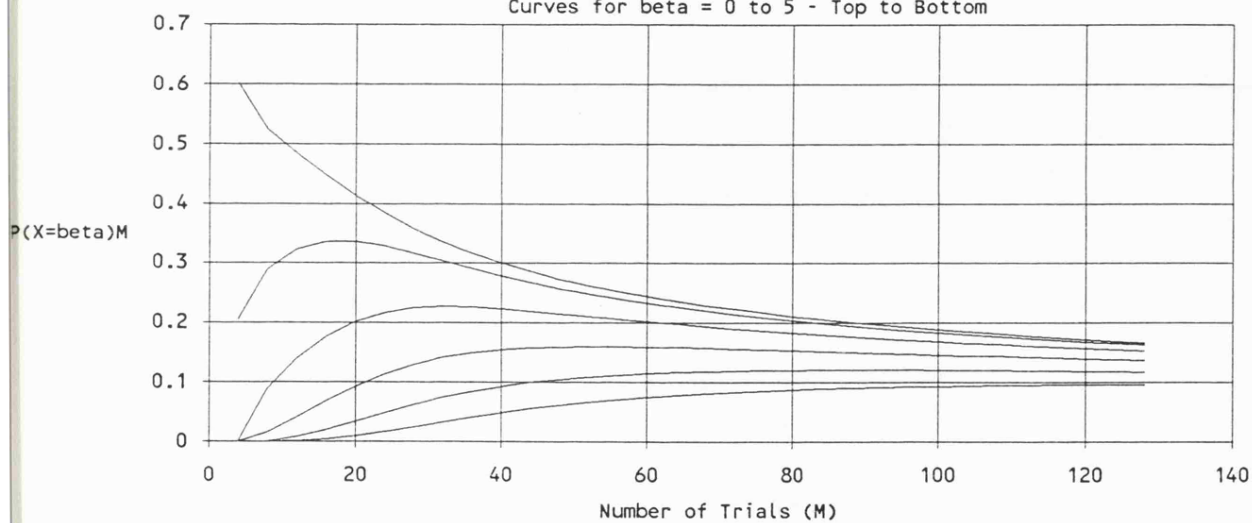


Fig.[8.15] Discrete binomial probability simulations for bin cancellation with noise events. Family of curves $P(X = \beta)M$, at $\beta = 0, 1, \dots, 5$ and $p = 0.1$.

Probability ($P(X \leq \beta)M$) of Bin Cancellation Error (β) for Increasing Numbers of Trials (M) at $p=0.10$.

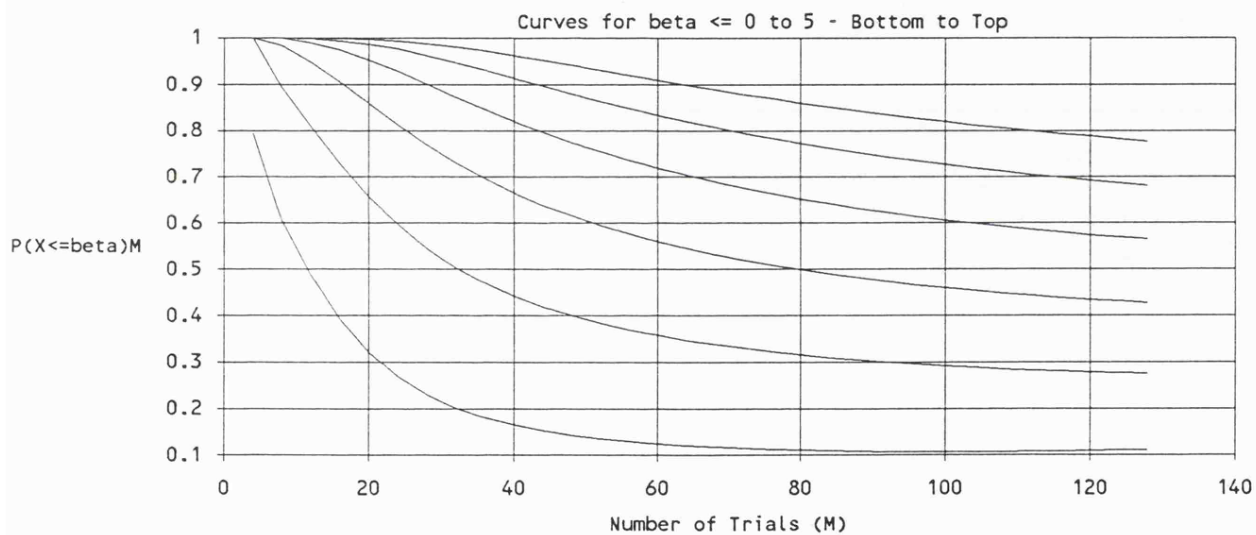


Fig.[8.16] Cumulative binomial probability simulations for bin cancellation with noise events. Family of curves $P(X \leq \beta)M$, at $\beta = 0, 1, \dots, 5$ and $p = 0.1$.

then run the event analysis procedure over a block of, say, 64 trials. If the dynamically computed value of p is greater than or equal to 0.1, then we can be reasonably confident that there is a low probability (less than 0.07) of obtaining an error of exactly five bin counts or events. Fig.[8.16], which shows the cumulative probability $P(X \leq \beta)_M$, reveals that there is a high probability (greater than 0.85) of obtaining at least an error of up to five events, and conversely a low probability of obtaining an error greater than five events.

We have seen from the above how it may be possible to implement a fast averaging procedure by using a dynamic check on the parameter p . The only change necessary for its implementation into event analysis, is to unify processes [A] and [B] in Fig.[8.6]. When sub-averaging and/or filtering are used, the criteria for stopping the averaging can be relaxed because of the increased SNR of the data.

The remainder of the discussion on event analysis will consider how latency variability estimates and the value of parameter p are obtained. Finally, the latency variability information will be used to generate enhanced averages of the BAEP through intelligent trial selection.

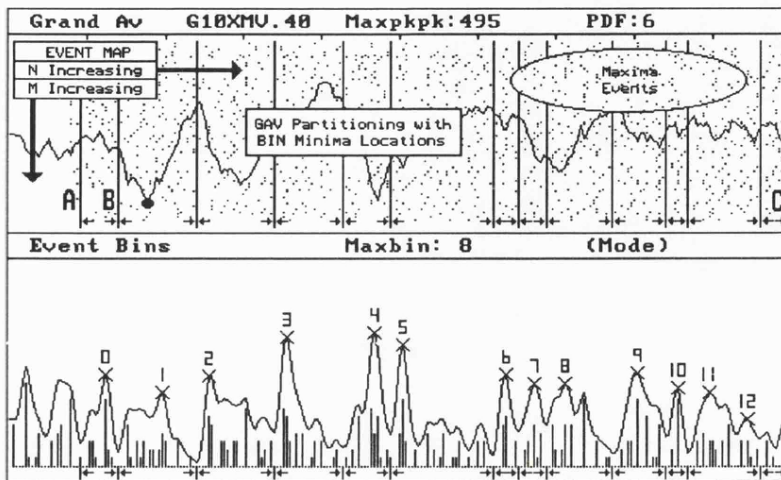
8.9 Latency Variability and Component Trajectories

During the event binning process, a two dimensional map of the events occurring within and across the single responses is maintained. This map, $T[M,N]$ is represented in the computer as an $M \times N$ bit array, whose elements $t_{m,n}$ represent markers for the events in the response sequences. A bit in this map is set to 1, only when event-maxima $\{E_{mx/m}\}_m$ are found. The row index m and column index n in $t_{m,n}$, correspond respectively to the response number and the time (sample point) at which an event-maximum has occurred. $T[M,N]$ is called the *trajectory* map for reasons which will become obvious later, and it is updated continuously during process [A] in Fig.[8.6].

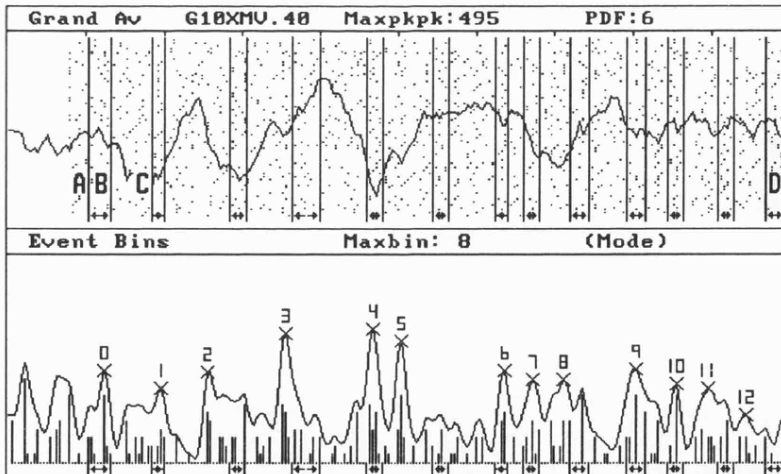
The reasons for the care taken to ensure that a good BIN structure was obtainable, become clearer at this stage of event analysis. Imagine a bit-mapped (pixel) image of $T[M,N]$, and consider only the post-stimulus portion $T[M,N/2]$. The space occupied by $T[M,N/2]$, in which maxima-events are set to 1, will resemble a peppered sheet of paper. If this were to be placed above the BIN of any of the example diagrams presented so far, i.e. pasted into the GAV window, then the minimum points in the BIN features will delimit several vertical segments in the space occupied by $T[M,N/2]$. These vertical segments will contain different proportions of the lit pixels depending on the individual widths of the delineating BIN features. The space that these vertical segments occupy is denoted by $T[M,\lambda N]$, or local trajectory space. The region bounded by the start of the first (leftmost) segment and the end of the last (rightmost) segment is denoted by $T[M,\gamma N]$, or global trajectory space, where γ is always less than $1/2$. The remaining space in $T[M,\gamma N]$, is delimited by the points between BIN features, and is called the inter-trajectory space $T[M,\iota N]$. In general $\lambda + \iota = \gamma$, and, furthermore because the delimitate points in the BIN are the adjacent minima, ι must be zero.

With Figs.[8.17 and 8.18], the author is not attempting to describe any EP-type dependent features, so we break from the normal, and use a pattern reversal visual evoked potential (PRVEP) data set (left eye, full-field, 56' check size, maximum contrast, $T_5 - F_z$ electrode derivation). The responses were inverted before analysis to obtain a BIN corresponding to the event-minima, thereby indicating where the P100 component is located (at the GAV label '●'). The use of a PRVEP also serves to demonstrate the generality of event analysis, except for the change in time scale required (i.e. in the case of the PRVEP, from 10ms to 500ms).

Fig.[8.17(a)] will help to familiarise the reader with the concepts of the trajectory map outlined above. This diagram shows the partitioning of the GAV window by the minimum points in the BIN features. Fig.[8.18(a)] is a filtered version of the same data set. The global trajectory space

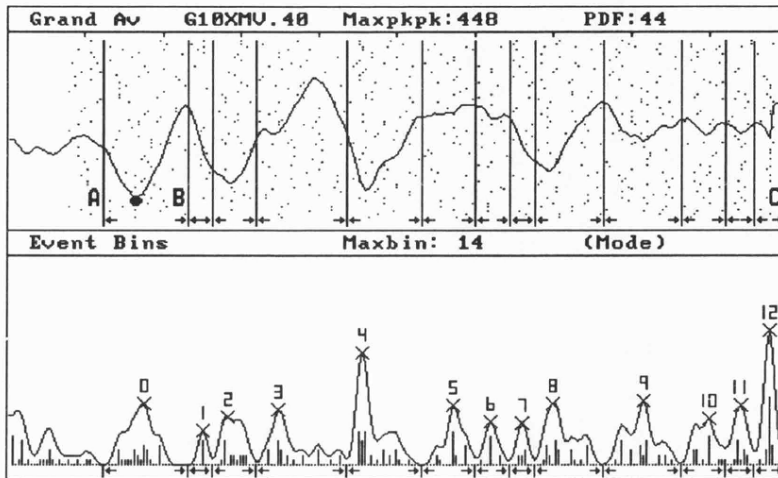


(a) Segmentation of the trajectory (event) map using BIN minima locations.

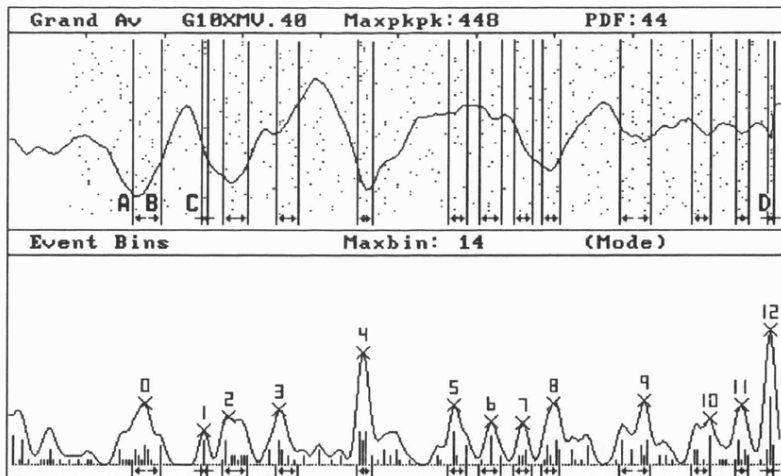


(b) Segmentation of the trajectory (event) map after iteration.

Fig.[8.17] Illustrations of the trajectory map obtained during event analysis, and their segmentation into global, local, and inter-trajectory spaces (see text). In (a), the label '●' indicates the location of the P100 PRVEP component (note: time scale is 50ms per division in this case).



(a) Segmentation of the trajectory (event) map using BIN minima locations.



(a) Segmentation of the trajectory (event) map after iteration.

Fig.[8.18] Illustrations of the trajectory map as in Fig.[8.17] using the same PRVEP data and filtering. There are fewer event-maxima in the map here compared to Fig.[8.17], and the P100 component is defined very well, in the BIN, GAV, and T[M, λ N] (note: time scale is 50ms per division in this case).

occupies a distance $C - A = \gamma N$, and the distance that a single vertical segment spans in local trajectory space is $B - A$. The sum total of these vertical segment spans is λN . In these examples there is no inter-trajectory space, so $\iota = 0$.

The regions bounded by the segments in local trajectory space contain significant GAV features, some of which might be of physiological importance. Each region also contains a population of latency markers, which were determined at the single response level, for the event-maxima that are part of the GAV feature contained in the region. The recognition of individual members of this *local population* of event-maxima, is reflected in the corresponding discrete BIN values. Each smoothed BIN feature can be viewed as an approximation to the distribution of the latencies in the local population of event-maxima. The peak in the smoothed BIN feature, therefore, represents the modal latency value of the local population of event-maxima. The mean latency of this local population, similarly, represents the mean latency value of the event-maxima which give rise to the corresponding GAV feature. It follows then, that the variance associated with each local population of event-maxima will approximate the variance of the corresponding GAV feature. This variance value is used as the estimate of component latency variability.

The effects of outlier observations on the mean latency estimate is minimised by performing an iterative procedure which converges to an unbiased mean estimate of the local population. This procedure first involves making an initial estimate of the standard deviation of the latency σ , and the mean latency μ , of the local population. The latency intervals (e.g. $B - A$ in Figs.[8.17(a) and 8.18(a)]), are then reset to $\mu \pm 1.65\sigma$ so as to enclose 95% of the population of event-maxima, assuming that they are normally distributed (c.f. spike rejection in Sec.[8.6]). This procedure is iterated through 10 cycles. The cycle count was determined through extensive tests with many data sets, and with iteration cycles reaching 50 in some cases. It was found that convergence to the local population mean and standard deviation could be achieved with cycle counts greater than seven. After this iterative process, the distributions of the *reduced* local populations are examined for any skew, and the latency intervals are adjusted to compensate for the original assumption of normality.

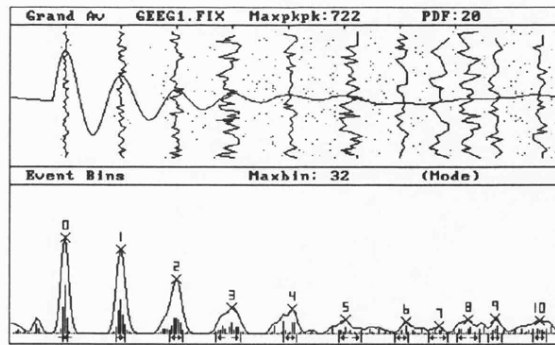
The resulting estimates for BIN segmentation are given in Figs.[8.17(b) and 8.18(b)] for the unfiltered and filtered PRVEP data respectively. In both these cases, the local trajectory space has been greatly compressed, and there is now an inter-trajectory space $T[M, \iota N]$. The distance that a single vertical segment spans in inter-trajectory space is $C - B$, and in local trajectory space this is $B - A$. The global trajectory space spans the distance $D - A$. The effectiveness of the iterative segmentation process is exemplified by examining the prior and post bounds of BIN peak '4' from Figs.[8.17(a) and 8.17(b)] respectively. We can see the common effect where prior bounds adjust to locate onto the most dense cluster of discrete BIN values. Further evidence of its

effectiveness is provided by counting the number of events in local and inter-trajectory space as the size of sub-averages increases and/or filtering is used. With the data sets of Fig.[8.9 and 8.13] (i.e. averaged and filtered data respectively), it was found that the *ratio* of the number of event-maxima found in local trajectory space to the number found in inter-trajectory space increased by nearly 400%. This means that the iterative segmentation process delimits local populations of events that are related to the components in the GAV, and that these events are not due to noise, since they persist with sub-averaging and filtering.

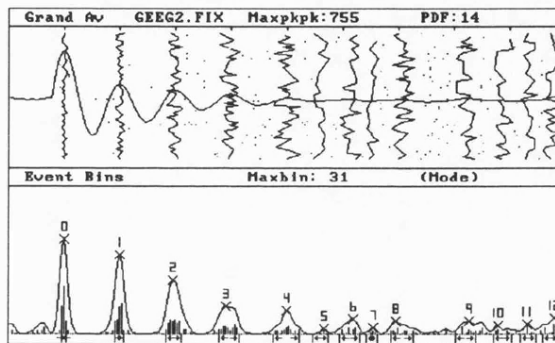
Having obtained the optimal bounds within $T[M,\lambda M]$, it is possible to plot the *trajectory* of the components in the single responses from one trial to the next using the latency values of the event-maxima in the segments of $T[M,\lambda M]$. This will provide the user with a graphical representation of where the components occur after the application of the stimulus and show how they progress across trials.

Fig.[8.19] illustrates the trajectory mapping obtained with the simulated data set described in Sec.[8.4]. We recall that this data set consisted of an invariant-signal file (i.e. in short: 64 trials of a 1 kHz, exponentially decaying, sine wave), combined additively with four different noise files to produce four ensembles of simulated responses. In Figs.[8.19(a) and 8.19(b)], where both the noise data are real, spontaneous, EEG records, the trajectories up to five milliseconds (i.e. at BIN peak '4' and a SNR of -14 dB in the GAV), contain high proportions of *active* periods and few *quiet* periods. Beyond this, as the SNR decreases, the trajectories become more variable and contain higher proportions of quiet periods. The detection and/or mis-detection of event-maxima is reflected in the activity of trajectories, and the omission of event-maxima is reflected in the quiet phases of the trajectories. In Figs.[8.19(c) and 8.19(d)], where the noise data are bandlimited, random, Poisson noise and random, gaussian noise respectively, the trajectories are highly variable and contain long quiet periods. This behaviour raises some questions about the accuracy of measurements of latency variability using the descriptive statistics of the trajectories, since, with the invariant underlying signal, the measured latency variability should be zero in all cases.

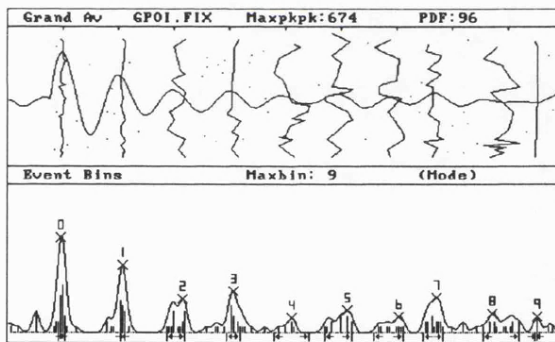
To a certain degree, the measured latency variability is driven by the additive noise characteristics, and it is important to determine the amount of error that is introduced into the measurement. The author has investigated this problem using the data from the simulations which were described in Sec.[8.4]. In addition, two more sets of data were generated, each, as before, consisting of four ensembles of simulated responses. These last two data sets were generated by adding the four individual noise files in turn to the signal file. However, prior to the addition, the single trials in the signal file were temporally shifted such that an artificial and pre-determined latency variability could be introduced into the signal peaks. In both data sets the mean signal latency was zero. In one of them, the induced standard deviation (Sd) in signal latency was 0.04ms, and in the other it



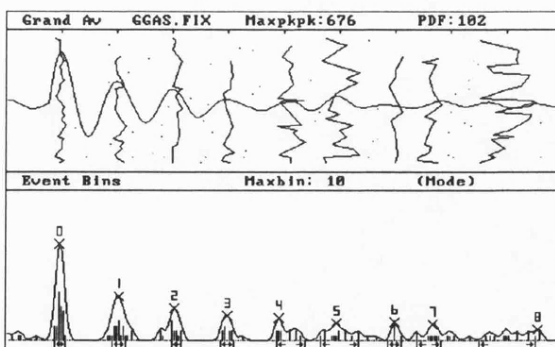
(a) Signal + Spontaneous EEG (1 response/sub-average)



(b) Signal + Spontaneous EEG (2 responses/sub-average)



(c) Signal + Poisson noise



(d) Signal + gaussian noise

Fig.[8.19] Trajectory maps obtained for one of the data sets used in the component latency variability recovery experiments. In each case, the simulated signal is invariant and combined with different noise data. The data set shown here is the same as that shown in Fig.[8.4].

was 0.08ms. Hence, in all, the three data sets consisted of data whose underlying signals had induced latency distributions $N(0,0)$ (i.e. an invariant signal), $N(0,0.0016)$, and $N(0,0.0064)$ respectively.

These data sets were passed through the event analysis procedures and the measured latency variability estimates were obtained for all the detected peaks. For each data set the measured latency variability of a peak was plotted against the SNR (and actual latency) at that peak. The three graphs obtained are reproduced in Figs.[8.20 - 8.22]. The errors in the recovery of the mean signal latency and the Sd of the signal latency are both $\leq 0.08\text{ms}$ for EEG noise and $\leq 0.16\text{ms}$ for the Poisson and gaussian noise, up to -10 dB. Beyond -10 dB the errors increase by approximately 50% with relatively worse errors occurring with Poisson and gaussian noise compared to those with EEG noise. The error values can be interpreted in terms of sampling points by dividing them by 0.04ms, i.e. the reciprocal of the sampling frequency (25 kHz). A complete set of results, including the numerical and graphical outputs of event analysis, is included in Appendix [D4].

McGillem et al. (1985) have derived an expression for the amount of error that additive noise introduces into latency measurements. Their approach was to compute the standard deviation of single trial peak latency measurements for an invariant signal plus random gaussian noise model. Latency measurements were made as was described in Sec.[7.2.2]. The resulting expression for the standard deviation of the latency (SDL) at a signal peak is as follows:

$$\text{SDL} = \frac{0.43 \cdot R \cdot f_s}{\sqrt{\text{SNR}}} \dots \dots \dots \text{Eq.[8.15]}$$

where R is the radius of curvature of the peak in sec^2 (i.e. a measure of its sharpness - the smaller it is the narrower the peak), f_s is the sampling frequency and it is assumed that this is at the Nyquist rate for the noise. For a typical BAEP, a single component might correspond to a loop of a 1 kHz sinusoid ($f_0 = 1 \text{ kHz}$). The corresponding radius of curvature $R = (1/2\pi f_0)^2 = 2.53 \times 10^{-8} \text{ sec}^2$, and for a sampling frequency of 25 kHz, the standard deviation of the latency would be:

$$\text{SDL} = \frac{0.43 \cdot 2.53 \times 10^{-8} \cdot 25000}{\sqrt{\text{SNR}}} = \frac{0.27}{\sqrt{\text{SNR}}} \text{ ms}$$

The value of the latency measurement error, as predicted by the expression above, would be much greater than that obtained in the experiments that have just been described for SNRs as low as -10 dB. Therefore, the careful application of adaptive PDF values in the selection of peaks, and the iterative component location procedures seem to work very well together when used to extract latency variability measures.

It is not known what effects a reduction in sampling frequency and sub-averaging and/or filtering will have on the latency variability estimates. However, if Eq.[8.15] is used as a guideline, then one can confidently predict that the outcome will be favourable, in that the latency variability estimates will be improved due to a reduction in the error through (a) an increase in SNR, and (b) a reduction in f_s . It is expected that changes in the analogue filter settings will affect the accuracy of the latency variability recovery due to the inclusion/exclusion of high frequency activity. In Figs.[8.20 - 8.22], the poorer estimates of latency variability obtained with the data containing Poisson and gaussian noise, are paradigmatic of the effects of noise bandwidth on the definition of the signal peaks (cf. R in Eq.[8.15]). In this respect pre-whitening the data may improve the estimate, provided no additional filtering is used, because the definition of peaks and bin cancellation will be enhanced, and the estimated PDF values will be lowered for increased sensitivity.

In the author's opinion, the latency statistics obtained with event analysis are sufficiently accurate to be used for assessing the latency variability associated with real BAEP signals. Since the SNR in other ERPs is generally much higher than in BAEPs, latency variability estimates can be determined in these cases also.

SNR (-dB) and Latency (ms)

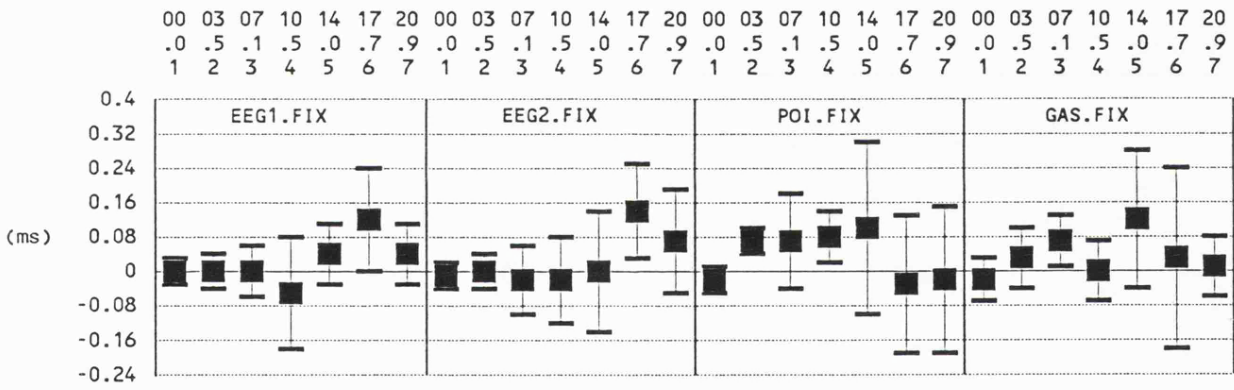


Fig.[8.20] Error in recovery of mean signal latency T (+/- 1Sd) in noise vs SNR. Signal latency distribution is N(0,0) and noise files are spontaneous EEG, Poisson, and gaussian.

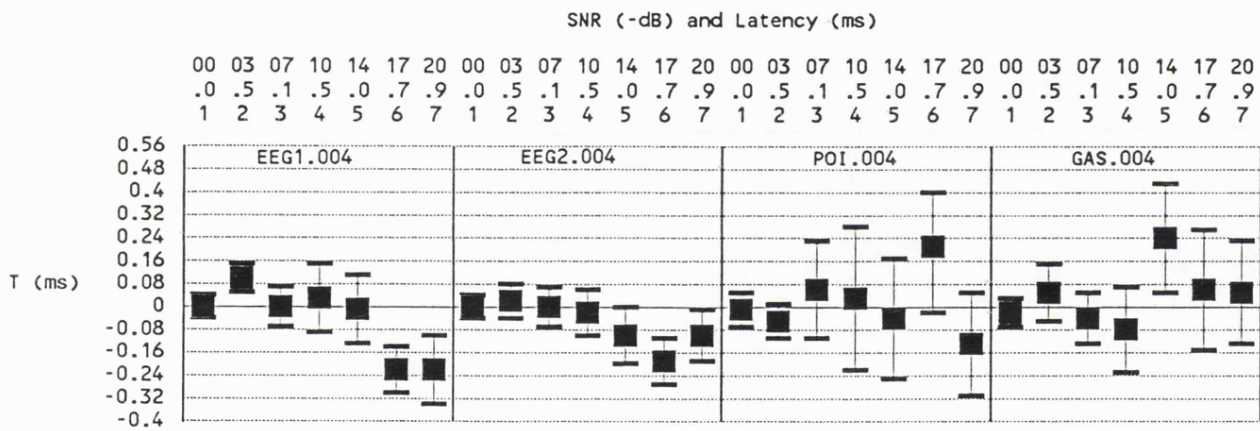


Fig.[8.21] Error in recovery of mean signal latency T ($\pm 1\text{Sd}$) in noise vs SNR. Signal latency distribution is $N(0,0.0016)$ and noise files are spontaneous EEG, Poisson, and gaussian.

SNR (-dB) and Latency (ms)

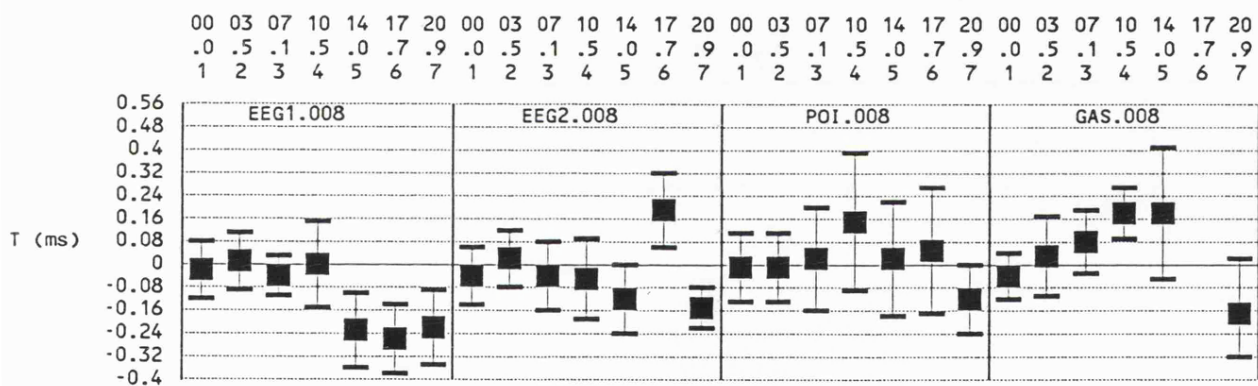


Fig.[8.22] Error in recovery of mean signal latency T ($\pm 1\text{sd}$) in noise vs SNR. Signal latency distribution is $N(0,0.0064)$ and noise files are spontaneous EEG, Poisson, and gaussian.

8.10 Significance Testing of BAEP Components

In this section the author will clarify the relationship between the various trajectory spaces and fast averaging. The local event-probability p , which connects the concepts of trajectory spaces and fast averaging, is described first. Following this, it is shown how p can be used in determining the significance of those trajectories associated with BAEP components. Extraction of the significant components (i.e. trajectories) enables one to reduce the number of candidate trajectories competing for definite assignment to individual components. This will be important in the enhancements that need to be incorporated into the prototype expert system (EPAXIS) for the automatic selection of BAEP components and their interpretation. The statistical properties associated with event-maxima in significant trajectories, provide the means of re-examination of the ensemble of single responses in order to create homogenous sets of single responses containing specific components and combinations of components. From an EP/ERP research point of view, this presents us with new and considerable possibilities to investigate the relationships between components.

Once the limits of global trajectory space $T[M,\gamma N]$ have been determined with the help of BIN features, we can calculate the probability of an event-maximum occurring anywhere within this space. This global event-probability p_g is given by:

$$p_g = \frac{\text{total number of event-maxima found in } T[M,\gamma N]}{\text{total number of event-maxima possible in } T[M,\gamma N] = M \cdot \gamma N}$$

A similar calculation is performed for the local event-probability p_l (previously denoted by p) in local trajectory space $T[M,\lambda N]$, and for the inter event-probability p_i in inter-trajectory space $T[M,\iota N]$. When the distribution of event-maxima in $T[M,\gamma N]$ is uniform, it is expected that $p_l = p_i$. This is a situation that is most likely to occur with single responses exhibiting white noise characteristics. In the presence of non-stationary signal activity, it is expected that p_i will be less than p_l , due to a *relative* increase in the total number of signal-related event-maxima found in $T[M,\lambda N]$. Achieving higher values for p_l , as the number of responses being analysed increases, is indicative of the presence of signal-related activity. Therefore, as described in Sec.[8.8], p_l can be used as a stopping criterion in fast averaging.

In order to test whether or not a trajectory is significant, we need to determine if the sample of event-maxima in the segments of $T[M,\lambda N]$ is drawn from the same population of event-maxima in $T[M,\gamma N]$ and/or $T[M,\iota N]$. The true distributions of events in the trajectory spaces are not really known. In the presence of non-stationary activity it is assumed that: (a) the distribution of events

in $T[M,\iota N]$ is uniform, (b) the distribution of events in the segments of $T[M,\lambda N]$ is binomial (cf. the model of bin-cancellation described in Sec.[8.8]), and (c) the distribution of events in $T[M,\gamma N]$ lies somewhere between (a) and (b). Without having to make any assumptions about the distributions of events, the significance of trajectories can be determined using a χ^2 tests for goodness of fit of the individual segment distributions in $T[M,\lambda N]$ to the *overall* distributions in either of, or each of $T[M,\gamma N]$, $T[M,\lambda N]$, or $T[M,\iota N]$ (i.e. using p_g , p_l , or p_i respectively). The trajectories can then be classified (graded) according to the degree of goodness of fit to these distributions.

To decide at the significance level α whether the trajectory events constitute a sample from a population with an arbitrary distribution $f(x)$, we first compute the expected number of observations that would fall in each category of the sample as predicted by $f(x)$. To compare the observed frequencies o_i , for the i^{th} category, with expected (theoretical) frequencies e_i , we compute the χ^2 statistic over the r categories:

$$\chi^2 = \sum_{i=1}^r \frac{(o_i - e_i)^2}{e_i}$$

A trajectory sample is comprised of two categories $r[1]$ and $r[2]$, where $r[1]$ is success $[o_1, e_1]$, i.e. containing those trajectory events that have been found, and $r[2]$ is failure $[o_2, e_2]$, i.e. containing those trajectory events that have not been found or, in fact, non-existent. For category $r[1]$, the observed frequency o_1 of events is obtained by simply counting the number of trajectory events. The expected frequency e_1 in $r[1]$ is computed by multiplying the width of the segment in the local trajectory by $p_e = p_g, p_l$, or p_i , depending upon which distribution is being fitted (i.e. $e_1 = \text{width of } T[M,\lambda N] \text{ segment} \times p_e$). For category $r[2]$, o_2 and e_2 are computed by subtracting o_1 and e_1 from the total number of trials being analysed M . Therefore, after simplification, the χ^2 statistic for a trajectory in a segment of $T[M,\lambda N]$ is given by:

$$\chi^2 = \frac{(o_1 - e_1)^2}{e_1} + \frac{(o_1 - e_1)^2}{M - e_1}$$

The null hypothesis, that the trajectory events are drawn from the distribution $f(x)$, is rejected at $\alpha = 90\%$ significance level, if χ^2 exceeds $\chi^2_{.9,1} = 2.71$ for one degree of freedom $\nu = 1$. The χ^2 probability value $P(\chi^2 | \nu)$ is numerically computed for the trajectories during event analysis using the incomplete gamma function provided in Press et al. (1988).

The results tables in Appendix [D4] show the χ^2 statistics for the data sets that were used to produce Figs.[8.20 - 822]. The values for χ^2 and $P(\chi^2 | \nu)$ in these tables were calculated using the local event-probability p_l so as to determine the trajectories with the highest grade. The values for χ^2 and $P(\chi^2 | \nu)$ which are computed using p_g and p_l are not yet available in event analysis. They can, however, be calculated very easily using the probability and span values which are available from the analysis (see result tables in Appendix [D4]).

In conjunction with the scheme proposed for dynamic data-quality monitoring for fast averages (Sec.[8.8]), this trajectory grading concept will have implications for the enhancements that are being incorporated into the EPAXIS expert system. The grading scheme is actually another form of measuring the quality of the data.

The next section discusses a method of generating enhanced averages of the BAEP by intelligent trial selection. The use of the word *intelligent* is deliberate, in order to emphasise the connection between event analysis and the EPAXIS expert system. The designs of both systems were complementary to one another. It is the author's intention that EPAXIS will automatically perform the decision process of trajectory selection and subsequent scoring of the BAEP, using the significance values for the trajectories, and BIN and GAV information, etc. as are output by event analysis. For the purposes of the following discussion on *intelligent averaging*, it is not important that EPAXIS and event analysis are functionally interfaced. The decision making intended for EPAXIS at this stage of event analysis has been performed manually.

8.11 Enhanced Averaging by Intelligent Trial Selection

The information, contained in the trajectories, which relates to the latency of events, is vital for enhanced averaging. We have seen how trajectories can be graded for quality and then manually selected (or automatically selected with EPAXIS) to be representative of specific components in the averaged BAEP. For each of the five major components in the BAEP, the corresponding trajectory contains information on:

- (a) the mean latency of the component,
- (b) the variance of the component,
- (c) the latency of each of the detected event-maxima that constitute the component, and
- (d) which trials in the ensemble of responses contain an event-maximum related to a specific component.

Item (d) is perhaps the most useful for enhanced averaging, since it enables one to selectively re-average the ensemble of responses. This is done by averaging only those trials that have a valid event in a trajectory. Since the five major trajectories are component-specific, the five new averages of the BAEP which can be produced, will each serve to enhance their own *source* component. An enhancement can be achieved because, only those trials with events are included, and more importantly, only those trials that contain noise-events and/or events due to spikes, are omitted. As the author shall demonstrate shortly, this simple procedure has proved to be surprisingly effective.

The five component-specific averages are called the *source averages*, and using their trajectories, the analysis has been extended to produce *derived averages*, which comprises an homogeneous set of trials containing pre-determined combinations of component-specific trajectories and their events. These derived averages allow for the investigation of the relationships that may exist between components.

In order to generate the above source and derived averages, the event analysis program first maps the events contained within the five pre-selected, component-specific, trajectories into the first five columns of an $M \times 13$ bit array, $C[M,13]$ (where M is the total number of trials). Bits in $C[M,13]$ are set to '1' in the five *source* columns corresponding to each of the component-specific trajectories, and in the M rows corresponding to the trial numbers that contain events in the trajectories. Second, the homogenous sets of trials that result in the derived averages are generated in the remaining eight *derived* columns in $C[M,13]$. The first five of the derived columns are generated by performing a bit-wise 'and' operation on selected combinations of source

columns. This operation produces the intersection-sets of homogeneous trials. The remaining three derived columns are generated by performing a bit-wise 'or' operation on selected combinations of source columns, and gives the union-sets of homogeneous trials.

The combinations of BAEP components chosen for the derived columns in $C[M,13]$ are formally specified as follows:

- The pre-selected component-specific trajectories T_t are:

$$T_t = \{e_1, e_2, \dots, e_{M-1}\} \text{ where } t = 0, 1, \dots, 5 \text{ and } e_m = 1 \text{ or } 0, \\ \text{and the overall source set } S = \{T_1, T_2, \dots, T_5\}.$$

- The intersection sets I_i are:

$$I_1 = T_1 \cap T_3, \\ I_2 = T_1 \cap T_5, \\ I_3 = T_3 \cap T_5, \\ I_4 = T_2 \cap T_4, \\ I_5 = T_1 \cap T_3 \cap T_5, \\ \text{and the overall intersect set } I = \{I_1, I_2, \dots, I_5\}.$$

- The union sets Y_u are:

$$Y_1 = T_1 \cup T_3 \cup T_5, \\ Y_2 = T_2 \cup T_4, \\ Y_3 = T_1 \cup T_2 \cup T_3 \cup T_4 \cup T_5, \\ \text{and the overall union set } U = \{Y_1, Y_2, Y_3\}.$$

- The universal combination set $C = \{S, I, U\}$, which is represented in the computer as the bit-mapped array $C[M,13]$.

The trajectory combinations in I and U were specified on the basis of what has been stated, about the manifestation of certain components in the presence of others, in numerous publications (e.g. Jewett, 1970; Picton, 1988). In particular, there is much quoted of the normal values for waves I, III and V, and their respective inter-peak latencies. This is because they have consistent representations in the averaged waveform at all stimulation intensity levels and stimulus repetition rates. Additionally, a normal data study (conducted by Robinson and Robinson of Medelec Ltd, Woking, Surrey, 1988) has also consistently shown high correlations between these waves and also between waves II and IV.

Apart from the intelligent averaging described above, it is also feasible to compute a form of latency corrected average (LCA) using the mean latencies of events in the component-specific trajectories. Since the total number of responses being analysed is small, it should be advantageous to temporally align events, that fall within the bounds of a component-specific trajectory, with the mean latency prior to re-averaging. The procedure used in this investigation does not *splice-out* segments of the LCA corresponding to each component-specific trajectory and then attempt to fit a curve to the segments (cf. LCA described in Sec.[7.2]). Instead, five *grand* LCAs are generated, which have each been, in-turn, corrected to the mean latency of one of the five component-specific trajectories. From each of these grand LCAs, a *source* LCA is produced using trials chosen from S as for the five source averages mentioned earlier. Selective re-averaging has to be performed several times using trials chosen from I_i or Y_i to generate each one of the *derived* LCAs. For these cases, to extract the corrected form of each component, re-averaging is performed however many times there are trajectories in the individual I_i or Y_i respectively. For example, if the derived LCA for I_1 was being generated, and the column vector for I_1 in the combination map showed 10 trials containing the combination of trajectories ($T_1 \cap T_3$), then the resultant LCA would be computed from the *same* 10 trials taken from *both* grand LCAs for T_1 and T_3 . This means that the derived LCA for I_i would eventually contain a total of 20 trials.

The latency alignment in LCA will exaggerate the contributions of trajectory events to the morphology of the corresponding components in the averaged BAEP. The peak of a latency corrected component will, in most cases, be found to exist at the mean latency of the trajectory used for the correction. Generally, one would attempt to select the trajectories corresponding to each of the five major components in the BAEP, so that the intersect and union sets of trials would be meaningful. To extend event analysis for intelligent averaging with other EPs would simply be a case of redefining the combinations of interest in I and U.

Some illustrative results for intelligent averaging and event analysis are given in the case studies that follow in the next section.

8.12 Event Analysis Case Studies

A complete set of results from event analysis of BAEPs can be overwhelming, especially if both ipsilateral and contralateral channels are being investigated. The case studies that are presented here will attempt to provide a global overview of the full event analysis procedure using contralateral channel data only. A small, but representative set of graphical and statistical output will be interspersed with short descriptions of the objectives, so that the reader may see how the event analysis programs can be used to find information in the BAEP.

8.12.1 Case Study A

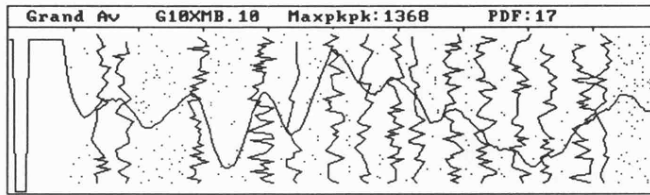
Background Information:

- **Data set:**
Name - 10xmb.10; Channel - contralateral; Stimulus intensity - 75 dBSL; Sex - male.
- **Data specification:**
16 responses / sub-average; 64 unfiltered sub-averages; 1024 responses in total.

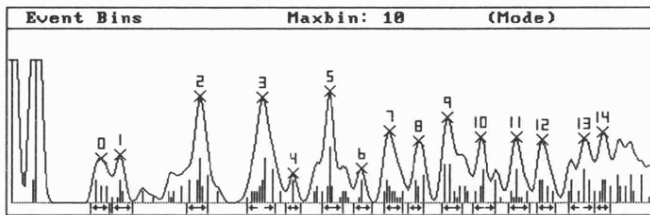
The diagrams in Fig.[8.23] show the general results obtained from the preliminary stages of event analysis. The reader should be familiar with their formats and meaning. Fig.[8.23(d)] shows the frequency distribution of latency intervals between adjacent maximum and minimum events, $H[(\Delta t)_p]_m$, which is used for spike rejection in, and adaptive low pass filtering of the ensemble of trials (Sec.[8.6]). The information in the event bins of Fig.[8.23(b)] suggests that significant activity exists in the GAV (Fig.[8.23(a)]) at latencies in the vicinity of BIN peaks '1', '2', '3', '5', and '7'. The trajectories in Fig.[8.23(a)] which correspond to these BIN peaks bisect the major components of the averaged BAEP.

The number of trajectories present in the latency interval occupied by the major BAEP components is low in comparison to the number of features of interest in the BAEP. This behaviour is expected, since the trials being analysed consist of small sub-averages (Sec.[8.7]), and the stimulation intensity is high which also serves to increase the SNR of the 1024 individual single responses. In this case, the benefits of bin cancellation were most likely to have been superseded by the benefits of having an increased SNR (Sec.[8.7]).

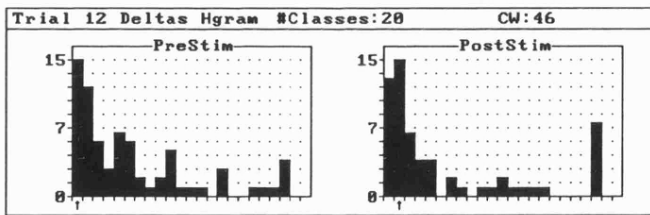
Wave I in Fig.[8.23(a)], at about 1.5ms, is broad and has a *ragged-top* consisting of multiple peaks. This is reflected in the bifid BIN peaks '0' and '1'. It would be a relatively simple matter to score (or label) this BAEP using information from the well-structured BIN in conjunction with normal values for the latency of components (given in Appendix [D5]). However, to gain a greater



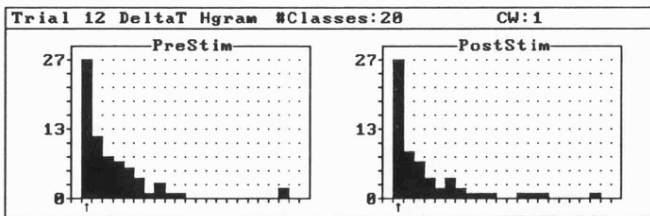
(a) GAV and Trajectory map $T[M, \gamma N]$.



(b) BIN and segment limits in $T[M, \gamma N]$ for $T[M, \lambda N]$.



(c) Frequency distribution $H[\Delta p]_m$.



(d) Frequency distribution $H[(\Delta t)_p]_m$.

Fig.[8.23] General results obtained from preliminary stages of event analysis.

understanding of the activity that produced the complicated wave I component, one must resort to an examination of the BAEP at the single-response or single sub-average level (Sec.[7.1]). We will use intelligent averaging to aid an investigation of the BAEP at this lower level.

The statistics for this data set, which were generated at the preliminary stages of event analysis, are shown below in Table [8.1] (see Appendix [D4] for an explanation of the attributes in the table):

Event Probabilities:

Max GPks possible (uniform) : 12800

Total GPks found : 684

Global Probability of Pk : 0.05

Max LPks possible (uniform) : 7424

Total LPks found : 493

Local Probability of Pk : 0.07

Max InterPks poss. (uniform) : 5376

Total InterPks found : 191

Inter Probability of Pk : 0.04

Item N ^o	GPkAmpl	GPkLat	BPkAmpl	BPkLat	Mn	SD	Q	E	ChiSq	ChSqP	BinomP	%Swps	CC	Span
0	. . . 162	1.72	1558	1.44	1.42	0.07	27	30	0.48	0.49	0.00	42.19	0.90	7
1	. . . 217	2.80	1683	1.72	1.76	0.09	23	34	7.59	0.01	0.00	35.94	0.88	8
2	. . . 230	3.96	3686	2.96	2.92	0.09	43	34	5.08	0.02	0.00	67.19	0.93	8
3	. . . 689	4.96	3641	3.92	3.90	0.12	47	47	0.00	0.94	0.00	73.44	0.89	11
4	. . . 392	5.92	1023	4.40	4.40	0.07	20	26	1.97	0.16	0.00	31.25	0.95	6
5	. . . 57	6.88	3858	4.96	5.00	0.09	37	34	0.56	0.45	0.00	57.81	0.93	8
6	. . . -372	7.68	1220	5.44	5.46	0.08	26	30	0.88	0.35	0.00	40.63	0.93	7
7	. . . -450	8.32	2475	5.88	5.95	0.08	35	30	1.73	0.19	0.00	54.69	0.85	7
8	. . . 208	9.48	2152	6.32	6.27	0.08	28	26	0.41	0.52	0.00	43.75	0.90	6
9	. . . 0	0.00	2947	6.76	6.82	0.10	40	34	2.26	0.13	0.00	62.50	0.93	8
10	. . . 0	0.00	2258	7.28	7.32	0.11	32	38	2.54	0.11	0.00	50.00	0.94	9
11	. . . 0	0.00	2282	7.84	7.87	0.09	32	34	0.25	0.62	0.00	50.00	0.94	8
12	. . . 0	0.00	2177	8.24	8.30	0.08	31	30	0.10	0.75	0.00	48.44	0.89	7
13	. . . 0	0.00	2240	8.88	8.85	0.12	40	43	0.44	0.51	0.00	62.50	0.80	10
14	. . . 0	0.00	2453	9.16	9.16	0.06	32	26	2.75	0.10	0.00	50.00	0.89	6

Table [8.1]

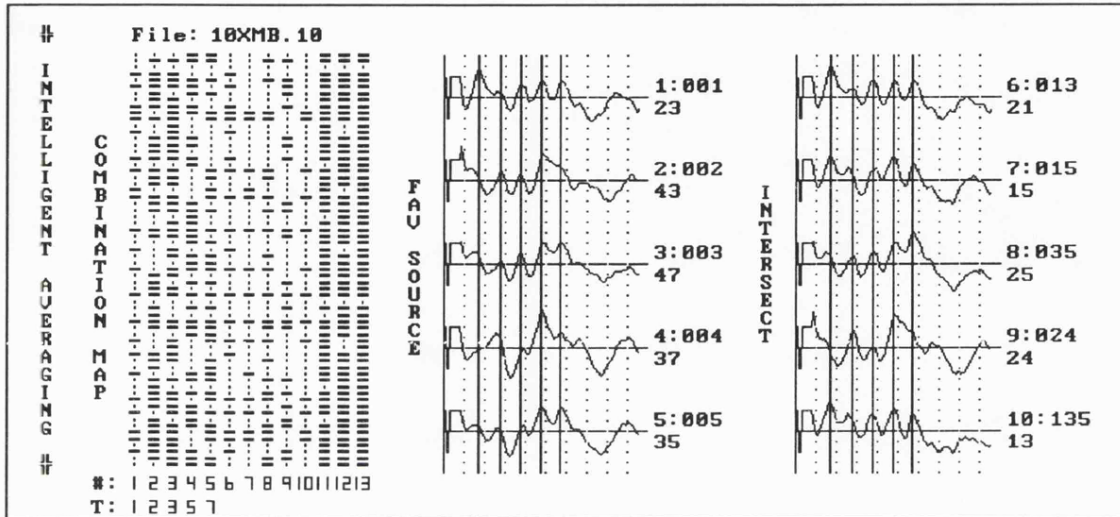
The number of events (peaks) found in local trajectory space $T[M,\lambda N]$ (493) is much higher than was found in inter-trajectory space $T[M,\iota N]$ (191). This indicates that there should be some non-stationary (i.e. signal-related) activity present. The local probability p_l of finding an event in $T[M,\lambda N]$ is 0.07, and from the bin cancellation simulation results in Appendix [D3] one can infer that the chance of obtaining an error of greater than five counts at one sampling point in the event

bin is less than 5% (using $P(X \leq 5)_{64}$ at $p = 0.06$). If the chance of an error was much higher, then it would be necessary to recompute the analysis with the inclusion of an additional ensemble of trials. With this particular data set, the error probability value $P(X \leq 5)_{64}$ is not strictly valid and/or representative of the bin cancellation process. This is because the probability distribution of the noise has been affected by the sub-averaging process (Sec.[8.8]). Nevertheless, it was beneficial to mention just how $P(X \leq \beta)_M$ is intended to be used when single-response data is being analysed with a fast averaging paradigm in mind.

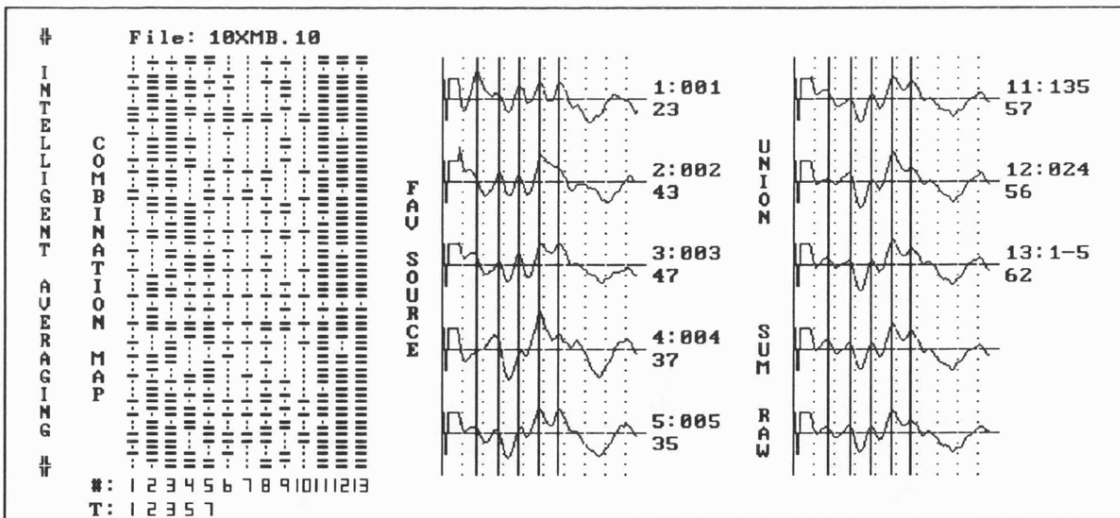
To proceed with the generation of intelligent averages, the individual T_i must be selected after consideration of the χ^2 values, the percentage of trials that contain an event, and above all, the mean latency values with respect to the standard normal values given in Appendix [D5]. If we manually assign the trajectories T_i corresponding to BIN peaks '1', '2', '3', '5', and '7' to the overall source set S, then the resulting combination set C will have a bit-mapped representation $C[M,13]$ as shown in Fig.[8.24]. The *fav-source* (fast average source) traces in both Figs.[8.24(a) and 8.24(b)] are the source averages computed from the individual T_i . The *intersect* traces in Fig.[8.24(a)] are the derived averages computed from the intersect sets I_i . In Fig.[8.24(b)], the *union* traces are the derived averages computed from the union sets Y_i . For comparisons, the average of the source averages and the conventional BAEP average are also provided. All the averages are delineated at the mean latency values of the selected trajectories. The numeric labels attached to the traces have the format - Column vector number in $C[M,13]$ which was used (trace number) : Combination *formula* | Number of trials contained in the average. An example of the latter for a trace in the intersect set is 9 : 024 | 24, which should be read as - column vector 9 (or trace 9) : from combination of trajectories 2 and 4 | contains 24 trials.

Trace 2 in Fig.[8.24], as expected, enhances wave 2, but it has no representation of the rightmost part of wave I which was selected in trace 1. This trace contains the leftmost part of the bifid wave I which was indicated by BIN peak '0' in Fig.[8.23(b)]. There is a marked showing of wave IV or a possible wave IV/V complex with a very weak showing of a wave V inflection. This is unusual, since there is a relatively high percentage of trials in the average (67%). By comparison, trace 1, which has just over half as many trials (36%), shows clear representations of all the waves.

In trace 4, wave II is very prominent and wave I is not present at all, even though the average contains 57% of the trials. When any of the waves I, III, or V are being enhanced, there appears to be a good representation of all other waves. When either waves II or IV are being enhanced, there appears to be a good representation of the other wave only. These phenomena have been repeatedly observed in other BAEPs. Trace 9 clearly supports the observation of an exclusive wave II and IV correlation. Traces 6, 7, and 8 show very good BAEPs, obtained from low numbers of trials, because of the enhancements included from either of waves I, III, or V. The BAEP in

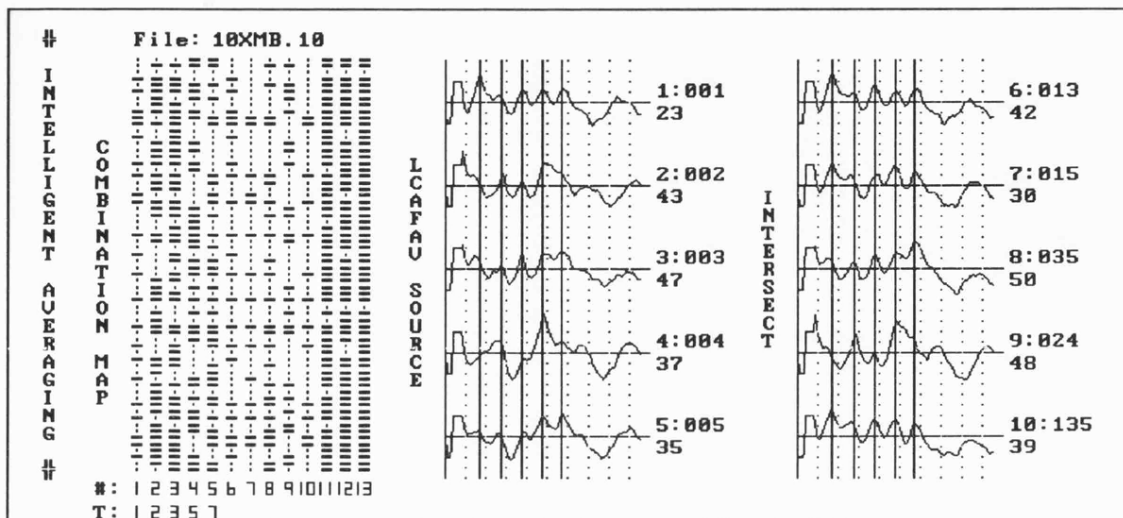


(a) Fav-source traces [1-5] and intersect traces [6-10].

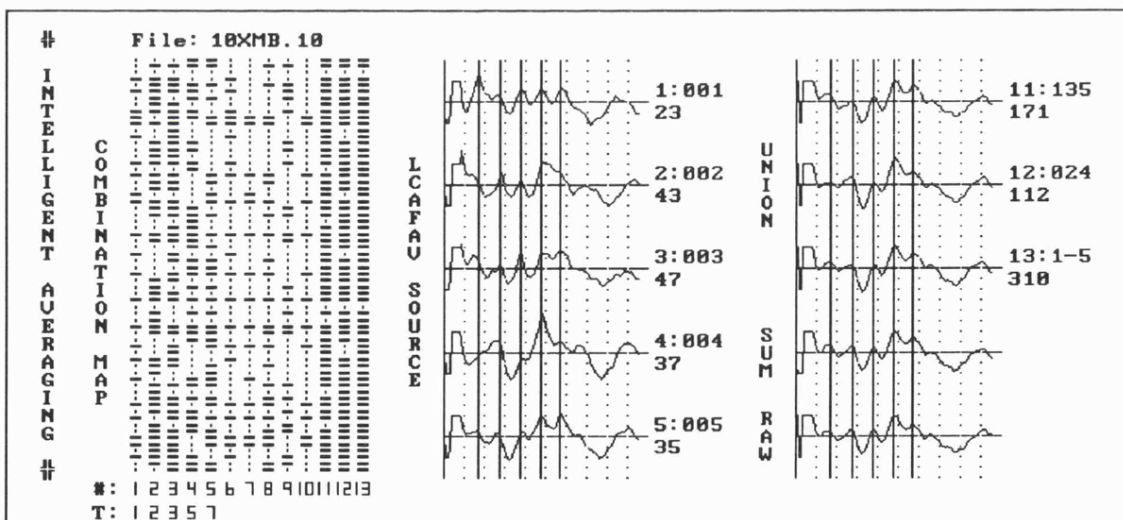


(b) Fav-source traces [1-5], union traces [11-13], sum of traces 1-5, and conventional average.

Fig.[8.24] Combination map and enhanced averages as obtained by assignment of the T_i for BIN peaks '1', '2', '3', '5', and '7' in Fig.[8.23(b)] to the overall source set S.

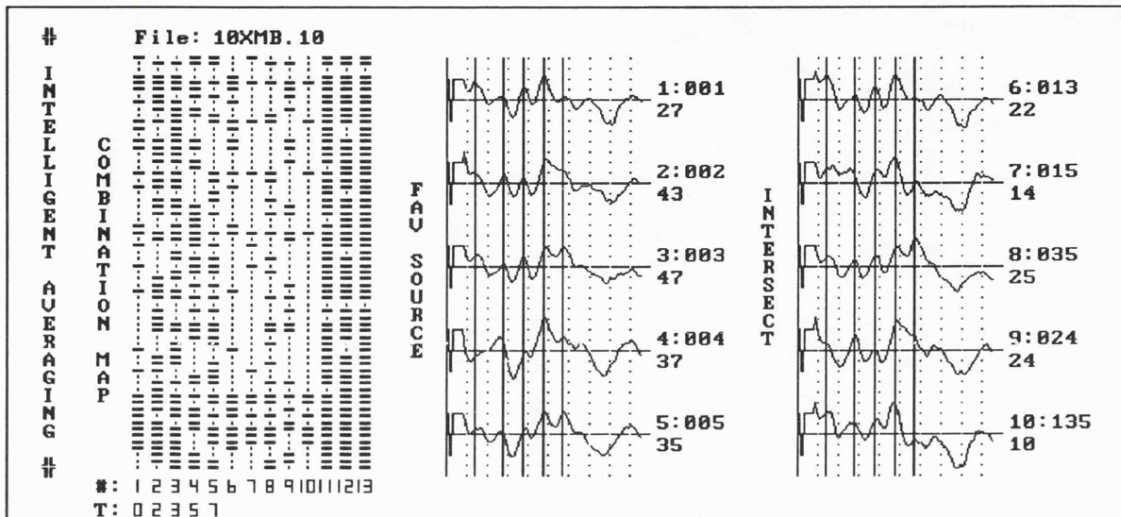


(a) Lcafav-source traces [1-5] and intersect traces [6-10].

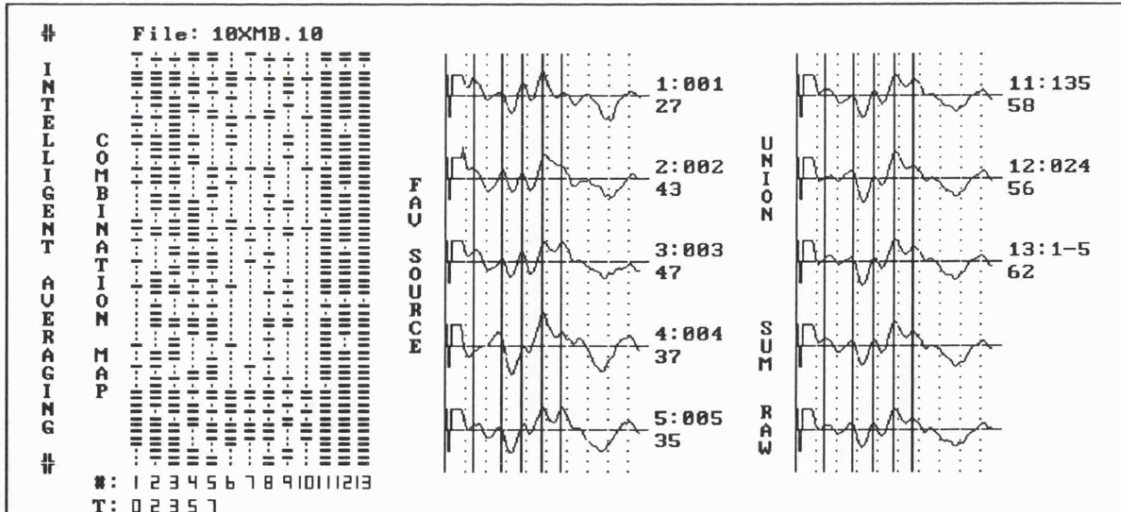


(b) Lcafav-source traces [1-5], union traces [11-13], sum of traces 1-5, and conventional average.

Fig.[8.25] Combination map and LCAs as obtained by assignment of the T_i for BIN peaks '1', '2', '3', '5', and '7' in Fig.[8.23(b)] to the overall source set S and corresponding grand LCAs.

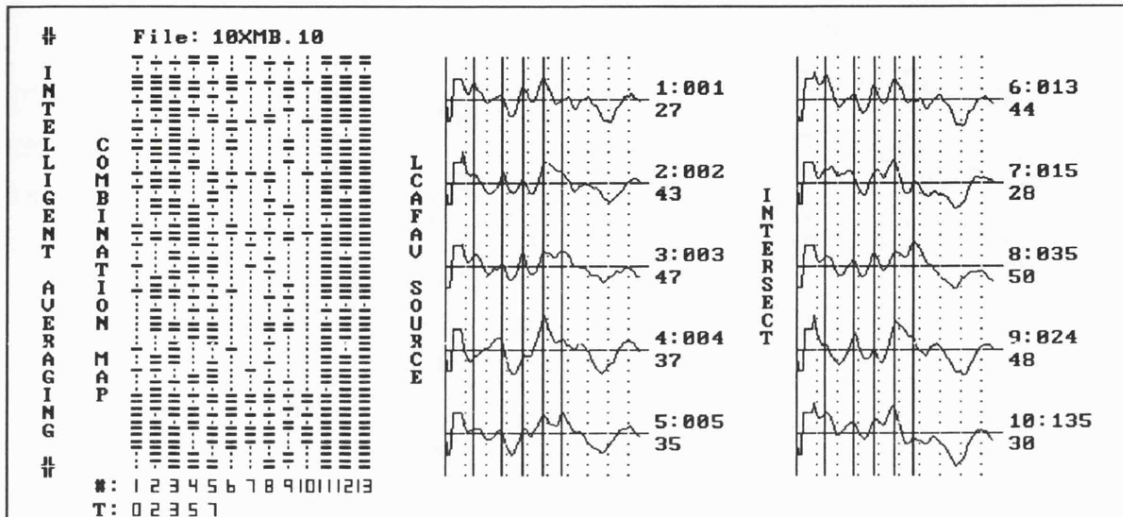


(a) Fav-source traces [1-5] and intersect traces [6-10].

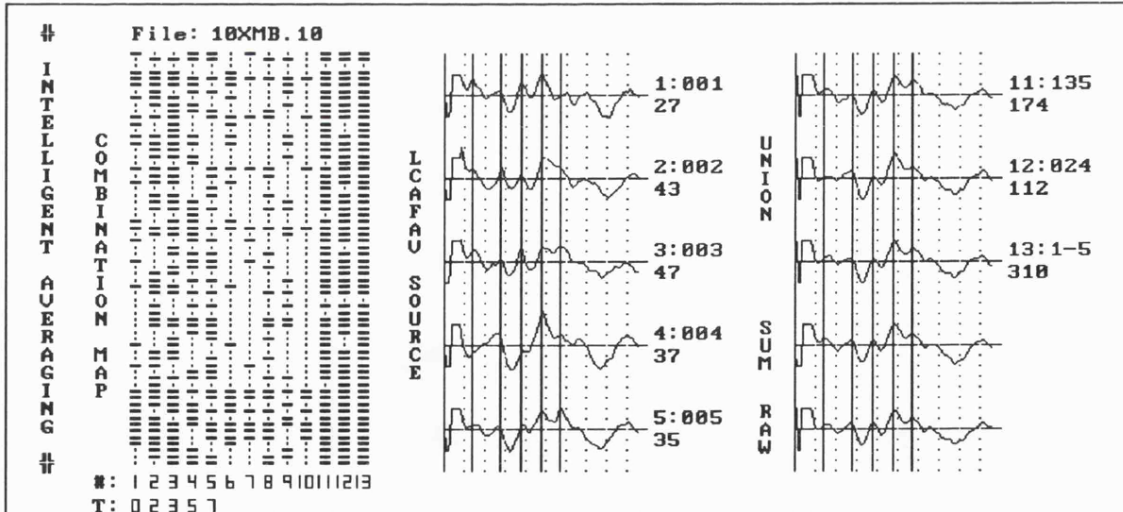


(b) Fav-source traces [1-5], union traces [11-13], sum of traces 1-5, and conventional average.

Fig.[8.26] Combination map and enhanced averages as obtained by assignment of the T_i for BIN peaks '0', '2', '3', '5', and '7' in Fig.[8.23(b)] to the overall source set S.



(a) Lcafav-source traces [1-5] and intersect traces [6-10].



(b) Lcafav-source traces [1-5], union traces [11-13], sum of traces 1-5, and conventional average.

Fig.[8.27] Combination map and LCAs as obtained by assignment of the T_i for BIN peaks '0', '2', '3', '5', and '7' in Fig.[8.23(b)] to the overall source set S and corresponding grand LCAs.

trace 10 is obtained from only 20% of the available trials, and it is has a much better morphology than the conventional raw average. Wave I is clearly defined and the strong negativity expected after wave V is also evident.

The difference in ensemble size between traces 12 and 13 is only six trials. These traces contain 88% and 98% of the available trials respectively, however, the waveforms are quite dissimilar. They both emphasise the waves II and IV, and the waves I, III, and V phenomena mentioned above.

Fig.[8.25] shows the latency corrected averages for this data set derived from grand LCAs using the *lcafav-source* trajectory information. They show neither significant improvements over the averages in Fig.[8.24], nor have they introduced any distortion. Examination of the standard deviations for the respective trajectories in Table [8.1] shows that trajectory five will cause a maximum latency correction in the ensemble of trials, since it has the highest variability. For 70% of these trials, the latency shift will be less than three sampling points, so the effects of latency correction will not be dramatic.

The traces in Figs.[8.26 and 8.27] show the *fav-source* and derived averages, and the *lcafav-source* and derived averages respectively for the data set in Fig.[8.23(a)]. The difference in this case, is that the trajectory corresponding to Bin peak '0' is used to generate traces 1, 6, 7, 10, 11, and 13 (i.e. all those traces that have trajectory T_1 in their combination set). On examination of the complete set of traces in both Figs.[8.26 and 8.27] which are generated using T_1 and not T_5 , it can be seen that their wave V representations are very small compared to their counterparts in Figs.[8.24 and 8.25]. This is not what is expected, given that waves I and V are highly correlated in the BAEP. All traces that are generated using T_5 help to *pull out* the rightmost peak in the bifid wave I component, which corresponds to the trajectory selected previously. One can strongly postulate therefore, that the leftmost peak in the bifid wave I component does not arise from the same polysynaptic chain in brainstem pathways as the rightmost peak.

8.12.2 Case Study B

Background Information:

- **Data set:**
Name - 3xmb.20; Channel - contralateral; Stimulus intensity - 65 dBSL; Sex - male.
- **Data specification:**
16 responses / sub-average; 64 filtered sub-averages; 1024 responses in total.

In this case study, the GAV peak in Fig.[8.28(a)] corresponding to BIN peak '5' in Fig.[8.28(b)] is a wave IV/V complex. The GAV component is broad and has prominent shoulders on each of its sides. These shoulders are reflected in the BIN structure by small peaks on either side of BIN peak '5'. All the other major components are noticeably represented in the BIN, though there is some erratic behaviour between waves II and III which tends to distort them. Wave I in the GAV is swamped by the presence of large stimulus-related artifacts. With intelligent averaging we hope to determine the precise locations of the peaks in the wave IV/V complex.

The statistics for this data set are given below in Table [8.2]:

Event Probabilities:

Max GPks possible (uniform) : 13824

Total GPks found : 462

Global Probability of Pk : 0.03

Max LPks possible (uniform) : 7616

Total LPks found : 348

Local Probability of Pk : 0.05

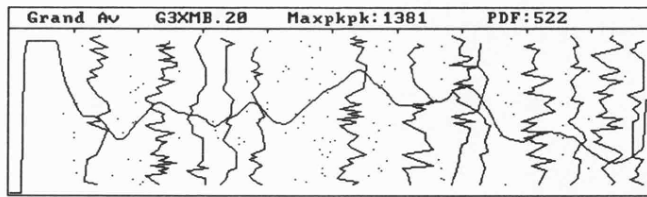
Max InterPks poss. (uniform) : 6208

Total InterPks found : 114

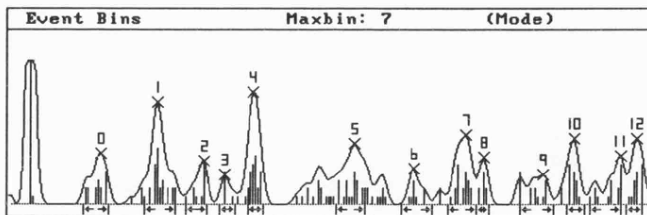
Inter Probability of Pk : 0.02

Item N°	GPkAmpl	GPkLat	BPkAmpl	BPkLat	Mn	SD	Q	E	ChiSq	ChSqP	BinomP	%Swps	CC	Span
0	. . . 212	2.36	2774	1.44	1.36	0.12	25	29	1.13	0.29	0.00	39.06	1.00	10
1	. . . 220	3.76	5596	2.32	2.36	0.14	41	35	2.20	0.14	0.00	64.06	0.98	12
2	. . . 771	5.44	2348	3.04	2.93	0.10	20	23	0.78	0.38	0.00	31.25	1.00	8
3	. . . 199	6.32	1623	3.36	3.40	0.07	17	18	0.02	0.88	0.00	26.56	1.00	6
4	. . . 505	7.04	6115	3.80	3.84	0.07	31	18	14.21	0.00	0.00	48.44	1.00	6
5	. . . -270	8.28	3324	5.36	5.31	0.13	33	32	0.04	0.84	0.00	51.56	1.00	11
6	. . . 0	0.00	1986	6.28	6.30	0.14	25	35	6.43	0.01	0.00	39.06	1.00	12
7	. . . 0	0.00	3825	7.08	7.02	0.12	30	32	0.29	0.59	0.00	46.88	1.00	11
8	. . . 0	0.00	2564	7.36	7.34	0.06	15	15	0.01	0.91	0.00	23.44	1.00	5
9	. . . 0	0.00	1654	8.28	8.17	0.16	32	38	2.35	0.13	0.00	50.00	0.97	13
10	. . . 0	0.00	3569	8.76	8.78	0.08	25	20	1.47	0.22	0.00	39.06	1.00	7
11	. . . 0	0.00	2680	9.48	9.26	0.16	34	35	0.08	0.78	0.00	53.13	0.97	12
12	. . . 0	0.00	3624	9.72	9.70	0.07	20	18	0.47	0.49	0.00	31.25	1.00	6

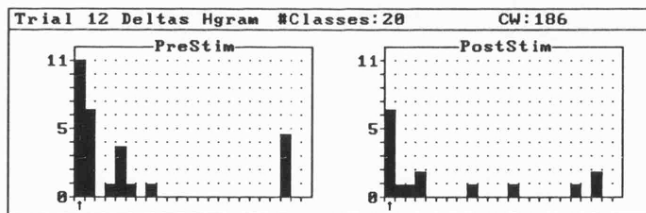
Table [8.2]



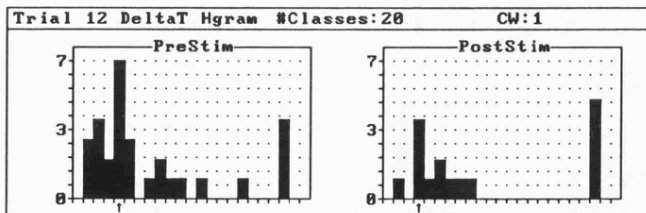
(a) GAV and Trajectory map $T[M, \gamma N]$.



(b) BIN and segment limits in $T[M, \gamma N]$ for $T[M, \lambda N]$.



(c) Frequency distribution $H[\Delta p]_m$.



(d) Frequency distribution $H[(\Delta t)_p]_m$.

Fig.[8.28] General results obtained from preliminary stages of event analysis.

To continue with the author's convention of assigning the five trajectories in the source set S to the major BAEP components, it will be necessary to omit assigning T₄ since a wave IV does not exist in this case. Therefore, the trajectories T₁, T₂, T₃, and T₅ corresponding to BIN peaks '0', '1', '4', and '5' only will be used.

In Fig.[8.29] the source and intersect traces that are computed from T₄ are obviously not available. Trace 2 shows a distinct wave IV component, despite there being a complex wave IV/V in the GAV. A note was made in case study A of the high degree of correlation that exists between waves II and IV. The separation between waves IV and V in trace 2 is only about 0.5ms. This can result in an apparent fusing of these potentials during averaging when either has an associated variability that causes their peaks to overlap. The small separation of waves in the complex is confirmed by trace 3, where the high correlation between waves III and V has caused an enhancement of wave V, and consequently a resolution of the complex.

The traces that enhance wave I, either directly through a combination formula containing T₁, or indirectly through a correlation with wave I, show little or no artifactual activity. The average of the fav-source averages (sum) contains cleaner wave I and wave II components than the raw average. This average is a form of weighted averaging, since some trials will be included more times than others, depending on the number of occurrences in the source set S. Favour is given to those trials with highly correlated components in the T_i contained in S.

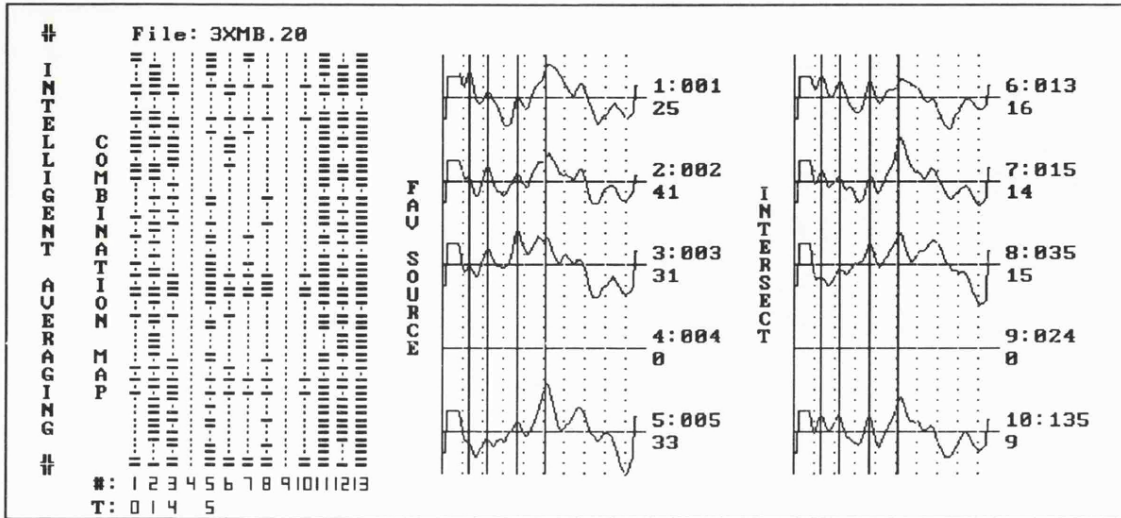
The LCAs for the data set in Fig.[8.28] are given in Fig.[8.30]. There is perhaps a very slight improvement in the sharpness of wave I and the resolution of the wave IV/V complex in these traces, but no other advantages over the averages in Fig.[8.29] are obvious.

8.12.3 Case Study C

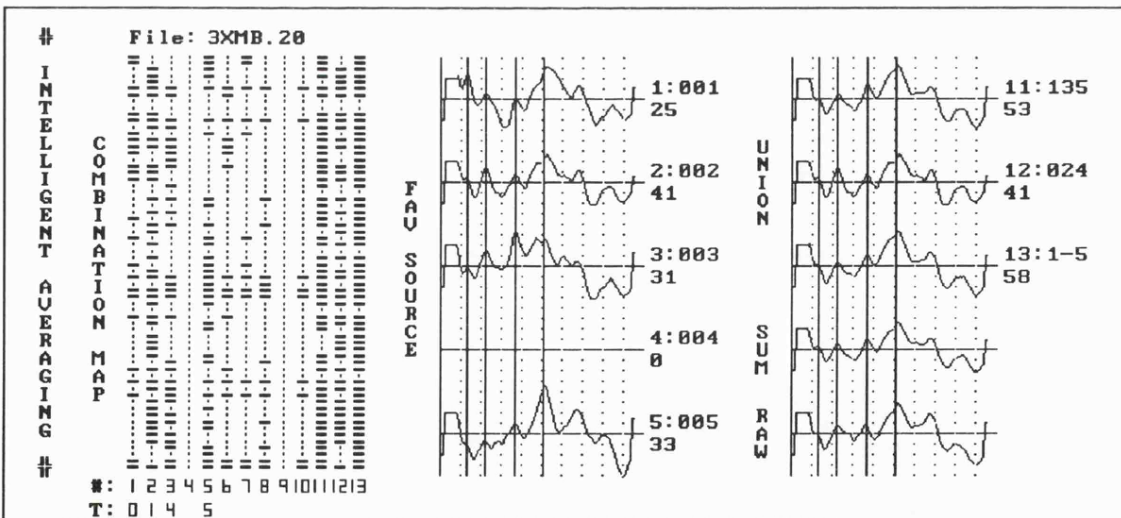
Background Information:

- **Data set:**
Name - comb4.dat; Channel - contralateral; Stimulus intensity - 65 dBSL; Sex - male.
- **Data specification:**
4 responses / sub-average; 64 filtered sub-averages; 64 responses in total. *
(* The sub-averages are combinatorially averaged)

The data set shown in Fig.[8.31] is produced from combinatorially sub-averaged data as described in Sec.[8.7.1]. The GAV in Fig.[8.31(b)] and the BIN in Fig.[8.31(c)] are the same as in Fig.[8.13(c)]. Since the total number of trials in this GAV is small (64), wave V at about 6.1ms is not yet represented by an obvious peak. The wave V shoulder in the GAV waveform emerges as a distinct peak after continued averaging (see Fig.[8.11(d)]). The task of assigning a latency label to

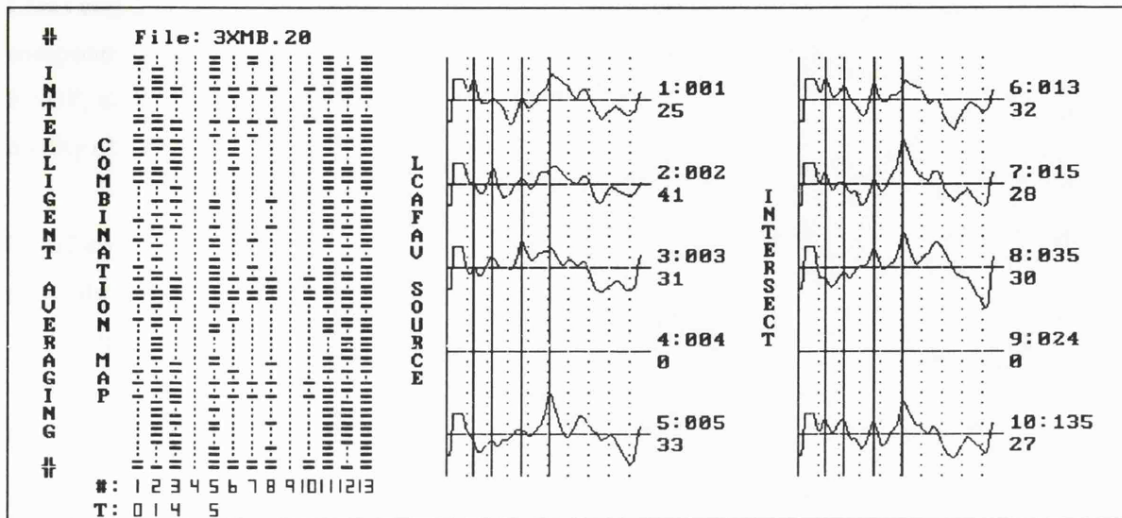


(a) Fav-source traces [1-5] and intersect traces [6-10].

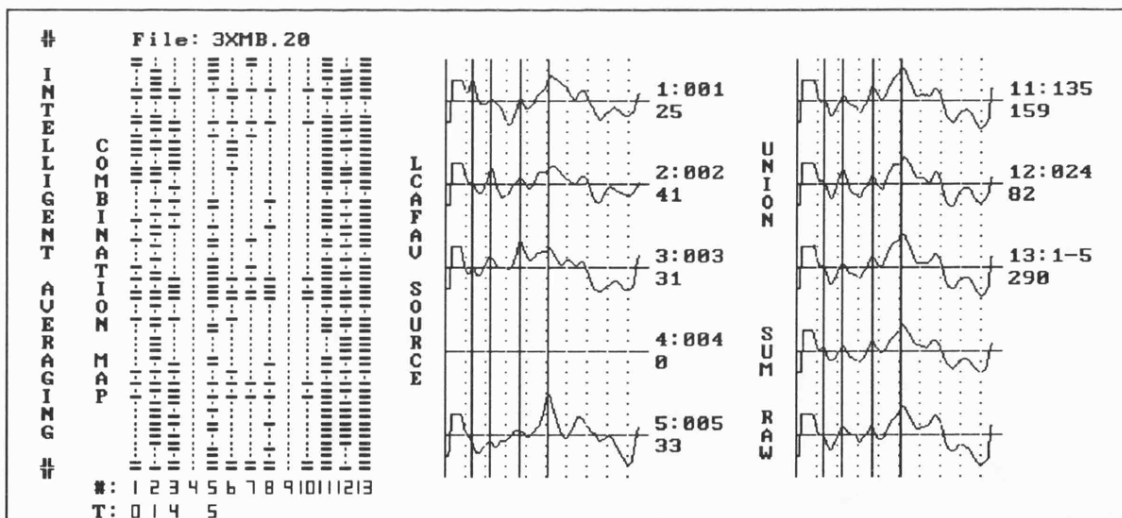


(b) Fav-source traces [1-5], union traces [11-13], sum of traces 1-5, and conventional average.

Fig.[8.29] Combination map and enhanced averages as obtained by assignment of the T_i for BIN peaks '0', '1', '4', '5', and '5' in Fig.[8.28(b)] to the overall source set S.



(a) Lcafav-source traces [1-5] and intersect traces [6-10].



(b) Lcafav-source traces [1-5], union traces [11-13], sum of traces 1-5, and conventional average.

Fig.[8.30] Combination map and LCAs as obtained by assignment of the T_i for BIN peaks '0', '1', '4', '?', and '5' in Fig.[8.28(b)] to the overall source set S and corresponding grand LCAs.

this shoulder is easily accomplished when the BIN information is used for guidance. Without it, the process of scoring this BAEP is open to some subjectivity. In addition, the GAV peaks around 1.5ms and 2.5ms are too broad to be regarded as good estimations of the wave I and wave II BAEP components. In a situation such as this, an experienced clinician might attempt to score the BAEP, although it is more likely that several more trials would be averaged to *hopefully* obtain the quality of average shown in Fig.[8.11(d)] (512 trials) so as to remove any need for subjectivity.

If real-time monitoring of patients using BAEPs is to be achieved in the future, we must attempt to generate good estimations of the components using a small number of responses. The intelligent averaging proposed in this section has shown some promise in this respect, and it is further demonstrated that the components of this GAV can be extracted from the small number of available responses. The statistics for this data set are given below in Table [8.3]:

Event Probabilities:

Max GPks possible (uniform) : 13440

Total GPks found : 476

Global Probability of Pk : 0.04

Max LPks possible (uniform) : 8000

Total LPks found : 415

Local Probability of Pk : 0.05

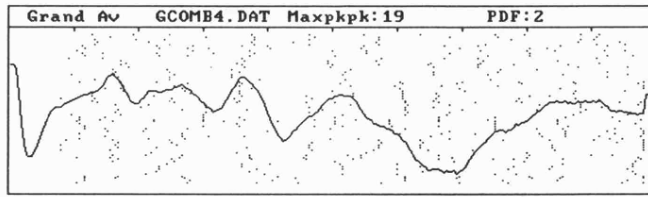
Max InterPks poss. (uniform) : 5440

Total InterPks found : 61

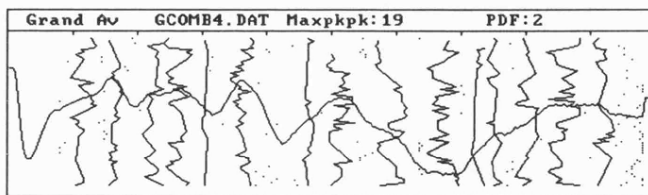
Inter Probability of Pk : 0.01

Item №	GPkAmpl	GPkLat	BPkAmpl	BPkLat	Mn	SD	Q	E	ChiSq	ChSqP	BinomP	%Swps	CC	Span		
0	.	.	10847	1.60	2645	1.08	1.16	0.12	31	33	0.30	0.58	0.00	48.44	1.00	10
1	.	.	8005	2.68	3833	1.64	1.65	0.06	27	17	8.80	0.00	0.00	42.19	1.00	5
2	.	.	9966	3.64	2075	2.28	2.24	0.09	23	27	0.82	0.37	0.00	35.94	1.00	8
3	.	.	5295	5.16	3690	2.72	2.62	0.13	37	37	0.01	0.90	0.00	57.81	0.97	11
4	.	.	3621	9.12	798	3.08	3.03	0.03	11	7	3.19	0.07	0.00	17.19	1.00	2
5	.	.	779	9.44	5328	3.60	3.63	0.10	42	30	9.22	0.00	0.00	65.63	1.00	9
6	.	.	0	0.00	1418	4.64	4.65	0.04	18	13	2.12	0.15	0.00	28.13	1.00	4
7	.	.	0	0.00	2869	5.04	5.14	0.13	34	37	0.40	0.52	0.00	53.13	1.00	11
8	.	.	0	0.00	4545	6.08	5.95	0.17	39	40	0.05	0.83	0.00	60.94	1.00	12
9	.	.	0	0.00	1557	6.80	6.71	0.14	38	40	0.23	0.64	0.00	59.38	0.97	12
10	.	.	0	0.00	1787	7.24	7.25	0.05	11	17	2.55	0.11	0.00	17.19	1.00	5
11	.	.	0	0.00	2708	7.52	7.52	0.07	19	20	0.06	0.80	0.00	29.69	1.00	6
12	.	.	0	0.00	1481	8.04	8.02	0.11	23	30	2.97	0.08	0.00	35.94	0.96	9
13	.	.	0	0.00	3226	8.52	8.59	0.16	42	43	0.10	0.76	0.00	65.63	0.91	13
14	.	.	0	0.00	1324	9.20	9.19	0.10	21	27	1.99	0.16	0.00	32.81	1.00	8

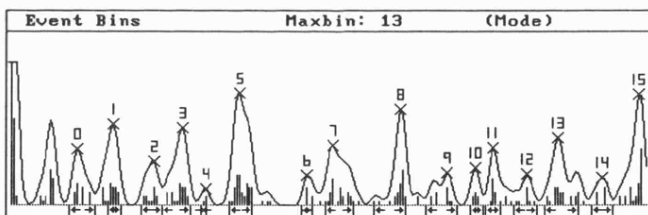
Table [8.3]



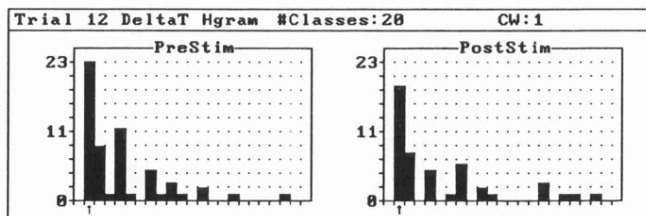
(a) GAV and Trajectory map $T[M,\gamma N]$ showing events only.



(b) GAV and Trajectory map $T[M,\gamma N]$.

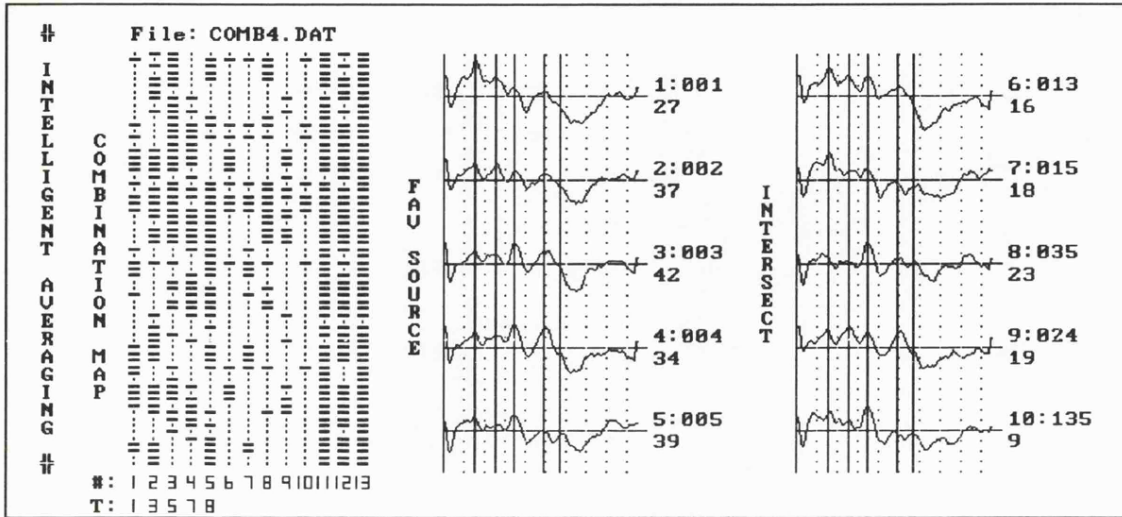


(c) BIN and segment limits in $T[M,\gamma N]$ for $T[M,\lambda N]$.

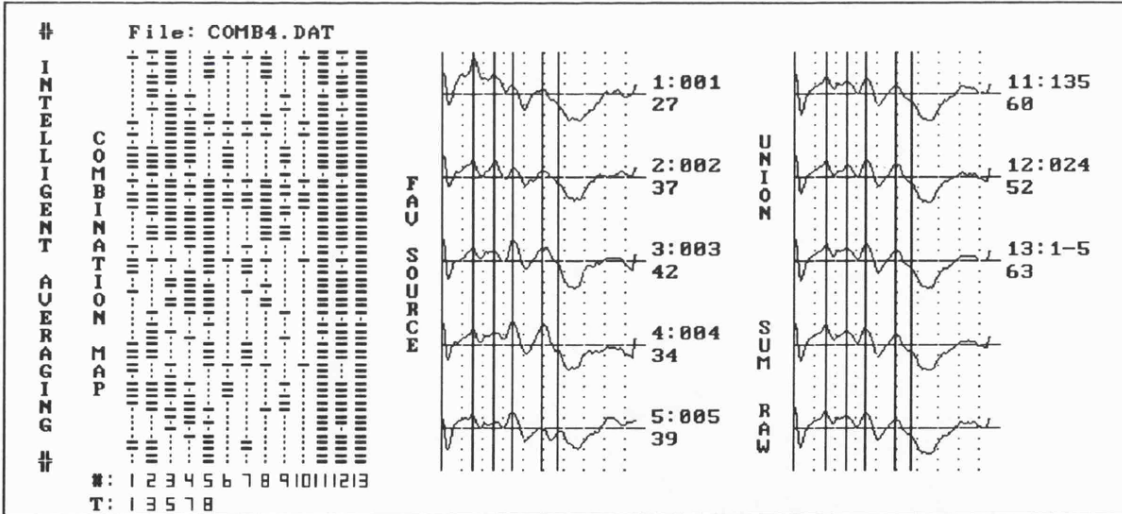


(d) Frequency distribution $H[(\Delta t)_p]_m$.

Fig.[8.31] General results obtained from preliminary stages of event analysis.



(a) Fav-source traces [1-5] and intersect traces [6-10].



(b) Fav-source traces [1-5], union traces [11-13], sum of traces 1-5, and conventional average.

Fig.[8.32] Combination map and enhanced averages as obtained by assignment of the τ_i for BIN peaks '1', '3', '5', '7', and '8' in Fig.[8.31(c)] to the overall source set S.

The distribution of events that have been found for this data set are shown in Fig.[8.31(a)]. There is a definite clustering of the events in the vicinity of the main components. A broad component (e.g. waves I, II, and IV) will have a correspondingly wide cluster of events and a sharp component will have a correspondingly narrow cluster of events (e.g. wave II and V). Broad components (and shoulders) appear in the average of small sized ensembles, when the underlying activity is either highly variable, consists of tightly-coupled bifid components, or contains few representations of the component. The wave V shoulder is an example of the presence of high variability in the underlying activity (standard deviation is 0.17ms). In Fig.[8.31(a)], this component, unusually, also shows large periods of non-activity between stimulus applications. Waves I and II are examples of bifid components.

Table [8.3] shows that the majority of events (87%) lie within local trajectory space which is most likely due to the low pass filtering used (Sec.[8.6]). Therefore, it follows that most of the trajectories should contain an event in a high percentage of the trials. The observed number of events for trajectories corresponding to BIN peaks '1', '3', '5', and '7' confirms this expectation. Selecting these trajectories for the calculation of the intelligent and LCA averages results in the traces given in Figs.[8.32 and 8.33].

The intersect traces that are generated with T₅ show marked enhancements of the wave V component. Again, as we have seen from the other case studies, wave II is clearly distinguished in the presence of wave IV, and there is a high degree of co-existence between waves I, III, and V. Trace 10 in Fig.[8.32], which is generated from only nine sub-averages, shows a very good BAEP in which all components are visible, including the bifid peaks that waves I and II contain. In Fig.[8.33], the sum of the lcafav-source averages (sum) is similar to the conventional average. Wave V, which was previously a broad shoulder, now exists as a small peak due to the latency alignment of its constituent events. The latency at which this wave V peak occurs is about 0.01ms earlier than the wave V peak in the fav-source average of trace 5 in Fig.[8.32]. It is evident therefore, that the subjectivity that might be involved in scoring the conventional average can be removed with a global examination of the averages produced by these forms of enhanced averaging.

8.13 Discussion

ERPs are used as non-invasive indicators of human brain function in both clinical and research applications. These electromagnetic signals directly reflect some aspects of the neural activity associated with the specific brain mechanisms that underlie sensorimotor and cognitive processing. Scalp recorded ERPs, however, provide an incomplete and distorted view of intracranial neural processes (Vaughan and Arezzo, 1988). These limitations are due both to the inability of some neural generator sites to produce electric fields that can be recorded at a distance on the scalp, and to the summation of different neural generator activities at the scalp.

Neurons that constitute a generator site exhibit some transmembrane ionic charge separation when depolarised through electrically excitable membranes or through chemically mediated synaptic effects. This charge separation initiates transmembrane current flows along the existing voltage gradient. The transmembrane current flow associated with the excitatory post synaptic potential (EPSP) depolarisation creates an extracellular negativity or *current sink*, flanked by relative increases in extracellular positivity or *current sources*. At the same time, extracellular current flows down the potential gradient created by the sink, at the site of active depolarisation, and the sources along the neural membrane extending outward from the sink.

Electrically depolarised membranes trigger action potentials that propagate along the axon and through its branches to the axon terminals. Some of this axonal current passes across the neural membrane in order to complete the circuit of current flow. The extracellular sink associated with this propagated depolarisation moves along the axon, flanked by sources that precede and follow the region of depolarisation.

Thus, the current sources and current sinks associated with the generator sites of ERPs are either stationary, in the case of EPSP induced excitations, or travelling, in the case of propagated action potentials. The spatial geometry of the stationary current sources and current sinks will affect the field potential recorded outside of the active neural tissue. If there is anatomical symmetry in adjacent activated neurones, then the sources and sinks will cancel one another, so that no significant extracellular current would flow beyond the dendritic field of the individual neurone. This concept of source-sink cancellation can be applied to groups of symmetrically activated neurones or generator sites which will have sharply localized extracellular field potentials. If there is an unequal distribution of sources and sinks in any dimension, then a potential field will be generated beyond the region of active tissue, and it will be measurable at the scalp. Unequal distributions of sources and sinks can be represented by a paired source and sink, which gives rise to the dipolar model of field potential generation. ERPs of cortical origin principally reflect

graded EPSPs that sum due to a common orientation of the active cellular elements. They have complex variations in magnitude, polarity and spatial extent over time as the intracortical patterns of sources and sinks change in strength and location. In contrast the fields set up by action potentials travelling along fibre tracts in subcortical structures (e.g. in the brainstem), obtain their complexity from the traversal of complex pathways with a number of synaptic relays and changes in orientation. The surface manifestation of potential fields generated within subcortical pathways and from cortical generators are therefore more complex than has generally been appreciated (Vaughan and Arezzo, 1988).

The identification of the anatomical generators of ERP components is essential for clinical applications in which ERPs are employed to aid in the localization of brain pathology. Very simply put, identification begins by mapping the surface ERP topography, and then, in conjunction with knowledge of the cellular anatomy of active structures, provides a basis for identifying the specific generators. Given any surface potential distribution, there are an infinite number of possible intracranial generator configurations, however constraints are imposed by known features of brain anatomy and physiology. The use of dipolar models of ERP generation can then be used to approximate an observed ERP distribution (Scherg and Von Crammon, 1985). For this form of modelling, the topographic data must be reliable and include all the major maxima, minima and points of inflection. It is in this latter respect, that the author believes the enhanced averages produced by event analysis can complement and extend the data obtained from such quantitative models of the electrogenesis of ERPs.

The methodology for event analysis described in this chapter has demonstrated how simple constructs can be combined to enhance features in BAEPs and other signals under the class of event related potentials. The stimulus-locked feature of BAEP components, and previous experience with turning points analysis in interference pattern EMG (Sec.[2.3.4]), has formed the basis for a representation of the BAEP as a sequence of events. Decomposition of the BAEP into event sequences throughout a series of stimulus-locked trials, means that at least one population of events will result for each component, if and only if that component is non-stationary and detectable. Analysis of these populations of events gives a set of sample statistics that provide component latency variability information and the ability to select the *best* trials from the ensemble for re-averaging, so as to enhance pre-selected components.

The problems of poor SNR were overcome by adaptively estimating the peak detection threshold value from one trial to the next, by sub-averaging and filtering, and by a process of event cancellation in the event accumulator bins. The use of these methods has been described in detail and some simulations were performed to determine their effectiveness. Combinations of these techniques can be used to analyse BAEPs using small numbers of responses. Results have been

given for 1024 and 64 trial BAEPs at 65 dBSL stimulus intensity which have demonstrated the ability to perform controlled *dissections* of the signal to extract information that is hidden by a conventional averaging process.

Control over a signal dissection is aided by the statistics that are generated during the analysis. Significant trajectories, corresponding to the major BAEP components, are chosen on the basis of their χ^2 probability values, the percentage of trials that contain an event, their mean latency values, and the structuring in the event bin. The significant trajectories are used to generate a trials-combination map which drives the construction of new enhanced averages from trials in the original ensemble.

In general, global consideration of all the enhanced averages provides more information than is available from the conventional average alone. The unfavourable effects of including a few low quality responses into the conventional average has been demonstrated. Conversely, it has been shown that there are significant advantages to be gained when responses that do not contain events are excluded from the average, and that this trial exclusion process can be performed on an automatic basis using event analysis and intelligent averaging. Selection of the correct trajectories for the computation of the enhanced averages is necessary to obtain any improvement of normal features. However, one can also select trajectories that do not correspond to normal features in the BAEP. This essentially serves to hypothesise that an underlying, and significant, component does exist in the region occupied by the trajectory. The hypothesis is tested by examination of the resulting averages, and severe distortion of previously observable normal (and/or well-formed) features will reject the hypothesis that a significant component does exist. The selection of statistically significant trajectories ($p = 0.05$, Sec.[8.10]) and/or trajectories containing greater than 40% of the available trials, appear to result in reliable enhancements to the components in the BAEP.

The results given in Sec.[8.12], suggest that BAEP generators are locked, in that strong synchronisation exists between certain generator sites and not others, e.g. between the generator sites for waves II and IV, and between the generator sites for waves I, III, and V. It is known that the BAEP components mainly reflect synchronised action potentials in afferent fibre tracts, and that these potentials are not representative of serial activation of the ascending pathways. The bifid components are possibly due to the different axonal conduction velocities in different afferent pathways. Compound action potentials in the separate pathways will become temporally dispersed, and this dispersion will be further complicated by the repeated firing of neurones within the sensory pathways following a single auditory stimulus. In addition, particularly in the auditory system, there are parallel bilateral projections that synapse within or bypass each relay nucleus (Stockard et al., 1978; Scherg and Von Crammon, 1985). So the simultaneity of surface and depth

potentials may be entirely due to chance, since the complexity of the intracranial signals and the shifts in timing of their peaks along their intracranial course leads to opportunities for synchronisation of the surface and depth recorded peaks that do not reflect activity within the same generator (Vaughan and Arezzo, 1988).

The effects of habituation and facilitation are not expected to contribute to this observed complex behaviour, since the process of acquiring the largest ensemble of responses (1024 trials) only lasts for 3¹/₂ minutes with the recording protocol used for these experiments (Sec.[8.2]).

The *knowledge* required to allocate a trajectory to a BAEP component is procedural in most cases. Sometimes, a deeper, more complex knowledge is required to arbitrate between multiple and equally likely trajectories. In order to effect this arbitration, additional channels of data may have to be examined. Following this, it would be necessary to score the data based on decisions made about the quality of the new, enhanced averages, and also to justify these decisions. These decision-making processes are difficult to specify and then encapsulate in a procedural paradigm. The EPAXIS prototype expert system is a first attempt to address this problem using techniques derived from the field of artificial intelligence. In the future, as more information becomes available (e.g. from multiple channels), the experience gained with EPAXIS should be used to intelligently contain the new problems that will arise with regard to the management of information and its comprehensive and comprehensible presentation to the user. The latter will no doubt involve the use of *intelligent graphical interfaces* that can be created in a small microcomputer-based environment. The graphical interfaces currently available for small computers, can be given an *intelligence* by embedding them into a knowledge-based environment that supervises and plans the presentation of graphic information (results and reports) based on a priori task specifications. In the author's opinion, the implementation of this type of concept (i.e. reasoning with graphical objects) is necessary if the benefits of event analysis are to be extended into the multiple channel and/or real-time monitoring regime.

Apart from the direct applicability of event analysis to other EP and ERP data, it should be possible to investigate data having similar characteristics derived from other areas of electrophysiology and engineering. For example, the basic ideas of coherent averaging followed by component variability analysis and improved waveform estimation can be employed in the extraction of the motor unit action potential jitter in single fibre EMG. From the engineering domain, fault diagnosis using data from vibration tests on rotating machinery (e.g. gearboxes), and intermittent fault analysis in the process industry are the most obvious application areas for event analysis.

A paper has recently been published (Sehmi et al., 1988, in Appendix [D6]) which describes the event binning processes summarised in Fig.[8.6].

Chapter Nine

Discussion and Conclusions

The research work described in this thesis has resulted in several new approaches to the investigation of neurophysiological data. The data of interest represent examples from two important classes of signal that are commonly encountered in neurophysiology and engineering. The characteristics of these signals differ significantly, though the techniques used by the author for their analysis have not differed to the same extent. The first class of signal, to which the EMG belongs, exhibits noise-like characteristics that have important implications when the dynamics of muscle are being modelled. EPs are drawn from the second class of signal which display non-stationary deterministic characteristics. Simulation experiments conducted by the author with spectral analysis of EMG turning points (Lago, 1979), provided a conceptual basis for the analysis of the (very different) EP signal.

Turning Points Spectral Analysis (TPSA) of the EMG was simulated on the small computer system (SPC) that was the subject of chapter three. The SPC is a multi-processor computer designed for flexible digital signal processing which incorporates ease of use and portability. The objectives for this computer were met by using a modular approach to the design of both hardware and software components. The author's involvement was mainly concerned with the design and specification of the software that allows for much of the flexibility that the SPC exhibits. Branching menus and built-in programmable interfaces between the host and slave processors allow the applications developer to re-configure the SPC rapidly for various, simple, data acquisition and analysis tasks. The signal acquisition rates are fast enough to cope with the majority of bioelectric signals to make the SPC a suitable machine for intra-operative data collection and on-line analysis. The on-line analysis capability of the SPC is achieved by a background tasking philosophy programmed into the host kernel programs. Background analysis tasks obtain data via a dual-plane memory which is symmetrically mapped into the address spaces of both the host and slave processors. The SPC development was taken to completion recently, at which point several applications in bioelectric signal analysis had been implemented successfully.

Apart from the four ADC inputs that the SPC contains, a pair of DAC outputs can be used to provide control signals to peripheral equipment (e.g. x-y plotter, EP stimulator). The SPC can, therefore, act as an intelligent host by providing pre-programmed control signals that adapt to changes in the status of measured input signals or in response to analyses performed on input signals. Examples for the use of the latter are transducer calibration and compensation during data acquisition tasks.

The noise-like features of EMG have been described in chapter two and their adverse effects in dynamic EMG-force modelling were shown to be of importance when specifying the model and its parameters. This identified the need to improve the quality of EMG and force data when EMG-force measurements were performed. The approach taken by the author to address this general problem has been to provide computer-controllable forcing protocols that, as far as possible, relieve the patient from the simultaneous pursuit and generation of dynamic force patterns in isometric dynamic loading experiments. Techniques from electromagnetic suspension theory were applied to solve this problem. Chapters four and five have described in detail how the highly non-linear force-airgap characteristic of an electromagnet can be manipulated in a negative flux-feedback control system to give isometric, dynamic control over muscle loadings of upto 250N. Small deviations from isometric conditions through patient movements are compensated by the control system for the electromagnet. The electromagnet feedback control signal is a direct measure of the delivered force, and it can therefore be used as the force output. In this sense, the system also behaves like a force transducer. The wide bandwidth of the system will allow numerous computer controllable forcing strategies to be adopted for EMG-force modelling experiments. The computer system described in chapter three is a very suitable vehicle to host the intelligent control process for this muscle load, and in addition, it could be used to simultaneously acquire the actual force and EMG signals during an experiment.

The loading system can be improved by changing the magnetic circuit as suggested in chapter five. Additionally, the mode of interaction with the device could be made simpler. This can be done by changing the position of the magnet in relation to the electronics housing so that the subject does not have to *reach-out* for the main assembly when interacting with the system. An ideal situation would be one in which the main assembly was remote from the drive electronics. A special frame-like structure could be constructed to hold the main assembly, within which the subject (possibly seated) competes against applied force variations. The major disadvantage of the muscle load is its expense. This can be reduced considerably by incorporating the new magnet design suggested in chapter five and by lowering the maximum load specification. As a result of this the magnet dimensions and power dissipation can be reduced, thereby enabling the use of cheaper power transistors and simpler drive and control electronics.

Common to the simulation program that was implemented on the SPC and the analysis procedure developed for EP signals, is a data reduction process that converts the digitised signals to a sequence of events. For EP data, this reduction process has the advantage of being tolerant to large noise-induced artifacts. In EMG analysis by the TPSA method, this has the additional advantage of providing information on the mean firing rate of the population of active motor units that give rise to the interference pattern (Lago and Jones, 1977, 1983). The original EMG reduction process applied to EP data has been extended to incorporate both positive and negative

events in the time-series. Since EPs are assumed to be non-stationary, deterministic signals, the bipolar event sequence can be synchronously summated across the ensemble of responses in a way analogous to the coherent time-averaging estimation process. This coherent summation of events results in a bipolar latency histogram which effectively delimits those regions in the averaged response that contain stimulus-locked activity.

Use of the latter delimiting information and the concept of a component trajectory, has enabled the author to extract EP component latency variability estimators which have proved to be accurate to within ± 2 sampling points (i.e. $\pm 0.08\text{ms}$ at 25 kHz sampling frequency) at signal-to-noise ratios as low as -10dB. More research work needs to be done to investigate the effects of changes in sampling rate on the extraction of these latency variability estimates. The component variability data is used to extract homogenous sets of trials from the original ensemble of responses that contain various combinations of components. The combinations of components that are selected depend on the type of EP that is being analysed and the statistics describing the component trajectories. The examples given in the thesis are specific to the BAEP. It has been shown that simple re-averaging of the trials contained in the homogenous sets can lead to a marked enhancement of underlying activity in the BAEP.

The results of experiments using real BAEP data are described in detail in chapter eight. Several conclusions can be made about this approach to EP analysis:

- (a) Resolution of the wave IV/V complex component is possible in situations where either wave IV or V exist as points of inflection in the complex.
- (b) Latency corrected averaging can be used to assist in the resolution of tightly coupled wave IV/V complex components.
- (c) It is possible to extract both wavelets in bifid components.
- (d) Event analysis highlights significant relationships between different components.
- (e) A priori knowledge of the correlation between components can be used to enhance the one, which is not clearly defined in the averaged response and/or the trajectory map, with a trajectory selection on the other.
- (f) The combination map provides a global overview of the trials that contain activations of the selected components. In the future, it may be feasible to use the combination map to perform a topographical correlation of events in multiple channel cognitive EP analysis. Given the recording geometry and the underlying brain anatomy regarding possible generator sites, an intelligent cluster analysis could be performed to extract the most likely groups of events from all combination maps that are related. In this respect, an inductive learning algorithm (Shepherd, 1985) may be applicable because of its ability to perform generalisations that will cope with the possibility of having noise-related events in the combination map. The induced pattern recognition rules could then be used as part of a rule-based system that also encapsulates the relevant anatomical knowledge.

- (g) It is common to find significant periods of non-activity in the combination map (even when sub-averages are used), which strongly suggests that the underlying neural generators do not contribute to the scalp-recorded field potential at every stimulus delivery.
- (h) The observation of silent periods means that there is little hope in achieving an EP estimation from a single stimulus (Madhavan et al., 1985). This will almost certainly be an impossibility with BAEPs due to the extremely low signal-to-noise ratios present in single trials. Several trials would have to be averaged to ensure registration of all components in the BAEP.
- (i) Event analysis can achieve high performance with a greatly reduced number of responses (up to 32 times lower against a conventional average using 2048 trials).

The selection of trajectories to represent the five most important components in the BAEP, requires a deep understanding of BAEP morphology and the underlying neuroanatomy of the brainstem pathways when meaningful interpretations are to be made from the resulting enhanced averages. Selection of trajectories is expected to be even more complicated in situations where pathology is evident. Symbolic representations of the parameters describing the trajectories, coupled with a shallow morphological knowledge of the normal BAEP have been used to build an expert system that will select those trajectories that are the most likely candidates for components. The expert system, called EPAXIS, incorporates reasoning with uncertainty using the theory of fuzzy logic, for which details were discussed in chapter seven.

More recently, the ideas behind EPAXIS have been used by Robinson and the author to implement a structured decision table for trajectory selection in a spreadsheet programming environment (Microsoft EXCEL). This pseudo-expert program takes as input compatible information files that are generated by the event analysis suite of programs.

It is quite clear that there is a large amount of information available from event analysis. Most of this information is contained in the morphology of the enhanced averages and the statistics for the trajectories. Sensible interpretations of this information rely on the special knowledge of the user who can use the suite of programs to dissect EPs at the single trial level. The process of exploring the multiple dimensions occupied by the parameters that are user-specified (currently there are five, each of which can usually have up to 10 possible values) can become unmanageable. Event analysis therefore needs extensions for pattern recognition incorporating heuristic search for features in the average using the event bin data and trajectory statistics. If we look at the expert system methodology as a means of coping with complexity in signal processing situations that require interpretation, management, planning, etc., then the methodology becomes more than just an increasing interest in computer science, it becomes essential.

This research has established, in theory and in practice, relationships between EMG analysis and controllable muscle loading, and between EP analysis and knowledge-based systems. A common factor in the work has been the integration of several analysis and control paradigms which are centred around small-computer technology. The integration of the analysis components is aided by the programming concepts and software structures that are used, and careful design of the user-machine interfaces. This has led to a high level of user controllability and ease of supervision during analysis procedures. The resulting environments provide valuable assistance in both clinical and research-orientated EMG and EP investigations.

The SPC is currently being used intra-operatively for jet ventilation studies in anaesthesia. The magnetic loading device is being used extensively in EMG-force modelling at the University of Leicester, and the event analysis suite of programs is being implemented on the next generation of EMG/EP machines at Medelec Ltd (Woking, Surrey, England). Four publications have been produced as a direct result of this research initiative. All of these papers are included in the Appendices.

References and Bibliography

ADRIAN, E.D. and BRONK, D.W., (1929), The discharge of impulses in motor nerve fibres, *J. Physiol.*, Vol 67, 119.

AGGARWAL, G.C. and GOTTLIEB, G.L., (1977), Oscillation of the human ankle joint in applied sinusoidal torque, *J. Physiol.*, Vol 268, 151-176.

AIKINS, J.S., KUNZ, E.H., SHORTLIFFE, E.H. and FALLOUT, R.J., (1982), PUFF: An expert system for interpretation of pulmonary function data, STA-HIPP-82-83.

ALTY, J.L. and COOMBS, M.J., (1978), *Expert Systems Concepts and Examples*, NCC Publications.

ANDREASSEN, S., WOLDBYE, M., FALCK, B. and ANDERSEN, S.K., (1987), MUNIN - A causal probabilistic network for interpretation of electromyographic findings, *IJCAI-87*, Milano, August 1987.

AUNON, J.I., MCGILLEM, C.D. and CHILDERS, D.G., (1981) *Signal Processing in Evoked Potential Research: Averaging and Modelling*, CRC Critical Reviews in Bioengineering, June 1981, 323-367.

AUNON, J.I. and SENCAJ, P.W., (1978), Comparison of different techniques for processing EPs. *Med. and Biol. Eng. and Comput.*, Vol 16, 642-650.

AUTOMATICA, (1981), Special issue: Identification and parameter estimation, Vol 17, Pt.1.

BARBER, C. (ed), (1980), *Evoked potentials*, MTP press Ltd, England.

BARR, A. and FEIGENBAUM, E.A., (1981), *The handbook of artificial intelligence*, Vol 1, Pitman, London.

BARR, A. and FEIGENBAUM, E.A., (1982), *The handbook of artificial intelligence*, Vol 2, Pitman, London.

BASMAJIAN, J.V., (1979), *Muscles alive*, 4th Ed., The Williams and Wilkins Co.

BASMAJIAN, J.V. et al., (1975), *Computers in electromyography*, Butterworth.

BAWA, P., MANNARD, A. and STEIN, R.B., (1976), Predictions and experimental tests of a visco-elastic muscle model using elastic and inertia loads, *Biol. Cybern.*, Vol 22, 139-145.

BEKEY, G.A. and MESSINGER, H.F., (1966), Analysis of continuous parameter identification methods, *Simulation*, Vol 5, 95-102.

BERGER, H., (1929), On the electroencephalogram of man. In P. Gloor (ed), *Hans Berger on the electroencephalogram of man*, *Electroenceph. Clin. Neurophysiol.*, Vol 28, 37.

BIEDERMANN, W., (1898), *Electrophysiology*, London.

BIGLAND, B. and LIPPOLD, O.C.J., (1954), The relation between force and integrated electrical activity in human muscles, *J. Physiol.*, Vol 121, 214-224.

- BLINOWSKA, A., VERROUST, J. and CANNET, G., (1979), The determination of motor unit characteristics from the low frequency electromyographic power spectra, *Electromyogr. and Clin. Neurophysiol.*, Vol 19, 281- 290.
- BOBROW, D.G. and WINOGRAD, T., (1977), An overview of KRL, a knowledge representation language, *Cognitive Science*, Vol 1, 3-46.
- BRANDSTATER, M.E. and LAMBERT, E.H., (1969), A histological study of the spatial arrangement of muscle fibres in single motor units within rat tibialis anterior muscles, *Bull. Amer. Assn. EMG Eletcrodiag.*, Vol 82, 15-16.
- BRIGHAM, E.O., (1974), *The Fast Fourier Transform*, Prentice-Hall.
- BRODY, J.A., (1976), Regulation of isometric contraction in skeletal muscle, *Experimental Neurology*, Vol 50, 673-683.
- BUCHANAN, B.G. and DUDA, R.O., (1982), Principles of rule-based expert systems, STAN-HIPP-82-14.
- BUCHANAN, B.G. and SHORTLIFFE, E.H., (1983), Rule-based expert systems: The MYCIN experiments of the Stanford heuristic programming project, Addison-Wesley.
- BUCHANAN, B. and SHORTLIFFE, E.H., (1984), Rule-based expert systems, Addison-Wesley (Mass., CA., Lon.).
- BUCHTHAL, F., GULD, C. and ROSENFALCK, P., (1954), Action potential parameters in normal human muscle and their dependence on physical variables, *Acta Physiol. Scand.*, Vol 32, 200-218.
- BUCHTHAL, F., GULD, C. and ROSENFALCK, P., (1957), Volume conduction of the spike of the motor unit potential investigated with a new type of multi-electrode, *Acta. Physiol. Scand.*, Vol 38, 331-354.
- BUCHTHAL, F. and MASDEN, A., (1952), Synchronous activity in normal and atrophic muscle, *Electroenceph. Clin. Neurophysiol.*, Vol 2, 425.
- BUCHTHAL, F. and PINELLI, P., (1953), Muscle action potential in polymyositis, *Neurology (Minneap.)*, Vol 3, 424-436.
- BUCHTHAL, F., PIRELLI, P. and ROSENFALCK, P., (1954), Action potential parameters in normal human muscle and their physiological determinants, *Acta. Physiol. Scand.*, Vol 32, 219-229.
- BUCHTHAL, F. and ROSENFALCK, P., (1966), Spontaneous electrical activity of human muscle, *Electroenceph. Clin. Neurophysiol.*, Vol 20, 321-336.
- BUNDY, A. (ed), (1980), *Artificial intelligence: An introductory Course*, Edingburgh University Press, Edinburgh.
- BUNDY, A., (1983), *The computer modelling of mathematical reasoning*, Academic Press.
- CATON, R., (1875), The electrical currents of the brain, *Br. Med. J.*, Vol 2, 287.
- CHRISTAKOS, C.N. and LAL, S.N., (1980), Lumped and population stochastic models of skeletal muscles, limitations and predictions, *Biol. Cybern.*, Vol 36, 73-85.
- CHRISTAKOS, C.N., (1982), A study of the muscle force waveform using a population stochastic model of skeletal muscle, *Biol. Cybern.*, Vol 44, 91-106.

- CHRISTAKOS, C.N., (1982), A linear stochastic model of the single motor unit, *Biol. Cybern.*, Vol 44, 79-89.
- CLAMMAN, H.P., (1969), Statistical analysis of motor unit firing patterns in human skeletal muscle, *Biophysical Journal*, Vol 9, 1233-1251.
- CLAMMAN, H.P., (1970), Activity of single motor units during isometric tension, *Neurology*, Vol 20, 865- 879.
- CLANCEY, W. and SHORTLIFFE, E.H., (1984), *Readings in medical artificial intelligence*, Addison-Wesley (Mass., Ca., Lon.).
- CLOCKSIN, W.F. and MELLISH, C.S., (1981), *Programming in PROLOG*, Springer-Verlag.
- COERS, C. and WOOLF, A.L., (1959), *The innervation of muscle: A biopsy study*, Blackwell Scientific Publications, Oxford.
- COHEN, B.A., (1977), Review of acquisition and analysis of the electromyogram, *Journal of Clin. Eng.*, April-June.
- COHEN, P.R. and FEIGENBAUM, E.A., (1982), *The handbook of artificial intelligence*, Vol 3, Pitman, London.
- COLSTON, J.R. and FEARNLEY, M.E., (1967), Preliminary experience with an experimental action potential analyser in clinical electromyography, *Annals. of Physical Med.*, Vol 9, No 4.
- COLWELL, H., (1992), *An essay on the history of electrotherapy*, London.
- DAVIS, R., BUCHMAN, B. and SHORTLIFFE, E.H., (1979), Production rules as a representation for a knowledge-based consultation program, *Artificial Intelligence*, Vol 8, 15-45.
- DAWSON, D.G., (1954), A summation technique for the detection of small evoked potentials, *Electroenceph. Clin. Neurophysiol.*, Vol 6, 65.
- De LUCA, C.J., (1979), Physiology and mathematics of myoelectric signal, *IEEE Trans. on Biomed. Eng.*, BME-26, No.6.
- De LUCA, C.J. and FORREST, W.J., (1973), Some properties of motor unit action potential trains recorded during constant isometric contraction in man, *Kybernetic*, Vol 15, 1167-1180.
- DENNY-BROWN, D., (1949), The interpretation of the electromyogram, *Arch. Neurol. Psychiat. (Chic)*, Vol 61, 99.
- DENNY-BROWN, D., (1953), Clinical problems in neuromuscular physiology, *Amer. J. Med.*, Vol 15, 368.
- DENNY-BROWN, D. and PENNYBACKER, J.B., (1938), Fibrillation and Fasciculations in voluntary muscle, *Brain*, Vol 61, 311.
- DESMEDT, J.E., (1983), *Progress in clinical neurophysiology: Computer-Aided electromyography*, Vol 10, Karger, Basel.
- DUDA, R.O., HART, P.E., KONOLIGE, K. and REBOH, R., (1979) *A Computer Based Consultant for Mineral Exploration, Final Report, Sept.*, SRI International, Menlo Park, CA.
- DURIEUX-SMITH, A. and PICTON, T.W., (1985), Neonatal hearing assessment by auditory brainstem response - the Canadian experience, *J.Otolaryngol. (Suppl. 14)*, 1-55.

- De VRIES, P.H., De VRIES ROBBE, P.F., (1985), An overview of medical expert systems, *Meth. Inform. Med.*, Vol 24, 57-64.
- De WEERD, J.P.C., (1981), Facts and Fancies about *Wiener* filtering, *IEEE Trans. Biomed. Eng.*, Vol BME-28, 3, 252-257.
- De WEERD, J.P.C. and MARTENS, W.L.J., (1978), Theory and practice of a posteriori *Wiener* filtering of average evoked potentials., *Biol. Cybern.*, Vol 30, 81-94.
- EDSTROM. L. and KUGELBERG, E., (1968) Histochemical composition distribution of fibres and fatigueability of single motor units, *J. Neurol., Neurosurg., Psychiat.*, Vol 13, 427-433.
- EDWARDS, R.G. and LIPPOLD, O.C.J., (1956), The relationship between force and integrated electrical activity in fatigued muscle, *J. Physiol.*, Vol 132, 667.
- ERB, W., (1883), *Handbook of electrotherapy*, New York.
- FAY, D.F., JONES, N.B. and PORTER, N.H., (1976), spectral analysis of the myoelectric activity of the pelvic floor during voluntary contraction, *Electromyogr. and Clin. Neurophysiol.*, Vol 16, 525-559.
- FEIGENBAUM, E.A. and McCORDUCK, P., (1983), *The fifth generation: Artificial Intelligence and Japan's computer challenge to the world*, Michael Joseph, London.
- FEX, J. and KRAKAU, C.E.T., (1968), Some experience with Walton's frequency analysis of the electromyogram, *Electroencephalogr. Clin. Neurophysiol.*, Vol 25, 570- 573.
- FLEISHER, S.M. and SHWEDYK, E., (1979), Sequential multistate EMG signal processor, *IEEE Trans. on Biomed. Eng.*, Vol BME-26, No 10 Oct 1979.
- FRENCH, A.S. and HOLDEN, A.V., (1971), Alias free sampling of neuronal spike trains, *Kybernetic*, Vol 8, 165-171.
- FUGLSANG-FREDERIKSEN, A. and JEPPSEN, S.M., (1987), An expert assistant for electromyography. In *Computer-aided needle and surface electromyography and expert systems*, DESMEDT, J. (ed), Elsevier.
- FUSEFELD, R.D., (1978), Instrument for quantitative analysis of the electromyogram, *Med. and Biol. Eng. and Comput.*, Vol 16, 290-295.
- GASSER, T., MOCKS, J. and VERLEGG, R., (1983), Salavco: A method to deal with trial-to-trial variability of EPs., *Electroenceph. and Clinical Neurophysiol.*, Vol 55, 717-723.
- GILMORE, L.D. and De LUCA, C.J., (1985), Muscle Fatigue Monitor (MFM): Second Generation, *IEEE Trans. on Biomed. Eng.*, Vol BME-32, No 1 Jan 1985.
- GLANTZ, S.A., (1977), A three element description for muscle with viscoelastic passive elements, *J. Biomechanics*, Vol 10, 5-20.
- GOODGOLD, J. and EBERSTEIN, A., (1978), *Electrodiagnosis of neuromuscular diseases*, 2nd Ed., The Williams and Wilkins Co.
- GOTTLIEB, G.L. and AGGARWAL, G.C., (1971), Dynamic relation between isometric and the electromyogram in man, *J. Applied. Physiol.*, Vol 30, No 3, 345-351.
- GRIMSBY, L. and HANNERZ, J., (1977), Firing rate and recruitment order of toe extensor motor units in different modes of voluntary contraction, *J. Physiol.*, Vol 264, 865-879.

HABRA, M.I.A. and IBRAHEEM, A.A., (1986), EMG processor based on the amplitude probability distribution, J. Biomed. Eng., Vol 8.

HAILSTONE, J.H., JONES, N.B., PAREKH, A., SEHMI, A.S., WATSON, J.D. and KABAY, S., (1986), Smart instrument for flexible digital signal processing, Med. and Biol. Eng. and Comput., Vol 24, 301-304.

HART, P.E. and DUDA, R.O., (1977), PROSPECTOR - A computer-based consultation system for mineral exploration, SRI computer Science Group Technical Report 155.

HAYES-ROTH, F., WATERMAN, D.A. and LENAT, D.B., (eds), (1983), Building Expert Systems, Addison Wesley.

HAYWARD, M., (1977), Automatic analysis of electromyograms in healthy subjects of different ages, J. Neurological Sciences, Vol 33, 397-413.

HEERKENS, Y.F. and WOLTTIEZ, R.D. et al. (1986), Passive resistance of the human knee: The effect of immobilization, J. Biomed. Eng., Vol 8.

HILL, A.V., (1970), First and last experiments in muscle, Camb. Univ. Press.

HOFF, A.C. and VAN DEN BERG, J.W., (1981), EMG to force processing, J. Biomechanics, Vol 14, pt 11, 747-792.

JAYAWANT, B.V., (1981), Electromagnetic levitation and suspension techniques, Edward Arnold.

JEWETT, D.L., (1970), Volume conducted potentials in response to auditory stimuli as detected by averaging in the cat., Electroenceph. Clinical Neurophysiol., Vol 28, 609.

JOHANSSON, S., LARSON, L.E. and ORTENGREN, R., (1970), An automated method for frequency analysis of myoelectric signals evaluated by an investigation of the spectral changes following string sustained contractions, Med. and Biol. Eng. and Comput., Vol 8, 257-264.

JOHNSON, J.C., (1978), Comparison of analysis techniques for electromyographic data, Aviation space and Environmental Medicine, January.

JONES, N.B. and LAGO, P.J.A., (1982), Spectral analysis and the interference EMG, IEE Proc., VOL 129, Pt A No.9.

JONES, N.B. and LAGO, P.J.A., Factors affecting the interpretation of emg spectra, IEE Conf. Publ., No 159, 65-81.

JONES, N.B. and LAGO, P.J., Characterising the interference EMG, an unpublished paper.

JONES, N.B., LISTER, P.F., LAGO, P.J.A. and RESTIVO, F.J. DeO., (1982), Microcomputer-based electromyographic signal analysis, Med. and Biol. Eng. and Comp., Vol 20, 649-652.

JONES, N.B., SEHMI, A.S. and LAGO, P.J., (1987), An EMG-force measuring system for assessing muscle condition, in Biomechanics in Sport, IMechE, September 1987, 1-6.

JONES, R.V., LAMBERT, E.H. and SAYRE, G.P., (1955), Source of a type of *insertion activity* in electromyography with evaluation of a histological method of localization, Arch. Phys. Med., Vol 36, 321-336.

- KAWAI, M. and BRANDT, P.W., (1980), Sinusoidal analysis: a high resolution method for correlating biochemical reactions with physiological processes in activated skeletal muscle of rabbit, frog, and, crayfish, *J. Muscl. Res. Cell. Motil.*, Vol 1, 279-303.
- KOMI, P.V. and CAVANAGH, P.R., (1977), Electromyochemical delay in human skeletal muscle, *Med. Sci. Sports*, Vol 9, Pt. 1, 49-?
- KUGELBERG, E., (1949), Electromyography in muscular dystrophies, *J. Neurol. Neurosurg. Psychiat.*, Vol 12, 129-136.
- KULIKOWSKI, C.A. and WEISS, S.M., (1982), Representation of expert knowledge for consultation: The CASNET and EXPERT Projects, 21-56, in *Artificial Intelligence In Medicine*, P. Szolovits (ed), Westview Press, Boulder, Colorado.
- LAGO, P.J.A., (1979), Mathematical models of aspects of the electrical and mechanical activity of human muscle, D.Phil. thesis dissertation, Univ. of Sussex, England.
- LAGO, P.J.A. and JONES, N.B., (1977), Effect of motor-unit firing time statistics on EMG spectra, *Med. Biol. Eng. Comput.*, Vol 15, 648-655.
- LAGO, P.J.A. and JONES, N.B., (1981) Technical note on low frequency spectral analysis of the emg, *ibid*, Vol 19, 779-782.
- LAGO, P.J.A. and JONES, N.B., (1982), Note on the spectral analysis of neural spike trains, *ibid*, Vol 20, 44-48.
- LAGO, P.J.A. and JONES, N.B., (1982), A study of the muscle force waveform using a population stochastic model of skeletal muscle, *ibid*, Vol 44, 91-106.
- LAGO, P.J.A. and JONES, N.B., (1983), Turning point spectral analysis of the interference myoelectric signal, *ibid*, Vol 21, 333-342.
- LANG, A.H., and TUOMOLA, H., (1974), The time parameters of motor unit potentials recorded with multi-electrodes and summation technique, *electromyogr. Clin. Neurophysiol.*, Vol 14, 513-525.
- LEBAILLY, J., MARTIN-CLOUAIRE, R. and PRADE, H., (1987), Use of fuzzy logic in a rule-based system in petroleum geology. In *SANCHEZ, E. and ZADEH, L.A. (eds), (1987), Approximate reasoning in intelligent systems, decision and control*, Pergamon press, Oxford.
- Le FEVER, R.S. and De LUCA, C.J., (1982), A procedure for decomposing the myoelectric signal into its consistent Action Potentials. Part 1: Technique, Theory and Implementation. Part 2: Execution and Test for Accuracy. *IEEE Trans. on Biomed. Eng.*, Vol BME-29, No.3.
- LENMAN, J.A.R., (1959), Quantitative electromyographic changes associated with muscular weakness, *J. Neurol. Neurosurg. Psychiat.*, Vol 22, 306.
- LICHT, S., *History of Electrodiagnosis*, Publisher unknown.
- LINDROSTROM, L., (1970), On the frequency spectrum of emg signals, *Res-Lab. Med. Electron.*, Chalmers Univ. Tech., Goteberg, Sweden.
- LINDSLEY, D.B., (1935), Myographic and electromyographic studies in myasthenis gravis, *Brain*, Vol 58, 470.

- LIPPOLD, O.C.J., (1952), The relation between the integrated action potential in human muscle and its isometric tension, *J. Physiol.*, Vol 117, 492-499.
- LIPPOLD, O.C.J., REDFEARN, J.W.T. and VUCO, J., (1957), The rhythmical activity of groups of motor units in the voluntary contraction of muscle, *J. Physiol.*, Vol 137, 473.
- LOWREY LEE THOMPSON, (1981), *The electromyographers Handbook*, Little, Brown and Company, Boston.
- LYNN, P.A., (1971), Recursive digital filters for biological signals, *Med. and Biol. Eng.*, Vol 9, 37-43.
- LYNN, P.A., (1977), On-line digital filters for biological signals: some fast designs for a small computer, *ibid*, Vol 15, 534-540.
- MADHAVAN, G.P., De BRUIN, H. and UPTON, A.R.M., (1985), Single Stimulus Evoked Potentials, Report No BMSP-EP-85-02, Jan 1985, Dept. of Med., Elect. and Comp. Eng., McMaster University, Canada.
- MAGORA, A., GONNEN, B., EIMERI, D. and MAGORA, F., (1976), Electrophysical manifestations of isometric contraction sustained to maximal fatigue in healthy humans., *Electromyogr. Clin. Neurophysiol.*, Vol 16, 309-334.
- MAGORA, A. and GONEN, B., (1977), Computer analysis of the relation between duration and decrease of superposition of electromyographic spikes, *electromyogr. Clin. Neurophysiol.*, Vol 17, 83-98.
- MANNARD, A. and STEIN, R.B., (1973), Determination of the frequency response of isometric soleus muscle in the cat using random nerve stimulation, *J. Physiol.*, Vol 229, 275-296.
- MARANZANA-FIGINI, M., BESTETTI, G. and VALLI, G., (1978), Measuring MUAP duration by means of surface electrode EMG, *Electromyogr. Clin. Neurophysiol.*, Vol 18, 45-46.
- MARMARELIS, P.Z. and MARMARELIS, V.Z., (1978), *Analysis of physiological systems: The white noise approach*, Plenum Press, N.Y..
- MARRINACI, A.A., (1968), *Applied electromyography*, Philadelphia PA, Lea and Febiger.
- Mc GILL, K.C., CUMMINS, K.L. and DORFMAN, L.J., (1985), Automatic decomposition of the electromyogram, *IEEE Trans. on Biomed. Eng.*, Vol BME-32, No 7.
- McGILLEM, C.D. and AUNON, J.I., (1977), Measurements of signal components in single visually evoked brain potentials, *IEEE Trans. on Biomed. Eng.*, Vol BME-24, 232-241.
- McGILLEM, C.D., AUNON, J.I., and POMELAZA, C.A., (1985), Improved waveform estimation procedures for ERPs, *IEEE Trans. on Biomed. Eng.*, Vol BME-32, No 6, 371-379.
- McGULLIVARY, R.V. and WALD, R.W., (1986), Digital peak detector for intracellular action potentials, *Med. Biol. Eng. Comp.*, 24, 319-334.
- MERLETTI, R., BIEY, D., BIEY, M., PRATO, G. and ORUSA, A., (1985), On-line monitoring of the Median frequency of the surface EMG power spectrum., *IEEE Trans. on Biomed. Eng.*, Vol BME-32, No.1.
- MILNER-BROWN, H.S., STEIN, R.B. and YEMM, R., (1973), The contractile properties of human motor units during voluntary isometric contraction., *J. Physiol.*, Vol 228, 285-306.

- MILNER-BROWN, H.S., STEIN, R.B. and YEMM, R., (1973 a), Changes in firing rate of human motor units during linearly changing voluntary contractions, *J. Physiol.*, Vol 230, 371-390.
- MIYAZAKI, S., (1977), An interactive mini-computer system for the analysis of EMG spikes and twitch waveforms of human motor units., *Computers and Med. Res.*, Vol 10, Pt.3, 287-296.
- MORECKI, A., EKIEL, J. and FIDELUS, K., (1983), *Cybernetic system of limb movement in man, animals and robots*, Ellis Harwood, Chichester.
- MORGAN, C.E., (1868), *Electrophysiology*, New York.
- MORRISON D.F., (1978), *Multivariate Statistical Methods*, Chapter 8, 2nd Ed., Mc Graw-Hill Inc.
- MORRISON, J.B., (1960), Electromyographic change in hyperkalemic familial periodic paralysis, *Ann. Phys. Med.*, Vol 5, 153-155.
- NANDEDKAR, S.D., STALBERG, E.V. and SANDERS, D.B., (1985), Simulation technique in electromyography, *IEEE Trans on Biomed. Eng.*, Vol BME-32, No.10.
- NORMAN, R.W. and KOMI, P.V., (1979), Electromechanical delay in skeletal muscles under normal movement conditions, *Acta. Physiol. Scand.*, Vol 106, 241-248.
- O'SHEA, TIM and EISENSTADT, MARC, (EDS), (1984), *Artificial intelligence, tools, techniques and applications*, Harper and Row.
- PAREKH, A.K., (1986), Computer analysis of EMG turning points process, D.Phil. thesis dissertation, Univ. of Sussex, England.
- PARKER, P.A. and SCOTT, R.N., (1973), Statistics of the myoelectric signal from monopolar and bipolar electrodes, *Med. Biol. Eng. Comput.*, Vol 11, 591-596.
- PARMIGIANNI, F., STEIN, R.B. and ROLF, R., (1981), Slow changes changes and Wiener Analysis of non-linear simulation in contractions of cat muscle, *Biol. Cybern.*, Vol 42, 177-188.
- PEARL, J., (1984), *Heuristics: Intelligent search Strategies for computer problem solving*, Addison-wesley (Mass., Ca., Lon.).
- PERRY, I.R., (1984), *Real-time clinical computing*, Reaserch Studies Press, J. Wiley and Sons. (N.Y., Brisbane, Chichester).
- PETERSON, L. and BROMAN, A.M., (1961), Electromyographic findings in a case of botulism, *Nord. Med.*, Vol 65, 259-261.
- PICTON, T.W., HUNT, M., MOWREY, R., RODRIGUEZ R. and MARU J., (1978), Evaluation of brainstem auditory evoked potentials using dynamic time warping, *Electroenceph. Clin. Neurophysiol.*, Vol 71, 212-225.
- PICTON, T.W. (ed), (1988), *Handbook of EEG and clinical neurophysiology, Human ERPs*, Vol 3, Elsevier.
- PRINEAS, J., HALL, R., BARWICK, D.D. and WATSON, A.J., (1968), Myopathy associated with pigmentation following adrenalectomy for Cushing's syndrome, *Quart. J. Med.*, Vol 145, 1.
- RICHARDSON, A.T., (1954), Muscle fasciculation, *Arch. Phys. Med.*, Vol35, 281-286.

RICHARDSON, A.T. and BARWICK, D.D., *Clinical Emg, in Disorders of voluntary Muscle*, J. Walton (ed), J and A Churchill Ltd.

RICHFIELD, E.H., COHEN, B.A. and ALBERS, J.W., (1981), Review of quantitative and automated needle electromyographic analysis, *IEEE Trans. on Biomed. Eng.*, Vol BME-28, No.7, 506-514.

RICKER, K., HERTEL, G. and STODIERCK, G., (1977), Increased voltage of the muscle action potential of normal subjects after local cooling, *J. Neurol.*, Vol 216, 33-38.

ROSENFALCK, P., (1969), *Intra and extra-cellular potential fields of the active nerve fibres*, Akademisk, forlag, Copenhagen, Denmark.

ROSSAMINTH, G.H., UNSWORTH, J. and BELL, R.D., (1983), Frequency domain study of the mechanical response of living striated muscle, *Experimenta*, Vol 36, 52-53.

RUCHKIN, D.S., (1988), Measurement of ERPs, in *Handbook of EEG and clinical neurophysiology, Human ERPs*, Vol 3, Picton, T.W. (ed), Elsevier, 7-43.

RUCHKIN, D.S., (1965), An analysis of average response computations based upon aperiodic stimuli, *IEEE Trans. on Biomed. Eng.*, Vol BME-12, 87-94.

SANCHEZ, E. and ZADEH, L.A. (eds), (1987), *Approximate reasoning in intelligent systems, decision and control*, Pergamon press, Oxford.

SADOYAMA, T. and MIYANO, H., (1981), Frequency analysis of surface EMG to evaluation of muscle fatigue, *Eur. J. Appl. Physiol.*, Vol 47, 239-246.

SCHERG, M. and VON CRAMMON, D., (1985), Two bilateral sources of the late AEP as identified by a spatio-temporal dipole model, *Electroenceph. Clin. Neurophysiol.*, Vol 62, 32-44.

SCHMIDT, E. and F.W., (1976), *Brief guide to practical enzyme diagnosis*, Diagnostica Boehringer Mannheim.

SCHMIDT, R.F. (ed), *Fundamentals of neurophysiology*, Springer-verlag (1975).

SCHULMAN-GALAMBOS, C. and GALAMBOS, R., (1975), *Recording the Brainstem Evoked Response: A Manual*, Dept. of Otolaryngology, Teikyo Univ. School of Medicine., Tokyo.

SEHMI, A.S. and JONES, N.B., (1985), *Artificial intelligence methods in quantitative electromyogram (EMG) analysis*, Grant Application to Medelec Ltd. (Old Woking, Surrey, England), September, Dept. of Engineering, University of Leicester.

SEHMI, A.S., (1988), *Epaxis: An expert system for automatic component labelling in evoked potentials*, Turing Institute research memoranda, TIRM-88-32, Turing Institute Press.

SEHMI, A.S., ROBINSON, N.L., CHARLES, A.J. and ROBINSON, P.M., (1988), *New developments in computer applications in neurology*, in *Digital signal processing: components and applications*, ERA report 88-0386.

SHEPHERD, B.A., (1985), *Computer induction versus statistical classifiers in the domain of shape recognition*, M.Phil. thesis dissertation, Univ. of Edinburgh, England.

SHERRIF, M.H., GREGOR, R.J. and LUI, L.M., (1983), Correlation of myoelectric activity and muscle force during selected cat treadmill locomotion., *J. Biomechanics*, Vol 16, 691-701.

SHIAMI, R. and NEGIN, M., (1975), Stochastic properties of motor neuron activity and the effect of muscle length, *Biol. Cybernetics*, Vol 19, 231-237.

SHIAMI, R. and GRIFFIN, P., (1981), Representing and clustering electromyographic gait patterns with multivariate techniques, *Med. Biol. Eng. Comput.*, Vol 19, 605-611.

SHORTLIFFE, E.H., (1984), Reasoning methods in medical consultation systems: AI Approaches, *Computer Programs in Biomedicine*, Vol 18, 5-14.

STACEY, R.W. and WAXMAN, B.D., *Computers in Biomedical Research*, Academic Press (N.Y.).

STEFIK, M., AIKINS, J., BALZER, R., BENOIT, J., BIRNBAUM, L., HAYES-ROTH, F. and SACERDOTI, E., (1983), The Architecture of Expert Systems, in *Building Expert Systems*, Hayes-Roth, F., Waterman, D.B. and Lenat, D.B., (eds), Addison Wesley.

STEIN, R.B., FRENCH, A.S., MANNARD, A. and YEMM, R., (1972), New methods for analysing motor functions in man and animals., *Brain Res.*, Vol 40, 187-192.

STEVENS, A.L. and FULTON, T.J., (1982), Digital processing of doppler signals, in *Digital Signal Processing*, Jones, N.B., (ed), IEE Control Eng Series 22, Peter Peregrinus Ltd.

STULEN, F.B. and De LUCA, C.J., (1981), Frequency parameters of the myoelectric signal as a measure of muscle conduction velocity, *IEEE Trans. on Biomed. Eng.*, Vol BME-28, No.7, 515-523.

SUSHEELA, A.K. and WALTON, J.N., (1969), Distribution of muscle fibres in normal human muscles., *J. Nuerol. Sci.*, Vol 8, 201-207.

TAYLOR, A., (1962), The significance of grouping of motor units activity, *J. Physiol.*, Vol 162, 259.

TAYLOR, T.P. and MacFARLANE, P.W., (1974), Digital filtering of the ECG - a comparison of low pass digital filters on a small computer., *Med and Biol. Eng.*, Vol 12, 493-502.

TRIBE, M.A. and ERAUT, M.R., (1977), *Basic Biology Course Unit 10*, Cambridge University Press.

TROJABORG, W. and BUCHTHAL, F., (1965), Malignant and benign fasciculations, *Acta. Neurol. Scand.*, Vol 41 (suppl.13), 251-254.

TUKEY, J.W., (1978), Measurement of ERPs: Commentary, a data analyst's comments on a variety of points and issues, in E.Callaway, P. Teutaing and S. Koslow (eds), *Event Related Brain Potentials in Man*, Academic Press, NY, 139-151.

VAUGHAN, H.G. and AREZZO, J.C., (1988), The neural basis of event-related potentials. In PICTON, T.W. (ed), (1988), *Handbook of EEG and clinical neurophysiology, Human ERPs*, Vol 3, Elsevier.

VOLTA, A., (1793), An account of some discoveries made by M. Galvani, *Philos. Trans.*, Vol 83, 10.

WALTON, J.H., (1952), The Electromyogram in myopathy: analysis with the audio-frequency spectrometer, *J. Neurol. Neurosurg. Psychiat.*, Vol 15, 219-226.

WALTON, J.N. and ADAMS, R.D., (1958), *Polymyositis*, Livingstone, Edingburgh.

WATERMAN, D. and HAYES-ROTH, F., (1978), Pattern directed inference systems, Academic Press (N.Y.).

WHORLOW, R.J., (1978), Design of magnetic suspension systems and control of vehicles in networks, D.Phil thesis dissertation, University of Sussex, England.

WILKE, D.R., (1956), The mechanical properties of muscle, British Medical Bulletin, Vol 12, Pt 3, 177-182.

WILLISON, R.G., (1964), Analysis of electrical activity in healthy and dystrophic muscle in man, J. Neurol. Neurosurg. psychiat., Vol 27, 386-394.

WOODY, C.D., (1977), Characterisation of an adaptive filter for the analysis of variable latency neuroelectric signals, Med. Biol. Eng. 5, 539-553.

ZAHALAK, G.I. and HEYMAN, S.J., (1979), A quantitative evaluation of the frequency response characteristics of active human skeletal muscle in vivo, Trans ASME, Vol 10, 28-37.

**NEW ENVIRONMENTS FOR NEUROPHYSIOLOGICAL
INVESTIGATIONS**

by
Arvindra Singh Sehmi

APPENDICES

Appendix [A]

Published Paper on the SPC

Smart instrument for flexible digital signal processing

J. G. Hailstone N. B. Jones A. Parekh
A. S. Sehmi J. D. Watson S. Kabay

Graduate Division of Biomedical Engineering, University of Sussex Centre for Medical Research,
Falmer, Brighton, E. Sussex BN1 9QT, UK

Keywords—Interactive signal processing, EMG analysis, Vascular impedance measurement

Med. & Biol. Eng. & Comput., 1986, 24, 301–304

1 Introduction

A significant problem with most digital signal processing systems so far introduced is the rigidity of the user interactive format adopted. As a result of this an inordinate amount of time is required to consult the system. This flexible signal processing instrument has been designed for use either by nonexperts or in situations where the user is unable to pay much attention to the instrument (for example in an operating theatre). The signal processing computer (SPC) is a friendly menu-driven system presenting the user with a page of options on the screen, allowing entry of analysis parameters, patient data etc. in a convenient manner through depression of the appropriate soft key. The relabelling of these buttons and the use of branching menus allows the user to progress through a signal acquisition, processing and display of results with the prior knowledge that all options have been considered previously in the laboratory during the program writing stage. Furthermore, the instrument exists as a single transportable unit, containing the display with its soft keys, a $\frac{5}{8}$ in disk drive and various data acquisition and processing cards. The small number of buttons used to control the instrument dispenses with the need for an alphanumeric keyboard, although this can be connected if required.

2 Instrument requirement and specification

The first field of instrument application was chosen to be medical signal acquisition and processing, particularly of blood flow and pressure during surgery. In this application, derived from BUTLER *et al.* (1980) and LAW *et al.* (1983), the surgeon could be presented with flow, pressure or ECG displays, or vascular impedance modulus or phase characteristics. An application area considered later is for future use in an electromyography outpatient clinic. This application is illustrated by Fig. 5 and is derived from

LAGO and JONES (1983). Consequently, the initial requirement placed upon the instrument was a capability to sample up to three channels of signal input (namely flow, pressure and ECG) at sampling frequencies of up to 2 kHz. To provide for the electromyographic application area and many other medical, biological and industrial applications, the present system facilitates acquisition of up to four multiplexed channels (8 or 12 bits) at a nominal sampling frequency of 3.3 kHz, the maximum for a single channel being 10 kHz. Apart from ease of use and safety in a clinical environment, the instrument should be portable, inexpensive and produce a visual display of computed results rather than numeric tabulation.

These requirements were derived from the current and proposed research work at the universities of Sussex and Leicester. Bearing in mind that other uses for the machine are envisaged besides that already mentioned, the instrument is amenable to expansion using commercial boards configured to the standard S-100 bus. It was also specified that programming of the machine could be done locally or remotely in a high-level language such as Fortran or in assembler via any CP/M compatible development facility. The full instrument specification is listed in the Appendix.

3 Hardware organisation

The specifications outlined have been translated into the hardware shown in Fig. 1, which portrays the front panel

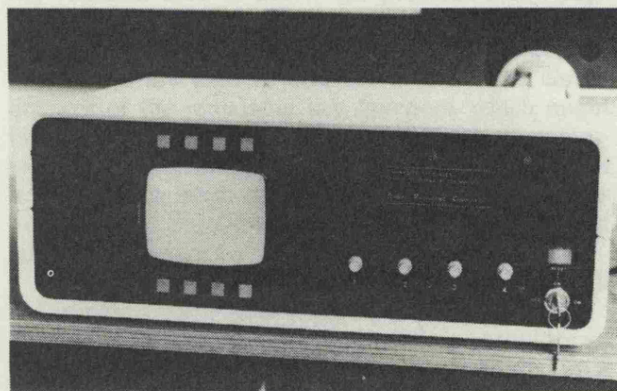


Fig. 1 Front panel of the signal processing computer

First received 26th March and in final form 15th July 1985.

J. G. Hailstone is now with West Glamorgan Health Authority, N. B. Jones, A. S. Sehmi and S. Kabay are now with the University of Leicester, and J. D. Watson is now with Eurotherm International.

Correspondence should be addressed to Prof N. B. Jones, Department of Engineering, The University, Leicester LE1 7RH, UK.

© IFMBE: 1986

the instrument. Its principal features are four input channels, for example, flow, pressure, ECG or other data, a floppy disk drive (FDC) for transferring programs and/or data to and from the remote research computers in the laboratory, a monitor and eight button keys. Fig. 2 is a schematic diagram of the system as a whole.

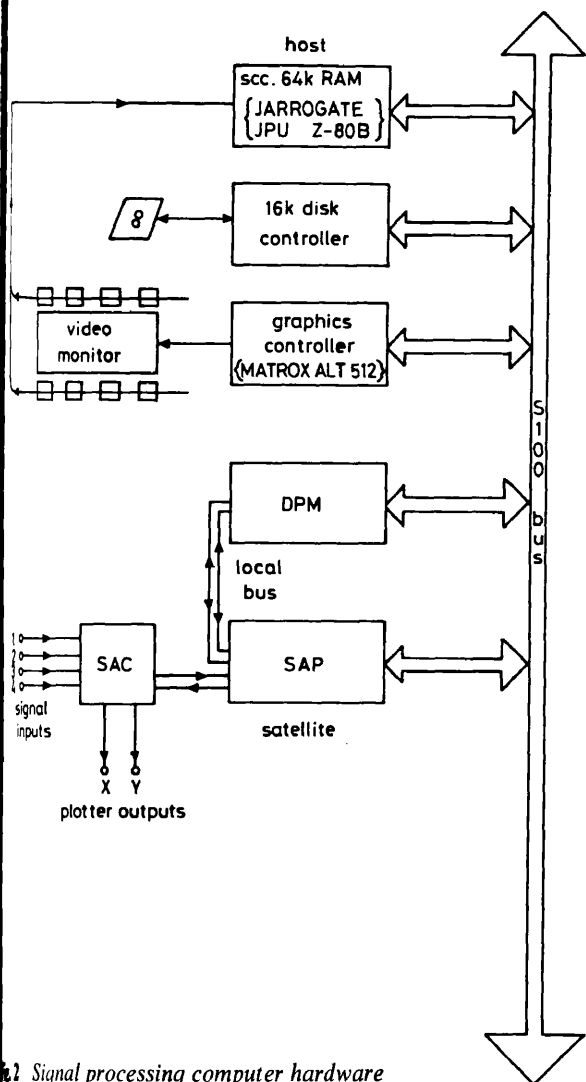


Fig. 2 Signal processing computer hardware

The host processor is a standard single-card computer incorporating a 6 MHz Z80B microprocessor, 64 kbytes of RAM and three each of serial and parallel ports and timers. A Matrox ALT-512 graphics board provides 640 x 256 resolution on a 5½ in display monitor. An RS232 connector allows a VDU and terminal to be connected if required for local program developments and debug facilities on the machine itself. It is not proposed that this should be used in clinical situations. The 16 kbyte FDC controls disk I/O. The front end or slave processor board is made up of 6 MHz Z80B microprocessor, 24 kbytes of RAM and 8 kbytes of PROM three parallel ports and three timers. This card controls signal acquisition of up to four channels of input data and xy plotter outputs for hard copy of results. Signal acquisition is performed using a software programmable analogue/digital convertor (ADC) with automatic offset and gain facility. This dual processor arrangement allows for signal acquisition on the front end and signal processing on the host. To facilitate the direct transfer of acquired/processed data to/from the host from/to the slave processor, the dual plane memory (DPM) is used. This feature provides data throughput at much faster rates than are obtainable through direct standard data bus utilisation techniques such as I/O and direct memory access (DMA). The dual plane memory is mapped

into both the host's and the front-end processor's memory spaces, occupying a 16 kbyte block in each. This arrangement allows data being acquired by the slave to be loaded into its half of the DPM through its local bus while the host concurrently performs data manipulation on its half of the DPM across the S-100 bus. Thus parallel processing can be achieved without bus contention problems. 'Phantoming' is used to switch out the pre-existed memory overlaid in the host computer. The dual-plane memory provides 32 kbytes of store in two 16 kbyte blocks which may be swapped between the memory maps of the two processors by means of one I/O instruction from the host. The transition time is approximately 1.7 s, thus enabling acquisition and processing of data requiring more than a 16 kbyte buffer space to be implemented in real time. DMA techniques having the same memory bandwidth would take typically 7-8 ms. Fig. 3 illustrates the idea presented above.

Programs to be run on the slave processor can be downloaded via disk to the host DPM memory space and then transferred to the slave by issuing a memory plane swap under program control.

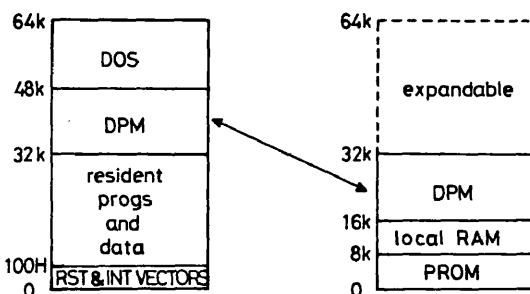


Fig. 3 Dual plane memory

4 Software organisation

Today instrumentation in almost every field is becoming increasingly smart or intelligent. This is primarily because the incorporation of a microprocessor, and its associated software, allows more complex configuration and analysis to be performed than in an instrument designed conventionally. There is little doubt that, through the use of suitable software and the associated interface hardware, instrument ergonomics can be high in terms of user friendliness.

The software driving the SPC can be divided into three major modules:

- (i) Host resident kernel program: this suite of macros and dedicated subroutines provides the nucleus of user-configurable programs to run on the SPC for the purpose desired. The kernel provides any number of pages in a menu. With each page is a reserved RETN key function used to access the previous menu page and seven programmer definable key functions, one of which provides up to three pages of HELP information. These are used to describe in detail the consequences of the remaining key functions which might be, for example, used to set various analysis parameters. This branching structure allows for numerous levels of depth in the tree just by specifying the macros during the program writing stage. A simple three-level structure is shown in Fig. 4.

The kernel program also handles the protocol with the acquisition processor.

- (ii) A host resident graphics utilities package provides an adequate facility to display computed results in a visual format. This is attractive to the examiner, e.g. surgeon or doctor, and has the advantage of being

able to convey trends or patterns in computed results more readily than a list of figures.

(ii) The monitoring program existing in the front end processor provides protocol handling with the host through which various functions may be set or slave processor status determined. The settable functions include the sampling frequency, ADC gain and offset, DPM plane swaps, plotting time base, signal acquisition initiation and termination, and input specification.

By combining these modules as an integrated whole during the program writing stage, most medical and biological signal acquisition and analysis packages can be assembled with ease. This will provide a complete menu driven system that is adequately user friendly and flexible. Programs used to provide key functions in the kernel can be written in a high level language for double precision number crunching in FFTs and matrix operations. Where speed is important, assembler programs can be used.

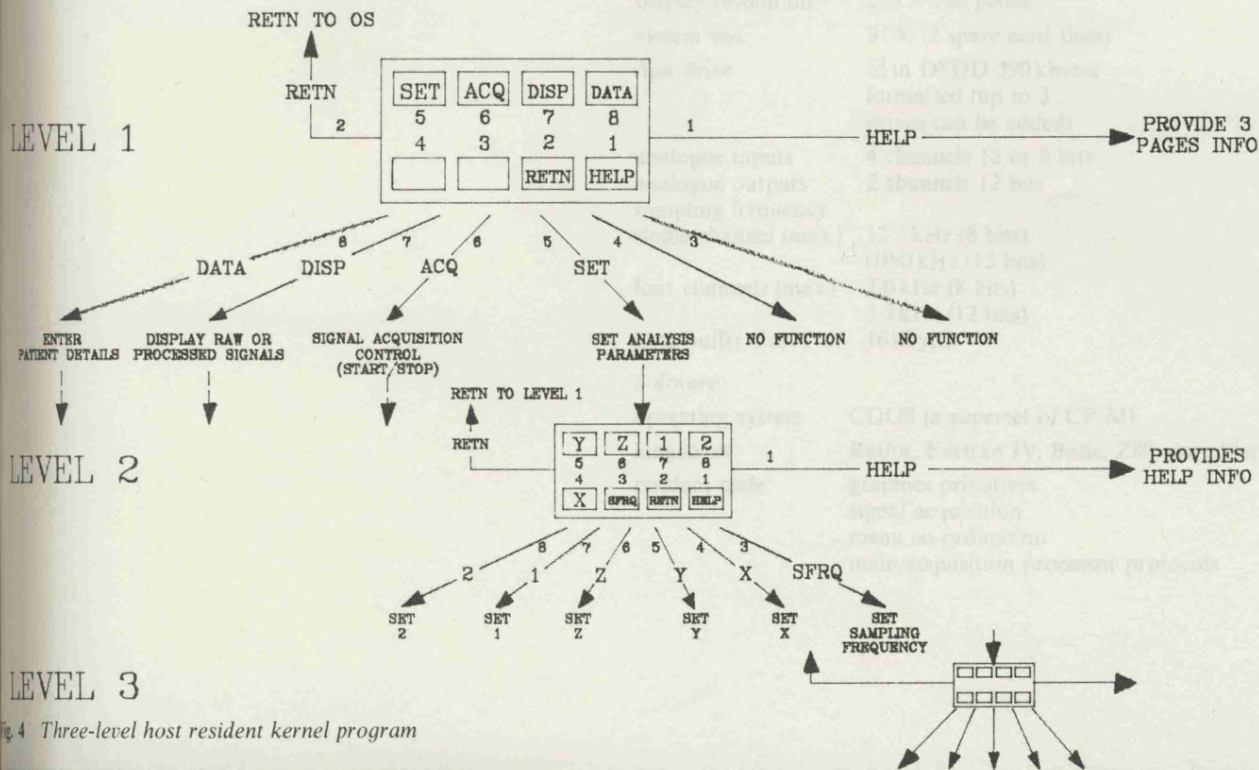
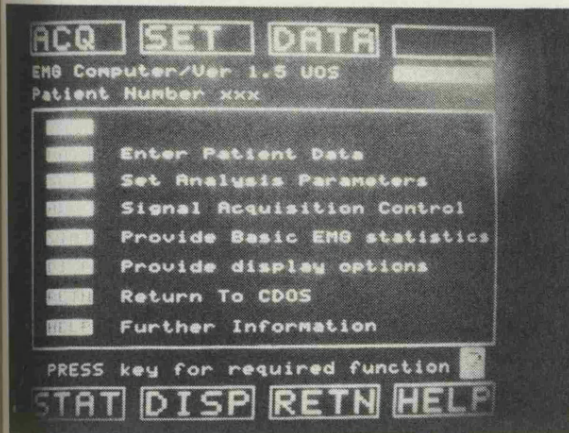
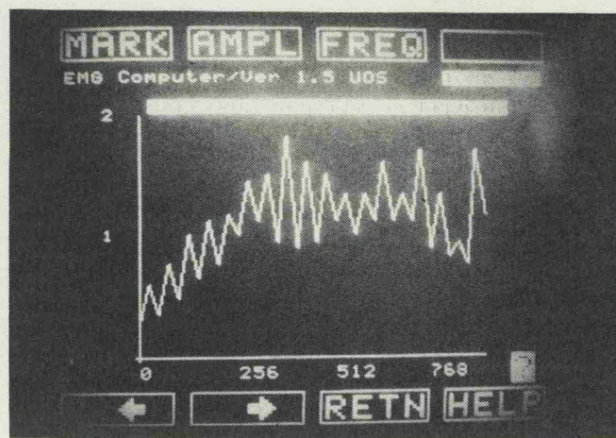


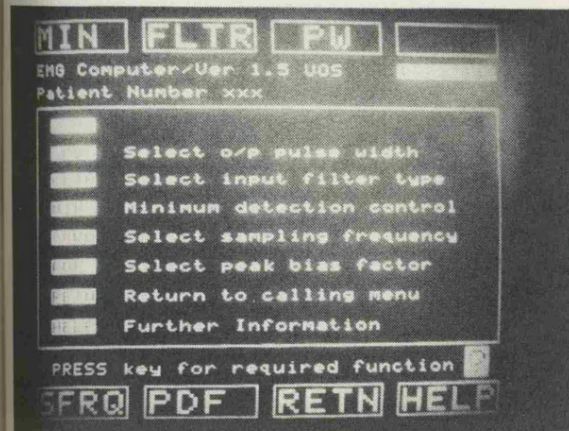
Fig. 4 Three-level host resident kernel program



a



c



b

Fig. 5 Examples of video display formats

Example of the video display formats that can be achieved are shown in Figs. 5a, b and c.

References

- WILKINSON, P. A., JONES, N. B., STRACHAN, C. and SOMERVILLE, P. (1980) 'Per-operative measurement of hydraulic vascular impedance'. Final Report, South East Thames Regional Health Authority 77/4 June 1980.
- WILKINSON, P. J. A. and JONES, N. B. (1983) 'Turning points spectral analysis of the interference myoelectric activity'. *Med. & Biol. Eng. & Comput.*, **21**, 333-342.
- WILKINSON, Y. F., GRAHAM, J. C., COTTON, L. T. and ROBERTS, V. C. (1983) 'Per-operative haemodynamic assessment of lower limb arterial surgery—Part 1: hydraulic impedance measurement'. *J. Biomed. Eng.*, **5**, 185-193.

Appendix

University of Sussex signal processing computer specification

Hardware:

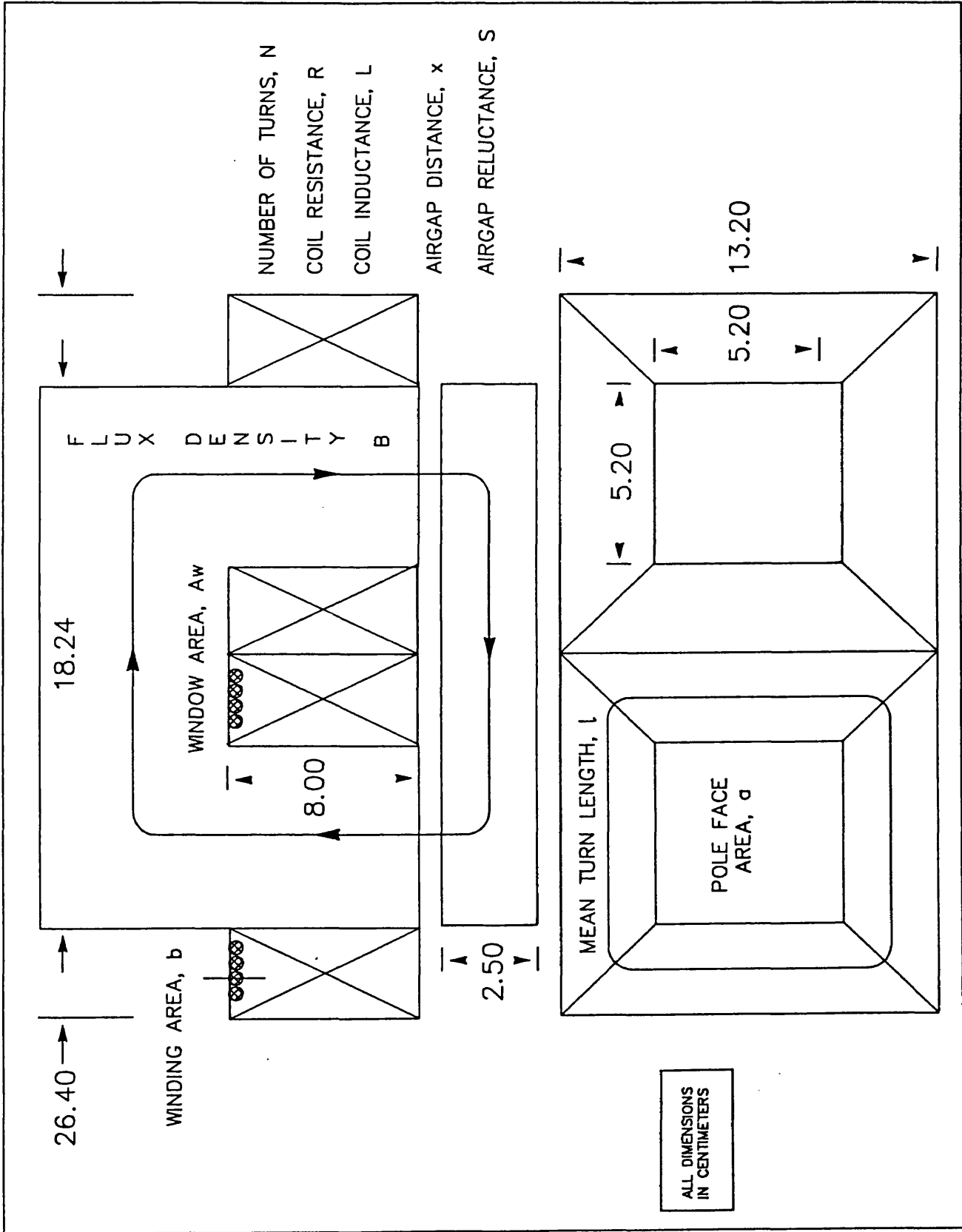
	<i>main processor</i>	<i>acquisition processor</i>
processor	Z80B	Z80B
memory	64 kbytes	32 kbytes
peripheral interfaces	3 × serial	3 × 8 bit parallel
timers	3 × 8 bit parallel	3 × 16 bit
display size	3 × 16 bit	
display resolution	5½ in diagonal	
system bus	256 × 256 pixels	
disk drive	S100 (2 spare card slots)	
	5¼ in DSDD 390 kbytes formatted (up to 3 drives can be added)	
analogue inputs	4 channels 12 or 8 bits	
analogue outputs	2 channels 12 bits	
sampling frequency		
single channel (max.)	12.5 kHz (8 bits)	
	(10.0 kHz (12 bits))	
four channels (max.)	7.0 kHz (8 bits)	
	3.3 kHz (12 bits)	
data buffer size	16 kbytes	

Software:

operating system	CDOS (a superset of CP/M)
languages	Ratfor, Fortran IV, Basic, Z80 assembler
resident code	graphics primitives signal acquisition menu co-ordination main/acquisition processor protocols

Appendix [B1]

MAGLOAD: Design Calculations



Design Calculations for MAGLOAD

The following notation is used in the electromagnet design which refers to the diagram in this appendix:

- a - Pole face area (m^2)
- A_w - Window area (m^2)
- B - Electromagnet flux density (T)
- F - Force produced by electromagnet (N)
- ξ - Forcing ratio
- I - Steady state load current (A)
- i - Instantaneous load current (A)
- l - Mean turn length (m)
- L - Inductance of coil windings (H)
- N - Number of turns
- NI - Ampere-turns
- P - Power dissipation (W)
- R - Resistance of coil (Ω)
- S - Reluctance of airgap
- V_p - Supply voltage (V)
- V_l - Load voltage (V)
- x - Airgap distance (m)
- μ_0 - Permeability of free space
- ρ - Resistivity of coil windings (m)
- b - Coil wire cross section area (m^2)
- τ - Coil time constant (Sec)

The force F for a single pole is given by:

$$F = \frac{B^2 a}{2\mu_0}$$

Therefore, the force per unit area F/a is:

$$\frac{F}{a} = \frac{B^2}{2\mu_0}$$

At a flux density of 0.65 T, the force per unit area is 168.11 kN/m². For the specified 500N forcing required (i.e. 250N per pole face with a U-shaped magnet) the pole face area a is calculated to be 14.87cm² (3.85² cm²)

The mean turn length l given a window area A_w of 4 x 4 cm² is therefore 23.4cm. The ampere-turns NI at the nominal airgap x of 2cm is:

$$NI = \frac{2Bx}{\mu_0} = \frac{2 \times 0.65 \times 2.0 \times 10^{-2}}{4\pi \times 10^{-7}} = 20690 \text{ At}$$

The power dissipation P that can be expected is:

$$P = \frac{(NI)^2 \rho l}{A_w} = \frac{(20690)^2 \times 1.78 \times 10^{-8} \times 23.4 \times 10^{-2}}{16 \times 10^{-4}} = 1.11 \text{ kW}$$

This power dissipation is obviously unmanageable without some forced cooling, so power reduction is achieved by doubling the poleface area and doubling the window dimensions.

$$\text{From } F = \frac{B^2 a}{2\mu_0}$$

Twice a implies twice the force F . Since $F \propto (NI)^2$ and we require the same force level with twice the poleface area $2a$, the ampere-turns NI must be reduced by $\sqrt{2}$. As a result of this, the original power dissipation will be reduced by 50%. The factor of 4 increase in the window area reduces the power dissipation by a further factor of 4. The increase in magnet dimensions, however, causes the mean turn length to go up by 25% of the original which results in a 25% increase in power dissipation. The overall reduction in power dissipation is, therefore: $0.5 \times 0.25 \times 1.25 = 0.156$.

The adjusted parameter values for the magnet are:

$$NI = 20690 / (\sqrt{2}) = 14630 \text{ At}$$

$$l = 23.4 \times 1.25 = 29.25 \text{ cm}$$

$$A_w = (2 \times 4)^2 = 64 \text{ cm}^2$$

$$a = 2 \times 14.87 = 5.45^2 \text{ cm}^2 \text{ (a standard 2 in}^2 \text{ section was used = 5.20}^2 \text{ cm}^2 \text{)}$$

$$P = \frac{(14630)^2 \times 1.78 \times 10^{-8} \times 29.25 \times 10^{-2}}{64 \times 10^{-4}} = 174.12 \text{ W}$$

When the magnet coils are wound, the circular cross-sectional area of the wire means that the full window area will not be filled. Approximately 60% of the available window area will be occupied by a perfectly wound coil. Errors in maintaining the alignment of adjacent windings increases the unoccupied window area. Hence a packing factor of 0.5 is introduced which means the actual power dissipation will be approximately twice the calculated value. So P becomes approximately 350 W.

To obtain a high bandwidth for the control system through voltage forcing we consider the behaviour of the magnet in relation to the supply voltage as follows (Whorlow, 1978):

The total force is given by:

$$F = \frac{(NI)^2 \mu_0 a}{4x^2} \dots \dots \dots \text{Eq.[B1.1]}$$

Therefore:

$$\frac{dF}{dt} = \frac{2N^2 \mu_0 a}{4x^2} \cdot I \frac{di}{dt} \dots \dots \dots \text{Eq[B1.2]}$$

Combining Eq.[5.5] and Eq.[5.10]:

$$\frac{dF}{dt} = \frac{2N^2 \mu_0 a I}{4x^2} \cdot \frac{(V_p - IR)}{L} = \frac{2N^2 \mu_0 a \cdot (I^2 R) \cdot (V_p / R - 1)}{4x^2 L}$$

Since $L = N^2 / S$, $S = 2x / \mu_0 a$, $P = I^2 R$, and $V_1 = IR$

$$dF / dt = (P / x) \cdot (V_p / V_1 - 1) \dots \dots \dots \text{Eq.[B1.3]}$$

The quantity V_p / V_1 describes the voltage forcing ratio ξ in the positive direction when the drive transistor amplifier is turned on. ξ is the ratio of the supply voltage to the steady state voltage drop across the resistive part of the magnet when a quiescent current I is being maintained with the full supply across the magnet. When the drive transistor amplifier is turned off this current still flows due to the inductance of the coils and is recirculated through the power supply by the freewheeling diode. By virtue of this recirculated current flow, a voltage V_1 will exist across the resistive part of the magnet and provides the negative voltage forcing of current through the coils since the inductive voltage drop is now in a direction opposite to that of the resistive voltage drop. The difference between V_p and V_1 determines the rate at which the decaying inductive current falls

when the drive transistor is off. The more V_1 approaches V_p , the less decay there will be in the inductive current; consequently there will be a lower current ripple. Values of V_1 less than one half of the supply voltage result in inadequate forcing and the ripple current increases.

This can be shown easily:

$$L \, di / dt = (V_p - V_1) \dots \dots \dots \text{Eq.[B1.4]}$$

This equation represents the forcing of current in the magnet in the positive direction. In the negative direction :

$$L \, di / dt = V_1 \dots \dots \dots \text{Eq.[B1.5]}$$

Hence for equal positive and negative forcing we equate Eq.[B1.4] and Eq.[B1.5] and it emerges that:

$$\xi = V_p / V_1 = 2 \dots \dots \dots \text{Eq.[B1.6]}$$

If ξ is required less than 2 then the circuit of Fig.[5.10(a)] is adequate. Otherwise the equal positive and negative voltage forcing circuit of Fig.[5.10(b)] must be implemented (Hodkinson, 1975). This circuit is more complex to drive however, requiring the use of an inverter amplifier to drive the topmost PNP transistor when an NPN type can not meet power requirements.

The required value of ξ is obtained by first defining the quantity dF / dt . This represents the slewing rate of force generated by the magnet-amplifier combination and is related to the forced current variations in the magnet. To demonstrate the selection of a slewing rate of force, we refer to Fig.[5.7] and assume we are operating at the nominal airgap of 20mm and at a force of 10N. A movement of 10mm, to 30mm, caused by the patient would make it necessary for the magnet to produce the equivalent of approximately 30N at 20mm. The period of growth for this force must be quicker than the time taken for an average isometric twitch response to rise and decay. Thus, taking 20ms as a reasonable response time for the build-up of magnetic force, we find that:

$$dF / dt = (200 / 20 \times 10^{-3}) = 10\text{kNs}^{-1} \dots \dots \dots \text{Eq.[B1.7]}$$

By substituting the power dissipation value of 350W and nominal airgap of 20mm in Eq.[B1.3], ξ is found to be approximately 1.5. Hence, it follows, that at the maximum specified force of 500N and nominal airgap of 20mm, a single-ended amplifier as in Fig.[5.10(a)] is sufficient for the current variations needed in this application.

The time constant of the magnet $\tau = A_w / S\mu_l$. From the reluctance $S = 2x / \mu_0 a$, the equation for the power dissipation $P = (NI)^2 \rho_l / A_w$, and Eq.[B1.1], it can be shown that there is a relationship $P\tau = 2Fx$. At a maximum force level of 500N, airgap of 20mm, and power dissipation of 350 W, this gives $\tau = 57.2$ ms. The actual power dissipation is an approximation so the time constant will be lower than the worst case of 57.2 ms.

Several iterations of the following calculation were necessary to arrive at a satisfactory choice for the power supply voltage and the coil wire gauge. Only the final iteration is given here:

If we start with 22 SWG (0.028 in / 0.07 cm diameter) enamelled wire then the cross-sectional area b will be $3.9 \times 10^{-7} \text{ m}^2$. Using the exact packing factor of 0.6, N can be estimated from:

$$N = 0.6 \times A_w / b = 9846 \text{ turns in total}$$

From $NI = 14630$, the steady state load current will be 1.5 A. V_l is therefore 235V, given a power dissipation of 350 W. This implies that the supply voltage of approximately 360V is needed to provide a voltage forcing ratio ξ of 1.5.

Connecting the coils in parallel results in an adjustment of I to 3A and V_l to 120V for approximately the same power dissipation (i.e. related to ampere-turns). The power dissipation must be kept constant to maintain both the coil time constant and the designed force. After the coils were wound, it was found that the number of turns actually achieved was 3100 per coil. Therefore, there is a further reduction by a factor of $3100/9846 = 0.63$ in the amount of window area A_w used by the coils. To maintain the ampere-turns, I must be increased to $3/0.63 = 4.8$ A. The load voltage per coil V_l is thus 73V and the required supply voltage V_p is thus 110V. These voltage and current values are used to assist in the selection of a drive transistor.

The resistance R_c of the coil windings can be approximated from:

$$R_c = \frac{N \rho (1 \times 0.63)}{b} = \frac{3100 \times 1.78 \times 10^{-8} \times (29.25 \times 10^{-2} \times 0.63)}{3.9 \times 10^{-7}} = 26.1 \Omega$$

and because the coils are in parallel $R = R_c / 2 = 13 \Omega$.

The reluctance of the airgap S is:

$$S = \frac{2x}{\mu_0 a} = \frac{2 \times 2.0 \times 10^{-2}}{4\pi \times 10^{-8}} = 1.3 \times 10^7$$

Therefore, at the nominal airgap, the inductance of the coils $L = N^2 / S = 0.75\text{H}$. The time constant of the coil can be checked by using $\tau = L/R = 57.7 \text{ ms}$.

As a way of checking the behaviour of the magnet against the design equations (i.e. to see if saturation and flux leakage is being avoided) several flux measurements were taken. The maximum force that will be produced at the design flux density of 0.65T is:

$$F = \frac{0.65^2 \times 0.052^2}{4\pi \times 10^{-7}} = 909.1\text{N}$$

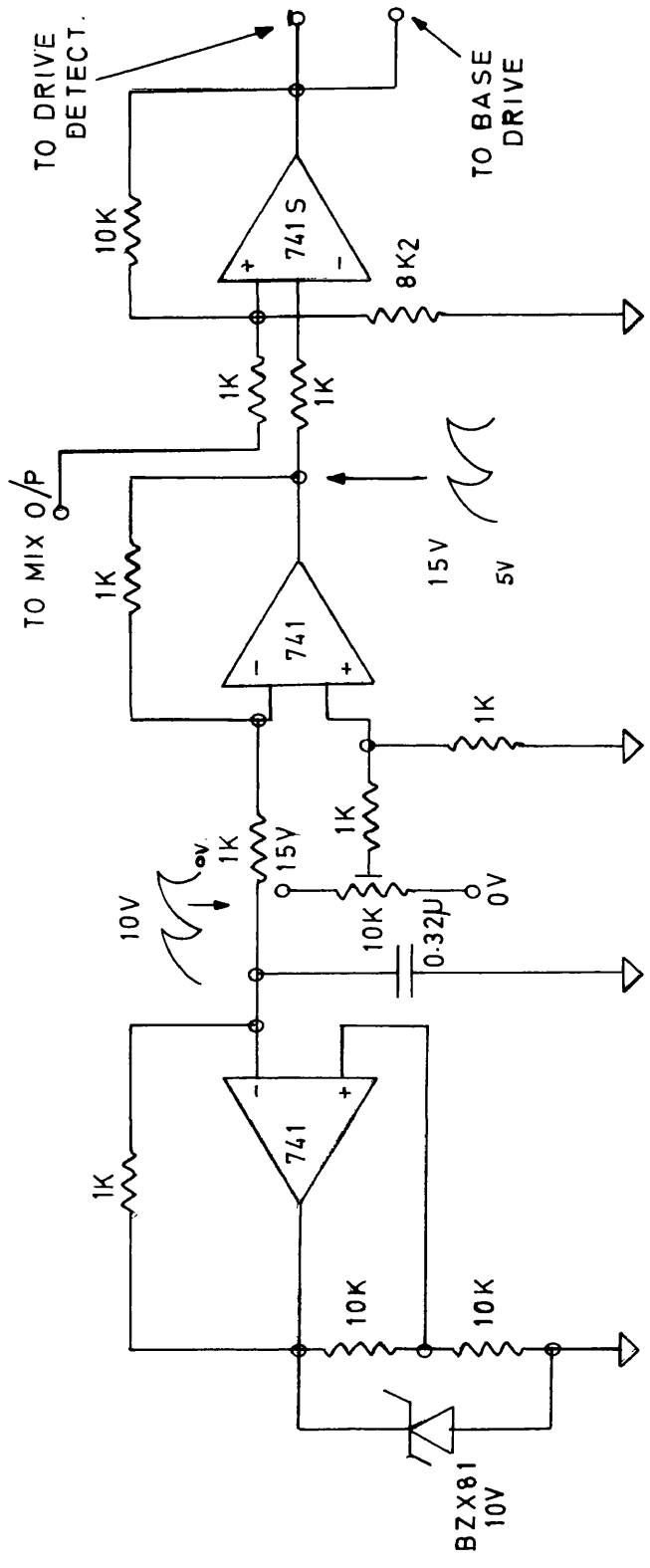
The flux density expected for 500N is $\{0.65 \times \sqrt{(500 / 909.1)}\} = 0.48\text{T}$. The expected ampere-turns is:

$$NI = \frac{2Bx}{\mu_0} = \frac{2 \times 0.48 \times 0.02}{4\pi \times 10^{-7}} = 15279 = 3100 \times I$$

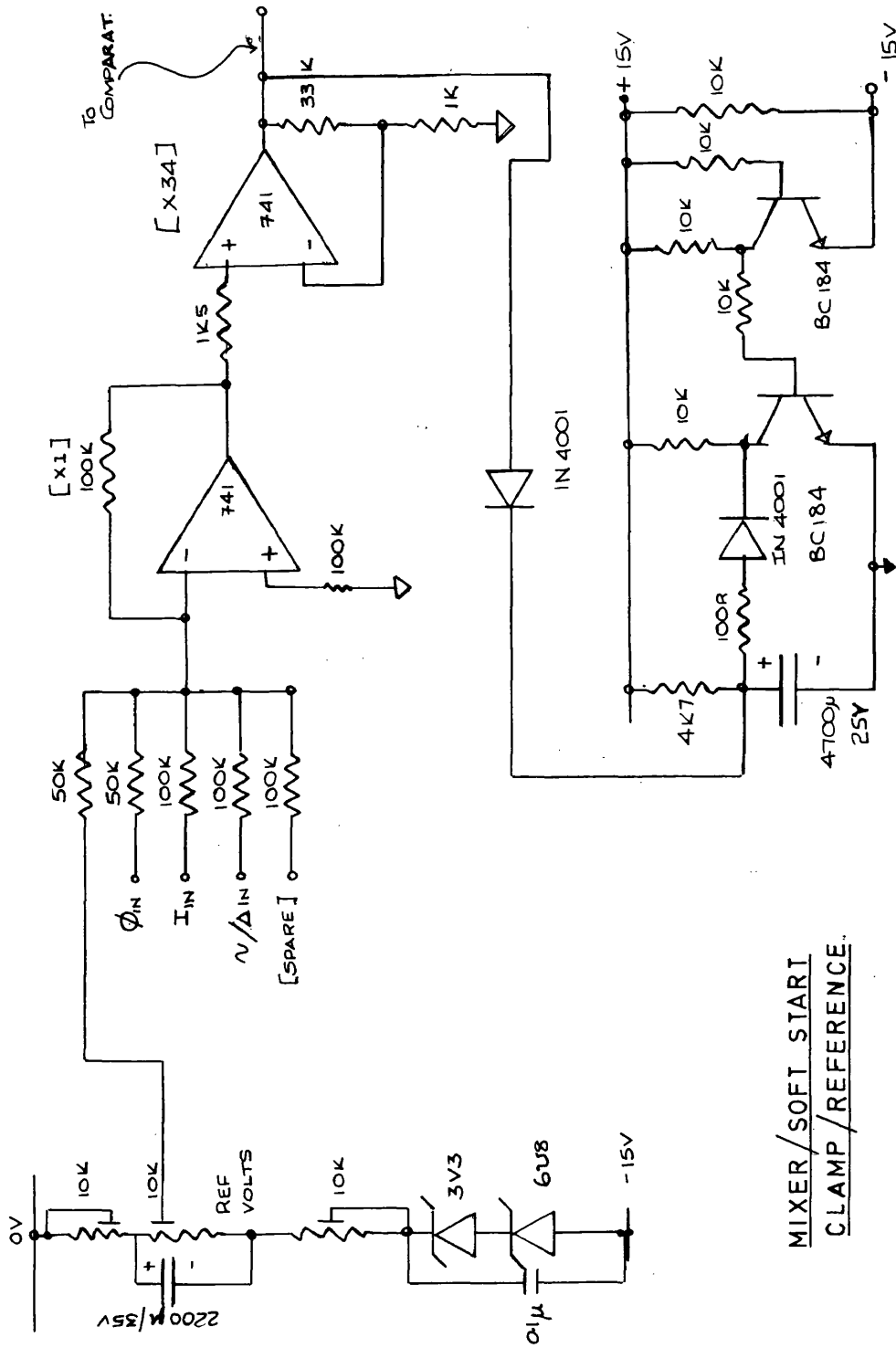
The load current I is therefore expected to be measured at 4.93A. From the results given in Fig.[5.7], I is 5.3A. The error is about 4.3% which is acceptable, and we can assume that flux leakage is minimal and that saturation is being avoided. The use of the equation $NI = 2Bx/\mu_0$ is therefore valid.

Appendix [B2]

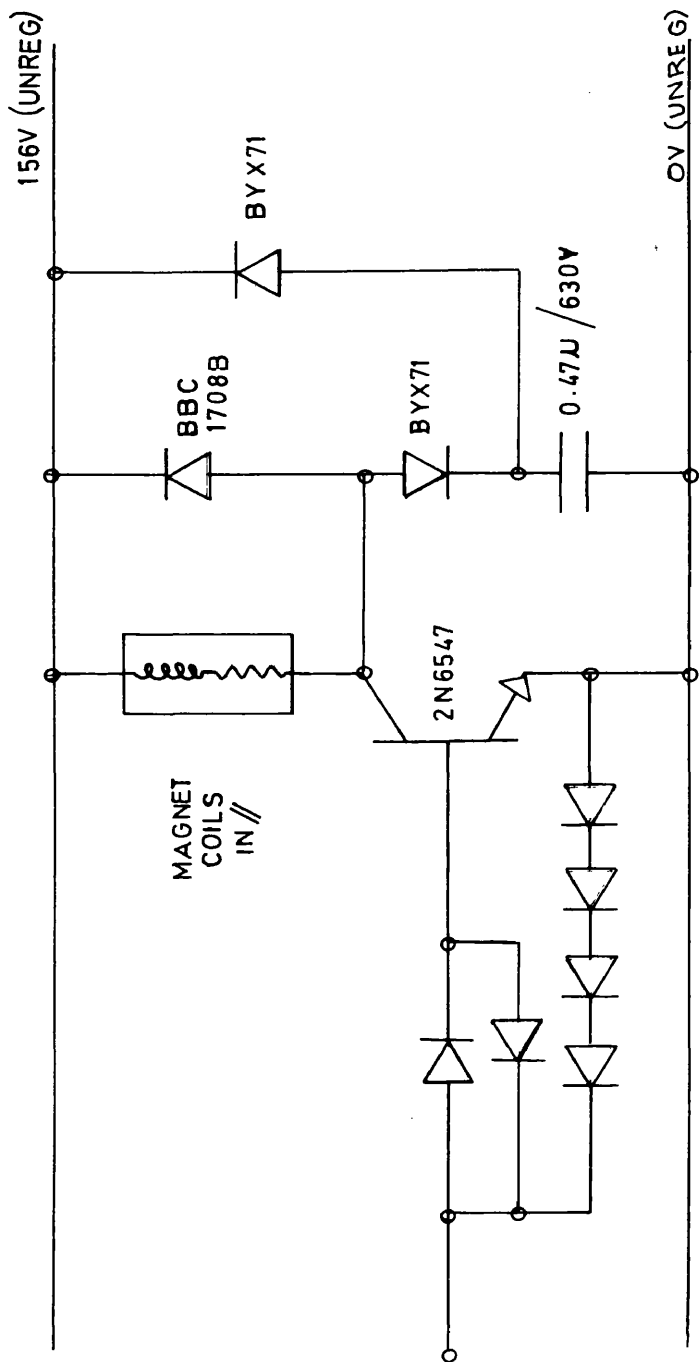
MAGLOAD: Circuit Diagrams



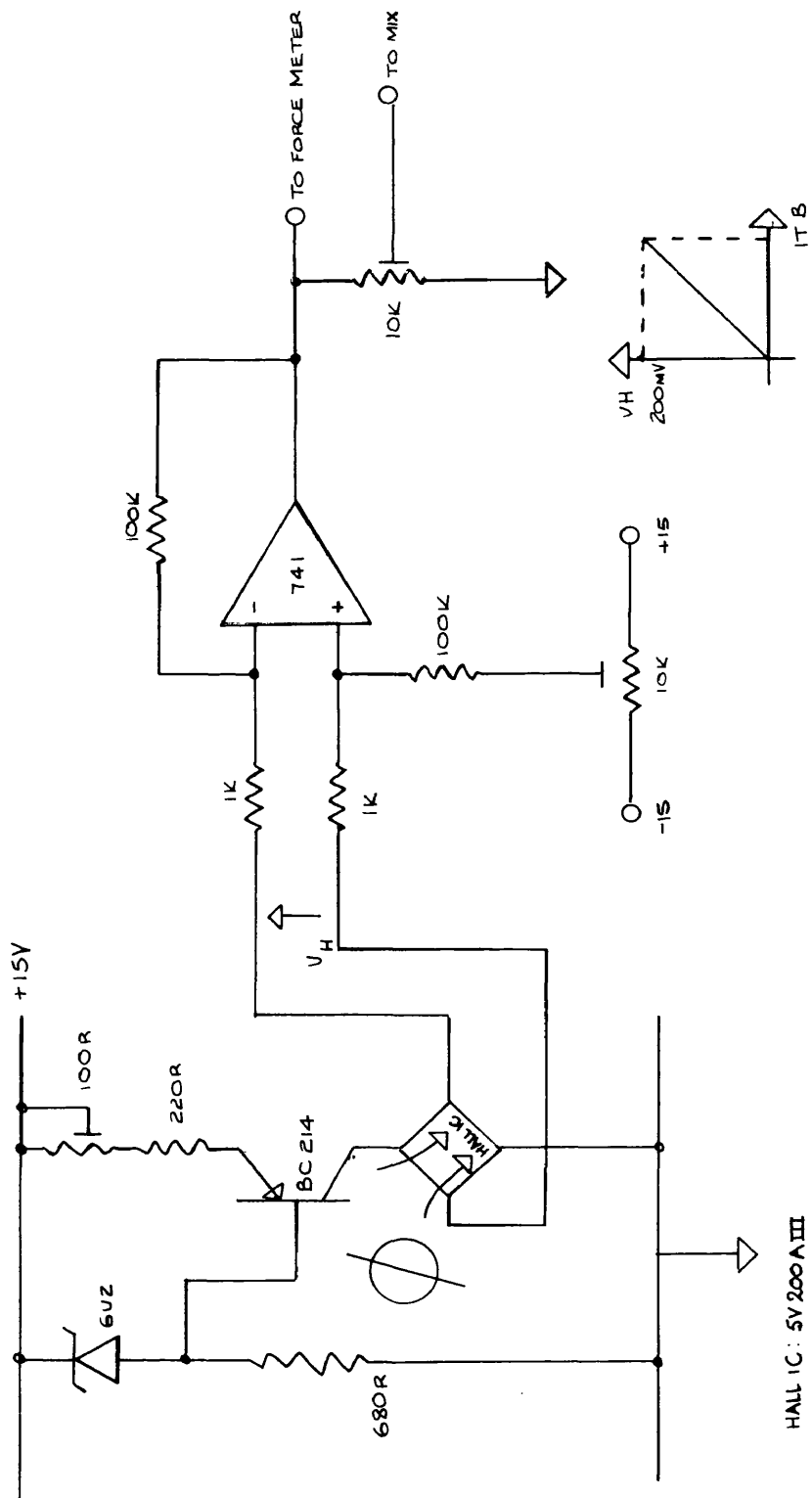
PWM AMPLIFIER.



MIXER/SOFT START
CLAMP/REFERENCE.

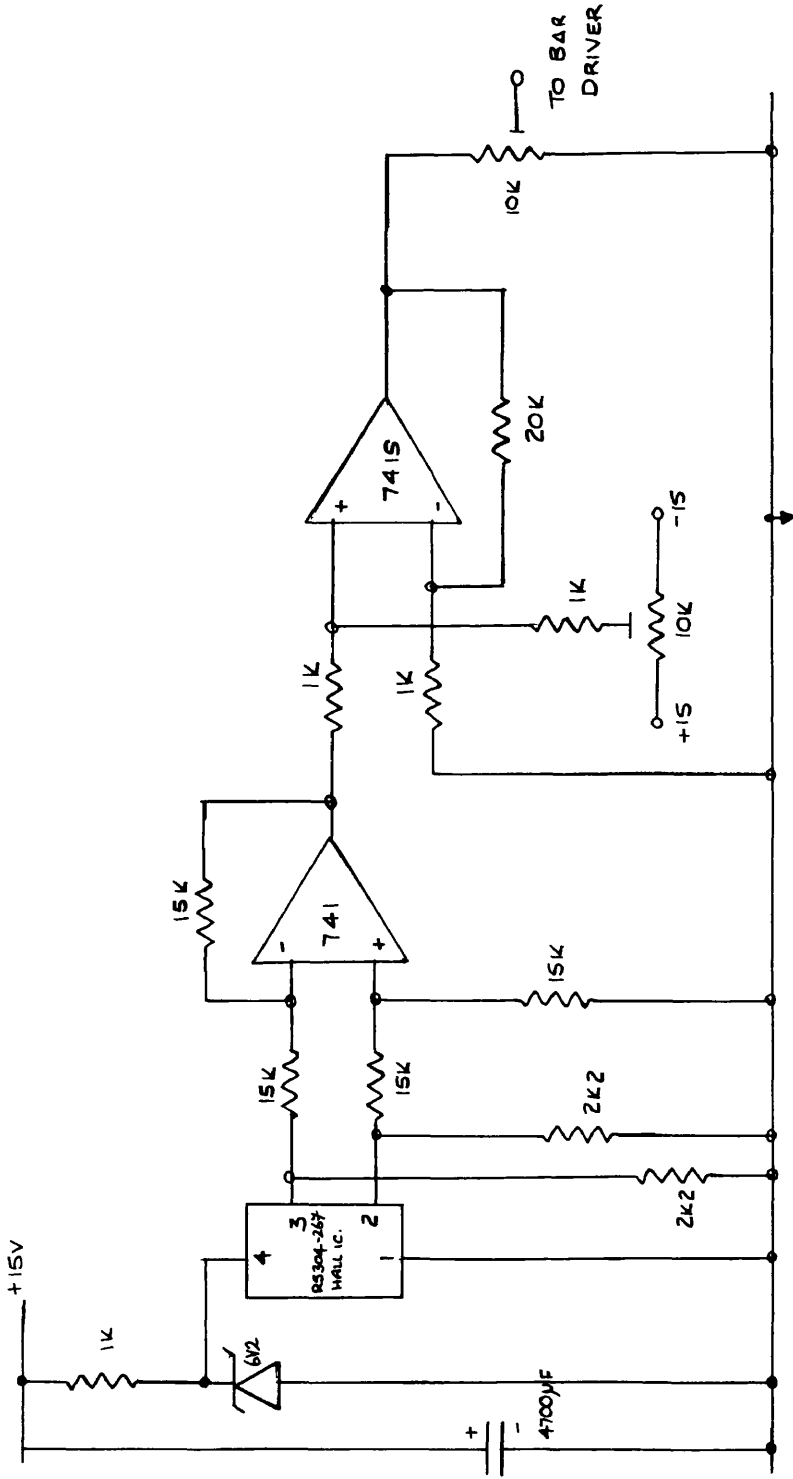


SINGLE ENDED MAGNET POWER AMPLIFIER.



HALL IC: 5V200AIII
 RH \approx 60R
 IH \approx 20mA

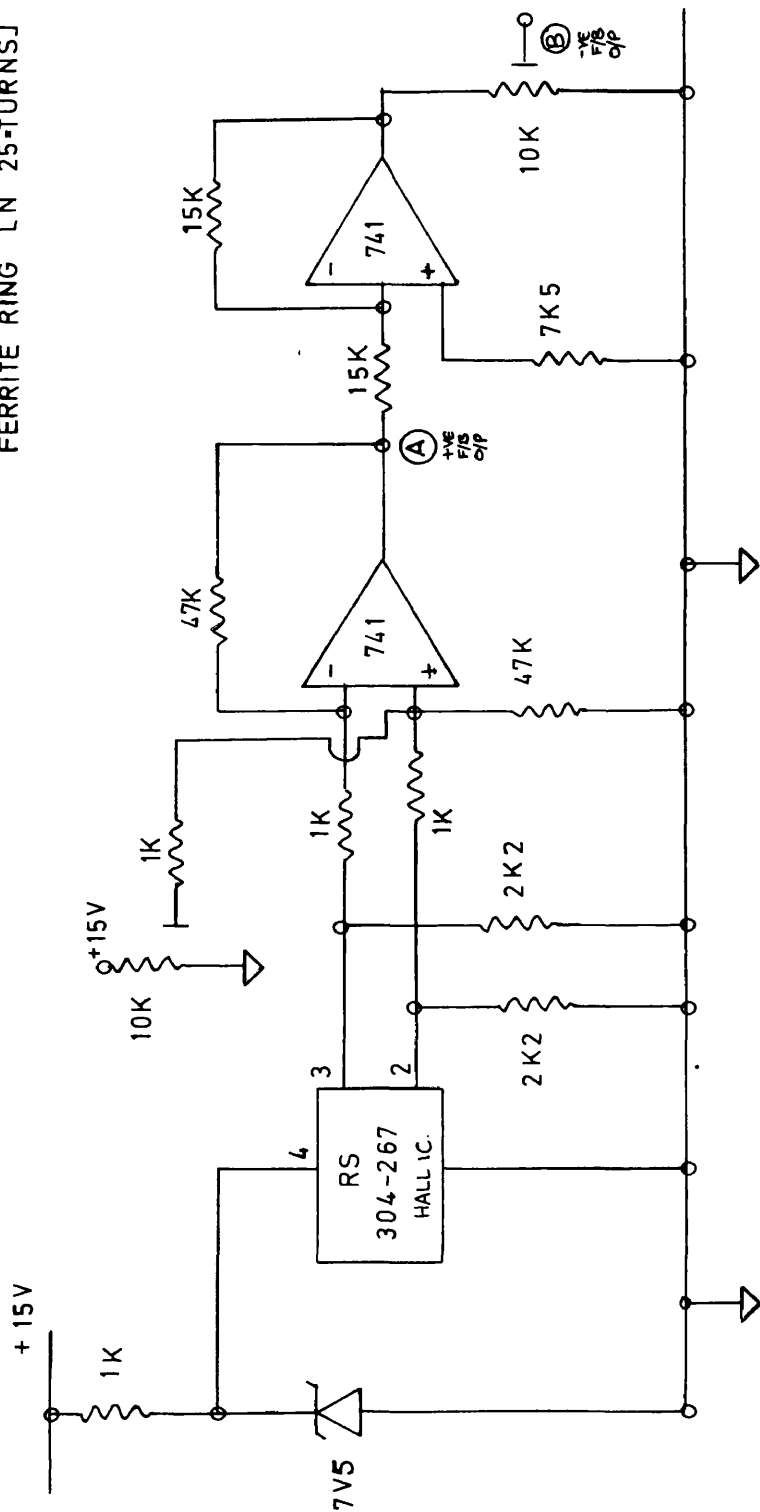
FLUX AMP



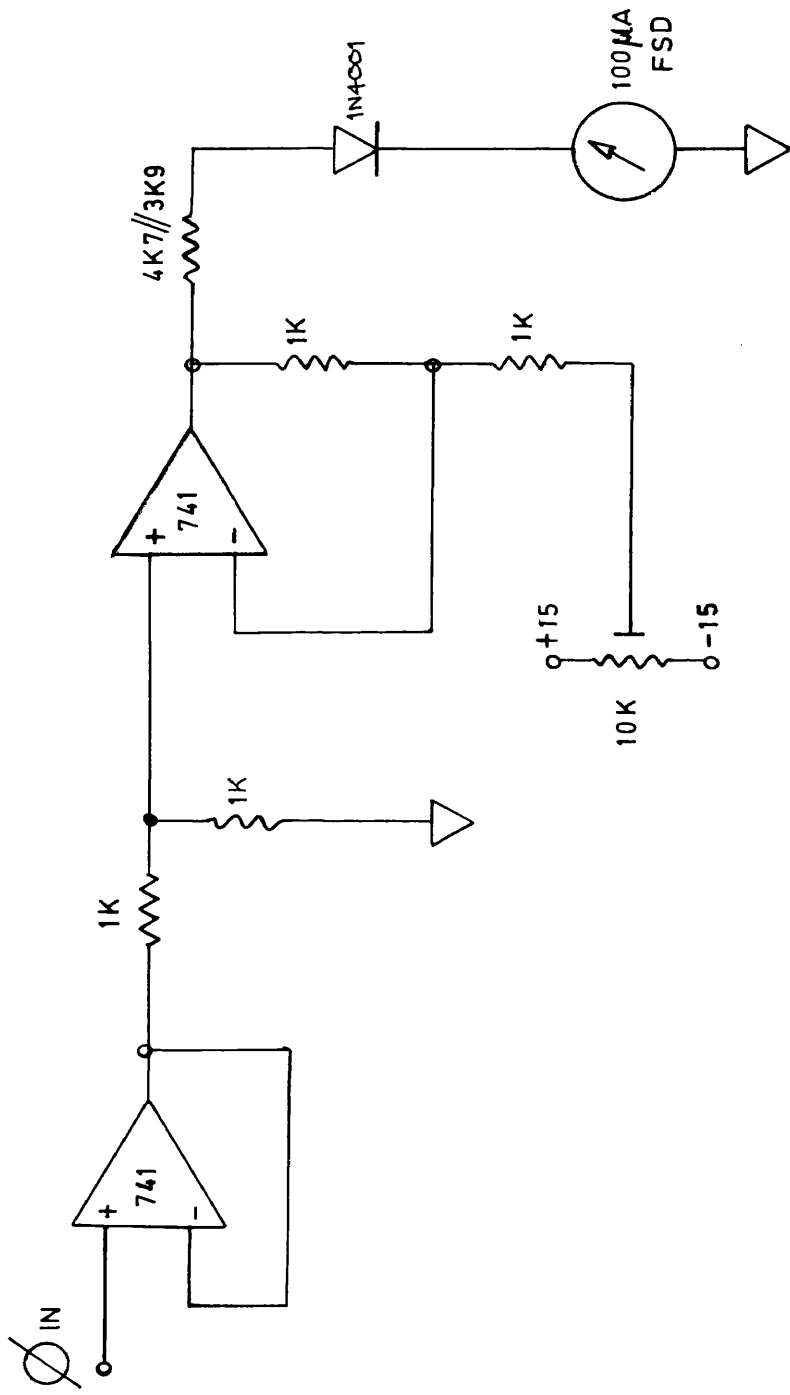
HALL PLATE MOUNTED
ON FACE OF PERMANENT
MAGNET.

POSITION AMP.

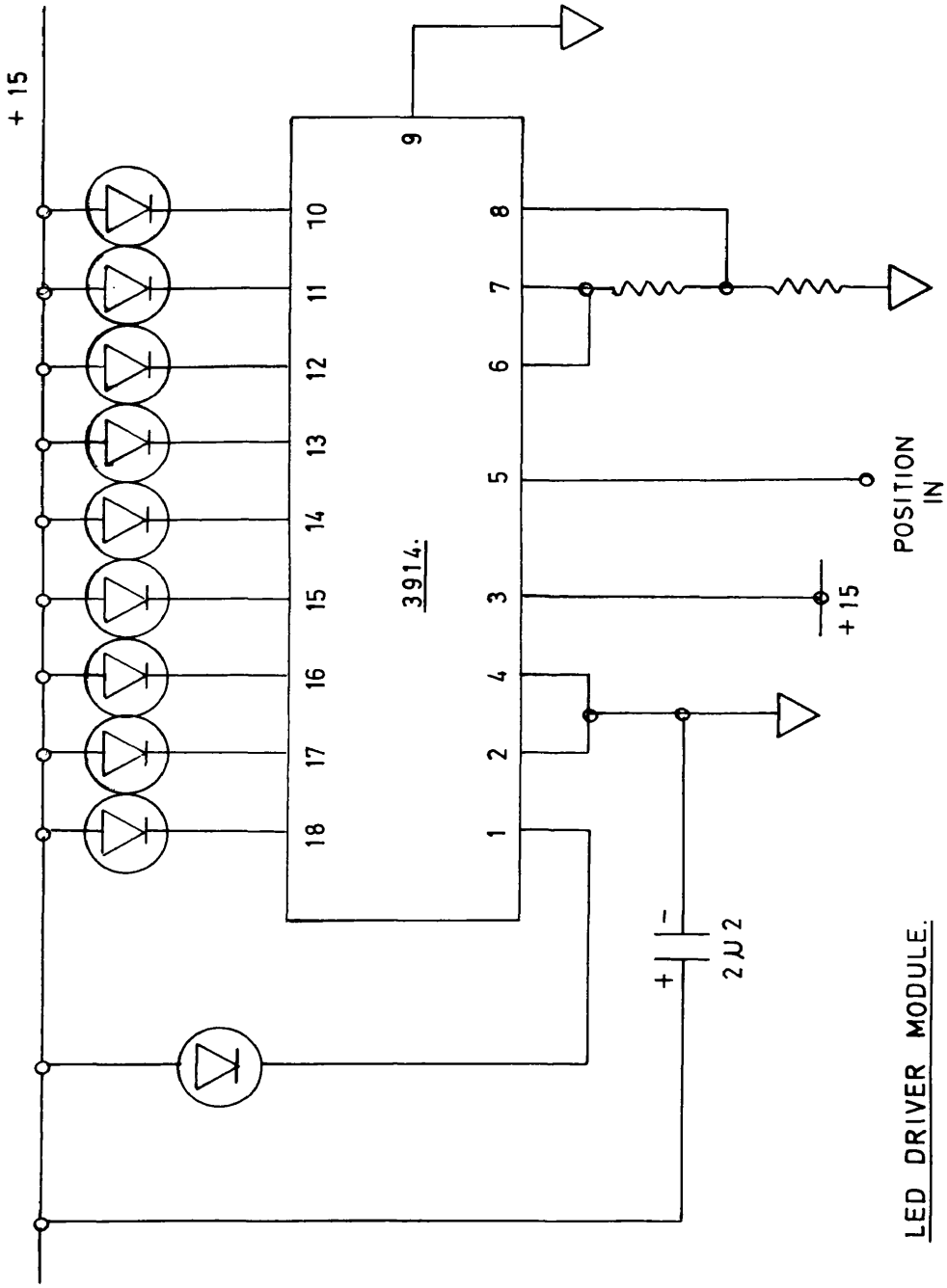
HALL PLATE MOUNTED IN
FERRITE RING [N 25-TURNS]



CURRENT AMP.

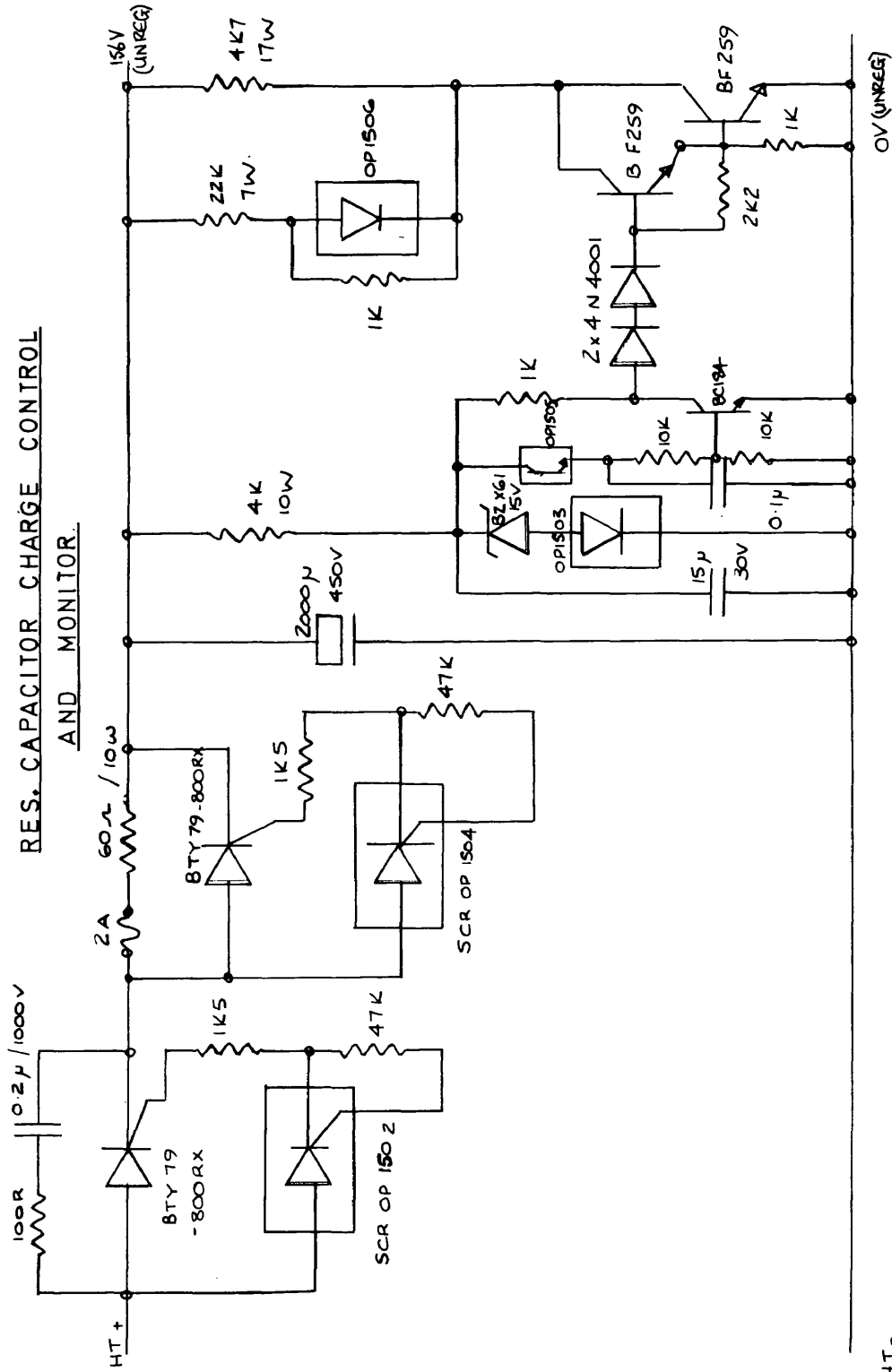


FORCE METER AMPLIFIER.



LED DRIVER MODULE.

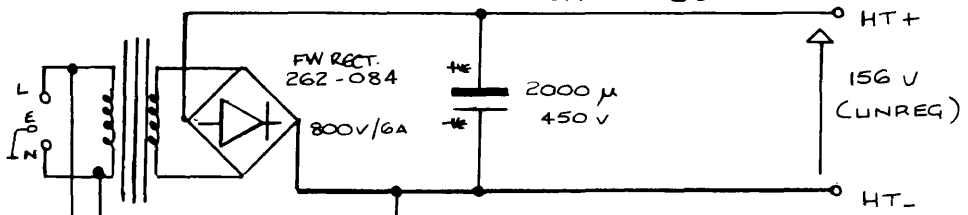
RES. CAPACITOR CHARGE CONTROL AND MONITOR



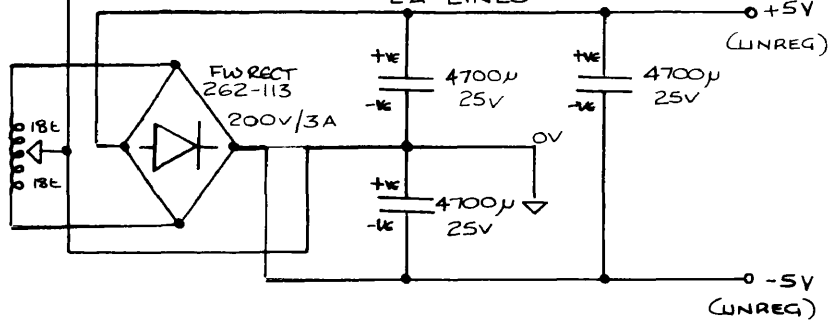
HT-

POWER SUPPLIES

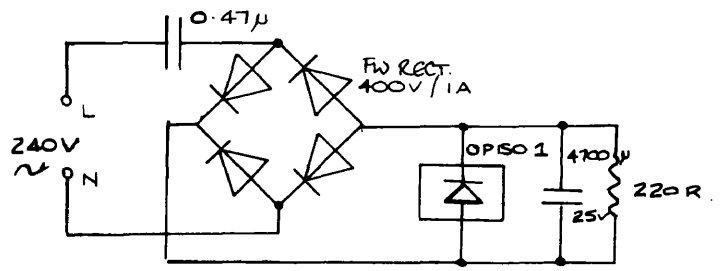
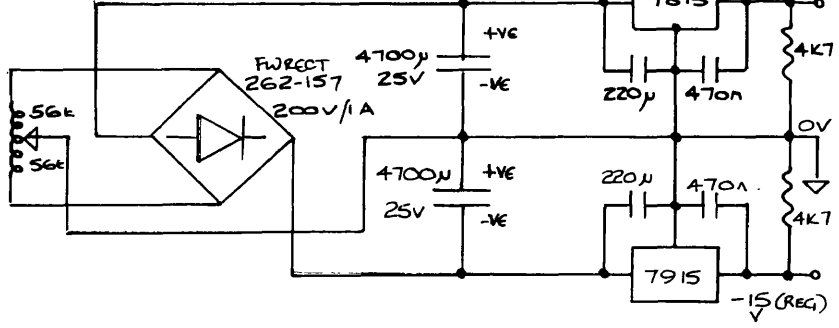
5A LINES



2A LINES



1A LINES



Appendix [B3]

MAGLOAD: Tabulated Results

MAGLOAD: Static Open-Loop Characteristics using Cantilever and Weights Holder Arrangement. Mass of Cantilever and Weights Holder, Mc = 4.3Kgf.				
Suspended Mass, Ms (5Kg to 50Kg). Therefore, Corrected Magnet Coil Current, Im is:				
$I_m = (M_s / (M_s + M_c))^{1/2} \times I$				
Where I is the measured Magnet Coil Current.				
The Following Results Provide the Force Vs Current at Constant AirGap Characteristic.				
Ms/Kg	AirGap x/mm	I/A	Im/A	
50	5	1.4	1.34	
	10	2.9	2.78	
	20	5.6	5.37	
25	5	1.2	1.11	
	10	2.1	1.94	
	15	2.9	2.68	
	20	3.8	3.51	
	25	4.9	4.53	
	30	6.1	5.63	
15	5	0.9	0.79	
	10	1.7	1.5	
	15	2.4	2.12	
	20	3.2	2.82	
	25	4	3.53	
	30	5	4.41	
	35	5.9	5.2	
10	5	0.8	0.67	
	10	1.5	1.25	
	15	2	1.67	
	20	2.7	2.26	
	25	3.4	2.84	
	30	4.1	3.43	
	35	4.9	4.1	
5	5	0.8	0.59	
	10	1.3	0.95	
	15	1.7	1.25	
	20	2.2	1.6	
	25	2.6	1.91	
	30	3.3	2.42	
	35	4	2.93	
0	5	0.6	0.6	
	10	1	1	
	15	1.2	1.2	
	20	1.5	1.5	
	25	1.8	1.8	
	30	2.2	2.2	
	35	2.5	2.5	

MAGLOAD: Static Closed-Loop Force Vs Airgap Distance Characteristic.							
Load Cell Calibration: 0.45mV/Kgf.							
Measurements of Force taken with Pull Rod at 255mm above pivot point. Values are then translated to 400mm. (Note: Reaction plate is 200mm below pivot point).							
Load Setting = 1Kgf at 15mm Nominal Airgap.							
#	1	2	3	4	5	6	7
Airgap Dist. X/mm	5	10	15	20	25	30	35
Magnet Current I/A	0.2	0.4	0.6	1	1.3	1.35	1.6
Load Cell Volts/mV	0.42	0.45	0.45	0.44	0.43	0.42	0.33
Force at 255mm/Kgf	1.5	1.57	1.57	1.56	1.55	1.5	1.2
Force at 400mm/Kgf	0.97	1	1	1	0.99	0.97	0.77
Load Setting = 2Kgf at 15mm Nominal Airgap.							
#	1	2	3	4	5	6	7
Airgap Dist. X/mm	5	10	15	20	25	30	35
Magnet Current I/A	0.2	0.5	0.8	1.3	1.6	1.7	2.1
Load Cell Volts/mV	0.89	0.96	1	0.95	0.95	0.9	0.8
Force at 255mm/Kgf	2.8	3.1	3.14	3.1	3.1	2.8	2.5
Force at 400mm/Kgf	1.79	1.98	2	1.98	1.98	1.79	1.59
Load Setting = 3Kgf at 15mm Nominal Airgap.							
#	1	2	3	4	5	6	7
Airgap Dist. X/mm	5	10	15	20	25	30	35
Magnet Current I/A	0.3	0.6	1	1.7	2.1	2.4	2.6
Load Cell Volts/mV	1.41	1.5	1.55	1.5	1.48	1.35	1.2
Force at 255mm/Kgf	4.3	4.6	4.71	4.6	4.6	4.1	3.7
Force at 400mm/Kgf	2.75	2.93	3	2.93	2.93	2.61	2.36
Load Setting = 4Kgf at 15mm Nominal Airgap.							
#	1	2	3	4	5	6	7
Airgap Dist. X/mm	5	10	15	20	25	30	35
Magnet Current I/A	0.4	0.7	1.2	1.9	2.4	2.6	2.9
Load Cell Volts/mV	1.95	2.05	2.1	2	2	1.9	1.75
Force at 255mm/Kgf	5.8	6.1	6.27	6.1	6.1	5.7	5.3
Force at 400mm/Kgf	3.7	3.89	4	3.89	3.89	3.63	3.38
Load Setting = 5Kgf at 15mm Nominal Airgap.							
#	1	2	3	4	5	6	7
Airgap Dist. X/mm	5	10	15	20	25	30	35
Magnet Current I/A	0.6	1.1	1.6	2.4	3	3.2	3.7
Load Cell Volts/mV	2.6	2.6	2.65	2.65	2.6	2.4	2.33
Force at 255mm/Kgf	7.7	7.7	7.84	7.84	7.7	7.1	6.9
Force at 400mm/Kgf	4.91	4.91	5	5	4.91	4.53	4.4

Load Setting = 6Kgf at 15mm Nominal Airgap.							
#	1	2	3	4	5	6	7
Airgap Dist. X/mm	5	10	15	20	25	30	35
Magnet Current I/A	0.7	1.1	1.8	2.7	3.1	3.7	3.8
Load Cell Volts/mV	2.95	3.1	3.2	3.15	3.15	3.1	3
Force at 255mm/Kgf	8.8	9.2	9.41	9.3	9.3	9.2	8.8
Force at 400mm/Kgf	5.61	5.87	6	5.93	5.93	5.87	5.61
Load Setting = 7Kgf at 15mm Nominal Airgap.							
#	1	2	3	4	5	6	7
Airgap Dist. X/mm	5	10	15	20	25	30	35
Magnet Current I/A	0.8	1.2	1.9	2.8	3.5	3.9	4.3
Load Cell Volts/mV	3.6	3.7	3.75	3.75	3.7	3.6	3.1
Force at 255mm/Kgf	10.6	10.9	10.98	10.98	10.9	10.6	9.2
Force at 400mm/Kgf	6.77	6.95	7	7	6.95	6.77	5.87
Load Setting = 8Kgf at 15mm Nominal Airgap.							
#	1	2	3	4	5	6	7
Airgap Dist. X/mm	5	10	15	20	25	30	35
Magnet Current I/A	0.9	1.4	2	3	3.7	3.9	4.3
Load Cell Volts/mV	4.2	4.27	4.3	4.3	4.3	4.2	3.6
Force at 255mm/Kgf	12.3	12.55	12.55	12.55	12.55	12.3	10.6
Force at 400mm/Kgf	7.84	8	8	8	8	7.84	6.78
Load Setting = 9Kgf at 15mm Nominal Airgap.							
#	1	2	3	4	5	6	7
Airgap Dist. X/mm	5	10	15	20	25	30	35
Magnet Current I/A	0.95	1.35	1.7	2.95	3.6	4	4.4
Load Cell Volts/mV	4.7	4.75	4.85	4.83	4.8	4.75	4.4
Force at 255mm/Kgf	13.8	13.9	14.12	14.12	14	13.9	12.9
Force at 400mm/Kgf	8.8	8.86	9	9	8.93	8.86	8.22
Load Setting = 10Kgf at 15mm Nominal Airgap.							
#	1	2	3	4	5	6	7
Airgap Dist. X/mm	5	10	15	20	25	30	35
Magnet Current I/A	1	1.6	2	3.2	4	4.35	4.6
Load Cell Volts/mV	5.35	5.35	5.4	5.35	5.3	5	4.3
Force at 255mm/Kgf	15.59	15.59	15.67	15.59	15.49	14.69	12.55
Force at 400mm/Kgf	9.88	9.88	10	9.88	9.82	9.31	8

Appendix [B4]

Published Paper on EMG-Force Modelling and MAGLOAD

An EMG-force measuring system for assessing muscle condition

RODRIGUES, BSc, MEng, DPhil, FIEE and A SEMHI, BSc
Department of Engineering, The University of Leicester, UK
MILAGRO, MSc, DPhil

Department of Applied Mathematics, The University of Porto, Portugal

ABSTRACT Previous studies are briefly described in which the dynamic relationship between emg and muscle force is estimated for isometric contractions. The need to design suitable experimental protocols and analysis algorithms is discussed and the need for careful control of the force pattern emphasised. Existing methods are considered and a new solution proposed. The new muscle load force transducer based on a controlled electromagnet is described. The advantages and disadvantages of the use of these machines in emg-force estimation experiments are discussed.

1 INTRODUCTION

The assessment of neuro muscular conditions in athletes by static testing is of limited value. The most athletic events involve dynamic contractions. Fatigue testing is important but does not monitor dynamic performance either. Attempts to characterise the dynamics of muscle are hampered by the difficulties of defining a simple enough model of sufficient generality and interpreting the results.

The only area where significant progress has been made in this direction is for isometric contractions as there now seems to be some theoretical basis for the experimental methods used thus allowing some insight into the reliability of the model and the interpretation of its parameters.

Two major effects which can be observed during the voluntary dynamic contraction of a skeletal muscle are the build up of the force and the associated emg signal. Both of these effects derive from the same cause, the increasing motoneurone bombardment.

It is known that the static relationship between force and force is linear for many, but not all, muscles when the contraction is isometric and surface electrodes are used (1) (2) and it has been proposed that a linear model can be usefully assumed as a means of characterising the dynamic relationship between emg and force.

The elementary force wave (force twitch) is generated as the result of a single motoneurone and lasts several hundred milliseconds while the corresponding component of the emg (the motor unit action potential) is over in much less than ten milliseconds. Hence, if a linear model can be assumed then its impulse response will have the characteristics of some "average" or "representative" force twitch.

It is also known that if the muscle changes length, particularly at variable speed then severe non-linearities are encountered (3) and as similar linear models cannot be postulated to describe contractions in non-isometric conditions.

The usefulness of a linear dynamical model in research into the biomechanics of sport can therefore be said to be somewhat limited. However, the potential value of knowing the dynamics of force build up and decay in athletes is such that a theoretically sound means of monitoring changes in muscle characteristics during training and recovery from injury is of value even if it is restricted to isometric conditions. This line of work is therefore worth pursuing.

This paper describes some experiments which have been tried to assess the problems of estimating the parameters of appropriate models relating force to emg and presents a new machine of considerable flexibility which may prove useful for this and for other related investigations.

2 PREVIOUS STUDIES

Experimental studies in this area date back to the late 1960's when parameter tracking on an analogue computer was used to produce a second order model relating the rectified emg to force for the human triceps (4). No account was taken of noise, nor of the choice of modelling algorithm. It was shown in 1971 that a second order model of the soleus muscle gave good results, but again the model was assumed to be overdamped a priori and the effect of the noise and modelling algorithm ignored (5). In 1976 and 1978 two attempts at using the rectified emg as a force predictor were reported (6,7). The first included some degree of non-linearity. The second used a linear second order overdamped model again, but in this case the results differed significantly from previous work on the same muscle using a different force pattern.

Experiments by the authors on the human deltoid muscle to help clarify the difficulties have shown that if an overdamped second order model is assumed then the model parameters are very dependent on the force pattern if an rms modelling technique is used.

Further pilot studies have demonstrated that the design of experiments, the modelling algorithms and the assumptions regarding the nature of the noise are crucial factors in defining the poles

the model (8) (9). An algorithm incorporating a modulation instead of an additive noise model has been shown to give an overdamped system expected even when the poles are unconstrained).

In 1985 other workers reported studies on human biceps anterior using auto-regressive moving average models (11). An attempt to have the patient follow a pseudo-random binary force pattern was made but abandoned because of difficulty in following the required pattern. An impulse followed by a sine wave was then used. The results obtained were often unrealistic (complex poles) and contained a pure time delay which was at variance with much of the previous work.

Research to date indicates that if an appropriate noise model is assumed and the identification algorithm designed to account for it correctly then it is possible to greatly reduce the dependence of the model on the force pattern. Most workers agree that a second order model is appropriate and that its impulse response is related to the muscle twitch response. No studies so far reported have however demonstrated that a linear emg-force model can be made totally independent of the force pattern.

The reasons for the residual dependence of the model on the force pattern demanded are still conjectural. However, the problems of emg-force non-linearity, which can be manifested as complicated noise models, is a likely cause. An example is shown in fig. 1 where bursts of emg can be seen when the force has dropped to almost zero. (The details of the emg are interpreted as noise as far as the identification algorithm is concerned).

Further development of this technique towards application in sports medicine as a means of measuring the dynamic performance of muscle thus still requires the accurate control and monitoring of the muscle load and hence, in isometric conditions, the muscle force.

3 METHODS OF MUSCLE LOADING AND FORCE MEASUREMENT

Most assessment of muscles currently used involve static isotonic and isometric tests to measure basic strength. The dynamic tests already referred to are still at the experimental stage. Loading methods should therefore take account of the requirement for static testing as well as allow for dynamic measurements.

Common methods presently used to achieve static loading include a set of standard weights, compressible load cells, and springs. In the case of load cells and springs the patient under test has to produce the correct amount of static or dynamic forcing by compressing the load cell or pulling the spring. The amount of force produced is monitored using strain gauge transducers and/or calibrated meters. Several workers have used elaborate techniques where contractions are performed isometrically against a load cell and the subject is asked to dynamically match a force pattern which is visually presented (11) (12). Appropriate apparatus is used to stabilise and support the joints.

All these techniques of muscle loading suffer from three major drawbacks. Firstly, and most importantly, is that the loading level remains within the subject's control. The success of the procedure depends on the ability of the subject to concentrate and to contract and relax his muscles in a controlled manner at the request of the examiner while maintaining an isometric situation. To some extent this is non objective.

Secondly, because tests need to be carried out under conditions of high force levels, the subject often cannot maintain a spring or load cell at a constant compressed length. At large static loading levels maintaining a standard weight motionless to minimise inertial forces also becomes difficult. For dynamic measurement on muscles, springs and weights are even more difficult to control.

Finally, when dynamic variations in the load are required, they must be repeatable during and between individual tests. This cannot be achieved with confidence using any of the current methods. The limitations can cause discrepancies when attempting to compare individual subject data from separate trials and muscle testing procedures due to the non-standardisation of investigative protocol.

It is therefore necessary to have a system where:

- i static levels and dynamic changes in muscle loading are under the control of the examiner,
- ii the load remains constant, if required, irrespective of small patient movements,
- iii static and dynamic in loadings are repeatable, and
- iv a virtually constant muscle length can be maintained during dynamic loading using some form of feedback, usually visual, via the subject, based on these constant length requirements only. That is, the subject is not asked to follow a moving force target but to maintain a constant position target.

4 THE MAGNETIC SUSPENSION BASED CONTROLLABLE MUSCLE LOAD

A useful loading device will produce a relationship between force and muscle length that is constant over a range of muscle length variation. To provide this characteristic and in addition provide dynamic loading, the control of a d.c. electromagnet is proposed. The familiar open-loop inverse square law characteristic of the solenoid (electromagnet) is reshaped over a limited airgap distance using closed-loop force feedback. The fluctuations in the airgap length about its nominal value are related to the variations in contracting muscle length. These airgap fluctuations are made available visually to the subject who will be required to maintain them at a minimum. Therefore, the muscle length is held approximately constant. If the muscle length changes, and in turn alters the airgap distance, the electromagnet control system adjusts to keep the force constant throughout the available airgap.

The electromagnet in the prototype is capable of providing 250N force at a nominal airgap of 20mm.

provide this comfortably and within acceptable power dissipation levels, a U-shaped magnet capable of providing up to 500N at this airgap is designed. An important factor contributing to the efficiency of the system is the power amplifier design. Here, considerations of forcing voltage capability in relation to the magnet inductance and in turn its time constant become important in order to maintain an adequate bandwidth of the control system.

The electronics to drive the magnet use the principle of Pulse Width Modulation. By varying the ratio of the ON-OFF time of the drive transistor amplifier a desired average current in the magnet can be maintained. As a result, a desired average force is produced by the magnet. The force needed at the nominal airgap can be set by adjusting this ON/OFF ratio. Instantaneous changes in airgap, and hence instantaneous force, result in this ON-OFF ratio being altered via a feedback loop to keep the force constant and equal to the demanded level. The controlling feedback signal can be derived from any transducible parameter proportional to force. In this design a measure of flux density in the airgap of the electromagnet was used. This was detected using a Hall effect transducer mounted at a pole face of the electromagnet. Fig. 2 shows a schematic diagram of the control scheme employed.

The magnet operates at 0.65 wb/m producing the designed maximum forcing level of 250N with a current of approximately 4.5A at the nominal airgap distance of 20mm. The choice of 0.65 wb/m ensures that the mild steel magnetic circuit remains in the linear region of the magnetisation curve for any transient changes in coil current and hence flux density. Power dissipation in the magnet is also reduced at a lower flux density. This is at the expense of increased magnetic circuit dimensions and a compromise had to be reached. Fig. 3 shows the results obtained of loading force against airgap distance at ten force levels in the closed-loop configuration. The non-linearity at large airgaps is mainly due to leakage flux and geometric misalignment of the pole faces and reaction plate through the available airgap. Minor positive position and current feedback loops of low gain can be added to boost the response in this region. This result constitutes the static performance of the magnet-amplifier configuration. The high degree of linearity has been achieved by paying close attention to the dynamic design considerations.

The electromagnet is part of a closed-loop control system which is required to adjust its current so as to maintain the flux density at the designed operating point. To obtain bandwidths of operation larger than that dictated by the magnetic circuit time constant, the amplifier gain becomes important. Larger bandwidths are only possible because of the capability of forcing current variations through the coils of the electromagnet. A rate of change of force of 1N/sec has been achieved. The former figure was calculated from the electromagnet static load characteristics assuming that a change in airgap of 20mm is matched by a change in force by the electromagnet of 200N in 20ms. The choice of this is to ensure that the build-up of force is quicker than the fastest average isometric twitch

response in human muscle. This is the region of 25ms for a group of very fast motor units in the muscle and it can rise to as much as 100ms with slower motor units.

Fig. 4 shows the frequency response of the system and the coherence function relating the test signal to the output. The input is a voltage comprising a d.c reference corresponding to a demanded force of 80N modulated by bandlimited white noise. The output is the feedback signal taken from the flux transducer mounted in a pole face of the electromagnet. The relationship is therefore between the demanded and delivered forces in the system. The phase plot is seen to be almost linear and rolls-off at $-2.25^\circ/\text{Hz}$ to -45° at 20Hz. The magnitude plot exhibits some minor resonances of unknown origin. The coherence remains very high throughout the frequency range but goes to zero at 50Hz (not shown) before returning to a high value and remaining above 0.75 up to 100Hz.

The system described has been designed for testing large muscles such as the biceps and the quadriceps and has been made geometrically adjustable to accommodate not only different muscles but different subjects as well. Two views of the device are shown in fig. 5.

A smaller device involving similar principles has been designed for testing muscles of the hand and other small muscles.

It is thought that this type of testing machine used either in its static or dynamic modes would also have medical and physiological applications.

The important advantage of the system in the present context is that the subject only needs to maintain a crude approximation to constant length using visual feedback. The force fluctuations are in the control of the operator or of a computer. Furthermore, the device also acts as a force transducer as the flux density in the airgap is measured for the purposes of control and this signal is an objective measure of force and its relationship to the demanded force is known via the transfer function of the system. This transfer function is seen to be satisfactory for the purpose. The machine is very well suited to computer controlled experimentation. The main disadvantage of the machine at present is its expense.

5 CONCLUSIONS

The testing of human muscle as a means of assessing training or treatment is of significance in sport. If the testing is limited to static measurements or crude dynamics involving considerable uncertainty due to the substantial subjective element present then the testing is of limited value.

A review of the literature and some pilot studies by the authors have shown that isometric emg-force modelling offers the possibility of a simple general model of muscle provided care is taken in the treatment of noise and in the design of the algorithm. Although this approach looks promising the models have some residual dependence on the force pattern and until such time as this can be resolved by further refinements of the model structure and identification

algorithms, careful control of the force is required.

The testing system presented based on controlled d.c. electromagnets is shown to have many of the characteristics required for the furtherance of this area of work.

REFERENCES

- (1) MILNER-BROWN, H. S. and STEIN, R. B. The relationship between the surface electromyogram and muscular force. J. Physiol., 246, 549-569, 1975.
- (2) LAWRENCE, J. H. and De LUCA, C. J. Myoelectric signal versus force relationship in different human muscles. J. American Physiol. Soc., 1653-1659, 1983.
- (3) WILKIE, D. R. The mechanical properties of muscle. British Medical Bulletin, 12,3 177-182, 1956.
- (4) COGGSHALL, J. C. and BEKEY, G. A. Emg-force dynamics in human skeletal muscle. Med. Biol. Eng., 8, 265-270, 1970.
- (5) GOTTLIEB, G. L. and AGARWAL, G. C. Dynamic relationship between isometric muscle tension and the electromyogram in man. J. Appl. Physiol., 3, 345-351, 1971.
- (6) WINTER, D. A. Biomechanical model relating emg to changing isometric contraction. Digest of 11th Int. Conf. on Med. Biol. Eng., Ottawa, 1976.
- (7) CROSBY, P. A. Use of surface electromyogram as measure of dynamic force in human limb muscles. Med & Biol. Eng. and Comput., 16, 519-524, 1978.
- (8) JONES, N. B. and LAGO, P. J. Dynamic estimators of muscle force from the emg. IEE Colloquium Digest 1981/57B Neuro Muscular Control Systems, 61-67, London, 1981.
- (9) JONES, N. B. and LAGO, P. J. Parametric models in the diagnosis of neuro-muscular disease. Inst. M.C. Symposium, Control Systems Concepts and Approaches in Clinical Medicine, 31-38, Univ. of Sussex, 1982.
- (10) LAGO, P. J. and JONES, N. B. Parameter estimation of system dynamics with modulation type noise-application to relationship between emg and force transient in muscle. IEE Proc. 13D, 6, 221-228, 1984.
- (11) REES, N. W., BASON, P. T. and SAMARASIRI, B. S. Muscle modelling and force estimation IFAC Conf. Proceedings, York, 1985.
- (12) De LUCA, C. J. Le FEVER, R. S, McCUE, M. P. and XENAKIS, A.P. Control scheme governing concurrently active human motor units during voluntary contractions. J. Physiol. 329, 129-142, 1982.

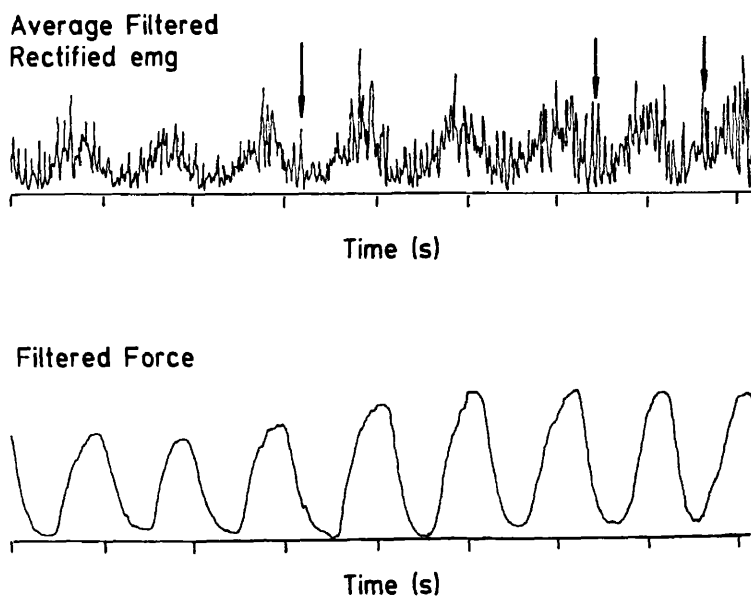


Fig 1 EMG and force waves. Departures from assumed model are indicated

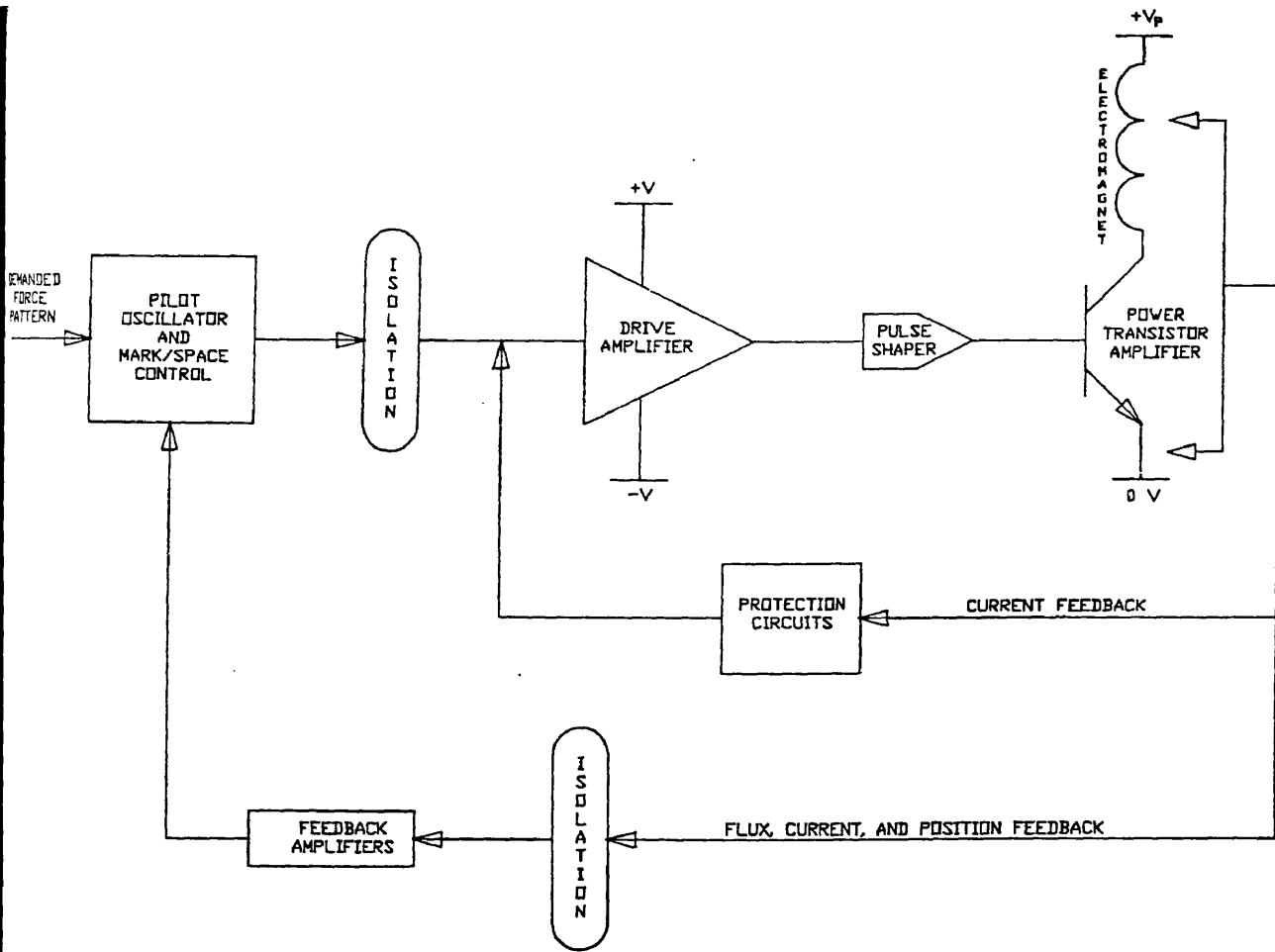


Fig 2 Schematic diagram of electromagnetic force generator and transducer

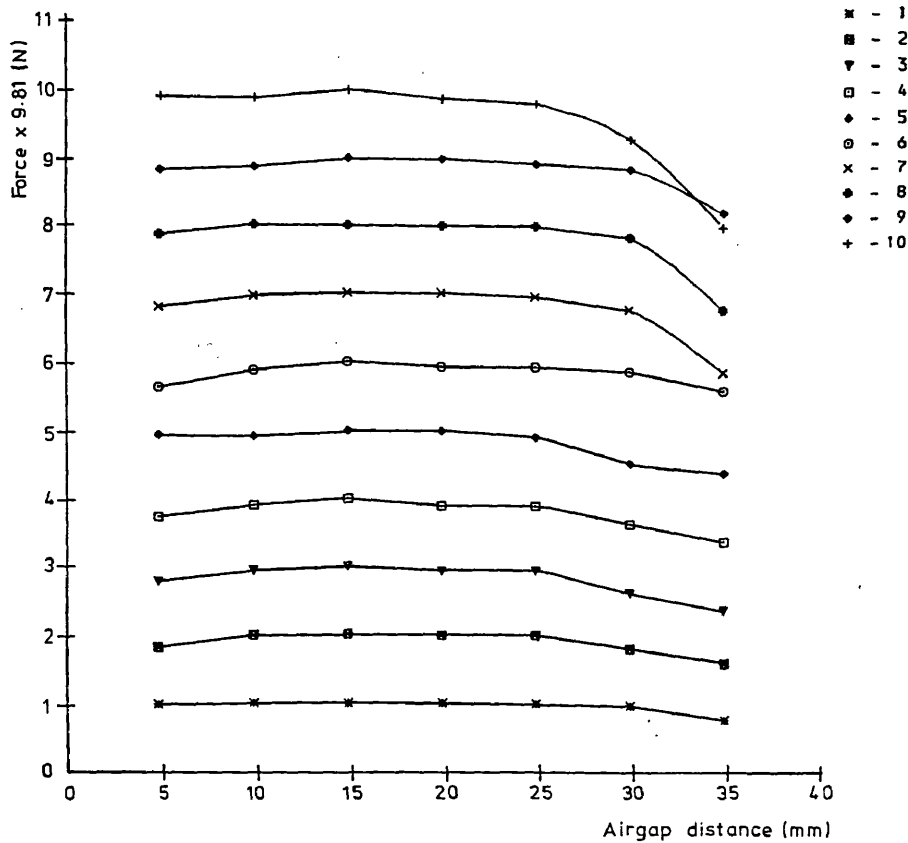


Fig 3 Generated force as a function of airgap for different demanded force levels

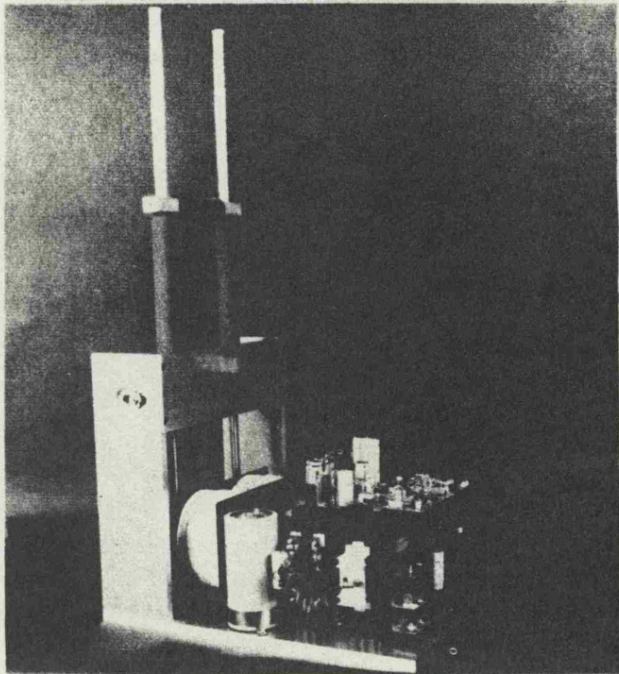
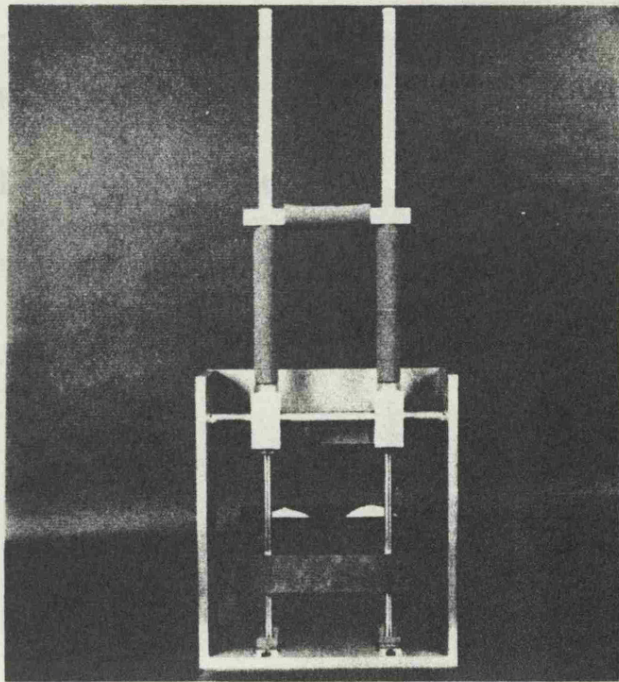
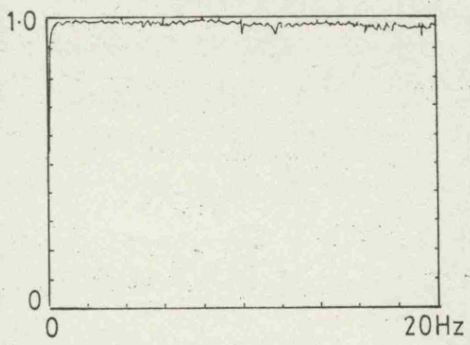
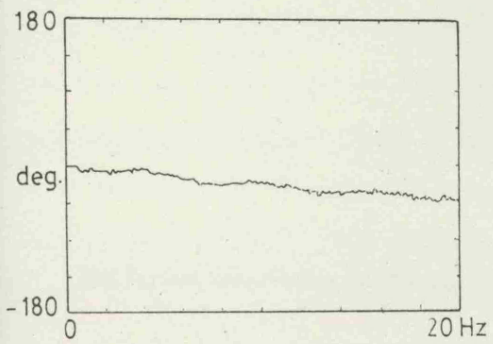
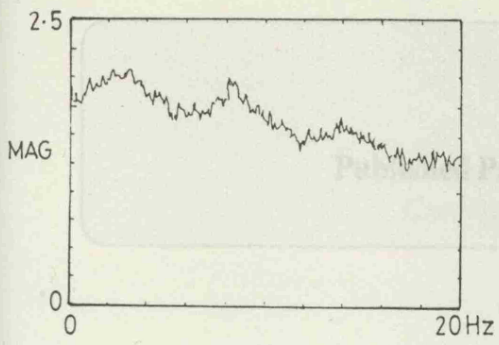


Fig 4 Frequency response of the system
 Top: Magnitude as a function of frequency
 Middle: Phase as a function of frequency
 Bottom: Coherence as a function of frequency
 All scales linear

Fig 5 Two views of the prototype machine

Appendix [C1]

Published Paper on EPAXIS Expert System

EPAXIS

An Expert System for Automatic Component Labelling In Evoked Potentials

TIRM-88-32

Sehmi, A

September, 1988

For further information on this and other Turing Institute Research Memoranda, please contact:

Turing Institute Press
George House
36 North Hanover Street
GLASGOW G1 2AD
Tel: 041-552-6400

Copyright Notice

No part of this publication may be reproduced, stored in a retrieval system, or transmitted, in any form or by any means, mechanical, photocopying, recording or otherwise without the permission of the Turing Institute.

ABSTRACT

Neuroelectric data assessment by human experts involves a complex process of data reduction and pattern recognition. This paper presents research in the development of a knowledge-based system for assisting an expert in the interpretation of a particular type of neuroelectric data, namely evoked potential (EP) data. This work constitutes part of a larger research effort currently being conducted by the University of Leicester and Medelec Ltd. The machine analysis consists of two main phases. Firstly, signal processing techniques are used to locate the major peaks (ie. 'components' or 'waves') in an averaged EP signal. This method is based on statistically estimating noise characteristics (Sehmi, 1987) suitable for detecting significant deflections in each EP signal, then constructing a histogram of deflections at each sampling interval summed over all individual signals. Peaks in this histogram correlate significantly with major peaks in the corresponding averaged EP.

The peak-finding algorithm provides input to the second phase of the analysis for labelling the peaks, performed by a knowledge-based system written in Prolog. The system comprises of some 50 rules that are driven by an interpreter that will allow for reasoning with uncertainty, using a method based on Zadah's (1965) theory of fuzzy sets. The system utilises a 'fuzzy model' of the EP containing both declarative and procedural knowledge. The declarative part contains a description of temporal relationships between significant EP components, and the procedural part defines demon procedures for computing values for EP attributes and certainty factors.

1 Introduction

The assessment of neuroelectric data by human experts is based upon complex processes of data reduction, feature extraction and evaluation, some of which are apparently subjective. The task of evaluating the data falls largely on the human expert. A greater part of the data reduction and some of the feature extraction processes are performed in dedicated computing machinery.

Our intention is to score and interpret EPs automatically. Clinical interpretation is a more ambitious goal that would have to use additional patient specific observations that are currently not available. Applications of a peak detection algorithm to analyse:

- [1] Short Latency Auditory Brainstem Potentials (Baeps),
- [2] Pattern Reversal Visual EPs (Prveps), and
- [3] Somatosensory EPs (Sseps),

have shown that underlying activity, not discernable by simple visual observation of the averaged EPs, can be extracted from the results. This information can be used to accurately locate *true* peaks in the averaged EP in conjunction with a simulation of the subjective methods of peak location which a human expert might use.

1.1 Solution Outline

Experienced clinicians working in the field of EP have a mental template of what to expect their data to look like on their CRT screens. The data is matched against this mental template and reduced to a sequence of latency and interval labels. The EP data interpretation by human experts relies on focussing first on the most prominent features in the data (i. e. *islands* of activity such as the largest peaks and troughs, the sharpest peaks, the broadest peaks, and '*the peak in the middle of the screen*'). Secondly, tentative labels are assigned to these peaks. Subsequent labelling of features is made with respect to the current decisions until the complete waveform is scored. Sometimes, intermediate decisions are discarded, and new reference features are selected.

To simulate this complex process a declarative model of expert reasoning is encoded as a collection of production rules. By allowing the attachment of certainty factors to the rule clauses, it is possible to weight the decisions being made on the data. This declarative model interacts with a procedural model of the data, which comprises of fuzzy membership functions describing each significant component of the data. The interaction between these models is achieved by a series of demon functions that contain algorithms for computing values for attributes and certainty factors, used in the reasoning process.

A common problem with the interpretation of data using a knowledge-based approach is the reduction of the raw data to a form that is usable by the reasoning modules. The technique

chosen depends largely on the type of information that is to be extracted during the reasoning process. We are interested in accurately labelling the major components in EPs and hence our data reduction method attempts to obtain peak information.

To provide input to the knowledge-based system, a non-linear adaptive algorithm has been developed to analyse the raw EP data. The algorithm statistically estimates certain noise characteristics in the single responses that constitute the averaged EP. These noise estimators are then used to detect all significant deflections (activity) in the individual responses. A histogram is then constructed from activity at each sampling interval. The peaks in this histogram have been found to correlate significantly with the major peaks (i. e. 'components' or 'waves') in the corresponding averaged EP. This then provides a good starting point for data input to knowledge-based system which will then attempt to assign labels to the corresponding deflections in the averaged EP response.

The following sections of this document will describe:

- [1] the application domain,
- [2] the data reduction algorithm,
- [3] the procedural model used to describe the data,
- [4] the declarative model (or knowledge base) used to describe the expert decision making process and,
- [5] the expert system interpreter and the propagation of certainty values.

2 The Application Domain

In order to test the knowledge-based paradigm of signal interpretation we shall use the Baep signal. This is perhaps the most complex of the EPs that have been mentioned. The Baep single responses are of low amplitude and signal to noise ratio. However, the data reduction algorithm performs well even under these circumstances. Hence, it should be possible to combine this information in the reasoning process to label Baep components accurately.

Below is a brief description of how EPs in general are obtained with an indication of the features of interest in Baeps for this study.

2.1 Evoked Potentials (EPs)

The application of sensory stimuli to the peripheral nervous system will, under normal circumstances, result in changes to the on-going activity of the central nervous system. These variations are known as evoked potentials (EPs). Some EPs can often be seen as a wave or group of waves in the electroencephalogram (EEG). Most EPs however, are indistinguishable in routine EEG recordings because of their inordinately low amplitudes (0.1 to 2 microvolts) and the interference of background cerebral electrical activity and electromyographic (EMG) artifacts (Chiappa and Ropper 1982).

By exploiting the non-stationary time locked nature of an evoked potential with its related stimulus and assuming that background EEG activity is a stationary random noise process, simple synchronous signal averaging can be used to extract the EP. The features of the electric potentials (waves) in the averaged EP brought out in this way are used in the assessment of neurological condition as each wave is generated by a specific anatomical structure within the nervous system. The presence or absence of the appropriate EP waves and their latencies are the primary characteristics used in clinical interpretation.

Several methods have been developed over the past decade to study the EP. Of these, pattern-shift visual, brainstem auditory, and short-latency somatosensory EPs have come into routine clinical use and are now well established as valuable clinical tools. EPs are used to reveal the presence of clinically unsuspected lesions in the sensory system when demyelinating disease is suspected because of indications in another area of the central nervous system. This is particularly relevant to

[1] the diagnosis of multiple sclerosis,

[2] determination of the anatomical distribution of a disease process,

and,

[3] to monitoring continuously the integrity of a pathway that cannot be examined clinically because of anaesthesia (Chiappa, 1982; Halliday, 1982; Colon et. al. , 1983).

Therefore, EPs are often used in patients with multiple sclerosis, nervous system tumors, trauma, stroke, in intra-operative monitoring procedures, and in intensive care environments, as well as in infants whose sensory systems cannot be accurately assessed. These tests provide sensitive, quantitative information complementing standard clinical neurologic examination.

Baeps

Evoked potential studies of the auditory system have proved extremely useful in the understanding of the physiological mechanisms of hearing in man. As a result of this they add to the diagnostic repertoire of the clinician for neurological and audiological investigation.

The Baep is best obtained with a high intensity click stimulus, and within the following 10 msec, could contain up to seven components labelled I-VII, according to Jewett's (1970) classification. There is considerable evidence that at least the first five components correspond to the successive activation of peripheral and pontomedullary (cochlea, spiral ganglion, and eighth nerve), pontine (cochlear nucleus, superior olivary nucleus, and lateral lemniscus tracts and nuclei), and midbrain (inferior colliculus) portions of the brainstem pathway (Stockard et al., 1978). This is shown in the diagram of Fig.[2.1], when these acoustic nerve and brainstem potentials are volume-conducted to recording electrodes at the vertex (electrode, Cz) and mastoid (electrode, Ai).

The components I-V in the Baep are those that are of most interest in audiological investigation as their variability under normal circumstances is low (about 300µsecs). It is quite possible though that the consistency of underlying activity is reflected in a distorted manner in the averaged response. This arises through a combination of averaging and the low signal to noise ratio of Baep single responses. The components (mainly the later ones above 4 msecs) then appear to be highly variable and/or fused. It is also possible that these components exist not as peaks, but as inflections on the rising or falling edges of a neighbouring component. This distortion in the Baep makes the task of assigning unique labels, I-V, difficult. Very often a clinician will have to perform multiple tests to gather evidence for the location of particular Baep components. The problem is magnified when the intensity of stimulus, and hence the amplitude of the responses, is reduced.

The data reduction algorithm described in the next section helps overcome these difficulties. It provides the type of data that can be used in an expert system for resolving possible ambiguities in the component labelling procedure.

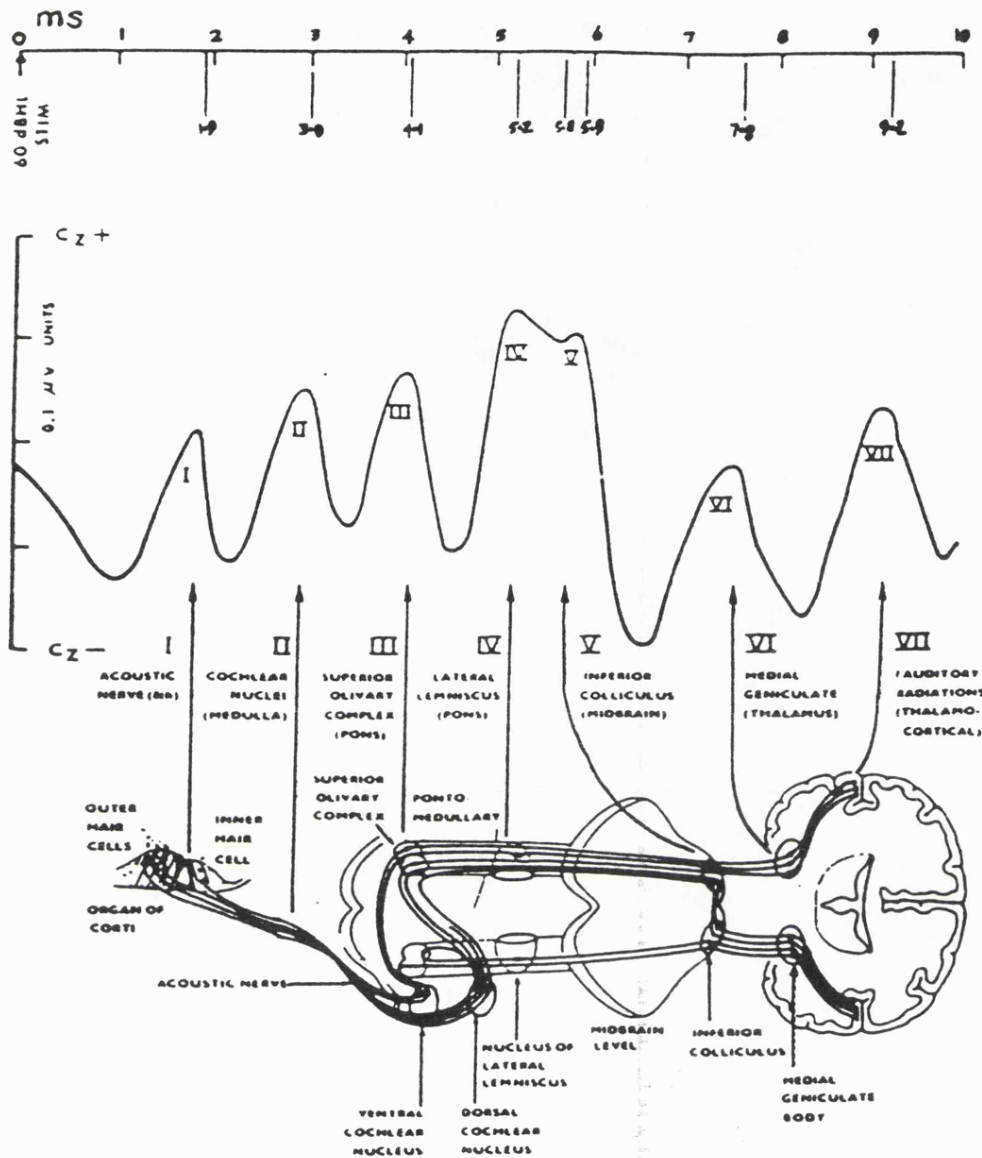


Fig. [2.1] Diagram of normal latencies at 60 dBSI for components I through VII. Lesions at different levels of the auditory pathway tend to produce response abnormalities in the components, although the affected component(s) does not specify the precise generator(s) of the response (taken from STOCKARD et al, 1977)

3 Measurements of Baeps from the Analysis of Single Response Data

The usual averaging process to extract the Baep waveform from an ensemble of individual responses assumes that the time-locked signal $s(t)$ repeats itself faithfully for each delivery of stimulus and that the mean value of the background EEG noise $n(t)$ will tend towards zero. If all of this were true, then averaging would be the optimal data analysis technique to implement prior to detection of significant components in the Baep. This, however, cannot be the case as there is considerable variability among responses (Aunon et al, 1981; Brazier, 1964) due to the effects of habituation, fatigue, and neuromuscular artifact. Distraction from the stimulus is a factor that may affect evoked potentials other than the Baep. In the averaged evoked potential the major features are due to components common to all the individual responses, and as such will obscure any subtle variations in the excitability of the central nervous system. The information contained in these variations could be as important as the gross information contained in the average. A procedure written in the C language is described for peak detection in the Baep. The individual responses to auditory stimuli are processed by a specialised peak detection algorithm. Estimates of the characteristic noise deflections contained within these responses are obtained from statistics of a frequency distribution of the amplitude differences between adjacent maxima and minima found in a 'noise-only' pre-stimulus run. These characteristic noise amplitudes are different for all subjects and different for all the individual responses in the same data set. With this noise amplitude information a second pass is made over the individual responses to determine the location of significant component peaks in the averaged response.

3.1 Outline of the Peak Binning Algorithm

The procedure relies on detecting the times of occurrence of significant events within the constituent sweeps of the Baep signal. These are defined as a pair of maxima enclosing a minimum such that the amplitude differences between the maxima and the enclosed minimum are larger than an arbitrary threshold value. This threshold value is termed the peak discrimination factor (PDF). The method of extraction of events in this analysis is similar to that used prior to the calculation of Turning Points Spectra of interference pattern EMGs (Lago and Jones, 1983). The difference lies in the attention paid to ensuring that an accepted event represents the maximum of highest amplitude and that the enclosed minimum is the deepest trough with respect to the chosen (peak discrimination factor or peak amplitude threshold level) PDF value. The sequence of N measured data points following the i th stimulus is $d_0, d_1, \dots, d_{N-1} = \{d_k\}_i$. The stimulus is delivered M times giving $N \times M$ data points in all. A turning point is defined as a change in slope; positive to negative slopes indicate maxima and the converse indicate minima. Maxima $d_{mx/j}, d_{mx/j+1}$, enclosing a minimum $d_{mn/l}$ have to satisfy all the following conditions:

$$|d_{mx/j} - d_{mn/l}| > \text{PDF} \dots\dots\dots \text{Eq. [3.1]}$$

$$|d_{mx/j+1} - d_{mn/l}| > PDF \dots\dots\dots \text{Eq. [3.2]}$$

$$|d_{mx/j+1} - d_{mn/l+1}| > PDF \dots\dots\dots \text{Eq. [3.3]}$$

such that a significant event is assigned to the maximum $d_{mx/j}$ at time mx/j (the real latency is the index value multiplied by the sampling interval and is assumed understood from here onwards). The algorithm commences with the maximum $d_{mx/j}$ set to the largest possible positive integer value the computer can hold ensuring that Eq. [3.1] is true at the start of analysis in the current sequence. Then the candidate minimum $d_{mn/l}$ is compared with the minimum that was found immediately prior to this to retain the lower of the two. This is used in the PDF comparison with candidate maximum $d_{mx/j+1}$ in Eq. [3.2]. As soon as this condition succeeds then a minimum $d_{mn/l+1}$ is found that makes Eq. [3.3] true thus confirming a significant event occurs at time mx/j . During this latter phase of analysis, any maxima found along the waveform are compared with the maximum $d_{mx/j+1}$ to retain the higher of the two. The updating procedure in effect '*slides*' this $1\frac{1}{2}$ wave template backwards by one wave and repeats the search for another pattern that fits the conditional tests just described. Implicit in this procedure is that the first condition automatically succeeds for all subsequent cycles. In this way accepted events represent those maxima enclosing the deepest troughs with respect to the chosen PDF value. In practice this method of peak detection is robust even with very noisy data.

It is apparent that this method relies on some knowledge of what value to assign to the PDF. Parekh (1987) and Lago and Jones (1983) have used similar peak detection algorithms in the analysis of turning point spectra of interference pattern EMG. Their choice of PDF value was largely empirical and was usually set to 3% of the maximum peak-to-peak deflection of the data. as this provided an adequate resolution for the subsequent classifications they were looking for.

The Baep has a high noise content (Fridman et. al., 1982) and a judicious choice of PDF value would be difficult to arrive at in the way it was above with EMG signals. The *Peak Binning* algorithm (Sehmi, 1987) assigns PDF values adaptively before analysing the single responses (or sub-averages of single responses) that make up a Baep. This is done by making an estimate of the '*noise*' in the sequence $\{d_k\}_j$. In this way any transient changes affecting the assumed statistical stationarity of background EEG activity can be partially compensated for.

The PDF assignment is determined from the '*modal*' value of the histogram computed from the amplitude differences between adjacent maxima and minima in a *noise only* pre-stimulus data sequence. The method assumes that the noise is additive to the signal in the post stimulus data sequence. This is not entirely true as the background EEG activity is *suppressed* (Berger, 1969) with sensory stimulation. This in fact helps the algorithm perform more efficiently.

The detection of positive peaks in the single responses lead to positive assignments in an accumulator or bin. An inverse assignment on negative peaks helps in the segmentation of the bin around major components in the Baep. Following the analysis of all single responses in the Baep, the bin is separated into positive and negative sequences. The positive bin sequence is convolved with a latency corrected 3-point backward moving average (twice), and further with a 3-point unit area triangular window (twice). The convolution process removes small baseline fluctuations produced in the second moment computation whilst preserving resolution, and maximising partitioning in the region of the major components in the corresponding Baep averaged response. Fig. [3.1] shows an averaged Baep response and the corresponding smoothed bin clearly indicating those *islands* of activity occurring in the averaged response. It should now be possible to use the bin information to *find* and *label* the major components in the averaged Baep response, whether they exist as true turning points or as points of inflection.

This data is written to files in the form of Prolog-readable terms. The structure of these terms have the following general format:

```
data(PeakType, NumberOfPeaks, ListOfPeaks).
ListOfPeaks = [Pos1/Ampl1, ... , ... , PosN/AmplN].
```

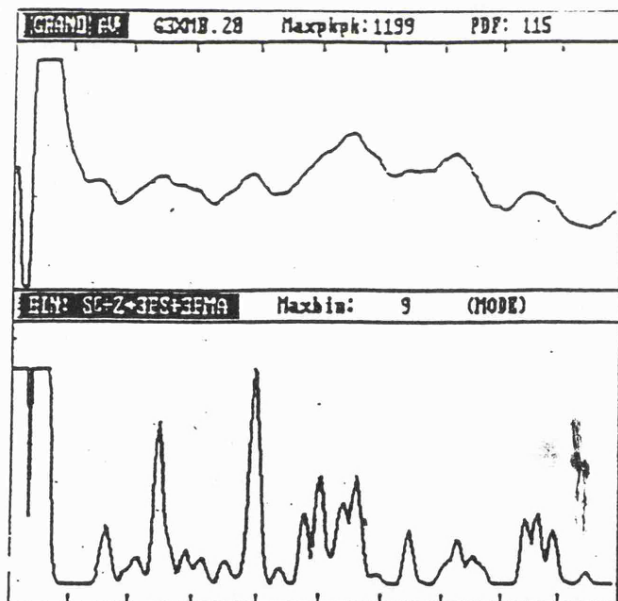


Fig. [3.1] An averaged Baep response in the upper window and the cooresponding smoothed bin histogram in the lower window. The peaks in the bin histogram correlate well with the major activity in the Baep. It is evident that activity not observable in the Baep is reflected in the fluctuations occurring in the bin.

(Because the algorithm attempts to disregard noise in the single responses, we assume that these fluctuations reflect activity obscured through the

averaging process)

4 A Fuzzy Model Description for Baep Interpretation

The Baep (and most neuroelectric data) can be highly contaminated with unwanted noise. This noise and the small variability in the times of occurrence of wave components in the single responses, almost always leads to a contaminated and distorted averaged response. It is however possible to extract general characteristics from the averaged response, only because our visual and mental faculties collaborate so well. Experts are able to perform correlations, selective filterings, weight assignments and generalisations quite naturally in order to identify and label wave components in a Baep.

The data reduction algorithm, described in section 3, makes it possible for a machine to get first estimates on where Baep components exist by examining peaks in the bin. The next problem we face is to resolve conflicts between *multiple* bin peaks that can cluster together in the immediate vicinity of *one* Baep component. This can be due to noise contamination that has not been completely removed with the data reduction method. It is also plausible to suggest that multiple peaks in the bin (especially in and around the later Baep components) are due to the activation of generator sites from the contralateral channel reflecting their activity in the recorded ipsilateral channel.

These problems have led to the specification of a *fuzzy* model describing Baeps. The model comprises two parts, namely the procedural and declarative components. The models employ techniques allowing *uncertain* descriptions of the data reduction output and the patterns of Baep components in the averaged response.

4.1 The Fuzzy Procedural Model (Data Base)

The fundamental primitive for information modelling in an expert system are propositional statements of the form: '*an attribute of an object has a particular value*'. This is represented in Prolog as the symbolic structure:

Object Attribute Value

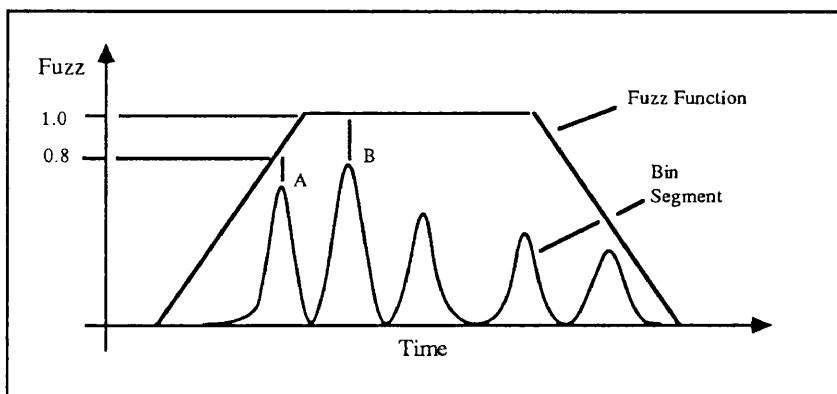
We may express that '*a component wave of the Baep occurs at position X*' by writing:

Wave position_is X

As soon as *Wave* does not occur exactly at *X* then we have introduced an amount of imprecision, where *X* does not exactly reduce to one element in the domain U_{Wave} (universe of discourse) of the variable *Wave*. *X* is then the set of mutually exclusive possible values for *Wave*.

In the imprecise proposition above, the set *X* may not have clear boundaries. Then *X* is what Zadeh (1965) has named a fuzzy set and *Wave position_is X* is said to be a fuzzy proposition. A fuzzy set *X* say, is described by means of a membership function μ_X . This is a function mapping from the domain U_{Wave} to the interval [0,1]. 1 represents full membership and 0 non-membership and intermediates represent partial membership.

The fuzzy set (π_X) of values which bin peaks (*X*) can take for a wave component (*Wave*) in the domain of Baep waves (U_{Wave}) is given uniquely by the fuzzy membership function (μ_X). The membership function for the domain U_{Wave} (our only domain) is shown in Fig. [4.1]. This is termed *fuzz function* and enables assignments of reliability or *fuzz* to the results of the data reduction algorithm and the peaks in the averaged Baep response



. [4.1] Mapping of Bin Peaks onto the Fuzz Function to obtain Peak Reliability measures.

Referring to Fig. [4.1], peaks in the bin segment shown, have their *fuzz* computed by a simple interpolation through a mapping of their times of occurrence onto the *fuzz function*. For example, the bin peak at 'B' maps to a *fuzz* of 1.0 indicating full membership of X in U_{Wave} and 'A' maps to a *fuzz* of 0.8 indicating partial membership of X in U_{Wave} .

Zadeh calls π_X the possibility distribution and its identification can be subjective as the definition of μ_X can be subjective. The importance of this distribution is the order it imparts on the domain U_{Wave} and it should contain all possible values of $Wave$. In this application, μ_X has been estimated from a linear approximation to the normal statistical distribution of the individual components in the Baep. This can be altered dynamically in the system since the model descriptions are generic. The flexibility that this imparts is important in maintaining the separation between the components in the expert system as a whole and its adaptability to other EP domains.

Fig. [4.2] illustrates the complete fuzzy procedural model for the Baep. The fuzz functions are located along the time axis at the normal mean values (initially) for each component wave of interest.

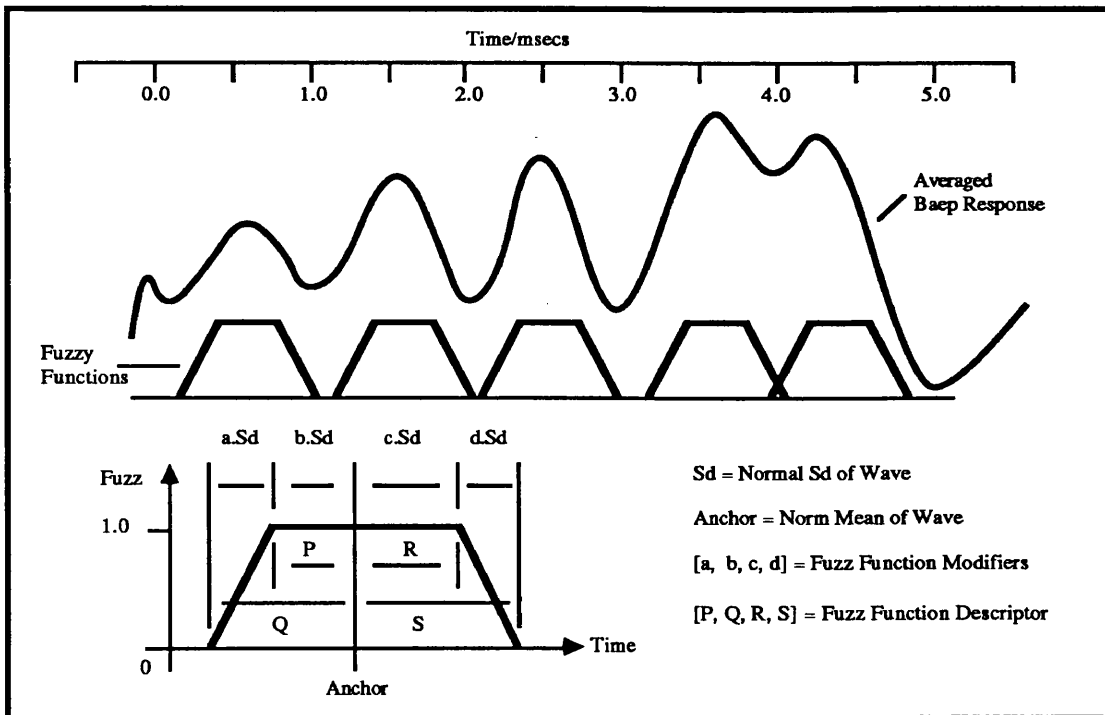


Fig. [4.2] A Fuzzy Procedural Model for Brainstem EPs.

Prolog descriptions for each wave are constructed via the execution of the declarative model (explained later) when and where required. The generic Prolog structures for a fuzzy function (or window) are:

fuzzwindow(WaveNumber, Anchor, [P, Q, R, S]).
modifs[WaveNumber, [a, b, c, d]).
current_shift(WaveNumber, Shift).

where [P, Q, R, S] are defined in terms of the modifiers [a, b, c, d]. These are set to constants, but conceptually they can be functions of time that modulate their respective fuzz function regions. The current shift is used to relocate the anchor point for the fuzzy function along the time axis.

This structure means that the fuzzy functions can adopt any suitable form and location. The description adopted for the prototype system is simple. The modifiers for each wave are: [0, 1, 2, 1], resulting in fuzzy function descriptions: [0, Sd, 2*Sd, Sd]. Hence, the total width of each fuzzy function is 4 standard deviations. The extent of the spread either side of the anchor point (normal mean latency value for the component wave) corresponds to the 99% confidence limits (note that the distribution of latencies for Baep components is assymetric).

We have seen how the results of the data reduction algorithm can be assigned reliability measures. To reason with these *'tagged'* data effectively requires that the declarative model and the inference machine (rule interpreter) are compatible at the higher level.

4.2 The Fuzzy Declarative Model (Knowledge Base)

This model attempts to capture the expert decision making processes used to interpret (label) a Baep. The fuzzy procedural model described in the previous section makes it possible to formulate propositions of the form:

Object Attribute FuzzyValue

FuzzyValue = Value + Fuzz

Furthermore we can formulate the consequence of fuzzy propositions by using rules or productions:

if: Object Attribute FuzzyValue
then: ObjectX AttributeX ValueX

The value *ValueX* of object *ObjectX* is concluded with the fuzziness *Fuzz* (in *FuzzyValue*) of object *Object*.

The certainty with which a proposition holds can be expressed with a propositional attachment called the *certainty factor*, *cf*. Therefore we can write:

if: ObjectX AttributeX FuzzyValueX cf CF
then: ObjectY AttributeY ValueY

The value *ValueY* of object *ObjectY* is concluded with a combination of the fuzziness *FuzzX* of object *ObjectX* and the *cf* attachment *CF*: [0.0, 1.0]. This in effect allows the modeller to express the reliability or confidence with which a proposition is being made when the object value is completely true. If the object value is fuzzy, then this is reflected nevertheless through a combination of fuzzy and certainty values.

The production '*if contralateral recording is available then contra_wave_V position is X*' represents knowledge that is applicable only if the antecedent is true. However we would like to express the influence of the antecedent on the consequent when the antecedent is false. To prevent the automatic assertion of the consequent with a low certainty value in the absence of a contralateral recording, another extension to our existing formalism is required. In this case we must assign a weighting to evidence for truth and to evidence for falsehood:

**if: ObjectX AttributeX FuzzyValueX of CF wt (WtT, WtF)
 then ObjectY AttributeY ValueY**

The combined fuzzy value for object *ObjectX* is calculated in two stages:

[1] $Fuzz = FuzzX * CF$

Introducing the clause weights (WtT , WtF) we obtain a total reliability for the antecedent proposition in the production rule. This is termed the *fuzzy reliability factor (FRF)*:

[2] $FRF = \frac{WtF + Fuzz(WtT - WtF)}{\max(WtT, WtF)}$

The value *ValueY* of object *ObjectY* is concluded with the fuzziness *FRF* of object *ObjectX*.

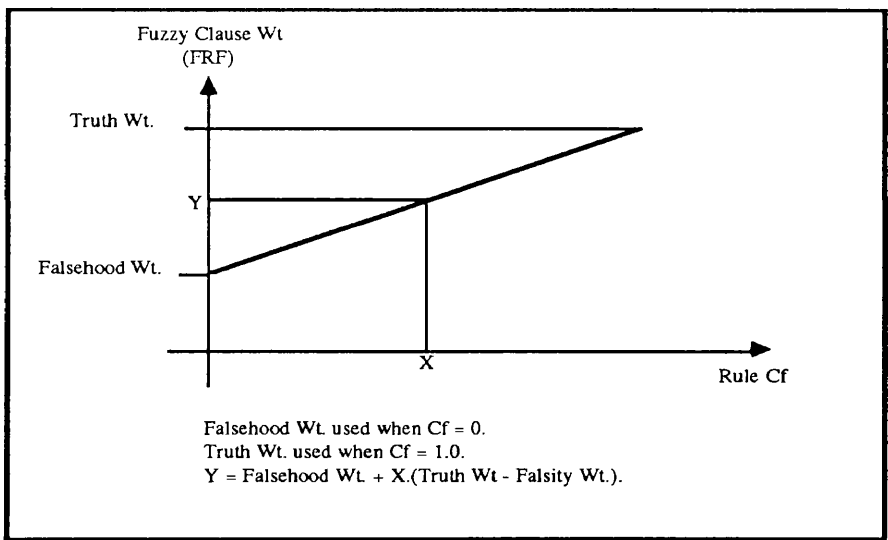


Fig. [4.3] Variation of FRF with rule certainty factor (or combined Fuzz).

Fig [4.3] illustrates the variation of the clause weight (FRF) with the certainty factor attachment (or combined fuzzy value) of the rule proposition. The contribution of truth and falsehood on the declarative interpretation of an antecedent proposition (and how much this contributes to the assertion of consequent propositions), is determined by the truth and falsehood weights. Adjustments of these weights is equivalent to an adjustment of the slope of the line in Fig. [4.3]. The steeper the positive slope, the higher is the contribution of truth of antecedents in the assertion of consequents, and the less falsehood detracts. Negative slopes have the same effect as negation of the antecedent propositions. Use of weights in this manner is not

recommended as it obscures the declarative content of the rules.

Rules containing conjunctions of antecedents get their individual FRFs combined before the assertion of a consequent:

$ClauseWtA = WtFA + FuzzA(WtTA - WtFA)$
 $ClauseWtB = WtFB + FuzzB(WtTB - WtFAB)$
etc...

$$FRF = \frac{ClauseWtA + ClauseWtB + \dots + \dots}{\max(WtTA, WtFB) + \max(WtTA, WtFB) + \dots + \dots}$$

If consequent have certainty factor attachments then the FRF calculated as above is combined with this as in stage [1] above.

These ideas are employed in a structured declarative model (knowledge base of rules) with a rich syntax. The grammar for the rules is summarised below in BNF:

Rule Grammar :-

**rule ::= <term> :: if <antecedent>
 then <consequent>.**

**antecedent ::= <antecedent> && <antecedent>
 | <antecedent> or <antecedent>
 | <antecedent> cf <number>
 | <antecedent> wt <weightT, weightF>
 | <antecedent> cf <number> wt <weightT, weightF>
 | <term>**

**consequent ::= <consequent> && <consequent>.
 | <consequent> cf <number>.
 | <term>.**

term ::= any Prolog term

number ::= [float : (0.0, 1.0)]

weightT, weightF ::= [float : (0.0, 5.0)]

Knowledge Base Structure

The rules contained in the knowledge base are structured into:

Control (meta) rules

These are rules that direct the search through the knowledge base when driven by the inference engine or rule interpreter. Our task requires some direction as to which Baep waves to look for in the absence of others. Examples are:

```
rule17 ::  
if  
channel = ipsi  
&& wave_I = found  
&& wave_II = found  
&& wave_III = found  
&& wave_IV = found  
&& wave_V = found  
then  
all_peaks = found.
```

```
rule18 ::  
if  
channel = contra  
&& wave_II = found  
&& wave_III = found  
&& wave_IV = found  
&& wave_V = found  
then  
all_peaks = found.
```

Descriptive rules

These are rule which produce qualitative descriptions for the Baep. They are generally higher level abstractions of the characterising rules below. Through backward chaining via the rule interpreter these rules activate the characterising rules. Descriptive rules are useful for two reasons. Firstly, they provide clear declarative semantics of what is being performed in the interpretation task which is useful in the debugging phase (notably understandable explanations). Secondly, the abstraction allows for increased generality and therefore application of the same rules in similar domains. Examples of these rules are:

```

rule02 ::
if
Wave list_of_pks_is ListOfPks+(bin_pks)
&& Wave best_pk_is Pos/Fuzz+(ListOfPks)
then
Wave position_is Pos cf Fuzz.

```

```

rule07 ::
if
Wave fuzz_window_is FuzzWindow
&& Wave pks_are ListOfPks+(PksType,FuzzWindow)
then
Wave has_pks_of_type PksType+(ListOfPks).

```

```

rule09 ::
if
Wave stats_of_are Stats
&& Wave modifiers_are Modifs
&& Wave is_described_by WaveModel+(Stats,Modifs)
then
Wave model_of_is WaveModel.

```

Characterising rules

The knowledge base can be considered as an AND/OR graph with its leaves being the conjunction of antecedents in these characterising rules. Specificity is handled here entirely. They are the interface with the data through procedural mappings that activate *demons*. These rules return the appropriate Prolog data structures which are examined and the results of which are propagated upwards from this level mechanisms. Examples of these rules are:

```

rule10 ::
if
Wave mean_is Mean
&& Wave sd_is Sd
then
Wave stats_of_are (Mean,Sd).

```

```

rule35 ::
if
channel = ipsi
&& wave_I position_is PosWave_I cf _Fuzz_
&& (

```

```

    wave_I is_expected_at EPos_I+Tol_I+(wave_III)
or
    wave_I is_expected_at EPos_I+Tol_I+(wave_V)
)
&& $(Diff is PosWave_I-EPos_I)
&& $(Diff =< Tol_I)
then
pos_wave_I_at = PosWave_I.

```

The corresponding demon procedure mappings are performed through a predicate defined as *external/2*:

```

external(Wave expected_at PosAndTol+(RefWave,RefPos),
external(Wave mean_is X, norm_mean(Wave, _,[X])).
external(Wave sd_is X, norm_sd(Wave, _,[X])).

```

The next section will go on to describe very briefly the top level interpreter used in this system.

5 The EPAXIS Interpreter

This interpreter shell is backward chaining and provides uncertain inference and explanation capabilities on the declarative model described in the previous section. It also provides the interfacing with the procedural model through invocation of the user-defined demon-procedures. The interpreter *executes* the declarative model (i.e. knowledge base) in much the same way as Prolog *executes* the interpreter itself. Hence, it is possible to pass goals to Prolog for execution. This is necessary for mathematical constructs and interfacing to other languages. An important specification for this implementation has been separation of all EPAXIS modules. In this respect the same interpreter can be used to execute knowledge bases that will be defined in the future for labelling different EPs.

The structure used in the shell derives from the work of Shapiro (1983) and Niblett (1984). The implementation of uncertain reasoning is a variant of that described by Lebailly et. al. (1987). The scheme below shows the basic structure of the EPAXIS interpreter:

```
% Top call
solve(X) :-
    solve(X, Fuzz, []).

% Is goal known
solve(X, Fuzz, _ ) :-
    known(X cf Fuzz),
    !.

% Is goal solvable using a procedural call
solve(X, Fuzz, _ ) :-
    external(X, Demon),
    !,
    execute_demon(Demon, Fuzz).

% Is goal solvable using a rule
solve(X, Fuzz, Stack) :-
    Rule :: if Conds then Goal,
    satisfy(Conds, CondsFuzz, [Goal+Rule|Stack]),
    conclude(Goal, CondsFuzz, Fuzz).

% Ask user for solution
solve(X, Fuzz, _ ) :-
    askable(X),
    !,
    certain(Fuzz).
```

Satisfy/3 attempts to solve the antecedent propositions by recursively invoking *solve/3* with each proposition in turn. A successful goal will cause *satisfy/3* to calculate its fuzzy value

(FRF) and eventually a combined fuzzy value (CondsFuzz) for all propositions. *Conclude/3* will then assert the conclusion with the fuzzy value of the antecedents.

In the case when goals are already known (i.e. they have been proved already) and the antecedent proposition has a certainty factor attachment, a simple product of fuzzy values performed before the calculation of the FRF. A similar multiplicative process is performed if the assertion of a particular consequent has a precedent. This latter process allows the accumulation of evidence for some items to strengthen or weaken evidence for others dynamically.

6 Results

The results of a consultation are given in Appendix [A]. This demonstrates the rudimentary explanation facility provided. Of greater interest is how the objects and values in the generic rules have become unified with data structures extracted from the raw Baep data. This has been performed using the procedural attachments interacting with the procedural model.

7 Conclusion

The use of an expert systems approach to automatic component labelling in evoked potentials has demonstrated several points:

[1] The use of a high level language (such as Prolog) has provided for rapid prototyping even in a complex domain. This can be attributed to the ease with which abstraction and separation of concepts is done.

[2] It should be possible to generate '*stand alone*' knowledge bases for other EPs using the one interpreter shell developed for this Baep domain.

[3] The use of a model of uncertainty for data description provides the sort of expressive power needed for reasoning in this noisy domain.

[4] The authors personal experience was that it is easier to modify the interpreter than it was to modify the knowledge base. Initial problems were concerned with defining a useful rule description language and designing a useful structure in which to fit the rules.

[5] There is a trade-off between the characterising and descriptive rules. They could really merge together, but this would be to the detriment of declarative understanding. It is entirely up to the rule writer (knowledge engineer) how far to pursue this separation. For debugging and explanations it is a task worth pursuing. If explanations *and* maintenance are unimportant, then a final version can contain a condensed rule set for faster rule execution. This is however unlikely.

Acknowledgements

The author would like to thank Peter Clark (TI) for his careful supervision and keen interest in this project. Thank you Jonathan Shapiro (TI) for being instrumental in porting the C programs from the IBM PC AT to the SUN workstations.

Thanks are also extended to Medelec Ltd., and in particular Dr. Neil Robinson, for allowing me to have the funds and time away from *normal* work to pursue this project. My apologies and sincere gratitude to Prof. Barrie Jones (Leicester University) who has been tolerant with my never ending delays in *getting that thesis done*.

Last and not the least, the author would like to acknowledge the invaluable sponsorship provided by the Department of Trade and Industry under their IKBS Turing Institute Journeyman Training Scheme.

References

- Avnon, J. I., McGillem, C. D. and Childers, D. G. (1981) Signal processing in evoked potential research: Averaging and Modelling.
- Berger, H. (1959) On the electroencephalogram of man. *Electroenceph. clin. neurophysiol.* 28, 37 ff.
- Brazier, M. A. (1964) Evoked responses from the depths of the human brain. *Electroenceph Clin. Neurophys.* 112, 33-59.
- Chippa, K. H. and Ropper, A. H. (1982) Evoked potentials in clinical medicine. *New England Journal of Medicine.* 306 (19), 1140-1150
- Colon, E., Visser, S., De Weerd, J. and Zonneveldt, A. (1983) *Evoked potential manual: a practical guide to clinical applications.* The Hague: Martinus Nijhoff.
- Fridman, J., John, E. R., Bergelson, J. B., Kaiser, J. B. and Baird, H. W. (1982) Application of digital filtering and automatic peak detection to brainstem auditory evoked potential. *Electroenceph Clin. Neurophys.* 53, 405-416.
- Halliday, A. M., ed. (1982) *Evoked potentials in clinical testing.* Edinburgh: Churchill Livingstone.
- Jewett, L. D. (1970) Volume conducted potentials in response to auditory stimuli as detected by averaging in the cat. *Electroenceph. clin. neurophysiol.* 28, 609 ff.
- Lago, P. J. A. and Jones, N. B. (1983) Turning points spectral analysis of the interference myoelectric signal. *Med. Biol. Engl Comp.* 21, 333-342.
- Lebailly, J., Martin-Clouaire, R. and Prade, A. (1987) Use of fuzzy logic in a rule-based system in petroleum geology. *Approximate reasoning in intelligent systems, decision and control.* Oxford: Pergamon Press. pp 125-144.
- McGillem, C. D. and Aunon, J. I. (1977) Measurements of signal components in visually evoked potentials. *IEEE Transactions on Systems, Man and Cybernetics.* 24, 232-241.
- Niblett, T. (1984) *YAPES - yet another prolog expert system.* Glasgow: The Turing Institute (TIRM-84-008).
- Parekh, A. (1987) *Computer analysis of the interference pattern.* Brighton: Sussex University (D. RhM thesis).
- Sehmi, A. (1987) *Automatic peak detection in evoked potentials.* Old Woking, Surrey: Medelec Ltd (Development Report).
- Shapiro, E. Y. (1983) *Algorithmic Program debugging.* Cambridge, MA: MIT Press.
- Stockard, J. J., Stockard, J. E. and Sharbrough, F. W. (1978) Non-pathologic factors influencing brainstem auditory potentials. *Am J EEG Technol.* 18, 177-209.
- Zadeh, L. A. (1965) Fuzzy sets. *Information and control.* 8, 338-353.

Appendix

% We enter the Prolog System and load the expert system (EPAXIS):

?- [makefile].

% To start the consultation we enter the query:

?- gotop(X).

% This activates the top level goal 'solve(baep_pks_found = X, Fuzz, [])'.

% A question is asked.

What channel is this recording taken from (ipsi/contra) ['why.' to see why] ? > why.

% We have typed in 'why' for an explanation.

% This is listed simply from an examination

% of the current goal stack.

In order to find the value of baep_pks_found,

I'm trying rule rule12T.

This concludes about baep_pks_found.

To prove the conditions of rule rule12T,

I need to know the value of labelling.

In order to find the value of labelling,

I'm trying rule rule13.

This concludes about labelling.

To prove the conditions of rule rule13,

I need to know the value of normal_interp.

In order to find the value of normal_interp,

I'm trying rule rule15.

This concludes about normal_interp.

To prove the conditions of rule rule15,

I need to know the value of all_peaks.

In order to find the value of all_peaks,

I'm trying rule rule17.

This concludes about all_peaks.

To prove the conditions of rule rule17,

I need to know the value of channel.

To find the value of channel, I'm asking you!

% After explanation the question is prompted again.

What channel is this recording taken from (ipsi/contra) ['why.' to see why] ? > ipsi.

% No more questions and the system attempts to solve the top level goal.

% The goal is successful after examining the Baep data

% using the fuzzy models described in the report.

% The reply from the system is:

The goal [baep_pks_found=yes] has been proved
The explanation for baep_pks_found=yes is as follows :

```
rule12T ::  
if  
  labelling=successful  
then  
  baep_pks_found=yes.  
  
% We can ask 'how' certain conclusions were reached.  
% e.g. by entering 'labelling=X.'
```

```
Which fact would you like to query ('end.' to end)  
  (eg. 'peak_5_found=magic.') -> labelling=X.
```

```
% This is how
```

```
rule13 ::  
if  
  normal_interp=yes  
then  
  labelling=successful.
```

```
% Again we have the option to query
```

```
Which fact would you like to query ('end.' to end)  
  (eg. 'peak_5_found=magic.') -> normal_interp=X.
```

```
rule15 ::  
if  
  all_peaks=found  
then  
  normal_interp=yes.
```

```
% Etc. ....
```

```
Which fact would you like to query ('end.' to end)  
  (eg. 'peak_5_found=magic.') -> all_peaks=X.
```

```
rule17 ::  
if  
  channel=ipsi  
  && wave_I=found  
  && wave_II=found  
  && wave_III=found  
  && wave_IV=found  
  && wave_V=found  
then  
  all_peaks=found.
```

```
Which fact would you like to query ('end.' to end)  
  (eg. 'peak_5_found=magic.') -> channel=ipsi.
```

annel=ipsi because you told me so!
Which fact would you like to query ('end.' to end)
(eg. 'peak_5_found=magic.') -> wave_I=X.

rule36T ::
if
pos_wave_I_at=284
then
wave_I=found.

Which fact would you like to query ('end.' to end)
(eg. 'peak_5_found=magic.') -> pos_wave_I_at=X.

rule35 ::
channel=ipsi
&& wave_I position_is 284
&& (wave_I is_expected_at 285.0+14.0+wave_III
or
wave_I is_expected_at 285.0+14.0+wave_V
)
&& \$(-1.0 is 284-285.0)
&& \$(abs(-1.0,1.0))
&& \$(1.0=<14.0)
then
pos_wave_I_at=284.

*§ We have asked to see how 'wave_I position is X' has been
§ found. Because this comes from the activation of a generic
§ rule, we have been given lots of other information.*

Which fact would you like to query ('end.' to end)
(eg. 'peak_5_found=magic.') -> wave_I position_is X.

wave_IV position has been found in the averaged Baep response
(grand_pks) with a certainty of 0.57. This was determined from the fuzzy
procedural model of the Baep.

rule01 ::
if
wave_IV list_of_pks_is[388/414/0.571428]+grand_pks
&& wave_IV best_pk_is 388/0.571428+[388/414/0.571428]
then
wave_IV position_is 388 cf 0.571428.

And so on for peak positions.
This data provides the component labels and
is of great importance for the future work
as a list of optional peaks is also attached.

rule01 ::
if

```
wave_V list_of_pks_is[388/414/1.0,411/ -43/0.857142,406/ -108/0.142857]+grand_pks
&& wave_V best_pk_is 388/1.0+[388/414/1.0,411/ -43/0.857142,406/ -108/0.142857]
then
wave_V position_is 388 cf 1.0.
```

```
rule01 ::
if
wave_II list_of_pks_is[320/ -234/1.0,326/ -300/1.0]+grand_pks
&& wave_II best_pk_is 320/1.0+[320/ -234/1.0,326/ -300/1.0]
then
wave_II position_is 320 cf 1.0.
```

```
rule01 ::
if
wave_III list_of_pks_is[345/ -105/1.0,347/ -90/1.0,358/ -340/1.0]+grand_pks
&& wave_III best_pk_is 345/1.0+[345/ -105/1.0,347/ -90/1.0,358/ -340/1.0]
then
wave_III position_is 345 cf 1.0.
```

```
rule01 ::
if
wave_I list_of_pks_is[284/ -177/1.0,286/ -182/1.0]+grand_pks
&& wave_I best_pk_is 284/1.0+[284/ -177/1.0,286/ -182/1.0]
then
wave_I position_is 284 cf 1.0.
```

% This is another generic rule which we query about.

Which fact would you like to query ('end.' to end)
(eg. 'peak_5_found=magic.') -> wave_I list_of_pks_is X.

```
rule06 ::
if
wave_IV has_pks_of_type bin_pks+
[370/10/1.0,376/15/1.0,390/15/0.857142,385/11/0.142857]
then
wave_IV list_of_pks_is[370/10/1.0,376/15/1.0,390/15/0.857142,385/11/0.142857]+bin_pks.
```

```
rule06 ::
if
wave_IV has_pks_of_type grand_pks+[388/414/0.571428]
then
wave_IV list_of_pks_is[388/414/0.571428]+grand_pks.
```

%%%% Etc. %%%%

% The rules are gradually chaining back to the point where
% the wave models are made.

Which fact would you like to query ('end.' to end)

(eg. 'peak_5_found=magic.') -> wave_I has_pks_of_type X.

```
rule07 ::
if
wave_IV fuzz_window_is[wave_IV,363.0/0.0,363.0/1.0,384.0/1.0,391.0/0.0]
&& wave_IV pks_are[370/10/1.0,376/15/1.0,390/15/0.857142,385/11/0.142857]+
    (bin_pks,[wave_IV,363.0/0.0,363.0/1.0,384.0/1.0,391.0/0.0])
then
wave_IV has_pks_of_type bin_pks+
    [370/10/1.0,376/15/1.0,390/15/0.857142,385/11/0.142857].
```

%%% Etc. %%%

% This is the point where we can query about the model.

Which fact would you like to query ('end.' to end)
(eg. 'peak_5_found=magic.') -> wave_I fuzz_window_is X.

% The fuzzy window is created from here onwards

```
rule08 ::
if
wave_IV current_shift_is 0
&& wave_IV model_of_is[wave_IV,363.0,363.0,384.0,391.0]
&& wave_IV window_is[wave_IV,363.0/0.0,363.0/1.0,384.0/1.0,391.0/0.0]+
    ([wave_IV,363.0,363.0,384.0,391.0],0)
then
wave_IV fuzz_window_is[wave_IV,363.0/0.0,363.0/1.0,384.0/1.0,391.0/0.0].
```

%%% Etc. %%%

% The model making rule is queried.

Which fact would you like to query ('end.' to end)
(eg. 'peak_5_found=magic.') -> wave_I window_is X.

% The reply is that this was calculated using fuzzwindow/4.
% This is an example of the activation of a demon through
% a procedural attachment to our declarative model of rules.

```
wave_I window_is[wave_I,282.0/0.0,282.0/1.0,297.0/1.0,302.0/0.0]+
    ([wave_I,282.0,282.0,297.0,302.0],0)
was calculated using fuzzwindow(wave_I,[wave_I,282.0,282.0,297.0,302.0],
    0,[wave_I,282.0/0.0,282.0/1.0,297.0/1.0,302.0/0.0])
```

% We end the consultation at this point.

Which fact would you like to query ('end.' to end)
(eg. 'peak_5_found=magic.') -> end.

% A listing of what has been determined globally is printed.

This is what is known in the working memory :

```
nown((baep_pks_found=yes)cf 0.999988,[rule12T]).
nown((labelling=successful)cf 0.99999,[rule13]).
nown((normal_interp=yes)cf 0.999992,[rule15]).
nown((all_peaks=found)cf 0.999994,[rule17]).
nown((wave_V=found)cf 1.0,[rule47T]).
nown((pos_wave_V_at=388)cf 1.0,[rule45]).
nown($(0.0=<15.0)cf 1.0,[calculated]).
nown($(abs(0.0,0.0))cf 1.0,[calculated]).
nown($(0.0 is 388-388.0)cf 1.0,[calculated]).
nown(wave_V is_expected_at 388.0+15.0+wave_I cf 1.0,[rule05]).
nown(wave_V expected_at 388.0+15.0+ (wave_I ' , ' 284)cf 1.0,[calculated]).
nown((wave_IV=found)cf 1.0,[rule44T]).
nown((pos_wave_IV_at=370)cf 1.0,[rule43]).
nown($(3.0=<17.0)cf 1.0,[calculated]).
nown($(abs(3.0,3.0))cf 1.0,[calculated]).
nown($(3.0 is 370-367.0)cf 1.0,[calculated]).
nown(wave_IV position_is 370 cf 1.0,[rule02]).
```

%% Etc. (Approx. 100 items) %%

```
nown(wave_I model_of_is[wave_I,282.0,282.0,297.0,302.0]cf 1.0,[rule09]).
nown(wave_I is_described_by[wave_I,282.0,282.0,297.0,302.0]+
      ((287.0 ' , ' 5.0) ' , '[0,1,2,1])cf 1.0,[calculated]).
nown(wave_I modifiers_are[0,1,2,1]cf 1.0,[calculated]).
nown(wave_I stats_of_are (287.0 ' , ' 5.0)cf 1.0,[rule10]).
nown(wave_I sd_is 5.0 cf 1.0,[calculated]).
nown(wave_I mean_is 287.0 cf 1.0,[calculated]).
nown(wave_I current_shift_is 0 cf 1.0,[calculated]).
nown((channel=ipsi)cf 1.0,[told]).
```

*% gotop(X) returns 'yes' as the answer to
% the goal 'solve(baep_pks_found = X, Fuzz, [])'.*

X = yes

| ?-

% Normal exit to the Prolog system.

Appendix [C2]
Source Code for EPAXIS Expert System Program

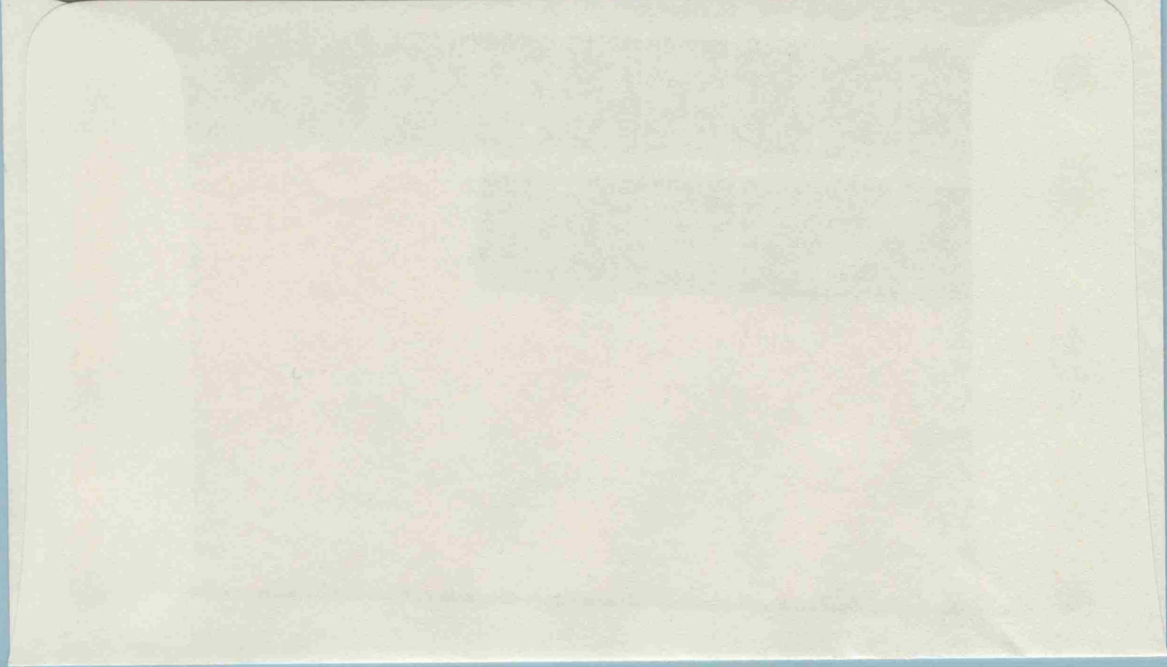
Appendix [D1]

Source Code for Event Analysis Program

Appendix [D2]

Source Code for Data Simulation and Related Programs

DATASIM.



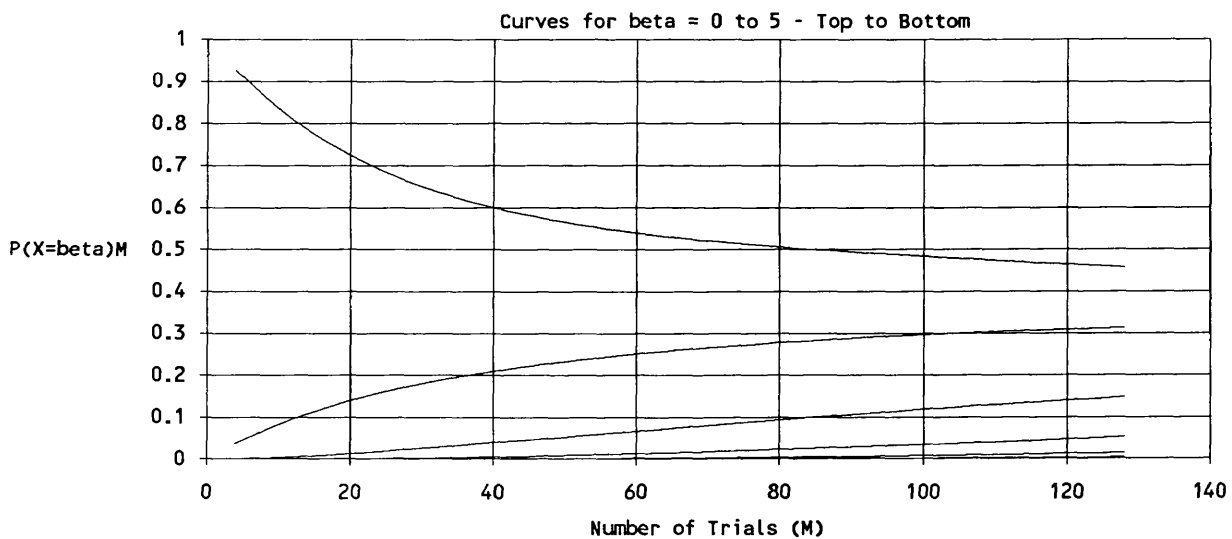
Appendix [D3]

Event Analysis: Results for Bin Cancellation Simulations

Probability (P(X=beta)M) of Bin Cancellation Error (beta) for Increasing Numbers of Trials (M) at Different Event Probabilities p.									
p=0.010									
M	4	16	32	48	64	80	96	112	128
P(X=0)M	0.926	0.763	0.638	0.571	0.532	0.506	0.488	0.472	0.457
P(X=1)M	0.0373	0.12	0.187	0.229	0.257	0.278	0.293	0.305	0.313
P(X=2)M	0	0.00901	0.0284	0.0506	0.0729	0.0942	0.114	0.132	0.148
P(X=3)M	0	0.000423	0.00282	0.00756	0.0143	0.0226	0.032	0.0421	0.0526
P(X=4)M	0	1.38E-05	0.000204	0.00084	0.00212	0.00416	0.00697	0.0105	0.0148
P(X=5)M	0	3.35E-07	1.15E-05	7.35E-05	0.000251	0.000614	0.00123	0.00214	0.0034
p=0.020									
M	4	16	32	48	64	80	96	112	128
P(X=0)M	0.862	0.638	0.533	0.49	0.459	0.432	0.405	0.381	0.359
P(X=1)M	0.0696	0.188	0.258	0.295	0.315	0.324	0.324	0.32	0.312
P(X=2)M	0	0.0278	0.0725	0.114	0.148	0.176	0.196	0.209	0.217
P(X=3)M	0	0.0026	0.0139	0.0315	0.0521	0.0731	0.0926	0.11	0.124
P(X=4)M	0	0.000171	0.00198	0.00669	0.0143	0.0243	0.0357	0.0475	0.0589
P(X=5)M	0	8.3E-06	0.00022	0.00114	0.00322	0.00669	0.0115	0.0174	0.024
p=0.040									
M	4	16	32	48	64	80	96	112	128
P(X=0)M	0.762	0.536	0.464	0.409	0.363	0.326	0.298	0.275	0.257
P(X=1)M	0.121	0.26	0.318	0.327	0.315	0.295	0.276	0.259	0.244
P(X=2)M	0	0.0717	0.148	0.196	0.218	0.224	0.221	0.215	0.208
P(X=3)M	0	0.013	0.051	0.0918	0.123	0.143	0.153	0.158	0.159
P(X=4)M	0	0.00169	0.0135	0.0346	0.0579	0.078	0.093	0.103	0.11
P(X=5)M	0	0.000164	0.00288	0.0108	0.0231	0.0368	0.0496	0.0604	0.069
p=0.060									
M	4	16	32	48	64	80	96	112	128
P(X=0)M	0.689	0.498	0.413	0.346	0.3	0.268	0.244	0.226	0.211
P(X=1)M	0.159	0.3	0.33	0.308	0.278	0.253	0.233	0.217	0.204
P(X=2)M	0	0.113	0.197	0.223	0.222	0.212	0.202	0.192	0.183
P(X=3)M	0	0.0293	0.0909	0.134	0.153	0.159	0.159	0.157	0.154
P(X=4)M	0	0.00555	0.0335	0.0674	0.0921	0.107	0.114	0.118	0.12
P(X=5)M	0	0.000798	0.0101	0.0289	0.0485	0.064	0.0749	0.0824	0.0875
p=0.080									
M	4	16	32	48	64	80	96	112	128
P(X=0)M	0.638	0.473	0.369	0.303	0.262	0.234	0.213	0.197	0.185
P(X=1)M	0.187	0.324	0.32	0.28	0.248	0.224	0.206	0.191	0.18
P(X=2)M	0	0.148	0.22	0.223	0.21	0.197	0.185	0.174	0.166
P(X=3)M	0	0.0486	0.122	0.153	0.16	0.158	0.154	0.15	0.145
P(X=4)M	0	0.0119	0.0556	0.0912	0.109	0.117	0.12	0.121	0.12
P(X=5)M	0	0.00223	0.0211	0.0474	0.0671	0.0794	0.0869	0.0915	0.0943

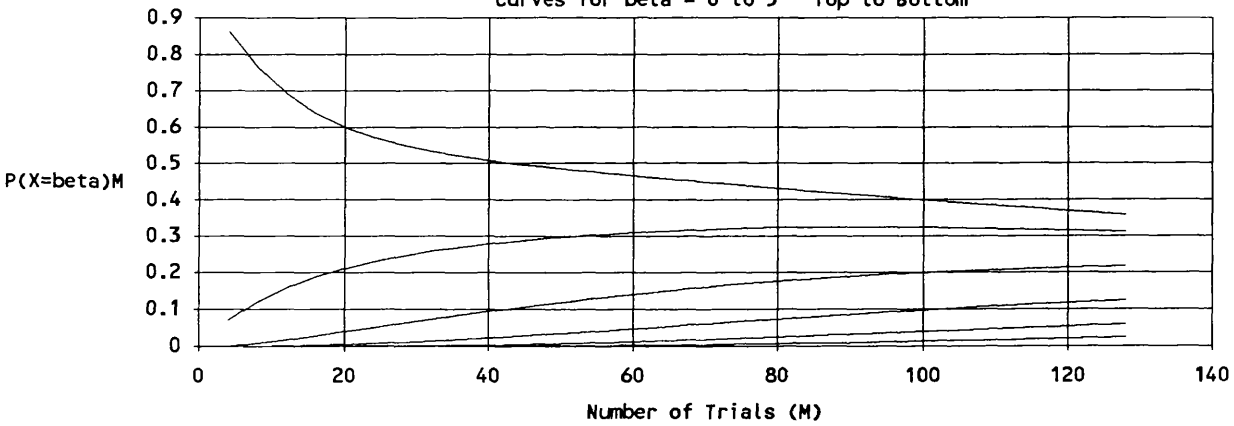
p=0.100									
M	4	16	32	48	64	80	96	112	128
P(X=0)M	0.603	0.448	0.335	0.273	0.236	0.211	0.193	0.178	0.167
P(X=1)M	0.205	0.336	0.303	0.257	0.226	0.204	0.187	0.174	0.163
P(X=2)M	0	0.177	0.227	0.215	0.198	0.183	0.171	0.161	0.153
P(X=3)M	0	0.0686	0.142	0.159	0.159	0.154	0.148	0.142	0.137
P(X=4)M	0	0.0202	0.0748	0.105	0.117	0.12	0.121	0.119	0.117
P(X=5)M	0	0.00463	0.0335	0.0619	0.0785	0.0877	0.0927	0.0953	0.0964
p=0.200									
M	4	16	32	48	64	80	96	112	128
P(X=0)M	0.527	0.352	0.249	0.204	0.176	0.158	0.144	0.133	0.125
P(X=1)M	0.231	0.317	0.238	0.197	0.172	0.155	0.142	0.131	0.123
P(X=2)M	0	0.232	0.205	0.179	0.16	0.146	0.135	0.126	0.119
P(X=3)M	0	0.138	0.161	0.152	0.142	0.132	0.124	0.118	0.112
P(X=4)M	0	0.0667	0.114	0.121	0.119	0.115	0.111	0.107	0.103
P(X=5)M	0	0.0254	0.0734	0.0902	0.0957	0.0968	0.0958	0.094	0.0919
p=0.300									
M	4	16	32	48	64	80	96	112	128
P(X=0)M	0.466	0.303	0.217	0.177	0.154	0.138	0.126	0.116	0.109
P(X=1)M	0.208	0.278	0.209	0.173	0.151	0.135	0.124	0.115	0.108
P(X=2)M	0	0.216	0.187	0.161	0.143	0.13	0.119	0.111	0.105
P(X=3)M	0	0.14	0.155	0.142	0.13	0.12	0.112	0.106	0.1
P(X=4)M	0	0.0739	0.119	0.119	0.114	0.108	0.103	0.0981	0.0937
P(X=5)M	0	0.0301	0.0842	0.0956	0.0967	0.0949	0.0922	0.0892	0.0862
p=0.400									
M	4	16	32	48	64	80	96	112	128
P(X=0)M	0.375	0.248	0.192	0.162	0.142	0.128	0.117	0.109	0.102
P(X=1)M	0.164	0.21	0.179	0.156	0.139	0.126	0.116	0.107	0.101
P(X=2)M	0	0.148	0.154	0.143	0.131	0.121	0.112	0.104	0.0983
P(X=3)M	0	0.0854	0.122	0.125	0.119	0.112	0.106	0.0996	0.0943
P(X=4)M	0	0.039	0.0881	0.103	0.104	0.102	0.0974	0.0931	0.089
P(X=5)M	0	0.0136	0.0575	0.0801	0.088	0.0893	0.0879	0.0854	0.0826
p=0.500									
M	4	16	32	48	64	80	96	112	128
P(X=0)M	0.27	0.14	0.0993	0.0812	0.0704	0.063	0.0575	0.0533	0.0498
P(X=1)M	0.109	0.0974	0.0779	0.067	0.0597	0.0545	0.0505	0.0472	0.0446
P(X=2)M	0	0.0553	0.0551	0.0515	0.0481	0.0452	0.0428	0.0407	0.0388
P(X=3)M	0	0.0251	0.0351	0.037	0.0368	0.036	0.035	0.034	0.033
P(X=4)M	0	0.00892	0.0199	0.0247	0.0267	0.0275	0.0276	0.0275	0.0273
P(X=5)M	0	0.00238	0.0101	0.0153	0.0183	0.02	0.0211	0.0216	0.0219

Probability ($P(X=\beta)M$) of Bin Cancellation Error (β) for Increasing Numbers of Trials (M) at $p=0.01$.

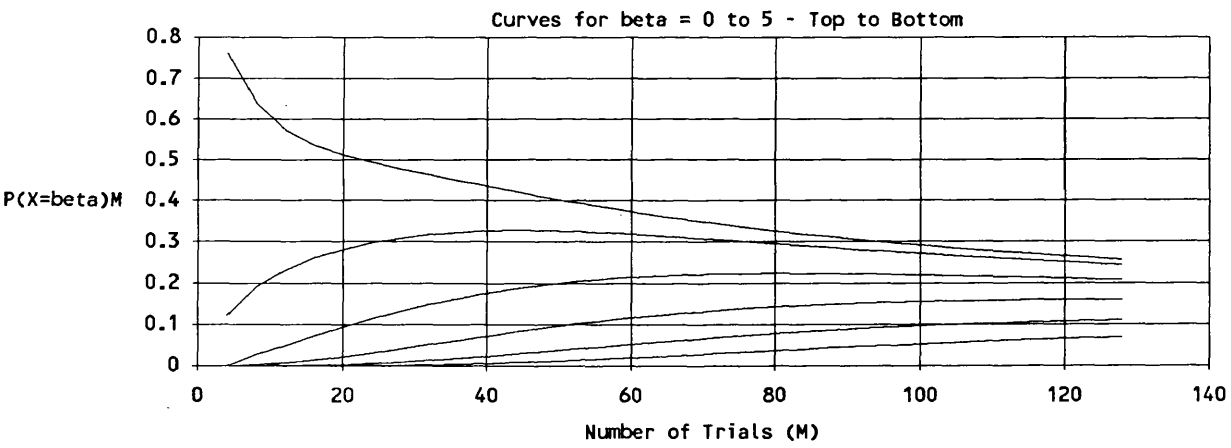


Probability $P(X=\beta)M$ of Bin Cancellation Error (β) for Increasing Numbers of Trials (M) at $p=0.02$.

Curves for $\beta = 0$ to 5 - Top to Bottom

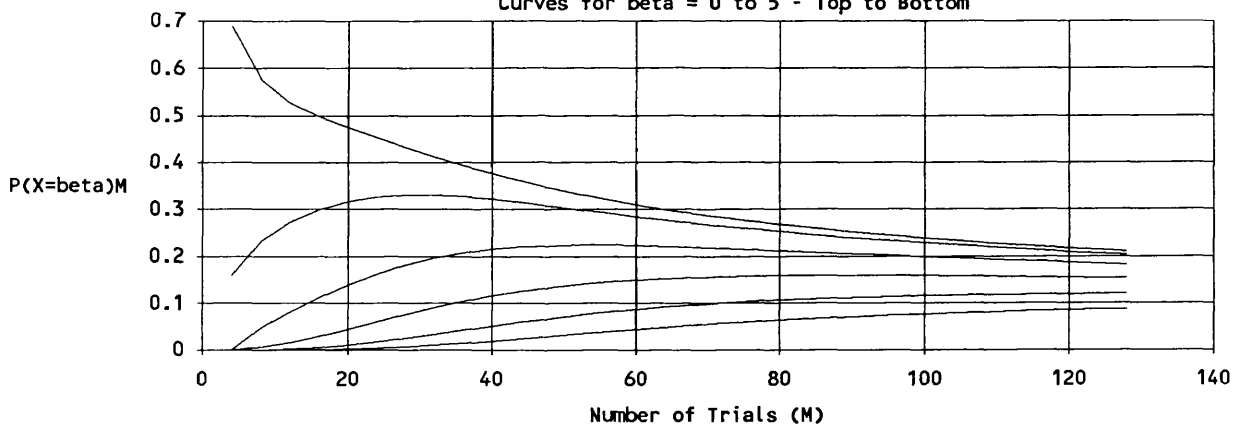


Probability ($P(X=\beta)M$) of Bin Cancellation Error (β) for Increasing Numbers of Trials (M) at $p=0.04$.



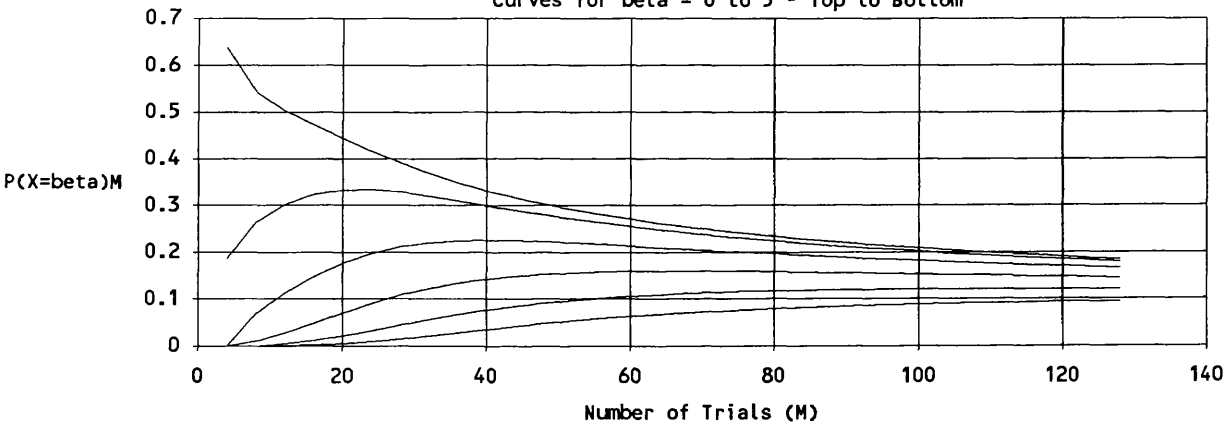
Probability $(P(X=\beta)M)$ of Bin Cancellation Error (β) for Increasing Numbers of Trials (M) at $p=0.06$.

Curves for $\beta = 0$ to 5 - Top to Bottom



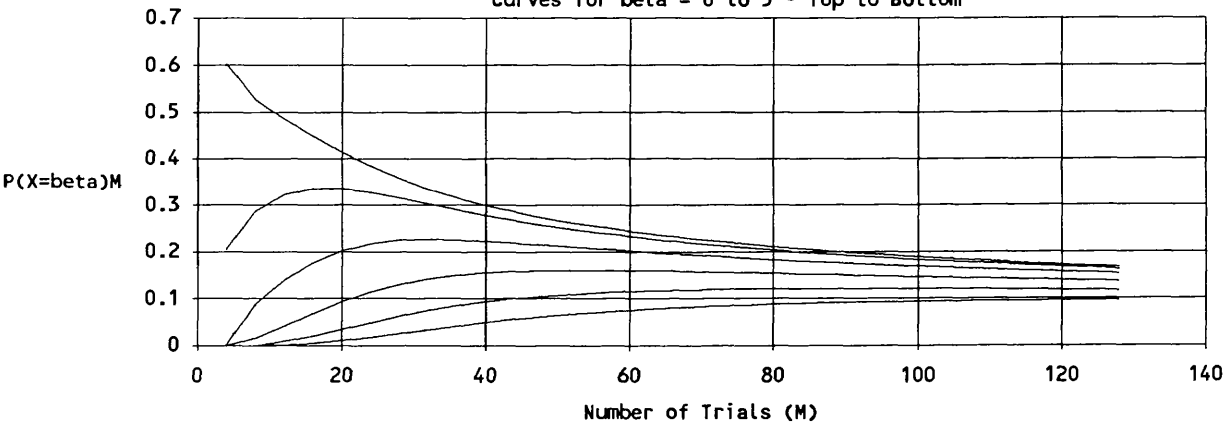
Probability ($P(X=\beta)M$) of Bin Cancellation Error (β) for Increasing Numbers of Trials (M) at $p=0.08$.

Curves for $\beta = 0$ to 5 - Top to Bottom

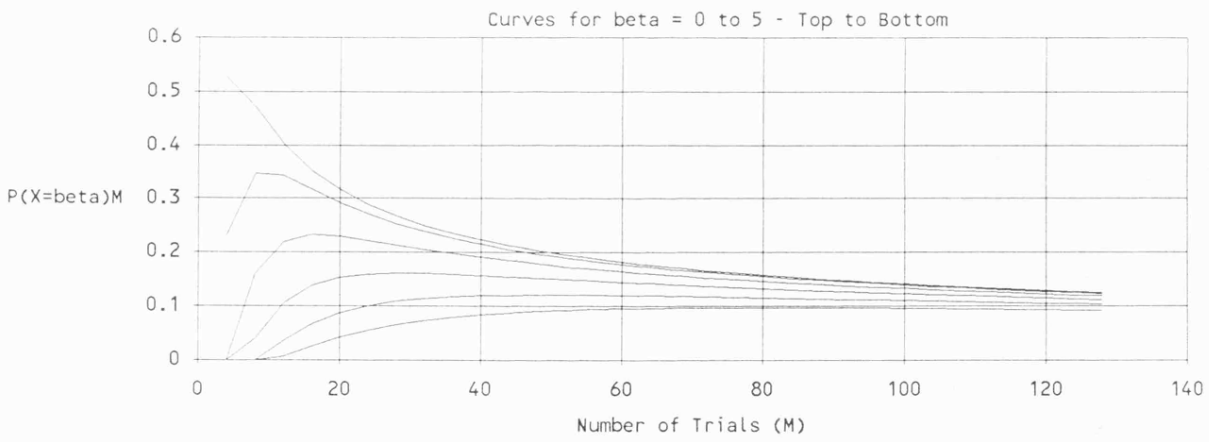


Probability ($P(X=\beta)M$) of Bin Cancellation Error (β) for Increasing Numbers of Trials (M) at $p=0.10$.

Curves for $\beta = 0$ to 5 - Top to Bottom

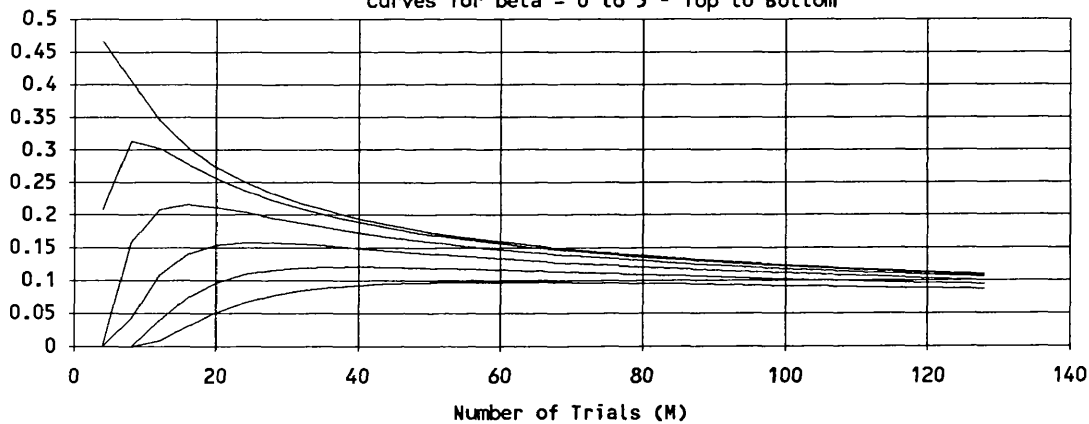


Probability $P(X=\beta)M$ of Bin Cancellation Error (β) for Increasing Numbers of Trials (M) at $p=0.20$.



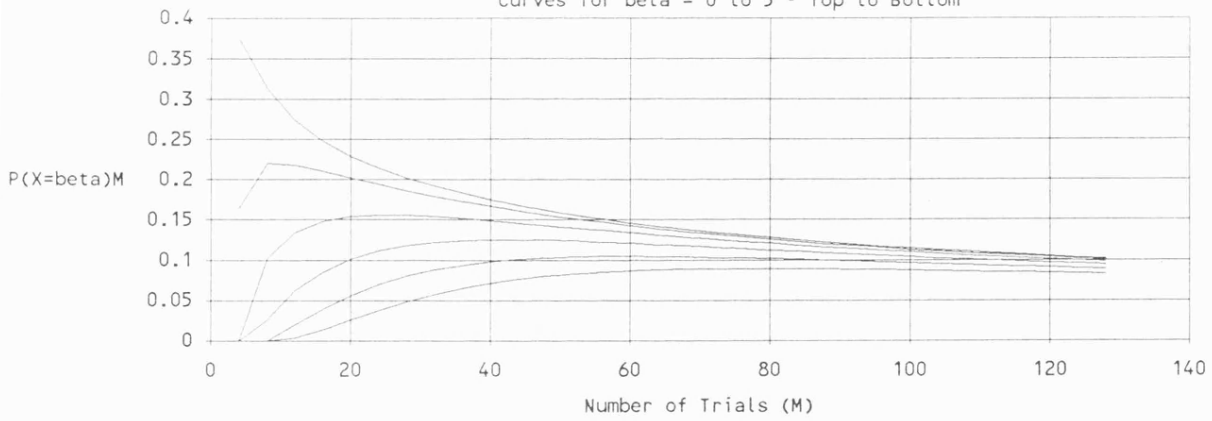
Probability ($P(X=\beta)M$) of Bin Cancellation Error (β) for Increasing Numbers of Trials (M) at $p=0.30$.

Curves for $\beta = 0$ to 5 - Top to Bottom



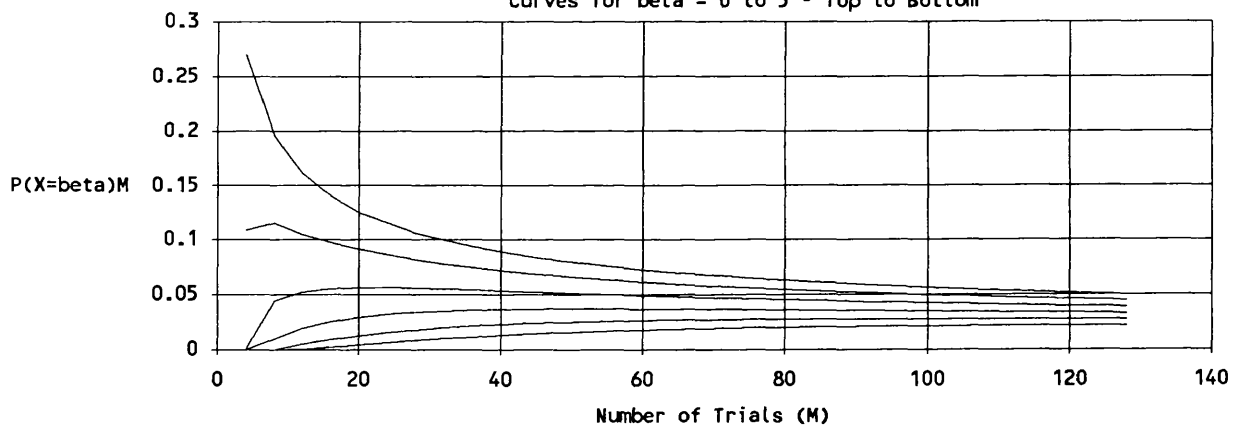
Probability ($P(X=\beta)M$) of Bin Cancellation Error (β) for Increasing Numbers of Trials (M) at $p=0.40$.

Curves for $\beta = 0$ to 5 - Top to Bottom



Probability ($P(X=\beta)M$) of Bin Cancellation Error (β) for Increasing Numbers of Trials (M) at $p=0.50$.

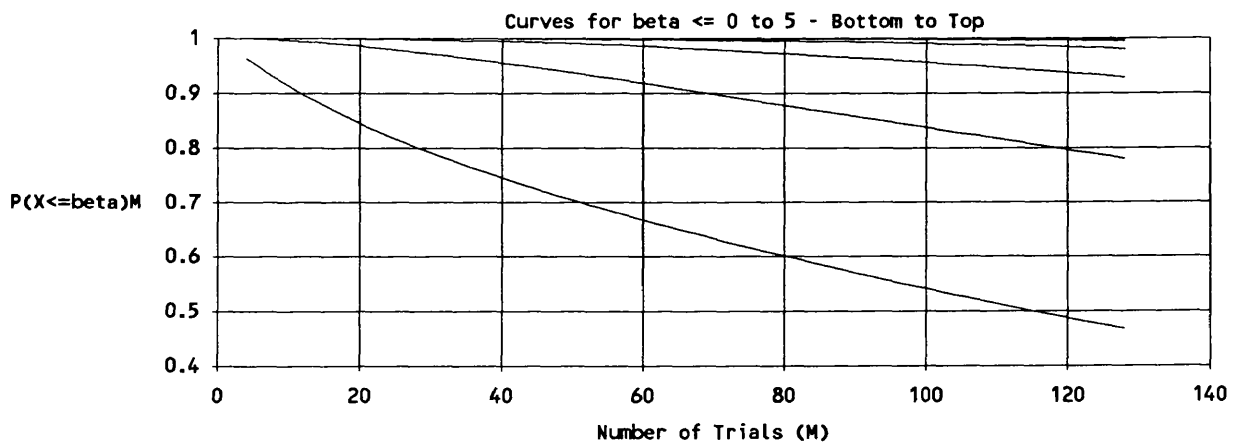
Curves for $\beta = 0$ to 5 - Top to Bottom



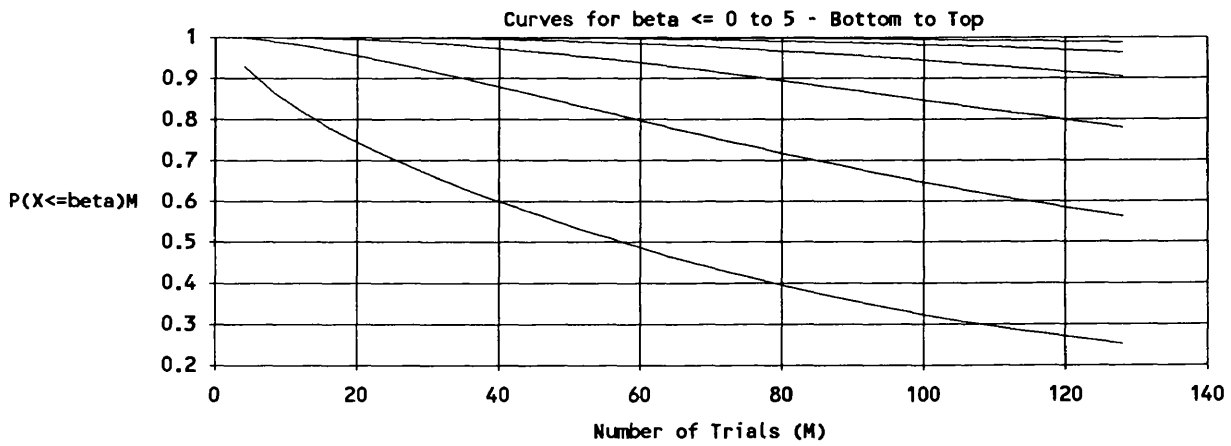
Probability (P(X<=beta)M) of Bin Cancellation Error (beta) for Increasing Numbers of Trials (M) at Different Event Probabilities p.									
p=0.010									
M	4	16	32	48	64	80	96	112	128
P(X<=0)M	0.963	0.871	0.781	0.712	0.653	0.601	0.552	0.508	0.467
P(X<=1)M	1	0.991	0.969	0.941	0.91	0.878	0.846	0.813	0.78
P(X<=2)M	1	1	0.997	0.992	0.983	0.973	0.96	0.945	0.928
P(X<=3)M	1	1	1	0.999	0.998	0.995	0.992	0.987	0.981
P(X<=4)M	1	1	1	1	1	0.999	0.999	0.997	0.996
P(X<=5)M	1	1	1	1	1	1	1	1	0.999
p=0.020									
M	4	16	32	48	64	80	96	112	128
P(X<=0)M	0.93	0.781	0.653	0.552	0.466	0.395	0.336	0.289	0.252
P(X<=1)M	1	0.969	0.911	0.847	0.781	0.718	0.661	0.609	0.564
P(X<=2)M	1	0.997	0.984	0.96	0.93	0.894	0.856	0.818	0.781
P(X<=3)M	1	1	0.998	0.992	0.982	0.967	0.949	0.928	0.905
P(X<=4)M	1	1	1	0.999	0.996	0.991	0.984	0.975	0.964
P(X<=5)M	1	1	1	1	0.999	0.998	0.996	0.993	0.988
p=0.040									
M	4	16	32	48	64	80	96	112	128
P(X<=0)M	0.879	0.653	0.466	0.335	0.252	0.2	0.169	0.148	0.135
P(X<=1)M	1	0.913	0.784	0.663	0.567	0.496	0.444	0.407	0.379
P(X<=2)M	1	0.985	0.932	0.859	0.785	0.719	0.665	0.622	0.586
P(X<=3)M	1	0.998	0.983	0.951	0.908	0.862	0.819	0.78	0.746
P(X<=4)M	1	1	0.997	0.986	0.966	0.94	0.911	0.883	0.856
P(X<=5)M	1	1	0.999	0.996	0.989	0.977	0.961	0.943	0.925
p=0.060									
M	4	16	32	48	64	80	96	112	128
P(X<=0)M	0.841	0.552	0.335	0.223	0.169	0.142	0.126	0.117	0.112
P(X<=1)M	1	0.851	0.665	0.531	0.447	0.395	0.359	0.334	0.316
P(X<=2)M	1	0.964	0.862	0.754	0.669	0.607	0.561	0.526	0.499
P(X<=3)M	1	0.994	0.953	0.888	0.822	0.766	0.72	0.683	0.653
P(X<=4)M	1	0.999	0.987	0.956	0.915	0.873	0.835	0.801	0.773
P(X<=5)M	1	1	0.997	0.985	0.963	0.937	0.91	0.884	0.86
p=0.080									
M	4	16	32	48	64	80	96	112	128
P(X<=0)M	0.813	0.465	0.252	0.17	0.136	0.121	0.112	0.109	0.108
P(X<=1)M	1	0.789	0.572	0.45	0.384	0.345	0.318	0.3	0.288
P(X<=2)M	1	0.937	0.792	0.673	0.595	0.541	0.503	0.474	0.453
P(X<=3)M	1	0.986	0.914	0.826	0.754	0.699	0.657	0.624	0.598
P(X<=4)M	1	0.997	0.97	0.918	0.863	0.816	0.777	0.745	0.718
P(X<=5)M	1	1	0.991	0.965	0.931	0.896	0.864	0.836	0.812

p=0.100									
M	4	16	32	48	64	80	96	112	128
P(X<=0)M	0.795	0.392	0.201	0.143	0.121	0.112	0.108	0.109	0.112
P(X<=1)M	1	0.729	0.504	0.401	0.347	0.315	0.295	0.282	0.275
P(X<=2)M	1	0.906	0.731	0.616	0.545	0.499	0.466	0.444	0.428
P(X<=3)M	1	0.974	0.873	0.775	0.704	0.652	0.614	0.586	0.565
P(X<=4)M	1	0.994	0.948	0.88	0.821	0.773	0.735	0.705	0.682
P(X<=5)M	1	0.999	0.981	0.942	0.899	0.86	0.828	0.8	0.778
p=0.200									
M	4	16	32	48	64	80	96	112	128
P(X<=0)M	0.769	0.212	0.127	0.109	0.108	0.117	0.13	0.146	0.163
P(X<=1)M	1	0.529	0.364	0.306	0.28	0.271	0.272	0.277	0.286
P(X<=2)M	1	0.761	0.569	0.485	0.44	0.417	0.406	0.403	0.405
P(X<=3)M	1	0.9	0.73	0.637	0.582	0.549	0.531	0.521	0.516
P(X<=4)M	1	0.966	0.844	0.758	0.701	0.665	0.642	0.627	0.619
P(X<=5)M	1	0.992	0.917	0.848	0.797	0.761	0.738	0.721	0.711
p=0.300									
M	4	16	32	48	64	80	96	112	128
P(X<=0)M	0.792	0.252	0.129	0.11	0.119	0.138	0.161	0.184	0.206
P(X<=1)M	1	0.53	0.338	0.283	0.27	0.274	0.285	0.299	0.314
P(X<=2)M	1	0.746	0.525	0.443	0.413	0.404	0.404	0.41	0.419
P(X<=3)M	1	0.886	0.68	0.586	0.543	0.524	0.517	0.516	0.519
P(X<=4)M	1	0.96	0.799	0.705	0.657	0.632	0.62	0.614	0.613
P(X<=5)M	1	0.99	0.883	0.801	0.754	0.727	0.712	0.703	0.699
p=0.400									
M	4	16	32	48	64	80	96	112	128
P(X<=0)M	0.836	0.5	0.335	0.245	0.203	0.193	0.201	0.217	0.236
P(X<=1)M	1	0.71	0.514	0.401	0.342	0.319	0.316	0.324	0.337
P(X<=2)M	1	0.858	0.669	0.544	0.473	0.44	0.428	0.428	0.435
P(X<=3)M	1	0.944	0.791	0.669	0.593	0.552	0.533	0.528	0.53
P(X<=4)M	1	0.983	0.879	0.772	0.697	0.653	0.631	0.621	0.619
P(X<=5)M	1	0.996	0.937	0.852	0.785	0.743	0.719	0.707	0.701
p=0.500									
M	4	16	32	48	64	80	96	112	128
P(X<=0)M	0.891	0.81	0.795	0.788	0.784	0.782	0.781	0.782	0.783
P(X<=1)M	1	0.908	0.873	0.855	0.843	0.836	0.832	0.829	0.827
P(X<=2)M	1	0.963	0.928	0.906	0.892	0.882	0.875	0.87	0.866
P(X<=3)M	1	0.988	0.963	0.943	0.928	0.918	0.91	0.903	0.899
P(X<=4)M	1	0.997	0.983	0.968	0.955	0.945	0.937	0.931	0.926
P(X<=5)M	1	1	0.993	0.983	0.973	0.965	0.958	0.953	0.948

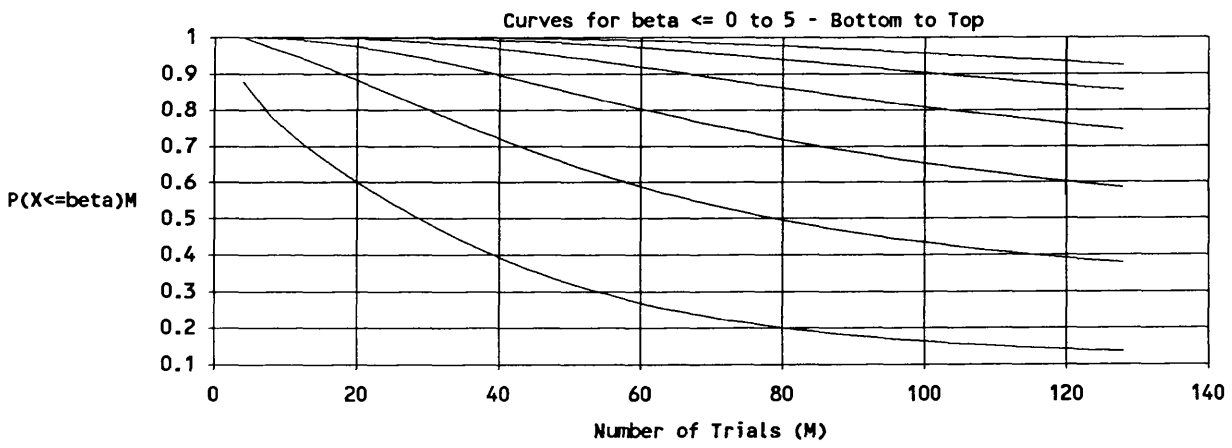
Probability $P(X \leq \beta)M$ of Bin Cancellation Error (β) for Increasing Numbers of Trials (M) at $p=0.01$.



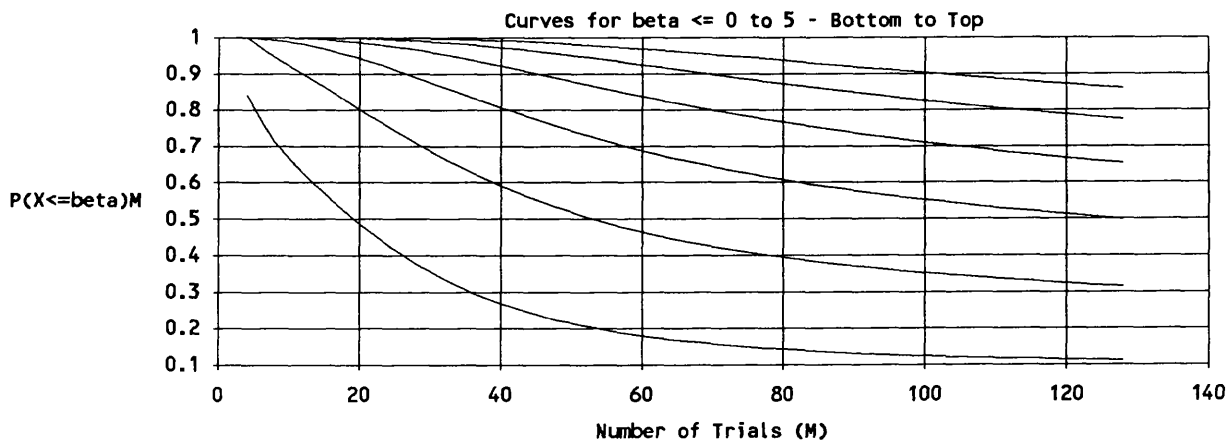
Probability ($P(X \leq \beta)M$) of Bin Cancellation Error (β) for Increasing Numbers of Trials (M) at $p=0.02$.



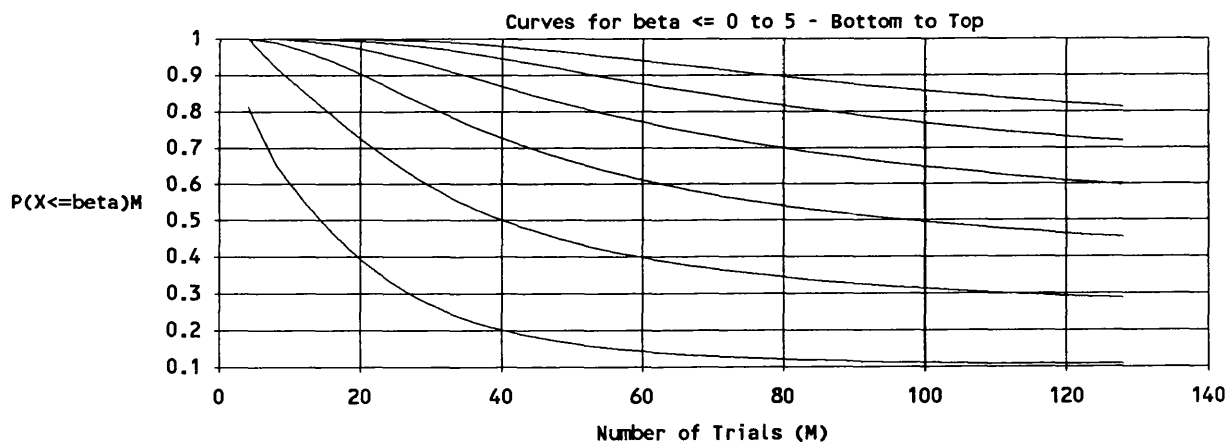
Probability ($P(X \leq \beta)M$) of Bin Cancellation Error (β) for Increasing Numbers of Trials (M) at $p=0.04$.



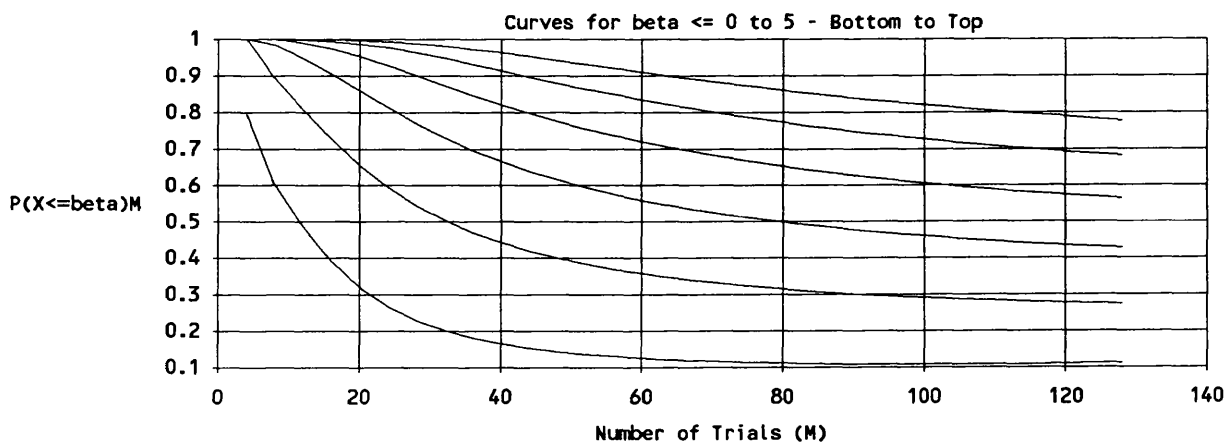
Probability ($P(X \leq \beta)M$) of Bin Cancellation Error (β) for Increasing Numbers of Trials (M) at $p=0.06$.



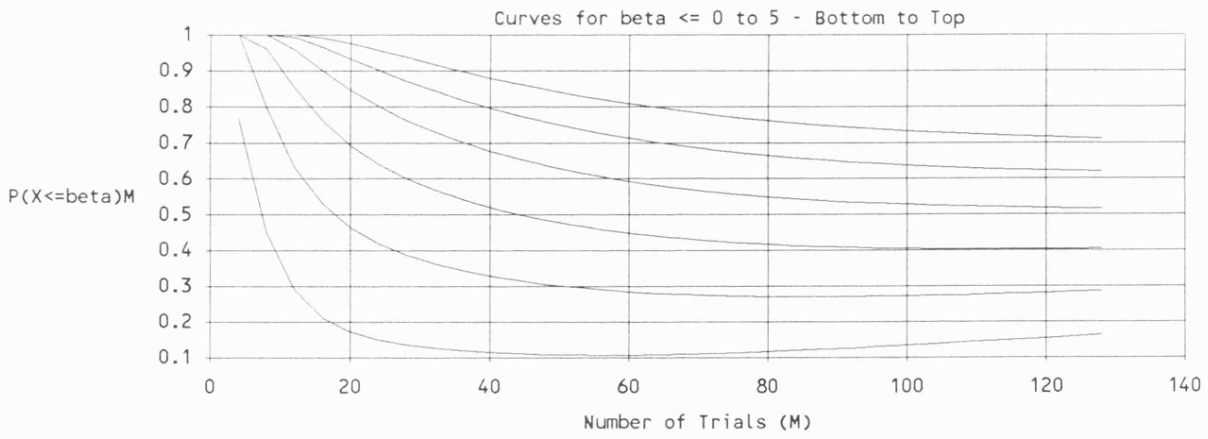
Probability $P(X \leq \beta)M$ of Bin Cancellation Error (β) for Increasing Numbers of Trials (M) at $p=0.08$.



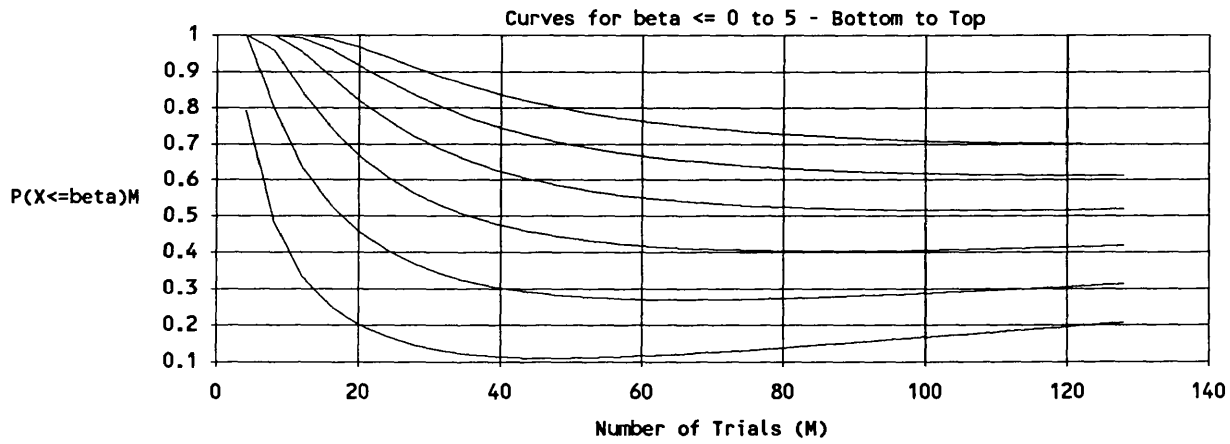
Probability $P(X \leq \beta)M$ of Bin Cancellation Error (β) for Increasing Numbers of Trials (M) at $p=0.10$.



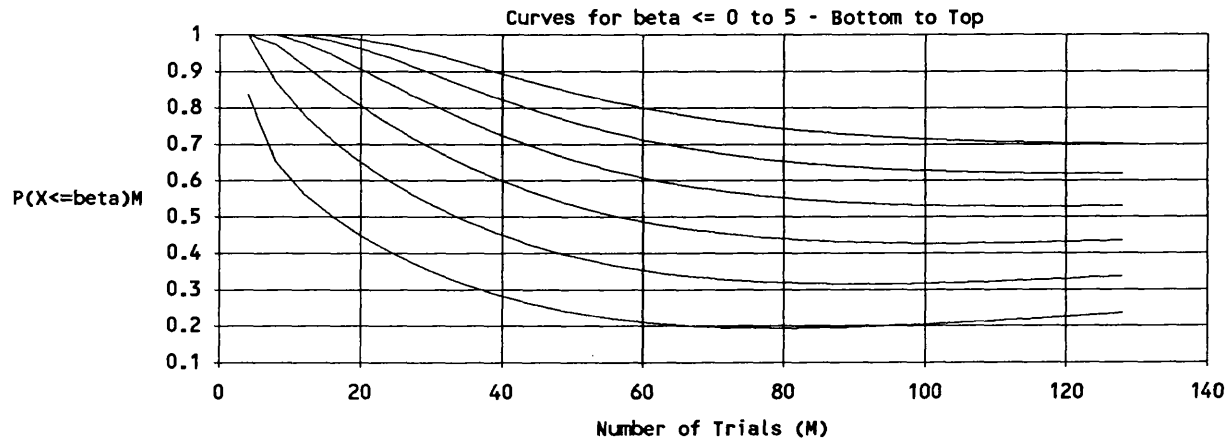
Probability $P(X \leq \beta)M$ of Bin Cancellation Error (β) for Increasing Numbers of Trials (M) at $p=0.20$.



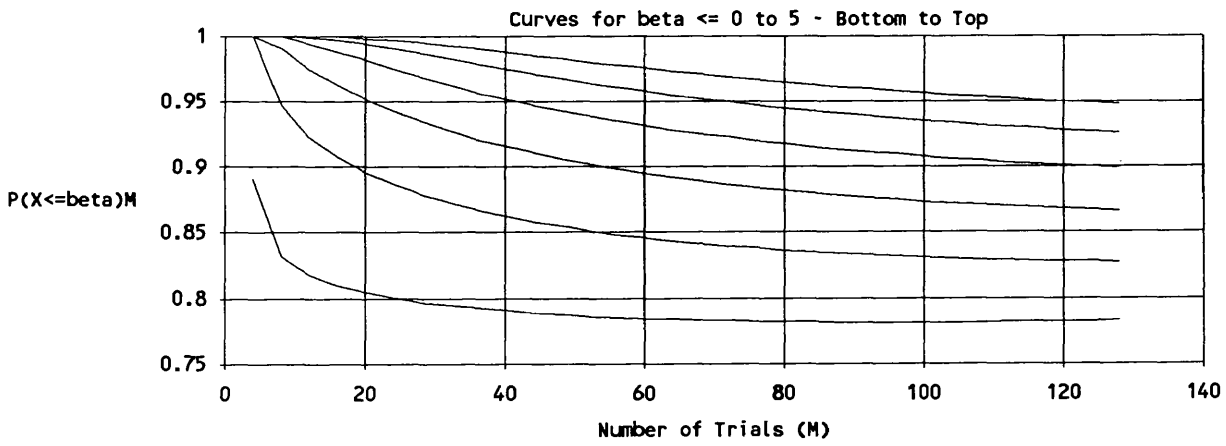
Probability ($P(X \leq \beta)M$) of Bin Cancellation Error (β) for Increasing Numbers of Trials (M) at $p=0.30$.



Probability ($P(X \leq \beta)M$) of Bin Cancellation Error (β) for Increasing Numbers of Trials (M) at $p=0.40$.



Probability $P(X \leq \beta)M$ of Bin Cancellation Error (β) for Increasing Numbers of Trials (M) at $p=0.50$.



Appendix [D4]

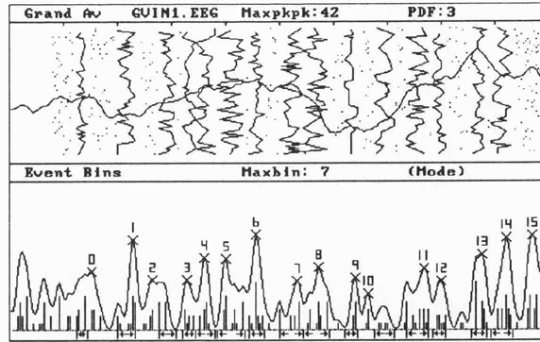
Event Analysis: Results for Latency Variability Recovery Experiments

Attribute Definitions for Event Analysis Result Tables

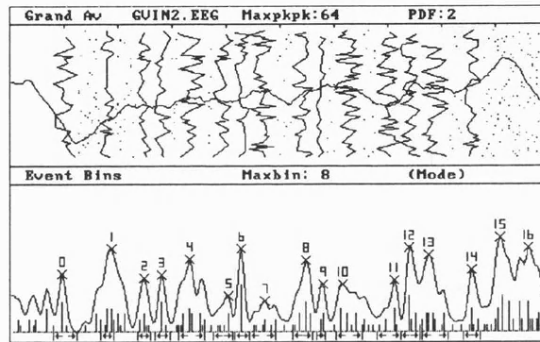
- **Item Nº**
Index number equivalent to the number of trajectories or BIN/GAV peaks
- **GPkAmpl**
Amplitude of peak in the GAV (1 unit = 25 nV)
- **GPkLat**
Latency of peak in the GAV (ms)
- **BPkAmpl**
Amplitude of smoothed peak in the BIN (arbitrary units)
- **BPkLat**
Latency of smoothed peak in the BIN (ms)
- **Mn**
Mean latency value of events in a trajectory (ms)
- **SD**
Standard deviation of latency of events in a trajectory (ms)
- **O**
Total number of observed events (after compression) in a trajectory
- **E**
Total number of expected events in a trajectory = (Span x Local event probability)
- **ChiSq**
 χ^2 statistic = $(O - E)^2 / E$
- **ChSqP**
Probability of χ^2 statistic with one degree of freedom
- **BinomP**
Binomial probability of finding an event in a trajectory
- **%Swps**
Percentage of trials containing an event in a trajectory
- **CC**
Compression coefficient = $1.0 - \{ (\text{Actual Number of Observed Events} - O) / \text{Actual Number of Observed Events} \}$.
- **Span**
Width of the region occupied by a trajectory after iterative convergence to the mean latency of 95% of the population of trajectory events.

[1] EVENT ANALYSIS RESULTS FOR NOISE DATA FILES														
[1A] Event Probabilities: Noise File VIN1.EEG Image Data Set Name GVIN1.EEG														
Max GPKs possible (uniform) : 12925														
Total GPKs found : 684														
Global Probability of Pk : 0.05														
Max LPks possible (uniform) : 8128														
Total LPks found : 512														
Local Probability of Pk : 0.06														
Max InterPks poss. (uniform) : 4500														
Total InterPks found : 172														
Inter Probability of Pk : 0.04														
ItemNum	GPKAmpl	GPKLat	BPKAmpl	BPKLat	Mn	SD	O	E	ChiSq	ChSqP	BinomP	%Swps	CC	Span
0	-441	0.92	6651	1.52	1.33	0.06	29	20	5.66	0.02	0	45.31	0.88	5
1	-441	1.48	10172	2.28	2.17	0.11	35	32	0.47	0.49	0	54.69	0.81	8
2	5675	4.6	5663	2.64	2.93	0.1	33	32	0.03	0.85	0	51.56	0.89	8
3	3696	5.2	5639	3.28	3.33	0.07	27	24	0.53	0.47	0	42.19	0.97	6
4	-11149	6.32	8181	3.6	3.62	0.11	32	36	1.17	0.28	0	50	0.89	9
5	16384	8.88	8030	4	4.1	0.15	44	52	7.45	0.01	0	68.75	0.85	13
6	6732	9.24	10809	4.56	4.58	0.07	36	28	3.94	0.05	0	56.25	0.84	7
7	0	0	5509	5.32	5.23	0.13	42	44	0.4	0.52	0	65.63	0.74	11
8	0	0	7079	5.72	5.66	0.15	39	48	7.45	0.01	0	60.94	0.81	12
9	0	0	5925	6.4	6.31	0.09	22	24	0.32	0.57	0	34.38	0.88	6
10	0	0	4040	6.64	6.94	0.11	32	36	1.17	0.28	0	50	0.89	9
11	0	0	7009	7.68	7.55	0.13	38	40	0.36	0.55	0	59.38	0.95	10
12	0	0	5529	8	7.96	0.07	32	24	4.05	0.04	0	50	0.97	6
13	0	0	8468	8.76	8.7	0.08	35	28	2.91	0.09	0	54.69	0.81	7
14	0	0	10480	9.2	9.12	0.12	35	40	1.89	0.17	0	54.69	0.92	10
[1B] Event Probabilities: Noise File VIN2.EEG Image Data Set Name GVIN2.EEG														
Max GPKs possible (uniform) : 12672														
Total GPKs found : 572														
Global Probability of Pk : 0.05														
Max LPks possible (uniform) : 8640														
Total LPks found : 450														
Local Probability of Pk : 0.05														
Max InterPks poss. (uniform) : 4032														
Total InterPks found : 122														
Inter Probability of Pk : 0.03														
ItemNum	GPKAmpl	GPKLat	BPKAmpl	BPKLat	Mn	SD	O	E	ChiSq	ChSqP	BinomP	%Swps	CC	Span
0	-2240	2.2	8503	0.96	1.02	0.13	28	37	4.8	0.03	0	43.75	0.88	11
1	-2441	2.48	12312	1.88	1.81	0.09	28	20	4.65	0.03	0	43.75	0.97	6
2	396	3.32	7952	2.48	2.48	0.07	25	20	1.82	0.18	0	39.06	1	6
3	-274	3.76	8445	2.8	2.82	0.08	25	23	0.19	0.67	0	39.06	0.93	7
4	2608	4.52	10752	3.32	3.35	0.15	37	40	0.6	0.44	0	57.81	0.77	12
5	4872	5.88	5362	4.04	3.95	0.11	25	30	1.57	0.21	0	39.06	0.86	9
6	4381	6.2	12358	4.28	4.3	0.08	25	23	0.19	0.67	0	39.06	0.93	7
7	5446	7.52	4585	4.72	4.68	0.14	34	40	2.4	0.12	0	53.13	0.83	12
8	13765	9.24	10548	5.48	5.43	0.11	29	30	0.06	0.8	0	45.31	0.88	9
9	0	0	7044	5.8	5.75	0.05	20	13	4.21	0.04	0	31.25	0.91	4
10	0	0	7057	6.16	6.28	0.14	41	40	0.07	0.8	0	64.06	0.85	12
11	0	0	7579	7.12	7.02	0.14	33	37	0.86	0.35	0	51.56	0.82	11
12	0	0	12505	7.4	7.41	0.11	36	30	2.26	0.13	0	56.25	0.86	9
13	0	0	11346	7.76	7.87	0.16	31	40	5.4	0.02	0	48.44	0.84	12
14	0	0	9119	8.56	8.56	0.1	29	27	0.35	0.55	0	45.31	0.97	8

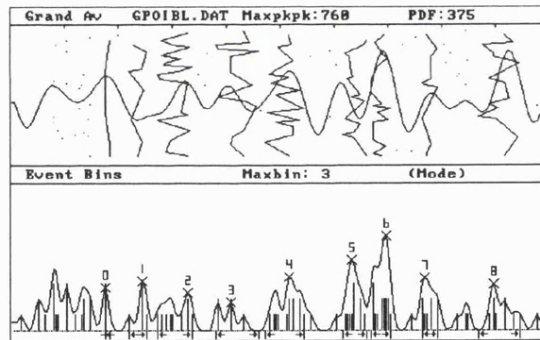
[1C] Event Probabilities: Noise File POIBLDAT Image Data Set Name GPOIBLDAT															
Max GPKs possible (uniform) : 12289															
Total GPKs found : 147															
Global Probability of Pk : 0.01															
Max LPks possible (uniform) : 7040															
Total LPks found : 125															
Local Probability of Pk : 0.02															
Max InterPks poss. (uniform) : 5248															
Total InterPks found : 22															
Inter Probability of Pk : 0.00															
ItemNum	GPKAmpI	GPKLat	BPkAmpI	BPkLat	Mn	SD	O	E	ChiSq	ChSqP	BinomP	%Swps	CC	Span	
0	7289	1.8	7454	1.76	1.79	0.04	0	5	2	0.12	0.73	0	7.81	1	2
1	5429	3.24	8620	2.44	2.38	0.11	9	9	0	0.97	0	14.06	1	5	
2	3983	4.04	6477	3.28	3.03	0.23	19	18	0.05	0.62	0	29.69	1	16	
3	8759	5.16	4979	4.08	4.2	0.25	15	23	4.07	0.04	0	23.44	1	20	
4	4937	6.12	9257	5.16	5.07	0.21	19	20	0.15	0.7	0	29.69	1	18	
5	15276	6.92	12110	6.32	6.37	0.14	15	13	0.62	0.43	0	23.44	1	11	
6	1513	7.9	16394	6.96	6.95	0.12	19	10	8.96	0	0	29.69	1	9	
7	-1192	8.44	9138	7.68	7.76	0.1	10	8	0.6	0.44	0	15.63	1	7	
8	15219	9.24	8092	8.96	9.06	0.22	14	22	4.03	0.04	0	21.88	1	19	
[1D] Event Probabilities: Noise File GASBLDAT Image Data Set Name GGASBLDAT															
Max GPKs possible (uniform) : 14080															
Total GPKs found : 192															
Global Probability of Pk : 0.01															
Max LPks possible (uniform) : 9536															
Total LPks found : 180															
Local Probability of Pk : 0.02															
Max InterPks poss. (uniform) : 4544															
Total InterPks found : 12															
Inter Probability of Pk : 0.00															
ItemNum	GPKAmpI	GPKLat	BPkAmpI	BPkLat	Mn	SD	O	E	ChiSq	ChSqP	BinomP	%Swps	CC	Span	
0	16165	0.84	16384	1	0.96	0.1	16	10	4.89	0.03	0	25	1	8	
1	5705	1.64	7172	1.48	1.56	0.18	11	17	2.81	0.09	0	17.19	1	14	
2	2239	3.6	15431	2.24	2.28	0.07	14	7	7.09	0.01	0	21.88	1	6	
3	9035	4.4	8829	2.88	2.89	0.06	8	6	0.7	0.4	0	12.5	1	5	
4	16384	5.2	12133	3.2	3.42	0.22	22	21	0.15	0.7	0	34.38	1	17	
5	8952	7.04	10138	4.56	4.4	0.16	14	16	0.25	0.62	0	21.88	1	13	
6	6686	7.88	8154	5.52	5.29	0.23	20	23	0.59	0.44	0	31.25	1	19	
7	2700	8.76	7080	5.92	6.12	0.21	14	19	2.1	0.15	0	21.88	1	16	
8	5954	9.56	10237	6.96	6.83	0.16	14	16	0.25	0.62	0	21.88	1	13	
9	0	0	8921	7.32	7.39	0.12	12	11	0.14	0.71	0	18.75	1	9	
10	0	0	10138	8.44	8.5	0.22	20	22	0.21	0.65	0	31.25	1	18	
11	0	0	9069	9.44	9.35	0.15	15	13	0.28	0.6	0	23.44	1	11	



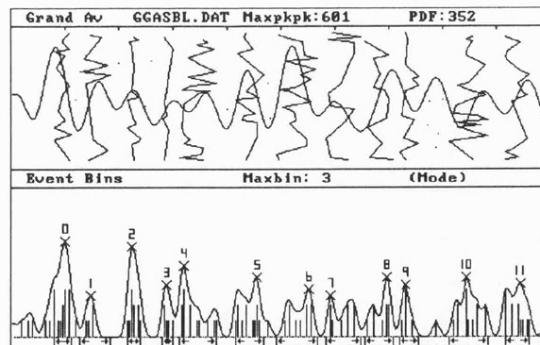
(a) Spontaneous EEG (1 response/sub-average)



(b) Spontaneous EEG (2 responses/sub-average)



(c) Band-limited random Poisson noise

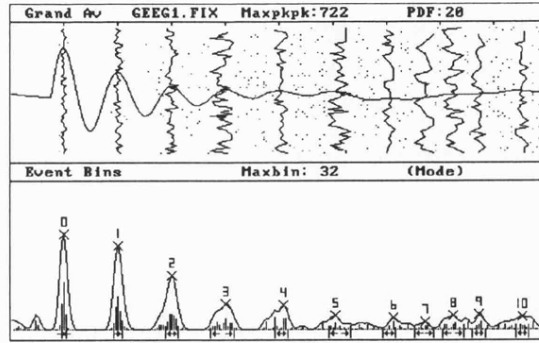


(d) Band-limited random gaussian noise

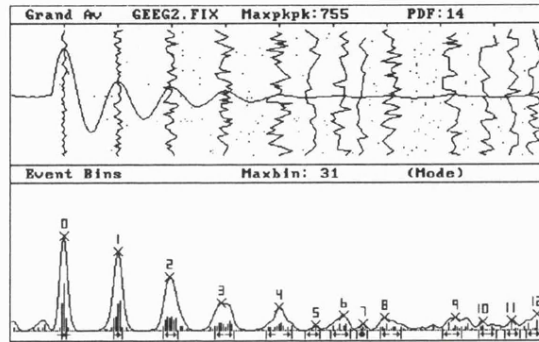
Trajectory maps obtained for the noise data sets used in the component latency variability recovery experiments.

[2] EVENT ANALYSIS RESULTS FOR FIXED LATENCY SIGNAL + NOISE DATA FILES																
[2A] Event Probabilities: Noise File VIN1.EEG Image Data Set Name GEEG1.FIX																
Max GPKs possible (uniform) : 13888																
Total GPKs found : 727																
Global Probability of Pk : 0.05																
Max LPks possible (uniform) : 4864																
Total LPks found : 455																
Local Probability of Pk : 0.09																
Max InterPks poss. (uniform) : 9024																
Total InterPks found : 272																
Inter Probability of Pk : 0.03																
ItemNum	GPKAmpI	GPKLat	BPKAmpI	BPKLat	Mn	SD	O	E	ChiSq	ChSqP	BinomP	%Swps	CC	Span		
0	16384	1	16384	1	1	0.03	59	12	227.2	0	0	92.19	1	2		
1	7975	2	14405	2	2	0.04	59	24	81.98	0	0	92.19	0.98	4		
2	2996	3	9303	3	3	0.06	52	36	16.4	0	0	81.25	0.93	6		
3	1893	4.04	4408	4	3.95	0.13	49	64	3.52	0.06	0	76.56	0.86	11		
4	1361	5	4214	5.08	5.04	0.07	39	36	0.6	0.44	0	60.94	0.85	6		
5	1081	6	2282	6.04	6.12	0.12	39	60	112.68	0	0	60.94	0.8	10		
6	-1335	7.08	2071	7.12	7.04	0.07	27	36	5.05	0.02	0	42.19	0.87	6		
7	120	8.16	1256	7.72	7.71	0.11	29	54	72.67	0	0	45.31	0.98	9		
8	1548	9.44	2308	8.24	8.24	0.12	38	60	123.74	0	0	59.38	0.93	10		
9	0	0	2606	8.72	8.72	0.07	32	36	0.98	0.32	0	50	0.91	6		
10	0	0	2175	9.52	9.52	0.07	32	36	0.98	0.32	0	50	0.78	6		
[2B] Event Probabilities: Noise File VIN2.EEG Image Data Set Name GEEG2.FIX																
Max GPKs possible (uniform) : 14272																
Total GPKs found : 597																
Global Probability of Pk : 0.04																
Max LPks possible (uniform) : 6144																
Total LPks found : 461																
Local Probability of Pk : 0.08																
Max InterPks poss. (uniform) : 8128																
Total InterPks found : 136																
Inter Probability of Pk : 0.02																
ItemNum	GPKAmpI	GPKLat	BPKAmpI	BPKLat	Mn	SD	O	E	ChiSq	ChSqP	BinomP	%Swps	CC	Span		
0	16384	1	16384	1	0.99	0.03	57	10	275.19	0	0	89.06	1	2		
1	5214	2	13636	2	2	0.04	56	19	100.69	0	0	87.5	0.98	4		
2	3364	3	9294	2.96	2.98	0.08	53	34	23.55	0	0	82.81	0.98	7		
3	1978	4	4778	3.92	3.98	0.1	44	43	0.04	0.83	0	68.75	0.9	9		
4	717	5.04	3949	5	5	0.14	39	58	60.43	0	0	60.94	0.85	12		
5	355	6.12	919	5.68	5.61	0.08	17	34	17.3	0	0	26.56	0.85	7		
6	273	7	2568	6.2	6.14	0.11	27	43	18.74	0	0	42.19	0.96	9		
7	742	8.24	1108	6.56	6.53	0.06	19	24	1.67	0.2	0	29.69	0.95	5		
8	-30	9.36	2120	6.96	7.07	0.12	35	48	14.14	0	0	54.69	0.9	10		
9	0	0	2114	8.28	8.21	0.11	34	43	6.06	0.01	0	53.13	0.81	9		
10	0	0	1411	8.8	8.86	0.1	25	38	11.72	0	0	39.06	0.93	8		
11	0	0	1726	9.32	9.34	0.08	24	34	5.79	0.02	0	37.5	0.89	7		
12	0	0	2687	9.8	9.74	0.08	31	34	0.43	0.51	0	46.44	0.86	7		

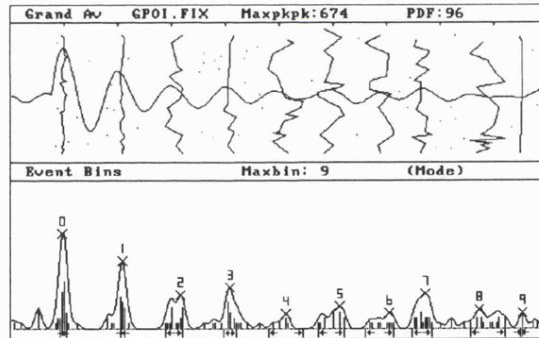
[2C] Event Probabilities: Noise File POIBL.DAT Image Data Set Name GPOL.FIX															
Max GPKs possible (uniform) : 13760															
Total GPKs found : 189															
Global Probability of Pk : 0.01															
Max LPks possible (uniform) : 5504															
Total LPks found : 148															
Local Probability of Pk : 0.03															
Max InterPks poss. (uniform) : 8256															
Total InterPks found : 41															
Inter Probability of Pk : 0.00															
ItemNum	GPKAmpl	GPKLat	BPKAmpl	BPKLat	Mn	SD	O	E	ChiSq	ChSqP	BinomP	%Swps	CC	Span	
0	16384	1	16384	0.96	0.98	0.03	21	5	52.84	0	0	32.81	1	3	
1	8558	2	11627	2.08	2.07	0.03	15	3	2.21	0.14	0	23.44	1	2	
2	3302	2.96	5907	3.16	3.07	0.11	15	14	0.14	0.71	0	23.44	1	8	
3	3052	4	7074	4.08	4.08	0.06	12	10	0.32	0.57	0	18.75	1	6	
4	1466	4.92	2621	5.12	5.1	0.2	15	28	10.02	0	0	23.44	1	16	
5	1978	5.96	3838	6.12	5.97	0.16	17	21	0.95	0.33	0	26.56	1	12	
6	682	6.88	2756	7.04	6.88	0.17	14	22	4.82	0.03	0	21.88	1	13	
7	2283	7.68	6079	7.72	7.66	0.11	18	15	0.54	0.46	0	28.13	1	9	
8	-628	9.2	3286	8.72	8.88	0.2	17	28	7.07	0.01	0	26.56	1	16	
9	0	0	2644	9.52	9.51	0.02	4	2	0.08	0.77	0.06	6.25	1	1	
[2D] Event Probabilities: Noise File GASBL.DAT Image Data Set Name GGAS.FIX															
Max GPKs possible (uniform) : 13624															
Total GPKs found : 207															
Global Probability of Pk : 0.01															
Max LPks possible (uniform) : 5952															
Total LPks found : 161															
Local Probability of Pk : 0.03															
Max InterPks poss. (uniform) : 7872															
Total InterPks found : 46															
Inter Probability of Pk : 0.01															
ItemNum	GPKAmpl	GPKLat	BPKAmpl	BPKLat	Mn	SD	O	E	ChiSq	ChSqP	BinomP	%Swps	CC	Span	
0	16384	1	16384	0.96	0.98	0.05	30	9	60.86	0	0	46.88	1	5	
1	7107	2	7460	2.04	2.03	0.07	18	10	6.66	0.01	0	28.13	1	6	
2	4542	3	5523	3.04	3.07	0.06	13	7	5.98	0.01	0	20.31	1	4	
3	1344	3.96	4234	4	4	0.07	13	10	0.78	0.38	0	20.31	1	6	
4	1444	5.08	3820	4.92	5.12	0.16	18	23	1.39	0.24	0	28.13	1	13	
5	2339	5.96	2871	5.96	6.03	0.21	21	29	4.47	0.03	0	32.81	1	17	
6	895	7.84	3032	7	7.01	0.07	9	10	0.22	0.64	0	14.06	1	6	
7	516	8.68	2670	7.68	7.62	0.13	15	19	1.22	0.27	0	23.44	1	11	
8	0	0	1844	9.56	9.03	0.3	24	43	26.53	0	0	37.5	0.96	25	



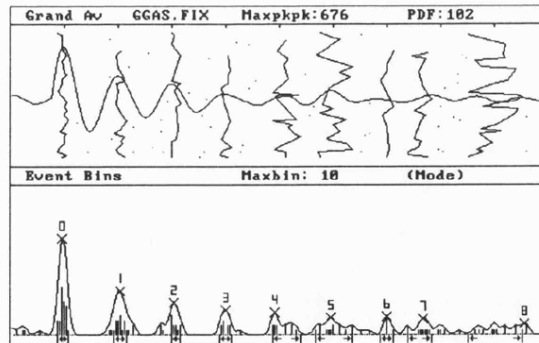
(a) Signal + Spontaneous EEG (1 response/sub-average)



(b) Signal + Spontaneous EEG (2 responses/sub-average)

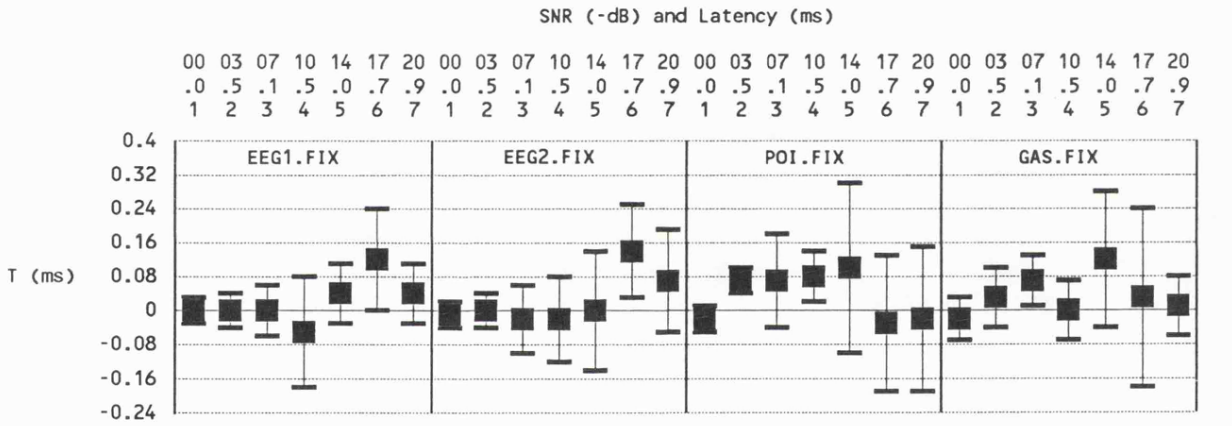


(c) Signal + Poisson noise



(d) Signal + gaussian noise

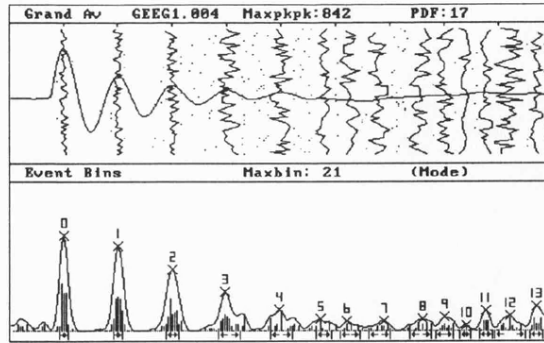
Trajectory maps obtained for one of the data sets used in the component latency variability recovery experiments. In each case, the simulated signal is invariant and combined with different noise data.



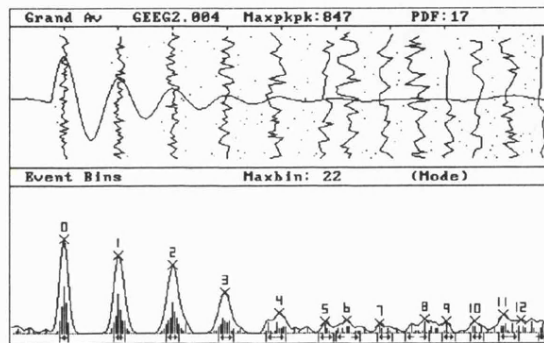
Error in recovery of mean signal latency T ($\pm 1Sd$) in noise vs SNR. Signal latency distribution $N(0,0)$ and noise files are spontaneous EEG, Poisson, and gaussian.

[3] EVENT ANALYSIS RESULTS FOR INDUCED LATENCY VARIANCE SIGNAL (SD = 0.04ms) + NOISE DATA FILES														
[3A] Event Probabilities: Noise File VIN1.EEG Image Data Set Name GEEG1.004														
Max GPks possible (uniform) : 14208														
Total GPks found : 707														
Global Probability of Pk : 0.05														
Max LPks possible (uniform) : 6976														
Total LPks found : 555														
Local Probability of Pk : 0.08														
Max InterPks poss. (uniform) : 7232														
Total InterPks found : 152														
Inter Probability of Pk : 0.02														
ItemNum	GPkAmpI	GPkLat	BPkAmpI	BPkLat	Mn	SD	O	E	ChiSq	ChSqP	BinomP	%Swps	CC	Span
0	16384	1	16384	1	1	0.04	60	20	113.12	0	0	93.75	1	4
1	7060	2	14647	2	2.01	0.05	57	20	96.65	0	0	89.06	1	4
2	3658	3	10586	3	3	0.07	52	31	28.81	0	0	81.25	0.96	6
3	2232	4	6668	3.96	4.03	0.12	50	51	0.08	0.78	0	78.13	0.89	10
4	1295	5.04	3572	4.96	4.99	0.12	44	51	4.6	0.03	0	68.75	0.9	10
5	-897	5.68	1912	5.72	5.78	0.08	29	36	2.79	0.09	0	45.31	0.97	7
6	244	8.08	1550	6.2	6.26	0.1	28	46	24.42	0	0	43.75	0.9	9
7	1165	8.68	1610	6.88	6.78	0.12	33	51	30.84	0	0	51.56	0.85	10
8	462	9.24	1924	7.6	7.57	0.12	35	51	24.34	0	0	54.69	0.88	10
9	0	0	2276	8	8	0.09	39	41	0.2	0.65	0	60.94	0.95	8
10	0	0	985	8.4	8.37	0.06	19	25	2.72	0.1	0	29.69	0.9	5
11	0	0	3464	8.76	8.76	0.07	33	31	0.38	0.54	0	51.56	0.89	6
12	0	0	2530	9.2	9.2	0.16	42	64	7.56	0.01	0	65.63	0.78	14
13	0	0	4119	9.68	9.69	0.07	34	31	0.75	0.39	0	53.13	0.81	6
[3B] Event Probabilities: Noise File VIN2.EEG Image Data Set Name GEEG2.004														
Max GPks possible (uniform) : 14272														
Total GPks found : 569														
Global Probability of Pk : 0.04														
Max LPks possible (uniform) : 5824														
Total LPks found : 431														
Local Probability of Pk : 0.07														
Max InterPks poss. (uniform) : 8448														
Total InterPks found : 138														
Inter Probability of Pk : 0.02														
ItemNum	GPkAmpI	GPkLat	BPkAmpI	BPkLat	Mn	SD	O	E	ChiSq	ChSqP	BinomP	%Swps	CC	Span
0	16384	1	16384	1	1	0.04	59	19	120.3	0	0	92.19	1	4
1	7952	2	13473	2	2.02	0.06	54	24	61.62	0	0	84.38	1	5
2	4271	3	11891	3	3	0.07	52	28	35.2	0	0	81.25	1	6
3	1724	4	7083	3.96	3.98	0.08	39	33	2.14	0.14	0	60.94	0.98	7
4	1049	5	3380	4.96	4.9	0.1	32	43	7.93	0	0	50	0.82	9
5	480	5.92	2092	5.8	5.81	0.08	23	33	6.45	0.01	0	35.94	0.96	7
6	474	7.52	2202	6.2	6.21	0.13	34	52	33.81	0	0	53.13	0.87	11
7	1409	9.28	1604	6.8	6.9	0.09	21	33	9.24	0	0	32.81	1	7
8	0	0	2342	7.64	7.49	0.13	31	52	45.95	0	0	48.44	0.84	11
9	0	0	2005	8.04	8.07	0.07	17	28	8.25	0	0	26.56	1	6
10	0	0	1970	8.56	8.6	0.08	21	28	3.48	0.06	0	32.81	0.91	6
11	0	0	3166	9.08	9.18	0.11	35	43	4.09	0.04	0	54.69	0.92	9
12	0	0	2168	9.4	9.78	0.04	13	14	0.13	0.72	0	20.31	1	3

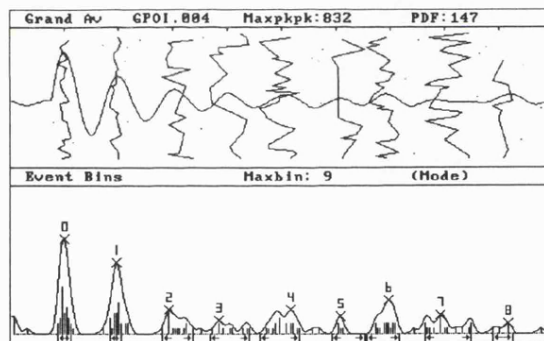
[3C] Event Probabilities: Noise File POIBL.DAT Image Data Set Name GPOL004															
Max GPks possible (uniform) : 13376															
Total GPks found : 188															
Global Probability of Pk : 0.01															
Max LPks possible (uniform) : 7744															
Total LPks found : 168															
Local Probability of Pk : 0.02															
Max InterPks poss. (uniform) : 5632															
Total InterPks found : 20															
Inter Probability of Pk : 0.00															
ItemNum	GPkAmpI	GPkLat	BPkAmpI	BPkLat	Mn	SD	O	E	ChiSq	ChSqP	BinomP	%Swps	CC	Span	
0	16384	1	16384	1	0.99	0.06	28	8	53.39	0	0	43.75	1	6	
1	8256	2	12378	1.96	1.95	0.06	20	7	27.55	0	0	31.25	1	5	
2	3759	3.04	4239	2.92	3.06	0.17	15	19	1.46	0.23	0	23.44	1	14	
3	2385	4.04	2318	3.84	4.03	0.25	14	25	7.93	0	0	21.88	1	18	
4	1855	5.08	4186	5.16	4.96	0.21	27	25	0.26	0.61	0	42.19	1	18	
5	728	6.08	3012	6.08	6.21	0.19	11	21	6.87	0.01	0	17.19	1	15	
6	2006	6.92	5794	6.96	6.87	0.18	23	21	0.34	0.56	0	35.94	1	15	
7	55	7.84	3346	7.92	8.06	0.28	21	29	4.19	0.04	0	32.81	0.95	21	
8	-694	8.44	1813	9.16	9.05	0.12	9	12	1.22	0.27	0	14.06	1	9	
[3D] Event Probabilities: Noise File GASBL.DAT Image Data Set Name GGAS.004															
Max GPks possible (uniform) : 12928															
Total GPks found : 194															
Global Probability of Pk : 0.02															
Max LPks possible (uniform) : 6400															
Total LPks found : 160															
Local Probability of Pk : 0.03															
Max InterPks poss. (uniform) : 6528															
Total InterPks found : 34															
Inter Probability of Pk : 0.01															
ItemNum	GPkAmpI	GPkLat	BPkAmpI	BPkLat	Mn	SD	O	E	ChiSq	ChSqP	BinomP	%Swps	CC	Span	
0	16384	1	16384	0.96	0.98	0.05	25	8	41.29	0	0	39.06	1	5	
1	7688	2	11009	2	2.05	0.1	24	14	8.26	0	0	37.5	1	9	
2	3721	3	5735	2.92	2.96	0.09	14	11	0.85	0.38	0	21.88	1	7	
3	753	4.04	3658	3.95	3.92	0.15	17	19	0.36	0.55	0	26.56	1	12	
4	2091	5.12	4404	5.24	5.24	0.19	20	26	2.04	0.15	0	31.25	1	16	
5	173	6	4214	5.92	6.06	0.21	20	27	3.31	0.07	0	31.25	1	17	
6	876	7.04	5703	6.96	7.05	0.18	23	24	0.07	0.8	0	35.94	1	15	
7	545	7.92	1912	8.44	8.6	0.24	17	30	11.25	0	0	26.56	1	19	



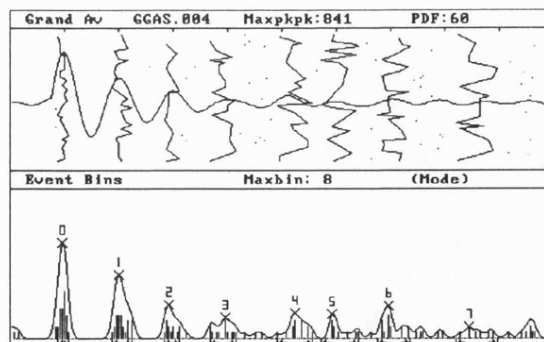
(a) Signal + Spontaneous EEG (1 response/sub-average)



(b) Signal + Spontaneous EEG (2 responses/sub-average)



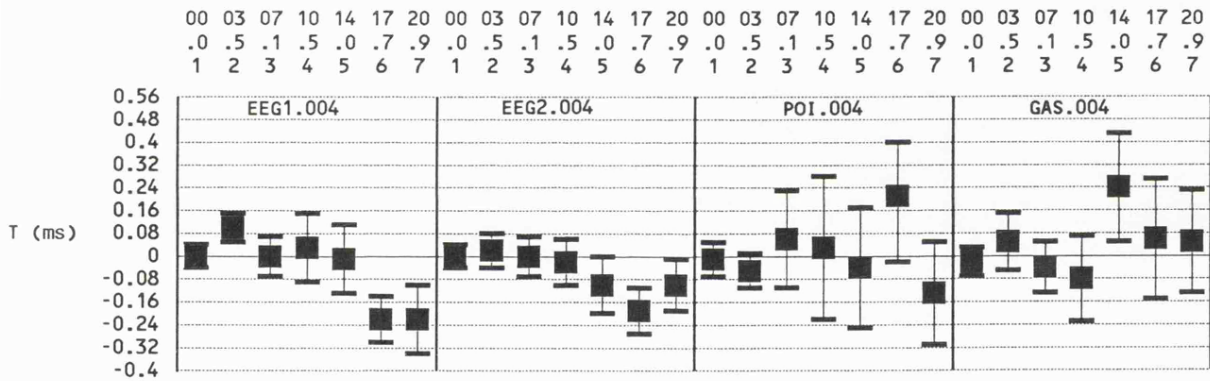
(c) Signal + Poisson noise



(d) Signal + gaussian noise

Trajectory maps obtained for one of the data sets used in the component latency variability recovery experiments. In each case, the simulated signal has been supplied with an artificial latency variability ($N(0,0.0016)$) and then it is combined with different noise data.

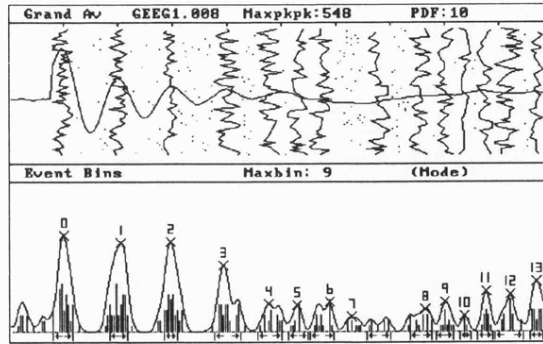
SNR (-dB) and Latency (ms)



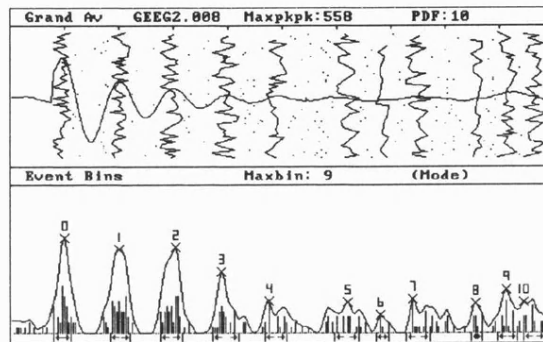
Error in recovery of mean signal latency T ($\pm 1sd$) in noise vs SNR. Signal latency distribution $N(0,0.0016)$ and noise files are spontaneous EEG, Poisson, and gaussian.

[4] EVENT ANALYSIS RESULTS FOR INDUCED LATENCY VARIANCE SIGNAL (SD = 0.06ms) + NOISE DATA FILES															
[4A] Event Probabilities: Noise File VIN1.EEG Image Data Set Name GEEG1.008															
Max GPks possible (uniform) : 14400															
Total GPks found : 687															
Global Probability of Pk : 0.05															
Max LPks possible (uniform) : 8064															
Total LPks found : 532															
Local Probability of Pk : 0.07															
Max InterPks poss. (uniform) : 6336															
Total InterPks found : 155															
Inter Probability of Pk : 0.02															
ItemNum	GPkAmpl	GPkLat	BPkAmpl	BPkLat	Mn	SD	O	E	ChiSq	ChSqP	BinomP	%Swps	CC	Span	
0	16384	0.96	16384	1	0.98	0.1	55	38	18.72	0	0	85.94	0.98	9	
1	6196	2	15174	2.04	2.01	0.1	49	34	14.53	0	0	76.56	1	8	
2	3364	3	15374	2.96	2.96	0.07	40	25	14.05	0	0	62.5	0.95	6	
3	2364	4	11274	3.92	4	0.15	50	51	0.04	0.84	0	78.13	0.88	12	
4	1523	5.04	4773	4.76	4.77	0.13	40	46	3.26	0.07	0	62.5	0.8	11	
5	431	8.08	4480	5.28	5.31	0.11	35	38	0.58	0.45	0	54.69	0.95	9	
6	1937	8.68	5063	5.88	5.74	0.12	38	46	5.6	0.02	0	59.38	0.93	11	
7	828	9.24	2480	6.28	6.78	0.13	32	46	18.38	0	0	50	0.89	11	
8	1417	9.64	3804	7.64	7.55	0.12	35	42	3.63	0.06	0	54.69	0.9	10	
9	0	0	5088	8	8	0.09	35	34	0.09	0.76	0	54.69	0.92	8	
10	0	0	2741	8.36	8.37	0.06	17	21	1.19	0.27	0	26.56	1	5	
11	0	0	6931	8.76	8.75	0.08	34	30	1.24	0.27	0	53.13	0.89	7	
12	0	0	6409	9.2	9.17	0.16	40	55	28.37	0	0	62.5	0.87	13	
13	0	0	8565	9.68	9.69	0.07	32	25	2.9	0.09	0	50	0.8	6	
[4B] Event Probabilities: Noise File VIN2.EEG Image Data Set Name GEEG2.008															
Max GPks possible (uniform) : 14464															
Total GPks found : 546															
Global Probability of Pk : 0.04															
Max LPks possible (uniform) : 6464															
Total LPks found : 374															
Local Probability of Pk : 0.06															
Max InterPks poss. (uniform) : 8000															
Total InterPks found : 172															
Inter Probability of Pk : 0.02															
ItemNum	GPkAmpl	GPkLat	BPkAmpl	BPkLat	Mn	SD	O	E	ChiSq	ChSqP	BinomP	%Swps	CC	Span	
0	16047	0.96	16384	1	0.96	0.1	49	30	23.6	0	0	76.56	1	8	
1	7250	2	14397	2	2.02	0.1	43	33	5.86	0.02	0	67.19	1	9	
2	4157	3	14693	3.04	2.96	0.12	48	37	7.71	0.01	0	75	1	10	
3	1512	3.96	10578	3.88	3.95	0.14	40	44	1.45	0.23	0	62.5	0.98	12	
4	1193	4.82	5523	4.76	4.88	0.12	27	37	6.45	0.01	0	42.19	0.84	10	
5	642	5.88	5352	6.2	6.19	0.13	32	41	5.15	0.02	0	50	0.91	11	
6	-249	6.96	3034	6.8	6.85	0.07	17	22	1.88	0.17	0	26.56	0.94	6	
7	980	7.52	5840	7.4	7.49	0.14	32	41	5.15	0.02	0	50	0.84	11	
8	2334	9.28	5184	8.56	8.59	0.07	20	19	0.17	0.68	0	31.25	0.95	5	
9	0	0	7440	9.12	9.15	0.1	36	33	0.45	0.5	0	56.25	0.95	9	
10	0	0	5189	9.44	9.44	0.12	30	37	3.17	0.08	0	46.88	0.83	10	

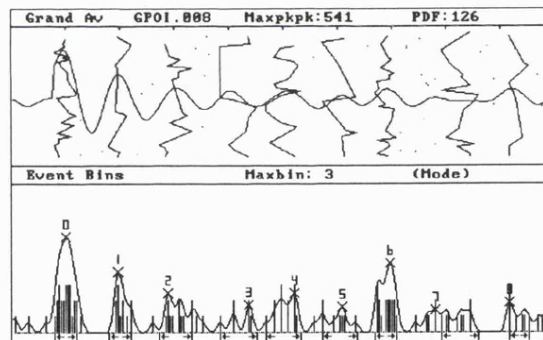
[1C] Event Probabilities: Noise File GASBLDAT Image Data Set Name GPOI.008															
Max GPKs possible (uniform) : 13952															
Total GPKs found : 166															
Global Probability of Pk : 0.01															
Max LPks possible (uniform) : 7680															
Total LPks found : 137															
Local Probability of Pk : 0.02															
Max InterPks poss. (uniform) : 6272															
Total InterPks found : 29															
Inter Probability of Pk : 0.00															
ItemNum	GPKAmpl	GPKLat	BPkAmpl	BPkLat	Mn	SD	O	E	ChiSq	ChSqP	BinomP	%Swps	CC	Span	
0	16384	0.96	16384	1	0.99	0.12	27	11	25.89	0	0	42.19	1	10	
1	8153	1.96	10399	1.96	1.99	0.12	13	11	0.27	0.61	0	20.31	1	10	
2	3534	3.04	6889	2.88	3.02	0.18	15	17	0.36	0.55	0	23.44	1	15	
3	2594	4.04	4646	4.36	4.15	0.24	11	19	5.23	0.02	0	17.19	1	17	
4	2400	5.08	6752	5.2	5.02	0.2	18	18	0.01	0.94	0	28.13	1	16	
5	956	6.08	4344	6.08	6.05	0.22	9	18	6.58	0.01	0	14.06	1	16	
6	3040	6.92	11835	6.96	6.88	0.12	21	11	9.79	0	0	32.81	1	10	
7	190	7.8	3806	7.8	8.27	0.21	16	19	0.86	0.35	0	25	1	17	
8	-682	8.44	5155	9.16	9.3	0.14	7	10	1.24	0.26	0	10.94	1	9	
[1D] Event Probabilities: Noise File GASBLDAT Image Data Set Name GGAS.008															
Max GPKs possible (uniform) : 14016															
Total GPKs found : 198															
Global Probability of Pk : 0.01															
Max LPks possible (uniform) : 6464															
Total LPks found : 137															
Local Probability of Pk : 0.02															
Max InterPks poss. (uniform) : 7552															
Total InterPks found : 61															
Inter Probability of Pk : 0.01															
ItemNum	GPKAmpl	GPKLat	BPkAmpl	BPkLat	Mn	SD	O	E	ChiSq	ChSqP	BinomP	%Swps	CC	Span	
0	16384	0.96	16384	0.96	0.94	0.08	26	8	44.91	0	0	40.63	1	6	
1	6993	2	8400	1.92	2.03	0.14	23	15	5.7	0.02	0	35.94	1	11	
2	3376	3	4997	2.96	3.08	0.11	14	11	1.1	0.29	0	21.88	1	8	
3	317	4.24	2626	4.2	4.18	0.09	8	9	0.28	0.6	0	12.5	1	7	
4	2732	5.16	3676	5.2	5.18	0.23	20	26	2.16	0.14	0	31.25	1	19	
5	100	5.96	4238	6.96	6.83	0.15	16	18	0.21	0.65	0	25	1	13	
6	1265	7.08	2775	8	7.83	0.36	23	41	21.12	0	0	35.94	0.92	30	
7	652	7.92	3988	9.36	9.41	0.09	7	9	0.77	0.38	0	10.94	1	7	



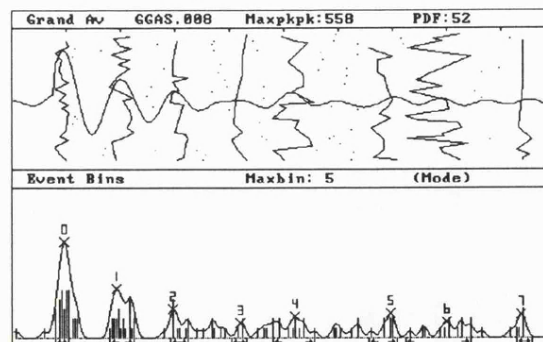
(a) Signal + Spontaneous EEG (1 response/sub-average)



(b) Signal + Spontaneous EEG (2 responses/sub-average)



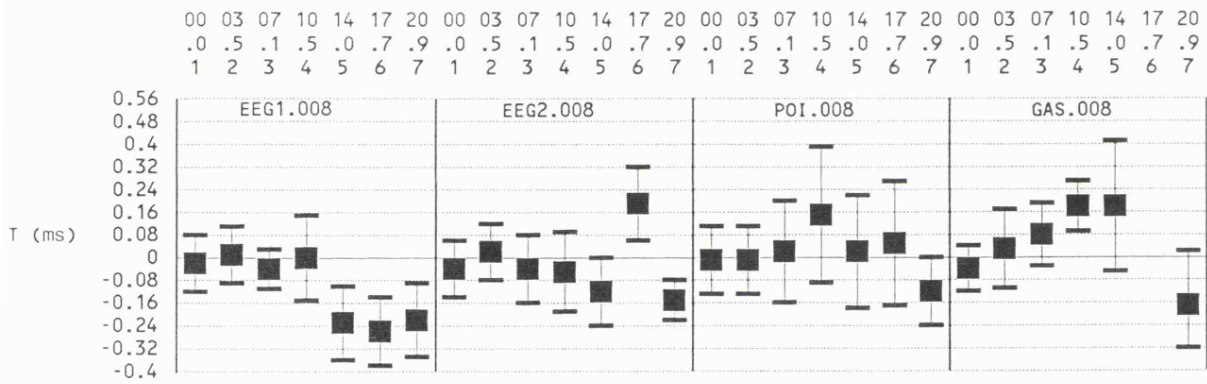
(c) Signal + Poisson noise



(d) Signal + gaussian noise

Trajectory maps obtained for one of the data sets used in the component latency variability recovery experiments. In each case, the simulated signal has been supplied with an artificial latency variability ($N(0,0.0064)$) and then it is combined with different noise data.

SNR (-dB) and Latency (ms)



Error in recovery of mean signal latency T ($\pm 1Sd$) in noise vs SNR. Signal latency distribution $N(0,0.0064)$ and noise files are spontaneous EEG, Poisson, and gaussian.

Appendix [D5]

Normal Latency Values for Short Latency BAEPs

Normal Latency Values for the Brainstem Auditory Evoked Potential (BAEP) / ms								
(Monaural Stimulation, Ipsilaterally, Ai - Cz)								
	Intensity Level dBSL							
Wave #	75	65	55	45	35	25	15	5
I	1.40	1.60	1.80	2.20	2.70	2.90		
II	2.60	2.80	3.00	3.30	3.60	3.80		
III	3.70	3.80	3.90	4.30	4.70	5.10	5.90	5.60
IV	4.60	4.80	5.00	5.40	5.80	6.60		
IV/V	5.20	5.20	5.60	5.90	6.40	7.00	7.70	7.80
V	5.40	5.50	5.80	6.00	6.60	7.10	7.70	8.10
VI	6.90	7.10	7.50	7.80	8.40	9.20	9.50	
VII	8.70	9.00	9.00	9.60				
Sd	0.20	0.20	0.20	0.30	0.30	0.40	0.40	0.40

Appendix [D6]

Published Paper on Event Analysis

NEW DEVELOPMENTS IN COMPUTER APPLICATIONS IN NEUROLOGY

A S Sehmi, University of Leicester,
N L Robinson, A J Charles, Medelec Ltd,
P M Robinson, University of Surrey.

1 Introduction

Clinical neurophysiology is concerned with making diagnostic inferences about diseases of the nervous system. A major procedure which is used in this process is the recording and analysis of the activity of the brain. This activity takes the form of electrical impulses which underlie the basic communication mechanisms of the central nervous system. It is frequently required that the activity of a specific part of the brain be assessed, and this is achieved by causing the structure under test to be activated by sensory stimulation. The resulting activity will then be synchronised in time with the sensory stimulus. Analysis of this activity is usually hampered by the fact that the size of the signal generated in response to sensory stimulation is very much smaller than the size of the other brain (EEG) and muscle (EMG) activity. The EEG and EMG are present all of the time and represent the major noise sources in any recording. In the past, the problems associated with distracting noise have been addressed by the use of coherent averaging techniques which enhance the signal to noise ratio (SNR). In this paper we shall discuss the use of some new approaches to signal estimation which provide additional information of clinical importance and has proved to be more effective than conventional averaging.

2 Evoked Potentials as a Measure of Brain Activity

Very simply, the brain can be considered to consist of a series of elements in which the basic unit is a neuron. Information is transmitted along the neurons in the form of digitally encoded electrical impulses. Communication between two basic units is effected through chemical release at the first unit and molecular recognition at the second. Molecular recognition results in the generation of a new electrical impulse which is then relayed via the cable network propagating from the second unit. When the brain acts as a system, populations of units act in unison, and it is unusual for units to function independently. The synchronous activation of substantial numbers of neurons generates a significant electrical field. As an electrical impulse moves through the specific population of neurons, which are themselves confined to discrete anatomical loci, the fluctuations, in the electrical field associated with impulse transmission, give rise to a change in the cortical surface potential. This change is measured as a potential difference between monitoring electrodes placed over a site anatomically close to the activity, and a remote reference site.

During the course of any sensory stimulation experiment, more than one anatomical structure in the depths of the brain are activated within the territory of the recording electrode geometry. This is reflected in the recordings of complex waveforms which may include activity from both serially and concurrently activated structures, which in turn, may or may not be activated in synchrony. In these recordings, known as evoked potentials, the activities of separate anatomical structures are described as individual components of the waveform. It is generally accepted that, provided exactly the same stimulus is applied repeatedly, the neuronal responses should be the same, i.e. the resulting signals are non-stationary and deterministic. A major limitation of this interpretation is the implicit assumption that the status of the neurons is constant across stimulation trials. This constraint limits the scope of investigation severely, and precludes investigation of one of the most important features of brain activity, namely the brain's ability to habituate to some forms of stimulus and to facilitate others. These types of change are known to be among the most sensitive to the disease process and, therefore, warrant the examination of new techniques which are less limited in their assumptions.

The complexity of evoked potentials poses significant signal processing problems. Solutions to these problems are of immediate clinical importance. It is possible that the approach described in this paper will have wider application to signals with similar characteristics derived from related areas in electrophysiology (e.g. in cognitive evoked potentials), and to signals derived from engineering (e.g. in fault monitoring and communications).

3 The Nature of the Analysis Problem

The aim of the clinical neurophysiologist is to gain the maximum amount of information about the effectiveness of signal transmission within the brain. These signals take the form of electrical impulses which, when recorded remotely from the scalp, are represented as maximum and/or minimum deflections in a time series voltage record.

Approaching the estimation problem from a signal processing viewpoint, a number of features in the data need to be considered:

- 1) It is often difficult to accurately predict the precise characteristics of the signal since these can change substantially with onset and progression of disease.
- 2) The signal itself should not be treated as entirely deterministic, as trial-to-trial changes are known to occur and these changes may carry important clinical information.
- 3) There is no substantial difference between the frequency content of the noise and that of the signal.
- 4) The signal to noise ratio is often very low ($< -20\text{dB}$).

The main approach to 1, 3 and 4 has been signal averaging, however this has precluded the possibility of estimating behaviour in 2. We have developed a new technique called Event Analysis¹, which allows all of the above points to be considered.

4 Recording Procedure

An ensemble of scalp-recorded potentials is amplified and then digitised using a Medelec Mystro MS25 connected to a CED1401 analogue to digital conversion system. Each trial in the ensemble consists of the time series related to a single sensory stimulus. During the course of an experiment, up to 1024 trials may be acquired. The electrode placements, sampling rate, and analogue filters are adjusted depending on the type of evoked potential recording which is being undertaken, and they are set according to the standard protocols. In simulation experiments, analogous data formats are used to allow simple mapping from simulation trials to experimental trials. For the purposes of this discussion, results will be limited to signals recorded following auditory stimulation, the corresponding evoked potential being known as the Brainstem Auditory Evoked Response (BAER). Fig.[1] shows the setup used for the acquisition of data. Elementary BAER characteristics and some clinical applications are described in the appendix.

5 Event Analysis

The data used in this analysis can be described by an additive noise model. The measured single response x , obtained after the delivery of one sensory stimulus, is the sum of a non-stationary signal s plus random noise n . The response is interpreted during analysis in terms of an additive combination of a signal event sequence $\{E_s\}$ and a noise event sequence $\{E_n\}$. The measured event sequence $\{E_x\}$ is then given by:

$$\{E_x\} = \{E_s\} + \{E_n\}$$

An event is assigned at a turning point where a pair of maxima are interleaved with a pair of minima, such that the amplitude differences between the adjacent turning points are greater than a threshold value².

5.1 Estimation of Peak Threshold

Separate peak threshold values are determined for *each* of the single responses in the data. The threshold value (or peak discrimination factor, PDF) is, therefore, adaptive on a trial-to-trial basis, and its computation is based on the assumption that the signal and noise are combined additively. This additive model predicts that, at points where signal and noise occur together, the resulting activity will be greater in amplitude than when the noise occurs alone. The amplitude deflections between turning points are calculated and a frequency distribution is constructed. The

proportional contribution of the noise-related deflections in the histogram bins is assumed to be high because of the low SNR of the single response data, and hence the modal class value will represent a measure for the noise-related amplitude deflections. The threshold used for the reduction of the individual responses to an event sequence $\{E_x\}$, is set to the upper value of the modal bin. The event sequence is thus limited to those turning points which fulfil the requirement that they are bounded by turning points with amplitude separation greater than the calculated threshold. Although, as is expected, this process will cause a rejection of some events which may be related to the true signal, it allows for adaptation to changing noise levels and protects the analysis from being biased towards the highest amplitude events. This bias is a major defect of conventional averaging, except in very large ensembles of data.

5.2 Estimation of Signal Component Locations

The event sequence at this stage consists of both true signal events and noise events extracted from a series of independent trials. The events are labelled either positive or negative depending on whether they resulted from a maximum or a minimum deflection. Signal-related events will be confined to a discrete time interval, and noise-related events will be randomly distributed. Polarised event-latency histograms are obtained from a synchronous summation of the bipolar events across all of the independent single responses (i.e. histograms of the number of times of occurrence of events at a time measured with respect to the onset of stimulus delivery). Modelling of this synchronous summation process has been performed to determine its effectiveness in the cancellation of noise-events¹. Results from this simulation show that there is an error in cancellation if the noise is wideband and stationary, and the number of trials is low. However, the error can be reduced by digital filtering and/or creating small sub-averages from the single responses prior to event analysis.

The positive half of the latency histogram is smoothed and its minima locations provide segmentation of the corresponding ensemble of single responses into component and non-component intervals. The unbiased mean latencies of these segments are determined by a convergent iterative procedure which uses the segment boundaries as initial values. Only those events in the ensemble that lie within the resulting latency intervals (usually described as trajectory events) are used in subsequent analysis. It is possible that some single responses will not yield a trajectory event. A summary of the event analysis procedure is shown in Fig.[2].

It will be clear that, throughout the procedure, the tendency has been to discard outlier data which is likely to contaminate results rather than to increase the size of the data set until the weighting of outliers is reduced. This has resulted in the ability to analyse signals using substantially smaller numbers of trials (64-128 trials for BAERs at 60 dB stimulus intensity), whilst retaining estimates of the underlying signal characteristics. Using the latencies of trajectory events, it is possible to

produce descriptive statistics for the signal components and to derive enhanced signal waveforms using latency corrected averaging³. This is performed by temporally aligning all events within a component interval by applying shifts to *selected* data trials which are then conventionally averaged. Trajectory events also enable one to extract and enhance specific components and/or combinations of components. These procedures have been implemented¹, and in conjunction with correlation analysis, they will allow for the investigation of relationships between different components, since some temporal synchronisation between trajectory events will exist across an ensemble of single responses and also within single responses.

5.3 Results of Simulation Experiments

In order to assess the effectiveness of the approach described above, a number of experiments have been performed using data simulations where both the SNR and latency variability of the *signal* can be controlled. The simulations have shown that it is possible to reliably estimate the latency variability of components to within two sampling points at a SNR as low as -15 dB. Examples of results from event analysis performed on a simulated BAER data set are shown in Figs.[3 and 4]. The data shown in Fig.[4] consists of 64 trials of an exponentially decaying, 1 kHz sine wave, which has been additively combined with spontaneous EEG. Prior to the combination, both the signal and the noise are normalised, so that the simulation experiments will reflect the performance of event analysis across a wide range of signal to noise ratios (i.e. 0 dB at 1ms to -21 dB at 7ms).

Following encouraging results obtained from single channel BAER recordings^{1,4}, it is intended to extend event analysis into the multi-channel recording regime. This will help to enhance the understanding of neuronal communication mechanisms in the brain, by analysing data containing temporal information which has been obtained spatially over the scalp.

6 References

1. Sehmi, A S: 'New environments for neurophysiological investigations', to be submitted for the degree of PhD. in Engineering at the University of Leicester, England, September 1988.
2. Lago, P J A and Jones, N B: 'Turning points spectral analysis of the interference myoelectric activity', *Med. & Biol. Eng. & Comput.*, 21, 333-342, 1983.
3. McGillem, C D, Aunon, J I, Pomalaza, C A: 'Improved waveform estimation procedures for event related potentials', *IEEE Trans. Biomed. Eng.*, BME-32, No. 6, 371-379, 1985.

4. Sehmi, A S: 'EPAXIS: An expert system for automatic component labelling in evoked potentials', TIRM-88-31, Turing Institute Press, Glasgow, September 1988.

Author Biography

Arvindra Sehmi

Graduate of the University of Sussex in Electronic Engineering with Medical Instrumentation and is at present submitting for the degree of PhD. in Engineering at the University of Leicester. Arvindra has worked extensively on instrumentation and signal processing applied to electromedical diagnostics both at Sussex and Leicester Universities. He is currently a Medelec Research Scientist and Research Associate of the University of Leicester.

Neil Robinson

Graduate of Liverpool University in Physiology with PhD in Biochemical Endocrinology from Hull University. He spent five years in postdoctoral research in neurophysiology at Nottingham University and Yale University before joining Medelec in 1982. He is currently Head of Clinical Research at Medelec.

Alison Charles

Graduate of the Open University in Applied Mathematics and graduate member of the IMA. Alison has worked as a Research Scientist at Medelec on the development of real-time signal processing applications in electrophysiology. She is hoping to pursue a PhD degree at the University of Surrey.

Paulette Robinson

Graduate of the Open University in Physiology. Paulette is Research Physiologist in the Medelec Clinical research team with responsibility for human subject research and experimental design. She is currently pursuing studies in the application of Brain Activity Analysis in Psychometric diagnosis and is a Senior Research Fellow at the Robens Institute at the University of Surrey.

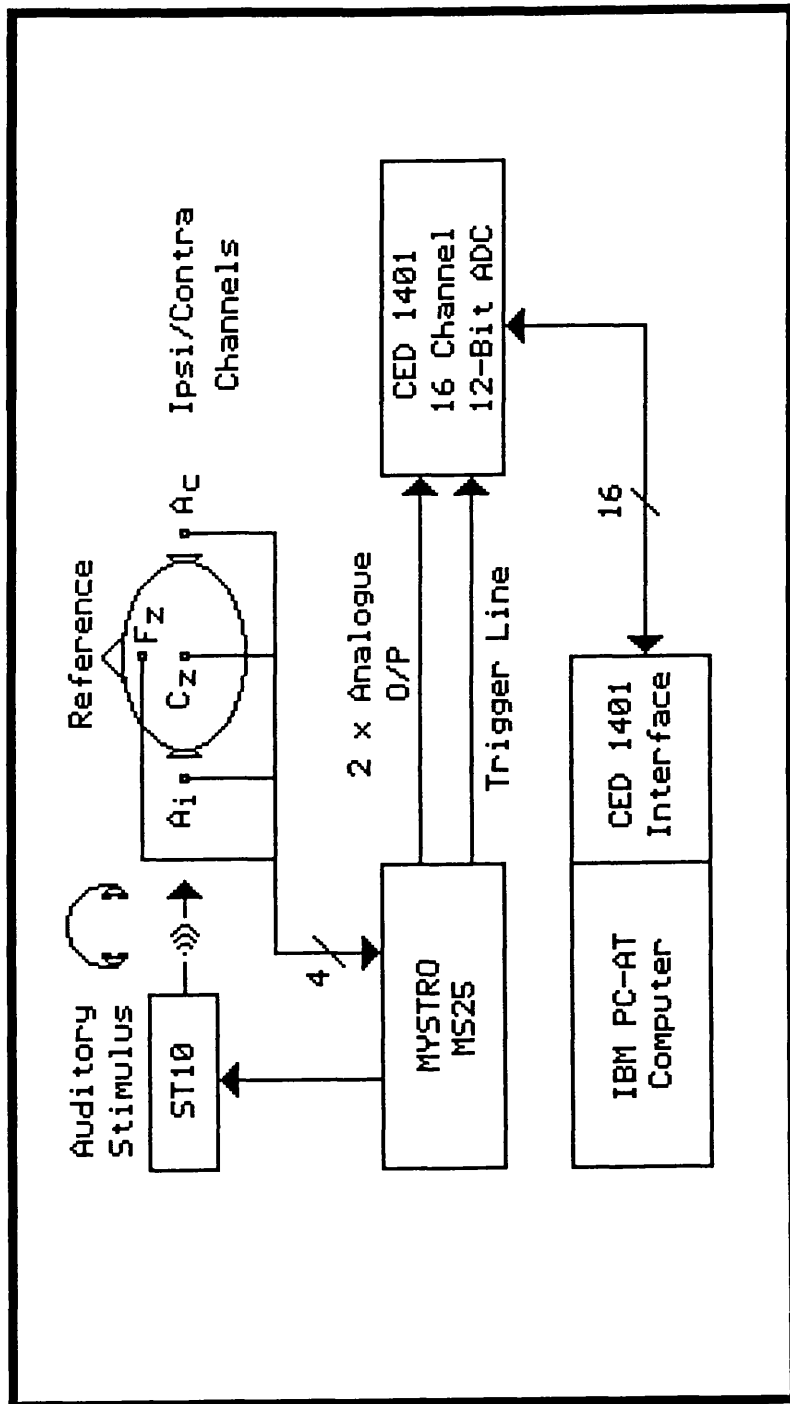


Fig.[1] The experimental setup used for the acquisition of BAER data. A similar setup can be used for all other ERPs when different stimuli and electrode derivations are employed (taken from Ref. 1).

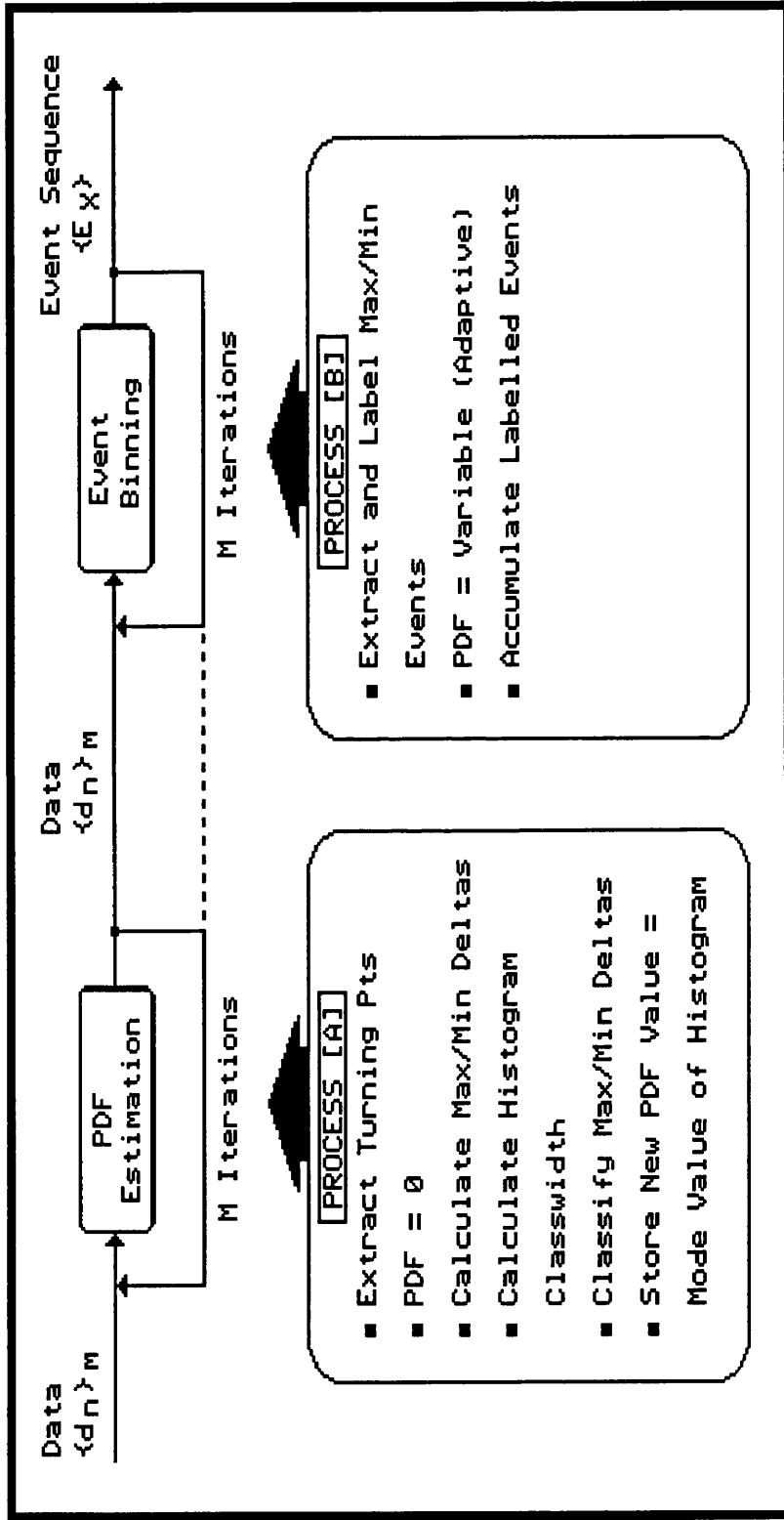


Fig.[2] Schematic diagram of the adaptive PDF calculation and subsequent event binning process. The dotted line indicates that the two separate iteration loops can be combined into one *super - process*, so as to enable a predominantly parallel execution architecture for more rapid execution in multi-tasking and/or multi-processor environments.

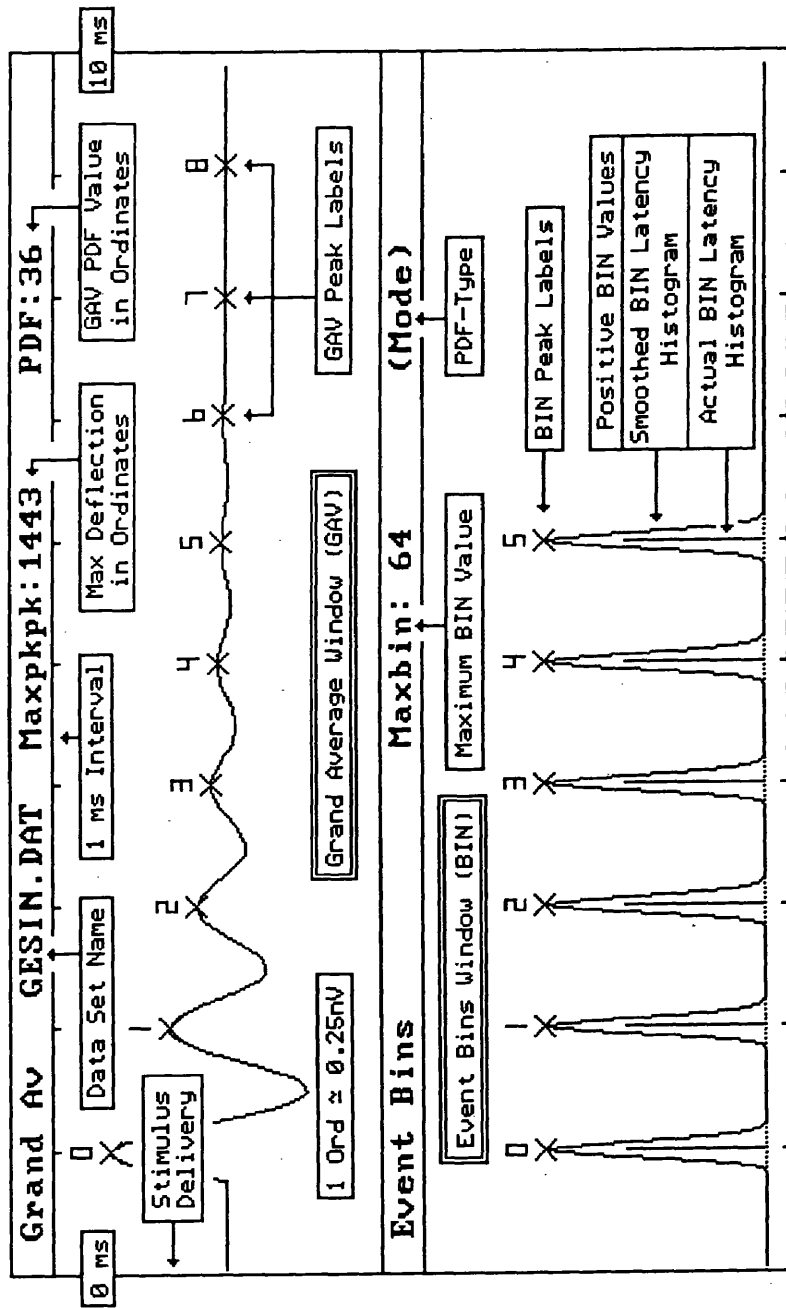
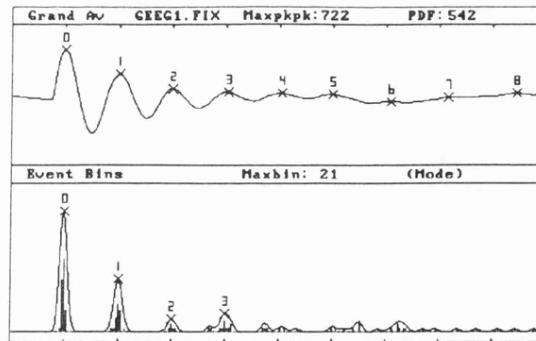
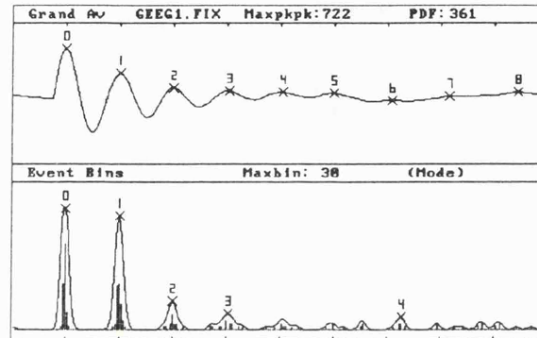


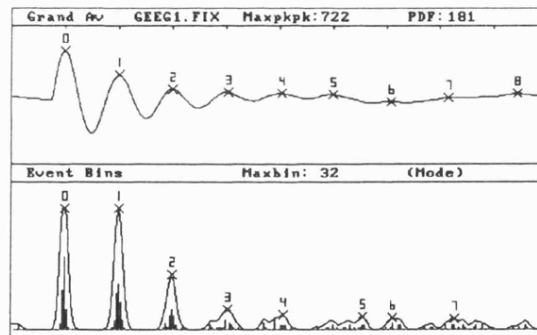
Fig.[3] A sample of the graphical display format for the results in the text. It shows explanations for the various screen attributes that are available. These displays have been derived directly from the Event Analysis result screens. The menu bars and cursors are not shown for clarity (taken from Ref. 1).



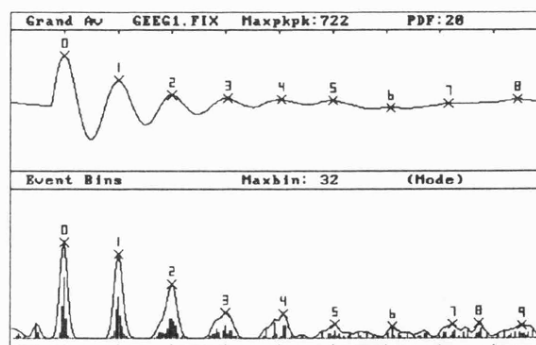
(a) PDF value = 75% of Maxpkpk.



(b) PDF value = 50% of Maxpkpk.



(c) PDF value = 25% of Maxpkpk.



(d) PDF value is determined adaptively.

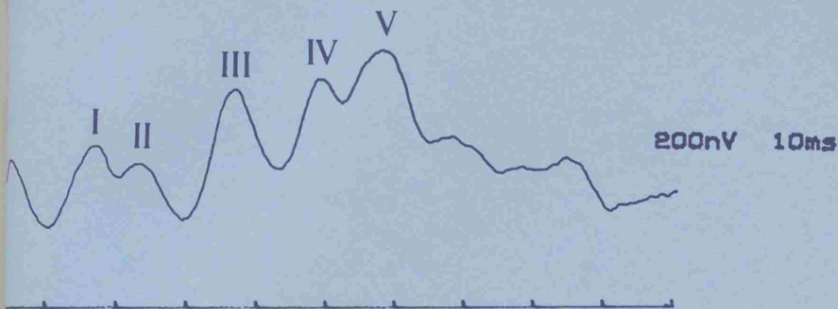
Fig.[4] The effect of the PDF value on the structuring that occurs in the event bin (BIN). The PDF value per single trial varies from 75% of the maximum peak-to-peak deflection, to one that is determined adaptively (taken from Ref. 1).

APPENDIX

Brainstem Auditory Evoked Response

CLINICAL APPLICATIONS

Brainstem Auditory Evoked Response

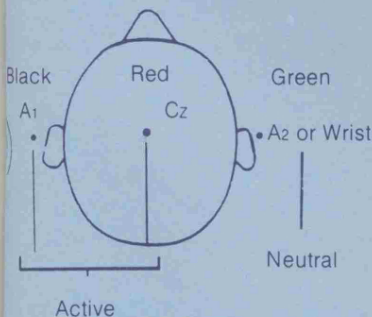


Assessment of the integrity of the auditory neural pathway can be performed by recording, using scalp electrodes, the far field potentials produced in the auditory nerve and brainstem.

Electrode Placement

The signal is produced at both A₁ and Cz. Both electrodes may be considered active. This may be confirmed by recording from A₁ and Cz independently referred to a remote (non-cephalic) recording site. The full signal may then be obtained by addition of the two traces. The signal arising from A₁ may also be investigated by recording both laterally and contralaterally (A₁-C_z and A₂-C_z). Subtraction of these traces (A₁-C_z) minus (A₂-C_z) would then show the signal on A₁.

Electrodes should be non-polarisable Ag/AgCl EEG type. Electrical contact is made using either electrode jelly or bentonite paste. Electrode resistances should be checked to be less than 6kΩ.



Stimulation

Monaural Clicks
 Black Polarity - rarefaction
 Duration - 0.1 ms
 Repetition Rate - < 10Hz
 Intensity - > 60dB HL
 BAER may also be recorded following the pip stimulation when some frequency discrimination may be possible.

Acquisition

Recording Sensitivity -> 20μV/div*
 Filter: Low Frequency cut off -< 300Hz
 High frequency cut off -> 3kHz

*Recording sensitivity may have to be adjusted to take account of muscle activity. In general it is best to use the highest sensitivity which does not cause the averager to overload.

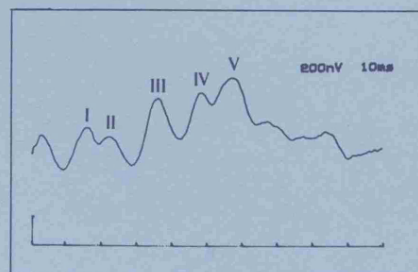
Averaging

Analysis time - 10 ms
 Sweeps - 1024
 Post Average
 Display Sensitivity - 200nV

Effect of filters on recording BAER

It should always be borne in mind that filtering, although often extracting a signal from the background noise, may alter the waveform recorded. In extreme cases alteration of wave latency of 1/8 - 1/4Hz of the signal frequency may occur. In the case of BAER this may amount to + 250 μs in latency. Filtering may also affect the relative amplitude of waves. These factors make it important to standardise recording parameters for all tests.

Identification of Waves



Waves I, III, V are the most consistently observed.

Wave I

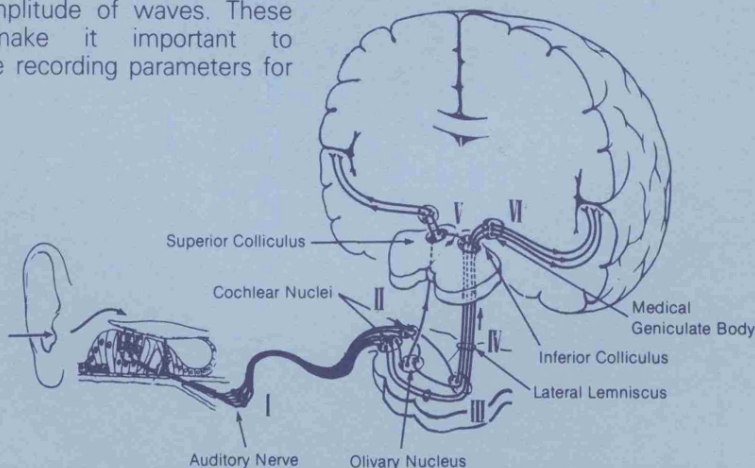
Thought to arise from activity in the VIIIth nerve. This potential is generated as a negativity at A₁ and its identity can often be confirmed by comparing the recording from the vertex to contralateral ear, when this wave will be considerably reduced.

Wave III

Proposed to reflect activity in Pons. This potential also arises largely as a negativity at A₁ and will therefore be reduced by recording from the vertex to the contralateral ear.

Wave V

Arising, it is thought, from activity in the midbrain, this potential is often the most reliable. Waves IV and V are often fused, hence wave V may well not be the fifth vertex positivity. A more characteristic feature is that it typically consists of a vertex positivity followed by a long, sharp negative potential.

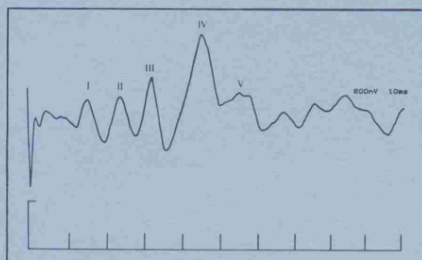


CLINICAL APPLICATIONS

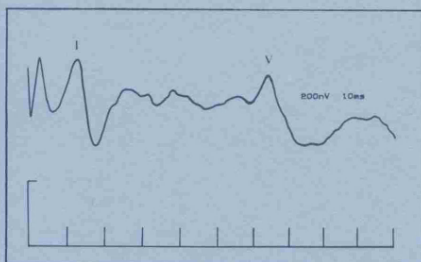
Multiple Sclerosis

BAERs are of most use when a non brainstem structure has a pathological profile since the tests then documents a second locus. It is not unusual to find patients with normal results from one ear and abnormal results from the other.

The most common change in BAER seen in MS is an increase in the I-V latency very often coupled with reduction in the amplitude of wave V.



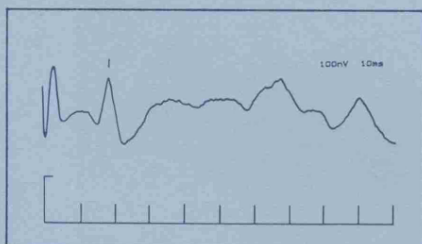
Typical trace obtained from a patient with MS showing reduction in wave V amplitude.



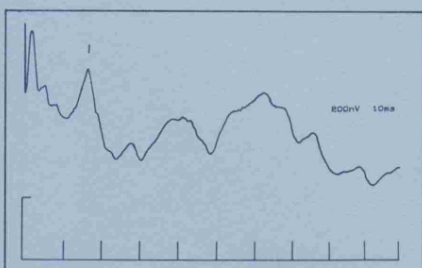
In an extreme case waves II, III, IV are almost absent but waves I and V are preserved.

Acoustic Neuromas

These usually develop in the internal auditory canal and can compress the eighth nerve, resulting in the complete abolition of all waves or an increase in the interpeak latency of early waves.



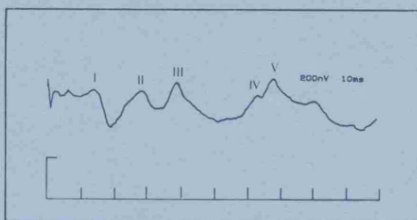
Acoustic neuroma associated with hearing loss abolishing all waves after component I.



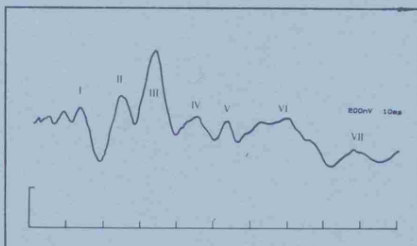
Wave I has normal latency but all other waves are abnormal.

Brainstem Tumours

Tumours intrinsic to the brainstem can increase the interpeak latency of the brainstem waves III and V or the waves subsequent to wave II may be abolished. In the case of multi-level tumours the position is considerably more involved and all waves except wave I may be absent.



A pontine tumour resulting in increased interpeak latency of waves III and IV.



A rostral pons-midbrain tumour resulting in diminished waves IV and V.

Objective Hearing Assessment

BAER can be used as a non-invasive measure of hearing threshold in both infants and adults; wave V being the most resilient component for this application.

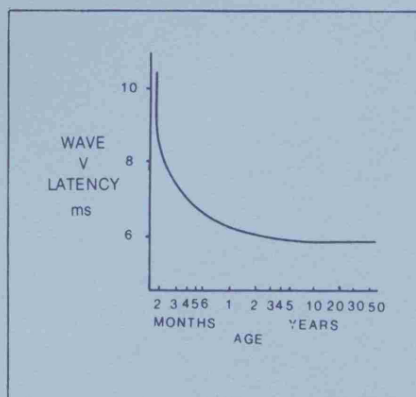
Other applications include intra-operative monitoring and assessment of patient status in intensive care and coma.

Also it is used to monitor development of auditory function in the very young.

Non-pathological factors affecting peak latencies

AGE

This is of particular importance with premature infants where wave V latency may be a useful parameter in assessing developmental age.

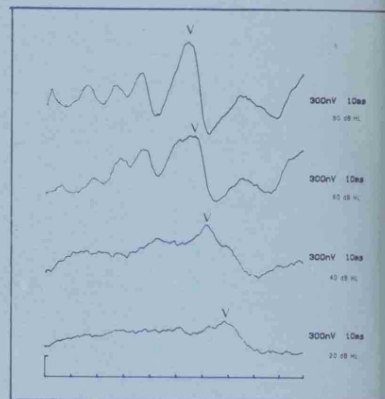


With patients over 50 years normal values also need to be increased.

SEX

Females have slightly shorter latencies

STIMULUS INTENSITY



Other factors influencing latency are temperature and repetition rate.

Further Reading

Chiappa K.H., Gladstone K.J. et al. Brainstem auditory evoked responses. Study of waveform variation in 50 normal human subjects. Arch. Neurology 1979 36, 81 - 87.

Chiappa K.H., Ropper A.H. — Evoked potentials in Clinical Medicine N.E.J.M. 1982 306 1140 - 1150.

Clinical applications of Evoked Potentials in Neurology, Edited by J. Courjon, F. Mauguier and M. Reval, Raven Press N.Y. 1982

Jewett D.L. and Williston J.C. Auditory evoked far fields averaged from the scalp of humans Brain 1971, 94, 681 - 696.

Kavanagh K.T. and Beardsley J.V. Brainstem auditory evoked responses. 1s basic principles in the assessment of patients with non-organic hearing loss. Ann. Otol. Rhinol. Laryngol. 1979 88 (Suppl 5) 1-10.

Ohlrich E.S. et al. Auditory E.P. development in early childhood: a longitudinal study EEG Journal 1978 44, 411 - 423.

Picton T.W. et al. Human Auditory E.P.'s: I evaluation of components, EEG journal 1974 36: 179 - 190.

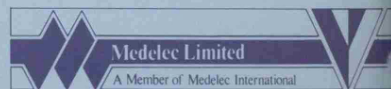
Robinson K. and Rudge P. Auditory Evoked Responses in MS Lancet 1, 1975, 1164 - 1166.

Starr A and Achor L.J. Auditory brainstem response in neurological disease. Arch. Neurol 1975 32, 761 - 768.

Stockard J.E. and Stockard J.J. Brainstem auditory evoked responses. Normal variation as a function of stimulus and subject characteristics. Arch. Neurol. 1979, 36, 823 - 831.

Stockard J.E. and Stockard J.J. et al. Non pathological factors influencing brainstem auditory evoked potentials. American J. EEG Technology 1978, 18, 177 - 209.

Stockard J.J. and Stockard J.E. et al. Detection and localisation of ocular lesions with brainstem auditory responses. Mayo Clinic proc. 52, 761 - 769



Manor Way Old Woking Surrey GU22 9JU England
Telephone: 04862 70331